THE EVOLUTION OF THE CONGO–KALAHARI WATERSHED:

AFRICAN MEGA–GEOMORPHOLOGY

By

Tyrel J. Flügel

Thesis Presented for the Degree of DOCTOR OF PHILOSOPHY

in the Department of Environmental and Geographical Science

UNIVERSITY OF CAPE TOWN

May 2014

Supervisors:

Dr Frank D. Eckardt

Department of Environmental and Geographical Science, University of Cape Town

Dr Fenton P. D. Cotterill

Africa Earth Observatory Network: Geoecodynamics Research Hub, Department of Botany and Zoology, University of Stellenbosch

DECLARATION

I, the undersigned, hereby declare that the work contained in this thesis is my own original work and has not been submitted in its entirety or in part at for examination. All external contributions are duly cited, referenced and acknowledged.

Signed:

T.J. Flügel

May 2014

ABSTRACT

Africa's bimodal elevation, low in the north and west, and high in the south and east, is globally unique. The Congo–Kalahari Watershed represents the transition between low and high Africa. This sub–continental drainage divide separates two of the world's large rivers: the Congo and Zambezi Rivers. This study focuses on the large rivers which form the Congo–Kalahari Watershed. The analysis of their longitudinal profiles, through the use of a geographic information system and remotely sensed imagery and elevation data, provides insights into this drainage divide. The creation of a geodatabase on river knickpoints, featuring geographic and geologic attributes for 18 longitudinal river profiles represented by 194 047 elevation points (19 700 km), identifies a total of 380 knickpoints, 243 of which have heights larger than 5 m. It is possible to assign a probable cause to 354 of all the knickpoints identified in this study, highlighting the underlying geology as a significant control with tectonics playing a secondary role. The following rivers are studied: Chambeshi, Congo, Kalungwishi, Kasai, Kwango, Luapula, Lufira, Lukuga, Lulua, Luvua and Wamba (Congo Basin) and the Cubango, Cuchi, Kabompo, Kafue, Luena and Upper Zambezi Rivers (Kalahari Basin).

It is argued that the Congo–Kalahari Watershed is a trimodal feature comprising of a western, central and eastern zone. The smooth central region of the divide is the oldest and has been relatively stable since the break–up of Gondwana. The western region is topographically rougher and has undergone substantial change in the Cenozoic becoming bifurcated by the headwater erosion of the coastal rivers. The eastern watershed is the youngest and topographically roughest, having been substantially modified in the Neogene due to tectonic activity associated with the extension of Western Branch. Due to the extensive modification, this eastern zone should be considered a new feature. The acknowledgment of these three landscapes may lead to the conciliation of various interpretations and suggested causes of Africa's present day continental geomorphology.

ACKNOWLEDGEMENTS

I would like to express my sincere gratitude to my supervisors, Dr Frank Eckardt (University of Cape Town) and Dr Woody Cotterill (University of Stellenbosch), for their support and guidance during my thesis. I would like to thank both of them for allowing me to a chance at that most crucial of activities when studying landscapes – field work. The opportunity to see both wet rivers (Woody) and dry rivers (Frank) was an invaluable experience and stimulated my thinking about landscapes. I have learnt much from both of them. I sincerely appreciate Prof. Maarten de Wit, who is thanked not only for his enthusiasm and support throughout my studies but also for the many learning opportunities he provided, especially for including me in a diverse research group in the form of the African Earth Observatory Network. I am grateful for his generosity.

I thank my fellow students from whom I learnt a lot. I would especially like to thank: John Decker for his advice, guidance and support, as well as teaching me that most vital of life skills, how to make proper coffee. Christian Mielke is thanked for his enthusiasm on all things related to technology and mapping. Steve Wessels is thanked for teaching me about geomatics. Kathryn Vickery is thanked for her encouragement and entertainment during two great field trips. Bastien Linol is warmly thanked for thoughtful discussions on the Congo Basin and for translating important French literature. I would also like to thank Nicholas Lindenberg and Tom Slingsby for their advice and commiseration for that wily program that is known as ArcGIS. Finally, I would like to thank all those academics and researchers who took the time to have stimulating and insightful conversations about Africa with me and for whom no question was too basic. Out of the many I extend my gratitude to John Ward, Mike de Wit and Hielke Jelsma for sharing their thoughts, ideas and views of the rivers of the south–central Africa.

I thank Caroline and Sarah for their extensive support and constructive criticism during the writing phase of this project. I thank my family and friends who have supported and encouraged me over the years. William is thanked for making the start of this journey possible. I give my heartfelt thanks and appreciation to Sarah for doing everything she could to help me complete my studies; without her help this work would not have been possible.

Financial support from the following institutions is gratefully acknowledged: The National Research Foundation (South Africa), the John Ellerman Foundation, the ERANDA Foundation, the Harry–Crossley Foundation, as well as the additional support from the University of Cape Town Doctoral Scholarship fund.

TABLE OF CONTENTS

LIST OF FIGURES

LIST OF TABLES

LIST OF ABBREVIATIONS

3D	three dimensional
AFTA	Apatite Fission Track Analyses
ASTER	Advanced Spaceborne Thermal Emissions and Reflectance Radiometer
ca.	Approximately
CB	Congo Basin
CGIAR	Consultative Group on International Agricultural Research
CKW	Congo-Kalahari Watershed
CSI	Consortium for Spatial Information
CSRS	Canadian Spatial Reference System
DEM	Digital Elevation Model
DGPS	Differential GPS
DTED	Digital Terrain Elevation Data
DRC	Democratic Republic of Congo
DSM	Digital Surface Model
DTM	Digital Terrain Model
EARS	East African Rift System
EGM96	Earth Gravitation Model 1996
ERS	European Remote-sensing Satellite
ETM+	Enhanced Thematic Mapper Plus
GCPs	Geodetic Control Points
G-DEM	Global Digital Elevation Model
GIS	Geographic Information System
GLCF	Global Land Cover Facility
GPS	Global Position System
ITCZ	Inter-Tropical Convergence Zone
KB	Kalahari Basin

LSM	Land Surface Model
NASA	National Aeronautics and Space Administration
NGA	National Geospatial-Intelligence Agency
NRCan	Natural Resources Canada
PPP	Precise Point ppositioning
RS	Remote Sensing
SAR	Synthetic Aperture Radar
SEM	Surface Elevation Model
SIR-C/X-SAR	Spaceborne Imaging Radar-C/X-band Synthetic Aperture Radar
SRTM	Shuttle Radar Topography Mission
SRTMv250m	SRTM version 4 at a 250 m resolution
SRTMv3	Third SRTM version at 90 m resolution
SRTMv4	Fourth SRTM version
USA	United States of America
USGS	United States Geological Survey
UTM	Universal Transverse Mercator
WGS84	World Geographic System

CHAPTER 1: INTRODUCTION

1.1 Africa's mega-geomorphology

Today Africa straddles the Equator, crossing 72 ˚ of latitude and 68 ˚ of longitude, and with a surface area of 30.3 million km^2, this continent thereby accounts for ca. 20 % of the Earth's landsurface. Incorporating the West African, Congo, Kalahari and Tanzania cratons, amongst others, Africa has its genesis in the formation and break-up of the super continent, Gondwana, which existed from ca. 510 Ma to 180 Ma (de Wit et al., 2008; Torsvik and Cocks, 2009). During this time the African continent formed the heartland of Gondwana and experienced multiple periods of tectonics, subsidence, uplift, denudation and deposition that modified its landsurface. After the break-up of Gondwana, Africa's surface continued to undergo significant changes, with modifications still occurring to this day. Thus, in order to understand Africa's present day continental and sub–continental geomorphology, its mega-geomorphology, Africa's geologic history must be acknowledged.

The African continent has a bimodal elevation distribution making it unique on a planetary scale (see **Figure 1.1**). By comparison, the rest of the world's continents have a unimodal distribution of elevation, with their zones of high elevation being associated with plate boundaries that have led to the formation of continental mountain ranges, such as the Andes, Himalayas and Rocky Mountains. On the planetary scale, Africa's elevation may be described as being composed of two flat lands: one of low elevation (averaging 400 m.a.s.l.) and one of high elevation (approximately 1000 m.a.s.l.). Low Africa consists of the western, northern and central regions while high Africa is formed by the southern and eastern regions (see **Figure 1.2**). Africa's bimodal topography, characterised by its high plateaus and flat lowlands, and the cause of this topography, has been described and debated in the earth sciences for close to a century now (e.g. du Toit, 1933; Veatch, 1935; Dixey, 1938).

Africa's bimodality was initially described in broad terms, with the drainage divide of the Congo and Zambezi Basins having been suggested as the boundary between low, central Africa and high, southern Africa (Dixey, 1938). This watershed in south-central Africa was first described and mapped by Steel (1917) and was later further described and referred to as the Great African Divide by Dixey (1943). Further investigations led Wellington (1955) to add several local watersheds east and west of the Great African Divide, thereby forming a regional watershed he named the South Equatorial Divide (Wellington, 1955). This South Equatorial Divide subsequently formed part of King's (1962) continent spanning West-East drainage divide (see **Figure 1.3**).

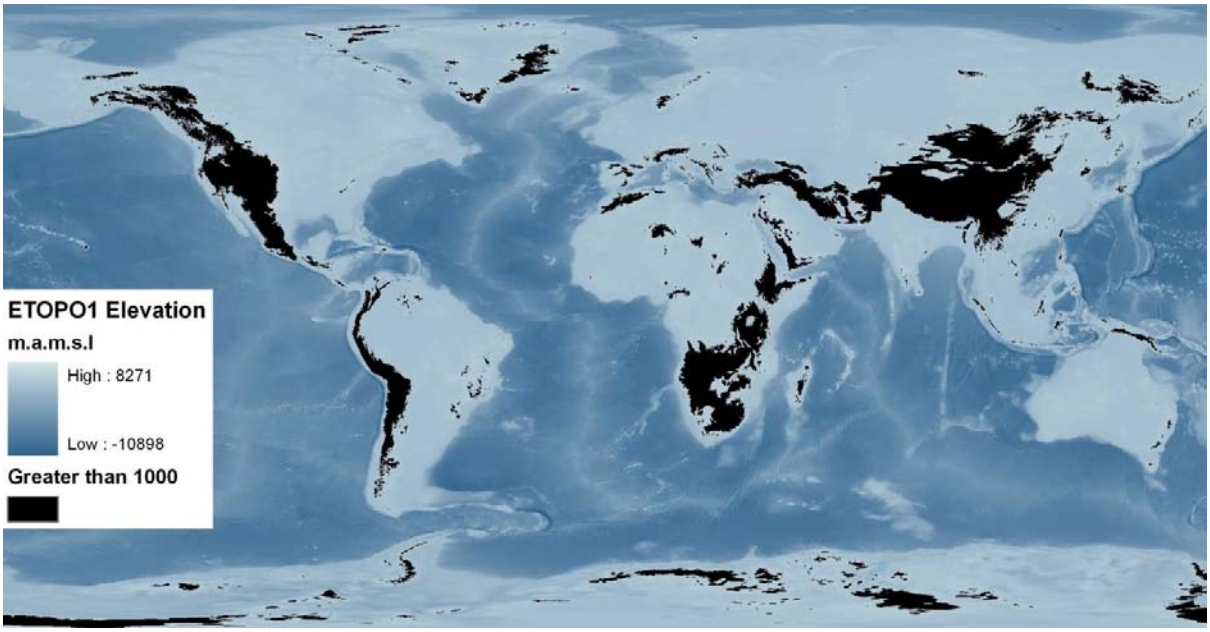

Figure 1.1: The topography and bathymetry of the world. Black regions indicate areas of elevation higher than 1000 m.a.s.l. These elevated zones corresponds to large mountains systems along the margins of continental boundaries, except for Africa. In the south and east, the majority of Africa's elevation is around 1000 m.a.s.l., being of low relief. The digital terrain model is from the ice free version of ETOPO1 2009.

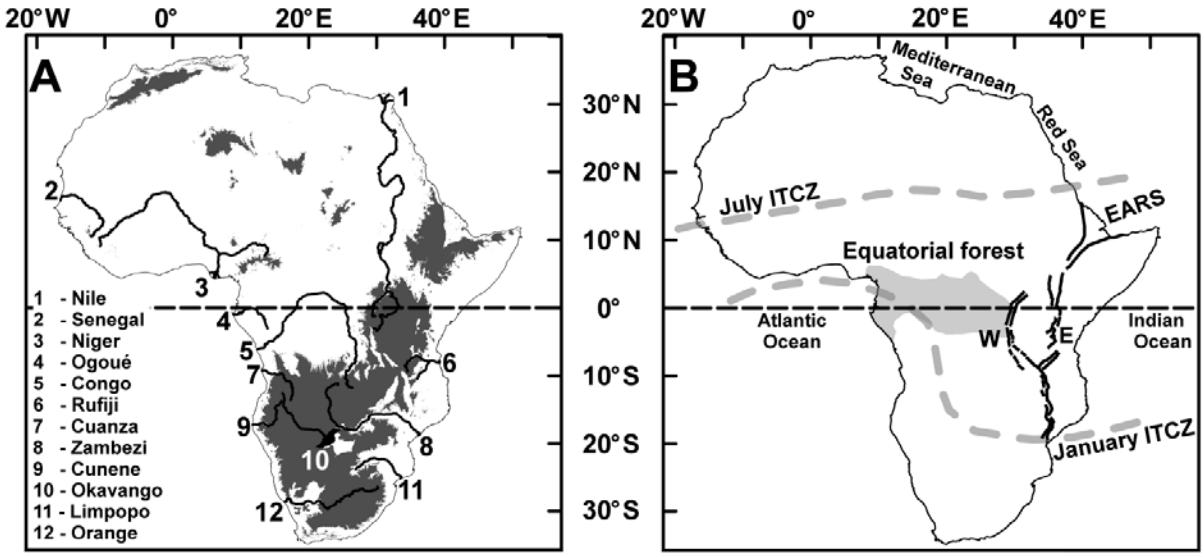

Figure 1.2: The geomorphic and climatic setting of Africa. (A) Dark grey shading indicates elevations above 1000 m.a.s.l. Major rivers are shown and numbered. (B) The climatic regime of present day Africa is related to the movement of the Inter-Tropical Convergence Zone (ITCZ); the maximum extent of which is indicated by the dashed grey lines. The abundant precipitation of central Africa has led to the formation of the Equatorial forest. The East African Rift System (EARS) runs the length of eastern Africa consisting of two branches, the Eastern (E) and Western (W) branches.

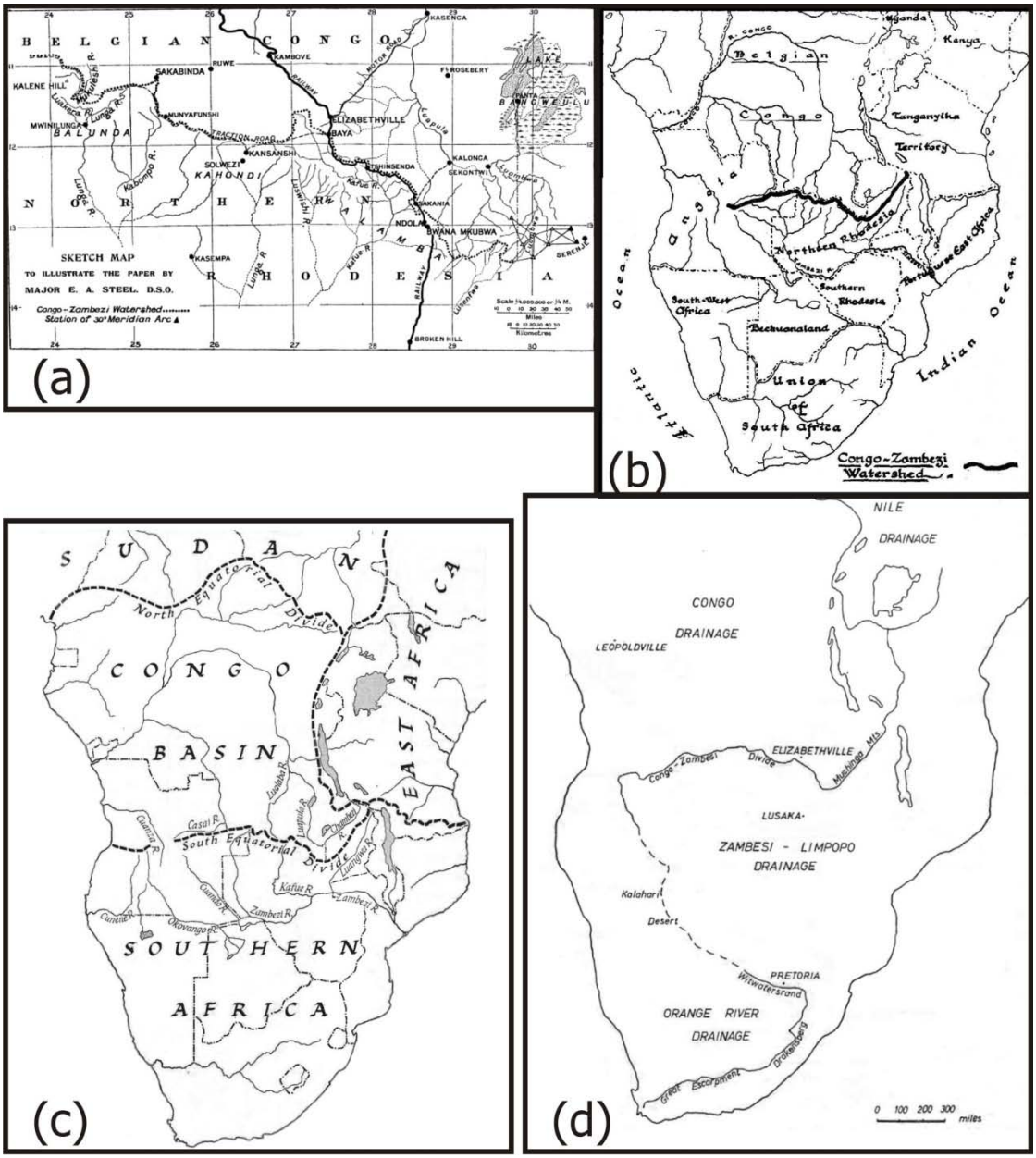

Figure 1.3: The increasing spatial context of the watershed between the Congo and Kalahari (Zambezi and Okavango) basins. (a) The Congo-Zambezi watershed as mapped by Steel (1917), (b) the Congo-Zambezi watershed of Dixey (1943) in context of central and south Africa. (c) The Great Equatorial Divide of Wellington (1955) and (d) the continental West–East Drainage divide of King (1962).

Initial studies in central and southern Africa focused on how these flat surfaces were formed in low and high Africa, with cycles of erosion and uplift being proposed (du Toit, 1933; Maufe, 1935; Veatch, 1935; Dixey, 1944; Robert, 1946; King 1951; Cahen, 1954). This led to attempts to identify and correlate common erosion surfaces in an effort to determine the sequence, duration, causes and magnitude of these periods of erosion and uplift, culminating in King's well known African surfaces (King, 1951; 1962). Recently, as more data and observations became available, the focus

has changed to the mechanism driving the overall process has been focussed on, with a mantle plume driver being suggested and debated (for example, see Nyblade and Roberts, 1994; Burke et al., 2003; Doucouré and de Wit, 2003; de Wit, 2007; Burke and Gunnell, 2008). Although the focus and techniques of inquiry have changed, it has been agreed that major elements of Africa's topography, such as its rivers, planation surfaces and depositional basins, formed in the Cretaceous or even earlier (for example, see King, 1953; Partridge and Maud, 1987; Doucouré and de Wit, 2003).

This recognition of old landscapes does not mean that Africa's landscape has not undergone drastic changes; perhaps the most dramatic geologically recent alteration is the formation the East African Rift System (EARS), whose extension has modified parts of central and southern Africa. The extension of the Rift in a general south–westerly trend (Gumbricht et al., 2001; Chorowicz, 2005) has major implications for the geomorphological evolution of central low Africa (Congo Basin) and southern high Africa (Kalahari Plateau), as it extends across the eastern boundary between the two (see **Figure 1.2**).

1.2 The Congo-Kalahari Watershed

On a sub–continental scale, the low African and high African flat lands making up bimodal Africa are not homogenous but rather comprise several basins and swells (see **Figure 1.4**). Thus, low Africa has seven basins and high, southern Africa is comprised of three basins; interestingly high, eastern Africa has no large, notable basins, consisting predominantly of a large swell (Holmes, 1965). The EARS is the primary cause for this eastern swell and the high elevations of eastern Africa (see **Figures 1.2b** and **1.4**).

This thesis focuses on the swell that separates the Congo and Cubango–Kalahari basins, which forms part of the West-East Drainage divide (see **Figures 1.2d** and **1.4**). This divide between the basins of low and high Africa presents a unique spatial location where the interaction between old, inherited landforms and younger, dynamic landforms (the EARS) can be investigated. An improved understanding of the origin and development of this divide is therefore of continental consequence when investigating Africa's mega-geomorphology.

For this study, the swell (basin divide) separating the Congo and Cubango–Kalahari Basins is termed the Congo-Kalahari Watershed (CKW). The term CKW is used in preference to the Congo-Zambezi

watershed and the Great African Divide as the region under study extends to the west of the Congo-Zambezi watershed; similarly the term South Equatorial Divide is unsuitable as it does not acknowledge the differences in the river systems both to the north and south of this swell. The use of CKW is an extension of the decision to collectively refer to the southern Cubango and Kalahari Basins as the Kalahari Basin. The word Kalahari is more easily associated with southern Africa and both basins occur on the region of high, southern Africa that is referred to as the Kalahari Plateau. Therefore, for the rest of this study the CKW will be used when referring to the drainage divide that separates the westerly flowing Congo Basin (CB) from the easterly flowing Kalahari Basin (KB).

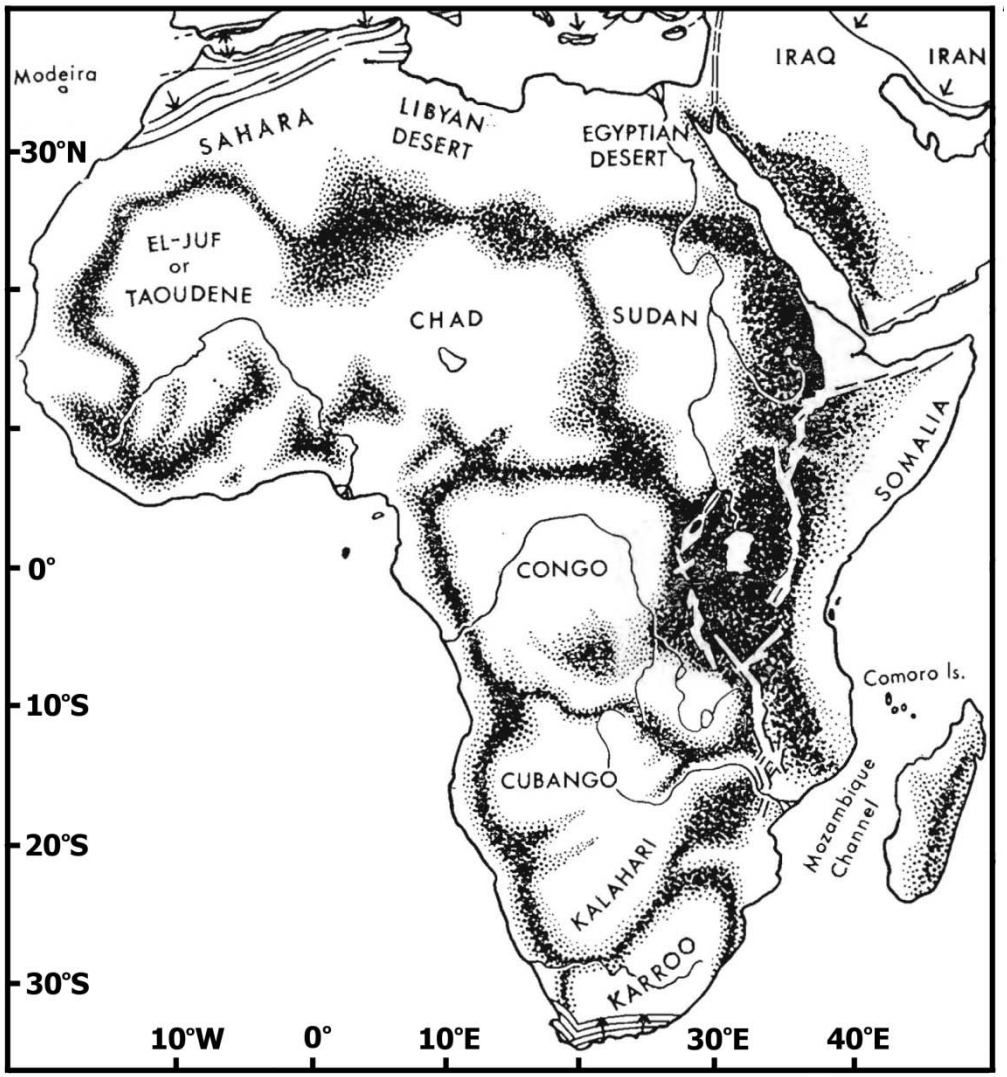

Figure 1.4: The present day continental geomorphology of Africa (after Holmes, 1965). Africa's geomorphology may be classified as basin (white) or swell (dark stippling). The Congo Basin is near circular apart from an extrusion in the south-east. By comparison the basins of the Cubango and Kalahari (Kalahari Basin) are kidney shaped. A thin swell divides the two basins.

The dominantly low relief CKW straddles the transition from low to high Africa, forming the divide between the Congo Basin and Kalahari Plateau. The CKW divides the northern flowing tributaries of the Congo River and the southern flowing rivers of the Okavango and Zambezi Rivers. Thus, the CKW separates the headwaters of the world's second and twenty-first most voluminous rivers, the Congo and Zambezi respectively (Meade, 1996; Gupta, 2007). The location and low relief of the CKW separating two of the world's most voluminous rivers is unexpected, as the majority of the world's large rivers are divided by mountain ranges (Tandon and Sinha, 2007). The CKW comprises principally the Angolan Highlands (in the west), the northern limit of the Kalahari Plateau (centre) and the margins of the Western Branch of the EARS.

The CKW marks the zone of a topographic transition from low to high Africa. It also divides two immense drainage basins, and, in addition forms a biological boundary. As one crosses this boundary from the southern KB into the CB there is a change in faunal assemblages, especially of fish (Roberts, 1975; Skelton, 1996). In the majority of cases, this faunal change corresponds to the threshold of the CKW. The CKW, therefore, represents three boundary phenomena: (1) the transition of low to high Africa; (2) the extension of the EARS and; (3) a continental biogeographical boundary. In this way the CKW forms a unique phenomenon where Africa's geomorphology, geology and biogeography are linked.

1.3 Scope, aims and objectives

In light of the unique spatial location and geomorphic attributes of the CKW, this region provides an opportunity to investigate the interplay of geomorphic and biological evolution at a (sub) continental level. As rivers are important geomorphic agents and play a key role in structuring biological habitats (e.g. Cullum et al., 2008; Doyle and Bernhardt, 2011), it is important to investigate the CKW in terms of its drainage geomorphology. While it has been possible in the past to investigate the planar river patterns of the Congo and Kalahari basins (Veatch, 1935; Dixey, 1943; Roberts, 1946; Cahen, 1954; Wellington, 1955; Deffontaines and Chorowicz, 1991; Potter and Hamblin, 2006; Stankiewicz and de Wit, 2006), the study of their rivers; longitudinal profiles has been more problematic. For the Congo Basin, the longitudinal studies of selected rivers by Robert (1946) appear to be the most detailed publically available profiles to date. The Kalahari Basin received attention in recent years in terms of its river's longitudinal profiles (e.g. Nugent, 1990; Moore et al., 2007). Yet, there appears to be no publically available, spatially referenced data comparing the river longitudinal profiles of the two adjacent but contrasting Basins.

1.3.1 Scope

This thesis focuses on the geomorphology of selected rivers whose headwaters originate along the CKW in order to better understand the geomorphic controls, processes and evolution of the CKW. The CKW is a multi-boundary feature, representing a transition zone in time (old and young landforms), space (low to high Africa) and a biological threshold (Congolian to Zambezian biodiversity (White, 1983; Olson et al., 2001). Being a transition zone in space and time, the CKW forms the boundary of interaction between Africa's three large scale geomorphic features: the Congo Basin, the Kalahari Plateau and East African Rift System. These three features make up Africa's anomalous bi-modal topography. The historical, structural and spatial relationships between these landforms, meeting along the CKW, enable us to ask overarching questions about why and how the CKW formed.

1.3.2 Aim

The aim of this thesis is to improve the understanding of the evolution of the Congo–Kalahari Watershed, and by extension, the development of Africa's topography. By exploring the landscapes of the CKW, information regarding the region's geomorphological evolution in terms of its rivers and drainage basins was obtained. This detailed empirical study of the land features of the CKW singles out rivers as proxy landforms to derive information on south–central Africa's geomorphology at a regional scale. It is argued that maps of quantified fluvial features will provide further insights into the geomorphic evolution of the CKW and its associated landscapes. Moreover, classification of these land features should shed light on the factors that control the evolution of the CKW and its associated mega-geomorphology. The specific aim of this study is as follows:

- To propose a conceptual model of the Neogene evolution of the CKW and its associated landforms

1.3.3 Objectives

In order to achieve this aim, it was necessary to create a spatially referenced database comparing the river longitudinal profiles of the two adjacent but contrasting basins. This database allowed for the following questions to be addressed:

- What are the spatial distributions and characteristics of the knickpoints of the studied rivers?
- Are these knickpoints controlled by structure (lithology and tectonics) or autogenic processes?
- How do pre-existing structures influence landscape and river evolution along the CKW?
- Is the evolution of the CKW related to the development of Africa's continental geomorphology?

1.4 Design of the study

This study, therefore, seeks to map and describe the meso– to macro–scale geomorphology of selected river long profiles. It is important to define the terms describing differences in landscape scale. The meso–scale geomorphologies are those features which may be measured in tens to hundreds of metres, whereas the macro-scale refers to those features measured in kilometres. The decision to create a geospatial database of meso–scale landscape features was based on three reasons: (1) a meso–scale resolution is required by biogeographic studies (mainly of fish), for example, Schwarzer et al. (2011); (2) it is hoped that a meso–scale would be sufficient to provide insights into the macro-scale evolution of the landscape (in terms of bimodal Africa and the development of the CKW and the role of the EARS); (3) new elevation data suited for meso-scale studies has recently become available. In order to achieve this description, the study made use of remotely sensed data, namely Landsat ETM+ images and Shuttle Radar Topography Mission (SRTM) elevation data using a geographic information system (GIS), with over 19 000 km of river being digitised and 380 knickpoints indentified. GIS has also been used to combine data from the literature and ancillary geological maps to create a geospatial database of the drainage geomorphology of the studied rivers. The synthesis of the various data sources, along with the characterisation of the knickpoints, is crucial in understanding the past and ongoing evolution of the CKW.

The individual landforms making up a big river (sensu Potter, 1978) provides the geomorphologist with a proxy of landscape history. The longitudinal profiles of selected rivers were thus investigated in order to better understand the CKW. More specifically, the knickpoints of the selected rivers were characterised. For this thesis, the term knickpoint refers to any significant break in the longitudinal

profile of the river (Gilbert 1877; Davis, 1899; Schumm, 1977; Leopold and Bull, 1979). The decision to focus on knickpoints was informed by geomorphic theory regarding the development of longitudinal profiles (Gilbert, 1877; King, 1951; Leopold et al., 1964; Hack, 1975; Schumm, 1977). This is because geomorphic theory suggests that, given sufficient time, tectonic stability and uniform conditions, river long profiles will become graded (concave in form). Yet, knickpoints are deviations from such graded profiles and therefore may serve as first order proxies for determining the state and evolution of a river system. Knickpoints may reflect bedrock changes, tectonic activity, past base-level changes and changes in sediment load from tributaries (Gilbert, 1914; Brundsen and Thornes, 1979; Schumm et al., 2005; Bishop, 2007). As river longitudinal profiles represent the integrated signal of geodynamic events and are themselves drivers of landscape development, an understanding of their anomalies may provide insights into their evolution. Thus the study of river longitudinal profiles and their knickpoints may elucidate key factors controlling the denudation and evolution of the broader landscapes through which they flow.

The ability to collect information through remote sensing and locate the data within GIS has allowed the studies of earth surface process to move from focus on individual features to regional scale studies (see, Jarvis et al., 2004; Iwahashi and Pike, 2007; Alexander, 2008). However, there are concerns that the use of GIS is focused on exploration and landscape classification rather than the investigation of the complex interdisciplinary issues required to solve geomorphic questions, with GIS outputs often being treated superficially with a disregard for the workings of the real world (Alexander, 2008; Remondo and Oguchi, 2009). In this thesis, GIS is used to achieve both types of investigation. Thus, the study seeks to explore and classify the selected rivers of the CKW and to investigate the mega-geomorphology of the CKW. The initial exploration and classification through the production of the GIS database was necessitated by the lack of publically available, spatially-referenced information for south–central Africa noted above. This geospatial database was then used to record the occurrence and investigate the cause of knickpoints of the studied areas, as well as to place the knickpoints in the context of the mega–geomorphic evolution of south–central Africa. Thus, this study utilises the inherently inductive approach of modern GIS to provide a base of evidence from which elements of the evolution of studied rivers of the CKW may be induced. The conclusions derived from the study of these rivers were then used in combination with other data sources to propose a deductive model (the conceptual framework of the aim) for the development of the CKW. This dual combination was used because, in order to develop a realistic deductive model (the model of the CKW evolution), there must be an inductive base of evidence grounded in field measurements (the river longitudinal profiles and knickpoint characteristics) (Bishop, 1980).

1.5 Thesis outline

This thesis is divided into nine chapters with the start of each chapter being indicated by a blue title page and the start of each appendix by a green title page. Each appendix has been numbered so that it corresponds to its relevant chapter, for the appendix for example Chapter 7 is numbered Appendix 7. Unless otherwise stated, all figures and maps in this thesis have been drawn by the author using ArcGIS, Corel Draw, Inkscape and GIMP. The geological time scale used in this study is that of Walker et al. (2009). This chapter (**Chapter 1**) has provided the overall context and indicated the importance of the CKW to an understanding of south–central Africa's geomorphic development. The conceptual framework of this thesis is dealt with in the second chapter (**Chapter 2**) which provides an overview of the geomorphic approach to understanding Earth's surface. In this chapter key concepts are highlighted and fluvial systems are focussed on.

Chapter 3 provides the regional geologic framework of the area under study, namely, south-central Africa. The general geology is of importance to geomorphology in two ways: firstly, it is the geologic units that comprise the landsurface upon which geomorphic processes act; secondly, the general geology provides a temporal aspect that is important in understanding the present day geomorphology. Furthermore, the lithospheric structure of the African continent may be important in understanding the landscapes response to geodynamic affects that appear to control the continental geomorphology of Africa.

Chapter 4 provides details regarding the data used for the study of the rivers in this thesis, namely Landsat 7 ETM+ imagery and SRTM elevation data. In any research making use of remote sensing, it is important to understand the data used, as the strengths and weaknesses of this data will affect the fidelity of observations derived from it.

Chapter 5 heralds the start of the original research conducted during this study. Here the Global Position System (GPS) survey conducted is described and discussed. This survey assessed the vertical accuracy of the SRTM data, which is an important consideration as it was used in conjunction with the Landsat imagery to digitise the river longitudinal profiles and derive the location and characteristics of knickpoints.

Chapter 6 forms the core novel contribution of this thesis in terms of the geomorphology of south–central Africa. This chapter describes the methods and results used to digitise the river longitudinal profiles and to characterise the knickpoints. It also assesses the use of standard GIS tools in terms of river profile extraction. A discussion of the results highlights key findings and provides a preliminary analysis of the geomorphic implications of the chapter's findings. The most important contribution of this chapter is the creation of the geodatabase of the river profiles.

Chapter 7 takes the geodatabase created in Chapter 6 and increases its value by adding geologic attributes to the knickpoints described. This chapter, thus, represents the second major contribution of this thesis. The addition of ancillary data to the knickpoint database has provided insights into the development and controls of the river systems under study. The process and results of adding this additional information is described in this chapter, along with a preliminary discussion that highlights the key findings of this chapter.

Chapter 8 builds on the preceding chapters (6 and 7) and synthesises their findings in order to gain valuable insights into the origin and evolution of the CKW. This is done through the blending of key elements of the literature covered in Chapters 2 and 3 and the main findings of Chapters 6 and 7. The development of a theoretical watershed is analysed and a conceptual model of the evolution of the CKW is proposed, contributing to an understanding of south–central Africa's development.

Chapter 9 concludes this study by re–affirming the key findings of this thesis. It ends with some concluding remarks and makes several recommendations for future geomorphic investigations in south-central Africa.

CHAPTER 2: THE GEOMORPHIC APPROACH AND LARGE RIVERS

2.1 Introduction

According to King (1951), geomorphology has two functions, namely, the description of present-day landscapes and the elucidation and explanation of their histories. However, Leopold et al. (1964) argue that in order to understand landforms, geomorphological studies should focus on understanding those processes acting on the landsurface. The difference between these two approaches stems from their treatment of time and space, a difference that has been apparent since the writings of Gilbert (1877) and Davis (1899), whose approaches show the same divergence. In fact it has been recognised that the reconciliation of a focus on landform (e.g. Gilbert, 1877; King, 1951; Hack, 1960) with a focus on process (e.g. Davis, 1899; Horton, 1945; Strahler, 1952; Leopold et al., 1964), across their respective spatial and temporal scales, both in observation and theory, is a key challenge in geomorphology (Church, 2010).

The relationship between landsurface processes and form, and spatiotemporal scales is an important consideration when studying Earth's topography in terms of the present, the past and the evolution of form over time (Gardner and Scoging, 1983). Owing to the possibility of convergent and divergent processes and causes, the interconnection of geomorphic processes and landforms histories may be a challenging task (Schumm, 1991). Convergence (equifinality) may result in similar landforms occurring through the action of diverse processes; for example, gentle sloping surfaces piedmont surfaces can be formed through parallel slope retreat, and lateral planation by stream or other, more complex processes (Schumm, 1977; 1991). There may be divergence of results where similar processes produce different landforms, for example, the variety of aeolian dune morphologies (Schumm, 1991). Furthermore, landscapes display variation in sensitivity to changes in the control of the system, resulting in substantial variation of previously similar morphologies (Brunsden and Thornes, 1979; Brundsen, 2001). Thus, any study of the Earth's surface needs to appreciate the role of spatiotemporal scales, as viewing the landscape utilising different scales may lead to substantially different interpretations.

As in this thesis an investigation of the CKW and its associated landforms will be undertaken, it is important to first establish the key components of the geomorphic approach. This chapter provides an overview of the main models of landscape evolution and the concepts of spatial and temporal scales, followed by a brief description of geomorphic processes, with a focus on fluvial systems. This account will of necessity be brief and it is not the intent to provide an exhaustive account of the

history, philosophical approach or a definitive treatment of the geomorphology, which may be found in Beckinsale and Chorley (1991), Schumm (1991), Summerfield (1991) and Huggett (2007) and references therein.

2.2 Geomorphology and models of landscape development

2.2.1 Models of landscape evolution

While both Davis (1899) and Gilbert (1877) identified landscapes as being a function of three variables, (1) structure (lithology and structural geology), (2) process and (3) time, Davis proposed that time was the primary factor of landscape evolution, whereas Gilbert favoured structure as being the dominant control of topographic development. This difference in emphasis has formed the two schools of geomorphic thought, namely, historical (or time–bound) geomorphology (Davis) and process (or timeless) geomorphology (Gilbert). Historical geomorphology is primarily focused on mapping of landscape features, whereas process geomorphology is most concerned with the phenomena responsible for landform development (Huggett, 2007).

Based on observations made in a humid environment, Davis (1899) proposed that landscape evolution is predominantly a function of time, with structure and process playing lesser roles. According to the geographic cycle of Davis, following a short-lived uplift event, the landsurface was lowered over time through denudation to form a single flat surface (peneplain) (see **Figure 2.1**). Landscapes could thus be assigned an age based on their degree of development, while making allowances for further uplift prior to a stage of maturity being reached; if uplift occurred after peneplains had formed, the landsurface would once again become youthful and all traces of the previous cycle would be eroded over time (Davis, 1899). Davis (1899) proposed that the rate of landscape rejuvenation would be in significant excess to the rate of downwearing, such that only a single process (either uplift or denudation) should be considered (Penck, 1953). Originally published in German in 1924 and translated in 1953, Penck's early investigations were made in a tectonically active setting, with the result that he differed from Davis (1899) on the premise of a single uplift event (Penck, 1953).

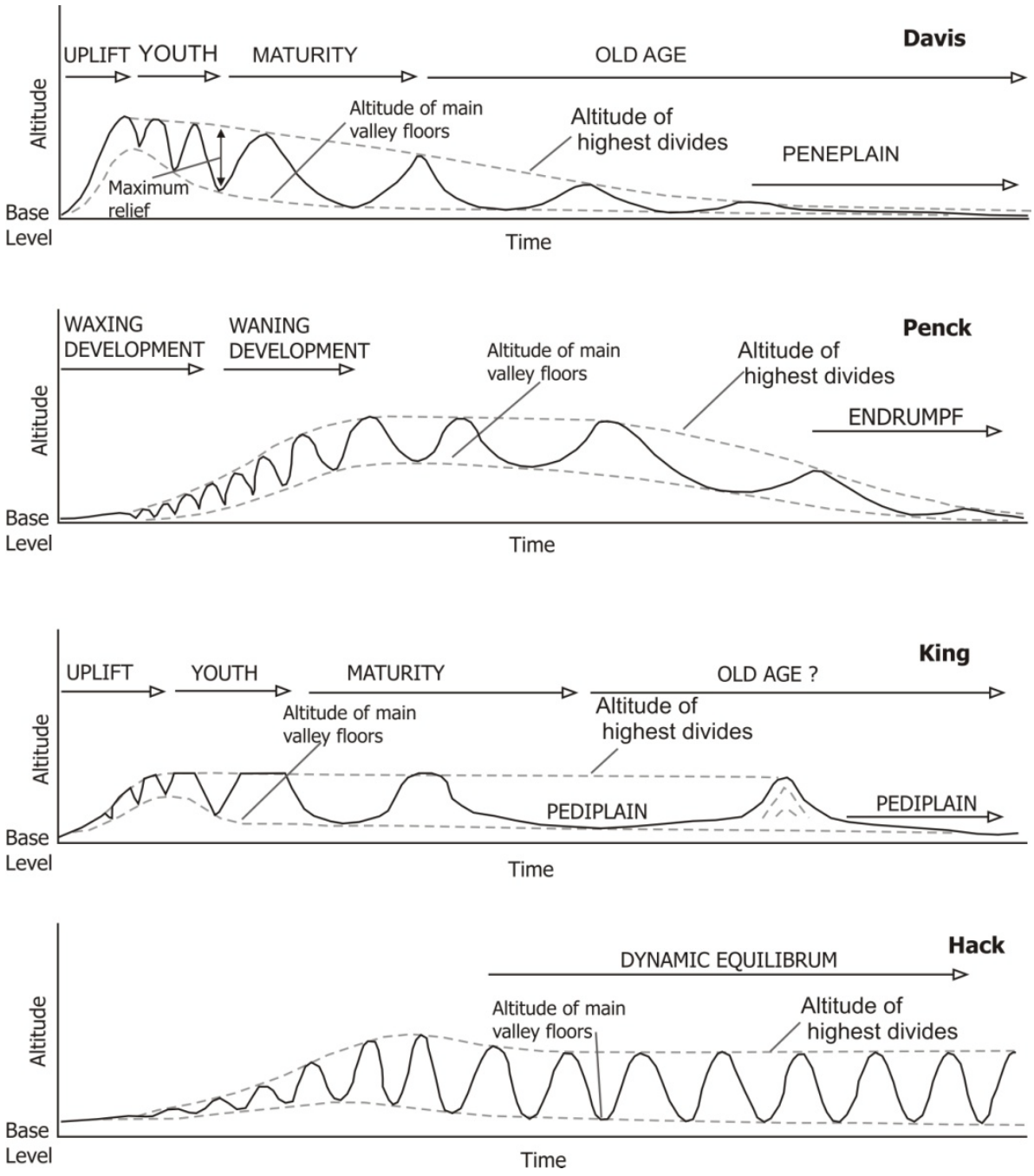

Figure 2.1: The four models of landscape evolution as proposed by Davis, Penck, King and Hack. The time scale is not necessarily comparable between the diagrams. Davis (1899) proposed the idealised geographic cycle in which a landscape experiences a phase of uplift followed by subsequent downwearing over time, to produce a peneplain. Penck (1953) proposed that uplift and denudation can occur simultaneously, and that once erosion exceeds uplift, slope recession and slope decline result in the flattening of the landscape and development of an *endrumpf*. King (1951) proposed that after uplift, the landsurface decrease in elevation through parallel slope retreats to form a pediplain. Hack (1960; 1975) explicitly deviated from the idea of a landscape forming a flat surface but held rather that rock uplift was long–lived, resulting in dynamic equilibrium where the landsurface is eroded only to experience subsequent uplift. Figure redrawn and modified from Summerfield (1991) and Burbank and Anderson (2001).

Penck (1953) argued that the rate of uplift was variable and that there existed an overlap between landscape rejuvenation (uplift) and the onset of denudation, where both processes were concurrent. In such a situation the removal of uplifted material enhances uplift, increasing the altitudinal gain of the landscape, as illustrated in **Figure 2.1** (Penck, 1953). Over time the rate of erosion, exceeds uplift resulting in a net lowering of landscape elevation. Unlike Davis (1899), Penck (1953) suggested that slope decline (downwearing) occurred in conjunction with slope recession (backwearing) (Huggett, 2007). Thus the uplifted landscape saw a simultaneous vertical and horizontal decrease in landmass (Penck, 1953).

King (1951), like Penck, was also critical of Davis's model of geographical cycle and landscape development through downwearing. King's model was grounded in observations made in dry southern Africa (King, 1951). Recognising the importance of the fact that rocks have varying resistance to mechanical and chemical weathering, King proposed that, following a period of landscape rejuvenation, landscape denudation was a function of parallel slope (scarp) retreat (see **Figure 2.1**). Thus portions of the landscape could maintain their elevations above the surrounding flat lands (pediplains) for long periods of time. The model of scarp retreat allowed for the persistence of landforms through multiple phases of uplift, which could then be used to provide a chronology of landscape development (King, 1962). King (1955) further proposed that successive phases of uplift could be initiated by the removal of a threshold amount of rock mass resulting in isostatic compensation, therefore acknowledging a degree of self–regulation.

During the 1950's the field of geomorphology moved away from the dominance of historical studies toward process geomorphology and the approach of Gilbert (1877, 1914) was revived (Beckinsale and Chorley, 1991). In 1914, Gilbert set out to quantify the movement of debris through a river system, making use of both analogue and mathematical models. The work of Horton (1945) and Strahler (1952) underwent a change of focus, and process geomorphology became a well-established field (Beckinsale and Chorley, 1991; Huggett, 2007). Hack (1960) built on Gilbert's (1877, 1914) work on landscape self–regulation. Based on observations of humid temperate landscape, Hack argued that in many cases rock uplift does not occur as a single, short-lived event but is a continuous process. The processes of weathering and erosion of each slope and channel are adjusted to one another (negative feedback or self–regulation), attaining an equilibrium (see **Figure 2.1**). The landscape experiences shear stresses (divided into gravitational and molecular stresses), which after a period of time attains a dynamic equilibrium or quasi–equilibrium (Hack, 1960; Leopold

and Langbein, 1962). Inheritance of a landscape may be possible. However, where uplift and rock resistance are matched by erosion and relief, a dynamic equilibrium is established, and the landscape will readjust should any disturbance occur, thus maintaining a steady–state landscape (Hack, 1960; 1975). Differences in form and relief are a function of spatial relation rather than an evolutionary path and so it is not necessary for landscapes to be investigated in historical terms (Hack, 1960).

These models have influenced how landscapes have been studied and interpreted and there have been variations of each (Schumm, 1991). The apparent conflict between the historical and process geomorphology suggests that landscapes may undergo progressive change over time but yet retain an equilibrium form (Summerfield, 1991). It has been suggested that the discrepancy between the process and historical geomorphology can be resolved once the issues of spatial and temporal scale are acknowledged (Schumm and Lichty, 1965; Summerfield, 2005). These issues are discussed below.

2.2.2 Issues of scale

Studies of the Earth's landsurface must deal with the issues of time (relative and absolute), space (scale and size) and location (placement), especially as an increase in the size of a geomorphic feature sees a concurrent increase in the complexity of the landscape (Summerfield, 2005). For example, a small drainage basin may occur within a single climatic and lithologic unit, whereas large drainage basins may incorporate several climate regions and geologic terranes. As the size and age of a landform increases, fewer of its characteristics can be explained by its present conditions and an increasing amount of information must be inferred about its past (Schumm, 1991). The relationship of increasing land feature size and age with concurrent reliance on historical explanations is illustrated in **Figure 2.2**. The acknowledgement of a spatial and temporal scaling of landscapes and their explanations provides a measure of consolidation of the process and historical geomorphological approaches.

Studies involving mega– and meso–scale geomorphology need to be especially cognisant of spatiotemporal and location components, since independent variables controlling the development of landforms may totally change as the scale of investigation changes from micro to mega scales

(Gardner and Scoging, 1983). Thus a consideration of space, time and location provides the basis of important considerations in the study of large scale features (see **Table 2.1**).

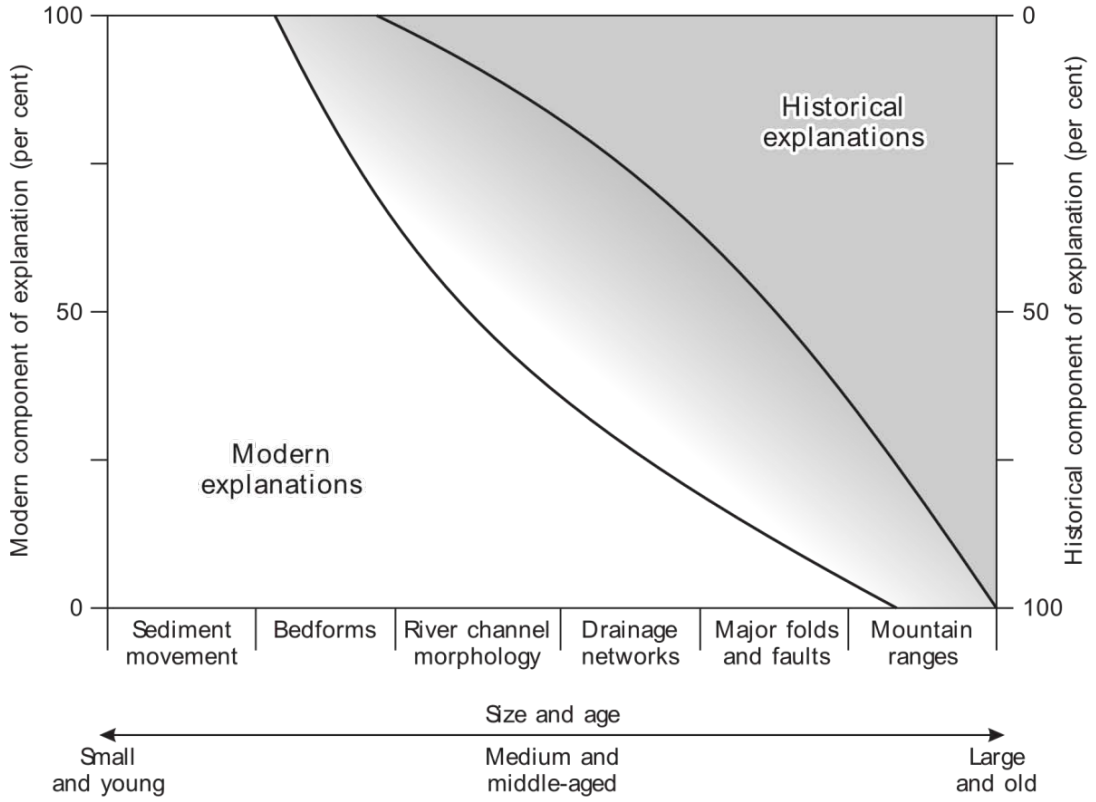

Figure 2.2: The components of historical explanation needed to account for geomorphic events of increasing size and age. Landforms falling within the top right can be explained by purely historical explanations, while features in the bottom left contain purely modern (process) explanations. The upper curve shows the maximum modern component and the lower curve indicates the maximum historical component. Landforms falling in the zone of overlap have a range of variability of historical and modern explanation. For example, 10 – 60 per cent of a given channel morphology may have a historical explanation (Schumm, 1991). Figure modified from Huggett, 2007.

Schumm and Lichty (1965) summarised the issue of scale by stating:

> The distinction between cause and effect in the development of landforms is a function of time and space (area) because the factors that determine the character of landforms can be either dependent or independent variables as the limits of time and space change (pp 110, Schumm and Lichty, 1965).

They focused on fluvial systems as a proxy for landscape development, and suggested that geomorphic systems should be viewed as being in one of three states, depending on the time scale involved (see **Table 2.1**). Thus landforms may be considered as open systems over long time periods, self-regulating over shorter periods of time, or in a steady state over even shorter periods of time (Strahler, 1952; Hack, 1960; Leopold et al., 1964; Schumm and Lichty, 1965; Hack, 1975). The

temporal component of landforms is of significance but it is vitally important when investigating river systems, especially large rivers, as large rivers exist both in present moment of geological time and as products of their history (Schumm, 2005; Tandon and Sinha, 2007). The spatial extent, and by extension the time span, of any landscape will, by inherent characteristics, determine the variables that are to be considered (see **Figure 2.2** and **Table 2.1**). For example, in cyclic time, vegetation is dependent upon all the features above it as listed in **Table 2.1** and in turn those basin variables below it show some dependence on vegetation. Thus the variables may be considered to form nested hierarchies, where the factors influencing a given variable are related to its ranking within the hierarchy (Schumm and Lichty, 1965). There are, however, limits to the system due to the relationship of the variables, in that causes may appear as effects and vice versa (Schumm and Lichty, 1965; Schumm, 1991; Summerfield, 2005). These limits are necessary as, on a drainage basin scale, the causes of climate, geology and the other variables individually are of no concern; rather it is the linkages between these variables that are important (Leopold et al., 1964; Brunsden, 2001).

Table 2.1: The status of drainage basin variables during time spans of decreasing duration. The variables of drainage basins occur in a hierarchical manner that approximates to the apparent increasing degree of dependence of considered variables. Table modified from Schumm and Lichty, 1965.

Drainage basin variables	Status of variables during designated time spans		
	Cyclic	Graded	Steady
1. Time	Independent	Not relevant	Not relevant
2. Initial relief	Independent	Not relevant	Not relevant
3. Geology (lithology, structure)	Independent	Independent	Independent
4. Climate	Independent	Independent	Independent
5. Vegetation (type and density)	Dependent	Independent	Independent
6. Relief or volume of system above base level	Dependent	Independent	Independent
7. Hydrology (runoff and sediment yield per unit area within system)	Dependent	Independent	Independent
8. Drainage network morphology	Dependent	Dependent	Independent
9. Hillslope morphology	Dependent		Independent
10. Hydrology (discharge of water and sediment from system	Dependent	Dependent	Dependent

Schumm and Lichty (1965) identified three temporal divisions in decreasing time length, namely, cyclic, graded and steady (see **Table 2.1**). The extent of the time spans of these divisions is not important; they serve to highlight that the same system can be considered at different lengths of time, influencing the relationship between the landscape variables. Cyclic time can effectively be thought of as geologic time, encompassing the period of landscape initiation to landscape termination (Schumm and Lichty 1965; Summerfield, 2005). In these terms, landscapes are considered cyclic when, for example, a tectonically inactive landscape (possess potential energy due to its current relief, which it transfers to the rivers flowing within it, and additional energy enters the system through the agency of climate (increased water availability) (Schumm and Lichty, 1965). Over a long period, the removal of the initial relief results in a net loss of potential energy and thereby alters the characteristics of the system. Therefore, a stable fluvial system can be conceptualised as an open system, undergoing continuous change; in such a system no constant relations between the dependent and independent variables can be discerned (Schumm and Lichty, 1965). On a cyclic scale, only time, geology, initial relief and climate are independent variables, with the passage of time being the most important, as the agencies of erosion require significant persistence to structure the morphology of the system. Over a shorter period of time, a geomorphic system may be considered to be graded.

On a graded time scale a quasi–equilibrium or dynamic equilibrium exists (Schumm and Lichty, 1965; Hack, 1975). Graded time is a common premise for fluvial studies that relate 'graded' (concave river profiles) to fluvial processes (e.g. Gilbert, 1914; Horton, 1945; Hack, 1960; Leopold and Langbein, 1962). Graded time exists to the point where existing landforms have reached a dynamic equilibrium with respect to the process acting upon them (Gilbert, 1877; Hack 1960). The landscape can be viewed as a series of fluctuations around, or approaching, a steady state as the landscape undergoes progressive, irreversible changes of cyclic time (Schumm and Lichty, 1965). Graded time is often a period of years or decades, although the time span may change depending on the landscape under investigation. During graded time some of the variables will change; time, for example, is eliminated (see **Table 2.1**), for at this scale, although the entire system will be undergoing some small magnitude changes, some of the components of the system will show no change at all, for example, slope angle (Schumm and Lichty, 1965). Thus some variables that are dependent during a long period of time become independent over this shorter time span (Schumm and Lichty, 1965).

The third division of time on **Table 2.1** is steady state time, a period where true steady states may exist in contrast with the dynamic equilibrium of graded time (Schumm and Lichty, 1965). Steady state time is a brief moment of time in the entire evolution of the system, so while the entire drainage system cannot be at a steady state, certain components may be (Hack, 1960; Leopold and Langbein, 1962). For example, while a stream over a short distance may export the same amount of water and sediment as introduced into the system, the river as a whole would not exhibit such a characteristic (Schumm and Lichty, 1965).

This multi–scalar approach to landscapes in both terms of space (see **Figure 2.2**) and time (shown in **Table 2.1**) allows for the Earth's topography to be understood in terms of the current (process geomorphology) and past development (historical geomorphology) of landscapes (Summerfield, 2005). The result is that geomorphological studies are not considered in terms of the linkages between the three time scales, but rather have been conceptualised as large (macro) scale processes (e.g. delta formation) or small (micro) scale processes (e.g. dune formation) instead of the consideration of fluvial systems as a continuum both spatially and temporally (Summerfield, 2005). Yet, by the nature of the interconnectedness of river systems, no meaningful explanation of large river evolution can be achieved by maintaining a single scale of thought and analysis rather rivers need to be viewed as a continuum. This multiple scales approach is required when investigating large rivers, as large rivers are the result of historical and current interactions of numerous variables, both within the drainage basin and within the river itself (Potter, 1978; Schumm 2005; Tandon and Sinha, 2007). This issue of scale not only determines the variables needed for consideration, but also dictates the direction of impact of the variables upon one another. Other important considerations when investigating the meso– to macro–scale landscape are: How much modification is required before a landscape may be considered to be new? What portion of a landsurface is inherited or persistent? What of landscape are resistant to modification in some parts and prone to it in others? This consideration of space, time and location provides the basis of important considerations in the study of large scale features and led Potter (1978) to suggest several important aspects that should be considered when studying large river systems. His questions have been re-phrased within the context of this study and are presented below:

(1) Is the Congo River the second largest river ever to exist? Were there bigger rivers on Gondwana?
(2) What conditions are required for large rivers to be long-lasting systems?
(3) Can Africa's large rivers be related to plate tectonics?

(4) What are the geological controls of Africa's large rivers?

(5) What is the relationship between depositional basins and their river systems?

2.3 Fluvial systems

Fluvial systems involve a series of time independent process that may act in parallel to, or independent of one another, as are discussed in detail below.

2.3.1 Overview of rivers

All rivers, both large and small, arise ultimately as a consequence of runoff generated by precipitation (Horton, 1945). Rivers are important components of the continental landforms, with river basins occupying approximately 69 % of the land area (Tandon and Sinha, 2007), which means that vast regions of the Earth's topography are moulded by rivers. The role of rivers and their sediment load is highly important in shaping the Earth's surface (Bridge, 2003; Schumm, 2005; Gupta, 2007; Tandon and Sinha, 2007), with large quantities of this sediment deposited in alluvial floodplains (Bridge, 2003; Schumm, 2005). It has been noted that in some cases the volume of deposited sediment is so vast as to cause neo-tectonic movements on the depositional plain as well as in the surrounding area (Brundsen, 1990; Gumbricht et al., 2001; Tandon and Sinha, 2007). Thus, depositional behaviour of large rivers may create a complex dynamic system, where a cyclic pattern of evolution endures such that deposition drives river change via localised tectonics which in turn further propagates subsequent deposition (Gumbricht et al., 2001).

Despite the importance of rivers, the current understanding of their evolution and geomorphology is limited (Dollar, 2000), with large rivers being the least understood of these landforms (Gupta, 2007). Much of the existing knowledge and theory regarding river geomorphology, form and function have been derived from the study of small rivers or from laboratory analyses (Gilbert, 1914; Dollar, 2000; Gupta, 2007). Rivers are highly dynamic features and as such undergo changes over time and in space (Dollar, 2002; Gupta 2007). These changes may be sudden events or slow, more progressive events and may be a direct result of the processes of rivers themselves or they may be caused by factors outside the rivers, for example, changes in the river catchment or global climate patterns (Tooth et al., 2002; Schumm, 2005). Therefore rivers can be seen as demonstrating the interplay between endogenic and exogenic processes. However, the way fluvial systems react is a function of the geomorphological setting of the system, which includes antecedent conditions (Dollar, 2002).

Rivers, especially large rivers, are often composed of several river channel elements, with some rivers exhibiting a wide range of these elements and other rivers exhibiting only a few of them. This is due partly to the fact that water and sediment supply to rivers and floodplains varies over time and space with differing time scales and magnitudes (Bridge, 2003). Further complexity is added by the natural changes that are brought about by flood events, autocyclicity and tributary-trunk stream relationships (Dollar, 2002). A variety of influences act upon a river system at given time, with these influences occurring as downstream and upstream controls (Piégay and Schumm, 2003). Downstream determinants generally occur as changes to baselevel and river length, whereas upstream controls include the historical, structural and climatic influences that act upon a river system (see **Figure 2.3**).

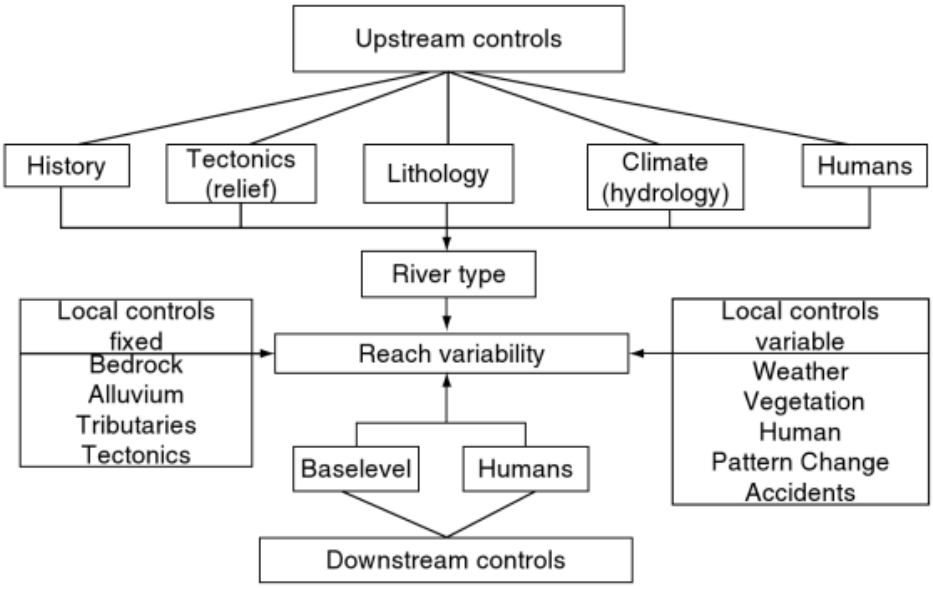

Figure 2.3: Chart showing various upstream and downstream controls of river morphology and behaviour (from Piégay and Schumm, 2003).

In recent studies much has been made about the fractal nature of river systems (Tarboton et al., 1988; Turcotte, 1992; Rodrígues-Iturbe and Rinaldo, 1997). However, few natural river systems display a true fractal nature at all scales, owing to deviations caused by non-linear dependence of river bed width and valley width, variability of a basin's geology and climate, basin shape and unequal channel formation conditions (Nikora, 1991). The causes of these deviations serve to highlight important controls on river systems (see **Table 2.2**) and will be discussed in turn below.

2.3.2 River channels

River channels are formed by the flow of water under the influence of gravity from higher to lower elevations and, over time, the formation of drainage networks (Leopold and Langbein, 1962). These river channels are incised into rock or sediment, this channel bed material accounting for the broad classification of channels into two types, namely, bedrock and alluvial (Schumm, 2005; Huggett, 2007). However, a single river can be a combination of segments of alluvial and bedrock typology, or a river may change from being predominantly bedrock to alluvial and vice versa, for example, bedrock may alternate with zones of alluvium (Tooth et al., 2002; Schumm, 2005).

Downcutting (vertical incision) of a river may be initiated by a variety of causes, and in some cases multiple causes act together to enhance incision (Schumm, 2005). These possible causes of vertical incision are indicated in **Table 2.2**. It should be noted that a river's response to these causes is a function of the internal and external thresholds of the fluvial system (Schumm, 1977). These thresholds act in conjunction to determine the magnitude and rate of response experienced by the system (Brundsen, 2001).

Table 2.2: Possible causes of river incision as classed according to field of study. Adapted from Schumm (2005, Table 3.2, pg 20).

Causes of incision			
Geologic	**Geomorphic**	**Climatic**	**Hydrologic**
1 – uplift	1 – stream capture	1 – drier	1 – increased discharge
2 – subsidence	2 – baselevel lowering	2 – wetter	2 – increased peak discharge
3 – faulting	3 – meander cutoffs	3 – increased intensity	3 – decreased sediment load
4 – lateral tilt	4 – avulsion		
	5 – lateral channel shift		
	6 – sediment storage (increase gradient)		
	7 – mass movement		
	8 – ground–water sapping		

2.3.2.1 Bedrock channels

In general, bedrock rivers are poorly researched (Huggett, 2007). They occur where bedrock channels have incised into rock and are resistant to erosion, generally having long persistence times (Schumm, 2005; Huggett, 2007). Most rivers have eroded into bedrock in their upper reaches, where gradients are steep and loads coarser (Schumm, 1977). The longitudinal profiles of bedrock rivers are more irregular than those of alluvial rivers (Huggett, 2007). These irregularities may take the form of downstream steepening of gradient below a knickpoint, with rapids and waterfall often marking the position of gradient change (Huggett, 2007).

2.3.2.2 Alluvial channels

Alluvial rivers are those whose beds are not in direct contact with the underlying geology; instead they flow on top of previously deposited sediments (Schumm, 2005). Due the variability of the sediments over which the river flows, alluvial channels may be highly variable (Huggett, 2007). Alluvial channels may be highly susceptible to changes in the system and have relative quick response rates to disturbances (Schumm et al., 2002).

2.3.2.3 Longitudinal profiles

A longitudinal profile of a river is the gradient of its water surface from source to end, as shown in **Figure 2.4** (Huggett, 2007). If river discharge increases downstream, the longitudinal profile is concave, owing to the interaction of water depth and sediment load (Schumm, 1977). A smooth longitudinal profile is the most common quasi–equilibrium shape of rivers, and is more readily associated with alluvial rivers (Sinha and Parker, 1996). Many river profiles are not smoothly concave but contain both flatter and steeper zones (Huggett, 2007). The steeper zones, which start at knickpoints, may be the result of resistant rock outcrops, tectonic activity, sudden changes in discharge or stages of valley development such as active headwater erosion (Huggett, 2007). Driving mechanisms of longitudinal profile development include (1) horizontal wavelike progradation of the river profile, (2) abrasion of bed particles, (3) aggradation of river profile balancing subsidence at constant speed, and (4) effect at tributaries adding sediment and water to the main stem of the river (Sinha and Parker, 1996). A graded river is one where the system is in equilibrium, and any changes to the controlling factors of the river system will be accommodated through a change in equilibrium (Hack, 1960; Leopold et al., 1964; Schumm, 1977). This disturbance of stream equilibrium can be brought about by a change in baselevel, thereby causing a change in slope or change in channel

pattern, width or roughness (Huggett, 2007). However, as changes to the equilibrium often occur at frequencies higher than the river can accommodate, a graded stream should rather be regarded as being in quasi–equilibrium as opposed to a true steady state (Hack, 1975; Schumm, 1977).

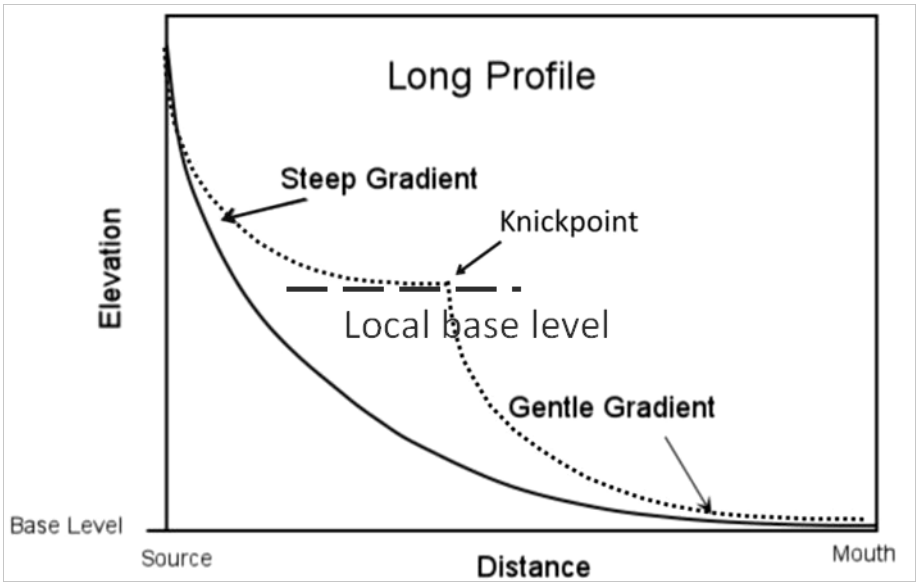

Figure 2.4: An idealised river longitudinal profile (heavy line) compared to a river longitudinal profile that exhibits a knickpoint (dotted line).

The decline of a river's gradient and its associated river sediment deposition (due to decreased river competence) controls the morphological formations and spatial distribution of fluvial features (Bridge, 2003; Brierley et al. 2006). This reduction in river gradient (and energy gradient) is associated with a baselevel (Dollar, 2002). Baselevel is the lowest elevation to which a river may vertically erode (incise) (Leopold et al., 1964). The ocean is the ultimate baselevel for all rivers, with local baselevels being formed by lesser water bodies, other rivers, resistant lithologies and, for some endorheic drainages, deltas and alluvial fans. Therefore two types of baselevel exist, namely, ultimate and local/relative baselevel. River gradient controls river morphology; for example, a river gradient cause the river to meander (Bridge, 2003).

Changes in the baselevel, either through continental uplift (isostatic change) or by sea–level drop (eustatic change), have an immediate effect on drainage systems (Schumm, 2005). The increase of the river's length, from its source to mouth, results in an overall increase in the speed, erosive powers and carrying capacity of the river (Schumm, 1977). The rejuvenated river begins incise downward, eroding a new valley within the old one, this incision migrating upstream from sea-level and possibly resulting in valley-in-valley forms (Hack, 1960; Leopold et al., 1964; Chorley et al.,

1984). Thus a young valley may develop within the confines of a broad floodplain of the original old section. A rapid change in gradient occurs where the headwaters of the rejuvenated stream are eroding backwards along the old longitudinal profile; this head of rejuvenation is a knickpoint. This advances upstream and the widening of the rejuvenated valley may be relatively swift because the rejuvenated river is working in the old river's sediments and weathered rocks (Davis, 1899; Leopold et al., 1964). As the new valley widens, the old valley surface is reduced to terraces and repeated rejuvenation results in subsequent terraces so that the valley sides begin to take on a stepped appearance (Schumm, 1977). In more arid regions where there is little surface water, rejuvenation may cause the deeper incision of the meander pattern of a through-flowing stream to form an incised meander (King, 1962).

Sea–level changes have been used to explain channel incisions, terrace development and long term aggradation in fluvial systems (Dollar, 2002). The affects of sea–level changes are often most noticeable in coastal floodplains (Dollar, 2002; Bridge, 2003). A rapid rise in sea–level causes prolonged reductions in gradients, with sea–level rise resulting in back flooding of channels establishing shallow, low energy depositional environments (Leopold et al., 1964; Schumm, 1977). This results in a lengthening of the low gradient section of the river's longitudinal profile upstream. Therefore, low gradient floodplains and other fluvial features will migrate upstream during sea–level rise. A decrease in sea–level will result in channel incision, terrace development and floodplain erosion (by scouring) (Dollar, 2002). As sea–level deceases there is an increase in the energy gradient, which initiates an increase in overall river gradient (Schumm, 2005). This results in a lengthening of the low gradient section of the river's longitudinal profile as fluvial features migrate downstream. The now incising river will erode the previously deposited sediment structures and carry them downstream, where they will be deposited in a new spatial context. When the sea–level rises, the resulting sedimentary features will consist of sediments from the catchment areas and not reworked sediments. This is important as river structures affect river functioning and *vice versa*, which in turn may have an impact upon the development of knickpoint features.

Local baselevels are temporary and rivers have the potential to continue flowing downstream of the baselevel, whereas rivers cease to flow in the ocean. While ultimate baselevel stops downward erosion, local baselevels only retard downward erosion (it is a matter of the time scale involved) (Tooth and McCarthy, 2007). Furthermore, a river that only has its baselevel at sea–level will (theoretically) be able to achieve an upward concaving profile (Dollar, 2002; Bridge, 2003; Schumm, 2005). However, a river with another baselevel other than sea–level may have two or more concave

upward profiles (Bridge 2003; Schumm, 2005). These baselevels may be due to a change in underlying rock resistance or may be due to the presence of a lake, dam, wetland or even a floodplain (Bridge, 2003; Schumm, 2005). These low gradient features may occur upstream of knickpoints serving as proxies for knickpoint identification. Local baselevels result in the same process of river grading and energy loss occurs.

2.4 Summary

This chapter has provided a brief account of the geomorphic approach to studying landscapes. It has also highlighted the fact that with an increase in the scale of feature under study, there is a concurrent increase in its complexity and reliance on historical explanations (see **Figure 2.2** and **Table 2.1**). An awareness of these spatial and temporal scale issues is important in investigating and understanding the Earth's surface. It is this multiple scale approach, both in terms of space and time, that was adopted for this study. The considerations of time (relative and absolute), space (scale and size) and location (placement) are significant for studies involving mega- and meso–scale geomorphology, since independent variables controlling the development of landforms may totally change as the scale of investigation changes from micro to mega scales (Gardner and Scoging, 1983; Schumm, 1991).

Huggett (2007) warned that the long profiles of large rivers may be difficult to interpret solely in terms of fluvial processes as large rivers are normally old, with lengthy histories and unique tectonic and other formative events, which have influenced their development. Ultimately the study of large rivers is a two-faceted endeavour involving issues of both their physical scale and their temporal scale (Schumm, 2005; Tandon and Sinha, 2007). This two-faceted approach addresses the issues raised by Potter (1978) and Huggett (2007) and, in order to understand the temporal scale of the Congo and Kalahari river systems, it is necessary to understand also the history of the continent in which these rivers formed. It is these historical geomorphic aspects that form the basis of the literature reviewed in **Chapter 3**. The literature indicates that the rivers of the Congo and Kalahari Basins are most probably of a dominant alluvial nature (at least for the most part) (Du Toit, 1933; Dixey, 1943; Moore et al., 2007; Runge, 2007).

While the landscape's history is important, an appreciation of the current processes acting upon the landsurface enhances understanding of given geomorphic features. This treatment of factors influencing fluvial evolution is required in order to understand a landform's past history and to

elucidate the role of Gondwana formation, evolution and break-up on Africa's mega-geomorphology and the possibility of those ancient landforms persisting into the present, being inherited by younger landforms or being completely reworked or obliterated.

CHAPTER 3: THE GEOMORPHOLOGY OF SOUTH-CENTRAL AFRICA

3.1 Introduction

The subject of this thesis is on the geomorphology of sub–Saharan Africa, with a focus on the landscapes of south–central Africa west of Lakes Tanganyika and Malawi. The topography of Africa's surface represents the interaction of exogenic and endogenic forces on the rocks of the continent, a relationship that is complicated by the immensity of time involved. Much of Africa's present day geomorphology is probably of great age, owing to the relative tectonic stability of most of the continent (King, 1951; Partridge and Maud, 1987). Therefore, for an understanding of Africa's geomorphology it is necessary to appreciate the formation of the continent, as characteristics that have been inherited during the development of Africa have significant influences on its ongoing evolution.

The African continent has its genesis in the formation and break-up the super continent Gondwana, which existed from ca. 510 Ma to 180 Ma (du Toit, 1933; de Wit et al., 2008; Torsvik and Cocks, 2009). During the time of Gondwana, the African continent formed the centre and experienced multiple phases of tectonics, subsidence, uplift, denudation and deposition that modified its landsurface. After the break-up of Gondwana, Africa's surface continued, and still continues, to undergo modification. Today the African continent comprises the West African, Congo and Kalahari Cratons (see **Figure 3.1**). It should be noted that, for the purposes of this thesis, the terms craton and shield are used to differentiated Archaen rocks from Proterozoic rocks that for the Precambrian Basement. These three cratons have been linked together since Gondwana formation and have subsequently been covered by Phanerozoic sediments. It has been suggested that events of the late Neoproterozoic that led to the formation of Gondwana have influenced subsequent Phanerozoic events (Partridge and Maud, 2000; Burke and Gunnell, 2008; de Wit et al., 2008). Wellington (1955) cautioned that the varied nature of southern and central Africa precludes any meaningful geographical (and geomorphological) separation of the two regions based on only one of the factors of elevation, relief, geology or climate. It is essential that any investigation of south-central Africa pursues a multi–faceted approach.

The divide between the northerly flowing Congo and southerly flowing Kalahari rivers is one of most clearly distinguishable geomorphic features of south–central Africa (Wellington, 1955). This chapter provides a broad overview of the events leading up the to present day regional geomorphology of south-central Africa, with the level of detail being discussed increasing concurrently with the

increase of the spatial and temporal scales being reviewed. The genesis of south-central Africa, with the formation and break-up of Gondwana is reviewed in **Section 3.2**; this fundamental geologic underpinning being important in terms of Africa's geodynamics, tectonic inheritance and landscapes development. Then the geology of south-central Africa is briefly covered in **Section 3.3**, as these rocks have been shaped into the present day geomorphology. Next, the geomorphology of CB and KB is described in **Section 3.4**, with a focus on the river systems of these basins. In **Section 3.5**, the CKW is treated in detail, and the chapter ends with a discussion of the choice of the rivers selected for this study (**Section 3.6**).

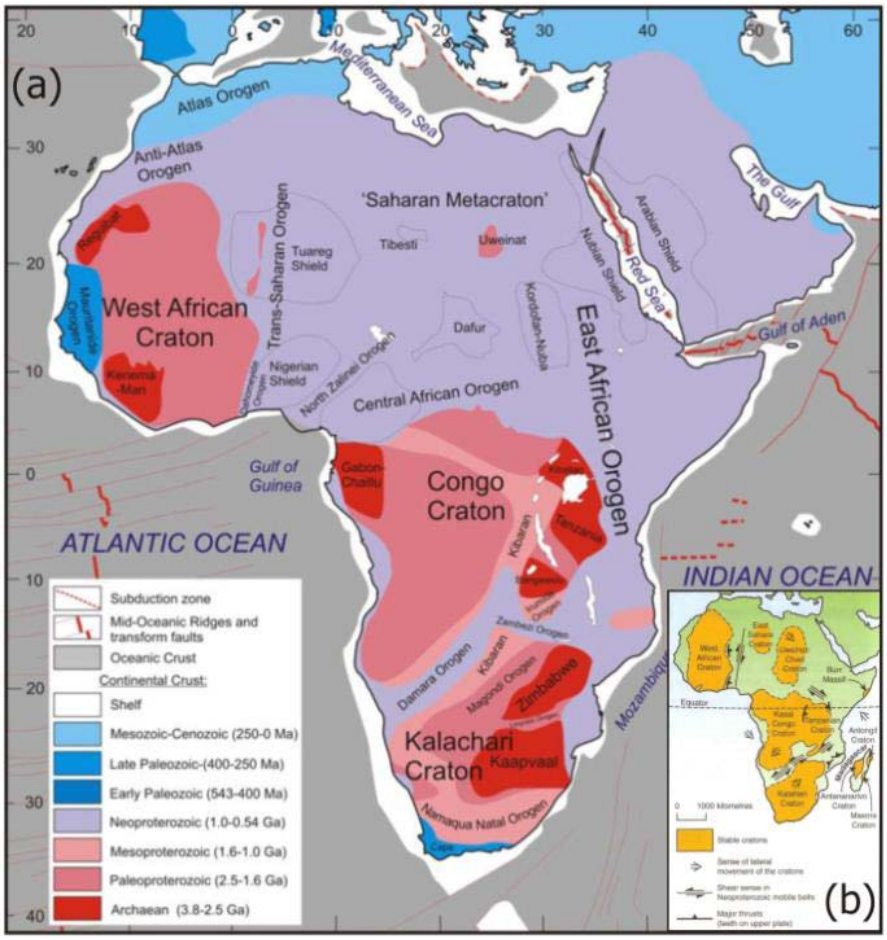

Figure 3.1: The extent and ages of Africa's orogens and cratons. (a) Ages indicate the time of formation or the time of thermal or tectonic reworking (after Gubanov and Mooney, 2009, in van Hinsbergen et al., 2011). Inset (b) Direction of lateral cratonic movements and shearing of the Neoproterozoic mobile belts (orogens). The East Sahara Craton and Uweinat–Chad Craton have yet to be confirmed (Key et al., 2011). Note that for this study the term craton is used for Archean rocks and shield for Proterozoic rocks that form the Precambrian Basement rocks.

3.2 Gondwana

3.2.1 Formation of Gondwana

The supercontinent Gondwana incorporated most of today's southern hemisphere landmasses, namely, Africa, South America, Antarctica, Australia, Madagascar, the Indian subcontinent and Arabian Peninsula (de Wit et al., 2008; Torsvik and Cocks, 2009). Du Toit (1937) was the first to suggest the existence of Gondwana based on the shared geological evidence and not continental geometry alone (Fuller, 1999). Du Toit (1937) found that several rock outcrops from South America and Africa are geologically identical, thereby providing evidence of their past connection, despite these continents being presently either side of the Atlantic Ocean. These two continents formed Western Gondwana (**Figure 3.2**), with Central and Eastern Gondwana consisting of the remaining landmasses. This section will focus on Western Gondwana as it contains the geographic area that corresponds to the present day Congo and Kalahari Basins.

Gondwana was formed through the relative rapid amalgamation of a number of continental fragments during the late Neoproterozoic (de Wit et al., 2008). It is probable that the Congo and Kalahari cratons were loosely joined along the eastern Zambezi Belt (see **Figures 3.1** and **3.3**) from 820 Ma (Hoffman, 1999). Subsequent reopening and closure of the western and central parts of the Zambezi Belt gave rise to the Damaran and Katangan Belts (see **Figure 3.3**), with a final closure occurring around 600 – 550 Ma, resulting in a continuous orogenic belt in southern African (Hoffman, 1999; de Wit et al., 2008). By ca. 510 Ma, after several orogenic phases, Gondwana had formed, although smaller blocks accreted to its peripheries throughout the Palaeozoic (Hoffman, 1999).

Over time, Gondwana underwent peneplanation, with the central region of Gondwana (Africa) remaining relatively undisturbed until the Mesozoic (de Wit et al., 2000). It is thought that Africa's position with regard to the Earth's deep mantle has remained the most stable of all the continents since the Permian and has possibly existed for much longer (Burke and Gunnell, 2008; Cocks and Torsvik, 2011). During the Palaeozoic, Gondwana slowly moved across the South Pole and, by the end of the Palaeozoic, the South Pole lay off the shore of Antarctica (Cocks and Torsvik, 2011). Apart from extensive shallow seas in the north in the Cambrian to Devonian, the majority of central Gondwana comprised land during the Palaeozoic (Cocks and Torsvik, 2011). During the upper Carboniferous and later, substantial non-marine lake basins in central and southern Africa appeared, in which the Karoo Supergroup was deposited (Cocks and Torsvik, 2011).

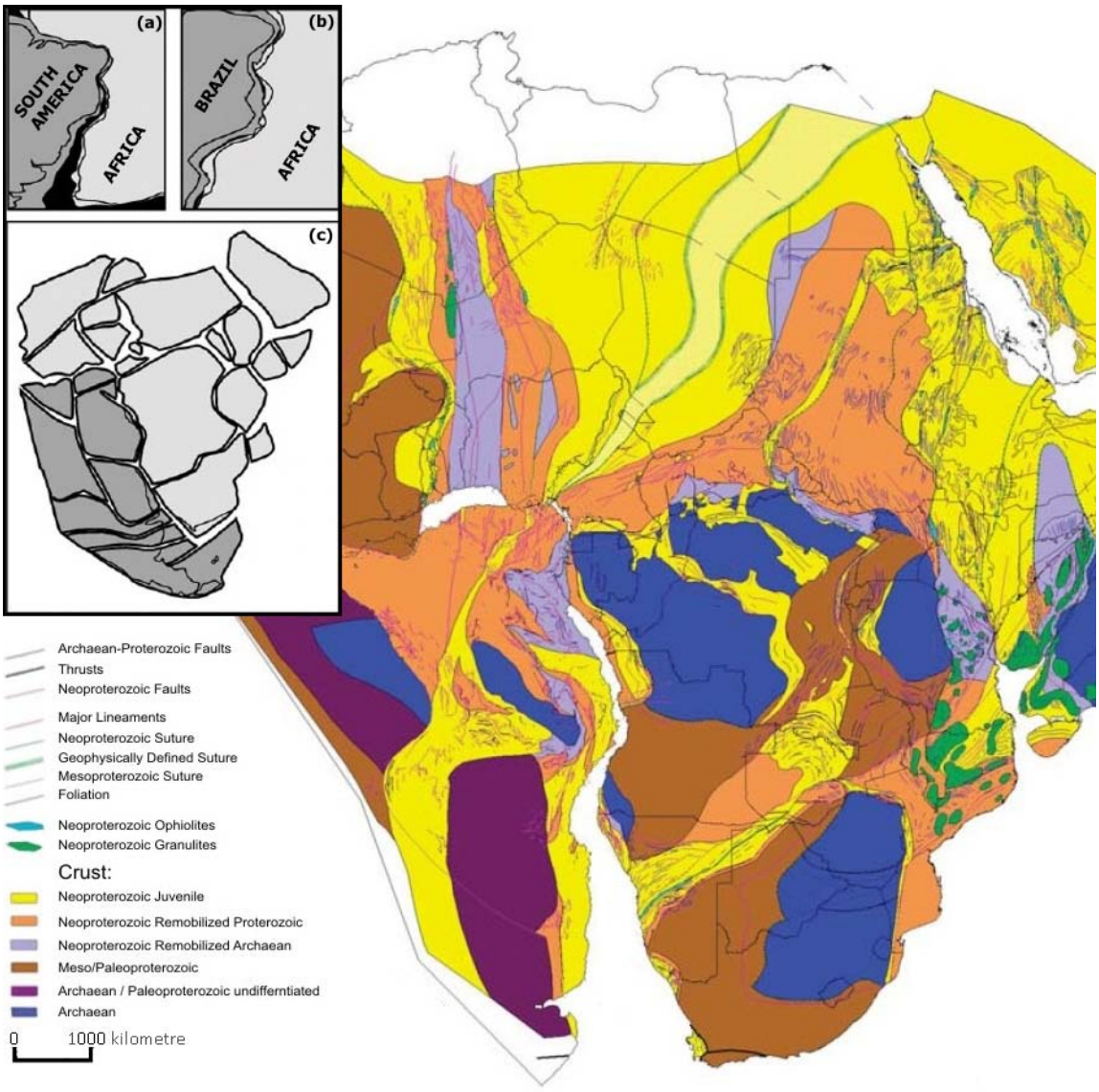

Figure 3.2: A simplified crustal geological map of Western Gondwana. The major embedded Archean cratons (blue), their Neoproterozoic shields (brown) and their Pan-African remobilised margins (yellow) are shown. Remobilised Archean-Proterozoic fragements are indicated by lilac and orange. Note that east-west striking central South Atlantic margins do not follow inherent lithospheric anistropy but rather cross cut major Pan-African tectonic belts and older Archean cratons and Palaeoproterozoic shields (de Wit et al., 2008). Inset: (a) schematic based on rigid plate rotations ca. 120 – 150 Ma; (b) possible tight fit between Nigeria and Namibia with c. 60 km separation between the edges of African and South American Precambrian blocks; (c) schematic of c. 150 -200 Ma fit of West Gondwana, after internal adjustments and rotation of the small Precambrian blocks have been undone. Figure adapted from Reeves et al., (2004), and de Wit et al., (2008).

It is thought that southern Africa was already substantially elevated during Gondwana's existence, with offshore sedimentation records and apatite fission track analyses (AFTA) providing support for an elevated southern Africa (de Wit et al., 2000). This evidence suggests that, in southern and central regions of southern Africa, several kilometres of rock had been removed prior to Gondwana's break-up. By comparison, the African inter-basin swells experienced less than 200 m of rock stripping (de Wit et al., 2000). During the Mesozoic a series of intra-continental rifts fractured the stability of Western Gondwana with break-up being completed during the Cretaceous (Reeves, 1999; de Wit et al., 2008).

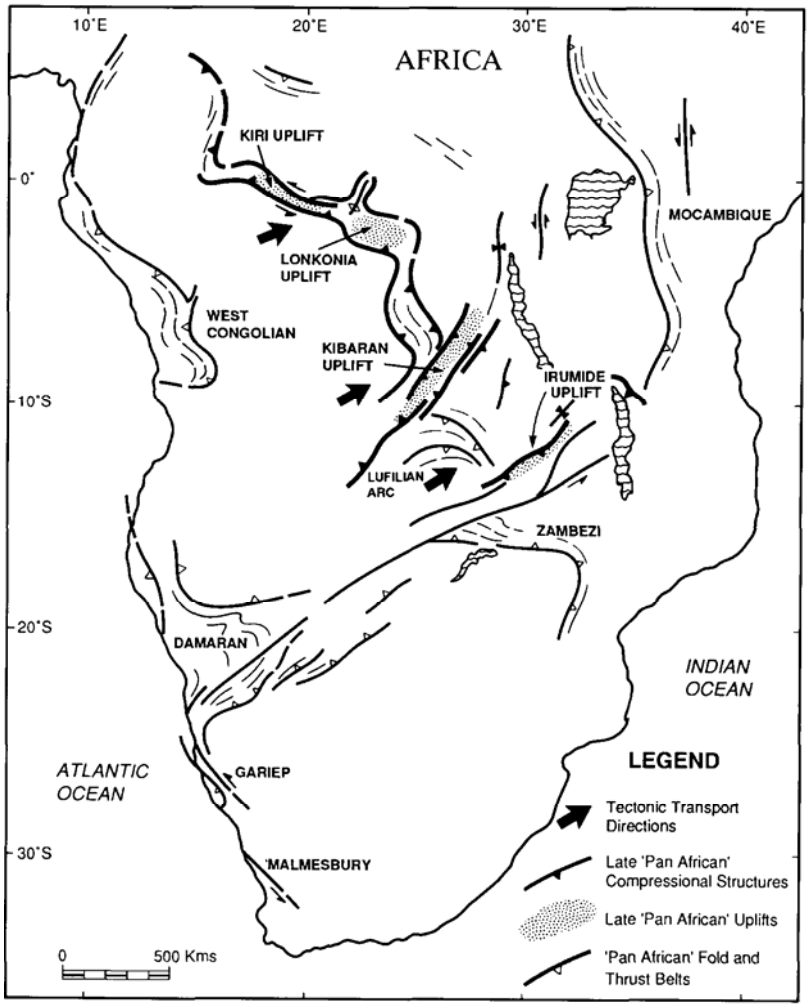

Figure 3.3: Regional tectonic setting of south and central Africa during the late Proterozoic to early Paleozoic. Kibaran belts are Mesoproterozoic in age. Note the distribution of basement uplifts in the foreland regions of the late Proterozoic fold and thrust belts. Figure from Daly et al. (1992).

3.2.2 Gondwana Break-up

Western Gondwana broke off from Eastern Gondwana during the Mesozoic, with the separation of South America and Africa occurring around 129 – 121 Ma, primarily through the opening of the Central Atlantic and South Atlantic Oceans (Fouche et al., 1992; van Hinsbergen et al., 2011). The rifting of South America and Africa involved uplift, which was higher in eastern southern Africa, resulting in the westerly flowing trend for the main drainage of southern Africa (de Wit et al., 2000). It is thought that this rifting created a marginal escarpment, which was driven backward during the Cretaceous (Partridge and Maud, 1987), and this erosion partly exhumed a pre-Karoo escarpment (de Wit et al., 2000). The cause of the breaking up of Gondwana along one of its five major Neoproterozoic Gondwana orogens is still unresolved (de Wit et al., 2008).

Rifting during the break-up of Western Gondwana mirrored the Neoproterozoic orogenic belts, with close to 65% of the total South Atlantic rift length trending approximately parallel to the Pan-African tectonic fabric (de Wit et al., 2008). However, not all the continental rifting followed the inherent lithospheric anisotropy of the separating fragments (as can be seen in **Figure 3.2**), with ca. 35 % of the South Atlantic rift being at a significant angle to pre-existing tectonic trends (de Wit et al., 2008). This resulted in rifting, cutting across major Pan-African/Brasiliano tectonic belts as well as older tectonic trends on Archean craton and Paleoproterozoic shields to form the present day east-west striking central South Atlantic margins (de Wit et al., 2008). It is possible that such a distribution of parallel and near-orthogonal rift patterns may play crucial roles in creating the *en echelon* rift geometries and overlap of early continental rifts (de Wit et al., 2008).

3.2.3 Motion of cratons pre- and post-Gondwana

Major continents do not always respond as single rigid blocks during plate motions and often there is internal movement of the continent itself resulting in distortions of the shape of the landmass (de Wit et al., 2008). Thus the edges of most cratons and shields have not been clearly defined and in many cases the Pan-African tectonothermal overprints and remobilizations have distorted their pre-Gondwana geometries, as illustrated in **Figure 3.2** (Reeves, 1999; de Wit et al., 2008). Reeves (1999) proposed the division of South America and Africa into a number of semi-independent Precambrian blocks to accommodate the internal deformations experienced by the continents subsequent to break-up. By allowing for small internal adjustments and rotations of the Precambrian blocks, known Mesozoic-Cenozoic rifts and slips along the major Pan-African, Brasiliano, Cretaceous and Miocene faults zones and tectonics lineaments were accounted for, allowing for tighter fit between the continents as shown in the inset of **Figure 3.2** (Reeves, 1999; Reeves et al., 2004). For Africa these

blocks correspond to the Congo and Kalahari Cratons amongst others (see **Figure 3.2 inset c**). Thus for part of their pre- and post-rift histories, Gondwana fragments have acted as a mosaic of blocks, with the cratons and shields having undergone some (mainly aborted) rifting and rotation (de Wit et al., 2008).

3.3. The geology of south-central Africa

The area under investigation in this thesis is the drainage divide of the CB and the KB and as such the pertinent geological elements of south–central will be highlighted (see **Figure 3.4**). Owing to the larger number of rivers under study occurring within the CB, its geology will be dealt with in greater detail than that of the KB.

Several of Africa's first–order features have yet to be explained and are still being debated (van Hinsbergen et al., 2011). Unresolved questions related to this study include what the role is (if any) of mantle processes in the formation of Africa's high elevation in eastern and southern Africa (e.g. Doucouré and de Wit, 2003; Pasyanos and Nyblade, 2007; Wichura et al., 2011), and what the mechanism is that controlled the formation and subsidence of the intracratonic sedimentary basin of central Africa, the CB (e.g. Daly et al., 1992; Giresse, 2005; Kadima et al., 2001b). A further unresolved issue of importance to this study is the trigger and formation of the EARS and how it developed on a continent largely surrounded by spreading centres and experiencing mainly compression (e.g. Chorowicz, 2005; van Hinsbergen et al., 2011; Delvaux et al., 2012). A final issue is the relationship between sedimentation and tectonics across Africa (e.g. Burke and Gunnell, 2008). These phenomena are significant to understanding Africa's unique topography, and the fact that they have yet to be fully explained is telling of the need for further research into Africa's evolution.

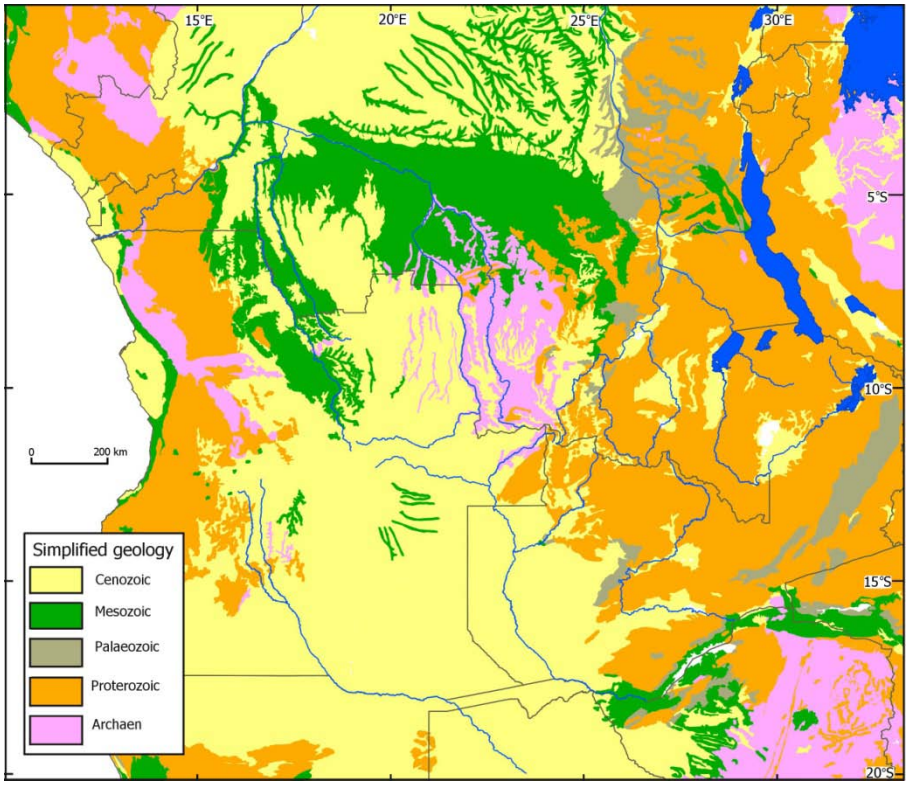

Figure 3.4: The simplified geology of south-central Africa. Political boundaries are indicated in black and waterbodies in dark blue. See legend for geological units (Hearn et al., 2001).

3.3.1 The significance of basin geology for this study

The review of the relevant geology of the Congo and Kalahari Basins in **Sections 3.3.2** and **3.3.3**, shows the varied and complex nature of the geology of south-central Africa. The review of the basins geology is important to this study as the development of river systems is often strongly associated with the lithologies over which they flow (see, for example, Zernitz, 1932: Leopold et al., 1964; Howard, 1967; Tooth et al., 2002). The varied nature of the sedimentary sequence, from localised silicification of sandstone to metamorphosis, may result in localised instances of hard rock that form a local base level of river erosion, thereby creating a knickpoint. Alternately the closer homogeneity of some units over others may result in river systems achieving a concave profile more easily. Furthermore, a river's ability to respond to any change, and by extension changes in its basin, may be strengthened or weakened by the geological setting of that river.

It is therefore reasonable to expect that the development of rivers of the Congo and Kalahari Basins, at least in some areas, would exhibit a degree of lithologic control. A sound geologic underpinning is crucial for understanding the development of the region's river systems as well as for identifying

possible controls. In order to be able to identify these cases of lithologic control, it is important to comprehend the geology of the basins, as described in **Sections 3.3.1** and **3.3.2**. This description will provide the basis for the investigation of the role of geology in the development of the river systems of the CB and KB, which is dealt with in **Chapter 7** of this thesis.

3.3.2 Overview of the geology of central Africa, Congo Basin

The CB is a large, roughly circular intracontinental basin, exceeding 3 million km^2 and measuring approximately 2600 km at its longest and 2400 km at it's widest, as shown in **Figure 3.5**. Although the details of the development of the CB are debated, it is thought that the initial basin was formed as a result of a Neoproterozoic failed rift (the concealed failed rift basin shown in **Figure 3.5**) and subsequent cooling of the stretched lithosphere during the Paleozoic, with several periods of basin inversion occurring thereafter (Daly et al., 1992; Giresse, 2005; Kadima et al., 2011b). This long lived intracratonic basin has a complex geologic history with sediment accumulation (up to 9 km), beginning in the Neoproterozoic and followed by phases of erosion, tectonic inversion and changes in the geodynamic processes of the region (Veatch, 1935; Roberts, 1946; Lepersonne, 1951; Cahen, 1954; Cahen and Lepersonne, 1978; Daly et al., 1992; Kadima et al., 2011a,b).

The CB exhibits ongoing tectonic activity, with a zone of high tectonic in the eastern basin that is linked to the development of the EARS (Mavonga and Durrheim, 2009; Delvaux and Barth, 2010). Throughout the rest of the CB there are sporadic tectonics, with the zone in the south-west *cuvette centrale* being of moderate activity; Delvaux and Barth (2010) suggest that this activity is associated with the deep thrust structure identified by Daly et al. (1992), as shown in **Figure 3.3**.

The underlying basement of the CB is overlain by extensive Phanerozoic sediments, which limits the number of exposures and in parts there has been extensive reworking of the uppermost sediments (Veatch, 1935; Cahen, 1951). This coverage and reworking combined with the large extent and complex geology of the CB, as well as limited exploration work, has hindered the creation of a definitive lithostratigraphy and the understanding of the basin's evolution remains incomplete (Daly et al., 1992; Giresse, 2005; Kadima et al., 2011a; Sachse et al., 2012).

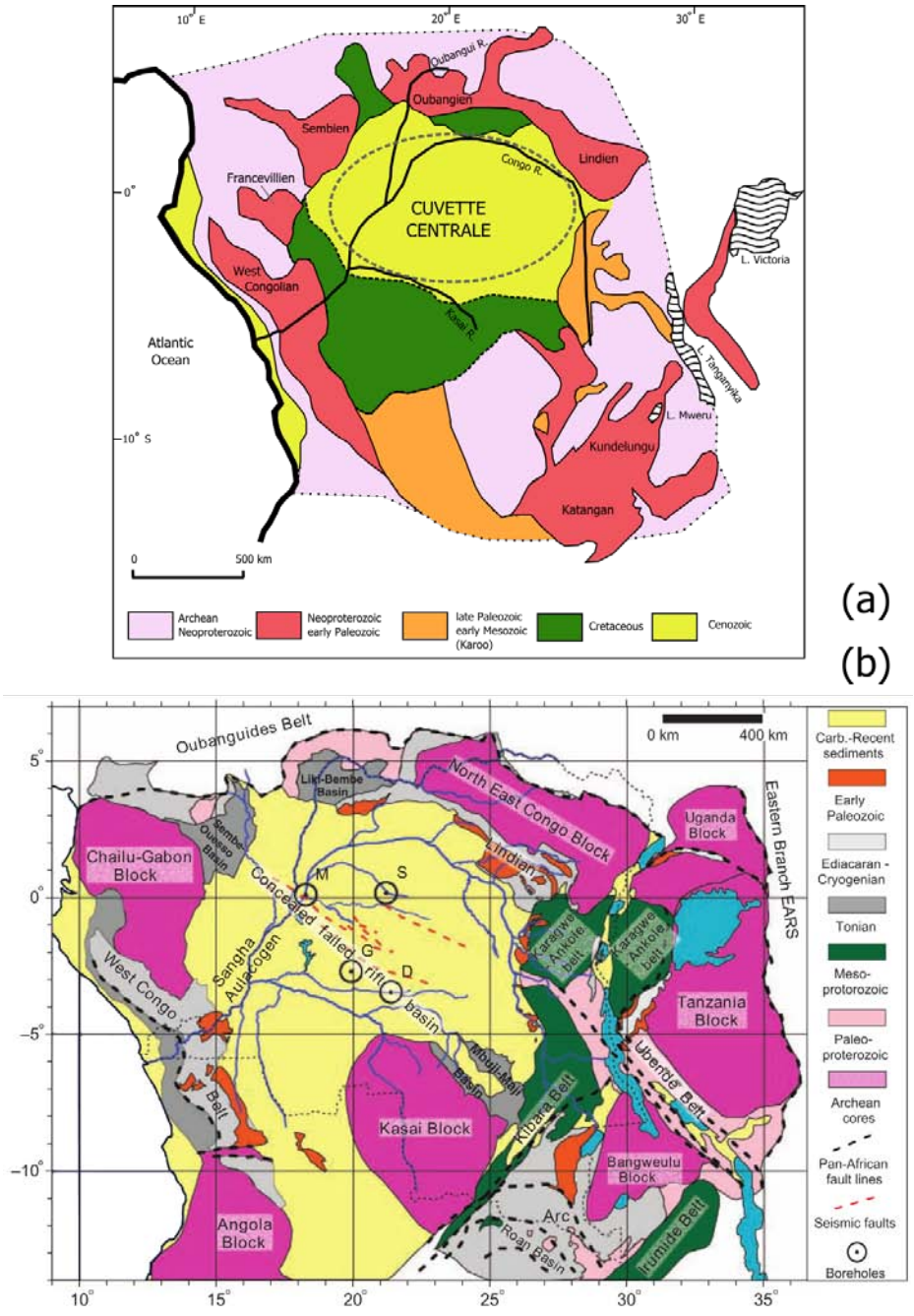

Figure 3.5: (a) Cartoon of the regional setting of the Congo Basin showing the extent of Karoo, Cretaceous and Cenozoic sediments (redrawn from Daly et al., 1992). The extent of the *cuvette centrale* (central basin) is shown by the dashed oval. (b) Tectonic setting of the Neoproterozoic basin of present day central Africa. Location of wells shown: M–Mbandaka, S–Samba, G–Gilson, D–Dekese. Figures modified from Kadima et al., 2011a.

Initial studies of the CB were focused around the peripheries of the *cuvette centrale* and stratigraphies were proposed based on the assumption of formations being continuous over large distances (Veatch, 1935; Roberts, 1946; Cahen and Lepersonne, 1954). However, the heterogeneity of these sedimentary formations has since been recognised and their lateral variation (both in facies and thickness) along with their unequal preservation (partially or completely absent at various locations) has limited the development of a robust, well correlated stratigraphy of the CB (Giresse, 2005; Sachse et al., 2012). The heterogeneity of the units and large distance between similar units led to various stratigraphies being proposed, as seen by comparing those of Lepersonne (1945), Cahen (1983), Daly et al. (1992), Colins (1994) and Kadima et al., (2011a). Recent attempts to provide an overall stratigraphy have been conducted by Giresse (2005), Kadima et al. (2011a) and Linol (2012). Giresse (2005) reviewed available regional Mesozoic–Cenozoic stratigraphies for the CB based on available literature. Kadima et al. (2011a) proposed an update stratigraphy (see **Figure 3.6**) using gravity, magnetic and reflection seismic in conjunction with a review of literature, map complications and partial re-examination of outcrop and core samples. Linol (2012) provided a new analysis of the sedimentology and sequence stratigraphy of the CB by revisiting various core samples and providing new detrital zircon age data. A detailed analysis of the geology is outside the remit of this study; however, Linol (2012), and Kadima et al. (2011a) have made an extensive analysis of the stratigraphy and geology of the CB. What follows here is a brief outline of the geology of the CB that seeks to highlight key events and its variable nature.

The CB's development appears to exhibit three first order sedimentary units which can be broadly correlated into Neoproterozoic, Paleozoic and Mesozoic-Cenozoic episodes (Sachse et al., 2012). These units and an updated stratigraphy of the CB are shown in **Figure 3.6** and the section below provides details of this lithologic record. The CB basement consists of two depocentres separated by a north-west to south-east trending ridge that is thought to be a horst block (the central African zones of uplift illustrated in **Figure 3.3**), which may have formed as a result of far-field stresses due to Neoproterozoic collisions around the Congo Craton (Daly et al., 1992). The sedimentary record of the basin has experienced varying degrees of deformation. For example, the c. 10 km thick late Neoproterozoic Kundelungu Formation was deformed during the formation of the Lufilian Arc (Lufilian Orogenic Belt) (Cahen, 1954). The CB's sedimentary record shows evidence of several marine transgressions, suggesting that the basin has remained near to sealevel for long periods of time (Colin, 1994; Giresse, 2005).

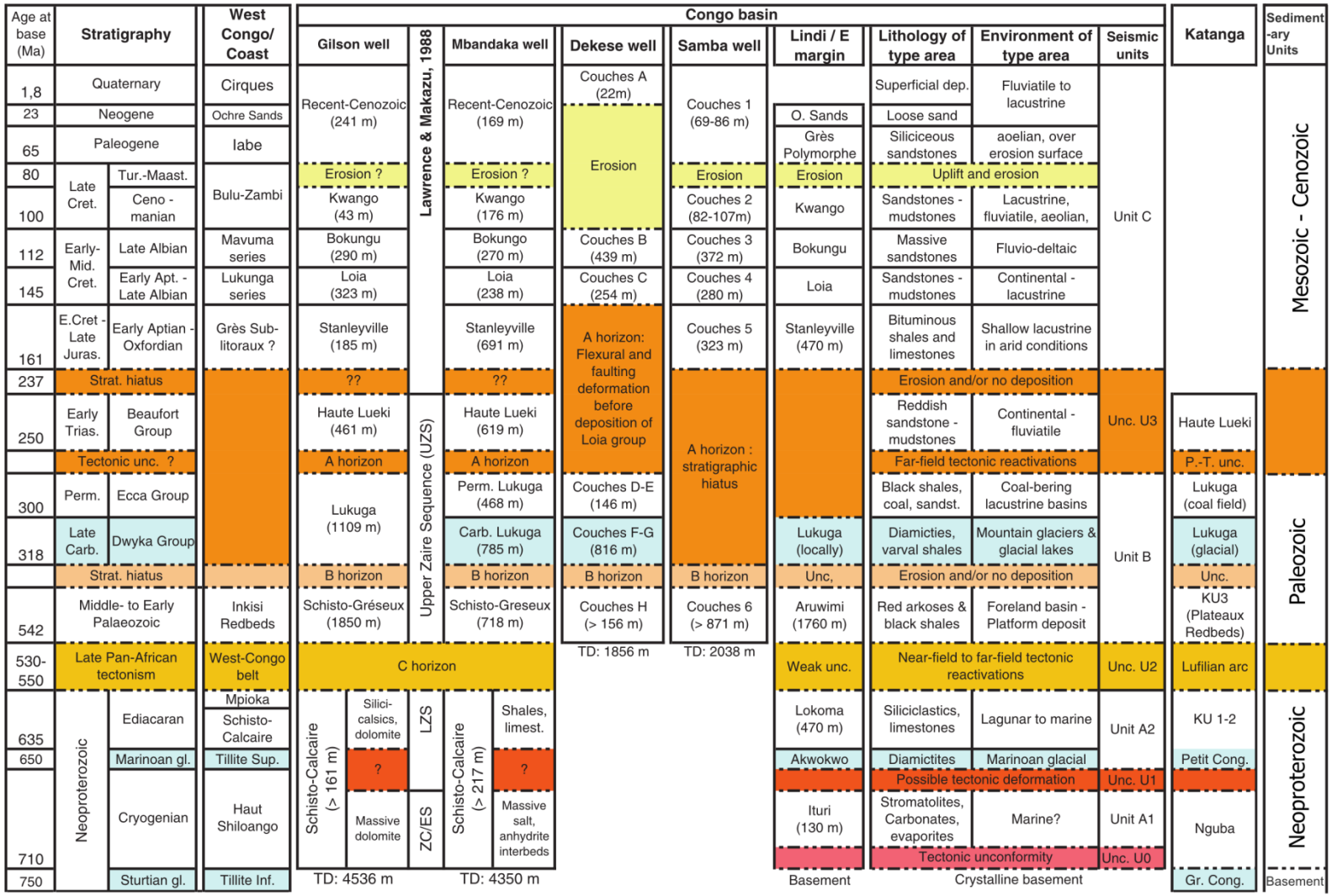

Figure 3.6: Proposed lithostratigraphy for the Congo Basin. The lithostratigraphic is based on four wells from the *cuvette centrale* and outcrops along the north-east (Lindi-Ubangi and Kisangani-Kindu regions) compared with the West Congo and Katanga stratigraphies. The term 'couches' is equivalent to 'beds'. Note the large variation in unit thicknesses. See Kadima et al., 2011a for details. Figure modified from Kadima et al. (2011a) and Sachse et al. (2012).

3.3.2.1 Neoproterozoic and Paleozoic geology

The Neoproterozoic to early Paleozoic sediments of the CB, see **Figure 3.6**, were deposited on a crystalline basement, having undergone several phases of erosion, uplift and tectonic activity, which has resulted in unequal preservation of these deposits (Cahen, 1954; Daly et al., 1992; Giresse, 2005; Kadima et al., 2011a,b). For example, in the Samba well data there is a notable absence of Triassic to Late Jurassic deposits and the Dekese well data lacks Permian and Triassic deposits, while early to mid-Mesozoic deposits are almost completely absent in the Kalemie region (near Lake Tanganyika) (Linol, 2012; Sachse et al., 2012). These missing deposits represent the Paleozoic-Mesozoic discontinuity which broadly corresponds to a major compressional basin inversion event (Daly et al., 1992; Linol, 2012; Sachse et al., 2012).

The first sedimentary sequences of the CB , as indicated in **Figure 3.6**, were deposited on top of the crystalline Precambrian basement rocks; these sequences include the Ituri Group found in the Lindi–Aruwimi region (in the north-east CB), the Haut-Shiloango Group of West Congo (the western margin of the CB) and the Nguba Group in the Katanga region (south-east CB) and are predominantly carbonates with stromatolites, and shales (Kadima et al., 2011a; Sachse et al., 2012). However, a recent re-evaluation of uppermost Haut-Shiloango, having being previously classed as stromatolitic carbonates, did contain evidence of these stromatolites (Delpomdor et al., 2014) and thus future analysis of the CBs early depositions may yet yield new interpretations of their depositional environments. Capping these Cryogenian deposits are Marionan glacial deposits (Kadima et al., 2011a). Overlying or, in some cases, in association with these glacial deposits are thick siliciclastics and limestones, known as the Lokoma Group (in total 470 m thick) in the north-east CB, the Schisto–Calcaire/Mpika in the west and the Kundelungu Kul and Kibuo (KU 1 and 2 in **Figure 3.6**) subgroups in the south-east (Kadima et al., 2011a). The Ituri Group consists of arkoses, carbonates, shales and sandstones, while the Lokoma comprises conglomerates, arkoses, gray shales, limestones and shales (Sachse et al., 2012). Above the Pan-African unconformity the c. 1000 m thick, fluvio–deltaic red arkoses known as Redbeds form the Inkisi Redbeds in West Congo, the Aruwimi Group (1760 m thick) in the Lindi–Aruwimi region and the Upper Kundelungu (KU 3) Group in Katanga (Kadima et al., 2011a). These Redbeds were largely deposited in a continental, lacustrine to fluvio–deltaic semi-arid environment (Kadima et al., 2011a). The Aruwimi Group may be subdivided into three units, namely, cross-bedded continental arkoses of a semi-arid fluviatile setting, a 100 m thick carbonaceous dark shale and sandstone unit deposited in a lacustrine to lagunar environment, and finally a 1000 m thick arkose unit consisting of aeolian and braided river facies with some cross-bedding (Kadima et

al., 2011a; Sachse et al., 2012). The age of the Aruwimi Group is problematic, being only constrained by the Pan-African unconformity at its base and the overlying glacial-interglacial and post-glacial sediments of the late Carboniferous Lukuga Group (Sachse et al., 2012). Together the Aruwimi and Lukuga groups represent the known Paleozoic deposits in the CB (Sachse et al., 2012). The Lukuga Group is preserved in grabens within the Lukuga River basin related to EARS development, the Upemba depression in the Luena River basin, and in U–shaped valleys on the eastern margin of the CB and within the southern *cuvette centrale* (Kadima et al., 2011a) At its base, the Lukuga Group displays diamictites and varval clays which are overlain by post-glacial claystones and sandstones (Kadima et al., 2011a). In the Dekese area the Lukuga Group is overlain by beds of postglacial black shales, whereas in the Kalemie (western Lake Tanganyika) region it is overlain by sandstones (Sachse et al., 2012). There is a marked discontinuity between the Paleozoic sedimentary unit and the overlying Mesozoic-Cenozoic series (Sachse et al., 2012).

3.3.2.2 Mesozoic–Cenozoic geology

The exposed Mesozoic and Cenozoic continental deposits of the *cuvette centrale* (see **Figure 3.6**) and its peripheries are composed mainly of clayey sands or soft sandstones, which are of dominantly fluvial and lacustrine origin with near-horizontal structuring (Veatch, 1935; Lepersonne, 1945; Cahen, 1951; Colin, 1994). The burial of planation surfaces (and their side slopes) by reworked superficial sediments and the relatively long distances (tens of kilometres) separating well-developed erosion surfaces has made correlation of the Mesozoic–Cenozoic challenging (Giresse, 2005). This burial and reworking combined with a lack dateable paleontological evidence has made the distinction between the Mesozoic–Cenozoic sediments difficult, adding further complications to geological studies of the CB (Giresse, 2005).

During the Triassic the Precambrian basement and Paleozoic deposits were planed followed by a period of sediments deposition, with the sedimentary succession of Carboniferous to Triassic sediments forming the Karoo Supergroup (Roberts, 1946; King, 1951; Cahen, 1954). Following deposition the Karoo sediments were tilted toward the centre of the CB and eroded and thus have limited preservation (Lepersonne, 1951; King, 1951; Cahen, 1954). This Karoo sequence is represented by Lukuga and Haute Lueki Groups in Katanga (Kadima et al., 2011a).

The Mesozoic sedimentation began in the eastern CB (the Kalemie region near Lake Tanganyika) with the deposition of Early Triassic reddish sandstones and mudstones of the Haute Lueki Group (Kadima et al., 2011a; Sachse et al., 2012). This Haute Lueki Group unconformably overlies the upper, Permian Lukuga Group with the unconformity being the result of a phase of erosion and/or no deposition in the Early Triassic (Kadima et al., 2011a; Sachse et al., 2012).

The formations of the Karoo Supergroup in the CB are overlain by a successive sequence of upper Jurassic, Cretaceous and Cenozoic continental deposits (Giresse, 2005; Kadima et al., 2011a), as shown on **Figure 3.6**.There is thus a stratigraphic hiatus, corresponding to at least the Early Jurassic, between the Early Triassic Haute Lueki Group and Late Jurassic sediments of the Stanleyville Group (Kadima et al., 2011a). Having limited preservation in the *cuvette centrale*, the Kimmeridgian (Late Jurassic) Stanleyville Group consist of sandstones with shales and limestones deposits (Lepersonne, 1951; Cahen, 1954; Colin, 1994; Kadima et al., 2011a). South of Kisangani, upstream of the Congo River to about 5° S, the Stanleyville Group occurs as an alternating succession of bituminous shales and limestone with a maximum thickness of 200 m, while in the Samba well it attains a thickness of 323 m and is dominantly composed of calcerous sandstones and shales (Kadima et al., 2011a). Evidence from the Samba well indicates a fluvial-lacustrine depositional environment for the Stanleyville Group, which sits directly on the Aruwimi Group (couches 5), while the Stanleyville is absent from the Dekese well (Kadima et al., 2011a; Sachse et al., 2012). Overlying the Stanleyville Group are the mid Cretaceous sediments of the Loia Group.

Cretaceous age sediments cover a large part of the CB and are well represented (Roberts, 1946; Cahen and Lepersonne, 1952; Cahen, 1954). These Cretaceous sediments are exposed in the marginal areas of the *cuvette centrale* see **Figure 3.5a)**. This Cretaceous sequence consists of the Loia, Bokung and Kwango Groups totalling a maximum of 750 m (Kadima et al., 2011a). The Loia Group consists of predominantly mud- and sandstones and is found widely in the *cuvette centrale*, with an enlarged depositional area that shows a shift in the depocentre toward the centre of the modern basin, while the southern and eastern basin rims underwent uplift (Lepersonne, 1951; Cahen, 1954; Colin, 1994). In the Dekese well (see **Figure 3.5b**) the Loia Group consists of aeolian sands dunes and shallow lacustrine sandstones and mudstones with bituminous shale levels (Linol, 2012; Sachse et al., 2012). Elsewhere it is formed by red shales, sandstones and shales (Colin, 1994). Sitting on top of the Loia Group is the Bokungu Group of massive sandstones that were deposited in a fluvio-deltaic environment (Giresse, 2005; Kadima et al., 2011a).

During the Cretaceous the CB region experienced a shallow-water marine intrusion, evidenced by marine deposits, being indicative of the basin's low elevation (Giresse, 2005). It is thought that the Congo surface experienced a slight uplift, experiencing some deformation and planation (Lepersonne, 1951). This Cretaceous surface probably occurred extensively in the northern and central part of the *cuvette centrale* but is neither well defined nor preserved in the southern regions (Lepersonne, 1951; Cahen, 1954). Consisting of fluvio-deltaic sandstones and siltstones, the Kwango Group was deposited directly on top of the truncated Loia Group that formed the Cretaceous surface (Lepersonne, 1951; Cahen, 1954). In the southern and south-western CB the Lualaba System is absent, with the Kwango Group lying directly on a very uneven and warped surface formed by either the Lualaba System or Precambrian basement (Giresse, 2005). Here the Kwango Group reaches a local thickness of 10 m and its basal conglomerate is thin and discontinuous (Giresse, 2005). The Kwango Group is dominantly composed of fluvio-deltaic sandstones and siltstones and can be subdivided into two units, the Inzia and Nsélé, which sit above a basal conglomerate, with diamonds occurring at the base of the Kwango Group (Lepersonne, 1951; Cahen, 1954). The Inzia unit is about 105 – 200 m thick and consists overall of fine argillaceous sands with interleaving shales (Lepersonne, 1951; Colin, 1994). The unit's succession sees fossiliferous shales (40 m) overlain by red sandstones (50 – 100 m) with localised pebbles and chert and a 15 – 40 m layer of shales overlain by red calcerous shales and red sandstones (25 m) (Colin, 1994). By comparison the upper Nsélé shows evidence of aeolian deposition, being approximately 100 m thick red fine-grained sandstone that is coarser and more varied than the Inzia sandstone and has locally silicificed deposits (Lepersonne, 1951; Colin, 1994). The Kwango Group is exposed along the Kwango and Kasai Rivers, in the southern rim of *cuvette centrale*, and in the Lukenie and Sankuru valleys and parts of the Congo River in the central basin (Lepersonne, 1951). The Kwango Group sands are more argillaceous, coarser and better sorted in the central and northern Kwango than in the assumed primary sediment source area of the south-western Kasai (Lepersonne, 1951). The Kwango Group, on the contrary, has been eroded from the Dekese well, and beds ('couches 2') in the Samba well consisting of pure quartz sand and kaolin-bearing clay have been correlated to the Kwango Group (Sachse et al., 2012). Overall the Mesozoic sediments of the CB are dominated by lacustrine or lagoonal deposition, having been close to sea level as indicated by a few marine intercalations (evidenced by marine deposits and fossils) (Colin, 1994; Giresse, 2005). There is a prominent erosion surface, marked by extensive silcretes, between the Late Cretaceous deposits and those of the Cenozoic (Lepersonne, 1945; Cahen, 1954; Linol, 2012).

The Cenozoic deposits of the CB have been equated to the Kalahari Group of southern Africa (Lepersonne, 1945), and both of these systems have been shown to lie on the same erosion surface (Cahen and Lepersonne, 1952). Roberts (1946) has suggested that the Kalahari sediments are an important feature of the plains and plateaus of the CB, especially the southern plateaus. The Kalahari Group is 200 – 300 m thick (Lepersonne, 1945; Cahen and Lepersonne, 1945) and in the CB has been sub-divided into two groups, namely, the *Grès polymorphe* (polymorph sandstone) and *Sables orces* (Ochreous sands) (Lepersonne, 1945). The *Grès polymorphe* are Paleogene in age, having being deposited on the Late Cretaceous surface (Lepersonne, 1945; Cahen and Lepersonne, 1952; Colin, 1994). Dominantly consisting of silicified aeolian sands, this group is found mainly in the southern part of the *cuvette centrale* and Angola, being especially well developed in the western Congo (Kwango Basin) (Roberts, 1946; Colin, 1994; Linol, 2012). The lower *Grès polymorphe* consists of a basal conglomerate, overlain by pale coloured sandstones, various silicified sandstones and limestones (chalcedony) and is up to 100 m thick (Lepersonne, 1945; Cahen and Lepersonne, 1952; Colin, 1994). Some of these silicified deposits have a large scale lenticular geometry and are the result of the silicification of limestone and the calcareous sandstone cement (Giresse, 2005). The *Grès polymorphe* is likely to be Eocene in age, having been tilted since its formation and exhibits vertical and horizontal homogeneity (Cahen, 1954; Colin 1994; Giresse, 2005). Overlying the *Grès polymorphe* are Neogene unconsolidated sands that form the *Sables orces* group, which can be distinguished from the *Grès polymorphe* based on physical characteristics (Lepersonne, 1945; Cahen and Lepersonne, 1952). Cahen (1954) differentiated the 100 m thick *Sables orces* into two sub-units, a lower unit of silicreted sandstones in contact with the *Grès polymorphe* and an upper unit of poorly consolidated ocherous sandstone. Toward the centre of the CB and on its western coastal plain, sediments post-dating the Kalahari Group may be found (Roberts, 1946).

3.3.3 Overview of the geology of northern Kalahari Plateau, south–central Africa

The geologic Kalahari basin is a large downwarped basin occupying the northern interior of high, southern Africa known as the Kalahari Plateau. The average surface elevation of the Kalahari Plateau is ca. 1000 m.a.s.l and is thus 600 m higher than the CB in the north. The Precambrian Basement rocks of the KB are covered by a succession of Paleozoic to Karoo age deposits (Jones, 1980; Haddon, 2001; Haddon and McCarthy, 2005). In brief, the geology of the northern KB is composed of the southern Congo Craton, the Damara, Lufillian and Zambezi Orogens and the northern extension of the Kalahari Craton (Zambezi Craton), as shown in **Figures 3.1**, **3.4** and **3.5** (Jones, 1980). The basin has been affected by phases of deposition, erosion, rift and non-rift tectonic activity and has been the site of continental sediment deposition since at least the Late Cretaceous (Lancaster, 2000).

Apart from Angola and the DRC, pre–Kalahari Cretaceous sediments are absent in most of the KB, occurring locally only in Zimbabwe and Namibia (Haddon, 2001). The lack of pre-Kalahari Cretaceous rocks suggests either minimal deposition was occurring during this period or that some of the basal Kalahari Group rocks may be equivalent to Cretaceous deposits further north (Haddon and McCarthy, 2005).

The Cenozoic Kalahari Group sediments cover a vast extent of the KB (see **Figure 3.7**) and were deposited on a (probably) Late Cretaceous surface that originated as a result of subsidence of southern Arica (Haddon, 1999; Haddon and McCarthy, 2005). The stratigraphy and sedimentology of these deposits are, however, poorly known as a result of a dearth of outcrop in most of the region and lack of dateable evidence (Lancaster, 2000). In the eastern region of the KB, there are no appreciable Kalahari Group deposits and the basement rocks are overlain by upper Carboniferous and later continental sediments loosely attributed to the Karoo Supergroup (Jones, 1980; Cocks and Torsvik, 2011).

3.3.3.1 Kalahari Group

The surface Kalahari Group sediments extend over an area of 2.5 million km^2 from the Orange River at 29° S in the south to 1° N in the western Congo and southern Gabon in north and from eastern Namibia to western Zimbabwe (Haddon, 1999; Haddon, 2000; Lancaster, 2000). Very little is known about the northernmost portion of the basin (Haddon, 2000). Along the north-western region of the Kalahari Plateau, the Kalahari Group sediments reach depths in excess of 250 m (Haddon, 1999). The thickness of the Kalahari sediments decreases eastward and apart from a limited number of locally preserved deposits they are absent from much of Zambia and Zimbabwe (Haddon, 1999; Haddon and McCarthy, 2005). Where the Kalahari Group sediments occur, they show a substantial variation in depth, exceeding 400 m near the Angola–Namibia border and being more than 200 m thick in central Angola and northern Botswana (Haddon, 1999). The Karoo age basalts and Proterozoic quartzites and volcanic rock outcrop locally through the Kalahari sand mantle (Wellington, 1949).

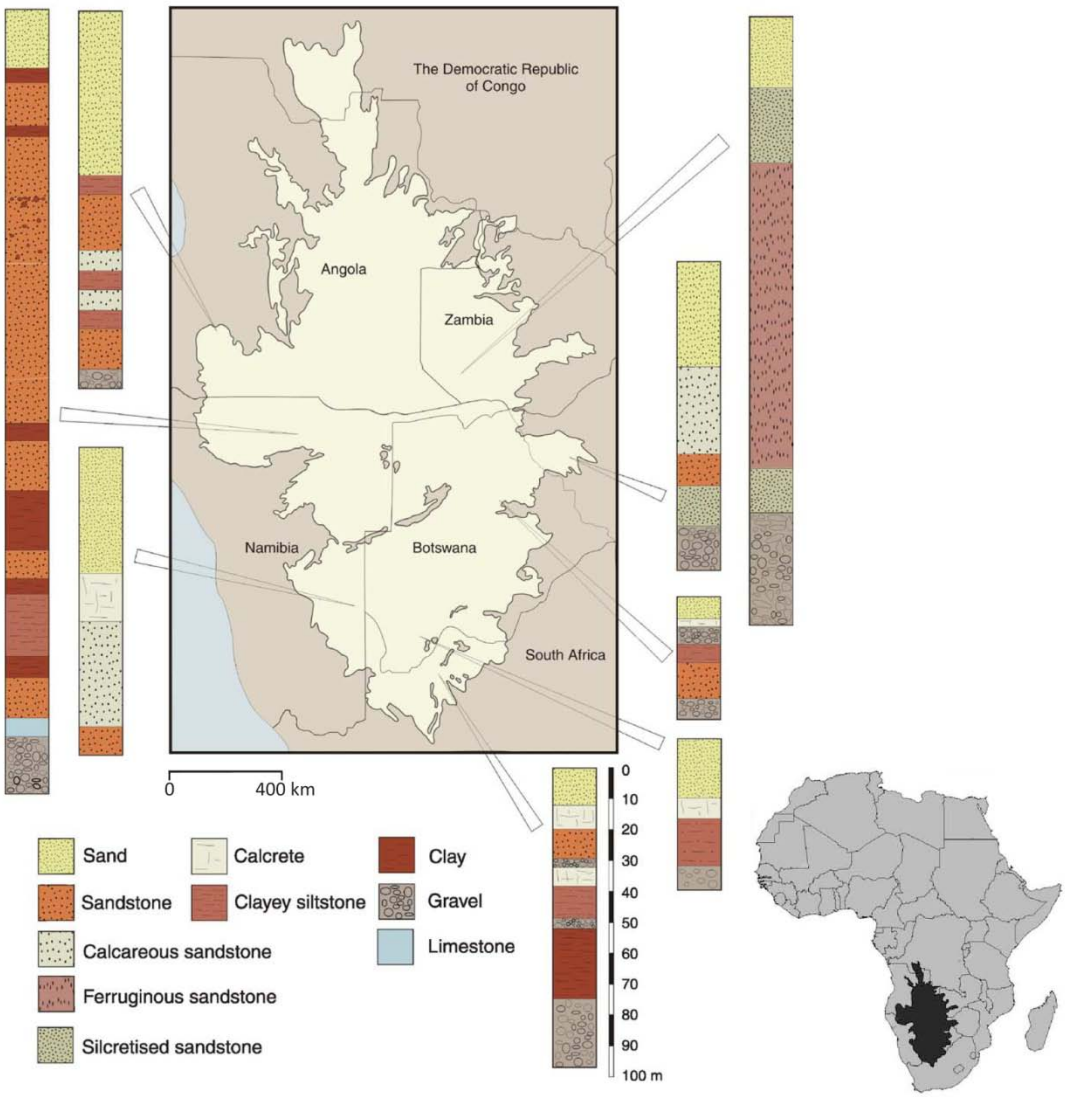

Figure 3.7: The extent of the Kalahari Group cover. The Kalahari Group sediments form a continuous cover from southern DRC, Angola, western Zambia, northern and eastern Namibia, Botswana, western Zimbabwe and northern South Africa, with some localised outcrops occurring elsewhere. Examples of borehole logs showing the Kalahari Group sediment succession. Modified from Haddon and McCarthy 2005.

Most studies have focused on the uppermost units of the Kalahari Group (i.e. the unconsolidated sands, duricrust and pan and lake sediments) as these are important for paleoevironmental information about the Quaternary and the underlying lithologies are exposed at few locations (Haddon, 2000). There is far more to the Kalahari Group than the Kalahari Sands and the complete succession is a complex and interesting sequence of sediments (Haddon, 2000). The Kalahari Sands are poorly documented, being largely unconsolidated and having a complicated stratigraphy with widespread calcretisation and silcretisation of the sediments (Jones, 1980; Haddon, 2000; Linol, 2012). Compared to the Kalahari Group sediments found in the CB, those found in the geologic Kalahari Basin show a greater areal coverage (shown in **Figure 3.7**), are thicker and are more varied

in nature (Haddon and McCarthy, 2005; Linol, 2012). Using mainly bore hole data Haddon (1999) derived an isopach map of the Kalahari Group thickness for the area south of DRC. The sedimentary thickness is highly varied from mantle covering to in excess of 400 m (Haddon, 1999). For a detailed account for the lithological characteristic of the Kalahari Group see Haddon (2000) and Linol (2012) and references therein.

At the base on the Kalahari Group are basal conglomerates and gravels which reach 90 m thickness in the south-west (Namibia) and up to 120 m in the south (South Africa) (du Toit, 1954; Haddon and McCarthy, 2005). Overlying these basal conglomerates is a combination of clays, limestones, clayey siltstone, calcrete, silcretised sandstone, ferruginous sandstone, calcareous sandstone and sandstones all capped by unconsolidated sands of variable thickness (Haddon and McCarthy, 2005). The clays may sit directly on top of the basal gravels or directly on the pre-Kalahari surface (Haddon and McCarthy, 2005). They may reach a thickness of up to 100 m and contain varying amounts of sand and silts, with some areas showing interbedding of sandy layers within the clay unit (Haddon and McCarthy, 2005). The sandstones may be poorly consolidated and easily weathered when duricrusts have not formed (Haddon and McCarthy, 2005). There is evidence of an aeolian origin of the sediments in some eastern parts (Zambia), with indications of fluvial origin in the southern regions (Haddon and McCarthy, 2005). The unconsolidated sands extend over a greater area than the underlying formations, varying from a few metres to over 30 m in many places with basins being deeper than 120 m (Jones, 1980; Haddon, 1999). Calcrete and silcrete layers are usually found where the sands exceed 30 m (Jones, 1980). It is thought that weathering of the bed rock underlying the unconsolidated sediments has significantly contributed to the unconsolidated sand deposits but there is evidence for transportation having occurred (Wellington, 1955; Haddon and McCarthy, 2005).

3.4 Cenozoic topography of south-central Africa

The modern topography of Africa may be considered as bimodal on the planetary scale and be described as basin and swell at the continental scale, as discussed in **Chapter 1**. This section will provide further details on Africa's topography and its post–Gondwana development during the Cenozoic. The discussion will be presented in three sections, starting with a geodynamic overview of the region, highlighting the proposed causes of south-central Africa's continental topography. This is then followed by an examination of the present day geomorphology, and finally a consideration of the Congo and Kalahari Basins and their rivers.

In common with many continental areas, much of Africa experienced a warm, humid climates during most of the Cretaceous (Tyson and Partridge, 2000). These humid conditions led to deep chemical weathering of the regolith and the formation of regional duricrusts and dense drainage networks across much of Africa followed by vigorous erosion (Partridge and Maud, 1987; 2000). This deep weathering profile with cappings of massive of laterite and silcrete is considered to be an identifiable datum referred to as the 'African Surface' by Partridge and Maud (1987). It has been suggested that this surface, first postulated for southern Africa by King (1951), represents a continent wide planation surface formed by multi–phase cycle of Cretaceous erosion, with remnants surviving later dissection (Partridge and Maud, 1987; Partridge, 2000).

The end of the Cretaceous saw a period of global cooling, with southern Africa experiencing desiccation since at least the Eocene and probably since the start of the Paleogene (Partridge and Maud, 2000). Africa's climate has been influenced by global and regional changes and it is likely that regional effects have been of equal (if not greater) importance of the development of southern Africa's climate (Partridge and Maud, 2000). In the late Oligocene to early Miocene, global oceanic warming and massive tectonic activity resulted in major changes, the warming of the oceans allowed rain producing weather systems to penetrate, on a regular basis, into the now arid western hinterland of southern Africa (Tyson and Partridge, 2000). Pre-dating the onset of cold upwelling in the Benguela Current system along the west coast, it is likely that both the Atlantic and Indian Oceans provided a source of moisture contributing to generally wetter environments in southern Africa (Tyson and Partridge, 2000). The humid interval was brought to an end and a strong longitudinal gradient in precipitation (south of ~20 °S) was established ca. 14 Ma with the initiation of the cold upwelling Benguela Current system (Tyson and Partridge, 2000). In the Miocene, regional uplift in east Africa related to the EARS resulting in orographic interception of advected moisture from the Indian Ocean, strengthening the east-west precipitation gradient (Tyson and Partridge, 2000). During the late Miocene to Plio-Pleistocene, a phase of warmer, more mesic conditions resulted in the rejuvenation of many of southern Africa's of drainage networks (de Wit et al., 2000; Tyson and Partridge, 2000). The general synchronicity of the uplift of eastern Africa and global cooling brought about major environmental responses, for example, the aridification of large tracts of sub-Saharan Africa (Partridge, 1998; Tyson and Partridge, 2000). This aridification led to the development of an extensive dune system and is thought to be exhibited by aeolian Kalahari sands in the KB and *Sables Ochres* in the CB, indicating the extension of this aridity beyond present day limits (Partridge, 1998; Tyson and Partridge, 2000). It is thought that the present day, worldwide climatic was established ca. 3 Ma (Partridge and Maud, 2000).

3.4.1 Geodynamic setting of the southern and central Africa

This section provides an introduction to the geodynamic setting of the three continental scale features associated with the CKW and highlights the ongoing debate regarding their age and cause. This is done by means of reviewing relevant literature on the possible timing of key events and mechanisms that have formed low central Africa (the Congo Basin, **Section 3.4.1.1**), high southern Africa (the Kalahari Plateau, **Section 3.4.1.2**) and high eastern Africa (the EARS, **Section 3.4.1.3**).

3.4.1.1 The Congo Basin

While the initial, Precambrian subsidence of the CB is thought to be related to failed intracratonic rift, the cause of the basin's Cenozoic subsidence is debated (Daly, et al., 1992; Kadima et al., 2011b; Buiter et al., 2012). While evidence of marine transgressions in the record of the CB suggests that the basin has undergone moderate subsidence, the cause of Cenozoic subsidence remains unresolved (Giresse, 2005; Kadima et al., 2011b; Buiter et al., 2012). Several driving mechanisms for the basin's subsidence have been proposed that include: thermal relaxation following initial rifting (e.g. Buiter et al., 2012); action of a downward dynamic force on the lithosphere, related to a high-density object at the base of the lithosphere (e.g. Downey and Gurnis, 2009; Crosby et al., 2010 Forte et al., 2010); downwelling of a mantle plume (e.g. Pasyanos and Nyblade, 2007); lithospheric delamination; and reactivation of tectono-thermal fabrics in combination with sediment load flexure (e.g. Kadima et al., 2011b).

Analysing available tomographic models, Buiter et al., (2012) did not find support for the sub–lithospheric mantle's playing a dominant role in the more recent subsidence of the CB. Furthermore, they propose that the present surface elevation of the *cuvette centrale* of the CB is due to the deposition of Mesozoic–Cenozoic sediments that raised the surface to 400 m.a.s.l. and that the last subsidence phase was due to this sediment loading.

However, offshore evidence suggests that the CB has experienced several uplifts during the Cenozoic rather than a single subsidence event. The offshore sedimentary record shows evidence of changes in geodynamic that have been enhanced by climatic regime shifts (Lavier et al., 2001). During the Palaeogene, there was a period of extensive reworking, transport and deposition of sediments within continental Africa and limited erosion of the cratonic areas, as evidenced by widely distributed Palaeogene sediments over continental Africa (Séranne et al., 2008). This suggests a system in equilibrium as no active erosion is apparent. A large amount of sediment was transported

into the coastal region of the CB during the Oligocene, which has been interpreted as a consequence of late Cenozoic uplift and formation of the Congo River (Anka and Séranne, 2004; Séranne et al. 2008; Anka et al. 2010). The Neogene saw a period of increased terrigenous sediment deposition in the coastal zone, which is thought to be a consequence a phase of sustained uplift in the Miocene, with sediment supply being further enhanced by a climatic shift (Lavier et al., 2001; Séranne et al. 2008). However, the origin and geodynamic evolution is still poorly understood and will be debated into the future as new data becomes available (Kadima et al., 2011b; Buiter et al., 2012; and Linol, 2012).

3.4.1.2 Kalahari Plateau

Southern Africa's high topography, here referred to as the Kalahari Plateau, has long been considered to be the result of regional uplift (du Toit, 1933; 1937; King, 1951; 1962), yet the timing and cause of this uplift is still debated. Two hypotheses regarding the uplift have been proposed, one arguing for a Mesozoic (Late Cretaceous) age (e.g. Doucouré and de Wit, 2003; de Wit, 2007; Flowers and Schoene, 2010 and Stanley et al., 2013), the other for a Cenozoic (early to mid Neogene) age (e.g. King, 1951; Partridge and Maud, 1987; Partridge and Maud, 2000; Burke and Gunnell, 2008). Those supporting a Mesozoic age of uplift, based dominantly on thermochronology evidence, suggest that the Plateau has remained stable since uplift (e.g. de Wit, 2007; Flowers and Schoene, 2010; Stanley et al., 2013), whereas those advocating a Cenozoic age have done so based on geomorphic evidence that includes correlation of regional erosion surfaces and laterised sediment layers and propose that appreciable amounts of uplift are still ongoing (King, 1951; Partridge and Maud, 1987; Burke and Gunnell, 2008). The two ages of uplift have resulted in fundamentally different mechanism of uplift being invoked.

The cause of Mesozoic uplift has been suggested to be the deep mantle processes associated with Gondwana break–up (e.g. de Wit, 2007), while the development of a Cenozoic swell ca. 30 Ma could be the result of the African continent becoming stationary with respect to the lithospheric mantle and experiencing shallow convection and thermal modification (e.g. Burke and Gunnell, 2008). A third option for a mechanism of uplift is the African superplume, which refers to a major seismic velocity anomaly in the deep mantle underneath the Plateau, which has been suggested to be a source of buoyancy for southern Africa's high topography (Nyblade and Robinson, 1994; Pasyanos and Nyblade, 2007). However, based on evidence indicating that this structure has remained stable

since the late Paleozoic, it is unlikely to be a dominant cause of southern Africa's high topography (Burke and Gunnell, 2008).

It must be noted that the body of thermochronology evidence (mainly apatite fission track (AFT) analysis data) has received recent criticism. It has been put forward that the technique is not sensitive to Neogene changes in topography where denudation is limited, that it does not differentiate between one– or two–stage models, and that it ignores 'informed' field based evidence demonstrating coexistence of surface of different ages (e.g. Moore and Blenkinsop, 2006; Burke and Gunnell, 2008; Partridge, 2010). This weakness means that the thermochronology data would have been unable to discern the major tectonics movements of the late Cenozoic that significantly altered the topography of eastern and southern Africa (Partridge and Maud, 2000).

However, studies making use of cosmogenic dating, which has a higher temporal resolution, allows for the determination of denudation ages of surfaces, thereby meeting most of the criticism levelled at other dating techniques. Three recent studies find no evidence of rapid Neogene uplift as proposed by Partridge and Maud (1987; 2000). Thus Erlanger et al. (2012) found incision rates for the Sundays River (near Port Elizabeth, South Africa) to be 16.1 ± 1.3 m/Myr for the past ca. 4 Myr; Decker et al. (2013) derived present denudation rates of < 4 m/Myr for sampled Karoo dolerites; and Scharf et al. (2013) calculated denudation rates < 8.8 m/Myr for the quartzitic Cape Mountains. The low denudation rates from these studies are in broad agreement with the average Cenozoic denudation for South Africa's southern coast, determined from AFTA and offshore sediment analysis, of 10 – 15 m/Myr (Tinker et al. 2008). Furthermore, an apatite dating (U-Th)/He study by Stanley et al. (2013) found, for the interior of the plateau, uplift at 117 – 90 Ma, with denudation at the surface with coeval lithospheric heating, metasomatism and thinning (increased buoyancy of lithospheric mantle) that might have resulted in elevation gain. Together these four recent studies from various parts of the southern Plateau provide convincing support for a high southern Africa of Mesozoic age, as suggested previously by other studies, such as Doucouré and de Wit (2003), de Wit (2007), and Flowers and Schoene (2010). Although some debate about the details of uplift remain, current evidence indicates that southern high Africa underwent uplift during the Late Cretaceous (termed the Kalahari epeirogeny) and has remained relatively stable since, with this Late Cretaceous high topography persisting into the present.

3.4.1.3 The Western Branch of the East African Rift System

At a length of 5200 km, the East African Rift System (EARS) spans eastern Africa, from the Red Sea to the coastal regions of Mozambique near Beira (see **Figure 3.8**). Where the EARS encounters the Tanzania Craton is separates into the Western and Eastern Branches, with the extensional structures in both rift branches exploiting pre-existing crustal anisotropies in Proterozoic mobile bets (Wichura et al., 2011). The rift structures of the Eastern Branch link with those of the Western Branch north of Lake Malawi, as indicated in **Figure 3.8**. The high topographies of the Western Branch, extending from Lakes Albert and Tanganyika southward to Lake Malawi, are related to volcanism and Cenozoic rift associated uplift (Cahen, 1954; Chorowicz, 2005; Ring, 2008; Wichura et al., 2011). The high topography of east Africa, as shown in **Figure 3.9,** spatially correlates with volcanism, extensional structures, long-wavelength negative gravity Bouger anomalies and reduced thickness of mantle lithosphere (Pasyanos and Nyblade, 2007; Wichura et al., 2011). It is thought that these thermal and dynamic processes associated with mantle plumes and active continental rifting are also the cause of widespread geophysical anomalies in the different branches of the EARS (Pasyanos and Nyblade, 2007; Wichura et al., 2011).

According to Wichura et al. (2011), the high topography of the East African Plateau (see **Figure 3.8**) and its related rift evolution has been commonly explained by two different mechanisms: (1) late stage rift flank uplift associated with major rift structures, regional-scale extensional detachments and mechanical relaxation and/or isostatic relaxation, as exemplified by the Kenya Rift; or (2) regional lithospheric (domal) uplift followed by extensional processes associated with mantle-plume impingement on continental lithosphere, with the Ethiopian Plateau serving as the type example. Yet the timing, the magnitude and the spatiotemporal characteristic of changes in topography of the East Africa Plateau have remained unclear (Wichura et al., 2011).

To the west of the high plateau topography of Ethiopia and Kenya, both traversed by Cenozoic EARS rifts, lies the Kivu dome of the Western Branch, whose geomorphic development remains unclear (Chorowicz, 2005; Wichura et al., 2011). This rift dome is associated with the Mitumba Mountain Range, of which the Rwenzori Mountains form a part (Chorowicz, 2005; Ring, 2008; Wichura et al., 2011). The Rwenzori Mountains form a horst between the Albert and Edward rifts and have resulted in Africa's highest uplift of Precambrian metamorphic basement rocks to ca. 5100 m.a.s.l, over the last 10 Myr (Bauer et al., 2010). However, it appears that a mature and topographically clearly defined graben structure did not form until Late Pliocene, the graben structure having formed as a

result of the tectonic pulse that was responsible for the uplift of the Rwenzoris (Ring, 2008; Roller et al. 2010). Phases of tectonics, rifting and associated uplift have resulted in several steep, incised valleys flowing west off the Mitumba Mountains into the CB (Bauer et al., 2010; Ring, 2008; Roller et al. 2010).

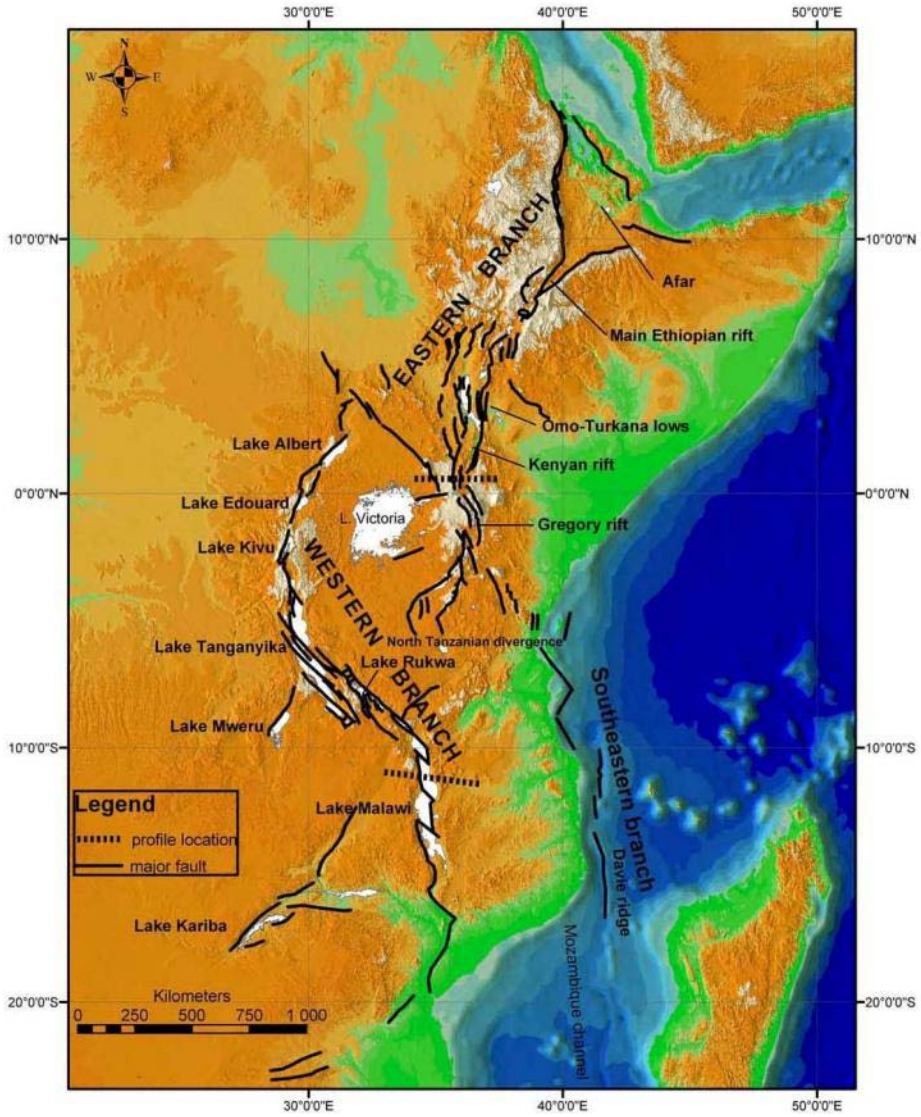

Figure 3.8: The Western and Eastern Branches of the EARS. Major faults and topographic features are named (Chorowicz, 2005). Note that Lake Edouard occurs within the Edward rift.

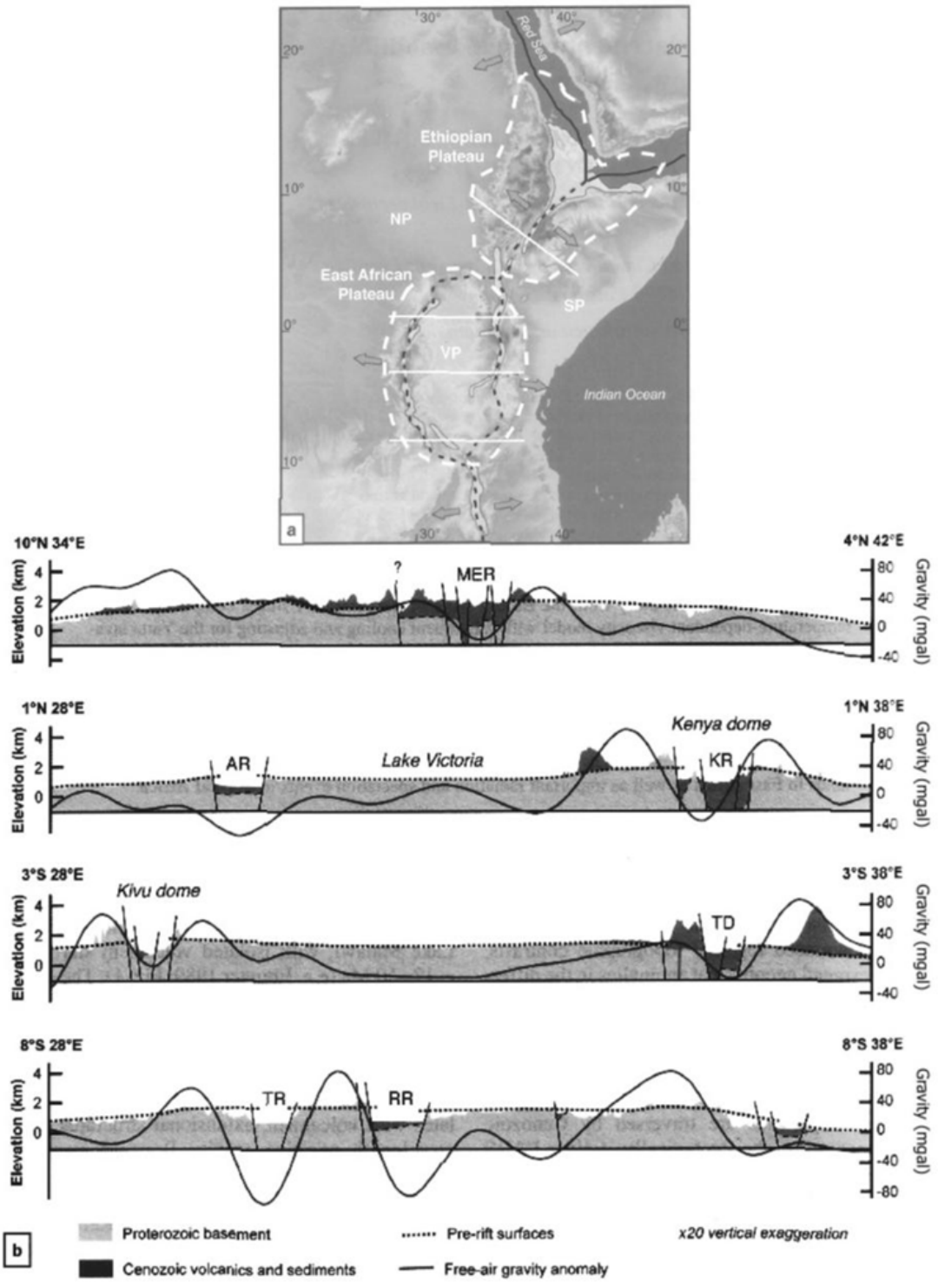

Figure 3.9: East African topography and free-air gravity anomalies. (a) Topography showing the main uplifted plateaus (white dashed lines) and dark lines mark the plate boundaries (solid) and developing plate boundaries (dashed). NP = Nubian, SP = Somalian and VP = Victoria plates. Arrows indicate the main extension direction. The eastern and western branches of the East African Rift System follow the dark dashed lines. White lines show the topographic profiles. (b) Four topographic and free-air gravity anomaly profiles from north to south. The topographic profiles (vertical exaggeration x20) integrate the potential pre-rift surface and contact between the Proterozoic basement and Cenozoic cover (MER = Main Ethiopian Rift; AR = Albert Rift; KR = Kenya Rift; TD = Tanzania Divergence; TR = Tanganyika Rift; RR = Rukwa Rift. Modified from Wichura et al., 2011.

The Western Branch of the EARS has been considered to be substantially younger than the Eastern Branch, with isolated volcanism starting at ca. 12 – 10 Ma (Cahen, 1954; Wichura et al., 2011). However, a recent study by Roberts et al. (2012), using detrital zircon ages, tephro– and magnetostratigraphy and sedimentary record, proposes that parts of the Western Branch, namely the Rukwa Rift (southern most Western Branch), show evidenced of volcanism ca. 25 Ma. This would make the age of initiation of the north–west to south–east trending Rukwa Rift to be at least 14 Myr older than previously thought, suggesting that the development of portions of the Western and Eastern branches were contemporaneous (Roberts et al., 2012). It is, however, a possibility that this initial rifting was confined to the Ubendian belt that separates the Bangweulu and Tanzanian Cratons (Roberts et al., 2012). Alternatively, as the Rukwa Rift forms part of the Tanganyika–Rukwa–Malawi (TRM) Rift, the history of the Rukwa Rift may be considered to be unrepresentative of the rest of the Western Branch. The TRM is one of the most seismically active regions of the EARS where several active faults and ongoing seismic activity affect most of the crust to ca. 30 km depths (Delvaux et al., 2012). The Rukwa Rift is at the centre of the TRM, along with the west bounding Ufipa Plateau (Delvaux et al., 2012). The Ufipa Plateau is a tilted block that uplifted during the late Cenozoic, largely within the Ufipa terrane, and the alignment of inselbergs and the footwall of faults systems illustrates the multi-stage tectonic history of the systems (Delvaux et al., 2012). Thus the Rukwa Rift may represent the anomalous scenario for the Western Branch's, having an earlier initiation age compared to the rest of the Western Branch due to its location within the TRM.

The development of the Western Branch created important relief in the regions with differing elevation. The creation of high topography in east Africa during the Ceonozoic uplift resulted in the formation of an efficient orographic barrier to moisture-bearing winds from the Indian Ocean and the Congo Basin, which has a strong influence on the region's rainfall (Wichura et al., 2011). This uplift and associated rift-shoulder uplift also affect the region's drainage system, as evidenced by the series of small lakes that forms the centre of internal drainage within the rift valleys (Chorowicz, 2005; Wichura et al., 2011). Our understanding of the timings and magnitudes of events of the Western Branch will only be improved by future studies that can definitely determine the age of rift initiation (e.g. Chorowicz, 2005 compared to Roberts et al., 2012).

3.4.2 The river systems of south–central Africa

South-central Africa is the boundary zone between the Congo and Kalahari Basins and the watershed between the Congo, Cuanza, Okavango and Zambezi river systems. The Western Branch of the EARS forms an eastern boundary for the CB that is only punctuated by the Malagarasi river system, and

the EARS continues further south to form an eastern barrier of the KB, pierced only by the Lower Zambezi River. Apart from the tectonic activity associated with the EARS, much of present day Africa is thought to be relatively stable.

The continental scale geomorphic features of the CB, KB (in the form of the Kalahari Plateau) and the EARS are important factors in the evolution of south–central geomorphology. However, the exact nature, timing and magnitude of their role in determining the development of the river networks of south–central require a better understanding of these features at a temporal and spatial resolution that is unavailable at present. It is thought that since the break-up of Gondwana, Africa's continental drainage systems have undergone substantial rearrangements (Goudie, 2005). However, the details of these rearrangements are poorly known.

Regardless of their timings and causes, the CB, KB and EARS have undergone alteration of their forms. One of the exogenic factors that act on the landscapes to result in geomorphic change is their rivers. It is the rivers that flow through south–central that are the primary focus of this thesis. Below an overview of previous work on the development of the region river networks is presented.

3.4.2.1 The Congo river system

The entire drainage network of the Congo Basin has been active (emergent) since the late Cretaceous (Roberts 1946; Cahen, 1954; Goudie, 2005). Yet Cahen (1954) suggested older ages for substantial portions of the river network, citing the occurrence of river flowing in east–west valleys, whose origin may be glacial, as an indication of at least Permian age of parts of the drainage network. Deffontaines and Chorowicz (1991) also highlighted the possibility of drainage inheritance, suggesting that much of the present day drainage is superimposed, having originated in at least the early Cenozoic. This section will provide an overview of the present day characteristics of the CB and highlight several theories put forward regarding the evolution of the hydrographic network of the CB, here referred to as the Congo River System.

General Overview

The combination of ongoing civil and political instability in the region and the difficult physical environment has translated to a scarcity of recent literature referring directly to geomorphological aspects of the CB. While there has been renewed interest in the last decade, much of this literature

relies directly on observations and studies conducted more than 50 years ago. Much of the older work was carried out during the period of colonial rule, for example, Veatch (1935), Dixey (1943), Roberts (1946), Cahen and Lepersonne, (1952) and Cahen (1954), with more recent studies drawing on the maps and building on this knowledge, such as De Dapper (1988), Runge (2007) and Linol (2012).

The present drainage area of the Congo River System (CRS) forms a circular intracontinental basin centred in the middle of Africa, which stretches from ~12 °E to ~34 °E and from ~9 °N to ~ 13 °S. The modern day climate of the basin is dominantly tropical (hot and humid) around the equatorial regions. The middle of the Congo Basin receives 1800 – 2400 $mm.yr^{-1}$ (Runge, 2007). The southern highlands are cooler and drier, while the eastern highlands are cooler but wetter. The seasonal movement of the Inter-Tropical Convergence Zone (ITCZ) is the dominant controlling factor of rainfall in the basin. South of the equator, the wet season is from November to March, with the dry season occurring from April to October, and *vice-versa* north of the equator. As the basin straddles the equator, some part of the basin is always experiencing a wet season. The water from this massive network ultimately flows westward into the Atlantic Ocean via the Congo River. Thus the outflow and sedimentary load of Congo River represents the integration of its diverse chemical and lithologic landscapes with the differing climatic and tectonic zones through which it flows (Dupré et al., 1996; Lavier et al., 2001).

The combination of the basin's circular shape, immense size and high precipitation allows the Congo River to achieve an annual discharge of 1250 x 10^9 m^3, making it Africa's largest river (and the globe's second largest) in terms of volume (Meade, 1996). In the vicinity of Kinshasa, the Congo River experiences a double discharge peak flow regime, although the variation in water level is limited, whilst exporting a total of 87 x 10^6 t of matter a year (Runge, 2007; Laraque et al., 2009). The majority of the Congo River's load appears to be mechanically derived, as indicated by measurements near Kinshasa that produced a mechanical erosion rate of 8 $t/km^2.yr^{-1}$, which is greater than the chemical erosion rate of 5 $t/km^2.yr^{-}$ (Gaillardet el al., 1995). This load is connected to one of the world's largest fan systems, the Congo Fan, by an active deep fan 1135 km long, meandering and deeply incised Congo Canyon (Uenzelmann–Neben, 1998; Baonneau, et al., 2002).

The Congo River is crescent shaped, being the only large river in the world to cross the Equator twice, and it flows through the world's second large continuous forest region that stretches from

~5° S to ~ 4° N. Interestingly most of the Congo River's major tributaries are orientated toward the CB centre and not the Atlantic Ocean in the west, making the CRS unique in Africa in respect to its drainage pattern (Goudie, 2005). Both the basin's extent and its vast, dense forests have impeded detailed geomorphic investigations, especially in the *cuvette centrale* and much of the existing data and chronology have been derived from studies closer to the basin's peripheries (see **Section 3.3.2**).

Geomorphic overview

The Congo Basin is centred in a series of swells and plateaus with rift valleys to the east (Holmes, 1965). The Basin ranges in elevation from sea level at the Congo River's outlet near Matadi (see **Figures 3.10** and **3.11**) to heights in excess of 3000 m.a.s.l. in the Mitumba Mountains (in the south-east) with the Rwenzori Range (lying just outside of the CB) exceeding 5000 m.a.s.l. Overall the Basin has a mean elevation of approximately 400 m.a.s.l. The *cuvette centrale* and northern areas of the Basin are low lying regions of subdued relief. They are bounded to the south by a dissected watershed comprised principally of the Angolan highlands, the northern limit of the Kalahari Plateau and margins of the EARS. This Western Branch of the EARS runs the entire length (ca. 2100 km) of the eastern margin of the Congo Basin. This rugged relief consists of a series of elongated, narrow rift valleys and scarps extending from Lake Albert (~3 °N) to Lake Malawi (10 °S) with the high topography forming the Mitumba Mountains along the eastern margin of the CB. The Western Branch converges with the Eastern Branch at the Tanganyika-Rukwa-Malawi (TRM) triple junction. In the west, the Congo basin is bounded by the Western Escarpment (Monts Crystal), which has been deeply incised by the channel of the Bas Congo. The Basin's northern extent is delimited by watersheds shared with the Ogoué River in the west, and extends east to form the Asande Rise (North Equatorial Plateau) in the north east.

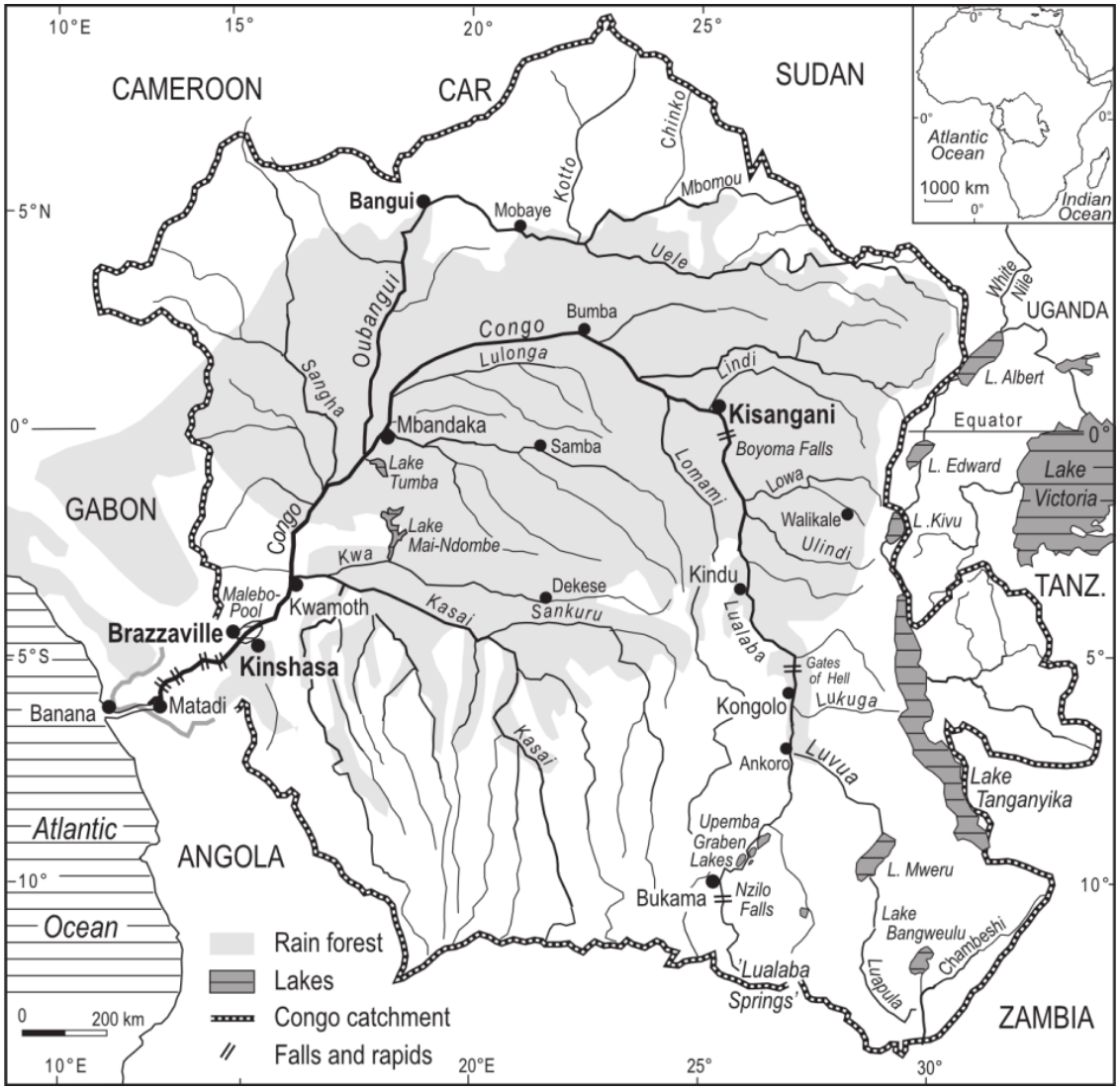

Figure 3.10: The Congo Basin and its rivers. Major rivers and known waterfalls are named. Of interest is the parallel flow direction of many of the southern tributaries of the Congo River. Figure from Runge (2007).

The western and eastern highlands of the Congo Basin (the West Congo Orogen and EARS respectively) exhibit high topographic roughness. The northern watershed incorporates parts of the Central African Shear Zone. The uplift associated with the EARS broke the drainage linkages to the Tanzanian plateau in the east, notably those of the Rufiji-Ruaha basin and is likely to be Pliocene in age (Cotterill and de Wit, 2011; Goodier et al., 2011; Delvaux et al., 2012). The Basin's highlands are dominated by the northern extensions of the Kalahari Plateau (ca. 1100 m.a.s.l.). At the centre of the basin are late Neogene and Quaternary alluvium mantling overlying thick continental sediments and it is thought these continental sediments, originating from erosion of the surrounding periphery, have been accumulating in the basin since Gondwana (Giresse, 2005; Runge, 2007).

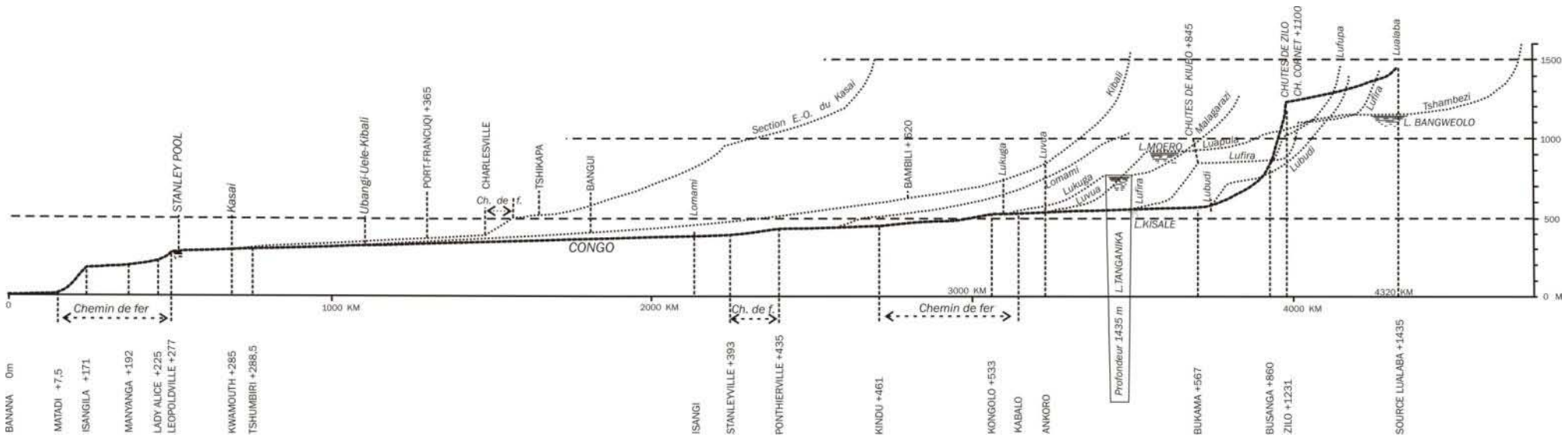

Figure 3.11: The longitudinal profiles of the Congo River and associated tributaries of Roberts (1946). Even though these profiles were drawn more than 50 years ago from topographic maps of the time, they represent the most detailed regional longitudinal river profile of the CRS previous to this study. This is evidenced knickpoints shown here still informing many modern maps in the location of waterfalls along southern rivers of the Congo Basin. As well as recent geographic and geomorphic studies of the CB continue to utilise these longitudinal profiles, for example Runge (2007). Redrawn from Roberts (1946).

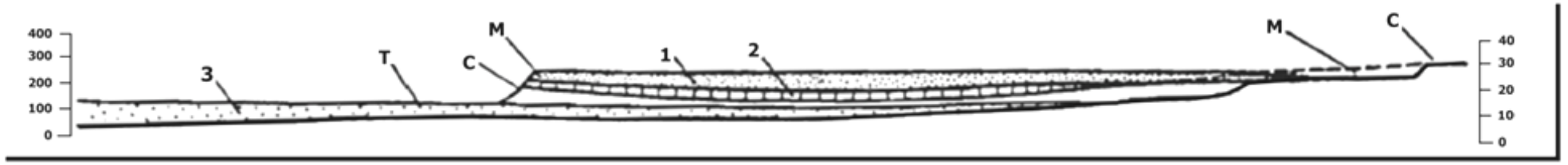

Figure 3.12: Schematic profile from the crest of the Congo–Zambezi watershed (right) towards the Congo Basin (left). C – end Cretaceous surface, M – mid Cenozoic planation, T – end Cenozoic planation. 1 – Ochre sands (*Ochres sables*), 2 - Polymorphic sandstones (*Grés polymorphes*), 3 – Plio – Pleistocene sands. Modified from Cahen (1954).

Previous work and proposed river development of river network

The complex nature of the CRS network has long been recognised (e.g. Veatch, 1935; Roberts, 1946; Cahen, 1954) and is evidenced by the juxtaposition of several apparently disparate drainage patterns (see Deffontaines and Chorowicz, 1991). Almost all of the studies of the CRS have proposed models of drainage evolution by focussing on the plan view of the river networks combined with sedimentary and other geomorphic evidence. This highlights the knowledge gap which this thesis aims to address by studying the river longitudinal profiles. Since Roberts (1946), for whom see **Figure 3.11**, there have been no regional attempts at determining longitudinal profiles of entire river lengths of the CB (as evidenced by recent studies, such as Runge (2007), which make use of his profiles). This is probably due to the quality of these longitudinal profiles at a regional scale and the difficulty of determining such profiles. Apart from Roberts (1946), most studies of the CRS have focussed on its drainage network pattern (e.g. Cahen, 1954; Deffontaines and Chorowicz 1991; Karner & Driscoll, 1999; Nibbelink and Budihardjo, 2002; and Stankiewicz and de Wit, 2006).

The offshore sediment accumulation of the northern Ogoué (relative to modern Congo River outlet) and southern Kwanza (relative to modern Congo River outlet) fans suggest that central Africa's continental drainage was different to the present (Leturmy et al., 2003). During the Late Cretaceous, the Ogoué and Kwanza Rivers were the dominant sources of sediments to the coast, suggesting that the (entire?) CRS was endorheic (Lucazeau et al., 2003; Leturmy et al., 2003). The progressive change of the depocentre from the Ogoué and Kwanza Rivers to the Congo during the Late Cretaceous to early Cenozoic indicates a capture of the endorheic CB (Baonneau et al., 2002; Anka et al., 2010). Today these southern and northern systems exhibit multiple incised valleys and gorges along the coastal areas, often occupied by underfit river channels. A variation of this model is that during the Late Cretaceous, the CB was not endorheic but was drained by an outlet at or near the present day Ogoué River (Karner and Driscoll, 1999; Nibbelink and Budihardjo, 2002). From the Late Cretaceous into the Cenozoic, the outlet of the CB migrated and by the mid-Cenozoic the CB was drained close to or by the present day Kouilou River channel and, with subsequent southerly migration, the CB, by the Oligocene, was drained by its present day outlet (Karner and Driscoll, 1999; Nibbelink and Budihardjo, 2002). This migration may be evidenced in the misfit of the present Ogoué and Kouilou Rivers that occupy abandoned channels, their valleys, relic drainage and the large estuary near Libreville, and the large size of the Late Cretaceous–early Cenozoic delta along the Gabon coast relative to present-day coastal river systems (Karner and Driscoll, 1999). Karner and Driscoll (1999) propose a positive feedback system between sediment loading and flexural uplift of the hinterland

as playing a role in this migration of the outlet, although the actual mechanism remains unclear. A further variation is that late Paleogene tectonic activity may have led to the capture of the interior drainage of the Congo Basin by a coastal valley (Cahen, 1954). Possible evidence for this is seen in the lower Congo River, which crosses an area of lower modelled flexural (Anka et al., 2010), suggesting that the lower Congo River comprises inherited drainage. This antecedent lower Congo River is evidenced by the deeply incised gorge and waterfalls downstream of Kinshasa (Anka et al., 2010).

O'Brien and Peters (1999) agree with an endorheic CB but propose that during the late Cenozoic (probably Pliocene) the central CB was still occupied by a large body of water. Taking the idea of a large body of water existing into the Quaternary, Stankiewicz and de Wit (2006) proposed that since at least the Late Cretaceous, the CRS was not endorheic. Rather, since the Late Cretaceous, the CRS drained eastward into the Indian Ocean via, or near, the present day Rufiji River in east Africa (Stankiewicz and de Wit, 2006). This easterly drainage was a consequence of the flank margin uplift associated with the opening of the Atlantic Ocean, with the CRS's eastward flow persisting through the Paleocene into the Late Eocene and the CB being drained via, or near, the present day Rufiji River outlet in east Africa (Stankiewicz and de Wit, 2006). During this time, the CRS drained into the Indian Ocean and not the Atlantic, thereby accounting for discrepancies of limited deposition on the Atlantic margin (Anka et al., 2010) and also accounting for the large Rufiji Delta (Stankiewicz and de Wit, 2006). This connection to east Africa was disrupted until the uplift of the EARS resulted in the CB becoming endorheic in the mid Paleogene, and a Miocene capture by a coastal stream saw the CB drain into the Atlantic (Stankiewicz and de Wit, 2006).

Regardless of the exact details, there were dramatic increases of terrigenous material being transported to the margin in the Neogene, implying that the CB was undergoing active erosion during this time (Lavier et al., 2001; Séranne et al., 2008). The offshore sedimentary record indicates changes in both sediment source and supply and in the dominance of contributing river systems; initiation of this change has been suggested to have taken place in the middle to late Miocene (Uenzelmann–Neben, 1998; Lavier et al., 2001). This increase of terrigenous sediment supply to the Congo Fan may have been enhanced by the uplift of the EARS (Uenzelmann–Neben, 1998). It is therefore probable that the modern day CRS formed during the Neogene, although elements of its drainage around the peripheries of the *cuvette centrale* had been established earlier (see **Figure**

3.12). By the early Quaternary, the Congo River was the dominant source of sediment to the deep sea fan (Uenzelmann–Neben, 1998).

3.4.2.2 Kalahari river system

General overview

The KB, as defined in this study, occurs in southern Africa and corresponds to the Cubango and Kalahari basins of Holmes (1965). To the east of the KB lies the southern zone of the EARS, as exemplified by Lake Malawi and the Luangwa Rift. The KB contains the Okavango and Zambezi rivers systems, which together are referred to as the Kalahari river system (KRS) for this study. Many of the present day southern tributaries of the KRS can be considered as fossil drainage as they rarely have flowing water in them (Dixey, 1955; Wellington 1955). The present day drainage of the KB is thought to have originated on the surface of the Kalahari Group, and has been and currently is being superimposed on the underlying rocks (Wellington, 1949; Haddon and McCarthy, 2005).

The Okavango river system lies to the west of the KRS and is hydrologically separate from the more extensive Zambezi rivers system (see **Figure 3.13**). Wellington (1949) classed the ca. 2750 km Zambezi River into three distinct morphological regions, namely, the Upper Zambezi ('Angola Plateau'), the Middle Zambezi and the Lower Zambezi ('Mozambique Plain'). The Upper Zambezi River extends from the watershed to ca. 100 km below the Victoria Falls and this upper course has been determined by the surface of the Kalahari Group (Wellington, 1949). Approximately 100 km upstream of the Victoria Falls, the Upper Zambezi River meanders through a 130 km sandy floodplain (the Shesheke plain) and, when it floods during the wet seasons, water flows from the plain into the Linyanti wetlands of the Cuando River.

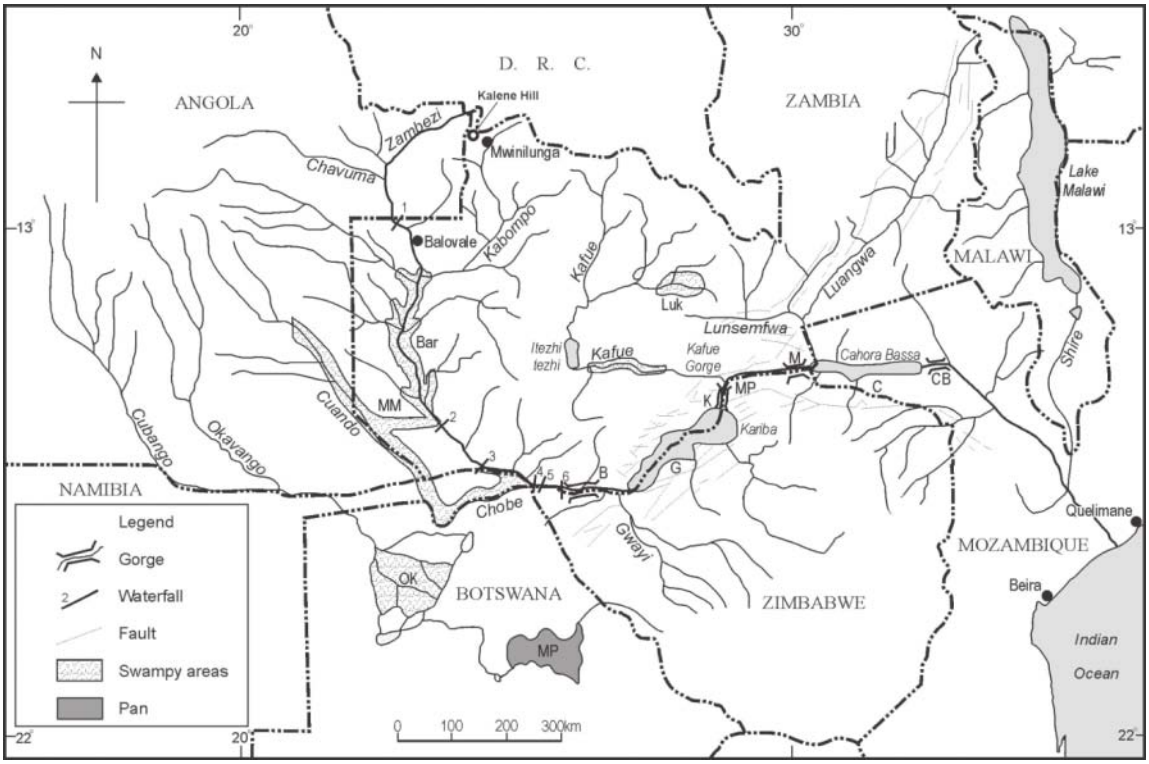

Figure 3.13: The Okavango and Zambezi river systems showing notable land features of the Kalahari Basin (modified from Moore et al., 2007). Together these river systems are referred to as the Kalahari river systems in this thesis.

Geomorphic overview

The subsidence of the KB during the Cenozoic in combination with uplift of its margins contributed to drainage disruption leading to the separation of links between the Limpopo and Okavango river systems and the Cuando and Zambezi–Luangwa river systems (Partridge, 1998; Partridge and Maud, 2000; Moore and Larkin 2001; Haddon and McCarthy, 2005). It has been suggested that doming (ca. 2000 km in diameter) in southern Africa is cause for the present day drainage, with the rivers flowing away from the centre of the these domes (Moore and Blenkinsop, 2002). The relevant drainages affected may have included the Okavango and Kwango Rivers as well as the Upper Zambezi and Congo headwaters, which would explain the absence of a major westward drainage system between the modern Orange and Congo river systems (Goudie, 2005).

Where the Zambezi and Cubango River is superimposed on resistant rocks, rapids or gorges form (Wellington, 1949; Nugent, 1990). Below the Popoa Falls (which occurs on an outcrop of quartzite), the Cubango River flows into the Nami depression, marking the start of the Okavango Delta and

associated wetlands (Wellington, 1949). The southerly flowing Cuito River is the only large tributary of the Cubango River; the southerly tributary rivers rarely flow (Wellington, 1949).

Previous work and proposed development of river network

Building on Wellington's (1949) idea of the Zambezi River comprising of three geomorphic units, Nugent (1990) identified the longitudinal profile of the Zambezi River as consisting of two concave sections whose boundary at the Victoria Falls represented the separating of the Upper Zambezi from the Middle and Lower Zambezi (see **Figure 3.14**). The Zambezi River's plateau and valleys occur across several continental rift structures that were active during Karoo and Cenozoic, with a south–west to north–east orientation (Nugent, 1990).

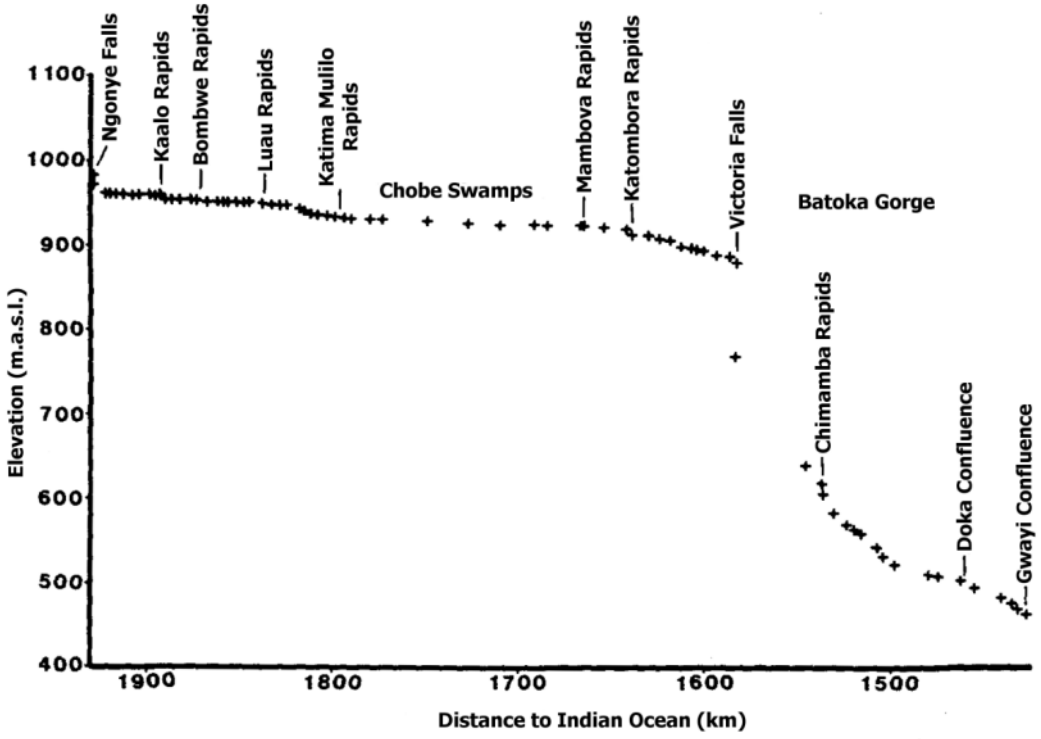

Figure 3.14: The longitudinal profile of the Zambezi River from Ngonye Falls to Gwayi Confluence (modified from Nugent, 1990). Heights and distances were determined from regional maps although the elevation downstream of the Victoria Falls may be subject to error (Nugent, 1990).

Similar to the CRS, much of the KRS has its origins in the Cretaceous, having being modified during and since the break–up of Gondwana. Haddon and McCarthy (2005) have proposed a possible model of drainage evolution of the KB from the Late Cretaceous to the early Cenozoic (see **Figure 3.16**). During the Cretaceous, much of the KRS had a south–east orientation, draining through a main

channel that is represented by the present day Limpopo River. Following a series of subsidence of the central KB, drainage reversal occurred resulting in the formation of interior drainage with the subsequent deposition of the Kalahari Group sediments (Haddon and McCarthy, 2005).

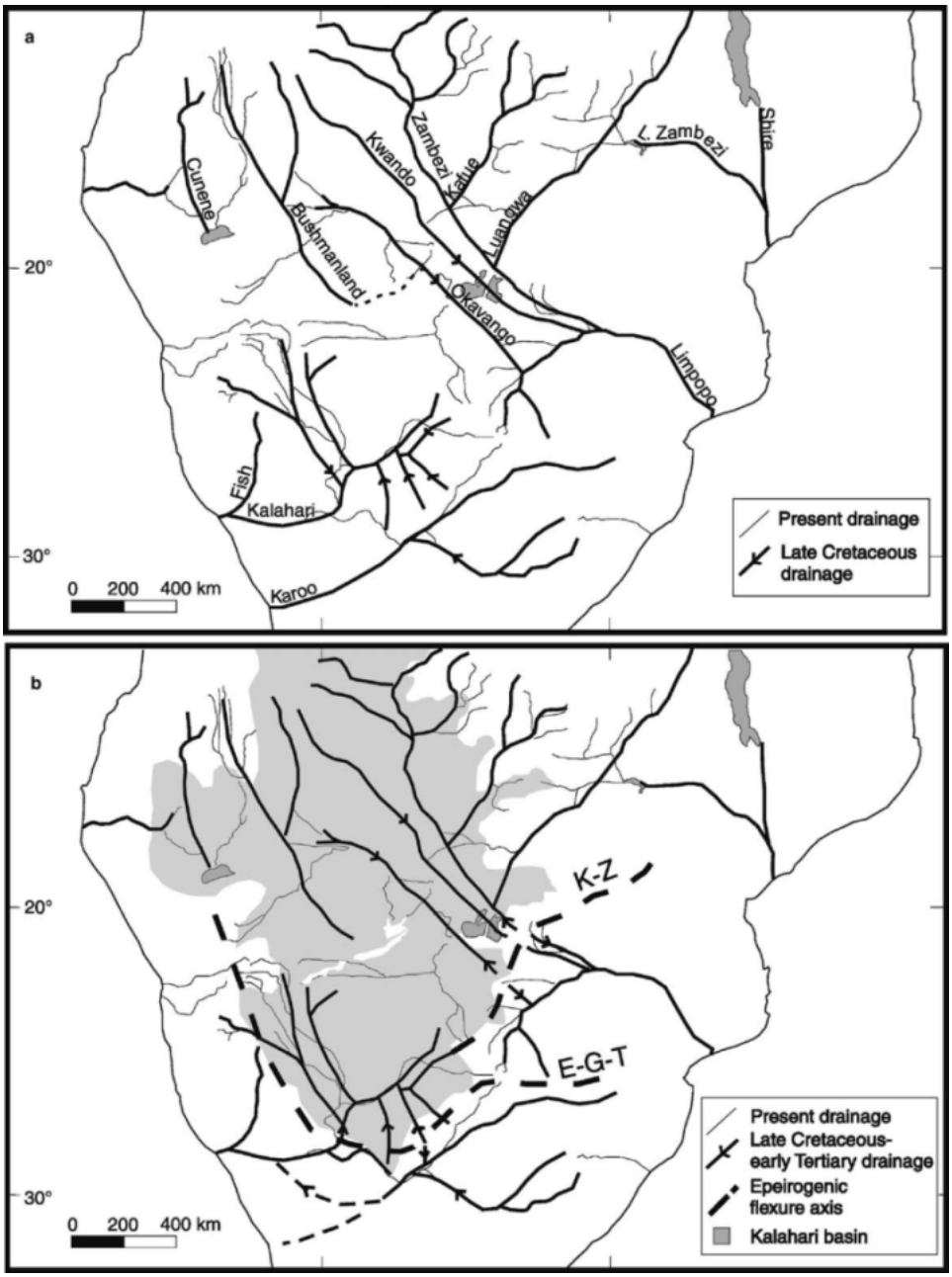

Figure 3.15: The stages of drainage evolution of the KB from the Early Cretaceous to early Cenozoic. (a) The drainage patterns of the Early– to Late–Cretaceous were dominated by several large rivers systems that drained into the Limpopo, Kalahari and Karoo Rivers. (b) Following subsidence of the Kalahari Basin in the Late Cretaceous or early Cenozoic, back–tilting of the landsurface leading to reversal of river flow directions and drainage disruption, and deposition of the Kalahari Group sediments. Figure from Haddon and McCarthy (2005).

This interior drainage became reconnected to the Indian Ocean via the Middle Zambezi River during the Cenozoic. Nugent (1990) suggests that the Upper Zambezi was captured by the Middle Zambezi River as a result of over topping of an Upper Zambezi lake, rather than through headward erosion of the proto–Middle Zambezi. This over topping better explains the concave profiles of both rivers section and the available alluvial evidence, the joining of these two river profiles having occurred in during the middle Pleistocene. By comparison, Moore et al. (2012) favours the capture of the Upper Zambezi by the headward erosion of the Middle Zambezi (see **Figure 3.16**). While acknowledging the existence of a lake occurring at the terminus of the Upper Zambezi, Moore et al. (2012) propose that the Middle Zambezi, due to westerly headward migration, captured the interior drainages through in the Miocene. Thus the Middle Zambezi captured the Pliocene Chambeshi with subsequent capture of the Upper Zambezi River (Moore et al., 2012).

Figure 3.16: The sequence of drainage re–arrangements in north–eastern Kalahari Basin since the Miocene. (a) The Late Miocene drainage formed as a result of drainage disruption related to late Paleogene uplift. (b) In the late Pliocene the westerly headward erosion of the Middle Zambezi resulted in the capture of the Pliocene Chambeshi and Upper Zambezi Rivers. (c) Drainage re–arrangement being associated with tectonic activity of the East African Rift System occurred during the early Pleistocene. (d) After several drainage disruptions the modern day drainage net work is established in the middle Pleistocene. Figure modified from Moore et al. (2012).

This series of capture events as proposed by Moore et al. (2012) has implications for the eastern CKW and drainage evolution in this region, significant changes in the drainage systems having occurred in the Plio–Pleistocene. The following section deals explicitly with the geomorphology of the CKW.

3.4.2.3 The Congo–Kalahari Watershed

The drainage divide separating the southerly flowing rivers of the KB from the northerly flowing rivers of the CB comprises several, related watersheds (Dixey, 1943; Wellington, 1955). In the west are the watersheds between the Congo and Cuanza Rivers and the Zambezi and Cunene Rivers (Dixey, 1943; Wellington, 1955). Here the headwaters of the Cuanza basin have eroded along the granite–Kalahari sand boundary resting approximately 190 km south of the general line of the CKW (Wellington, 1955). East of the Cuanza basin, the watershed separates the Zambezi headwater tributaries, the Lungwabungu, Luena and Chavuma Rivers from the east–flowing headwaters of the Kasai River (Wellington, 1955). Further eastward, near Kalene Hill (24° E), the rise of the watershed on the Congo side is abrupt whereas the Zambezi side is very flat and shows a gradual rise (Steel, 1917). Here the Zambezi River is already a large stream (Steel, 1917). East from Kalene Hill, the source of the Zambezi tributaries, the Lunga and Kabompo Rivers are within 3 km of one another, separated by a dome-shaped ground rising (Steel, 1917). Yet the Kabompo headwaters flows due south while the Lunga headwaters flow due north, similar to the Zambezi headwaters, toward the CB (Steel, 1917). On the CB side, near the Upper Congo River (Lualaba River), the major landforms are a plateau complex, the result of the south–west extension of the Western Branch (De Dapper, 1988). Cahen (1954) suggested that the east – west and west – east flowing rivers of the CKW represent an end-Cretaceous surface that has been cross cut by south – north rivers that have created a mid–Cenozoic surface.

Moving west from Kalene Hill to Baya (about 27° 30’ E and close to Lubumbashi (Elizabethville), at about a distance of about 325 km from Kalene Hill, Steel (1917) found the ground surface changes from an indurated layer of soft sands to be replaced by hard red, clay soils. During the rainy season this route along the divide is completely flooded, up to a depth of 0.15 – 0.2 m, but quickly dries once the rainy season is over as the deep sandy soils absorbs the water (Steel, 1917). At Irumi Hills (29° 30‘ E, near Mkushi along the DRC – Zambia border), CKW is sharply defined (Steel, 1917).

There appears to be very little published work conducted on the CKW east of 31E, a region that is characterised by the rough topography of the Luangwe Rift Valley, with the Luangwe River forming part of the Zambezi drainage. On the Congo side, several short, streams flow north–west off the rift flank to form part of the Chambeshi River sub-catchment.

With regard to the divide between the Congo and Zambezi river systems, the Congo–Zambezi watershed, it has been suggested that this zone was further north than it is presently and that is was formed by warping of the sub–Kalahari surface during the Cretaceous (Dixey, 1943; Wellington, 1949; King, 1951). According to King (1951), the Bia and Kibara Plateaus contain strongly silicified surface deposits with freshwater shells (suggestive of a wetland environment) and a gentle northward rise, despite the concavity of the CB and the slight convex nature of the Congo–Zambezi divide in this region. King (1951) proposed that the Congo–Zambezi divide (the central and eastern zone of the CKW) formed as a result of a late Cenozoic warping event.

The Kasai River provides the only definitive example of capture in the region. Its long, eastward flowing headwaters contrast with the general northward flow of the Kasai (and other northerly flowing rivers of the CB), the direction change occurring at a major elbow of capture, the Kasai River having beheaded the Chavuma River of the Zambezi system (King, 1951; Wellington, 1955). In the region of the Kasai and Zambezi River sources, extreme planation and lack of definitive flow directions of the river courses prevent the determination of other river captures (King, 1951), although the presence of the wetlands (swamps) in many headwater regions of the CB along this divide, such as the Lulua, Lueo and Lualaba (Upper Congo) Rivers, may indicate stream diversion away from the KB by back tilting of the watershed (King, 1951). Veatch (1935) had previously suggested back tilting of this planed region of the Congo–Zambezi based on the 1 $m.km^{-1}$ slope gradient he calculated. Veatch (1935) suggested that this slope gradient was too low for a watershed region and concluded that tilting was the cause, a finding that King (1951) supported. Westward of the Congo–Zambezi, the headwaters of the CB rivers (in Angola and DRC) have deeply incised valleys suggesting river rejuvenation that is presently moving the CKW southward (King, 1951).

3.5 Justification of rivers studied

The rivers' position relative to other major topographic features was an important consideration in selection. Despite the debate surrounding the timings and mechanisms of the CB, KB and EARS, their impact upon the Neogene geomorphology of southern and central Africa is inescapable. For

example, Karner and Driscoll (1999) advocate that understanding the interplay between rift-induced topography and geomorphic responses of fluvial networks can reveal where and when important events occurred in fluvial evolution; this affected the decision to chose several rivers thought to be likely influenced by the EARS in this study. The chosen rivers and their longitudinal profiles are likely to provide insight into the development of their respective basins and by extension their shared watershed, the CKW. The decision to explore the individual rivers are summarised below.

Congo river system

Chambeshi, Luapula and Luvua Rivers: These rivers occur wholly or partially within the zone of a south-westerly trending incipient rift, the Mweru Rift, that branches from the Western Branch in the region of south Lake Tanganyika (Gumbricht et al., 2001). Thus investigating these rivers may provide insights into how the EARS has affected the geomorphology of south–central Africa during the Neogene. The Mweru Rift zone is characterised by enhanced seismicity with the zone including Lake Mweru and the Lufira (Tack et al., 2003).

Congo River: Being the Africa's most voluminous river, the Congo River is one of the main drivers of landscape change in central Africa. Its immense length, high volume and position in an intracontinental basin makes this river the effect baselevel of all its tributaries, as the Congo River is the only river of the CB that is connected to the Ocean (ultimate baselevel). This connection takes the form of the lower Congo River (downstream of Malembo Pool) and as such any sea level fluctuations would have to be translated upstream past Malembo Pools to affect the rest of the rivers of the CB. Therefore, the Congo River is the controlling baselevel of the other studied rivers. It headwaters occur in the plateau complex that is a result of an incipient south–west extension of the Western Branch (De Dapper, 1988).

Kalungwishi River: Occurring in the plateau complex of the south–eastern CB, this river may provide insights into the region's tectonic history. Additionally, the Kalungwishi was an accessible river to allow ground truthing of the remote sensing analysis (see **Chapter 5** and **Chapter 6**).

Kasai River: Its headwaters are thought to have captured a Zambezi tributary (e.g. Dixey, 1943; Wellington, 1955) and thus this area may be a zone of ongoing drainage capture. Furthermore the

Kasai may be considered a large river in its own right and its headwater region occurs in an important aquatic eco–region (Skelton, 1996).

Lufira River: This eastern headwater tributary of the upper Congo River is affected by enhanced seismicity related to the Mweru Rift (Tack et al., 2003). It headwaters occur in the plateau complex that is a result of an incipient south–west extension of the Western Branch (De Dapper, 1988). This makes this river a good candidate for exploring any tectonic controls.

Lufupa River: This river occurs both on the west of the upper Congo River and is marginally to the plateau complex that is a result of an incipient south–west extension of the Western Branch (De Dapper, 1988). It therefore acts as a control to observations made for the Lufira River.

Lukuga River: Being the sole outlet of Lake Tanganyika, and flowing through the rift related Mitumba Mountain range, the Lukuga may provide insights in how a river's longitudinal profile is affected by the EARS.

Lulua River: Flowing parallel to the northerly flowing Kasai River but without the Kasai's extensive west to east headwater, the Lulua may provide insights into the development of both the central CKW and the Kasai River.

Kwango and Wamba Rivers: The Kwango was chosen owing to the presence of a large topographic depression of 150 – 200 km, averaging an elevation close to 400 m, which was incised on the north-west flank of the Kalahari Plateau. It is a significant tributary of the Congo River. Furthermore, the Kwango River and valley have been a type locality for earlier studies of the CB, such as Robert (1946), Lepersonne (1945, 1951) and Cahen (1954), having the Kwango Group named after it. Additionally, it formed part of the then ongoing study of Linol (2012) and creating the profile would be useful for that study (e.g. Linol, 2012 Figures 4-25 pp 107 and 4-37, inset, pp 107). Furthermore, the river is of economic interest due to its diamondiferous alluvial deposits. The Wamba was a tributary selected to serve as a control to the Kwango River as the Wamba does not have any major valleys and, for much of its course, flows on top of the flat lands of the northern Kalahari Plateau.

Kalahari river system

Cubango and Cuchi Rivers: These two rivers form part of the Okavango–Cunene drainage divide. The characterisation of their longitudinal profiles may provide insights into the development of the western KB.

Kabompo River: This eastern tributary of the Upper Zambezi River falls within the region of enhanced seismicity that is associated with the Mweru Rift (Tack et al., 2003). It may therefore provide insights into how the EARS has affected the KB as well as serving as a comparative foil for the upper Congo and Lufira Rivers.

Kafue River: The upper Kafue occurs in a region of tectonic activity (see Gumbricht et al., 2001) and has been associated with the Chambeshi River in the past (Moore et al., 2012). It may therefore provide insights into the development of the eastern KB as well as the occurrence of the CKW in eastern south–central Africa.

Luena River: Flowing parallel to the Kasai River, the Lulua represents an important area of possible river captures. Its profile may enable a better understanding of the upper Kasai River. Furthermore, as no tectonic activity has been assigned to the Luena River region, this westerly tributary of the Upper Zambezi may provide details on how the Kabompo River has been influenced by tectonic activity.

Upper Zambezi River: Southern Africa's largest river, the Upper Zambezi River characterises the central KB. Improved understanding of this river is likely to provide insights into the development of the central KB and by association the central regions of the CKW.

3.6 Synthesis

The unique situation of the tributaries of the Kalahari and Congo river systems, containing the world's 2nd and 25th most voluminous rivers, share a common source region with headwaters less than 3 km apart and this makes the CKW an interesting feature (Steel, 1917; Dixey 1943; Meade, 1996; Gupta, 2007). The fact that the CKW is not the expected form of divide between two large rivers, which is normally a mountain chain (Tandon and Sinha, 2007), further enhances the remarkable nature of this watershed.

This chapter has sought to illustrate why the evolution of the CKW is of importance in understanding the development of south–central Africa. The second purpose of the chapter was to provide the reasoning behind the choice of the rivers that were studied and in conjunction with Chapter 2, to explain why their longitudinal profiles were of interest. Africa's geological history was briefly outlined and the development of the CB and KB were covered, drawing on the work of de Wit et al. (2000), who have illustrated the impacts the Mesozoic and Cenozoic have on drainage evolution. The exhumation of the pre-Karoo surface by Mesozoic and Cenozoic drainages of southern Africa led to subsequent modification of drainage patterns due to the exposure of the relief and structure of this pre-Karoo surface (de Wit et al., 2000). This chapter has sought to provide both the geologic (temporal) and geographic (spatial) background of the study area, which has served to indicate when and where these landscape may have developed and been modified.

CHAPTER 4: REMOTE SENSING IMAGERY

4.1 Introduction

Remote sensing is a technique that involves the use of instruments to collect data about features without touching the object under study (Lillesand et al., 2004; Jensen, 2007). The present study made use of two types of space-based (orbital) imagery, namely: Landsat 7 Enhanced Thematic Mapper Plus (ETM+) and Shuttle Radar Topography Mission (SRTM) imagery. The Landsat 7 ETM+ imagery provided the spectral context for the rivers studied while the SRTM imagery provided data on river elevation. When using data from remote sensing, it is important to understand how the information was acquired and processed, as the various remote sensing techniques have different inherent strengths and weaknesses associated with them. These differences in acquisition and processing may result in a situations where a single natural phenomenon could have different signatures depending on the sensor used, thereby allowing for multiple interpretations of the studied object. The strengths and limitations of these various sensors must be explicitly acknowledged when interpreting the data produced. This is to ensure that the remotely sensed data was applied to the problem being investigated was appropriate and that interpretations of the data are correct.

This chapter provides the background of Landsat ETM+ and SRTM imagery, highlighting key aspects that made the data suitable for the study. The selection and acquisition of the data, and any processing required prior to the imagery being used for the river long profile digitisation is also dealt with.

4.2 Landsat 7 ETM+

Landsat 7 ETM+ imagery was selected for use in this study owing to its extensive coverage, relatively high resolution and public (free) availability and accessibility. The Landsat 7 ETM+ satellite was launched on 15 April 1999 as a continuation of the Landsat series that began in 1972 (Jensen, 2007). The Landsat 7 ETM+ uses a multispectral sensor (a scanning mirror spectrometer with a discrete detector) allowing it to record data across eight bands (Global Land Cover Facility Landsat Technical Guide, 2004; Jensen, 2007). A summary of the band properties and utilities of Landsat 7 ETM+ imagery is provided in **Table 4.1**. With its circular, sun-synchronous orbit at an altitude of 705 km, Landsat 7 ETM+ achieves a 16 day revisit time and covers a ground area (footprint) of 170 x 183 km (Global Land Cover Facility Landsat Technical Guide, 2004; Lillesand et al., 2004). The 183 km image

swathe size allows for reasonable overlap between adjacent images (see **Figure 4.1**). Prior to a mechanical failure in May 2003 which impaired imagery quality, Landsat 7 averaged 250 images per a day (Global Land Cover Facility Landsat Technical Guide, 2004; Jensen, 2007).

The three bands used to make image composites for this study were band 2, band 4 and band 7 (see **Table 4.1** for details). The effective horizontal spatial resolution (pixel size) of each band used is 30 x 30 m (the absolute pixel size is 28.5 x 28.5 m), with a positional accuracy of 50 m root-mean-square error, although average horizontal displacement is often substantially better (Lillesand et al., 2004; Tucker et al., 2004). Band 2 (green) is useful for vegetation discrimination and cultural feature identification (i.e. roads and buildings) while band 4 (near infra-red) is suited for delineating water bodies, vegetation types and soil moisture (Lillesand et al., 2004; Jensen, 2007). Band 7 (mid infra-red) is useful for the discrimination of mineral and rock types (Lillesand et al., 2004; Jensen, 2007). These bands were chosen to make image composites as they allow for the greatest contrast between water and vegetation (bands 2 and 4) and bare soil/rock (band 4 and 7).

Table 4.1: Overview of the band properties and utilities of Landsat 7 ETM+ imagery (Global Land Cover Facility Landsat Technical Guide, 2004; Jensen, 2007). Bands marked with an asterisk (*) were used in this study.

Band	**Spectral Resolution (µm)**	**Spatial Resolution (m) at nadir**	**Spectrum**	**Band utility**
1	0.450 – 0.515	30 x 30	Blue	Useful for land-use, soil and vegetation characteristic studies due to high degree water body penetration.
2 *	0.525 – 0.605	30 x 30	Green	Spans the regions between blue and red chlorophyll absorption and contrasts the green reflectance of healthy vegetation.
3	0.630 – 0.690	30 x 30	Red	Useful for vegetation discrimination, soil-boundary and geological-boundary delineation. This band corresponds to the red chlorophyll absorption of healthy green vegetation.
4 *	0.750 – 0.900	30 x 30	Near-infrared	Useful for emphasising soil/crop and land/water contrasts as well as crop identification. This band is responsive to the amount of vegetation biomass and/or leaf area.
5	1.55 – 1.75	30 x 30	Mid-infrared	Useful for plant vigour and crop-drought studies as well as cloud, snow and ice discrimination. This band is sensitive to the amount of water in plants.
6	10.40 – 12.50	60 x 60	Thermal-infrared	Spectrum corresponds to the infrared radiant energy emitted from surfaces, making it useful for locating geothermal activity, geology based thermal inertia, vegetation classification and stress analysis and soil moisture. This band often captures unique information on differences in topographic aspects in mountainous areas.
7 *	2.08 – 2.35	30 x 30	Mid-infrared	Important for discriminating geologic rock formation. This band has been shown to be effective for identifying zones of hydrothermal alteration in rocks.
8	0.52 – 0.90	15 x 15	Panchromatic	Higher spatial resolution allows for greater differentiation of image features.

4.2.1 Landsat 7 ETM+ image selection

The required imagery was downloaded from the Global Land Cover Facility (GLCF) hosted at University of Maryland USA. The images were searched for and selected using the GLCF's Earth Science Data Interface website (Global Land Cover Facility Earth Science Data Interface, no date). The Landsat 7 ETM+ imagery was mainly acquired during 2000, although some of the scenes were acquired from 1999, 2001 and 2002 (Tucker et al., 2004). The image search criteria were as follows:

1) orthorectified, GeoTiff file format (Landsat GeoCover images);
2) must have limited cloud cover; and
3) must have been captured *circa* 2000 to be as close a temporal match to the capture date of the SRTM data, which was undertaken in February 2000.

Orthorectification is important to eliminate or minimise misregistration by removing erroneous image displacements caused by topographic relief and sensor orientation variations (Tucker et al., 2004). Images were selected first by minimum cloud coverage, determined by visual inspection of the browse image, and then by closest date to February 2000. Owing to cloud density and frequency in the tropics, two or more images with different cloud locations were occasionally required for a single scene. This ensured that there was sufficient overlap of cloud-free zones in the images so that heavy cloud did not interfere with delineation of the studied rivers. A total of 106 Landsat 7 scenes, covering the rivers of a region ranging from ~3 °N to ~20 °S and ~12 °E to 32 °E, were used for this study (**Figure 4.1**). For each scene, three bands (namely 2 – green, 4 – near-infrared and 7 – mid-infrared) were downloaded (**Table 4.1**). Each band was ca. 60 MB in size and therefore each scene amounted to ca. 180 MB. For this study ca. 20 GB of Landsat imagery was downloaded.

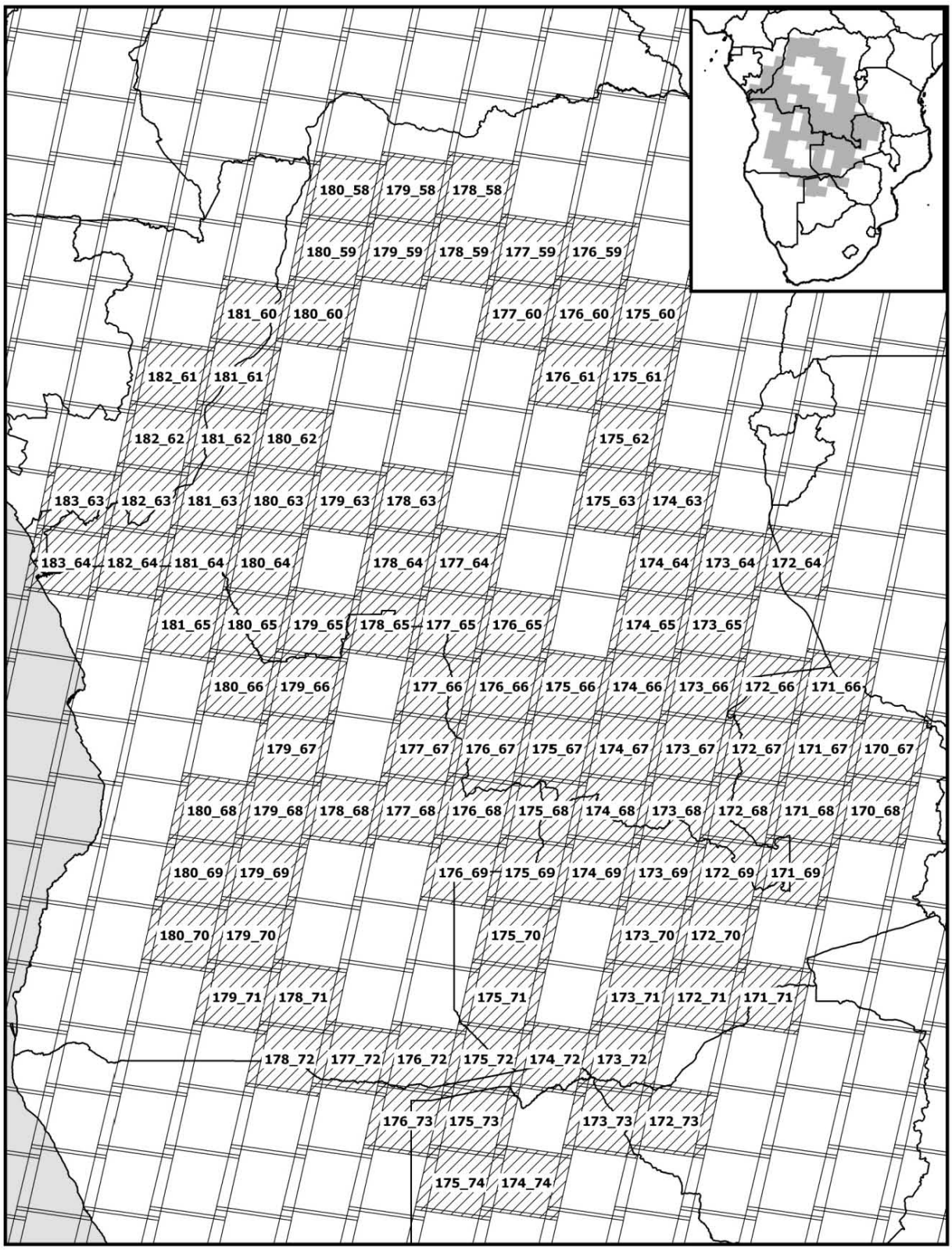

Figure 4.1: The footprint of Landsat imagery over central Africa. A total of 106 images, indicated by block hatching, were used in this study. The path and row number of each image is giving in the format PATH_ROW. Note the overlap of margin edges. Inset indicates used Landsat imagery (grey shading) in sub-Saharan context.

4.2.2 Landsat 7 ETM+ image processing

The georeferenced Landsat 7 images from the GLCF have been processed for atmospheric effects and are projected to UTM using a WGS84 datum and ellipsoid (GLCF Landsat Technical Guide, 2004). Thus, the Landsat 7 images from GLCF may be considered ready to use within a GIS without further end-user processing being required. See Tucker et al. (2004) and GLCF Landsat Technical Guide (2004) for further details regarding the processing and quality of Landsat 7 ETM+ imagery.

As the Landsat 7 ETM+ imagery had been extensively corrected and processed by the United States Geological Survey (USGS) and GLCF, for this study the bands only needed to be imported and combined (stacked) to form a single image. This was done using ERDAS IMAGINE 9.1, producing a single, false colour composite image, where band 7 was displayed as red, band 4 as green and band 2 as blue. In the resulting false colour composite images, water and saturated soils appeared in shades of blue, vegetation in shades of green and bare soil/rock and other hard surfaces (such as buildings) in shades of pink. Each scene was colour-contrasted to enhance the visual differences between water, vegetation and hard surfaces so as to allow for easier differentiation of the river channel and its features.

For each river, several scenes were stitched together to create a mosaic. Although mosaicking images results in a minor compromise of the positional accuracy of the images (Tucker et al., 2004), it allows for quicker river digitisation. Mosaics of eight scenes or less were created (see, for example, **Figure 4.2**), although in areas with complex river channels images were used individually, to ensure the fidelity of the digitisation process. The false colour composites were used during the river digitisation and knickpoint characterisation in combination with the SRTM imagery.

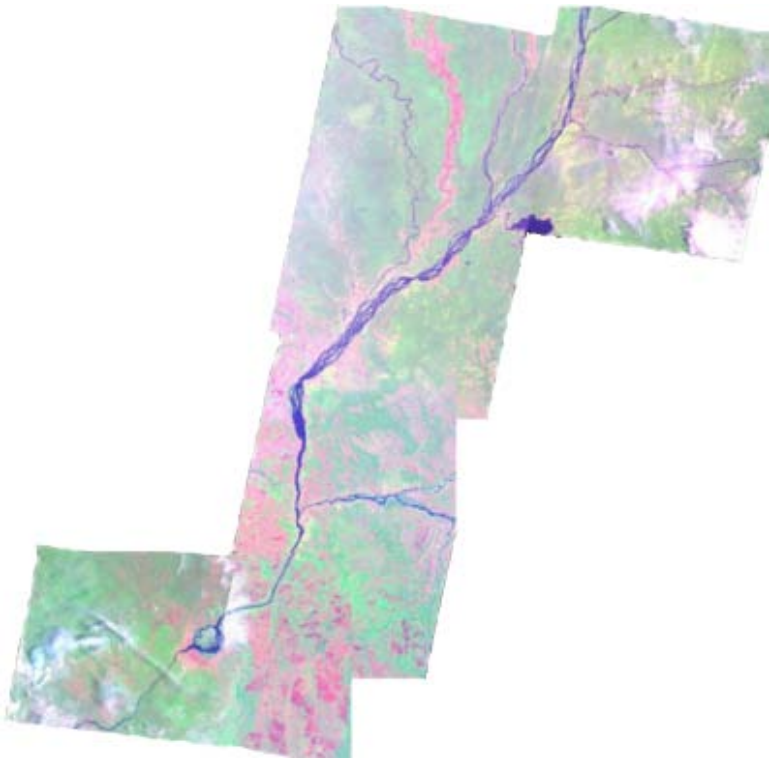

Figure 4.2: An example of a 6 tile false colour composite mosaic showing the lower Congo River. Bands 2, 4 and 7 of the Landsat ETM+ imagery were used. Water is in shades of blue, vegetation in shades of green with bare soil, hard surfaces in shades of pink and clouds cover in white.

4.3 Shuttle Radar Topography Mission

The Shuttle Radar Topography Mission (SRTM) has provided unprecedented globally uniform digital elevation data. The mission was flown in February 2000 on the Shuttle Endeavour and covered about 80% of the Earth's land surface over an 11 day period (Kobrick, 2006). The Mission used single pass synthetic aperture radar (SAR) interferometry to collect radar echo data allowing for the determination of elevation data. This involved use of a C-band antenna on an extended 60 m mast, scanned in unison, with an active phased-array antenna housed in cargo bay of the Shuttle Endeavour (Consortium for Spatial Information (CGIAR-CSI), n.d.; Jarvis et al., 2004; Kobrick, 2006). The radar echo data allowed for differences in the elevation of the Earth's surface to be measured at a resolution of 1 arc-second (30 m pixel size) with a 6 m relative vertical accuracy (Jarvis et al., 2004; Kobrick, 2006). The elevation differences were indexed to specific points on the ground in a uniform matrix. The National Aeronautics and Space Administration (NASA) processed the raw radar images, with further quality control and finishing steps by the National Geospatial-Intelligence Agency (NGA) of the United States of America (USA) (US Geological Survey, n.d.). The horizontal datum of the SRTM data is World Geographic System (WGS84) and the vertical datum is referenced to mean sea

level as determined by the WGS84 Earth Gravitational Model (EGM96) geoid (US Geological Survey, n.d.; Nelson et al., 2009). The use of radar meant that the elevation data represents a reflective surface; in other words, the detected elevations are the sum of the land surface elevation (bare earth) plus the height of any feature that may overlie the land surface, such as vegetation (depending on its density), ice, water and man-made features (US Geological Survey, n.d.; Lillesand et al., 2004; Nelson et al., 2009). The model is known as a digital surface model (DSM) as the radar measures the elevation of a reflective surface. DSMs are discussed in more detail in **Section 4.3.1**.

The original 1 arc-second DSM was released only for the USA, with access restricted to the USA Defence Department (Kobrick, 2006). In 2003, NASA publically released a down-graded 3 arc-second version global product (about 90 m pixel size at the Equator). The grid dimensions of the global SRTM data are a 3 arc-seconds spacing between latitudes 0 ° and 50 ° and 3 arc-seconds in latitude and 6 arc-seconds in longitude between 50 ° and 60 ° latitude (US Geological Survey (n.d.)). This gives an on-the-ground spatial resolution range from 90 to 92 m depending on the latitude (Jarvis et al., 2004). The reported overall absolute vertical (height) accuracy is significantly better than mission required 16 m (90 % confidence limit), with Africa having an absolute vertical error of 5.6 m and a relative vertical error of 9.8 m (at 90 % error limits) (US Geological Survey (n.d.); Jarvis et al., 2004; Rodríguez et al., 2006). In terms of absolute horizontal location (at 90 % error limits), Africa has an 11.9 m error (Rodríguez et al., 2006). As shown in Figure 4.3 below, apart from the desert regions of Africa, void occurrence in the SRTM data was limited with the majority of Africa having no voids (Reuter et al., 2007).

While there was a 30 arc-second elevation model available for Africa (GTOPO30) prior to the SRTM model, it had been cobbled together by the USGS using a variety of sources of differing quality (Gesch et al., 1999). The resolution and inherited errors, artefacts and asystematically distributed distortions of GTOPO30 meant it was of limited use for investigating meso-scale earth surface process and features (for example, Iwahashi and Pike, 2007; Hebeler and Purves, 2009). This limited research into meso-scale geomorphology over Africa. The giant leap forward in spatial resolution of digital elevation data represented by the SRTM allowed, for the first time, the possibility of the study of earth process on a local catchment and subcatchment scale in a global context which was required by this research. Since the release of the SRTM data, it has been used in various geomorphic studies, ranging from aeolian to fluvial and geomorphometric analysis at the meso- to

macro-scale (Jarvis et al., 2004; Blumberg, 2006; Iwahashi and Pike, 2007; McFarlane and Eckardt, 2007; Rossetti and Valeriano, 2007; Bubenzer and Bolten, 2008; Kenny et al., 2008).

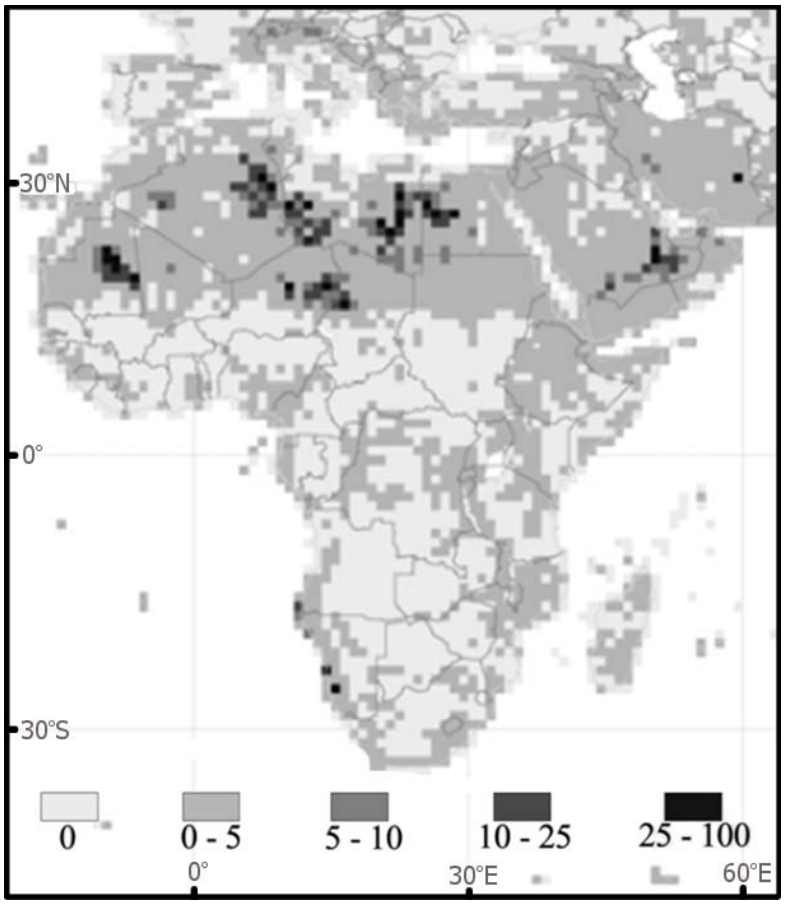

Figure 4.3: The distribution of voids in the SRTM data over Africa. Grey scale indicates the proportion of void area in each 1 x 1 degree SRTM tile. The absolute vertical and horizontal errors for Africa are 5.6 m and 11.9 m (at 90 % error limits Jarvis et al., 2004; RodrÍguez et al., 2006). Void occurrence for most of Africa is 0 % (light grey), with the Escarpment, EARS and parts of the Equatorial forest having a void occurrence of 5 % or less (darker grey). Note the higher void occurrence in the desert regions of Africa (black) (modified from Reuter et al., 2007).

4.3.1 DSM versus DEM

There appears to be some confusion about terminology regarding remotely sensed elevation models. Digital Elevation Models (DEMs) are often derived from topographic data and ground point elevations and thus represent the bare surface of the land. In contrast, remotely sensed Digital Surface Models (DSMs) report the elevation as seen by the instrument. Thus, elevations indicated by DSMs are often ground elevation plus vegetation, ice or building height where present. The height

added to the elevation is dependent on the properties of the material covering the ground. For example, in a densely forested region the elevation of a DSM may be 10 – 15 m higher than a DEM due to the height of the forest, whereas a DSM area with grass cover will have the same height as the DEM (on a metre scale at least). An additional consideration regarding DSMs is the penetrative ability of the sensor being used. For example, radar penetration of the vegetation canopy will be less in areas of moderate vegetation density compared to areas of high vegetation density (Miliaresis and Delikaraoglou, 2009; Huang et al., 2010), whereas with a laser based approach it may be possible to determine the vegetation height using the lasers signal phase different and correct the elevation reading for this offset (Huang et al., 2009). In cases where the height of the objects have been corrected for through the use of control points, the DSM will represent a bare earth model and could be referred to as a DEM (e.g. Miliaresis and Delikaraoglou, 2009; Huang et al., 2010).

While it has been argued above that the terminology employed for elevation models needs to be defined with care, the research literature demonstrates a less than systematic use of a variety of terms. These terms include not only DEM and DSM but also Land Surface Model (LSM), Surface Elevation Model (SEM), Digital Terrain Model (DTM) and Digital Terrain Elevation Data (DTED). For example, Ludwig and Schneider (2006) insist on DSM and Jarvis et al. (2004) use DEM, while NASA uses DTED (US Geological Survey (n.d.), all the while referring to the SRTM elevation data.

4.3.2 Characteristic of radar imagery

The use of radar to determine Earth surface elevations was established prior to the SRTM by missions such as European Remote-sensing Satellite (ERS) 1 and 2, launched in 1991 and 1995 respectively, Spaceborne Imaging Radar-C/X-band Synthetic Aperture Radar (SIR-C/X-SAR) in 1994 and Radarsat-1 in 1995. The advantages of using radar-based techniques to collect elevation data are the speed and systematic method of acquisition and the fact that they are not affected by cloud cover or sunlight availability and intensity (Lillesand et al., 2004).

The disadvantages associated with radar techniques are the possibilities of relief displacement and radar shadow (Lillesand et al., 2004; Nelson et al., 2009). These disadvantages have been illustrated by Lillesand *et al*. (2004), as shown in **Figure 4.4** below. This figure illustrates how relief displacement occurs when there is a substantial time difference between the radar return signals from the top and bottom of an object. If the return signal from the top of an object reaches the antennae before the return signal from the object's base, layover results; this creates a situation

where direction of relief displacement is toward the sensor and vertical features appear to lean toward the antenna nadir, thereby masking less elevated features closer to the antenna. The relief displacement of an objective increases with decreasing distance from the antenna (due to higher incident angles) with layover occurring when the terrain slope is steeper than a line perpendicular to the direction of the radar pulse. If the return signal from the base of the feature reaches the antenna before the signal from the top, foreshortening (relief compression) may occur; thus, the slopes of the surface will be compressed, with compression most evident in areas of steep slopes that are closely perpendicular to the radar pulse. The severity of foreshortening increases as the slope steepness approaches perpendicularity to the look direction. Therefore the type and severity of relief displacement is dependent on the topography and may be an issue in regions of rapid elevation change and high topographic roughness.

Figure 4.4 also illustrates how, in cases where slopes face away from the radar antenna, the return signal may be weak or non-existent, resulting in radar shadows. If the feature slope is less steep than the look direction, the return signal will be weak and the feature will be weakly illuminated; where the slope is steeper than the look direction, the area of non-illumination will extend beyond the slope, resulting in a shadow masking down range features. Nelson et al. (2009) point out that radar shadowing may result in data holes in the DSM of the features themselves or of other masked downrange features.

Another potential issue with the radar derived SRTM DSM is noise related to the inclusion of non-topographic features, such as trees and bridges. This noise, along with relief displacement and shadowing, may result in elevation peaks and sinks, which, when combined with zones of little elevation change (flats), make the use of automatic hydrological modelling problematic when using a DSM and may prevent the derivation of a fully connected hydrologic network (Jarvis et al., 2004; Ludwig and Schneider, 2006; Kenny et al., 2008). However, as the SRTM data was the best publically available data for the study area and as the modelling of stream networks was not the main aim of this research, the issue of using raster terrain surfaces was considered secondary. While regions of high noise in the elevation data may negatively impact on the hydrology of small creeks in steep mountainous terrain, it is not likely to affect higher-order streams (for example, Jarvis et al., 2004; Hancock et al., 2006; Hebeler and Purves, 2009).

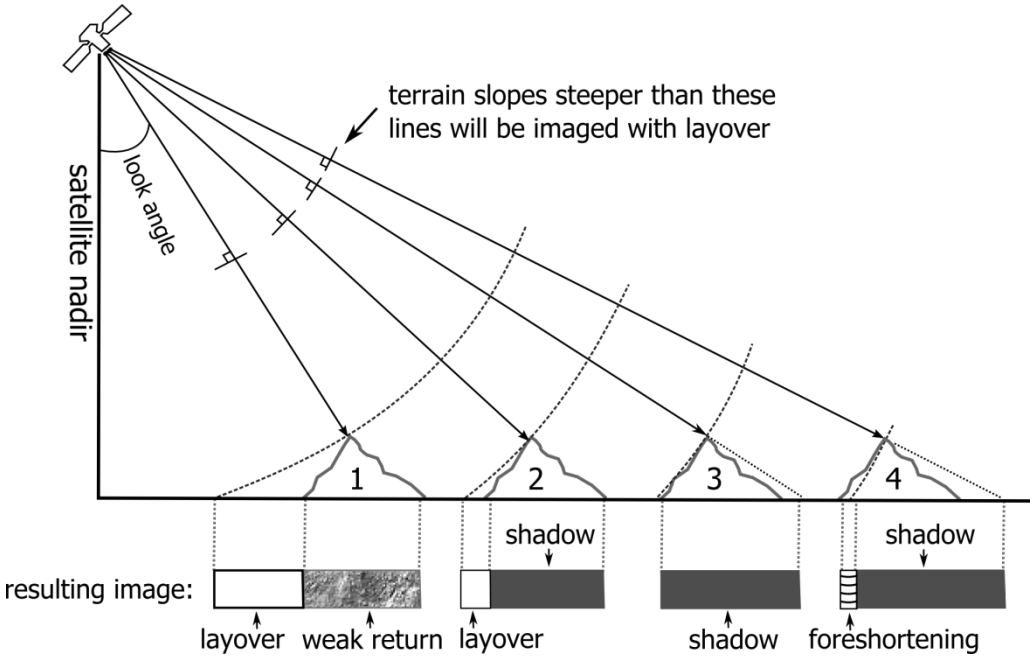

Figure 4.4: A cartoon illustrating potential issues of radar derived images. The severity and type of problem is dependent on the characteristics of the topography being measured relative to the look angle. Modified from Lillesand et al., 2004.

4.3.3 CSI-CGIAR SRTM

While the 2003 SRTM release by NASA was the best available DSM at the time, it still presented numerous issues. These issues were mainly the result of data holes in the radar image due to a lack of contrast, the presence of water or excessive atmospheric interference (Jarvis et al., 2004). As a result, areas along rivers, lakes and steep regions (especially hillsides with similar aspect ratios due to radar shadowing) were often highly problematic (Jarvis et al., 2004). The occurrence of these non-random data holes, ranging from 1 pixel to 500 km^2 (as shown in **Figure 4.3**) and the problem of how to account for them have been investigated (see Jarvis *et al,.* 2004; Reuter et al., 2007).

The Consultative Group on International Agricultural Research (CGIAR) decided to undertake further processing of the NASA released SRTM data. This processing was undertaken by the CSI and resulted in several releases and resolutions of processed SRTM and released through their online CSI Geoportal (Consortium for Spatial Information (CGIAR-CSI), n.d.). The CGIAR-CSI SRTM was processed using the methods developed by Reuter et al. (2007) and based on the earlier work of Jarvis et al. (2004), making use of a number of hole-filling algorithms in the data processing in conjunction with various spatial techniques (spatial filters, iterative hole-filling and interpolation

techniques) to correct these problems (see Gamache (2004), Jarvis et al. (2004) and Reuter et al. (2007) for further details).

Three versions of the CSI-CGIAR SRTM data were made use of in this study. The SRTM version 3 (Jarvis et al., 2006) with a 90 m pixel resolution was the best available version at the start of this research. Owing to the limited occurrence of voids in central and southern Africa, void filling was limited (Reuter et al., 2007). At the beginning of 2009, a SRTM version 4 (also 90 m resolution) was made available for Africa (Jarvis et al., 2008). The differences between the two versions are an additional half pixel shift and the use of extra auxiliary DEMs to fill holes (Consortium for Spatial Information (CGIAR-CSI), (n.d.)). As a third of the rivers in the study had already been digitised by the end of 2008, the third SRTM version (SRTMv3) was used to digitise the rest of the rivers in order to maintain uniformity of the data source for the river-long profiles. Thus, all data relating to the studied rivers is based on SRTMv3. The SRTM version 4 (SRTMv4) and the DSM of a 250 m resolution (SRTMv250m), a resampled version of SRTMv4, were used for the elevation data of all maps and displays, unless otherwise stated. This was done because of the more pleasing aesthetic of SRTMv4 for sub-regional and finer scale maps. For regional and larger overview maps, SRTMv250m was used due to its smaller file size, which lowered computational requirements and resulted in more efficient rendering.

It may be noted that in 2009, during the data collection phase of this study, the Advanced Spaceborne Thermal Emissions and Reflectance Radiometer (ASTER) Global Digital Elevation Model (G-DEM) (ASTER Global DEM Validation, 2009) was released. The ASTER G-DEM had been expected to be a substantial improvement on the SRTM data, with a predicted vertical accuracy of 7m (Hayakawa et al., 2008). Additional advantages of the G-DEM data were to be their higher resolution, 1 arc-second (30 m), less missing data and better topographic representation (Hayakawa et al., 2008). However, on its release the ASTER-GDEM was found to have a 20 m vertical accuracy and a 30 m horizontal accuracy (at 95 % confidence intervals). Additionally the G-DEM had several anomalies, the most significant being ‘step anomaly’ offset (ASTER Global DEM Validation, 2009). Created at image boundaries these step anomalies create offsets of around 10 m between continuous land surfaces (ASTER Global DEM Validation, 2009). The ASTER G-DEM thus had a lower vertical accuracy than the SRTM data and, as the SRTM for Africa had few areas without data holes, it was decided not to make use of this new, 30 m global dataset in the study.

4.3.4 SRTMv3 image processing

As the SRTMv3 data had been extensively processed by CGIAR-CSI, it required little processing for this study. The SRTMv3 data was downloaded as 5 x 5 ° GeoTiff tiles (geographic coordinates WGS84 datum) from the CGIAR-CSI. Only tiles falling within the regions of ~6 °N to ~21 °S for Africa were selected. All the GeoTiff files were imported into ERDAS 9.1 and converted into a single IMAGINE (.img) file to allow for greater interoperability across programs.

For the SRTMv4 and SRTMv250m, the total datasets for the African block were downloaded. These datasets were also converted to IMAGINE file formats. A detailed coastline polygon shapefile was created by accurately tracing the SRTMv4 coastline thereby removing all the islands, including Madagascar, and parts of the Arabian Peninsula from the SRTM data to reduce the file size. This shapefile was used to extract the data for the African continent.

Separate hillshaded images were created for the three SRTM DSMs in ERDAS. This involved reprojecting the DSM from a geographic coordinate system to a projected one, so that the horizontal and vertical units were both in metres. This was necessary for an accurate derivation of hillshading, slope and aspect. Owing to the large geographic coverage (terms of latitudes and longitudes crossed by the study area), a Robinson UTM projection (UTM Zone 33 south was chosen as it represented the middle zone) was used with nearest neighbour resampling. A hillshade relief image was created from the resulting projected DSM. The vertical scale was set as three and the solar azimuth and elevation were set to 45 °. The hillshaded relief output was then reprojected back to WGS geographic coordinate system, so that it referenced to the same spatial frame as the DSMs. By reprojecting the file twice, minor horizontal spatial offsets may have been introduced but as the hillshaded relief was used in an interpretive manner, offsets were considered negligible.

4.4 Conclusion

This chapter has indicated the ability of remote sensing to provide information on inaccessible areas and, moreover, that the use of Landsat and SRTM data is of adequate resolution ground (30 and 90 m, respectively) for the investigation of meso–scale features. Owing to the extensive processing of the Landsat 7 ETM+ and the CGIAR-CSI SRTMv3 DSM, further processing of the imagery itself was not required in this study. Rather, processing involved the creation of several derivative products, including Landsat 7 ETM+ false colour composites and the hillshading of the SRTMv3. These were

used in combination with the SRTMv3 DSM to digitise the rivers of interest, extract their associated elevation data and make observations on fluvial characteristics, such as abrupt changes in flow direction and knickpoint characteristics. This process is dealt with further in **Chapter 6**.

However, it is important before conducting any analysis to determine the accuracy of the data. Owing to the Landsat's long mission record, extensive processing and documentation, Landsat 7 ETM+ imagery was assumed to be accurate. Regarding the SRTM data, the reported overall absolute height accuracy for Africa was significantly better than mission required 16 m (90 % confidence limit), having an absolute height error of 5.6 m and a relative height error of 9.8 m (at 90 % error limits) (US Geological Survey (n.d.); Jarvis et al., 2004). This is a continental estimate and, at the start of this research, little had been published on the local accuracy of the SRTMv3 data for south-central Africa. It was therefore necessary to test the local accuracy in order to have a better understanding of its quality. The next chapter (**Chapter 5**) will describe how the quality of the SRTM data in south-central Africa was assessed using the precise point positioning (PPP) global position system (GPS).

CHAPTER 5: PRECISION GPS SURVEY

5.1 Introduction

Although the quality of input data for any study making use of remote sensing (RS) usually receives limited attention (Remondo and Oguchi, 2009), the ability to understand landscape processes is dependent on the quality of the topographic data used (Jarvis et al., 2004; Iwahashi and Pike, 2007; Pike et al., 2009). It is therefore crucial to understand the limitations of the input data through validation. In order to assess the suitability of the DSM, derived from Shuttle Radar Topography Mission data, for studying geomorphology in southern Africa and for use in this study, precision GPS surveys were conducted. These surveys are discussed in detail in this chapter.

The first field campaign of the GPS survey, which had as its main purpose of determining the vertical fidelity of the SRTM DSM, was conducted during the last quarter of 2008, with the majority of the positions surveyed being in north-east Zambia. A second field campaign took place in the third quarter of 2009, with all of the surveyed positions being in north-east Botswana. The positions in both surveys are indicated in **Figure 5.1** below. The elevation acquired by the precision GPS survey was compared to the elevation of the same location on the CSI-CGIAR DSM, SRTMv3 (see **Chapter 4** for details on SRTMv3). A secondary function of the GPS survey was ground truthing of fluvial features, where possible. As such, a number of the 2008 positions were sited near to fluvial features of interest, such as waterfalls, with characteristics of interest being noted.

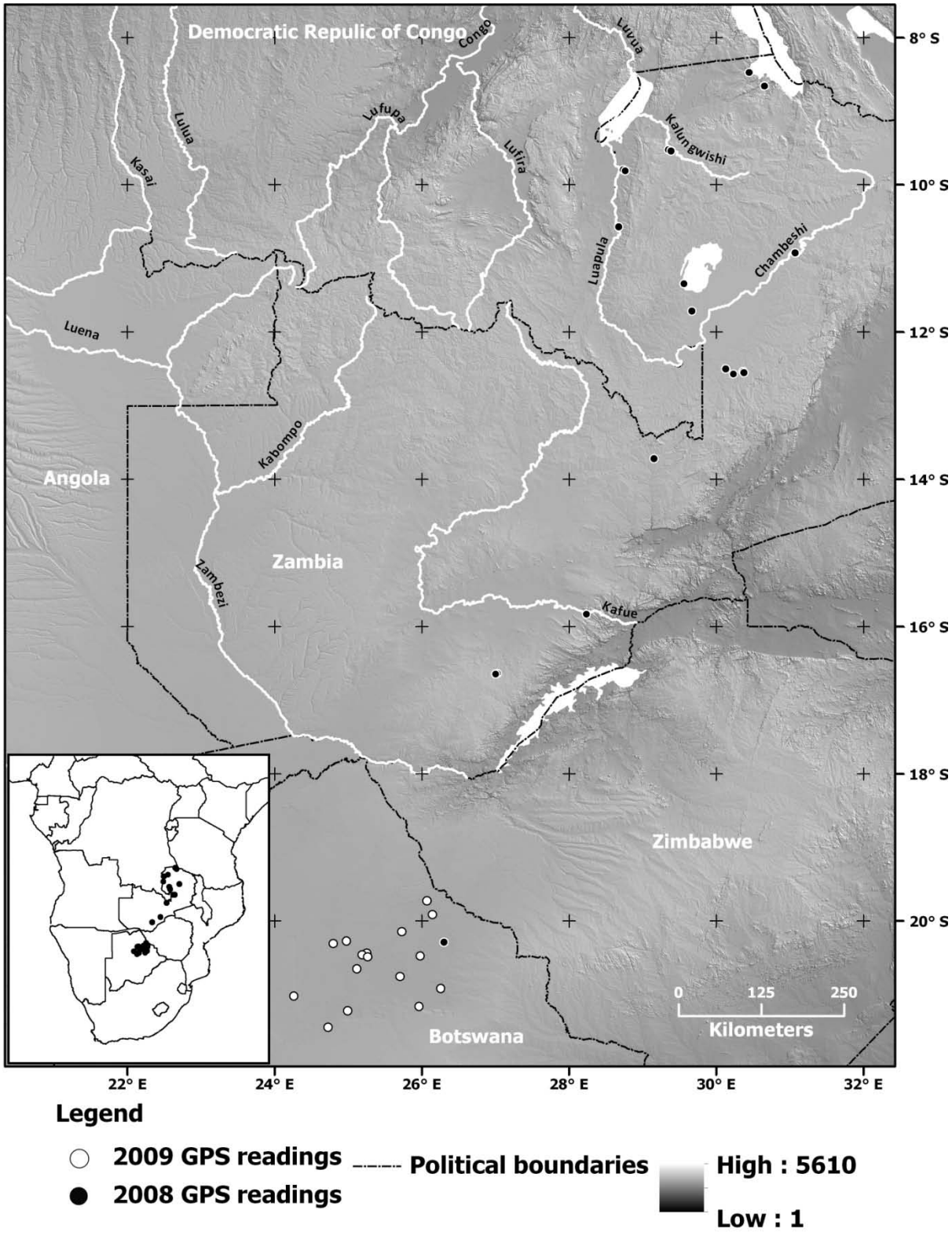

Figure 5.1: The location of GPS surveyed positions. Positions surveyed in 2008 are indicated by a black dot and those recorded in 2009 by a hollow white dot. A total of 39 field readings were recorded in a variety of landscapes. Studied rivers and large water bodies indicated in white. Inset shows location of all 39 surveyed positions (black dots) in context of sub-Sahara Africa (hillshaded relief created from SRTMv4 250 m, Jarvis et al., 2011).

5.2 Precise Point Positioning

In order to determine accurate location, this study has made use the Precise Point Positioning (PPP) approach. PPP utilises the carrier phase data of the GPS in combination with the precise satellite orbit and clock products (Héroux and Kouba, 1995). This contrasts with traditional positioning methods, such as differential GPS (DGPS), which determines accurate positions by differentiating between location errors of two (or more) known locations (geodetic control points - GCPs). Precise point positioning thus bypasses the need for GCPs, achieving positional accuracies at a decimetre level in areas lacking GCPs (Héroux et al., 2001; Castleden et al., 2004). Currently, the GCP coverage for large portions of central and southern Africa is inadequate for the effective use of DGPS and other non-PPP GPS positioning techniques, requiring the establishment of local GCPs and post-processing which would be labour intensive. Because it does not require GCPs, PPP is an ideal method for establishing three dimensional (3D) positional locations in remote regions using a single GPS receiver.

By using the combination of GPS carrier phase data with the precise satellite orbit and clock products, PPP allows for GPS positional accuracies to be improved to at least decimetre scale in horizontal (latitude and longitude; x and y) and vertical (elevation; z) (Héroux and Kouba, 1995; Kouba and Héroux, 2001; Héroux et al., 2001; Bisnath and Collins, 2012). Under ideal conditions, PPP can provide single point accuracies of 5 – 10 cm in all three coordinate components (x, y and z) irrespective of the measurement baseline length, which is a limitation of DGPS (Castleden et al., 2004). This correction of decimetre accuracy can be further improved to millimetre accuracy, depending on the environmental conditions at measurement (Bisnath and Collins, 2012).

In order for PPP to work, the receiver needs to record positional data for a minimum period of time to allow for positional convergence. As the initial convergence period can vary significantly depending on receiver location (Bisnath and Collins, 2012), long recording times are necessary, with longer logging times resulting in higher 3D (x, y and z components) accuracies. In most cases horizontal (x and y) accuracy is improved from 10 cm to 2 cm after 60 minutes, with the vertical component showing comparable, albeit larger, centimetre accuracies after 60 minutes (Bisnath and Collins, 2012). In most cases data convergence occurs after 40 minutes, with single digit centimetre improvement for both the horizontal and vertical components occurring thereafter (Bisnath and Collins, 2012). It is thus possible to achieve centimetre accuracy over long static data sets of

uninterrupted measurements (minimum 40 minutes) using the PPP approach and post-processing (Bisnath and Collins, 2012).

5.3 Survey

A total of 39 positions (as indicated in **Figure 5.1**) were surveyed using a Leica GS20 handheld GPS receiver with a calibrated AT501 single frequency antenna. In the majority of the cases the AT501 antenna was placed on the ground; when the antenna was not on the ground, the height of the object it was placed on was measured and recorded. Before the static positions were recorded the Leica GPS was allowed to record position data for a minimum of 5 minutes or until at least 4 satellite locations were locked. This was done to ensure uninterrupted measurements. Additionally, a 15 ° restriction (from the horizontal) on satellites utilised was set in order to limit the influence of satellite signal errors, as GPS satellite geometry is an important consideration for PPP (Héroux et al., 2001). Positional data was logged for 1 hour 15 minutes for the 22 positions surveyed in 2008, while the 17 positions of 2009 were logged for 1 hour. A minimum of an hour was chosen to ensure position convergence was attained, as 40 minutes is usually sufficient for data convergence (Bisnath and Collins, 2012). Longer recording times may have resulted in improved positional accuracies but, as the SRTM elevations have been rounded to the closest metre (Jarvis et al., 2004; Reuter *et al*., 2007), only sub-metre accuracies were required, which was exceeded by the one hour recording time. Where possible, positions were chosen to represent a wide range of landscape types from areas of little vegetation to areas of dense canopy cover. At each site, a field log was recorded with the weather, conditions of interest, date, time started and time ended as well as the final, on-the-fly position correction computed by the Leica. This display indicates the co-ordinates, elevation and accuracy as determined by the Leica firmware.

5.4 Post-processing

In order to attain PPP for this study, the GPS data was post-processed using the free online service provided by service Canadian Spatial Reference System (CSRS) of Natural Resources Canada (NRCan) (Natural Resources Canada, 2010). The NRCan makes use of the decoupled clock model, error modelling and satellite information to make corrections to the GPS data (Bisnath and Collins, 2012). A study conducted in Australia by Ebner and Featherstone (2008) found that the CSRS PPP produced horizontal coordinates within 1 cm of the horizontal coordinates derived from a geodetic survey control network. Vertical heights were within 2 cm of heights measured by a geodetic surveys

control network (Ebner and Featherstone, 2008). Therefore, the PPP method used by the CSRS produces 3D positions with single digit centimetre accuracies, which is an order of magnitude greater than the decimetre accuracy required for the survey.

In order for the GPS points to be post-processed, it was necessary for the Leica GPS data files to be converted to a RINEX format as this is the file format required by the NRCan site for processing (Natural Resources Canada, 2012). The LEICA Geo Office 2006 suite was used to convert the native Leica file format to the RINEX format after which it was uploaded to the NRCan site. The 3D positional output from the NRCan site was referenced to the global integrated reference frame (ITRF) (Natural Resources Canada, 2013). The processed elevations from NRCan are referenced to the ellipsoid (GPS height) as is usual for GPS heights; the relationship between ellipsoid and geoid height is shown in **Figure 5.2** below. Yet the elevation data of SRTMv3 was referenced to the Earth Gravitation Model 1996 (EGM96) geoid vertical datum (Jarvis et al., 2004). There can be substantial differences between ellipsoid and geoid heights, with differences between geoid and the WGS84 ellipsoid ranging between -100 m to +70 m over the globe (Lemoine et al*.,* 1998; Li and Götze, 2001; Hengl and Evans, 2009; Chandler and Merry, 2010). It is therefore important that heights were referenced to the same vertical datum in order to correctly compare the vertical accuracy of the SRTMv3 elevations to the GPS surveyed elevations. After subtracting the height of the antenna (where required), the resulting NRCan elevations were referenced to the EGM geoid using an online calculator (National Geospatial-Intelligence Agency, 2013). The coordinates of the GPS points were entered and the calculator provided the EGM96 height. The EGM96 height was subtracted from the GPS heights to give the orthometric height; see Lemoine et al*.,* 1998 and **Appendix 5** for further details regarding the EGM96 and the African geoid model. By referencing the GPS elevation to the geoid, the orthometric elevations of surveyed positions were obtained, which allowed for comparison to the SRTMv3 elevations.

5.4.1 Firmware issue

During the 2009 field campaign, there was a worldwide issue with the onboard software (firmware) of the Leica GS20 receiver. This firmware issue resulted in the date settings being rolled back to the start of the Leica GS20 calendar so that the incorrect dates were recorded for the 2009 readings. The firmware issue was problematic as the PPP approach requires accurate date and time information in order for the processing to occur. However, as the time data recorded for the positions was acquired from the satellites themselves, the firmware issue did not affect the time stamps. The firmware issue

was only discovered subsequent to the field work; this required the use a text editor and field notebook to correct the dates on the RINEX files allowing the data to be successfully processed.

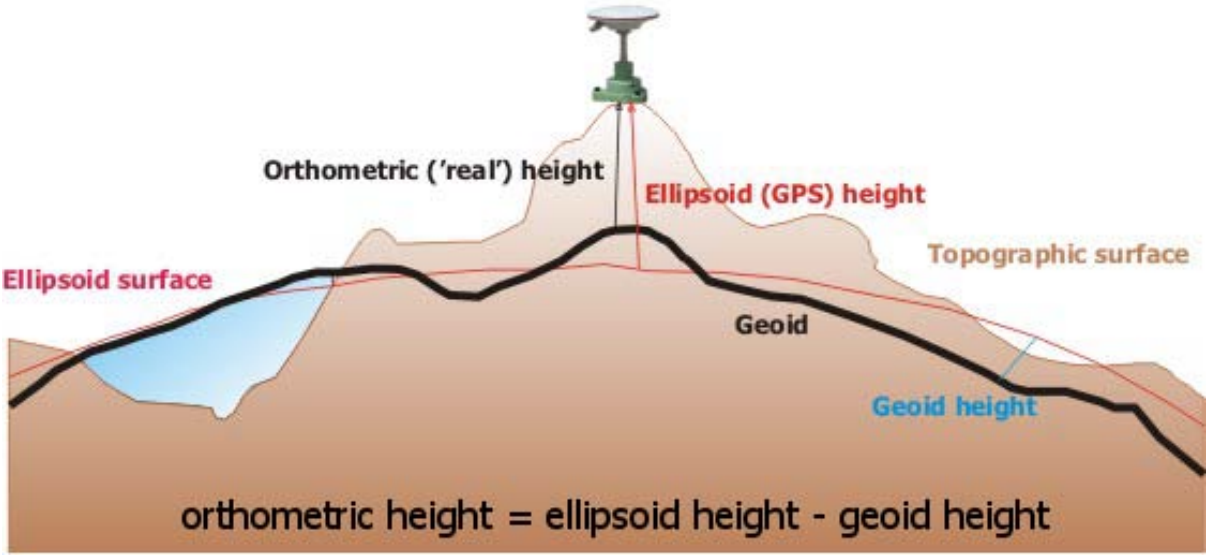

Figure 5.2: Cartoon showing the difference between ellipsoid heights (red line) and geoid heights (heavy black line). By accounting for differences in the ellipsoid (GPS) height as 'seen' by GPS (the AT501 antenna is shown) to the geoid height results in orthometric height. The ellipsoid surface represents the even, mathematical elevation with the Earth's centre used as a reference point, which may be above or below the Earth's surface (Featherstone, 2001; Li and Götze, 2001). In order to attain a true elevation, the difference between ellipsoidal and geoidal elevations (geoid height) must be accounted for (Li and Götze, 2001; Chandler and Merry, 2010). This difference exists due to the Earth's uneven gravitation field, with geoid heights being based on a surface that represent the elevation of a hypothetical free-flowing ocean (mean sea level) (Featherstone, 2001; Li and Götze, 2001). This geoid surface may be above or below the ellipsoid surface (see **Appendix 5, section 5.1** and **Figure A5.1** for further details).

5.5 Results

The 22 points of the 2008 GPS survey were collected from a wider range of spatial locations than the 17 points of the 2009 survey, as is shown in **Figure 5.1**. The co-ordinates of the 39 GPS locations and the results of post-processing as well as their corresponding SRTMv3 pixel elevation are shown in **Table A5.1 (in Appendix 5**). After post-processing, the vertical (z) precision GPS survey has an average error of 0.406 m with a range of 0.252 – 0.627 m. This sub-metre accuracy of the GPS exceeds the required 1 m accuracy of the SRTMv3 elevation data, which has been rounded to the closest metre (Jarvis et al., 2004; Reuter et al., 2007).

As the surveyed GPS elevations have been corrected to the geoid (resulting in orthometric heights), they are able to be compared to the SRTMv3 elevations (see **Table A5.1** in **Appendix 5**). The comparison of elevations shows that the average difference in elevation between the GPS derived orthometric and SRTMv3 elevations is +5 m. In other words, the SRTMv3 over-reports elevations by 5 m on average when compared to the GPS surveyed points. The differences between the SRTMv3 and orthometric elevation range from -1 to +34 m (see **Table A5.1** in **Appendix 5**), indicating that SRTMv3 elevations can and do vary substantially from orthometric elevations in the survey area, being generally higher.

The comparison of all 39 orthometric elevations to the SRTM elevations shows a near linear relationship (R^2 = 0.998) as shown in **Figure 5.3** below. This relationship allows the orthometric elevation height to be predicted for a given SRTM elevation ('**Predicted orthometric**') by the following:

Predicted orthometric = (0.990 x SRTM elevation) + 4.498 (1)

The calculation used to predict the orthometric elevation (1) includes seven points with higher elevations than the corresponding orthometric elevations due to either high topographic relief, riparian forest or dense, sustained tree cover, all of which affected the GPS reading (see **Table A5.1** and **Appendix 5**). The R^2 value of 0.998 suggests a near linear fit between the SRTMv3 and orthometric elevations, although the best-fit line shown in **Figure 5.3** plots below the line of unity, indicating that on average SRTMv3 values are higher than the corresponding orthometric values.

The SRTMv3 and predicted elevations (based on equation 1) were compared to the orthometric elevation (see **Table A5.2** in **Appendix 5**). This was done in order to determine if the accuracy of the SRMv3 data would be improved using the near linear relationship between the SRTM and orthometric elevations indicated in **Figure 5.3**. The range of values of the predicted orthometric compared to orthometric elevations is -7 m to +27 m, whereas the range for the SRTMv3 data is -1 m to +34 m. However, the average difference between the SRTMv3 elevations and the orthometric elevations is 5 m with the predicted orthometric elevations showing no appreciable mean difference to the surveyed orthometric elevations. Both the predicted orthometric and SRTMv3 elevations show similar variances, of 36 and 38 respectively (see **Table A5.2**, **Appendix 5**). Similarly, both elevations achieve a 6 m absolute accuracy at the 68 % confidence limit (1σ standard deviation) and

a 12 m absolute accuracy at the 95 % confidence limit (2σ standard deviation) compared to the surveyed orthometric elevations (see **Table A5.2**, **Appendix 5**). Therefore, using equation 1 to predict the orthometric elevations does not significantly increase the accuracy of the SRTMv3 elevations and results in a similar variance of elevations as found in the SRTMv3 data.

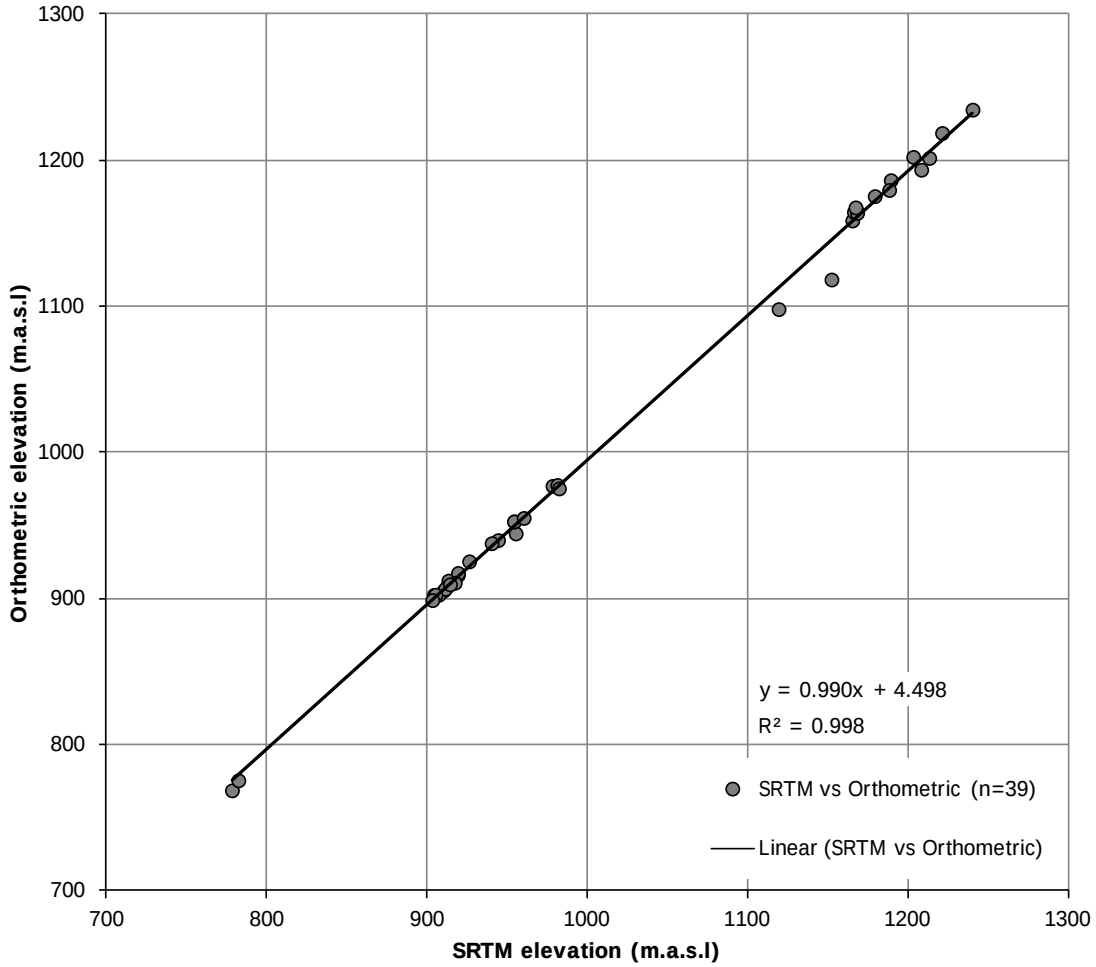

Figure 5.3: SRTM elevations plotted against orthometric heights for all 39 measurements. Field measured Leica GS20 elevations were corrected to orthometric heights using the EGM 96 geoid. The R^2 value of 0.998 indicates a near linear correlation of SRTM height versus orthometric height. The trend line having the equation **y = 0.990x + 4.498** indicating the SRTM elevations are, on average, higher compared to orthometric elevations.

By applying equation 1 to a set of given SRTMv3 elevations it can be seen that SRTMv3 accuracy is related to the overall elevation of the data. The elevations of the two correction factors as well as the difference between the given SRTM elevation and the corrected elevations are set out in **Table 5.1** below. For areas higher than 750 m.a.s.l., the predicted orthometric elevations indicate that, for the SRTMv3 data, when elevation increases so too does its positive elevation offset. Elevations at 500 m.a.s.l. show no difference between the two, with SRTMv3 elevations lower than 500 m.a.s.l.

being below the predicted orthometric elevation. **Table 5.1** also indicates that, up to 1750 m.a.s.l., the difference between the predicted orthometric and SRTMv3 elevations fall within the 12 m absolute accuracy at the 95 % confidence limit.

Table 5.1: Table showing the resulting elevations of the two correction factors and the difference between given SRTM elevation and corrected elevations.

SRTMv3 (m.a.s.l.)	Predicted orthometric (m.a.s.l.)	Difference (SRTM – predicted)
2000	1985	+15
1750	1738	+12
1500	1409	+10
1250	1242	+8
1000	995	+5
750	747	+3
500	500	0
250	252	-2
100	104	-4
50	54	-4
10	14	-4
5	9	-4
0	4	-4
Average difference		**+2**

5.6 Discussion

As equation 1 did not increase the accuracy of the elevation data, it was not necessary to apply it to the SRTMv3 data. In addition, as most of the rivers studied have the majority of their elevations between 200 and 1500 m.a.s.l., the expected difference between orthometric and SRTMv3 elevations would fall within the 12 m absolute accuracy at the 95 % confidence level (see **Tables 5.1** and **A5.2** in **Appendix 5**). Therefore, no benefit would be achieved by applying equation 1 to the SRTMv3 data. Interestingly, of the seven areas that were thought likely to have produced abnormal elevations based on the field observations, only three fell outside of the 12 m absolute accuracy (at the 95 % confidence interval)(see **Table A5.1**, **Appendix 5**). These three points are Kabawene Falls (+21 m), Below Lumangwe Falls (+34 m) and Malembo River (+14 m). Both Kabawene Falls and Below Lumangwe Falls are noticeable on **Figure 5.3** as the two points that do not fall near the trendline. These two points were taken in an incised gorge along the Kalungwishi River, with dense riparian vegetation along the river margins. If these three readings are disregarded, the average difference between the SRTMv3 and orthometric heights decrease from 5.3 to 3.8 m (a 1.5 m change) and the absolute accuracy increases to 6 m at 95 % confidence level. This highlights the role vegetation (increase in heights) and topography (radar shadow effects within the gorge) may play when using a radar–based DSM, such as the SRTMv3. Therefore, these two factors need to be borne

in mind when digitising the river longitudinal profiles, as rivers flow through zones of high to low topographic relief and dense to sparse vegetation.

An additional reason for not using a correction factor is that maintaining the 'original', uncorrected elevations of the SRTMv3 data allows for easier comparison between the results of this study and others. Furthermore, if improved (and more accurate) correction equations become publically available in the future they may easily be applied to the river elevations of this study, without the need to undo any previous correction.

The PPP GPS survey lends confidence to the absolute accuracy (at a ~90 m^2 resolution) of river elevations determined from SRTMv3 data. Outside of areas of dense, high forest and complex relief, the PPP GPS survey indicates that the absolute vertical accuracy of the SRTMv3 data is 12 m at the 95 % confidence limit and 6 m at the 68 % confidence limit. This vertical fidelity is supported by other studies on the SRTM elevation data, particularly the version of the SRTM data as released by CGIAR-CSI, for other parts of the world (Gamache, 2004; Jarvis et al., 2004; Gorokhovich and Voustianiouk, 2006; RodrÍguez et al., 2006; Reuter et al., 2007) which have shown a vertical accuracy between 8 m to 4 m (often at 90 % error limits). This is comparable to the vertical accuracy shown for the locations surveyed (see **Table A5.2** in **Appendix 5**). The difference between the processed PPP surveyed elevations and SRTMv3 elevations is probably due to the SRTM being a DSM and not DEM. As the SRTMv3 DSM is not a bare earth model (like orthometric elevation) it incorporates elevated surfaces. In areas of low vegetation height, such as grasslands, the SRTMv3 (having been previously corrected to the geoid) would closely correspond to orthometric elevations. However, in densely forested regions, the SRTM elevation represents the uppermost elevation band of the tree cover (due to partial radar penetration of the vegetation (Sun et al*.,* 2003). This elevation offset (compared to orthometric heights) may be 10 m ore more depending on canopy density and tree height. Several studies have also found that slopes greater than 10 ˚ and slope aspect may influence the vertical accuracy of the SRTM data (e.g. Sun et al*.,* 2003). This affect of slope and aspect are likely related to the radar based nature of the SRTM data as described in **Chapter 4**, **section 4.3.2** and **Figure 4.4**. Jarvis et al. (2004) noted that in absolute terms the SRTM tends to underestimate elevations in peaks and ridges, while overestimating the elevation of valley bottoms. The GPS survey generally agrees with these findings.

It must be remembered that the SRTM elevation represent an average surface elevation over a ~8100 m^2 area (90 m pixel resolution), whereas the GPS elevation is a single point elevation and so

local topographic vagaries within the pixel may contribute to the differences in SRTMv3 and orthometric elevations. In general terms, the SRTMv3 elevations will, for regions of low or sparse vegetation cover and low, homogenous relief in southern Africa, closely approximate orthometric heights, especially due to the scarcity of data voids in southern Africa (Reuter et al., 2007). This would be the case for the majority of the rivers, where river width is greater than fringe forest heights, as a 'bare' water surface is represented. Yet, areas that incorporate large areas of dense forest or woodland or areas of high topographic relief that form the majority of the 3 arc–minute pixel are unlikely to furnish orthometric or near orthometric elevations (Sun et al., 2003). This is the case for headwater regions and zones where river widths are smaller than vegetation heights. Overall, the SRTM data should be considered of sufficient quality for most geomorphic studies. This is especially true in Africa where no better, contiguous DSM is publically available.

The GPS survey shows that the vertical accuracy of the SRTMv3 data for southern Africa averages +5 m compared to orthometric heights. This represents a better vertical accuracy than has been reported for other regions (e.g. Jarvis et al., 2004; Ludwig and Schneider, 2006; Gorokhovich and Voustianiouk, 2006; Reuter et al., 2007). As long as the potential problems (as shown by the -1 to +34 m range of the SRTM elevation compared to orthometric heights) of radar derived DSM are acknowledged, it is considered that the CSI-CGIAR SRTM data shows a high degree of fidelity at its given resolution. The SRTMv3 data should therefore be considered sufficiently accurate to investigate meso-scale geomorphic features, such as the characterisation of knickpoint height and derivation of longitudinal river profiles, being a near (within 12 m) true reflection of the reality of the rivers. Due to both the resolution and accuracy of the SRTM data, it is unlikely that future data of better pixel resolution will lead to significant differences with regard to the production of entire river profiles and investigation of geomorphic features at a 10 to 100 m scale (meso-scale) over a sub-continental area.

The following conclusions can, therefore, be made regarding the accuracy and suitability of the SRTMv3 data for this study:

- Correction of SRTMv3 elevations based on the surveyed PPPC points does not improve the overall accuracy of the SRTMv3 data.
- SRTMv3 elevation data is highly accurate relative to the geoid, with most of the errors being small (12 m and 6 m at 95 % and 68 % confidence level respectively) compared to the 90 m pixel resolution and the meso-scale nature of the features being investigated.
- If the three elevation points that fall outside of the 95 % confidence are disregarded, the absolute accuracy increases to 6 m at 95 % confidence level and 3 m at 68 % confidence level.
- The 95 % confidence limit closely approximates the 5 m average difference between the SRTMv3 and the 39 orthometric elevations.
- The systematic positive shift of the SRTMv3 elevation is mainly due to canopy effects, although, in a few, more extreme cases, local topography (i.e. the river gorge) had an influence.
- SRTMv3 has sufficient vertical accuracy and the spatial resolution to make it suitable for the mapping and classification of topographic features in south-central Africa.

CHAPTER 6: RIVER LONGITUDINAL PROFILE AND KNICKPOINT MAPPING

6.1 Introduction

This chapter outlines and explains the GIS analysis of the Landsat imagery, SRTM data and other associated data sources (**Section 6.2**). The analysis of the rivers of the CKW in a spatial context utilises the strength of geographical information systems (GIS), which allows for the creation of spatially correct data (feature) and the addition of non-spatial data (attributes). Therefore, the creation of this geodatabase (both feature and attribute data) allows for analyses of landscapes both spatially and contextually. This chapter details and discusses the creation of geospatial datasets, long profiles and knickpoints, which forms the core data contribution of this thesis (**Sections 6.3** and **6.4**). Thus, this chapter adds to the limited existing body of knowledge of river longitudinal profiles in south-central Africa by providing new observational information to the form of feature and attribute data related to those features.

For this study, river long courses and long profiles were manually digitised using the data described in **Chapter 4**, namely SRTMv3 and related products as well as Landsat 7 ETM+ imagery. As manual digitisation is time intensive, it is important to compare it to more computationally intensive approaches. A comparison was made for two reasons: to determine the potential benefit of manual digitisation and to act as a quality control method; the latter is described in **Section 6.3.2.3** below. Both the long profile digitisation and the knickpoint identification and characterisation are dealt with. This chapter is presented as two thematic sections: the methods and results section and a preliminary discussion and summary section.

The new geospatial data created here will form the foundation of **Chapter 7**. **Chapter 7** details the enhancement of the geodatabase created in **Chapter 6** by the addition of data from various existing maps and literature. This chapter also informs the understanding of the geomorphic development of south-central Africa proposed in **Chapter 8**.

6.2 Methods

Unless otherwise stated, all of the data (both raster and vector types) were referenced to the World Geodetic System 1984 (WGS84), a geographic coordinate system. The reason is threefold: 1) over large areas, the spacing of longitudinal spacing of raster using a rectangular grid projection (such as

Universal Transverse Mercator) changes with latitude; 2) internationally, many of the world's medium resolution DSMs (10 – 100 m) use geographic coordinates; and 3) Guth (2009) has shown that reinterpolation may contribute to anomalies in the resulting analysis. Furthermore, Hengl and Evans (2009) suggest that for a fine grid resolution (less than 100 m) raster, the use of a metric (projected) or degree (geographic) coordinate system is of little consequence. Thus, using WGS84 ensured that all of the data was spatially compatible and avoided issues of reinterpolation.

The remainder of this section describes in general terms the steps and processes used. For a more detailed description, see **Appendix 6**.

6.2.1 Software

This study made use of two different geospatial programs, namely ERDAS IMAGINE and ArcGIS. ERDAS is geospatial imagery software that focuses on raster analysis; it was used to manually digitise the river courses and extract the relevant elevation data from SRTMv3. Two versions of ArcGIS (9.2 and 10.0) were used during this research. ArcGIS is predominantly focussed on vector data (point, lines and polygons) analysis. ArcGIS was used for the creation, curation and interrogation of the various shapefile dataset as well as map production. The spreadsheet program, Excel, was used for attribute data creation and the graphical representation of the long profiles in conjunction with a graphics editing programs, CorelDraw and Inkscape.

6.2.2 Digitising of river courses and longitudinal profiles

6.2.2.1 River digitisation

The rivers profiles were digitised following a method similar to that used by MacFarlane and Eckardt (2007). This method involved the use of Landsat ETM 7+ imagery, the SRTMv3 DSM and its hillshaded product (see **Chapter 4**). A total of 18 river long profiles and courses were manually digitised from July 2008 until August 2009. These digitised rivers formed part of the Congo-Kalahari Watershed (CKW) that divides the CB from the Zambezi and Okavango Basins. The rivers are shown on the map in **Figure 6.1** below.

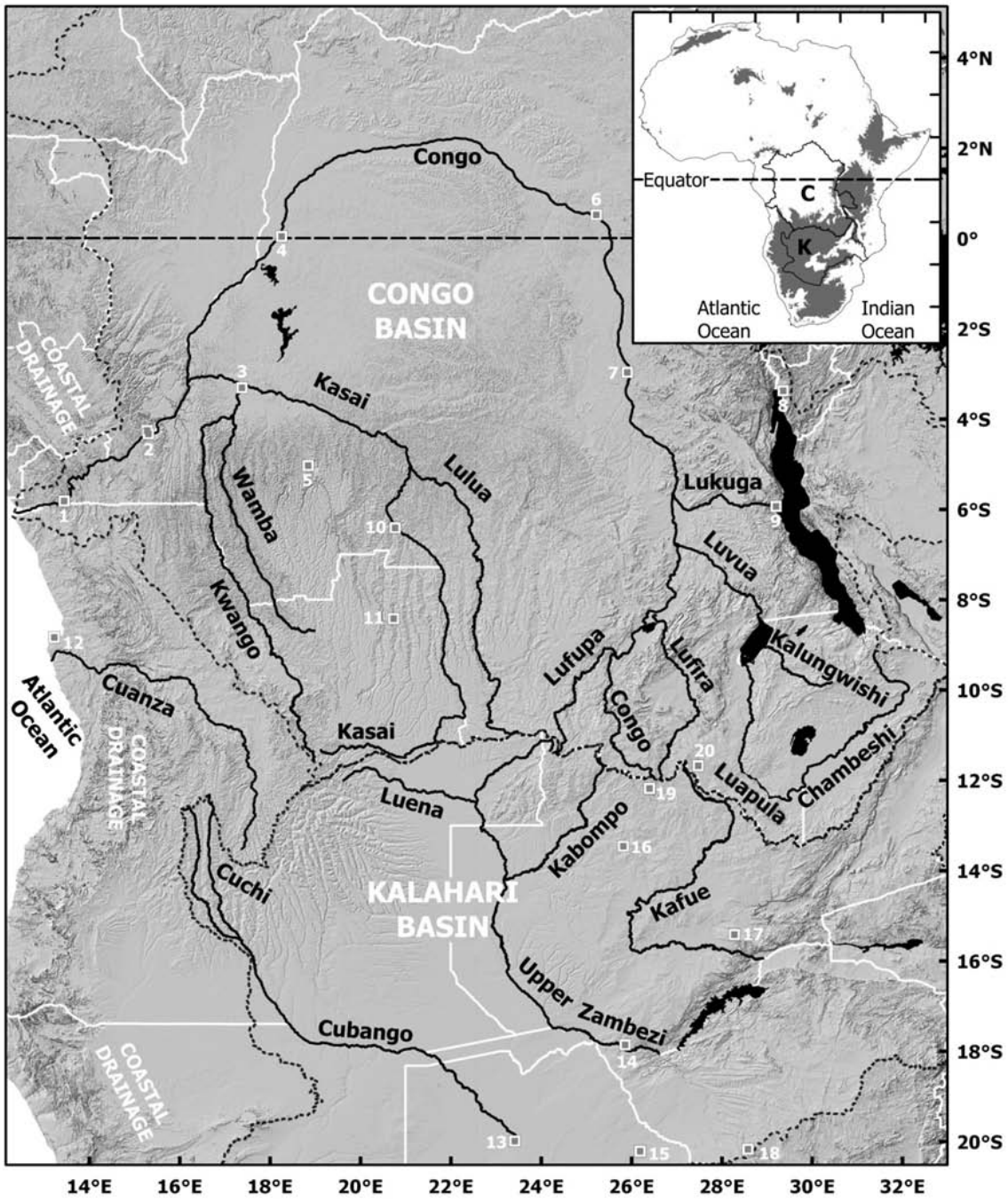

Figure 6.1: Map of the rivers digitised in this study. Inset shows the digitised rivers and their basins (C – Congo Basin, K – Kalahari Basin) in the context of Africa's topography (grey shading indicates elevations 1000 m.a.s.l. and higher. Heavy black lines indicate the river courses, water bodies shown in black and political boundaries in white. The dotted lines indicate the drainage divides of the CB, KB and coastal river systems and were created as part of this thesis. Several towns and settlements of interest have been shown: 1– Matadi; 2– Brazzaville / Kinshasa; 3– Bandundu; 4– Mbandaka; 5– Kikwit; 6– Kisangani; 7– Kindu; 8– Bujambura; 9– Kalemie; 10 – Tshikapa; 11 – Lucapa; 12 – Luanda; 13– Maun; 14– Livingstone; 15– Nata; 16– Kasanka; 17– Lusaka; 18– Bulawayo; 19– Solwezi; 20– Lubumbashi.

The three imagery products (Landsat, DSM and hillshaded) were geographically linked together and used simultaneously to digitise rivers as demonstrated in **Figure 6.2** below. This process made use of three separate ERDAS viewer windows with the geographic linking allowing the cursor position to have the same geographic coordinates in all three windows. In the window showing the DSM, the 'Profile Tool' was used to manually digitise the river course by following the lowest elevation in the DSM (see **Figures 6.2** and **6.3**). For the digitising of the CKW and coastal watersheds, the same method was applied but instead of using Landsat imagery and aspect raster was used as it allowed for better discrimination of hill slope direction.

Owing to the scale of the SRTMv3 pixel (90 m) and issues of using radar to produce a DSM, as discussed in **Chapter 4 (Section 4.3.2**) it was necessary at this point to manually adjust the digitised course based on the Landsat image to ensure the greatest horizontal accuracy of the digitised rivers. Landsat 7 ETM+ imagery was considered to be a better indicator of river course due to its horizontal spatial accuracy, 30 m resolution and its more extensive quality control methods (see **Chapter 4**, **Section 4.2**). Thus, the final river course, as seen in the Landsat imagery, was considered the most accurate and given preference over the SRTM data. This means that the digitised rivers did not always follow the thalweg (the line of downslope gravitational flow which the river follows) as indicated by the DSM but instead followed the river course as indicated by the finer resolution Landsat 7 ETM+ imagery. If the apparent valley thalweg had been exclusively followed, as indicated by the lowest DSM valley elevations, the latitude and longitude of the river course would have been incorrect due to the DSM's 90 m resolution and radar affects (lay over and shadowing). This type of error might have resulted in the misplacement of the river course (and associated features such as knickpoints) in terms of their horizontal location. Therefore, the Landsat 7 ETM+ imagery had the secondary purpose of providing a quality check of the SRTMv3 data. The accuracy of the SRTMv3 has already been established in **Chapter 5**, **Section 5.5**.

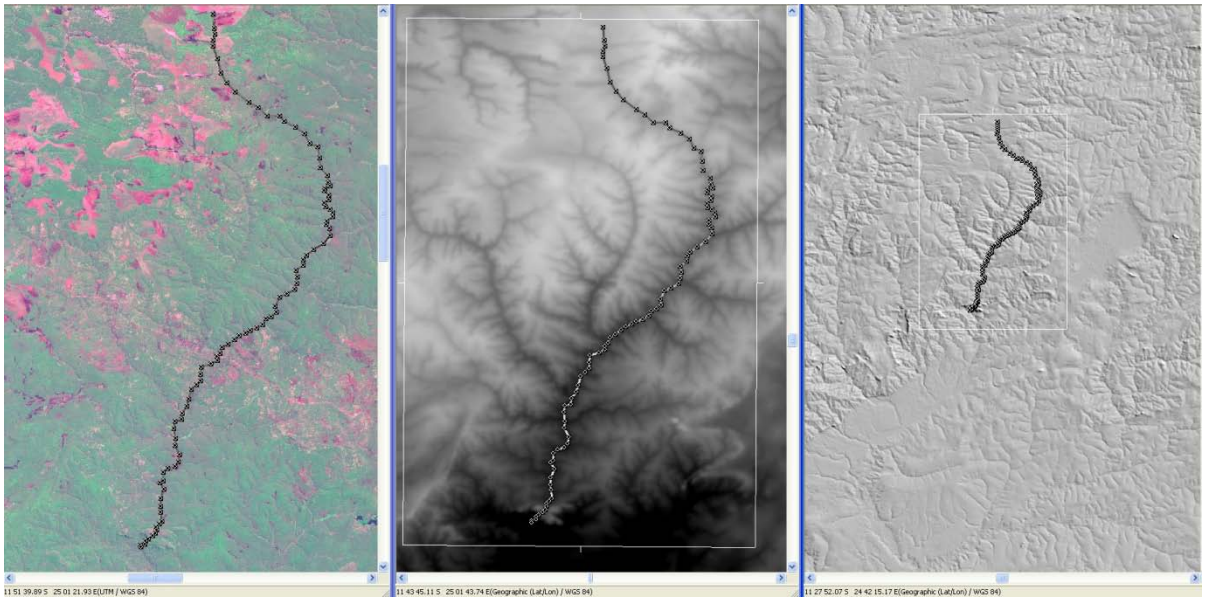

Figure 6.2: The digitisation of rivers with the Landsat 7 ETM+ false colour image on the left, the SRTMv3 DSM in the centre and the hillshaded product on the right. The three windows are geographically linked; the spatial extent of the Landsat and SRTMv3 are similar, with the hillshading showing a larger extent (white box). This example is from the Kabompo River.

The manual digitisation of the rivers using the Profile Tool produced a table of point data, each with an associated 'Map X' (longitude), 'Map Y' (latitude), 'Distance' (straight line distance), 'Surface Distance' (on the ground difference) and elevation ('Layer 1'). As all the imagery was in the WGS84 geographic coordinate system, the distances were measured in decimal degrees. The data was displayed using WGS84 as most of the studied rivers crossed several degrees of latitude and longitudes; using a single projection on rivers of such immense length would likely have introduced spatial errors (as illustrated by the Landsat image mosaicking in **Chapter 4**, **Section 4.2.2**). Furthermore, as river networks and their lengths have fractal properties (e.g. Tarboton et al., 1988; Turcotte, 1992; Rodríguez-Iturbe and Rinaldo, 1997), measured river lengths would be dependent on raster resolution. Therefore, any river length calculations based on the SRTMv3 data will differ from river lengths derived from a raster at a different resolution.

During the digitisation processes, screen image captures were taken and points of note recorded. For example, possible causes of knickpoints, singular river morphology and apparent quality of data (elevation spikes and sinks), were recorded. An example is displayed in **Figure 6.3**. Due to the complexity of the river courses it was often necessary to have points at high densities (a point every ~30 m) while in some areas a low point density (a point every ~1 km) was sufficient. The Profile Tool in ERDAS the Profile Tool extracts all of the elevation data falling on a straight line between the two

manually placed nodes. In zones of high sinuosity in floodplain areas, not all of the small meanders were followed (meanders with a wavelength of <50 m were straightened out) or if the meanders were large (wavelength of ca. 100 m), the average curve was followed. To accurately follow the small meanders, often associated with localised floodplains and wetlands, was too time consuming. In these areas of low relief, with little change in elevation, following these meanders did not provide insight into the interpretation of the overall profile as the meanders were likely due to vegetation and/or short term, highly dynamic depositional environments such as floodplains (see, for example, **Figure 6.3**). Therefore the straightening of these short-lived meanders did not impact on the accuracy of the date or detract from the geomorphologic interpretations of the river systems. In areas where the meanders were incised (indicated by a large change in elevation of river surface and surrounds) this method was not followed as it would lead to artificial knickpoints and so meanders were accurately traced.

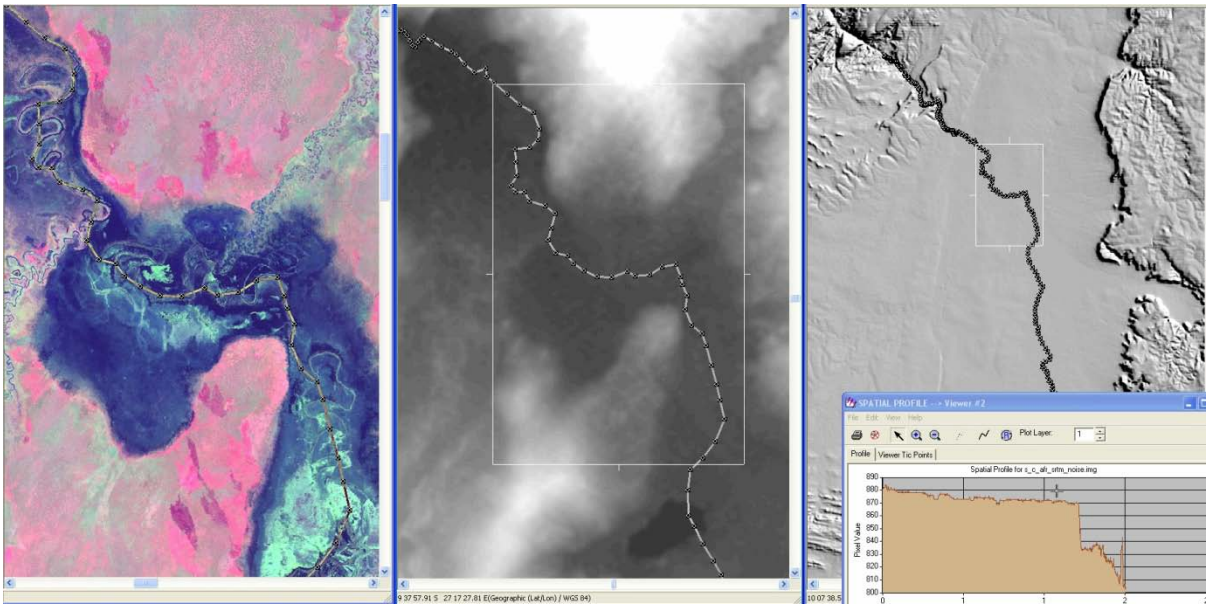

Figure 6.3: Example of the 'straightening' out of the river course in low gradient areas. Landsat false colour image showing minor meanders in a floodplain setting shown on the left and SRTMv3 DSM showing lack of elevation differential in the floodplain is in the centre. The lack of elevation change is further shown by the profile inset (bottom right) with the cursor showing location of the floodplain. Example from the Lufira River.

6.2.2.2 Longitudinal profiles

The tabular data created through the manual digitisation was copied and imported into a spreadsheet. This allowed for the digitisation process to be carried out in small, manageable sections adding each subsequent section in turn to the preceding records. In addition, it was found that ERDAS would crash due to memory constraints when long river sections were being digitised, so shorter sections were undertaken to avoid this problem and sections were kept below 50 km in length. Once the river digitising was complete, a graphical representation of each long profile, plotting elevation against pixel number, was created. This allowed for the comparison of rivers and aided the analysis.

6.2.2.3 File conversion and river length determination

The digitisation of the river in ERDAS provided point data, with each river having thousands of elevation points (some had tens of thousands of individual points). This point data was imported into ArcGIS by plotting the coordinates of each elevation point from the spreadsheet and converting it to a point shapefile (see **Appendix 6**, **Section 6.1.1**). High density point shapefiles are not only cumbersome to work with but offer limited analysis capacity. Therefore, these point shapefiles were converted into polyline shapefiles using a free GIS extension, namely, Hawth's Analysis Tools (Beyer, 2004). It should be noted that Hawth's Analysis Tools does not work in ArcGIS 10 (and later versions) and, as of December 2009 has been formally discontinued to be replaced by the Geospatial Modelling Environment software (http://www.spatialecology.com/htools/tooldesc.php). This was done for each river, resulting in 18 named polyline shapefiles. It must be noted that the conversion from point to polyline resulted in the loss of the elevation attribute data of the point shapefiles. Thus two sets of shapefiles were created for each individual river: point shapefiles (which had elevation attribute data) and polyline shapefiles (which allowed for easier mapping and spatial analysis).

In order to determine the length of each digitised river course, the river polyline shapefiles were duplicated and projected to a south Universal Transverse Mercator (UTM) zone. The UTM zone used was the one closest to the river course mid-point, which allowed each river's length to be calculated in kilometres using Hawth's Analysis Tools (see **Appendix 6**, **Section 6.1.1**). As minor meanders were not followed when digitising the rivers, the determined lengths represent minimum river lengths. Additionally, it must be kept in mind that using a raster of significantly different resolution compared to the SRTMv3 may result in substantial differences in length. Once all the river lengths were calculated, the individual shapefiles were merged and the river names added to the attribute table.

6.2.3 Generating river networks and profiles

The quality of the results of the manually digitised river courses and long profiles were compared to river networks and long profiles generated from a DSM using the standard tools in ArcGIS. In order to simulate the process of the manual river digitisation, limited pre-existing data and knowledge was used. This was done to replicate the explorative nature of the manual process. Moreover, there are very few readily and publically accessible GIS databases for south-central Africa. The automated process required two steps: (1) the determination of the river course; and (2) the subsequent extraction of elevation (while maintaining their spatial attributes). The details of this process of generation of river networks and profiles are discussed below.

6.2.3.1 Generating river networks

The ArcGIS hydrology toolset in Spatial Analyst was used to generate the river networks. An attempt was made to run the tools on the entire SRTMv3 (3 arc-seconds or about 90 m pixel resolution) data for the study area. However, the size of the input file rendered this approach inoperable as ArcGIS would either crash or fail to produce outputs even after an 18 hour run. This was probably due to the inadequate processing power of the computer being used and also the limitations of ArcGIS 9 in terms of raster processing (the SRTMv3 file exceeded 2 GB in size). In an attempt to resolve the issue, the study area was then split into its two large drainage basins, with some overlap along the watershed to simulate a lack of data for the watershed location. Several processes were tried, such as the tool Fill and Flow Direction, with the SRTMv3 data but ArcGIS was still unable to resolve the required outputs. In order to achieve a result, the DSM was downgraded to a ~900 m (30 arc-seconds) resolution by resampling the 90 m SRTMv3 data. This resampled SRTM DSM was used to generate the river networks.

In the generation of river networks, several tools had to be used to create the intermediary output files required as inputs for other processes (see **Table A6.1** in **Appendix 6**, **Section 6.1.2.1**). The Hydrology Tools require the DSM to be 'filled' and thus any elevation holes in DSM data were filled in, based on the elevation of the surrounding pixels, which effectively smoothed out some of the topographic relief. It should be noted that this tool does not affect spikes in elevation. The smoothing process allowed for creation of linear rasters representing the flow of adjacent pixels that form a river network for both the Congo and Kalahari Basins. These linear rasters were created at a variety of pixel accumulations. To allow for the use and analysis of these linear networks, these linear rasters were converted into shapefiles (see **Table A6.1** in **Appendix 6**, **Section 6.1.2.1**). The

drainage networks of each river were constructed by merging the corresponding stream shapefiles, from those of highest flow accumulation to the lowest flow accumulation. This process resulted in the creation of river networks based on a 900 m pixel resolution DSM for the rivers studied in both basins.

6.2.3.2 Generating river longitudinal profiles

The stream network shapefiles (based on the filled 30 arc-second DSM) were used to extract elevation values from the 900 m DSM and the SRTMv3 90 m DSM, using the Spatial Analyst Tools (see **Appendix 6**, **Section 6.1.2.2**). Elevation data was extracted from both DSMs (900 and 90 m) for two reasons: firstly, to compare the longitudinal profiles to the manually digitised rivers and, secondly, to serve as some degree of quality control of generated river course fidelity. The quality control was premised on the fact that, while the long profile on the hole-filled 900 m DSM should be smooth (that is without holes and spikes), the long profile from the SRTMv3 data would be likely to show holes and spikes (noise) which would serve as a rough proxy of river course accuracy. The generated river networks were also spatially compared to the digitised river courses.

The extraction process did not prove to be straightforward. The use of the stream rasters in drawing the river long profile was problematic as the elevation ordering of the raster output attribute was from highest to lowest (see **Appendix 6**, **Section 6.1.2.2** for further details). Several methods were tried to overcome the raster ordering issue. It was established that the DSM raster itself was responsible for the incorrect elevation ordering. This was because, when the raster output is converted to a shapefile, the information (including elevation) is written in row-column order as it occurs in the raster grid and not in sequential order as it occurs along the river. Thus, a preference is assigned to row number, resulting in the ordering of any cells with the same row number but different column numbers as if they occur as adjacent cells. Thus, elevation values in the extraction of the data were ordered according to their row number, resulting in segments of river being recorded out of order when converting from a raster to a shapefile. This resulted in the generation of incorrect longitudinal river profiles. An example of such incorrect ordering is demonstrated in **Figure 6.4**.

It was, therefore, not possible to automatically generate accurate river longitudinal profiles from the complex rivers courses using the standard tools available in ArcGIS. In order to create the required

longitudinal profiles, new polyline shapefiles were created by tracing the relevant generated river courses. This more time-intensive approach resulted in a single polyline shapefile for each of the 18 rivers. Details of this and the following aspects of the process are provided in **Appendix 6**, **Section 6.1.2.2**. After a unique identifying number was assigned to each shapefile, they were projected into UTM using the closest zone that approximated the centre of the river polyline. The shapefiles were projected into UTM to allow for the correct linear spacing of the points along the polylines. Hawth's Tools was used to convert the polyline into point data so that a single data point corresponded to a single pixel. This was done for all 18 rivers, at 900 m and 90 m intervals.

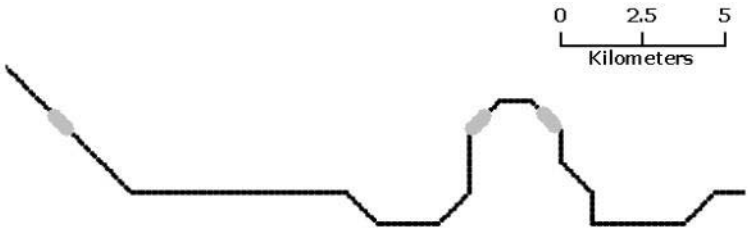

Table

kaf_3pt

FID	Shape *	POINTID	GRID_CODE
1021	Point	1022	1267
1022	Point	1023	1270
1023	Point	1024	1276
1024	Point	1025	1270
1025	Point	1026	1272
1026	Point	1027	1274
1027	Point	1028	1271
1028	Point	1029	1272
1029	Point	1030	1271
1030	Point	1031	1271
1031	Point	1032	1270
1032	Point	1033	1269
1033	Point	1034	1270
1034	Point	1035	1268
1035	Point	1036	1267
1036	Point	1037	1270
1037	Point	1038	1268
1038	Point	1039	1268
1039	Point	1040	1270
1040	Point	1041	1269
1041	Point	1042	1270
1042	Point	1043	1270
1043	Point	1044	1271

(15 out of 11488 Selected)

kaf_3pt

Figure 6.4: An example of incorrect ordering of pixel value from the Kafue River. The grey highlight points correspond to the 15 selected table records highlighted in grey. Using elevation ordering would have resulted in incorrect long profiles.

A point shapefile was thus created for each river. Each point had its own unique StepID, with this StepID being in sequential order; thus, the starting point of the river was assigned a value of 1, the second point a value of 2 and so on until the end of the river polyline was reached. The point shape was re-projected back to WGS 84to match the DSM. This point shapefile was used to extract

elevation data from the DSM. This resulted in two separate point shapefiles – one with the correct sequence of points but no elevation data and the other with out-of-sequence elevation data. To combine the two data sets and ensure the correct elevation was assigned to the correct StepID, a spatial join in ArcGIS was used (see **Appendix 6**, **Section 6.1.2.2**).

The spatial join created a new shapefile which had both elevation and StepID information for both the 900 m and 90 m interval point shapefiles. As a quality control, two of the final shapefiles were manually inspected for irregularities in the ordering of the elevation data (based on comparison of the StepID as well as the longitude and latitude data). No problems were observed. The attribute tables were exported to a database file (.dbf), opened as a spreadsheet, ordered according to the StepID and then plotted.

6.2.3.3 Comparing the generated rivers to the digitised rivers

The plots of the generated profiles were compared to the manually digitised long profiles. This was done by plotting the three profiles of each river on the same axes and visually inspecting them. As the 30 arc-second profile had 1/10 of the point density of the 3 arc-second, it needed to be scaled to the 3 arc-second profiles.

In order to compare the generated river networks to the digitised course, a spatial join using closest distance was used to compare the point data of the automatically extracted river courses to the polyline shapefile of the manually delineated river. Both the Auto30 networks and digitised courses were projected to UTM, with the zone closest to each river's middle point being chosen. Point data to polyline data was compared instead of point data to point data as the manually delineated river had substantially more data points, and so the line of the manually generated river is considered the 'true course'. The location of the point data determines the shape of the line (course) of the generated river, as these elevation points form the vertices on which the automated river course is built; they are the determining factor in terms of the fidelity of the generated profile. Therefore, while the minimum distance when comparing line to line data would be 0 m, as the lines will cross, the maximum distances would still be the same. Point to line was used as it was the quickest method that still gave accurate results and allowed for additional statistics to be determined.

6.2.4 Knickpoint characterisation

6.2.4.1 Knickpoint categorisation and description

During the river digitisation process, when knickpoints were encountered, their coordinates, height category and description were recorded and a screen capture of the scene taken. The knickpoint height was manually determined from the SRTMv3, as shown by the ERDAS section profile, and the elevation of start of the knickpoint was recorded. An example of this process is provided in **Figure 6.5**. The knickpoint heights were binned into height categories at 5 m intervals and described by their characteristics as seen on the Landsat 7 ETM+ imagery (see **Table 6.1** below). Knickpoints heights were assigned in multiples of 5 due to the absolute vertical error of the SRTMv3 approximating 5 m for the majority of central and southern Africa (Rodrĺguez et al., 2006). This has been discussed in **Chapter 5**. For example, a knickpoint with a 7 m height would be categorised as 5, whereas a knickpoint with 8 m height would be classed as 10. Where knickpoints occurred as a long series of highly connected rapids, cascades and falls, the coordinate for the central section within the window was recorded.

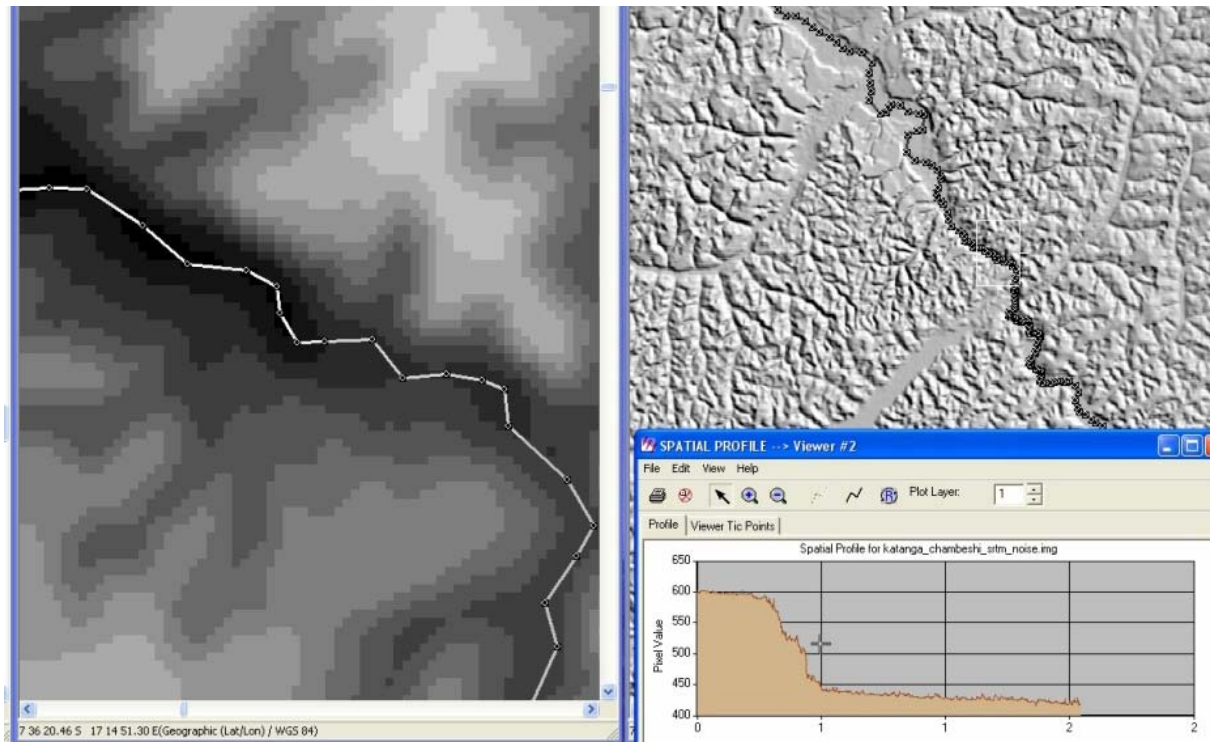

Figure 6.5: An example of knickpoint height (50 m) and elevation (460 m.a.s.l), indicated by the cursor, as determined from the ERDAS profile tool (bottom right) from the Kwango River. The SRTMv3 data is on the left and the hillshaded output for the larger area is on the right.

Table 6.1: The categorisation of the knickpoint height category and the attributes used to assign each knickpoint to a height class.

Knickpoint category	Definition
-5	Minor knick point; drop in elevation is visible on DSM, but less than 5 m, and visible on Landsat imagery.
-1	Knickpoint is likely; it is visible on Landsat imagery as white water but there is no drop in elevation on the DSM.
0	Knickpoint easily visible in Landsat imagery, much white water. Height is indeterminable as the DSM is too noisy at this point (i.e. area of elevation spikes and sinks).Usually other discernible knickpoints close by.
Multiples of 5 from 5 to 90	Knickpoints visible, both with white water and noticeable drop in DSM. Knickpoint heights are binned into 5 m categories, beginning at 5 m and ending at 90 m.

Not all the evidence for the occurrence of the knickpoints was equal. In the ideal situations, both the SRTMv3 and Landsat 7 ETM+ imagery showed strong evidence for a knickpoint, for example a substantial, sudden drop in river long profile elevations (SRTMv3) and white water (Landsat). In other cases, the evidence was not so clear. In **Table 6.1** three category numbers are used. If the knickpoint was visible on the Landsat image and had a height less the 5 m, it was classed as -5. Both aspects of the categorisation are necessary because, if the knickpoint height is below 5 m, it is within SRTMv3 vertical error and these small knickpoints may be undetectable when the river is in flood. Therefore, the -5 category attempts to deal with river water levels and seasonality of the river flows where the occurrence of the knickpoints is not disputed. The remaining two categories, -1 and 0 are used when, for various reasons, the presence of a knickpoint or its height may be disputed. A knickpoint is categorised as -1 in cases where there is evidence from the Landsat imagery (proxy evidence) but no decrease in the river long profile is noted (no SRTMv3 evidence) and its context does not provide further evidence (for example, no nearby knickpoints present). A knickpoint is categorised as 0 in cases where Landsat imagery, along with secondary lines of evidence (i.e. nearby knickpoints, bare rock and dramatic changes in river direction) supported knickpoint occurrence but its height could not be resolved from SRTMv3.

6.2.4.2 Image library and directory creation

Whenever a knickpoint or potential knickpoint was encountered, a screen capture of all three windows, along with the displayed profile (and cross hair indicating the position of the knickpoint along the profile) was taken. Examples of these images can be found in **Figures 6.3** and **6.6**. Other features were also noted for those locations. In this way, a catalogue of images and notes for each knickpoint was created as a reference. This allowed a database of all the knickpoints along with associated screen captures to be created. This directory contains eight entries per knickpoint detailing the height, location (in decimal degrees), qualitative description, distance (horizontal and surface) and feature name, as indicated in **Table 6.2**.

Table 6.2: The name and explanation of the knickpoint directory associated with a knickpoint shapefile. Note that column names cannot be more than 10 characters long.

Column name	Explanation
Name	The name of the river that the knickpoint is on and its broad category (viz. knick, minor knick, minor knick likely, knick likely)
Height_m	Height of the knickpoint in metres according to category (see **Table 6.1**)
Longitude	In decimal degrees
Latitude	In decimal degrees
Descriptio	Short description and notes on the knickpoint
Hor_Dis_dd	Horizontal distance in decimal degrees from the start of the profile (calculated by the Erdas Profile Tool)
Sur_Dis_dd	Surface distance in decimal degrees from the start of the profile (calculated by the Erdas Profile Tool)
Fall_Name	Common/given name of selected falls (if available).

The directory allowed for the creation of a knickpoint shapefile for each river, with the eight entries in Table 6.2 forming the associated attribute columns. This process was followed for each digitised river to allow for the knickpoint data to be spatially queried and analysed. The resulting shapefiles were checked for errors manually as well as by using the "select by attributes" function. Several of the files were found to have a limited number of missing values, which were manually corrected by cross-checking the original spreadsheet files and original notes taken during the digitisation process.

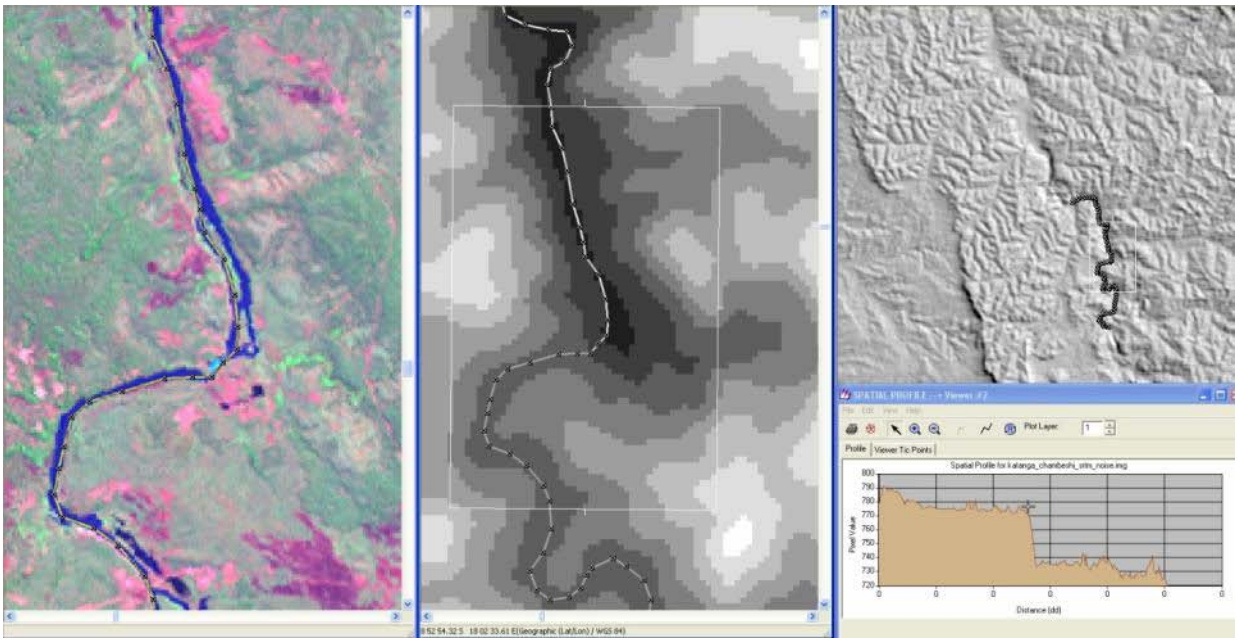

Figure 6.6: An example of the digital image library created during the characterisation of the knickpoints. From left to right: Landsat ETM+ (bands 2, 4, 7), SRTMv3 and SRTMv3 hillshaded with the vertical profile for the digitised section shown (the cursor marks the location of the knickpoint on the profile). This example is of a knickpoint along the Kwango River (8.885638 °S, 18.010738 °E) that was categorised as having an elevation of 756 m.a.s.l. and a height of 45 m. On the Landsat image it can be seen that this is a single fall (highlighted by the lighter blue of the river) that splits into two channels after the fall. The light pink on the Landsat image indicates bare rock or soil. The SRTMv3 indicates a rapid change in elevation in the same area (as seen on the in situ profile).

6.2.4.3 Spatial correction of knickpoint locations

All the separate knickpoint shapefiles were merged into a single shapefile resulting in one file with all the identified knickpoints. This knickpoint shapefile was overlaid on the river course shapefiles. The resulting composite was then visually analysed. It was noted that numerous knickpoints did not occur exactly on the river course polyline. This was due to a rounding error when manually recording the knickpoint coordinates (locations were recorded only to the third decimal degree). In some cases this rounding caused an offset of several tens of metres but it was usually less. River widths in some areas were an additional complication as the digitised river polyline was not always in the centre of the river channel (as seen on the Landsat imagery). The culminate offset of river width and rounding error may have led to erroneous spatial analysis; some knickpoint locations were 100 m from the polyline, although the majority were closer than 20 m to the polyline. To account for this offset issue, all of the knickpoint shapefiles were corrected by spatially adjusting the knickpoint shapefiles to the river course shapefiles using a spatial join. This was done for every knickpoint shapefile as well

as the merged knickpoint shapefile. After this correction the elevation of each knickpoint was extracted from the DSM and added as an attribute field to the knickpoint shapefiles. This was done using the Spatial Analyst tool and using the knickpoint shapefile as a mask to extract the corresponding SRTMv3 pixel elevation. Thus, a final knickpoints shapefile was created for knickpoints recording their height category, elevation, location, description and measures of horizontal differences as well as available names. These corrected knickpoint shapefiles along with the knickpoint directory were further used to explore spatial relationships of the knickpoints in relations to the digitised longitudinal profiles and river courses.

6.3 Results

The digitisation of rivers during this study resulted in a total of ca. 19 900 km of river course being digitised with 380 knickpoints being categorised and described as shown in **Figure 6.7**. Thus, a new and large geospatial database of the studied rivers was created. The results presented in this section are primarily concerned with the spatial nature of this database. The results presented here form the basis of the more detailed analysis in **Chapter 7**, where the landscape context of these results is discussed. In order to avoid duplication of figures and maps the reader is directed to Chapter 7 as appropriate.

6.3.1 Digitised rivers

The various rivers studied and described are shown in **Figure 6.7** and **Table 6.3** below. A total of 12 river profiles were investigated in the CB, with ca. 13 300 river kilometres being digitised and characterised. The CB's three longest rivers are the Congo (ca. 4100 km), Kasai (ca. 2100 km) and Kwango (ca. 1400 km) rivers. In the KB, a total of six rivers were digitised, covering ca. 6300 km. The three longest rivers of the KB are the Cubango (ca. 1700 km), Kafue (ca. 1500 km) and Upper Zambezi (ca. 1500 km) rivers.

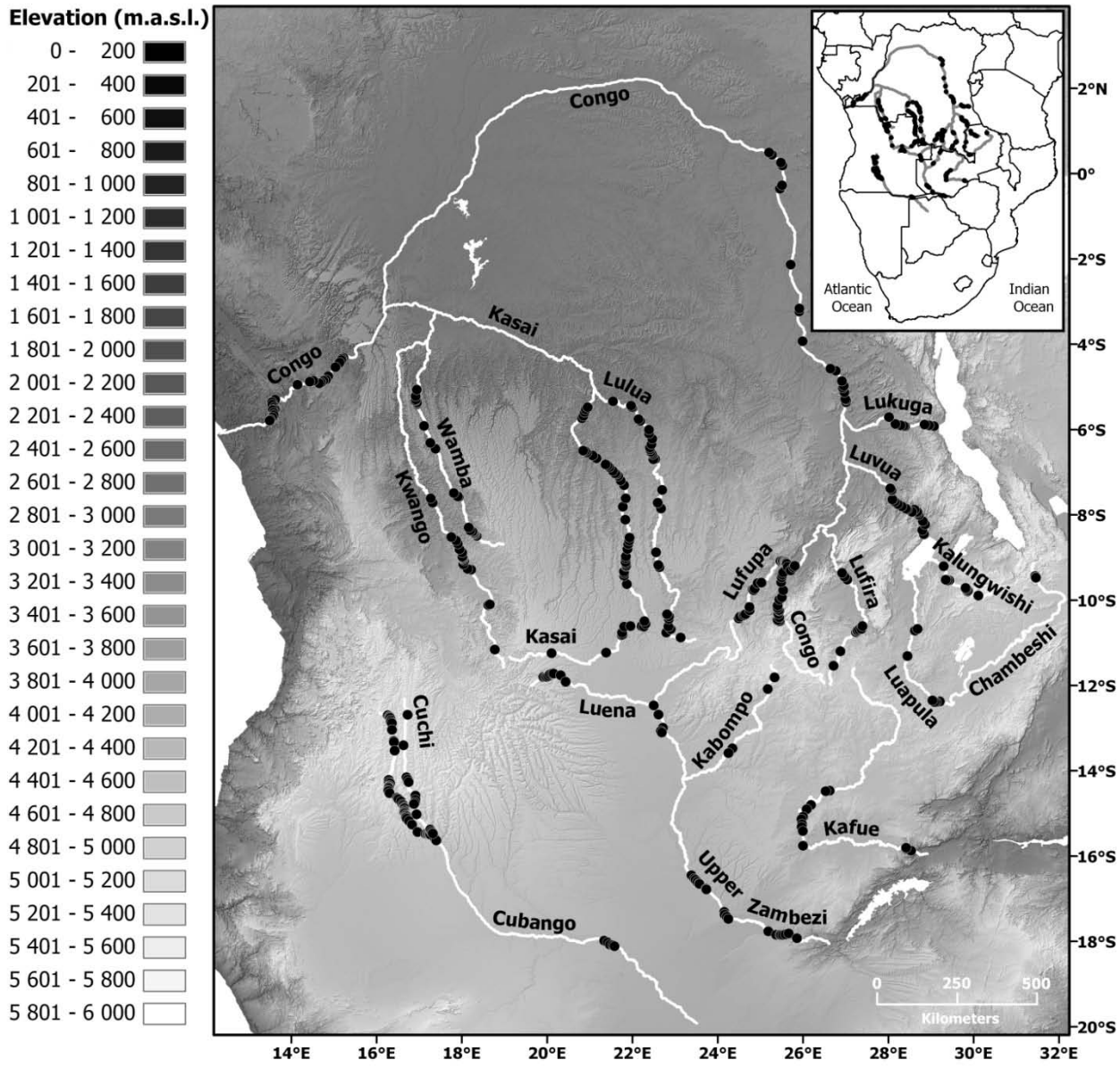

Figure 6.7: The geographic distribution of the 380 knickpoints identified in this study. Studied rivers are named and shown in white, with major water bodies in white. Grey circles indicate location of individual knickpoints. The inset is the political map of central and southern Africa with the rivers and knickpoints shown. See loose map in back sleeve. Hillshading is based on the SRTM 250 m data; the DSM used is SRTMv250m.

Table 6.3: A summary of important longitudinal profile characteristics of the digitised rivers. See relevant sections for details of each river. Rivers are ordered alphabetically. See **Chapter 7** for larger graphical displays of the longitudinal profiles.

River name	Pixel No.	Length (km)*	Start elevation (m.a.s.l)	Finish elevation (m.a.s.l)	Total drop (m)
Congo Basin					
Chambeshi	6683	668	1576	1160	416
Congo	42715	4150	1526	0	1526
Kalungwishi	2686	291	1592	921	671
Kasai	20718	2064	1348	272	1076
Kwango	14661	1465	1395	292	1103
Luapula	5969	604	1162	921	241
Lufira	6558	681	1415	562	853
Lufupa	5168	530	1485	562	854
Lukuga	3283	338	767	547	220
Lulua	11290	1137	1225	381	844
Luvua	3932	507	921	556	365
Wamba	8869	922	1183	312	871
Kalahari Basin					
Cubango	17074	1708	1834	937	897
Cuchi	5118	524	1757	1191	566
Kabompo	6568	653	1495	1031	464
Kafue	14744	1529	1375	369	1006
Luena	4313	430	1403	1063	340
Upper Zambezi	12600	1522	1464	505	959

***** see **Chapter 5** for details on how river lengths were calculated in kilometres

6.3.1.1 River longitudinal profiles

The manually extracted elevation data for each of the rivers allows for the graphing of their longitudinal profiles. This section will provide a brief description of the profile of each river as listed in **Table 6.3**. The profiles can also be viewed in combination with the automatically extracted profiles as described in **Appendix 6 (Section 6.2)** or in combination with plotted knickpoints as described in **Section 7.3.1.3** in **Chapter 7**. Where relevant to the descriptions in this section, cross references will be made to figures in these sections. In **Table 6.3**, the rivers are described by basin and arranged alphabetically. The river pixel numbers are reported, as opposed to length in kilometres, as the pixel number represents the number of elevation readings for each river and therefore pixel number can be used as a proxy of river length (each pixel is ~ 90 m long). The river lengths are shown in kilometres.

The Congo river system

Chambeshi River: Of the river's total 416 m change in elevation (see **Table 6.3** and **Chapter 7**, **Figure 7.7**), a ca. 300 m decrease occurs over first ca. 100 km. The river's three knickpoints all occur in the headwater regions. Thereafter, the profile is extremely flat as the river flows into Lake Bangweulu. The entire river is above 1100 m.a.s.l.

Congo River: The Congo River's profile is complex; this large river experiences a 1526 m change in elevation over its entire course of ca. 4000 km (see **Table 6.3** and **Chapter 7**, **Figure 7.8**). It has two major zones of elevation decrease, with the first being a ca. 800 m change that occurs ca. 480 km from the headwater region. Thereafter, the river's gradient is gentle, until the second major zone of decrease. This second zone begins about 500 km upstream of the river's mouth, with a ca. 350 m decrease in elevation. A mere 980 km of the Congo River's course accounts for ca.1150 m of its elevation decrease (that is 75 % of its elevation change occurs over 25 % of its course), with almost all of the rivers 64 knickpoints occurring within this 980 km zone. The remaining 400 m of elevation change occurs over 3200 km of river, which is largely knickpoint-free. Several elevation spikes are noted, corresponding to tall and dense riparian forest cover along the banks and on large in-stream islands.

Kalungwishi River: The profile has three major steps, with the first elevation drop, ca. 200 m over a short distance, occurring ca. 60 km from the headwaters. The second step is ca. 60 km downstream of the first, with an elevation decrease of ca. 150 m. About 60 km downstream of the second is the third and final step, with ca. 100 m drop in elevation. These three major steps account for 450 m of the total 671 m of elevation decrease (see **Table 6.3** and **Chapter 7**, **Figure 7.9**). The majority of the Kalungwishi River's nine knickpoints occur in steep gorges and valleys, with only the first knickpoint (a 30 m fall) not occurring in a cataract scenario.

Kasai River: The Kasai, with a total decrease of 1076 m (see **Table 6.3** and **Chapter 7**, **Figure 7.10**), is one of the four rivers studied which shows an elevation change exceeding 1000 m. Most of this change occurs in the first two-thirds of its course. The upper ca. 1000 km of the Kasai has an overall convex shape, dropping ca. 500 m. After this upper 1000 km, the river experiences a rapid decrease in elevation, dropping ca. 350 m over ca. 400 km. Thereafter, it flattens out, flowing ca. 1000 km with only a 200 m elevation drop. The Kasai's 47 knickpoints predominantly occur in its middle

reaches, being densely clustered in the more convex parts of the profile. The river's last 1000 km, where it flows in the *cuvette centrale*, is free of knickpoints.

Kwango River: The Kwango also has an elevation change exceeding 1000 m, dropping 1103 m along its course (see **Table 6.3** and **Chapter 7**, **Figure 7.11**), mostly over the first half of the river. Four major drops are discernible along the Kwango's entire profile. The first, at ca. 55 km from the headwaters, is a ca. 30 m drop over ca. 10 km. The second, around ca. 300 km from the headwaters, shows a 50 m decrease. The third zone of decrease occurs over ca. 130 km (starting about 440 km from the headwaters) with an elevation change of over 200 m. The fourth drop is found ca. 710 km from the headwaters; here the with river drops more than 120 m over ca. 17 km. These zones of decrease are separated by low gradient stretches of river. Downstream of the fourth zone of major elevation decrease, the river has a gentle, slightly convex shape until its end. The majority of the Kwango's 18 knickpoints occur where the river flows off the plateau to enter the Kwango valley, with two major knickpoints occurring within the valley. There are no knickpoints in the lower reaches of the river.

Luapula River: The 600 km Luapula has two major drops, which gives it a step-like shape, accounting for nearly all of its 241 m of elevation change (see **Table 6.3** and **Chapter 7**, **Figure 7.7**). The first drop sees a ca. 100 m decrease in elevation over ca. 35 km (starting at about 115 km from its source). The second drop sees a ca. 80 m elevation decrease over a 30 km stretch of river, starting ca. 390 km from the river's headwaters. After the second drop the profile is very flat, with little elevation change. The two major drops, over a combined distance of 60 km, account for over 180 m of the total 241 m elevation change. Four of the Luapula's seven knickpoints occur as it flows out of Lake Bangweulu, with the remaining three knickpoints found just before the river flows into the valley of Lake Mweru.

Lufira River: The upper and lower reaches of the Lufira are predominantly convex and it has two zones of elevation decrease. The majority of the river's total 853 m elevation change (see **Table 6.3** and **Chapter 7**, **Figure 7.12**) occurs within the two major zones of elevation drop. The first drop is of ca. 100 m, over 30 km, starting ca. 220 km from the river's headwaters. The start of this drop corresponds to a dam wall. Separating the first major step from the second is a large flat, depositional plain containing numerous wetlands and open water-bodies (the Kundelungu Swamps). The second drop, starting 430 km from the headwaters, sees a ca. 80 m decrease over ca. 40 km.

Thereafter, the lower Lufira has a concave profile, initially flowing through steep–sided valleys (topographic interference is the responsible for elevation spikes) that widen progressively until the river finally flows into Upemba Swamps. Nine of the 11 knickpoints occur in the zones of rapid elevation decrease.

Lufupa River: The upper half of Lufupa is convex, with a zone of major decrease in elevation terminating this convexity. This zone begins ca. 170 km downstream of headwaters; here, the river drops ca. 200 m over about 37 km. Thereafter, the river experiences a fairly constant decrease in elevation, until the last ca. 40 km of the river, where it drops ca. 100 m. It is over the last 40 km that nine of the 21 knickpoints occur. Seven of the remaining 12 knickpoints occur on the zone of convexity. The river's total elevation decrease is 854 m (see **Table 6.3** and **Chapter 7**, **Figure 7.13**).

Lukuga River: The Lukuga comprises two sections. The first section is predominantly convex, forming the first third of the river (ca. 100 km) while the remaining two-thirds of the river (ca. 220 km) is dominantly convex. Most of its 220 m elevation decrease (see **Table 6.3** and **Chapter 7**, **Figure 7.14**) occurs in the first half of the rivers course. The first third (220 km) of the river experiences an elevation decrease of ca. 60 m. Most of the elevation decrease occurs along the second third, over a ca. 58 km zone, beginning ca. 100 km from the headwaters) with ca. 100 m of the total decrease occurring in this zone. All of the Lukuga's eight knickpoints occur along the upstream half of its profile, with no knickpoints occurring once it reaches the CB level.

Lulua River: The Lulua has four zones of notable elevation decrease, two of which are major. The first zone begins ca. 90 km from the headwaters, with the river dropping ca. 230 m over ca. 80 km. A small distinct drop of 30 m over 12 km occurs about 280 km downstream of the first. Starting ca. 900 km from the headwaters, the third drop has an elevation change of ca. 270 m over ca. 135 km. The river experiences its fourth drop ca. 30 km downstream from the third; here, the river drops ca. 40 m over ca. 18 km. The two major zones of elevation change account for 500 m of the total 844 m change in elevation (see **Table 6.3** and **Chapter 7**, **Figure 7.15**). Of the Lulua's 30 knickpoints, 24 occur within the two major zones of elevation decrease, with six knickpoints corresponding to the two minor elevation drops.

Luvua River: The Luvua has five drops over its 506 km course, with all of its 20 knickpoints occurring in these zones. These five steps account for ca. 305 m of the rivers total 365 m decrease in elevation (see **Table 6.3** and **Chapter 7**, **Figure 7.7**). The first step occurs ca. 120 km from the profile start, dropping ca. 45 m over ca. 16 km. The second is ca. 15 km downstream, where the river drops 71 m over ca. 12 km. Downstream of the second step, (ca. 15 km) the third drop, of 69 m, occurs over ca. 26 km. In terms of elevation change, the fourth step (ca. 300 km from the headwaters) is the largest, dropping ca. 95 m, but is this change occurs over ca. 50 km and so this step has a lower slope. The last drop is ca. 30 km downstream of the fourth drop, with a ca. 25 m elevation change over ca. 15 km.

Wamba River: In terms of elevation, the Wamba River is the noisiest of the rivers, with numerous and frequent elevation spikes. This makes the interpretation of the river's total 871 m drop difficult (see **Table 6.3** and **Chapter 7**, **Figure 7.16**). This noise is probably due to the interplay between channel width and the proximity of dense, tropical forest along the middle and lower sections of the river. This forest canopy is probably the dominant cause of the large elevation spikes. The Wamba's upper region is convex, with the river decreasing ca. 470 m over its first ca. 130 km; half of this elevation decrease occurs in the last 40 km of the 130 km stretch, producing a convex shape. Eight of the Wamba's knickpoints occur along the convexity of the profile in the rivers upper reaches. Thereafter, the river gradually drops ca. 400 m over ca. 660 km to enter the Kwango River at an elevation of 312 m.a.s.l. The remaining knickpoints are distributed, seemingly randomly, in the middle to lower reaches, with no knickpoints being found where the Wamba flows in the *cuvette centrale*.

The Kalahari river system

Cubango River: The Cubango River experiences an 897 m change in elevation (see **Table 6.3** and **Chapter 7**, **Figure 7.17**), with three of the four main zones of elevation decrease occurring in its upper reaches. The first two zones are the largest, both exceeding 200 m. The first decrease is ca. 240 m over the first ca. 85 km of the river. The second drop is found ca. 465 km downstream, with a ca. 250 m change over ca. 180 km. About 60 km downstream of the second, the third zone of change occurs, with the river decreasing ca. 60 m over 60 km. Thereafter the Cubango has a shallow gradient, only broken by the fourth and final drop of ca. 20 m over 35 km. This final drop begins ca. 400 km upstream of the river's end, representing the start of the Okavango Delta. The distinct

nature of these decreases in elevation is highlighted by the fact that all of the Cubango's 55 knickpoints are confined to these zones.

Cuchi River: The profile of Cuchi is broken by three zones of change, with the toe of the profile being slightly convex. These breaks disrupt the low gradient of the Cuchi, with the middle stretch being almost flat. The river sees a 566 m decrease in elevation over its course (see **Table 6.3** and **Chapter 7**, **Figure 7.18**). Of the 14 knickpoints, eight are associated with the steps, four with the convex toe end and two occur along otherwise low gradient sections.

Kabompo River: The river falls a total of 464 m over its course (see **Table 6.3** and **Chapter 7**, **Figure 7.19**), having only four knickpoints. The upper profile of the Kabompo is convex, with the river's second knickpoint marking the end of this convexity and the start of a very low gradient profile (about 85 km from its headwaters). This convex zone accounts for ca. 325 m of the total 464 m drop, representing the river's major zone of elevation decrease.

Kafue River: The Kafue River is the fourth of the rivers studied (and the only Kalahari river) that experiences an elevation change greater that 1000 m, with a 1006 m change in elevation (see **Table 6.3** and **Chapter 7**, **Figure 7.20**). About 600 m of this elevation decrease occurs in the Kafue Gorge near the river's end. This gives the profile a single large step in elevation, with the upstream zone of the river being relatively flat. The middle portion of the river is where 10 of the Kafue's 14 knickpoints occur, although they only account for a ca. 115 m fall over ca. 280 km.

Luena River: The ca. 430 km Luena River profile is overall concave, with the upper and middle reaches being concave and its extensive lower reach nearly flat. The lower, low gradient portion, experiences a ca. 70 m elevation change over ca. 300 km, whereas the first ca. 130 km accounts for ca. 260 m of the river's total 340 m drop (see **Table 6.3** and **Chapter 7**, **Figure 7.21**). Nine of the river's ten knickpoints are found in this upper concave region, with a single knickpoint occurring close to the river's end, before it flows into the Upper Zambezi River.

Upper Zambezi River: For the most part the Upper Zambezi has a low gradient profile. The majority of the river's 959 m decrease in elevation occurs at the start and finish of the longitudinal profile (see **Table 6.3** and **Chapter 7**, **Figure 7.22**). Although a gradient change is visible, the upper reaches

do not have any discernible knickpoints. The lower reaches are the location of 20 of the 24 knickpoints, with the lower third of the river accounting for most of the elevation decrease.

6.3.2 Generated rivers compared to digitised rivers

In order to determine if the cost-to-benefit (in terms of time) of manually delineating rivers was worth the increased accuracy compared to automatically extracted river profiles, profiles produced by each method are compared (see **Tables 6.4** and **6.5**; also see **Appendix Chapter 6** for graphical representations). The manually determined profiles were compared to the automatically extracted profiles at 30 arc-second ("Auto30") and 3 arc-second ("Auto3") resolutions (see Section **6.2** for how these profiles were determined). In terms of length, the difference between manually versus automatically extracted rivers is, on average 7 % (**Table 6.4**). In terms of basin-wide length differences, the CB averages an ~ 6 % difference and the KB has an ~ 8 % difference. Therefore, on a regional scale the differences appear acceptable.

Nevertheless, in terms of individual rivers, there is a large degree of variation of difference in river length (see **Table 6.4**). Comparing the lengths of the automatically and manually extracted rivers, for the CB, the Chambeshi River has the least percent difference (~ 0.5 %) while the Lukuga River has the largest (~ 13 %). For the KB, the Luena showed the least difference (~ 1 %) and the Kabompo showed the largest difference (~17 %). Five rivers have variations of around of 10 % or more, these being the Luapula (~ 11 %), Lukuga (~ 13 %), Kabompo (~ 17 %), Kafue (~ 11 %) and Upper Zambezi (~ 10 %). The automatically extracted versions of the Luapula and Lukuga Rivers are longer (indicated by the negative sign in **Table 6.4**) than their manually extracted equivalents, whereas the Kabompo, Kafue and Upper Zambezi automatically extracted rivers are shorter than their manually derived courses. This may be due to the nature of the surrounding topography, with the Luapula and Lukuga having large portions of their course in topographically rough areas, while the Kabompo, Kafue and Upper Zambezi Rivers have extensive floodplains and wetlands for large portions of their length (see **Appendix 6,** and **Section 6.2**). Therefore, in terms of river length (as measured by number of pixels crossed) there is substantial variation, both between the lengths of manually and automatically generated rivers and also in terms the percent of difference in lengths of the rivers. This makes it difficult to define a standard error in terms of river length.

Table 6.4: Comparison of river lengths, as measured in the number of 3 arc-second pixels. A negative sign indicates cases where the generated profiles are longer than the manually determined profile.

River name	Digitised pixel No.	**Auto30 pixel No.**[1]	Auto3 pixel No.	**Percent difference (auto30/manual)**	Percent difference (auto3/manual)
Congo Basin					
Chambeshi	6683	**666**	6651	**0.3**	0.5
Congo	42715	**4492**	44920	**(-) 5.2**	(-) 5.2
Kalungwishi	2686	**255**	2548	**5.1**	5.1
Kasai	20718	**2179**	22177	**(-) 5.2**	(-) 7.0
Kwango	14661	**1382**	13813	**5.7**	5.8
Luapula	5969	**660**	6595	**(-) 10.6**	(-) 10.5
Lufira	6558	**607**	6063	**7.4**	7.5
Lufupa	5168	**480**	4794	**7.1**	7.2
Lukuga	3283	**370**	3700	**(-) 12.7**	(-) 12.7
Lulua	11290	**1134**	11333	**(-) 0.4**	(-) 0.4
Luvua	3932	**390**	3894	**0.8**	1.0
Wamba	8869	**806**	8060	**9.2**	9.2
Kalahari Basin					
Cubango	17074	**1685**	16841	**1.3**	1.4
Cuchi	5118	**469**	4683	**8.4**	8.5
Kabompo	6568	**548**	5477	**16.6**	16.6
Kafue	14744	**1313**	13124	**10.9**	11.0
Luena	4313	**436**	4352	**(-) 1.1**	(-) 0.9
U. Zambezi	12600	**1386**	13852	**(-) 10.0**	(-) 9.9
		Congo average		**5.8**	6.0
		Kalahari average		**8.1**	8.1
		Total average		**6.6**	6.7

[1] Auto30 had a 30' pixel size, which is 10 times the size of Auto3 and digitised pixels

6.3.2.1 Comparison of generated longitudinal profiles to digitised longitudinal profiles

A comparison of the automatically generated profiles to the manually digitised profiles allows for the assessment of longitudinal fidelity of the automated method. Differences between generated and digitised longitudinal profiles are of primary concern. The automatically generated profiles consist of two pixel resolutions: a 30 and a 3 arc-second resolution, referred to as Auto30 and Auto3, respectively. The profiles that are manually digitised are interchangeably referred to as manual or digitised. **Table 6.5** summarises the comparisons of the river profiles from the hole-filled 30 arc-second SRTM data and the 3 arc-second SRTMv3 data (for graphic comparisons of individual rivers see **Appendix 6**, **Section 6.2**). The table shows that there is a smaller variation in the profile finish (end) elevations between the manually digitised and the generated rivers compared to their start (source) elevations. The headings D-30 and D-3 refer to the elevation difference between digitised ("D") and generated ("30" for Auto30 and "3" for Auto3) river elevations for the same location along the profile. For example, the elevation of pixel 320 for the automatic profile is subtracted from pixel

320 of the manual profile. Subtraction is, therefore, only done when pairs of cell exist as the aim of the analysis is to determine the accuracy, in terms of elevation, of the automatically extracted profiles.

Table 6.5 shows that the overall variation of elevation for the generated rivers of the CB is 230 m for Auto30 profiles and 269 m for Auto3 profiles, whereas in the KB, the variation for Auto30 profiles is 244 m and for Auto3 profiles it is 297 m. Taking results for both basins, Auto30 averages a 234 m elevation variance, with Auto3 showing a 277 m variation. This variation in elevation relative to the digitised profiles is negatively skewed, that is, elevations are higher than the corresponding manually derived elevation. This variation represents the extreme spikes and holes present in the automatically generated extracted river elevations and a visual inspection of the profiles (see **Appendix 6**, **Section 6.2**) shows that there is no systematic distribution of these spike and holes. However, spikes are often (but not always) associated with narrow valleys and gorges, and represent introduced errors from the hole-filling of the SRTMv3 data required to produce the hydrological analysis (see **Section 6.2**). Holes are not an issue for the Auto30 profiles but occur along the Auto3 profiles, likely representing areas where the generated river course crosses valleys.

In terms of individual rivers in the CB, the generated Congo River has the greatest variation at 683 m (Auto30) and 676 m (Auto3), being ranked 1 for both types of long profiles (see **Table 6.6**). Being in a zone of high relief, the Lukuga River unexpectedly has the lowest variation for Auto30 (44 m, D-30 rank 12), while the Luapula is the lowest for Auto3 at 132 m (D-3 rank 12) (see **Table 6.6**). For the KB, the Kafue River shows the greatest total variation at 508 m (for Auto30) and 670 m (for Auto3), being ranked 1 for both (see **Table 6.6**). The Luena River with 75 m (Auto30) and 79 m (Auto3) is the river of lowest variation in elevation, being ranked 6 for both (see **Table 6.6**).

Table 6.5: Comparison of digitised and automatically derived river elevations[a]. The start and finish elevation of each river profile is shown. The minimum and maximum differences between digitised and Auto30 (D-30) and digitised and Auto3 (D-3) is indicated.

River name	Start digitised	**Finish digitised**	Start Auto 30	**Finish Auto 30**	D-30 Max	**D-30 Min**	Start Auto 3	**Finish Auto 3**	D-3 Max	**D-3 Min**
Congo Basin										
Chambeshi	1576	**1160**	1558	**1163**	7	**-106**	1565	**1160**	21	**-143**
Congo	1526	**0**	1471	**1**	371	**-312**	1486	**3**	404	**-272**
Kalungwishi	1592	**921**	1536	**1015**	40	**-106**	1539	**994**	53	**-94**
Kasai	1348	**272**	1331	**307**	5	**-166**	1318	**272**	69	**-154**
Kwango	1395	**292**	1329	**307**	122	**-202**	1329	**297**	158	**-258**
Luapula	1162	**921**	1163	**1015**	19	**-94**	1163	**921**	39	**-93**
Lufira	1415	**562**	1390	**565**	172	**-309**	1376	**564**	187	**-125**
Lufupa	1485	**631**	1454	**639**	92	**-38**	1454	**640**	106	**-43**
Lukuga	767	**547**	797	**554**	-4	**-48**	783	**547**	6	**-137**
Lulua	1225	**381**	1209	**415**	57	**-59**	1218	**401**	65	**-112**
Luvua	921	**556**	1015	**562**	34	**-256**	977	**560**	56	**-397**
Wamba	1183	**312**	1095	**324**	75	**-64**	1099	**311**	95	**-137**
Kalahari Basin										
Cubango	1834	**937**	1773	**942**	97	**-56**	1780	**938**	105	**-45**
Cuchi	1757	**1191**	1734	**1197**	55	**-63**	1737	**1197**	67	**-64**
Kabompo	1495	**1031**	1493	**1034**	33	**-116**	1495	**1033**	57	**-192**
Kafue	1375	**369**	1352	**505**	477	**-31**	1352	**430**	615	**-55**
Luena	1403	**1063**	1381	**1076**	7	**-68**	1401	**1062**	13	**-66**
U. Zambezi	1464	**505**	1408	**857**	33	**-429**	1391	**882**	73	**-430**
Average variation of elevation										
	Congo Basin			Auto30	83	**-147**	Auto3		105	**-164**
	Kalahari Basin			Auto30	117	**-127**	Auto3		155	**-142**
	Total average				94	**-140**			121	**-156**

[a] Where generated rivers where shorter/longer than manual rivers, elevation differences are not reported for these mismatching sections, as comparing a known to an unknown is not informative in this case.

Variation of elevations is not systematically related to river length or to the difference in generated river length relative to digitised river length, as shown in **Table 6.6**. For example, the 6th longest river (the Chambeshi River), being ranked 10th and 8th for Auto30 and Auto3 respectively, has the smallest difference in length (ca. 0%) but is ranked 10th (Auto30) and 8th (Auto3) in terms of elevation variation. While portions of several of the longitudinal profiles may be within acceptable limits of variation (see **Appendix 6**, **Section 6.2**), the occurrence of large, non-systematic variations, as evidenced in **Table 6.5** and **Table 6.6**, means that for studies requiring the accurate placement of river elevation, automatically generated river long profiles, as conducted in this study, are of limited use. As the quality of automatically extracted elevations remains uncertain, the only observation that can be made is that there is a likelihood that the elevation will be shown to be higher than the real elevation.

Table 6.6: The total variation of elevation for automatically generated rivers, compared to manually digitised rivers. Rank of variation and length as well as average percent difference in length of automatically versus manually extracted rivers.

River name	Total M-30 variation (m)	**Rank (largest to smallest D-30)**	Total D-3 variation (m)	**Rank (largest to smallest D-3)**	Length rank (manual)	**Average length percent difference (nearest %)**
Congo Basin						
Chambeshi	113	**10**	164	**8**	6	**0**
Congo	683	**1**	676	**1**	1	**5**
Kalungwishi	146	**6**	147	**10**	12	**5**
Kasai	171	**5**	223	**6**	2	**6**
Kwango	324	**3**	416	**3**	3	**6**
Luapula	113	**11**	134	**12**	8	**11**
Lufira	481	**2**	312	**4**	7	**8**
Lufupa	130	**8**	149	**9**	9	**8**
Lukuga	44	**12**	143	**11**	11	**13**
Lulua	116	**9**	177	**7**	4	**0**
Luvua	290	**4**	453	**2**	10	**1**
Wamba	139	**7**	232	**5**	5	**10**
Kalahari Basin						
Cubango	153	**3**	150	**4**	1	**1**
Cuchi	118	**5**	131	**5**	5	**9**
Kabompo	149	**4**	249	**3**	4	**17**
Kafue	508	**1**	670	**1**	2	**11**
Luena	75	**6**	79	**6**	6	**1**
U. Zambezi	462	**2**	503	**2**	3	**10**

While further analysis of each river to see where exactly the major deviations of elevation occur would be interesting (for example, investigating the deviations of elevations of manual and automatically extracted elevation data normalised to elevation histograms), this would not add to the overall assessment of the quality of automatic elevation extraction. The variation of elevation of automatically extracted rivers (as seen in **Table 6.5**, **Table 6.6** and **Appendix 6**, **Sections 6.2.1** and **6.2.2**) is sufficiently variable to be of concern in achieving one of the primary objectives of this study, which is the precise location and characterisation of knickpoints along these rivers. The findings for the comparison of the profiles for each river are discussed in detail below, firstly for the Congo rivers and subsequently for the Kalahari rivers.

Comparison of Congo rivers

Chambeshi River: In terms of overall shape, the two automatically generated profiles are similar to the manual profile (see **Appendix 6**, **Section 6.2.1**, **Figure A6.1**) with total length showing less than 1 % difference (see **Table 6.4**). The generated river profiles, Auto30 and Auto3, have a positive elevation offset in the upper and middle reaches (see **Appendix 6**, **Section 6.2.1**, **Figure A6.1**). In the lower reaches the difference in elevations is minimal. The increased noise for Auto3 in the middle and upper reaches suggests that this offset in elevation is probably a function of the required hole-filling of the DSM. This offset is highlighted in the range of values shown in **Table 6.5**, with both automatically generated profiles having similar terminal elevations (within a 5 m error) but a wide range of elevation mismatches. The Auto30 and Auto3 profiles start at 18 m and 11 m, respectively, below the digitised Chambeshi start. The range of elevation offsets (elevation at the same location in terms of distance) is 7 m below and 106 m above for Auto30, compared to the corresponding manually extracted elevation points. For Auto3 this range is 21 m below and 143 m above. The mismatch is skewed to over-reporting the elevation of the same location.

Congo River: The two generated profiles maintained the overall profile shape with respect to that generated manually (see **Appendix 6**, **Section 6.2.1**, **Figure A6.2**). Compared to the manual profile, the automated profiles are positively offset (higher elevation) in the middle and lower reaches of the river, being ~ 5 % longer than the manually determined river (see **Table 6.4**). For the lower reaches of the Congo, the generated profiles are extremely noisy compared to the manual profile. This is probably a function of the rough relief of the Western Rise. Overall, Auto3 is the nosiest profile. Elevation comparisons indicate that Auto3 has large variation from the manual profile, with a maximum underestimation of -404 m and overestimation of +272 m (**Table 6.5)**. The results for Auto30 show a similar overall elevation variation (~ 680 m) with an under-reporting of -371 m and over-reporting of +312 m.

Kalungwishi River: A good fit exists for the upper and middle reaches in terms of shape for the three profiles, yet the shape of the lower reaches is dissimilar (see **Appendix 6**, **Section 6.2.1**, **Figure A6.3**). The automatically generated profiles are ~ 5 % longer than the manually delineated river (see **Table 6.4**). The Auto30 and Auto3 profiles under- and over-report elevations relative to the manually derived elevations, having a range of +40 and -106 m, and +53 and -94 m respectively (see **Table 6.5**). The last section of the Auto30 profile is highly elevated compared to the manual profile, while the Auto3 is very noisy in the lower section.

Kasai River: The upper and middle reaches of the three profiles have good fit in terms of shape, with the lower reaches beginning to diverge with regards to shape, especially for Auto3 (see **Appendix 6**, **Section 6.2.1**, **Figure A6.4**). Auto3 is extremely noisy, with large 'holes' in the foot of the profile. The automatically generated profiles return lengths (Auto 30 ~5 % and Auto3 ~7 %) longer than the manually extracted river (see **Table 6.4** and **Appendix 6**, **Section 6.2.1**, **Figure A6.4**). The elevation range of Auto30 is -5 to +166 m with the profiles terminal elevation being 35 m higher than the manual river (see **Table 6.5**). For Auto3, the profile under- and over-reports elevations by a maximum of 69 and 154 m, relative to the manually delineated river elevation.

Kwango River: The generalised shapes of the three profiles are comparable for the upper and middle reaches (see **Appendix 6**, **Section 6.2.1**, **Figure A6.5**). There are large deviations in terms of shape between the three, especially in the lower-middle and lower reaches (see **Appendix 6**, **Section 6.2.1**, **Figure A6.5**, and **Table 6.5**). The range of elevation deviations is in excess of 320 m, with the lower reaches of Auto3 and Auto30 accounting for most of this deviation. The lower reaches of Auto3 are too noisy to be useful (see **Appendix 6**, **Section 6.2.1**, **Figure A6.5**, and **Table 6.5**). The manually derived river profile is ~6 % longer than the automatically extracted rivers (**Table 6.4**).

Luapula River: Both the Auto3 and Auto30 profiles show large deviations from the shape of the manually derived profile from the middle reaches downstream (see **Appendix 6**, **Section 6.2.1**, **Figure A6.6**). The lower reaches of Auto3 has numerous spikes and holes, while Auto30 has a distinct stepped form with its lower reaches 94 m higher than the manual profile (see **Appendix 6**, **Section 6.2.1**, **Figure A6.6,** and **Table 6.5**). The range of the deviation of elevation for Auto3 is -19 and +94 m and Auto30 is -39 and +93 m and both generated profiles are ~11 % longer than the digitised river length (see **Table 6.4**). It is the flatter regions that appear to be most problematic in terms of elevation, and the filling of the central basin has led to the +96 m offset.

Lufira River: In terms of shape, there is close agreement between the three profiles for the upper reaches (see **Appendix 6**, **Section 6.2.1**, **Figure A6.7**). The middle and lower reaches of Auto3 and Auto30 are very noisy with large spikes in elevations, the spikes being a maximum of 125 and 309 m for Auto3 and Auto30 respectively (see **Appendix 6**, **Section 6.2.1**, **Figure A6.7**, and **Table 6.5**). In addition, Auto3 and Auto30 both underestimate the length of the Lufira by ~7 %, showing an offset in terms of the elevation changes compared to the manual profile (see **Table 6.4** and **Appendix 6**, **Section 6.2.1**, **Figure A6.7**).

Lufupa River: Overall, there is close agreement between the three profiles in terms of shape and elevation values (see **Appendix 6**, **Section 6.2.1**, **Figure A6.8**, and **Table 6.5**). The generated profiles under-report the elevation in the middle and lower reaches with the lengths being ~7 % shorter than the digitised river (see **Table 6.4** and **Table 6.5**). This deviation of the middle and lower reaches and shorter length is probably due to the hole-filling of the DSM.

Lukuga River: There is a consistent positive offset in terms of elevation of the Auto30 profile relative to the manual profile (see **Appendix 6**, **Section 6.2.1**, **Figure A6.9,** and **Table 6.5**). The profile of Auto30 closely agrees with the shape of the manual profile (see **Appendix 6**, **Section 6.2.1**, **Figure A6.9**). Auto3 has numerous large elevation spikes making most of its profile ill-defined and only the lower reaches match the shape of Auto30 (see **Appendix 6**, **Section 6.2.1**, **Figure A6.9,** and **Table 6.5**). Both Auto3 and Auto30 are ~13 % longer than the digitised profile (see **Table 6.4**).

Lulua River: The three profiles are similar in shape with only the extreme lower section of Auto3 and Auto30 differing substantially from the digitised profile (see **Appendix 6**, **Section 6.2.1**, **Figure A6.10**). The greatest difference in elevation occurs in the lower section of the profiles, with Auto3 largest elevation spike being +112 m (see **Table 6.5**). The three river lengths are nearly equal, with 0.4 % difference (see **Table 6.4**). The variations in elevation seem to be most noticeable in areas where the river enters the central CB. The generated profile of the Lulua River appears to be the most accurate of the generated profiles.

Luvua River: There is significant mismatch in the upper and middle reaches of the three profiles in terms of elevation and shape (see **Appendix 6**, **Section 6.2.1**, **Figure A6.11**).Large elevation spikes are present in the upper and middle zones of both Auto3 and Auto30 profiles (see **Appendix 6**, **Section 6.2.1**, **Figure A6.11,** and **Table 6.5**). The variation of elevation is an under- and over-reporting of -34 and +256 m for Auto30 and -56 and +397 m for Auto3 (see **Table 6.5**). The lower sections of the three profiles are similar, with little difference in length between the digitised and generated rivers (see **Table 6.4**).

Wamba River: While the digitised profile is itself noisy, the Auto3 profile has no clear, discernible profile due to noise (see **Appendix 6**, **Section 6.2.1**, **Figure A6.12**). Auto30 has a markedly stepped nature, with elevations above the manual profile in the upper and middle reaches and elevations below the manual profile in the lower reaches (see **Appendix 6**, **Section 6.2.1**, **Figure A6.12,** and

Table 6.5). The total range of elevation variation of Auto30 and Auto3 is 139 and 292 m, respectively, with both profiles being ~9 % shorter than the digitised river (see **Table 6.4**).

Comparison of Kalahari rivers

Cubango River: There is a general similarity in the shape of the three profiles. However, the middle reaches show a major discrepancy with the generated profiles showing a negative elevation offset relative to the digitised profile. This discrepancy is associated with a deviation in shape from the digitised convex to more concave profile in Auto30 and Auto3 (see **Appendix 6**, **Section 6.2.2**, **Figure A6.13**). The automatically generated rivers are slightly longer (~1 %) compared to the digitised river (see **Table 6.4**). The starts of the generated profiles are offset by 61 m (Auto30) and 54 m (Auto3) relative to the digitised profile (see **Table 6.5)**. Auto30 under-reports elevation values by a maximum of 97 m and over-reports by a maximum of 56 m, while Auto3 has offsets of -105 m and +45 m (see **Table 6.5**).

Cuchi River: Apart from the stepped nature of Auto30, the three profiles match in terms of overall shape (see **Appendix 6**, **Section 6.2.2**, **Figure A6.14**). The stepped nature of Auto30 is probably due to the hole-filling algorithm used on the DSM. This has also led to the lower reaches of the generated profiles having lower gradients compared to the manual profile. Both generated profiles are noticeably shorter (~8.5 % shorter) and noisier compared to the digitised river, even though they have similar ending elevations (see **Table 6.4** and **Table 6.5**). For comparative elevations, the largest offsets of Auto30 are -55 m and +63 m. For Auto3 this offset is similar, being -67 m and +64 m.

Kabompo River: The upper and upper-middle zones of the three profiles match in overall shape, although the generated profiles are noticeably noisier and of lower elevation than the manual profile (see **Appendix 6**, **Section 6.2.2**, **Figure A6.15**). The Auto30 profile has a distinct stepped nature. Both generated rivers are substantially shorter (~17 % shorter) than the digitised river (see **Table 6.4**). This is probably because the channel of generated rivers takes a straight course across a large floodplain through which the Kabompo flows, resulting in an underestimation of the river's length. The elevation offsets of the generated profiles are -33 m and +116 m for Auto30, and +57 m and -192 m for Auto3 (see **Table 6.5**). This large range of elevations of Auto3 is seen in the noisiness of its profile (see **Appendix Chapter 6**).

Kafue River: All three profiles have similar shapes but owing to the shorter lengths (~11 % shorter) of the generated profiles, there is a large elevation offset in the lower reaches (see **Appendix 6**, **Section 6.2.2**, **Figure A6.16,** and **Table 6.4**). This gives the generated river a more compressed form relative to the digitised profile. The Auto3 profile is the noisiest, ranging from -615 m (in the Kafue Gorge region) to +55 m in terms of elevation offsets (see **Table 6.5**). The maximum under- and over-reporting for Auto30 is -477 m and +31 m, with the Auto30 profile ending 108 m higher than the digitised profile (see **Table 6.5**). This significant under-reporting and the decreased lengths are due to the infilling of the Kafue Gorge and the shortening of the river course in the floodplain regions, especially in the Kafue flats.

Luena River: Both the Auto3 and Auto30 profiles are very noisy with numerous small spikes in elevation (see **Appendix 6**, **Section 6.2.2**, **Figure A6.17**). It has the least variation in terms of elevation of all of the KB rivers and, for Auto3, of all studied rivers (it is second smallest for Auto30) (**Table 6.6**). The Auto30 profile under- and over-reports the elevations by -7 and +68 m, with Auto3 having offsets of -13 and +66 m (see **Table 6.5**). There is some agreement of profiles for the lower section of the river, with most of the difference in shapes between the profiles occurring in the upper reaches (see **Appendix 6**, **Section 6.2.2**, **Figure A6.17**).

Upper Zambezi River: Apart from the extreme lower reaches of the profiles, the shape of the three profiles is comparable, although the Auto3 and Auto30 profiles have positive elevation offsets (see **Appendix 6**, **Section 6.2.2**, **Figure A6.18**). Both Auto3 and Auto30 show spikes in elevations for the upper and middle reaches, with profiles becoming more similar in shape relative to the digitised profile downstream. The large variation of elevation, 462 m for Auto30 and 503 m for Auto3, is due to longer length of the generated rivers (~10 %) compared to the digitised river (see **Table 6.4** and **Table 6.6**). This results in a large portion of the lower reach being offset, as shown by the terminal elevations of the generated rivers 857 and 882 m.a.s.l. for Auto 3 and Auto30 respectively, compared with the digitised that ends at 505 m.a.s.l. (see **Table 6.5** and **Appendix 6**, **Section 6.2.2**, **Figure A6.18**).

6.3.2.2 Generated river networks versus digitised courses

The vertical accuracy of the generated rivers is not the only important consideration. The rivers' horizontal accuracy is a key factor and assessment of this accuracy is required in order to have any confidence in the spatial relationship of one profile compared to another. The horizontal accuracy of

the generated rivers compared to the manually digitised rivers is shown in **Table 6.7,** and **Figure 6.8** shows a comparison of the river courses**.** The assessment is based on distances (a UTM projection was used) of the automatically extracted elevation point data to the digitised river courses (polylines). The point data extracted from the generated raster network represents the vertices of the generated river network (polylines), that is, while generated point data were compared in terms of distance, polylines have been used for network display, as seen in **Figure 6.8**, where the generated river course has been derived from the point data.

The assessment of horizontal accuracy was undertaken in order to spatial differences of the generated river elevation points relative to the manually determined river courses. Several generated river point tracks do not have points falling on the digitised rivers courses at all, with these points having minimum distances ranging from 1 to 10 m, although most are less than 5 m but greater than 2 m (see **Table 6.7**). This is not to say that the polylines derived from these data tracks do not cross the digitised rivers but that the vertices (nodes) of these polylines do not fall on the digitised river courses. There is greater variation in terms of maximum distances (see **Table 6.7**).

The five largest maximum distances of deviation are 64 km (Luapula), 62 km (Cubango), 51 km (Kafue), 21 km (Lufira) and 19 km (Congo). The shortest maximum distance was 0.9 km (Cuchi), although this is the only river that has a sub-kilometre maximum distance, the second lowest being the Wamba at 1.4 km. In terms of basin averages, the CB rivers average a 12 km maximum distance, whereas the KB rivers achieve 23 km (almost double that of the Congo rivers). This difference in basins is most likely due to the Kalahari having three rivers with maximum distances greater than 15 km, two of which exceed 50 km (the Cubango, Kafue and Upper Zambezi Rivers). In comparison, the CB has only two rivers exceeding 15 km (Luapula and Congo), with only one over 50 km. While some generated rivers are within acceptable limits of error at a regional scale (i.e. sub 1 km), there is a large variation in terms of the maximum distance (ranging from 0.9 km to 64 km). A 1 km error represents a single pixel offset on the 30 arc minute hole-filled version of the SRTMv3 data. Therefore, horizontal accuracy of the generated rivers, for specific portions of the river course, is questionable.

Table 6.7: The deviation of generated river courses compared to manually digitised river courses. The point data (extracted from the 30 arc seconds DSM) that form the vertices of the generated river courses are spatially compared to the line data of the manual rivers.

River	Minimum (m)	**Maximum (m)**	Mean (m)	**Standard deviation (m)**	Number of elevation points	**Length (km)**
Congo						
Chambeshi	1	**7 425**	1 324	**1 506**	666	**668**
Congo	0	**19 448**	1 663	**2 709**	4492	**4151**
Kalungwishi	10	**4 743**	592	**716**	255	**291**
Kasai	0	**8 852**	711	**1 086**	2218	**2064**
Kwango	0	**7 245**	764	**893**	1382	**1465**
Luapula*	3	**64 294**	5 230	**11 895**	660	**603**
Lufira	2	**20 638**	2 636	**4 118**	607	**681**
Lufupa	1	**2 543**	348	**308**	480	**530**
Lukuga	5	**1 856**	498	**331**	370	**337**
Lulua	1	**5 365**	501	**451**	1134	**1137**
Luvua	3	**5 903**	603	**886**	390	**507**
Wamba	0	**1 446**	382	**269**	806	**922**
Average	2	**12 480**	1 271			
Kalahari						
Cubango	0	**61 929**	3 980	**9 643**	1685	**1708**
Cuchi	2	**949**	300	**207**	469	**524**
Kabompo	1	**2 579**	550	**486**	548	**653**
Kafue	0	**51 077**	3 038	**6 519**	1313	**1529**
Luena	1	**5 200**	1 288	**1 178**	436	**430**
U. Zambezi	0	**15 163**	1 238	**2 101**	1386	**1522**
Average	1	**22 816**	1 732			

*The generated Luapula was longer than the manually delineated river as it only terminated at the end of Lake Mweru; it actually contains 660 elevation points.

Using the mean distance and the standard deviation to analyse the overall accuracy of the river courses as a whole, the horizontal fidelity of the generated river courses is found to be problematic. The rivers of the CB have an average mean distance of deviation of 1.2 km, with individual rivers' means ranging from 0.3 km to 5.2 km. For the KB, the rivers average a mean distance of deviation of 1.7 km, while individual rivers have means that range from 0.3 to 4 km. While some of these means are within acceptable limits at a regional scale, several of them are larger. Furthermore, there is substantial variation in terms of all the distances from the manually delineated rivers as shown by the standard deviation. In the CB, the Chambeshi, Congo, Luapula and Lufira all have standard deviations of greater than 1.5 km (see **Table 6.7**). This means that the elevation points of the majority of these rivers are more than 1.5 km from the manually delineated courses. Similarly, in the

KB, the standard deviations of the Cubango, Kafue and Upper Zambezi are greater than 1.5 km. Thus, majority distribution of the elevation points of seven of the rivers is further than 1.5 km away from the manually delineated courses.

The overall deviation of these generated rivers from the manually digitised rivers is substantial, with seven of the profiles having deviations greater than 1.5 km. This variable quality of the horizontal accuracy of the generated profiles may result in the placement any fluvial features varying substantially.

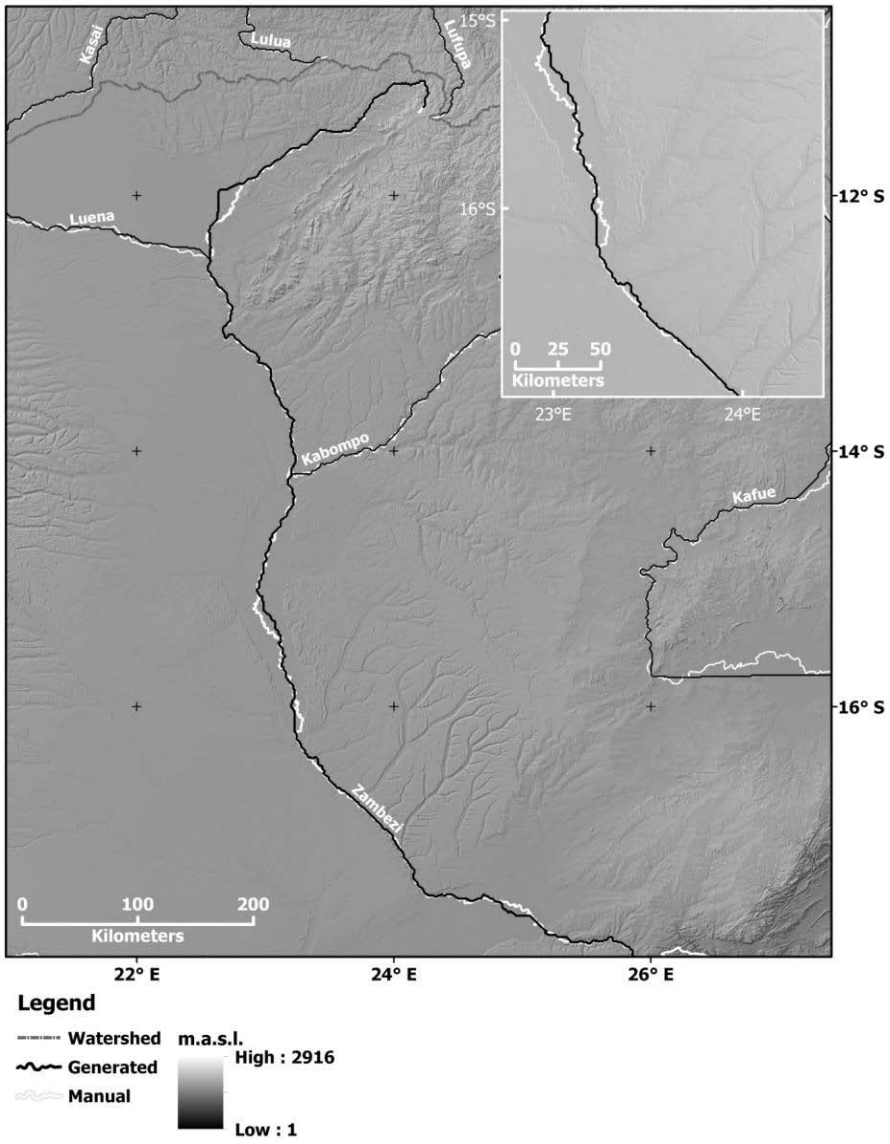

Figure 6.8: Comparison of the manual versus generated river courses. In terms of horizontal accuracy, the generated courses (heavy black line) may deviate substantially from the manually defined courses (heavy white lines), especially in floodplain and low relief zones. Inset shows a magnified section of the Upper Zambezi. Hillshading based on the SRTM 250 m data; elevations from SRTMv3.

6.3.3 Knickpoint categorisation

A total of 380 knickpoints have been identified and characterised across the studied rivers. The overall geographic distribution of these knickpoints is shown in **Figure 6.7**. Often, the knickpoints are clustered spatially, with many zones of high knickpoint density being associated with areas where the rivers cross the escarpment in the CB (see **Figure 6.7**). In addition to the recording of each knickpoint's location, a digital record for each knickpoint was created. An example is shown in **Figure 6.6**. These digital records allow for the characterisation of the qualitative aspects of the knickpoints and provide a checkable reference to any classification made in this study. Additionally, this digital image library also captures interesting or anomalous river and landscape features with the possibility of several of these being studied further in the future.

6.3.3.1 Classification and distribution of knickpoints

A database containing the qualitative and quantitative characterisation of knickpoints was created (see **Table A6.2** in **Appendix 6**, **Section 6.3**). The purpose of this database was to aid with assigning a likely cause for the occurrence of the knickpoints and it provides insights into what may be inferred from these knickpoints (see **Chapter 7**). **Table A6.2** (in **Appendix 6**, **Section 6.3**) lists all 380 identified knickpoints, first in river alphabetical order and secondly in descending elevation. It thus provides the sequential order of a river's knickpoints from headwater (source) to mouth (end). This directory details the local height of a knickpoints (the vertical decrease in elevation of the river), the elevation of the start of the knickpoint (m.a.s.l.), its location (in decimal degrees) and a brief description. Due to the size of this database (**Table A6.2** in **Appendix 6**, **Section 6.3**) a summarised version is presented as **Table 6.8**. Of the 380 characterised knickpoints, the heights of 15 (4 %) knickpoints could not be determined and were assigned a **knickpoint category of 0** (see **Tables 6.1** and **6.8**). For example, knickpoint **272**, on the **Lufupa River**, occurs on an anomalous elevation spike (see **Table A6.2** in **Appendix 6**, **Section 6.3**). A second group of problematic knickpoints were designated as having a **Knickpoint category of -1**, with 26 knickpoints (7 % of the identified knickpoints) being assigned this designation (see **Tables 6.1** and **6.8**). This category incorporates the knickpoints that are evidenced by features on the Landsat imagery that have, through the course of this study, been associated but not definitely shown to be knickpoints and thus are disputable. For example, knickpoint **68** on the **Cubango River** is suggested by its river channel geometry (a straight channel between two meander zones) in combination with Landsat characteristics (light pink suggesting bare rock) and SRTMv3 data (elevations drop rapidly (see **Table A6.2** in **Appendix 6**, **Section 6.3**). Combined, **category 0** and **-1** knickpoints represent 11 % of the total knickpoints

studied. Thus, the heights of 42 knickpoints are uncertain and so do not have a height assigned to them. The remaining 339 knickpoints have heights assigned to them.

Table 6.8: A matrix showing the categorisation of all the knickpoints identified in this study. The number of each knickpoint is given per category and per river and also for the two basins. The total number of knickpoints per river is given on the right with the total number of knickpoints per category given at the bottom of the table. See text for further details regarding categorisation as well as **Table 6.1** and **Table A6.2** in **Appendix 6**, **Section 6.3**.

Feature	**Knickpoint category**																		
	-1	**0**	**-5**	**5**	**10**	**15**	**20**	**25**	**30**	**35**	**40**	**45**	**50**	**60**	**70**	**75**	**80**	**90**	**Total**
Chambeshi	-	-	-	-	1	1	-	-	-	-	-	-	1	-	-	-	-	-	**3**
Congo	2	1	17	17	10	5	2	1	3	-	3	-	1	-	-	-	1	1	**64**
Kalungwishi	-	-	-	-	1	-	2	1	1	-	1	-	1		-	-	2	-	**9**
Kasai	1	-	9	16	11	4	4	1	1	-	-	-	-	-	-	-	-	-	**47**
Kwango	-	-	1	5	1	1	4	1	1	-	-	1	1	-	-	1	-	1	**18**
Luapula	-	-	-	-	1	3	2	-	-	-	-	-	-	-	-	-	1	-	**7**
Lufira	-	-	3	1	1	1	1	-	-	-	-	1	2	-	-	-	-	1	**11**
Lufupa	3	6	3	1	1	2	-	3	1	1	-	-	-	-	-	-	-	-	**21**
Lukuga	-	1	-	2	1	4	-	-	-	-	-	-	-	-	-	-	-	-	**8**
Lulua	3	-	9	3	6	1	5	-	2	-	1	-	-	-	-	-	-	-	**30**
Luvua	-	1	5	3	3	1	5	-	1	-	-	-	1	-	-	-	-	-	**20**
Wamba	6	-	4	2	3	1	2	1	-	-	-	-	2	-	-	-	-	-	**21**
Cubango	9	4	19	4	4	2	8	-	2	1	2	-	-	-	-	-	-	-	**55**
Cuchi	2	-	4	1	-	-	2	-	-	1	1	-	1	2	-	-	-	-	**14**
Kabompo	-	1	1	-	-	-	1	-	-	-	-	-	-	-	1	-	-	-	**4**
Kafue	-	-	2	4	2	1	1	-	-	1	1	-	-	1	1	-	-	-	**14**
Luena	-	1	2	1	4	1	-	-	-	-	1	-	-	-	-	-	-	-	**10**
U. Zambezi	-	-	15	7	1	-	-	-	-	-	-	-	1	-		-	-	-	**24**
Congo Basin	15	9	51	50	40	24	27	8	10	1	5	2	9	-	-	1	4	3	**259**
Kalahari Basin	11	6	43	17	11	4	12	-	2	3	5	-	2	3	2	-	-	-	**121**
Totals	**26**	**15**	**94**	**67**	**51**	**28**	**39**	**8**	**12**	**4**	**10**	**2**	**11**	**3**	**2**	**1**	**4**	**3**	**380**

The knickpoints evidenced in both Landsat and SRTMv3 with heights less than 5 m are designated **category 0** knickpoints and are usually rapids or small cascades (**Knickpoint category 0**, **Tables 6.1** and **6.8**). For example, knickpoint **140** on the **Kabompo River** is characterised by anabranching (angular, island fan), with white-water and a change in direction at the knickpoint (see **Table A6.2** in **Appendix 6**, **Section 6.3**). In total, 94 knickpoints (25 % of all studied knickpoints or 28 % of the 339 knickpoints to which heights were assigned) are categorised as **category -5** (see **Table 6.8**). In terms of occurrence these **category -5** knickpoints are approximately equally distributed, with 54 % being found in the CB and the remaining 46 % in the KB. The remaining knickpoint categories show in

Table 6.8 indicates the height group to which the other 245 knickpoints were assigned (see **Table 6.1** for details). Therefore 64 % of all the knickpoints identified had heights of 5 m or greater (or 72 % of the knickpoints to which heights could be assigned).

The general trend for **category 5** or higher knickpoints is that knickpoint frequency decreases with increasing height; thus, **category 5** has 67 knickpoints, whereas **category 90** has 3 (**Table 6.8**). There is some variation within this overall trend, as categories **20, 30, 40, 50** and **80** all have more knickpoints than the preceding category (see **Table 6.8**). This is probably due to the classification scheme used (see **Table 6.1**) and the nature of the SRTMv3 data that appears to favour the classification of knickpoints into multiples of 10 in terms of elevation bins.

Comparing the basins, the CB has more identified knickpoints, with 259 (68 %) of all the knickpoints categorised (see **Table 6.8**). Of these Congo knickpoints, 235 (91 %) are assigned heights, with 184 (71 %) of these being 5 m or higher (see **Table 6.8**). Looking at the KB, it has 121 (32 %) of the total number of knickpoints identified (see **Table 6.8**). It is possible to assign a height to 104 (86 %) of these knickpoints, with 61 (50 %) having heights of 5 m or higher. The difference in terms of total knickpoint numbers between the Congo and Kalahari Basins is likely a function of more river kilometres being investigated in the CB compared to the KB (for comparative knickpoint frequency see **Table 6.9** and **Figure 6.12** below). While the **category -5** numbers are similar for both basins, there is a greater difference in category numbers for the large height classes (see **Table 6.8**). The CB has 35 (14 %) knickpoints with heights of 30 m or larger (eight of them are 70 m heights or larger), whereas the KB has 17 (14 %) knickpoints with 30 m or larger heights (but only two with 70 m heights and none larger) (see **Table 6.8**).

Looking at the rivers individually, it can be seen in **Table 6.8** that the top five rivers (in terms of total identified knickpoints) are: (i) Congo (64 knickpoints); (ii) Cubango (55); (iii) Kasai (47); (iv) Lulua (30) and (v) Upper Zambezi (24) rivers. Three of these rivers are in the CB and two are in the KB. If categories **-1** and **0** are discounted, the top five rivers stay the same but the order changes to: (i) Congo (61); (ii) Kasai (46); (iii) Cubango (41); (iv) Lulua (27) and (v) Upper Zambezi (24) (see **Table A6.3** in **Appendix 6**, **Section 6.3**). The Cubango River is the only river where the number of knickpoints changes substantially if categories **-1** and **0** are removed. In general, the exclusion of these categories does little to change river rank based on knickpoint numbers, as these categories represent a limited percentage of the total knickpoints identified, although they are more prevalent

in some rivers than others, for example Cubango (13), Lufupa (9) and Wamba (6) (see **Table 6.8** and **Table A6.3** in **Appendix 6, Section 6.3**).

6.3.3.2 Ground truthing of knickpoint heights

During the precise GPS survey (**Chapter 5**), three of the identified knickpoints were visited. Two were along the Kalungwishi River (see **Figures 6.9** and **6.10**) and the third was along the Luapula (see **Figure 6.11**). In-field height estimations were made, with the knickpoints shown in **Figures 6.9** and **6.10** approximating heights as determined from the SRTMv3 data. The field estimation for the height of the Lumangwe Falls was 45 to 50 m (see **Figure 6.9**). The corresponding description for this fall, knickpoint **161** on the **Kalungwishi River,** gives the height as >50 m (but <60 m) and identifies a single fall, with a small angular island above and below an angular channel, with the fall forming the start of a gorge (see **Table A6.2** in **Appendix 6**, **Section 6.3**). Field observations (done after the digitisation of the Kalungwishi River) support the above description for Lumangwe Falls, although field height estimations were lower. This difference between field and SRTMv3-based heights is probably due to the added elevation of the riparian fringe (as seen in **Figure 6.9**) to the SRTMv3 elevations. Further downstream along the Kalungwishi River, the Kaweluma Falls are found (**Figure 6.10**). This knickpoint was estimated as having a height around 35 to 40 m. The SRTMv3 based characterisation, knickpoint **162** on the **Kalungwishi River**, (see **Table A6.2** in **Appendix 6**, **Section 6.3**) puts the height as greater than 40 m (but less than 45 m). The description includes an angular channel with an island fan above the falls, with the falls representing the point where the river enters a second gorge (see **Table A6.2** in **Appendix 6**, **Section 6.3**). There was evidence of radar shadowing in the SRTMv3 data. This, along with the dense riparian fringe (see **Figure 6.10**), is the most likely cause of over reporting of the elevation by SRTMv3 compared to the field estimation.

Figure 6.11 presents a different situation, as it shows some rapids along the Luapula River. The photograph was taken between a well-known set of cataracts known collectively as the Mambilima Falls. The observations of this zone, made during the digitisation of the Luapula River, report a total drop of >80 m (but <90 m) that occurred as several large drops, knickpoint **235** on the **Luapula River** (see **Table A6.2** in **Appendix 6**, **Section 6.3**). The Mambilima Falls is described as having large and small angular islands (see **Table A6.2 in Appendix 6, Section 6.3**), which are visible in **Figure 6.11**. Therefore, while the entire observation for Mambilima Falls was not validated by field observation, some of its associated characteristics were.

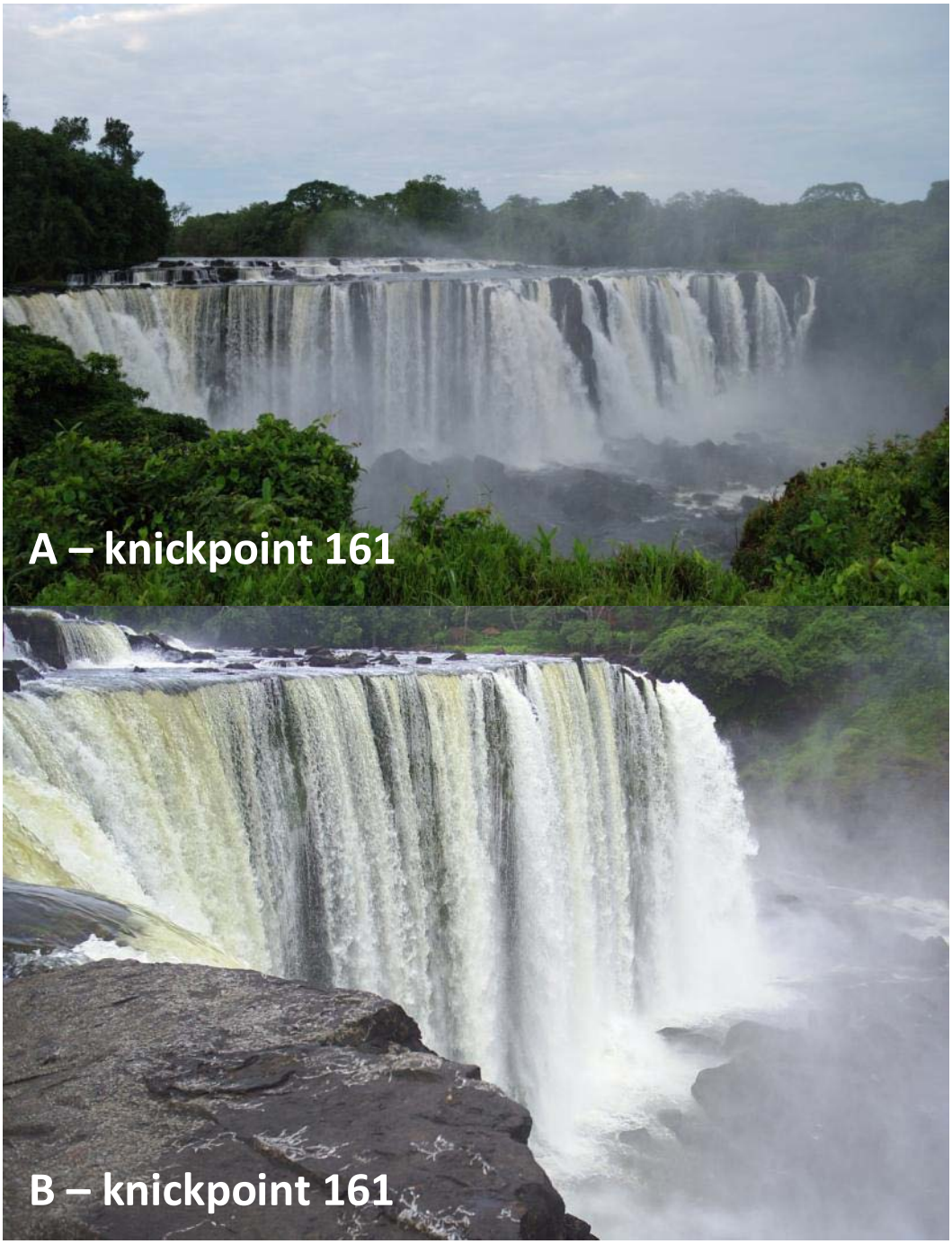

Figure 6.9: Two views of Lumangwe Falls along the Kalungwishi River. (A) Shows the face of the fall looking upstream (photograph: F.P.D. Cotterill). (B) Shows a closer side on view of the fall (facing upstream looking right) (photograph: T.J. Flügel). In field estimation of fall height was 45 to 50 m.

Figure 6.10: Kaweluma Falls looking upstream along the Kalungwishi. In field height estimation of the fall was 35 to 40 m (photograph: T.J. Flügel).

Figure 6.11: Rapids along the Luapula River, looking upstream. These rapids are upstream of a major waterfall of the Mambilima Falls (photograph: F.P.D. Cotterill).

6.3.3.3 Knickpoint density per a river

As the kilometres of digitised river courses were not equal for the two basins in this study, the knickpoint density of the rivers from Congo and Kalahari Basins were compared. In aggregate terms, one may find a knickpoint every 52 km on the studied rivers of the CB and every 53 km in the KB (see **Table 6.9**). Thus, the average knickpoint density for each basin is comparable. Considering knickpoint density per river, there is a broad trend of higher knickpoint densities being associated with longer rivers, and this is more noticeable with rivers of the CB (see **Table 6.9**). Yet, this trend is not prescriptive and the Kafue Rivers' low knickpoint density is a notable exception. Further analysis of the knickpoint number compared to river length reveals that this relationship is not simple (see **Figure 6.12**). While there is a linear trend in terms of knickpoint number compared to river length, this relationship is weak and not systematic. This is particularly true for the KB where the apparent correlation is weak, being 50 % (see **Figure 6.7**). The correlation appears to be stronger in the CB (82 %) but this relation may be due to the greater number of rivers digitised (**Figure 6.7**).

Table 6.9: The length (in km) of each of the digitised rivers, with the number of knickpoints and average knickpoint density per kilometre. See **Section 6.2** to see how the length was determined in km.

River name	Length (km)	No. of knickpoints	Knickpoint density (km.knickpoint^{-1})
Congo Basin			
Chambeshi	667.773	3	223
Congo	4151.306	64	65
Kalungwishi	290.696	9	32
Kasai	2063.770	47	44
Kwango	1465.326	18	81
Luapula	603.450	7	86
Lufira	681.438	11	62
Lufupa	529.951	21	25
Lukuga	337.475	8	42
Lulua	1136.703	30	38
Luvua	506.878	20	25
Wamba	922.304	21	44
Totals	**13357.071**	**259**	**52**
Kalahari Basin			
Cubango	1707.530	55	31
Cuchi	523.667	14	37
Kabompo	653.434	4	163
Kafue	1529.148	14	109
Luena	430.225	10	43
Upper Zambezi	1521.957	24	63
Totals	**6365.962**	**121**	**53**

In the Congo and Kalahari Basins, it appears that river length is not the sole (or even the dominant) controlling factor on knickpoint number. This is especially evident on an individual river scale, where the true heterogeneity of the knickpoint distribution is seen (see **Table 6.9**). For example, the Cubango River has three times the number of knickpoints compared to the Kafue River, even though they are comparable in length; on the other hand, the Kwango and Luapula Rivers have similar densities of knickpoints, even though the Luapula is half the length of the Kwango, and both have higher knickpoint densities than the Congo River. This spatial variability of knickpoints can be seen graphically on **Figure 6.7**.

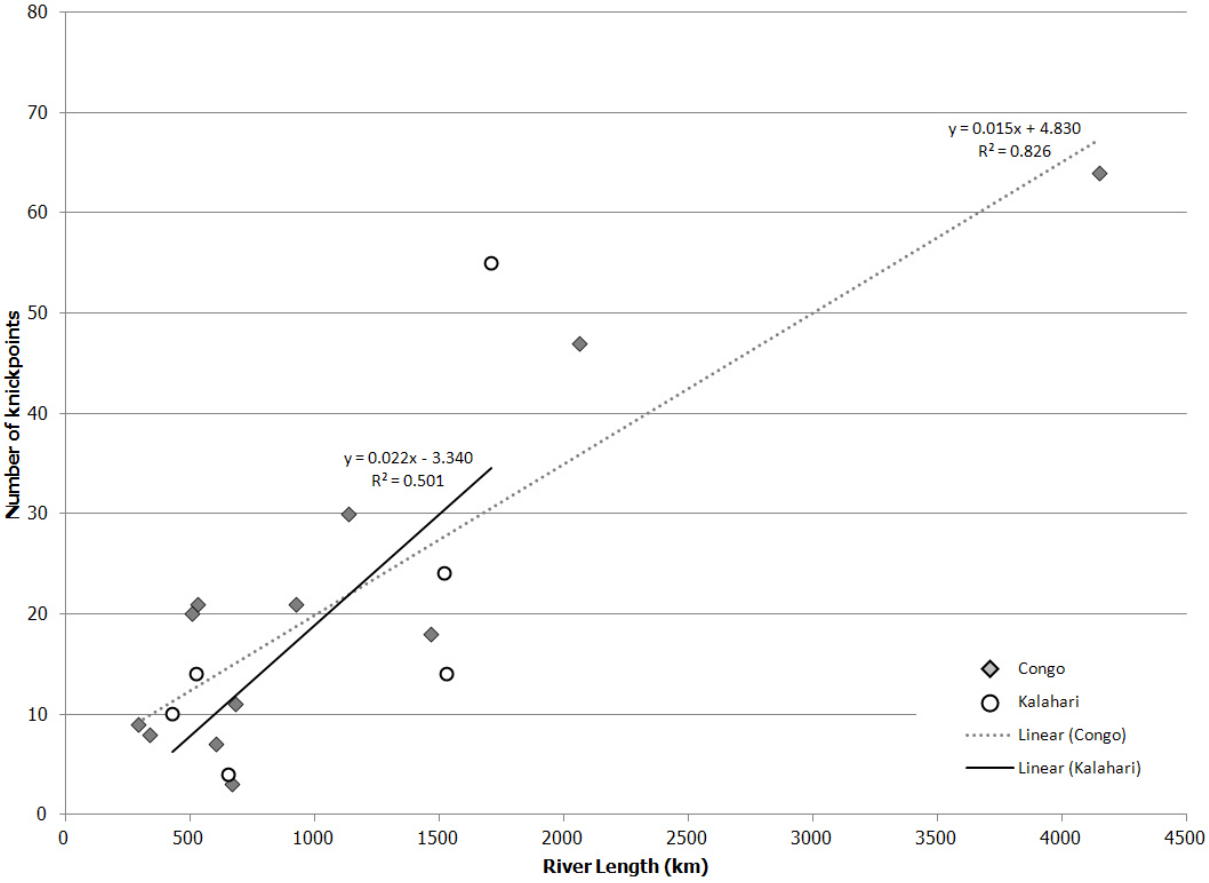

Figure 6.12: The number of knickpoints as a function of river length. While a general trend of increasing river length results in increasing number of knickpoints, this relationship does not appear to be systematic. Therefore, river length is not the sole determining factor of the number of knickpoints in the Congo and Kalahari Basins (based on the studied rivers).

6.4 Discussion of river longitudinal profiles and their associated knickpoints

A total of 18 river profiles were delineated, with ca. 19 900 km of river being digitised and 380 knickpoints characterised (see **Figure 6.7** and **Table 6.7**). In terms of river length, the CB has the two longest rivers, namely, the Congo (ca. 4100 km) and the Kasai (ca. 2100 km), with the other rivers of the CB being less than 1500 km. In the KB, three rivers are 1500 km or longer, namely, the Cubango (ca. 1700 km), the Kafue (ca. 1500 km) and the Upper Zambezi (ca. 1500 km). By comparing the number of knickpoints that occur along a river it can be concluded that, for the studied rivers, river length is not a systematic indicator of knickpoint number nor does it play a dominant role in knickpoint location (see **Figure 6.7** and **Figure 6.12**). This is highlighted by the large variation in knickpoint density across the rivers (see **Table 6.9**).

The discussion below will deal, firstly, with the results of comparing the digitised rivers to the generated rivers. This comparison justified the benefits of the enhanced accuracy of the manual digitisation over its costs in time. Secondly, the digitised river long profiles and knickpoints will be discussed and, in the final sub-section, some of the potential geomorphic implications as evidenced by the digitised long profile and knickpoint data will be assessed.

6.4.1 Comparing digitised rivers to generated rivers

In order to determine if the high degree of accuracy attained by manually digitising rivers was effective in terms of time-to-benefit, the digitised river courses and profiles were compared to a commonly utilised method for generating river courses and profiles (see **Table 6.4** and **Table 6.5**; and see **Appendix 6**, **Section 6.2** for graphical representations). The comparison led to several findings that are discussed here in terms of the river courses and longitudinal profiles.

With reference to the accuracy and usability of the profiles, an important caveat regarding the generated profiles is that elevation points were extracted for a river course that was generated on a 30 arc-second DSM (about 900 m), which is 10 times that of the DSM resolution for the manual rivers (3 arc-second). This introduced the first source of error. The need to hole-fill the 900 m DSM (see **Section 6.2**) provides a second source of error but was necessary because of limited computing power.

6.4.1.1 River courses

Firstly, the initial computational requirements for the generation of the river courses were problematic. Several issues arose owing to the size of the data used (2 GB) in order to cover the study area. This necessitated the degradation of the SRTMv3 3 arc-second (90 m pixel size) to a 30 arc-second (900 m pixel size) DSM. This probably introduced a first layer of potential error in that a single pixel shift in river course translates to a ca. 900 m offset, this shift being due to averaging of the elevation over a 900 m pixel. This is likely to have propagated any elevation artefacts of the SRTMv3 data, especially in flat, homogenous areas, as the SRTM data has been shown to have deviations in flat valley bottom regions, such as floodplains, which may lead to artificial pathway diversions (e.g. Jarvis et al., 2004; Ludwig and Schneider, 2006). A second source of error was introduced through the filling in of the holes of the DSM in order to ensure a hydrologically–sound DSM. While it is possible to do this hole-filling without major topographic infilling using customised methods (e.g. Reuter et al., 2007), this computational approach was outside the scope and feasibility of this thesis. Instead, the standard hydrological tools of ArcGIS 9.3 were used to hole-fill the DSM. The required steps to generate rivers using the hydrological tools in ArcGIS 9.3 have thus introduced potential for errors in both the vertical and horizontal accuracy. Yet this 30 arc-second resolution is comparable (and of better vertical accuracy) to the best available pixel of DEMs prior to SRTMv3 data, for example, GTOPO30.

An example of this horizontal river (pathway) diversion can be seen in the flatter regions of the CB rivers where several rivers show substantial horizontal distance offsets from the manually delineated course. These offsets are the most likely cause of the large differences between the lengths of several generated rivers compared to the digitised rivers (see **Table 6.4** and length of profiles compared in **Appendix 6**, **Section 6.2.1**). This led to the under-reporting (e.g. Kafue River) or over-reporting (e.g. Congo River) of the total river lengths (**Table 6.4**). The under-reporting of lengths was often due to the hole-filling process that artificially straightened the channel, especially in areas of low relief. These offsets are especially significant for rivers with extensive floodplains, for example the Kafue and Upper Zambezi Rivers. The automatically generated river course makes a straight line through these regions as the definitive channel cannot be determined (e.g. **Figure 6.8**). The over-reporting of river lengths was probably due to the infilling of high relief areas and deviation of the river course around topographic features through which they flow in reality. For example, the lower portion of the Congo River has been extended due to infilling and course deviation, leading to its increased length (see **Table 6.4**). These offsets, in combination with the degraded resolution of the DSM, also explain the differences in the river profiles start and finish elevations (see **Table 6.5**).

Furthermore, the difference in distance of cardinal and diagonal directions from between pixel centres negatively impacts on the precision of hydrological modelling (Hengl and Evans, 2009).

The above has consequences for the horizontal accuracy of the river courses (see **Table 6.7** and **Figure 6.8**). The variation of the horizontal accuracy makes the determination of spatial relationships between rivers problematic. Thus the comparison of features related to the rivers' x and y components can have substantial errors. For example, the maximum horizontal error of the Congo is 19 km and the Luapula is 64 km and, therefore, comparing the morphology of portions of these rivers may result in an error of greater than 60 km.

6.4.1.2 Rivers' longitudinal profiles

The most important point to be made regarding the generation of river long profiles is that it could not be done in a straightforward manner and posed several problems (see **Section 6.2**). A second consideration is related to the same issue of generating river courses, but in relation to pixel degradation, hole-filling and the displacement of the river course. As is shown by the comparisons of the profiles, this processing of the DSM introduced substantial, non–systematic errors in the generated profiles (see **Table 6.5** and **Table 6.6** and **Appendix 6**, **Section 6.2**). For example, the use of the hole-filling algorithm led to a +96 m offset of the elevations of the central regions of the CB (see **Appendix 6**, **Section 6.2.1)**. This offset is in part due to the rough relief of the Crystal Mountains through which the lower Congo River flows, with narrow valleys which were filled in. There was a noticeable bias in terms of filling when it came to several of the flatter regions that had rough topography downstream of them, such as Lake Mweru and the Upemba Swamp region, resulting in a subsequent positive offset throughout most of the profile (see **Appendix 6**, **Section 6.2.1**). The issues of horizontal channel offset are further highlighted by the large amount of noise in most of the Auto3 profiles, especially in the middle and upper regions of the rivers.

Overall, the generated river profiles do resemble the shape of the digitised profiles but often with large variations in elevation and/or length. The larger pixels size of the 900 m DSM resulted in the loss of profile detail, which in turn led to a simplification of the long profile, for example, with the Luapula River (see **Appendix 6**, **Section 6.2**). Whereas the nose of the Auto3 profiles made determining of profile trends problematic in some cases, for example, with the Wamba River (see **Appendix 6**, **Section 6.2.1**, **Figure A6.12**). Furthermore, owing to the offsets, several fluvial features were incorrectly located; for example, elevation changes happen further upstream on the Lufupa

River or further downstream on the Lukuga River compared to the digitised profile (see **Appendix 6**, **Section 6.2**). However, these trends were often strongest in the middle and lower reaches of the profile, with the upper reaches of many of the generated profiles comparing favourably to the digitised profiles.

6.4.1.3 Problems associated with automatically generated rivers

While it may have been possible to generate river courses from the 3 arc-second SRTMv3, this was not computationally achievable in this study. A second option would have been to have generated each river separately based on individual catchments. This would probably have increased the accuracy of the automated process but it would have required *a priori* knowledge of the river involving pre-existing GIS data, for example, accurate catchment shapefiles of each river. This, however, would have negated the purpose of the comparison of trying to compare both techniques (generation and digitisation) using the same exploratory approach.

Most worryingly is the issue of using derivation of the generated profiles, owing to the sequential ordering of the elevations data upon extraction (see **Section 6.2**). This issue of the sequential ordering when using the generated courses is illustrated in **Figure 6.13**. Whenever the rivers courses did not show a constant, uniform direction, the extracted elevation for those portions is incorrect when using ArcGIS 9.3 (this was tested and confirmed three times in ArcGIS 10.0) (see **Figure 6.13**). Here, the automatic extraction of the elevations from the raster grid has been sequenced primarily according to its row order and then secondarily according to column order. Therefore, the elevation values are presented in the incorrect order (i.e. first A 1 – 8 than B 1 – 8), which often results in smoother than expected profile sections. This incorrect sequencing was only noticeable when the digitised profiles were used as a reference profile. Overcoming the incorrect sequencing required further manual processing to ensure that the elevation data was in the correct hydrological order (see **Section 6.2** for full details).

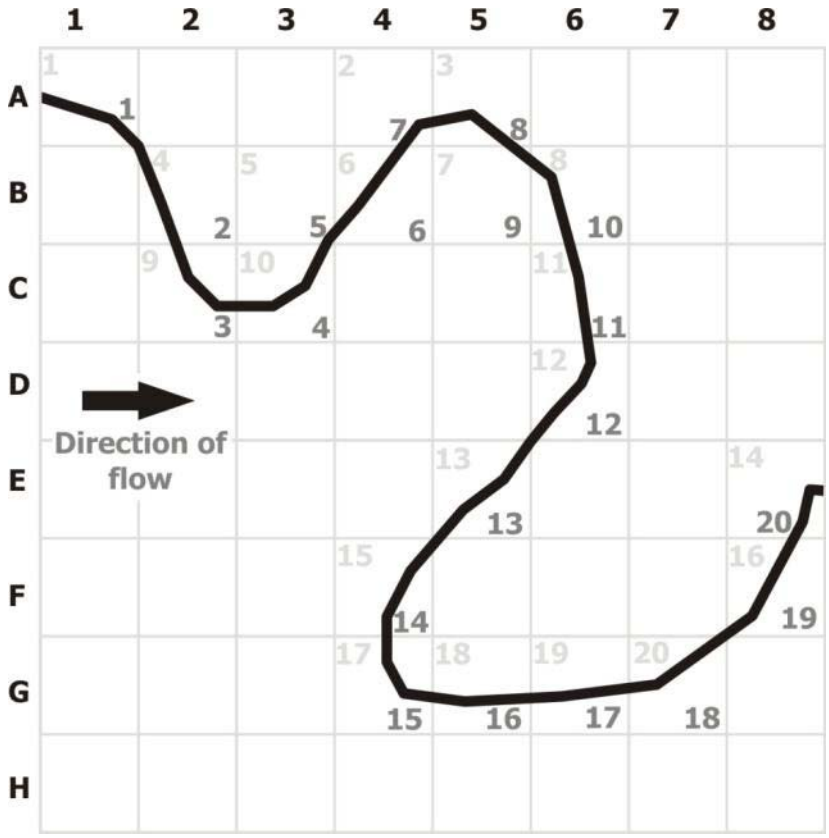

Figure 6.13: A schematic diagram of a river super imposed on a grid, flow direction is from left to right. The light numbers in the upper left hand side of the squares represent the value order of the river as seen by the extraction tool in ArcGIS 9.3. Darker numbers in the lower right hand side of the square is the true sequential value order of the river. Row order is represented by letter and column order by numbers.

Overall, the limited vertical and horizontal accuracy of the generated profiles and courses leaves much to be desired and renders these results of limited use. Thus, when using standard hydrological tools to generated profiles these issues must be borne in mind, as there are substantial variations in the z-values (elevation) between the three profiles. This variation in accuracy has an impact on the interpretation of the longitudinal profiles of the generated rivers, as they are often oversimplified and lose the resolution necessary for being able to indentify knickpoints. These profiles may, therefore, be of limited use for interpreting the geomorphology of individual rivers; however, they may have sufficient detail and accuracy if a researcher is only concerned with profile generalities.

While it should be noted that some of the generated rivers are of useable quality, owing to the non-systematic variation there is no way of knowing which of these rivers are accurate and/or where accuracy within a river may be an issue (when following the method described in the this study, in **Section 6.2**). This means that the generated river courses and profiles should be treated cautiously

and with an appreciation of their surrounding landscape if they are to be used for studies on a meso-scale or finer.

6.4.2 Digitised rivers and knickpoint characterisation

As shown above, the use of standard tools to generate river courses and profiles may lead to incorrect spatial placement and non-detection of fluvial features such as knickpoints and river junctions. It therefore follows that in situations where there is limited accurate and accessible spatial data regarding the catchments of the rivers system, and where a high level of vertical and horizontal accuracy is required, river profiles should be digitised manually. However, the processes differ in terms of time required for completion, with the manual digitising taking 60 days while river generation took 25 days to complete; this includes time taken for attempting to find solutions to the profile issues (see **Section 6.2**).

Although comparatively time intensive, the manual digitisation has the advantage of including the characterisation of the knickpoints and the creation of an image library with descriptions, which provide important context for the features. The automatic extraction does not include the creation of such metadata (nor can it), it does not identify all the knickpoints and it shows a large variation in terms of accuracy.

6.4.2.1 River longitudinal profiles

The use of SRTMv3 in conjunction with Landsat ETM 7+ imagery proved successful in determining the longitudinal profiles of rivers from the Congo and Kalahari Basins. While the SRTMv3 DSM showed some minor deviations from true courses, especially in low relief areas such as floodplains (Jarvis et al., 2004; Ludwig and Schneider, 2006) the use of Landsat ETM 7+ data negated this issue (e.g. **Figures 6.3** and **6.6**) thereby allowing the river courses and longitudinal profiles to be accurately digitised.

In broad terms, the nature of elevation changes for the rivers of the KB were more varied than those of the CB. The Kalahari rivers showed significant changes both their upper and lower reaches, whereas rivers from the majority of rivers from the CB experienced most of their elevation decrease in their upper reaches. An exception to this is the Chambeshi-Luapula-Luvua system that has notable elevation decreases before and after each local base level (i.e. Lake Bangweulu and Lake Mweru). In terms of the river's longitudinal profiles, only four of the studied rivers had a change in elevation of

greater than 1000 m, namely, Congo (1526 m), Kwango (1103 m), Kasai (1076 m) and Kafue (1006 m). The Lukuga River had the smallest elevation change, experiencing a fall of only 220 m. The rest of the rivers had changes in elevation greater than 220 m but less than 900 m.

6.4.2.2 Knickpoints

Of the total 380 knickpoints, 26 (7 %) were classed as **category -1** and therefore may be disputed. However, as **category -1** knickpoints were identified based on visual interpretation of several proxy data that have been seen to correlate with known knickpoints, they probably do represent real knickpoints. The second problematic set was the 15 **category 0** knickpoints, whose heights were not resolved. The combination of **category -1** and **0** knickpoints, represent 11 % of the total studied knickpoints; they may be considered of limited usability for future work and geomorphic interpretation. It should be noted that the rivers with the largest number of **category 0** and **-1** are the ones with the nosiest overall profiles, namely, the Cubango, Lufupa and Wamba Rivers (see **Appendix 6**, **Section 6.2** and **Chapter 7)**. Part of the inability to resolve knickpoint category may be related to the date that the SRTM elevation data was collected. The SRTM was collected during February 2000 (Kobrick, 2006), which is near the end of the southern hemisphere wet season. Therefore, it is likely that several of the rivers are at their yearly high stands which may obscure smaller knickpoints. This may explain some of the discrepancies between SRTMv3 and Landsat evidence. Nevertheless, the use of a combination of Landsat 7 ETM+ and SRTMv3 data allows for more than 85 % of knickpoints present along the river to be confidently identified.

Owing to the vertical resolution of the SRTMv3 data, which is approximately 5 m (see **Chapter 5**), there was a possibility of under–counting the number of knickpoints. Yet the low percentage (11 %) of inferred or unresolved knickpoints (**category -1** and **0**) indicates that the knickpoints missed would be in the minority. It should be noted that the height categories of some of the knickpoints with lower heights may change substantially during the southern hemisphere dry season. The uncertainty of knickpoint height and number appears to be associated with zones whose elevation data was extensively noisy. Therefore, knowing the longitudinal profile of a river will help in the assessment of the quality of knickpoint categorisation for that river. Of the 339 knickpoints to which height categories were assigned, 72 % were 5 m or higher.

Added to above assessment of the accuracy of knickpoint characterisation, field observations confirm the fidelity of descriptions and characterisations of the knickpoints possible from Landsat

and SRTMv3 data (see **Figures 6.9**, **6.10** and **6.11**). This demonstrates that accurate categorisation of knickpoints is possible using the technique of manual digitisation of the river profiles. Furthermore, the manual extraction of knickpoint location and heights as used in this study, although time consuming, is important to achieve accuracy, robustness and greater context of the result.

While the manual recording of knickpoint coordinates led to minor offset of knickpoint locations (due to rounding up of numbers), this had no bearing on the characterisation. Furthermore, correction of knickpoint location to the rivers course ensured spatial fidelity at the level of the Landsat resolution (see **Section 6.2**).

6.4.3 Geomorphic implications

The river longitudinal profiles shed light on the geomorphic evolution of these systems. Although the rivers of the CB exhibit large variation in profile style, some generalisations may be made. Rivers flowing into the Congo River from the south tend to experience the largest decrease in elevations in their first third to half of the river length, while over the remainder of the rivers' course, they experience a low gradient and limited change in elevation. Comparing the rivers of the KB, if the ends of the Kafue and Upper Zambezi are ignored, these rivers have flatter profiles, with profiles generally consisting of long stretches of little decrease in elevation interspersed with zones of rapid elevation decrease.

The knickpoints are often spatially clustered, with many of the larger clusters associated with zones where the river crosses the escarpment in the CB (see **Figure 6.7**). However, the number of knickpoints shows no systematic relation to river length (see **Figure 6.12**). Additionally it appears that purely process based explanations (that is, river capture and trunk-tributary relationships) are insufficient to account for the knickpoints distribution. For example, in the CB, no knickpoints were discerned to be associated with trunk-tributary interactions in the *cuvette centrale*. This lack of expected knickpoints is probably due to a combination of the rivers being of comparative size in the *cuvette central* (except for the Congo River) and the fact that the material over which they flow consists of sandy, alluvial deposits. When combined with the very low gradients of rivers in this region (i.e. the lower reaches of the Kasai and Kwango) which limit elevation differentials, it is probable that all the rivers are able to quickly adjust their profiles. This would limit the development of trunk-tributary knickpoints on the unconsolidated Cenozoic alluvial deposits of the central basin. Additionally, any trunk-tributary knickpoints that did form would likely migrate rapidly upstream

until they encounter more resistant lithologies. In terms of the Kalahari rivers, the end of the Cubango has several knickpoints associated with localised faulting, while the end of the Upper Zambezi, the Victoria Falls, is controlled by the large rift related valley into which it flows. Therefore there is a need to further investigate possible causes of the knickpoints and their patterning, such as lithologic, structural and geodynamic controls, which will be examined in **Chapter 7**.

6.5 Chapter conclusion and summary

Overall, the river profile data can be considered useful in describing the longitudinal morphology of the rivers, even in cases with numerous elevation spikes, for example, the Wamba. The cause of this noise in terms of elevation is partly due to the precedence given to the Landsat 7 imagery over the DSM in terms of determining the course of the river channel. This means that in some regions the digitised course did not always follow the thalweg as indicated on the SRTMv3 but followed the channel as indicated by the higher resolution Landsat 7 imagery, which is considered to have a greater fidelity than the SRTMv3 DSM. The rivers of the CB were generally nosier, this being due to the dense tropical forests that may result in large positive errors in elevation (Sun et al., 2003; Ludwig and Schneider, 2006; Nelson et al., 2009). Nelson et al. (2009) report that SRTM elevations are on average of 4.66 m higher than bare earth models in forested regions due to the forest canopy. Yet, several large elevation spikes are noticeable in the Kalahari rivers. These spikes appear to be associated with zones of radar shadowing (see **Chapter 4**), where the river flows close to a large topographic feature. The majority of the noise is in the form of elevation spikes and not elevation holes; therefore, it would be possible to increase overall profile shape accuracy by using a filtering window to remove these spikes. However, the longitudinal elevation data represented here is the data, as is, from SRTMv3. It is suggested that further processing of the data would not aid interpretation and usability of the river profiles and may in fact introduce more error (see **Chapter 5**). Further processing would thus be of a cosmetic nature rather than adding data accuracy, since most data spikes are relatively minor.

The river profiles digitised for this thesis are highly accurate and may be the most detailed GIS versions yet produced of these rivers in terms of the whole river, due to SRTMv3 being the best publically available. While it is acknowledged that not every meander in the smaller floodplains was captured, a comparison of these areas to the features shown on older maps shows that often the meanders on the printed maps do not accurately represent their locations. This is to be expected as often it is these smaller floodplain that are areas of most dynamic change, with meanders being the way in which the river accommodates systems changes (Schumm, 1977; Schumm et al., 2005).

Therefore, the digitised rivers presented here may be claimed to be the most accurate and complete river courses and profiles developed, at least compared to the data in the public domain.

The manual digitisation, categorisation and cataloguing of the rivers using radar based elevation data and optically remote sensing data is undoubtedly the best approach for studying rivers over a large, inaccessible area such as central Africa. Manual digitisation of the rivers not only allows for the context of fluvial morphological features to be noted, it also provides a higher degree of accuracy both in the horizontal (x and y values) and vertical (z values). Therefore, if vertical accuracy and sub-kilometre horizontal accuracy is required, manual digitisation of the rivers should be used rather than the automatic generation of rivers.

The main findings of this chapter can be summarised in the following points:

- The horizontal fidelity of generated river courses is problematic, with the majority of rivers having deviations greater than 1.5 km relative to the digitised course (see **Table 6.7**).
- There are numerous issues involving the vertical accuracy of generated profiles, in particular the sequential ordering of their elevations (see **Figure 6.13**, **Appendix 6**, **Section 6.2**).
- The combined use of Landsat ETM+ and SRTMv3 allows for accurate long profile digitisation and knickpoint characterisation.
- The creation of a geospatial database is crucial to a better understanding of the studied rivers.
- The longitudinal profiles of studied rivers are similar to one another in each basin but differ between the Kalahari and Congo Basins.
- River length is not the sole determinant of knickpoint number (see **Table 6.9** and **Figure 6.12**), nor do purely fluvial processes appear to account for knickpoint location and height.
- Nevertheless, knickpoints show distinct spatial clustering (see **Figure 6.7**)
- There is a need to further investigate the cause and context of these knickpoints (**Chapter 7**).

CHAPTER 7: GEOSPATIAL DATASETS

7.1 Introduction

The creation of the GIS database in **Chapter 6** provides important and new spatial information for rivers across the CB and KB. However, these datasets lack important temporal and attribute information which would significantly add to our understanding of the evolution of the landscapes of south–central Africa. While previous studies attributed well known knickpoints in south–central Africa to the underlying geology (Wellington, 1949; King 1951), these preceding studies did not provide a regional analysis of the knickpoints in terms of their geology for entire rivers and across the KB and CB. Moreover, this previous work did not result in the development of a geospatial database that included both geomorphic and geologic observations.

A better understanding of the evolution of south-central African landscapes requires additional information beyond the geomorphic classification of knickpoints. In this study the additional information came from available geologic and biogeographic data, mainly in the form of maps, as well as additional geomorphic data. It is the integration of this information (attributes) to the knickpoint geodatabase that forms the core focus of this chapter.

This chapter describes the process of capturing and collating the additional information and presents the integration of new and existing datasets, thereby presenting a novel amalgamation of original and published knowledge. Here, key maps that provide the wider context of the studied rivers are presented. This section may be viewed as a geospatial synthesis of the original knickpoint geodatabase created during this study (**Chapter 6**) with geological and biological data. This blending of original and published datasets forms the second original contribution of this study in terms of GIS datasets, extending our current understanding of landscape evolution in south–central Africa.

Chapter 3 of this study highlighted the various factors that may influence the present day geomorphic evolution of the CKW. These factors range from the genesis of the African plate during the formation and break–up of Gondwana (see **Section 3.2**), the varied nature of the geology of the CB and KB (see **Section 3.3**) and the region's present day topography (as discussed in **Section 3.4**), and how these factors have influenced south–central Africa's drainage. The review in Chapter 3 of these factors in south–central Africa form the rationale for looking at geological maps in relation to

two river longitudinal profiles and all of the identified knickpoints as detailed in the current chapter, in order to ascertain what the controls are (if any) which act on these landforms in south–central Africa.

7.2 Geological and biogeographic data used

7.2.1 Geological maps

The geomorphic evolution of landforms is related, in varying degrees, to the geological and geographical setting of these landforms (Gilbert, 1877; Zernitz, 1932, Horton, 1945, Howard, 1967, Holbrook and Schumm 1999). In order to better understand the geological setting of the knickpoints, detailed geological maps of the relevant countries were used. Due to the lack of publically accessible digital geologic datasets for much of the study area at scales better than 1:5 000 000, available hardcopy geologic maps were scanned and georectified. The geological maps scanned for this study were (as shown in **Figure 7.1**):

- the Democratic Republic of the Congo, scale 1:2 000 000 (Lepersonne, 1974a),
- the Republic of the Congo, scale 1:1 000 000 (Desthieux, 1995)
- Angola, scale 1:1 000 000 (de Carvalho, 1981)
- and Zambia, scale 1:1 000 000 (Thieme and Johnson, 1975)

For Zambia, only the northern most section was a scanned map, for the rest of Zambia, a digitised shapefile of the 1:1 000 000 was used. For Botswana, a 1: 500 000 geology shapefile (Key and Ayes, 2000) was used. For a small section of the Cubango River (in the region of the Caprivi corridor of Namibia), a printed geologic map of Namibia (Miller, 1980) was visually inspected.

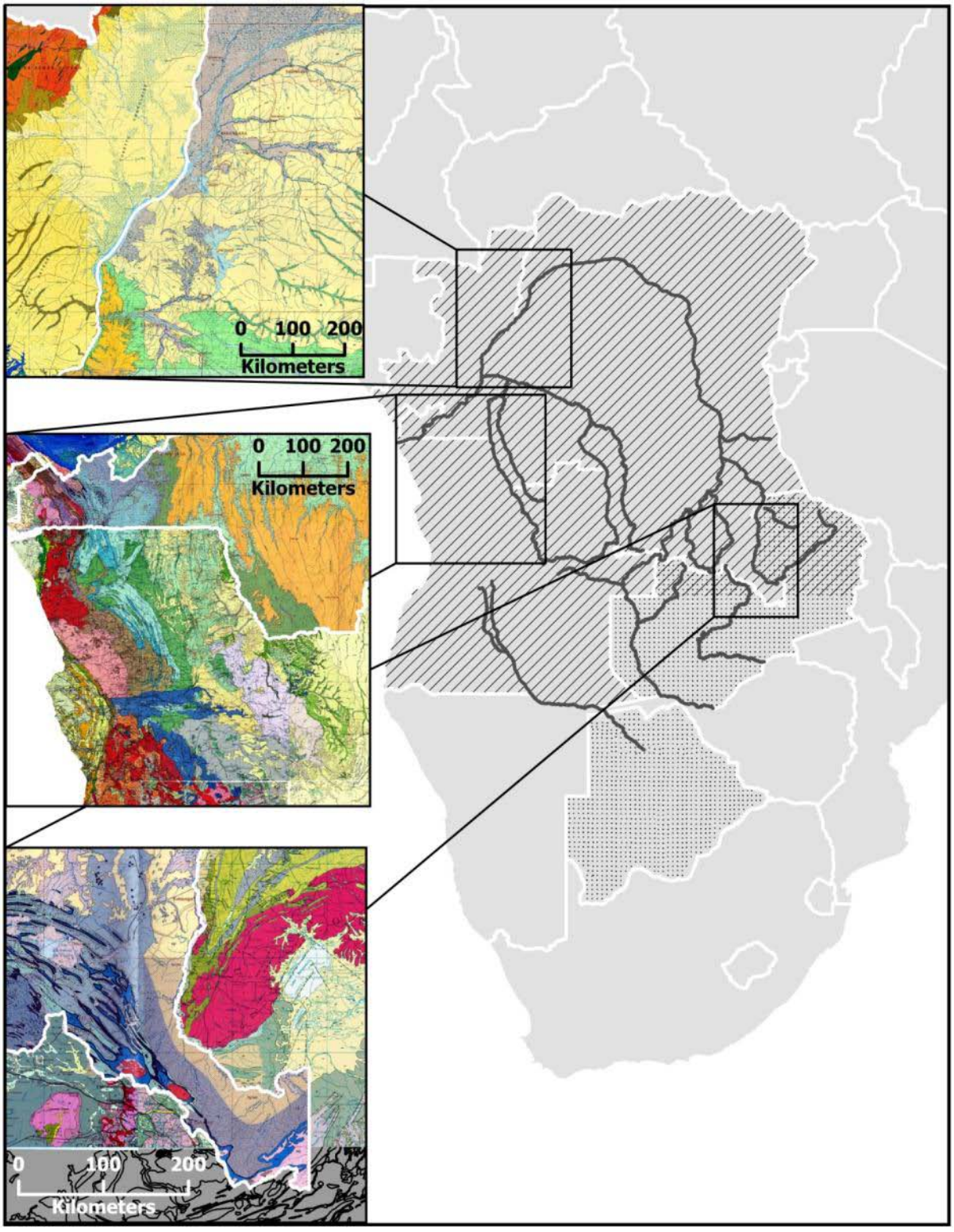

Figure 7.1: The extent and location of geology maps used in this study. Maps that were scanned and georectified are indicated by the black hatching (Angola, DRC, Republic of the Congo and northern Zambia). Stippling indicates the coverage of geology GIS shapefiles used (Botswana and Zambia). Heavy dark grey lines indicate studied rivers. The three insets show examples of the actual georeferenced scans (Lepersonne, 1974; Thieme and Johnson, 1975; de Carvalho, 1981; Desthieux, 1995). Note the change in classification, extent of outcrops and representation at country borders.

The need to use several geological maps from different countries, due to the extent of the study, made the assignment of geology to the knickpoints challenging as the geological terminology and classifications varied amongst the countries. Furthermore, the DRC and Republic of the Congo maps were in French and the Angolan map was in Portuguese. These difficulties were dealt with by, firstly, translating the relevant maps and, secondly, by maintaining the native geologic unit names, ages and definitions of the maps utilised when entering this information into the relevant attribute field of the geodatabase. An advantage of using the names and terms as shown on the reference maps is that it allows for the revisiting and updating of the geologic information should changes to classification occur in the future, thus ensuring the increased longevity of this geodatabase. An example from the DRC map is the geological unit named Kb on the map with its given age, Kibarien; this unit was entered into the GIS as Kb and Kibarien. The translation of the maps allowed for the lithological descriptions to be entered, which for the above example is schists and quartzites. The use of lithological descriptions was adopted as the development of an equivalent and unifying geological classification was outside the scope of this study. For details regarding the geology of the study areas, see the geological descriptions of each basin found in **Chapter 3**, **Sections 3.2.1** and **3.2.2**. Following from the literature reviewed in **Chapter 3** and the lack of uniform terminology across the maps, it was determined that the age (e.g. Kibarien) and rock type (e.g. schist and quartzite) would be most appropriate for comparing the knickpoints in this thesis. In addition to the recording of this geologic information, the presence and proximity of mapped or inferred faults was noted. The simplified lithology and observations regarding the presence of faults allowed for the probable cause of each knickpoint to be determined using a combination of geologic and geomorphic evidence. The probable cause of each knickpoint was than plotted onto the longitudinal profiles of each river (see **Chapter 6**, **section 6.3.1.1** for the description of each longitudinal profile).

This study required the creation of three geology geodatabases:

1) a primary, detailed geology shapefile, providing detailed geologic information as shown on the relevant maps;
2) a derived, simplified lithostratigraphy shapefile, with the rock descriptions and ages; and
3) a derived, probable causes shapefile, where the lithology descriptions, age and fault information was combined with the geomorphic description of the original knickpoint geodatabase (as described in **Chapter 6**, **Section 6.2.4** and shown in **Table A6.2**, **Appendix 6**).

7.2.1.1 Detailed geology

The lithologies of each knickpoint were manually determined using the scanned geological maps and this data was entered into the knickpoint shapefiles. The geologic information was recorded both at the knickpoint location and also upstream and downstream, using the maximum search distance of 1 km or until a change in lithology was encountered. If no change was encountered within this 1 km search distance, than the geological characteristic of the upstream and/or downstream field was entered as the same for the knickpoint. This allowed for the recording of geologic information, such geological unit name, age and lithological description, to be captured against the knickpoint location, as determined for this study (see **section 6.2** in **Chapter 6** and **Table A6.2** in **Appendix 6**). Additionally, features such as faulting, nearby intrusions and channel morphology features, such as change in flow directions, were also recorded.

In order to assess the role of the underlying geology on the profile as a whole, the geology of the Kwango and Kasai Rivers were mapped and plotted onto their longitudinal profiles.

7.2.1.2 Simplified lithostratigraphy

The terms used in the detailed geology database were too variable to allow for categorisation of knickpoints into common groups, which was required to allow for comparisons across river systems. Following from the research literature (see **Chapter 3**), it was decided to class these lithologies into age and rock types. This involved correlating the map lithostratigraphies and grouping the lithology descriptions by utilising available explanatory notes. As the studied rivers occurred dominantly in the DRC and due to the more extensive explanatory note for the DRC geologic map (Lepersonne, 1974b), it was decided that the rock types of other regions should mirror those given in the DRC geologic map. This correlation and grouping of rock types was done with the assistance of Dr. Bastien Linol (Linol, personal communication, January 2011). The simplification of the geological data was based primarily on the age of the lithological unit (e.g. Precambrian, Kalahari) as provided on the maps and, secondarily, on lithology type (e.g. sedimentary, granitic). While the aggregation of the detailed geology attributes has caused some loss of detail, aggregation was essential to characterise knickpoints so they could then to be compared and the possible cause of knickpoints to be examined.

7.2.1.3 Probable causes of knickpoint occurrence

The simplified lithostratigraphic geodatabase was required to assign likely causes for the knickpoints. This was done based on the interpretation of the geologic context of the knickpoint, such as lithology type, age, size of outcrop, proximity of faulting, surrounding changes in lithology and river morphology. In cases where no causes could be readily ascertained from geological maps, the causes were classed as 'unidentifiable'; while a cause for many of these unidentified knickpoints could possibly be proposed using finer scale studies, this was considered to be outside the remit of this thesis. Allowance was made for three types in descending influence. Of the three knickpoint geodatabases created in this study, it is the 'Likely Causes' that is the most subjective, requiring interpretation of both geomorphic and geologic information. However, an attempt to minimise subjectivity was made by incorporating both geologic and geomorphic evidence in as much detail as possible and assigning a confidence score to each cause. This score ranged from 1 to 5, with 1 being the most confident and 5 the least. Cases where knickpoints had a single clear cause were scored as 1, whereas knickpoints with more than one equally strong cause (e.g. both lithology and a fault) were assigned a score of 5. Knickpoints whose cause was unidentified were not assigned a score.

By exporting the resulting knickpoint shapefiles as databases (.dbf format) their information could be plotted using spreadsheets. This allowed for the 'Likely Causes' (of knickpoint location) to be plotted onto the longitudinal profiles of the rivers in order to quantify and compare each river's geomorphic development. The knickpoint locations were plotted utilising the surface distance values, which allowed for the accurate placement of knickpoints along the longitudinal profiles of each river. For each knickpoint the most likely cause was chosen and entered into one of six categories, these being faulty, likely fault, lithology, lithology change, unidentifiable and large dam. The cause was classed as lithology if the knickpoint occurred within a resistant lithology, for example, Precambrian granites. Lithology change was used whenever knickpoints occurred in a zone of change from one rock type to another, the assumption being that the different shear strengths of the rock types may have resulted in knickpoint occurrence. If a knickpoint was located on a fault and was associated with a change in flow direction, it was considered probable that the knickpoint was a result of faulting. If the knickpoint occurred downstream or upstream of a fault or corresponded to an inferred fault line, its cause was classed as likely fault. In cases where the knickpoint could not be classed as one of the previous categories it was labelled unidentified.

7.2.2 Evidence from biogeography

One method to determine the age of geomorphic changes in landscape is to make use of the geographic distributions of the fauna that inhabit them. This approach is exploits the relationship between gene genealogies (phylogenetics) and geography, known as phylogeography (Avise, 2000). As discussed in Avise (2000), the phylogeographic approach exploits the historical information accumulated in genetic lineages that often display distinct and persistent geographic associations. A hypothetical example is illustrated in **Figure 7.2**. A population of species is geographically isolated by a barrier that limits the gene flow as individuals are unable to move between the two descendent populations (subgroup). The barrier to dispersal may be purely physical, such as large rivers that primates are unable to cross (e.g. Harcourt and Wood, 2012), or a combination of factors, for example, the adaptation to environmental niches that collectively decrease gene flow between populations (e.g. Joyce, et al., 2005). Over time, through the accumulation of genetic differences (through mutations) and the lack of gene flow between the two lineages, the single ancestral genetic lineage evolves into two distinct, albeit related lineages, that occupy different geographic spaces (Avise, 2000), as illustrated in **Figure 7.2**. It is possible to determine the total time geographical isolation for these two, now separate genetic lineages, thereby providing a time estimate (on the range of ka to Myr time scales) when the two lineages last experienced a substantial flow of genes (Avise, 2000). There has been an increase in the complexity of these methods, relying on various genetic techniques and analyses, with the disciplines of population genetics and molecular systematic experiencing rapid improvement (see DeSalle and Rosenfeld, 2013). It is possible to determine the average rate at which a species has accumulated genetic differences (mutation rate) over time. By measuring the number of genetic differences between two related groups and applying the average mutation rate, a time estimate of when the two populations were once freely breeding can be calculated (Avise, 2000). This process gives the approximate age of genetic divergence of the two groups from their last shared common population, or most recent common ancestor (MRCA) (Avise, 2000). The use of Bayesian methods allows for age estimates to be assigned a measure of statistical error, usually expressed at the 95 % error, which constrains the probability of the true age value (DeSalle and Rosenfeld, 2013).

By combining geologic and geomorphic evidence with such phylogeographic information, it is possible to quantify estimated times of changes in the landscape (e.g. Goodier et al., 2011), as illustrated in **Figure 7.3**. An important consideration in using phylogeographic data is the degree of association of a species with a topographic feature (landform) as this will determine how effectively

the species has tracked changes in the landscape (Cotterill and de Wit, 2011). Thus, such analyses focus on stenotopic species, which are species with a narrow environmental niche and definitive geographic range. This approach is not without criticism, owing especially to the assumption of average mutation rates being applicable to different species and to the fact that this mutation rate is often based on paleontological evidence, which in turn makes use of geological data, leading to the possibility of circular reasoning and a possible incorrect age estimation of the MRCA. These two criticisms may be met by using multiple, unrelated taxa, making use of species calibration points that have been determined through conventional geologic dating methods and cross–checking the ages against available, established geologic and geomorphic evidence. Thus a more robust interpretation of landscape events can be attained (see Cotterill and de Wit, 2011).

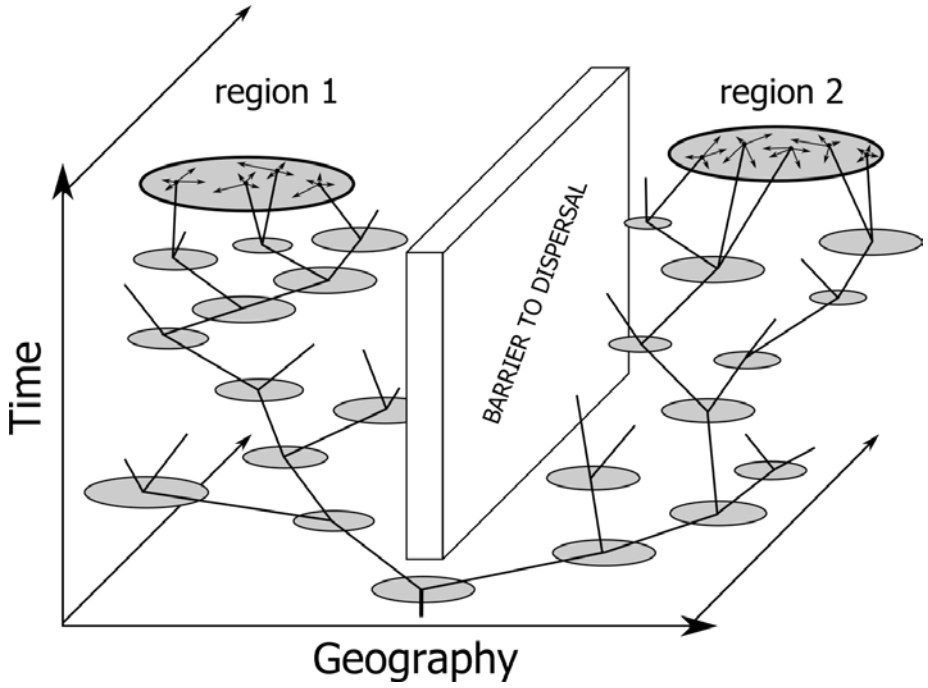

Figure 7.2: A hypothetical gene genealogy for species whose gene flow is restricted between two regional populations. Through time the geographic range of the species changes in both size and extent. In the case of stenotopic species these changes represent definitive changes in the landscape. Shaded ovals indicate geographic range of particular lineages, with the top large ovals representing the extant populations present day range and the bottom oval indicating the most common recent ancestor. The arrow vectors in the top, extant populations indicate the current dispersal of individual from their natal sites within their geographic range. Figure after Avise (2000).

Phylogeographic data used in this study was drawn from the research literature and no original phylogeographic work was conducted. The primary focus for this thesis was on studies that had mapped species distributions and used species which exhibit definitive geographic relationships to

the landscape and to rivers in particular. Aquatic species were selected because they are confined to rivers and lakes. The data from aquatic species is complemented with by studied mammals whose mapped distributions reveal isolation by major rivers. Thus not all available phylogeographic studies from southern and central Africa were suitable. The rationale behind using phylogeographic data was twofold: firstly, the lack of available Neogene geologic dates in the study area; and, secondly, the fact that the phylogeographic approach explicitly acknowledges temporal (gene lineages) and spatial (species ranges) scales, making it well aligned to the geomorphic approaches used in studying landscapes. Phylogeography can, therefore, provide novel insights into the development of the landscape.

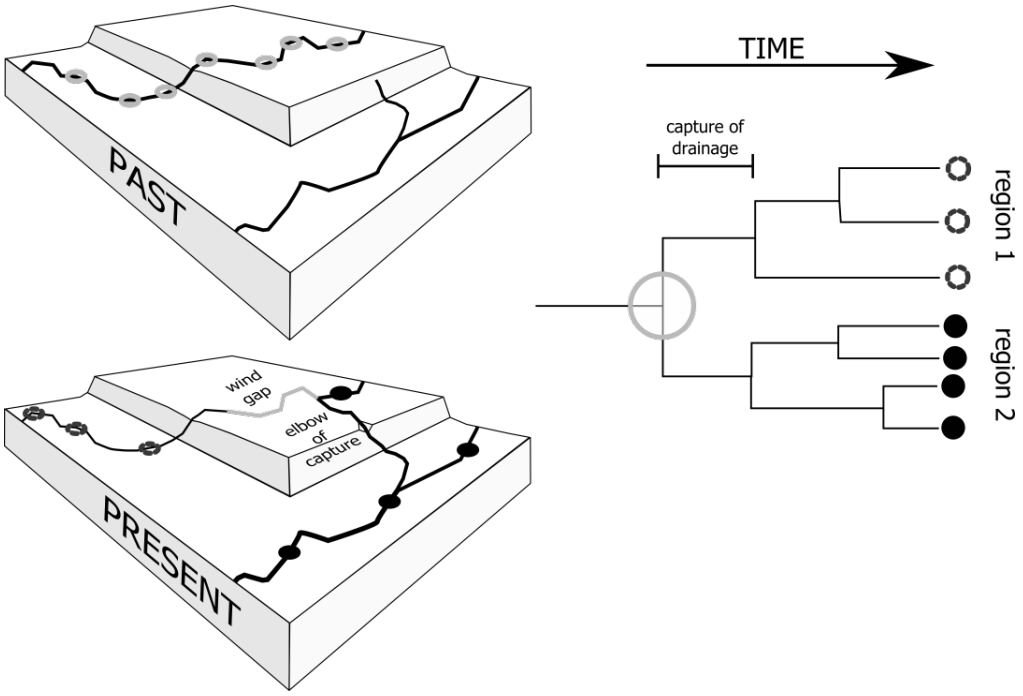

Figure 7.3: By combining geomorphic and phylogeographic evidence the age of a drainage capture may be determined. The occurrence of two related fish populations (black circles and dashed grey circles) in currently unconnected river systems (heavy dark lines) and geomorphic evidence of river capture (the presence of a wind gap and elbow of capture) in the present suggest a past capture event. The use of phylogenetic data allows for the creation of a gene tree (right) that provides a time constraint (capture of drainage bar) on the river capture event. This is done by determining the genetic divergence of the two populations found presently in the upper river (region 1) and lower river (region 2) and using a molecular mutation rate to determine the age since the most recent common ancestor (light grey circle).

7.3 Results

7.3.1 Knickpoint geodatabase

7.3.1.1 Detailed geology of the knickpoints

The results of the creation of the detailed geology GIS database for each knickpoint are shown in **Table A7.1** in **Appendix 7**, **Section 7.1** (due to the appendix's length it is on a data CD-R). In order to evaluate the role of the underlying geology, as well as the complexity of using geological maps from different countries, the detailed rock types were plotted against the entire river longitudinal profiles for the Kasai and Kwango Rivers. The outcome of this exercise is shown in **Figures 7.4** and **7.5**. Both of these rivers have parts of their upper courses in Angola and their middle to lower course in the DRC. In addition, the middle courses of both rivers form part of the international boundary between the two countries. This makes these two rivers good examples of the difficulties of using geological classifications across political divides. An example of the differences of geological classifications is shown in the middle inset in **Figure 7.1**.

The Kasai River flows over 16 different rock types, as revealed on the Angola and DRC geological maps, and has 47 knickpoints (see **Figure 7.4**). The longitudinal profile of the Kasai reveals a clear association of knickpoints and zones of convexity of the longitudinal profile with the resistant rock types of dolerite, granitic rocks, gabbro and charnockite, granite and migmatite, gneiss and migmatite, basalt and dolerite. The occurrence of river convexity and resistant lithologies indicates that these rock types, many forming the crystalline basement of the study area (as discussed in **Chapter 3.3**), are strong determinants of the shape of the rivers longitudinal profile by controlling the location of well established knickpoints. The lack of knickpoints in the lower regions of the Kasai is interesting, here the river flows into the *cuvette centrale* over poorly consolidated Cretaceous sandstones (marked as "red sdstone", "red sdstone C2" and "red sdstone C3"), Plio–Pleistocene alluvium (indicated as "alluvium (PlPl)") and the Holocene alluvium (marked as "modern alluvium (Ho)").

The Kwango River flows over 10 rock types and has 18 knickpoints, as can be seen in **Figure 7.5**. Similar to the Kasai River, the underlying geology controls the morphology of the Kwango's longitudinal profile and position of at least 14 of the knickpoints. The majority of the 18 knickpoints are clustered within a zone of mixed geology comprising alternations between schist and sandstones

with gabbro and charnockite, as well as a mix of schist and sandstone outcrops in a region of Cretaceous red sandstone (marked as “red sandst” on **Figure 7.5**). The largest knickpoints are associated with granite and migmatite. These two regions, consisting of gabbro and charnockite alternating with schist and sandstones, and the granite and migmatite region also form a zone of convexity (gabbro–schists region) and a large step (granite region) in the profile. Interestingly, in the Kwango’s upper region there is a large knickpoint occurring on Kalahari Sands, and the region of convexity is restricted to rocks consisting of sandstone and shales. Here the change in river gradient is coincident with a change from sandstone and shales to bedded claystones and sandstones (“bedded clayst and sandst”). In addition, like the Kasai River, the Kwango River’s longitudinal profile gradient decreases and knickpoints become absent as it flows into the central CB over poorly consolidated Cretaceous sandstones (marked as “red sandst” and “red sandst 3”) and alluvium of Plio–Pleistocene and Holocene age (“alluvium (PlPl)” and “modern alluvium”).

The river longitudinal profiles of the Kwango and Kasai indicate that, for rivers flowing in the CB, the underlying geology has a strong influence on the shape of the river’s longitudinal profile, and location of its knickpoints. The role of geology in knickpoint occurrence is exemplified in **Table 7.1**, which illustrates how knickpoint location corresponds to rock type for the Kwango River. It is important to note that the Precambrian rock, while only forming 11 % of the lithologies over which the Kwango flows, accounts for 12 of the 18 knickpoints, with a further 2 knickpoints occurring on the boundary between the Precambrian schist and quartzites and the poorly consolidated Cretaceous red sandstones. Thus three rock types are associated with 14 of the 18 knickpoints of the Kwango but restricted to only 157 km of the Kwango’s approximately 1450 km length.

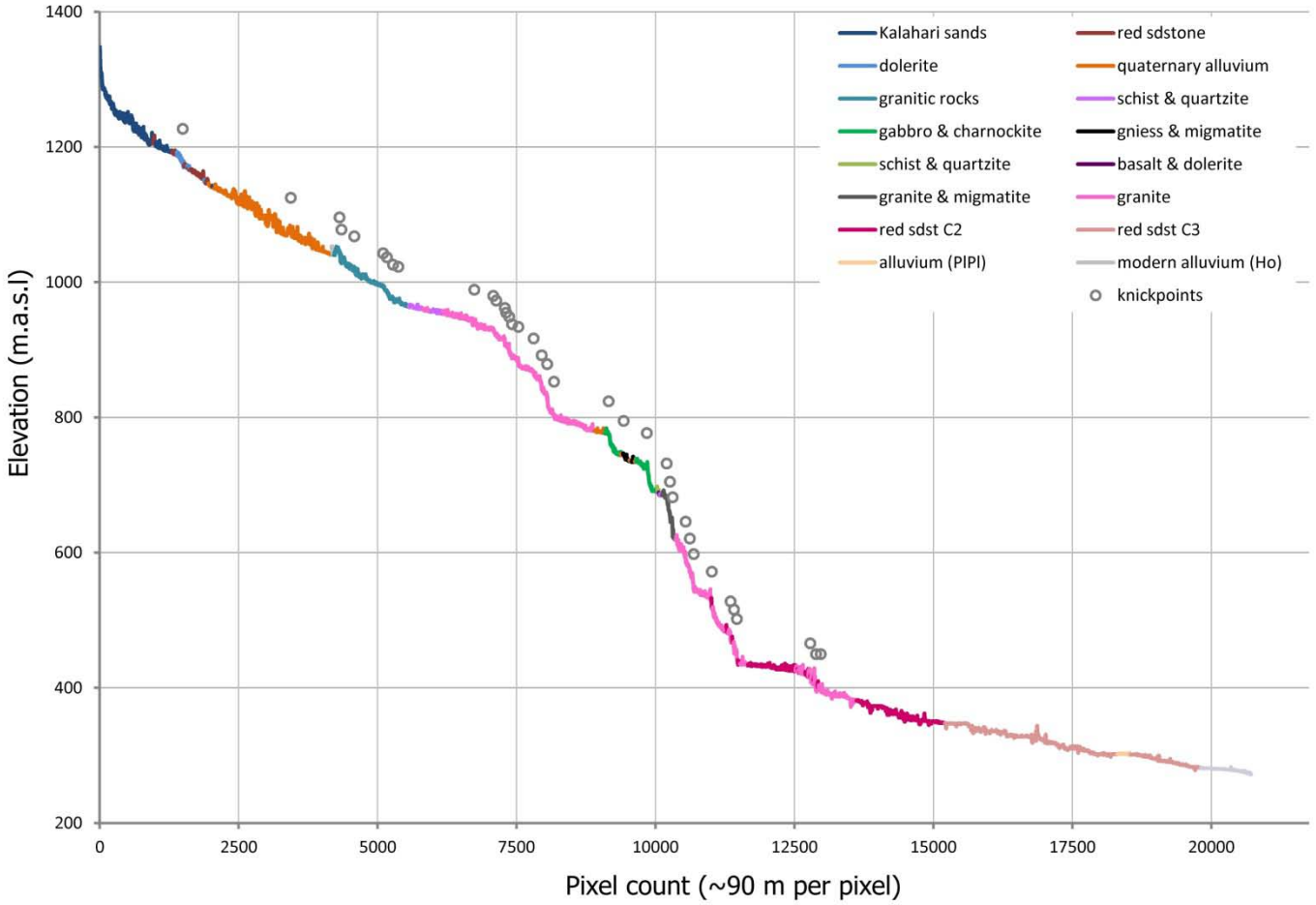

Figure 7.4: The geology of the **Kasai River** mapped onto its longitudinal profile. The rivers 47 knickpoints have been vertically offset to for improved clarity. The rock types shown were derived directly from the geological maps of Angola and the Democratic Republic (see **Section 7.2.1** for details). The approximately 2000 km Kasai flows over 16 different rock types throughout its course. Of interest is the preferential clustering of the knickpoints associated with granites, gabbro and charnockites, granitic rocks, granites and migmatites, basalt and dolerites and dolerites rock types. These rock types are also zones of convexity of the river longitudinal profile. In a few instances knickpoints occur on unexpected rock types such as quaternary alluvium.

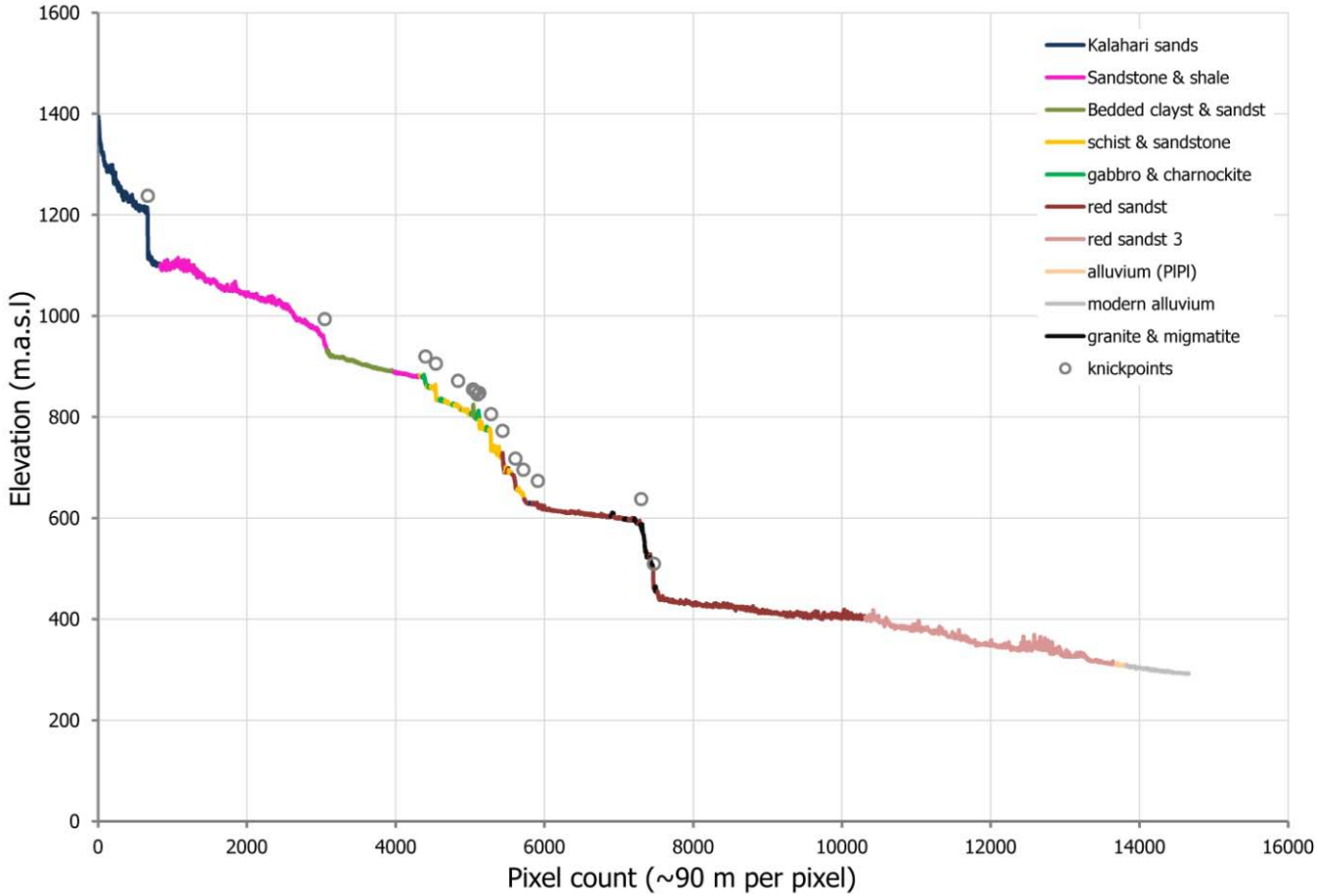

Figure 7.5: The geology of the **Kwango River** mapped onto its longitudinal profile. The river's 18 knickpoints have been vertically offset for improved clarity. The rock types shown were derived directly from the geological maps of Angola and the Democratic Republic (see **Section 7.2.1** for details). The approximately 1500 km Kwango flows over 10 different rock types throughout its course. Of interest is the preferential clustering of the knickpoints associated with the zone where schists and sandstone alternate with gabbro and charnockite, and the region of granite and migmatite. River convexity is also associated with these rock types. Note the occurrence a large knickpoint on Kalahari Sands and the change of gradient from sandstone and shale to bedded claystone and sandstone in the rivers upper reaches.

Table 7.1: The rock types on which knickpoints occur in the Kwango River. It can be see that of the ca. 1450 km long Kwango, that majority of knickpoints (12) are associated with rocks that outcrop only along 157 km of the river, with another two occurring on the boundary between two rock types. The remaining four knickpoints occur on rock types that are exposed along 493 km of the river course.

Age	Rock type	Length (km)	Proportion (%)	Number of knickpoints
Precambrian	• granite and migmatite • schist and quartzite • gabbro and charnockite	157	11	12
Phanerozoic	• Kalahari sands • sandstone and shale • red sandstone 1	493	34	4
Lithology change	• schist and quartzite upstream and red sandstone 1 downstream • red sandstone 1 upstream and schist and quartzite downstream	-	-	2
	Lithologies with knickpoints	650	45	18
	Lithologies without knickpoints	794	55	-

Ideally all of the studied rivers should have had their geology plotted against their longitudinal profiles, as shown in **Figures 7.4** and **7.5**, but this process is very time intensive due to the length of the studied rivers and the need to manually extract the lithology types from the geological maps. As knickpoints can provide insights into the development of a river when taken in context with the rivers longitudinal profile, and as knickpoints are themselves influenced by geology, as shown in **Figures 7.4** and **7.5** and **Table 7.1**, it was decided to focus on the geology of knickpoints. In summary, the combined evidence of knickpoint location and associated geological control together improve our understanding of the dominant controls of the river longitudinal profiles across south–central Africa.

7.3.1.2 The simplified lithostratigraphy of knickpoints

As shown in **Section 7.3.1.1**, many of the knickpoints can be related to the geology into which the river channel has incised. By simplifying geology into rock types and age groups, it has proved possible to compare different rivers within and between the two basins. The rock ages were considered important, owing to the different conditions under which these rocks formed, which controls the rocks petrology and mass shear strength and thus resistance to erosion. The following paragraph qualifies this statement.

The Precambrian rocks are divided into three groups: (1) the granitic and gneissic rocks that form the crystalline basement of the crustal shields; (2) the sedimentary deposits that were laid prior to Gondwana formation and have been substantially altered since; and (3) volcanic sedimentary complexes that contain a mixture of both volcanic rock and sedimentary types, for example, rhyolite mixed with tuffs. Knickpoints occurred on Karoo age rocks consisting of sandstones and glacial deposits. The Kalahari Group, consisting of sandstones and silcretes formed the third age group. Intrusive rocks played a role in knickpoint occurrence and thus formed the fourth age group, these being of various ages. The last age group is the recent alluvium which incorporates the bulk of the non–Kalahari Group sediments and consists mainly of reworked sediments. The number of knickpoints found on each lithology is shown in **Figure 7.6**.

Of the 380 knickpoint identified (including the 6 knickpoints that are large dams), 253 occurred on Precambrian rocks, with a 132 of the knickpoints falling on the granitic basement rocks (see **Figure 7.6)**. Therefore, more than 66 % of the studied knickpoints occur on Precambrian rocks. This percentage changes at the basin level, with 73 % (188 of 259) of the CB knickpoints being associated with the Precambrian basement, whereas only 54 % (65 of 121) of the KB knickpoints are found on Precambrian rocks. There were no knickpoints identified within the Karroo age group in the KB, while 42 knickpoints of the CB are found on this lithology. In terms of the Kalahari Group, only three CB knickpoints were found within these sandstones and silcretes while 17 (14 %) of the KB knickpoints occur within the Kalahari rocks. In total the igneous and metamorphic rocks associated with intrusions accounted for 11 % (40 of 3800 of the knickpoints), which, considering the areal coverage of these intrusive rocks compared to the other lithologies, is a significant number of knickpoints. No knickpoints were found on recent alluvium in the CB while 25 knickpoints of the KB can be found within this Quaternary sedimentary cover.

Most (18 of 25) of the knickpoints associated with recent alluvium occurred in Angola and 14 knickpoints were classified as having heights of 5 m or less, although two were 15 m and another two were 20 m (see **Appendix 7**, **Section, 7.2**, **Table A7.2**). These four large knickpoints occur in the upper reaches of the Cubango River above elevations of 1350 m.a.s.l. Of the 37 knickpoints with heights of 40 m or more, 30 occurred on the Precambrian lithologies with 10 occurring on granitic and gneissic rocks, 9 on sedimentary rocks and 11 on the volcanic–sedimentary. Of the remaining seven knickpoints, four are found on the intrusive igneous and metamorphic rocks, one on the Karoo age rocks and two on the Kalahari Group rocks.

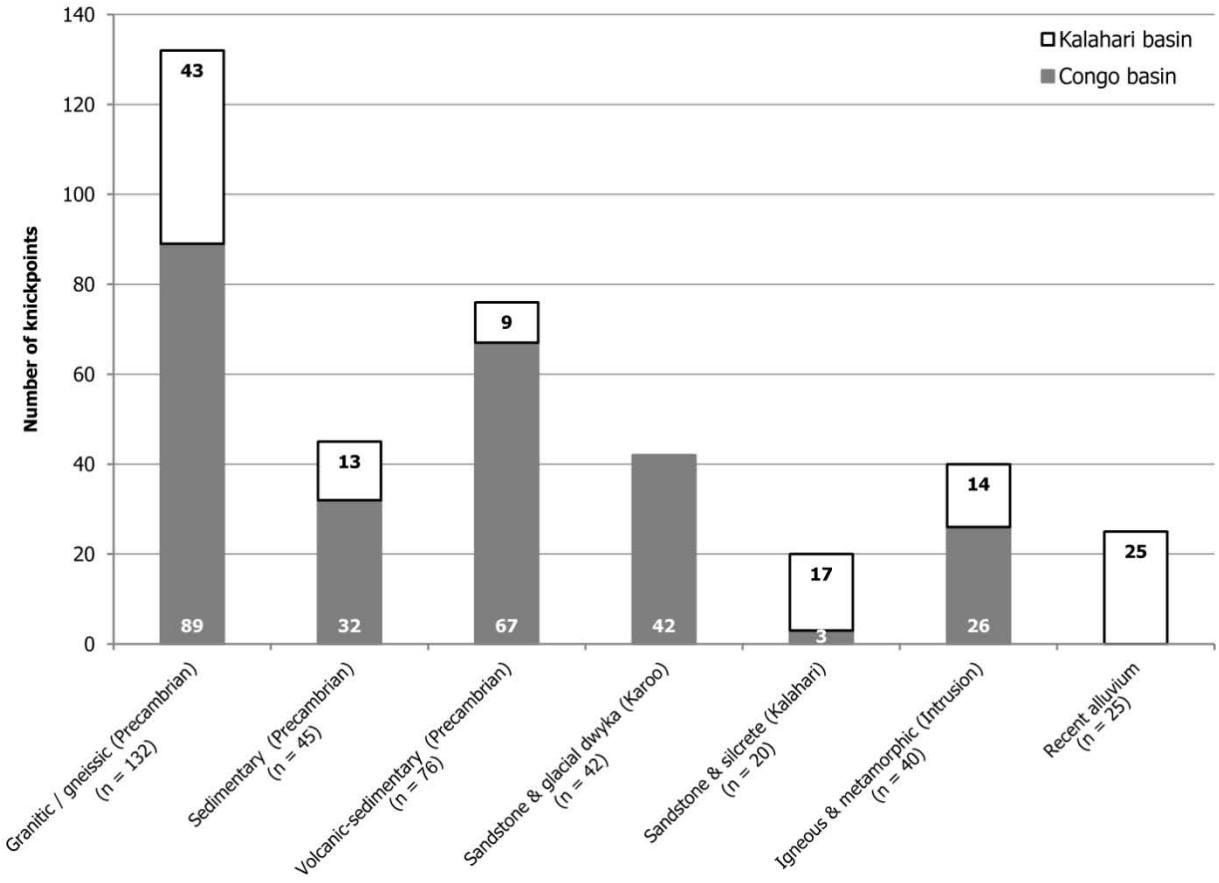

Figure 7.6: The simplified lithologies of the 380 knickpoints identified in this study. The categories are based on lithology age and grouped type, as derived from the detailed geology of each knickpoint. The Congo Basin is indicated in grey and the Kalahari Basin in white.

7.3.1.3 The probable causes of knickpoint occurrence

This section deals with the knickpoint causes with regard to the Congo and Kalahari basin and their relative position along the individual longitudinal profiles rivers. The combined use of the simplified lithology database and the geomorphic evidence captured in the knickpoint geodatabase allowed for possible causes to be assigned to 354 of the 380 knickpoints identified in this study. As the longitudinal profiles have been described in **Chapter 6, Section 6.3.1.1** and the knickpoints in **Table 6.8 Chapter 6, Section 6.3.4.1** (and in greater detail in **Table A6.2** in **Appendix 6, Section 6.3**), the focus here will be on the possible causes of the knickpoints in relation to the longitudinal profile of the rivers. The categorisation of knickpoints was explained and presented in **Sections 6.2.4.1** and **6.3.4.1**. See **Table A7.3**, in **Appendix 7**, **Section 7.3** for the confidence scores for the cause of each knickpoint.

The longitudinal profiles and probable causes of the knickpoints in the CB

Of the 259 identified knickpoints in the CB, 222 could be assigned possible causes, as shown in **Table 7.2**. Lithology is to the most common cause, accounting for 62 % of the knickpoints identified in the CB, with a variety of knickpoint categories being associated with the underlying geology. Knickpoints occurring at the boundaries of different lithologies are responsible for 23 % of the knickpoints and also exhibit a wide range of knickpoint categories. Only 5 % of the knickpoints occur on known faults, with a further 10 % of the knickpoints located in close proximity to faulting or on inferred faults and are thus probably caused by tectonics ('likely fault' in **Table 7.2**). While faulting appears to be responsible for 6 of the knickpoints with heights in excess of 30 m it is mainly a cause of smaller knickpoints. However, 17 % of the knickpoints could not be assigned a cause, either in areas of poorly consolidated material, such as the Cretaceous red sandstones, or lithologies that are not considered to be highly resistant, such as glacial deposits and Kalahari Group sandstones. It is possible that these knickpoints represent areas of localised resistance or are of a purely fluvial origin, such a knickpoint migrating upstream due to a baselevel change.

Table 7.2: The most likely causes of knickpoint occurrence in the Congo Basin. Lithology appears to be the cause for the majority of the knickpoints identified in the Congo Basin.

Knickpoint category	Primary likely cause of knickpoint						
	Fault	**Likely fault**	**Lithology**	**Lithology change**	**Unidentifiable**	**Large dam**	**Total**
-5	1	3	26	12	9	-	**51**
-1	1	-	7	2	5	-	**15**
0	1	2	5	1	-	-	**9**
5	1	6	25	11	7	-	**50**
10	2	5	23	7	5	-	**42**
15	-	1	8	9	3	1	**22**
20	-	2	18	2	5	-	**27**
25	-	1	4	1	1	1	**8**
30	2	-	8	2	-	-	**12**
40	-	-	2	2	-	-	**4**
45	-	-	2	-	-	-	**2**
50	1	-	4	2	1	1	**9**
75	-	-	1	-	-	-	**1**
80	-	2	2	-	-	-	**4**
90	1	-	-	-	1	1	**3**
Totals	**10**	**22**	**135**	**51**	**37**	**4**	**259**

Individual rivers of the CB

Chambeshi-Luapula-Luvua Rivers: While the Chambeshi, Luapula and Luvua were digitised separately, and may be justified as three separate rives on hydrological aspects (each river section has its own distinct baselevel), a better understanding of their evolution can be achieved when they are considered together as a single river system. Of the 30 knickpoints in this system, lithology and changes of lithology account for 21 knickpoints, with 4 being related to tectonics and 5 having causes that were not identifiable (see **Table 7.3)**. Almost all of the knickpoints occur where one river changes to the next; albeit the cause for the knickpoints between the Chambeshi and Luapula sections being unidentifiable, as can be seen on **Figure 7.7**. Downstream of Lake Mweru, the knickpoints of the Luvua River occur on Precambrian rocks and several igneous intrusions.

Table 7.3: The likely causes of the 30 knickpoints of the Chambeshi-Luapula-Luvua river system. Lithology appears to be the largest contributing factor to the occurrence of knickpoints, accounting for 17 knickpoints.

Knickpoint category	Most likely cause of knickpoint : Chambeshi-Luapula-Luvua						
	Fault	Likely fault	Lithology	Lithology change	Unidentifiable	Large dam	Total
-5	-	-	3	2	-	-	**5**
0	-	1	-	-	-	-	**1**
5	-	0	2	1	-	-	**3**
10	1	1	5	-	-	-	**7**
15	-	-	-	-	3	-	**3**
20	-	-	5	-	2	-	**7**
30	-	-	-	1	-	-	**1**
50	-	-	2	-	-	-	**2**
80	-	1	-	-	-	-	**1**
Totals	**1**	**3**	**17**	**4**	**5**	**-**	**30**

Congo River: Of the Congo River's 64 knickpoints, 32 are associated with resistant lithologies or lithological changes (see **Table 7.4**). Tectonic influences play a role in the occurrence of 19 of the knickpoints, while the cause of 11 of the knickpoints could not be identified. The distributions of these knickpoints is shown in **Figure 7.8**, where it can be seen that upper and lower reaches of the Congo River are dominated by tectonic causes, whereas the lithology plays an important role downstream of the faulted zone in the upper regions. The knickpoints whose cause could not be identified occur within the shallow gradient middle reaches.

Table 7.4: The likely causes of the 64 knickpoints of the Congo River. The dominant cause of knickpoint occurrence appears to be lithological, accounting for half (32) of the knickpoints.

Knickpoint category	Primary likely cause of knickpoint : Congo						
	Fault	Likely fault	Lithology	Lithology change	Unidentifiable	Large dam	Total
-5	-	3	3	6	5	-	17
-1	1	-	1	-	-	-	2
0	1	-	-	-	-	-	1
5	1	5	5	3	3	-	17
10	1	3	1	2	3	-	10
15	-	1	-	3	-	1	4
20	-	-	1	1	-	-	2
25	-	-	-	-	-	1	0
30	1	-	4	1	-	-	6
50	1	-	1	-	-	-	2
90	1	-	-	-	-	-	1
Totals	7	12	16	16	11	2	64

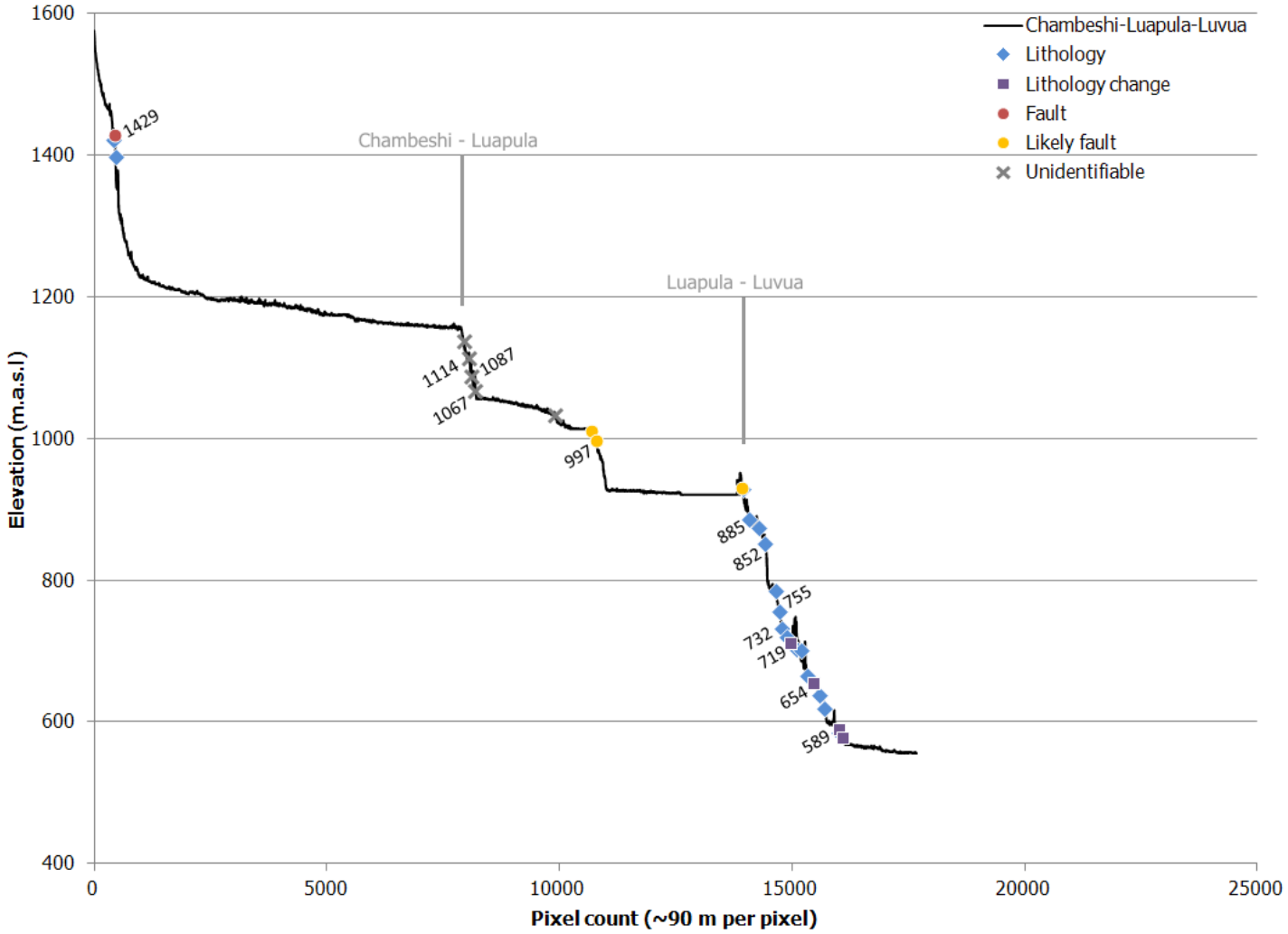

Figure 7.7: The longitudinal profile of the **Chambeshi-Luapula-Luvua** river system. The three sub-profiles cover a distance of ~ 1800 km, having elevation decreases of 416 m (Chambeshi), 241 m (Luapula) and 365 m (Luvua) giving the overall profile a 1022 m decrease in elevation. The location, elevation and most probable cause of knickpoints is indicated. **Thirty** knickpoints occur along the course of the river, with the majority being a result of resistant lithology (**Table 7.3**). Other causes include faulting and differential erosion resistance. The cause of the knickpoints that occur at the transition of the Chambeshi to Luapula could not be determined

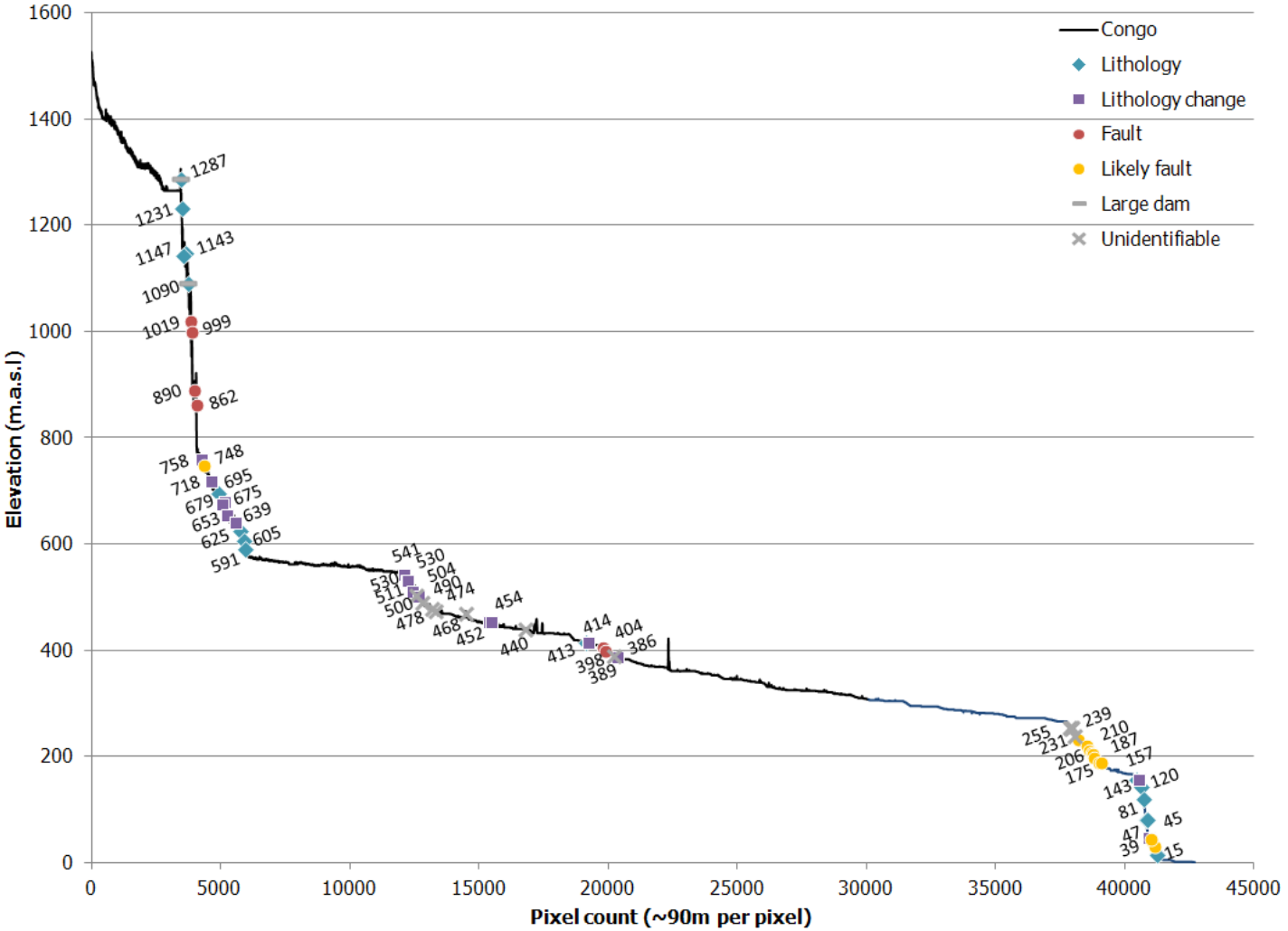

Figure 7.8: The longitudinal profile of the **Congo** River. Over its ~ 4200 km course it drops in elevation is 1526 m. The location, elevation and most probable cause of the Congo's **64** knickpoints is shown. Lithology and lithology change account for the largest proportion of knickpoints: 16 each (**Table 7.4**). The knickpoints of the upper and middle zones appear dominantly related to lithologies while the lower Congo knickpoints are mainly fault related.

Kalungwishi River: The stepped profile of the 290 km Kalungwishi River contains nine knickpoints, eight of which of occur on its three major drops in elevation (see **Figure 7.9**). Of the five knickpoints with heights larger 30 m, four are associated with the underlying geology and one with fault activity, as shown in **Table 7.5**. While faulting may only be associated with a third of the Kalungwishi knickpoints, the three knickpoints are of substantial heights being 20, 25 and 80 m, suggesting that, although limited in number, knickpoints related to faulting can be significant in terms of size.

Table 7.5: The possible causes of the 9 knickpoints of the Kalungwishi Rivers. Lithology appears to be a dominant control, accounting for 6 of the 9 knickpoints, with faulting accounting for the other 3 knickpoints.

Knickpoint category	Primary likely cause of knickpoint : Kalungwishi						
	Fault	Likely fault	Lithology	Lithology change	Unidentifiable	Large dam	Total
10	-	-	1	-	-	-	**1**
20	-	1	1	-	-	-	**2**
25	-	1	-	-	-	-	**1**
30	-	-	1	-	-	-	**1**
40	-	-	-	1	-	-	**1**
50	-	-	1	-	-	-	**1**
80	-	1	1	-	-	-	**2**
Totals	**-**	**3**	**5**	1	**-**	**-**	**9**

Kasai River: As shown in **Figure 7.4**, the geological formation incised by the channel of the Kasai River exercise significant influences on the shape of its longitudinal profile and the occurrence of knickpoints. Of the 47 knickpoints, 43 are associated with the underlying lithology (resistant lithologies and change in lithology), see **Table 7.6**. These lithological controlled knickpoints form the convex regions of the Kasai River, highlighting the influence of geology on the development of the Kasai River.

Table 7.6: The likely causes of the 47 knickpoints of the Kasai River. Knickpoints are dominantly associated with lithology, with 43 of the knickpoints being controlled by the underlying geology.

Knickpoint category	Primary likely cause of knickpoint : Kasai						
	Fault	Likely fault	Lithology	Lithology change	Unidentifiable	Large dam	Total
-5	1	-	7	2	-	-	**10**
-1	-	-	1	-	-	-	**1**
5	-	1	13	2	-	-	**16**
10	-	1	8	2	-	-	**11**
15	-	-	2	2	-	-	**4**
20	-	1	3	-	-	-	**4**
25	-	-	1	-	-	-	**1**
Totals	**1**	**3**	**35**	**8**	**-**	**-**	**47**

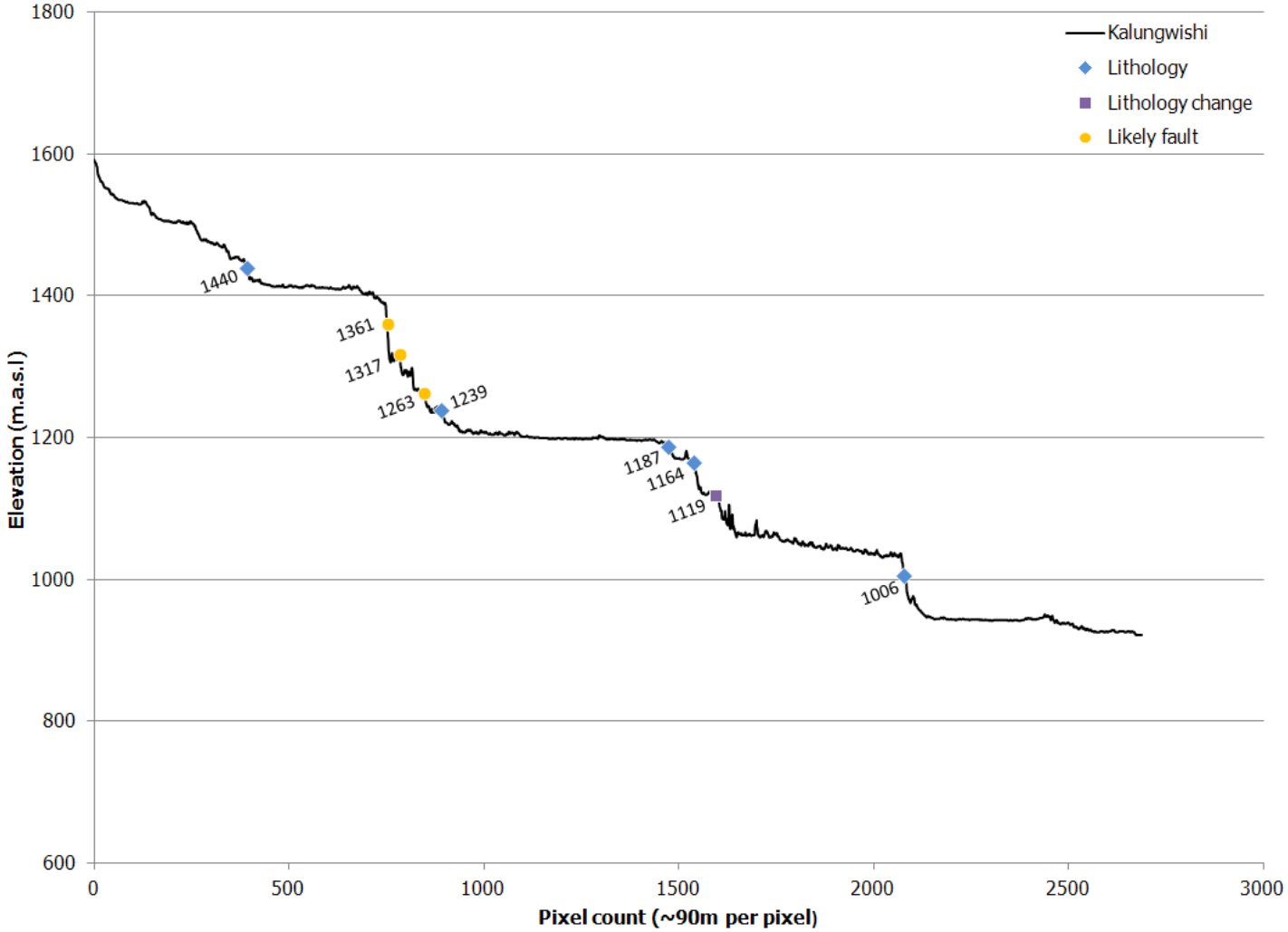

Figure 7.9: The ~290 km long profile of the **Kalungwishi** River experiences a 671 m drop in its elevation over its ~ 300 km course. The location, elevation and most probable cause of the **nine** knickpoints of the river are shown. The nine knickpoints are related to lithology (6) and faults (3) (**Table 7.5**). Two of the three largest knickpoints are due to lithology (category 50 and 80), while the third appears to be related to faulting (category 80).

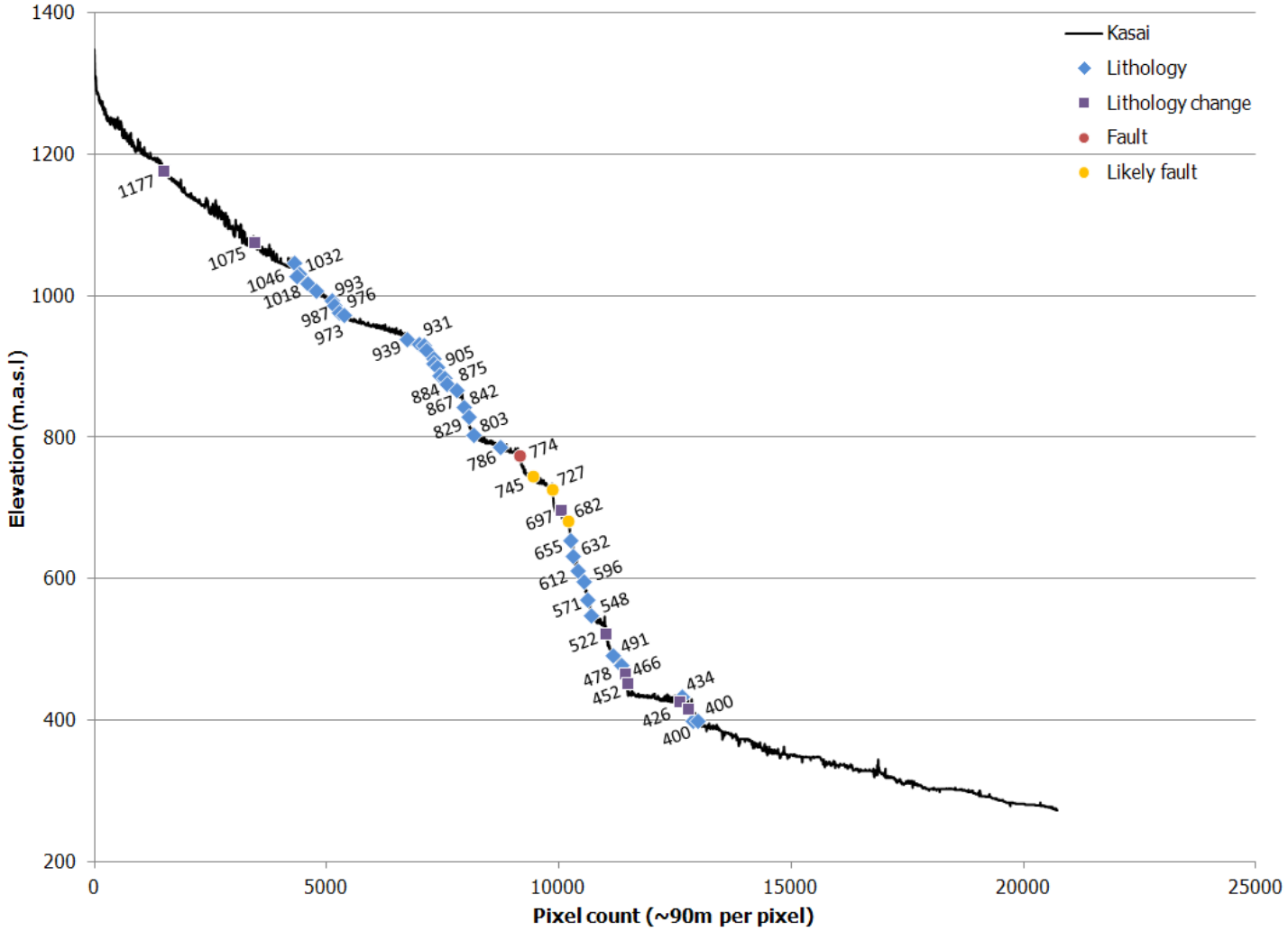

Figure 7.10: The longitudinal profile of the **Kasai** River. Over its ~2100 km course it drops in elevation is 1076 m .The location, elevation and most probable cause of its **47** knickpoints is illustrated. The majority of the knickpoints are associated with lithology (43) with faulting be associated with only 4 of the knickpoints (see **Table 7.6**). The dominating influence of the Precambrian basement is the likely contributes to the rivers overall convex shape. After the last knickpoint at 400 m.a.s.l., the Kasai flows in the *cuvette centrale* that is dominated by unconsolidated alluvium.

Kwango River: The 14 knickpoints of identified along the Kwango are controlled by the lithology (see **Table 7.7**) with the four knickpoints with unidentified causes in the river's upper reaches in Angola (shown in **Figure 7.11**). The control of knickpoints by lithology is confirmed by the plotting of the geology on the river longitudinal profile (see **Figure 7.3)** and the comparisons of the rock type to the proportion of outcrop where knickpoints are found as indicated in **Table 7.1**. Most of the knickpoints are grouped in middle of the river profile (see **Figure 7.11**) where the longitudinal profile is convex.

Table 7.7: The probable causes of the Kwango River's 18 knickpoints. The majority of the knickpoints (14) are associated with lithological controls, with the causes of the remaining knickpoints not being readily identifiable.

Knickpoint category	Primary likely cause of knickpoint : Kwango						
	Fault	Likely fault	Lithology	Lithology change	Unidentifiable	Large dam	Total
-5	-	-	1	-	-	-	**1**
5	-	-	1	3	1	-	**5**
10	-	-	-	1	-	-	**1**
15	-	-	-	1	-	-	**1**
20	-	-	1	1	2	-	**4**
25	-	-	-	1	-	-	**1**
30	-	-	-	1	-	-	**1**
45	-	-	1	-	-	-	**1**
50	-	-	1	-	-	-	**1**
75	-	-	1	-	-	-	**1**
90	-	-	-	-	1	-	**1**
Totals	**-**	**-**	**6**	**8**	**4**	**-**	**18**

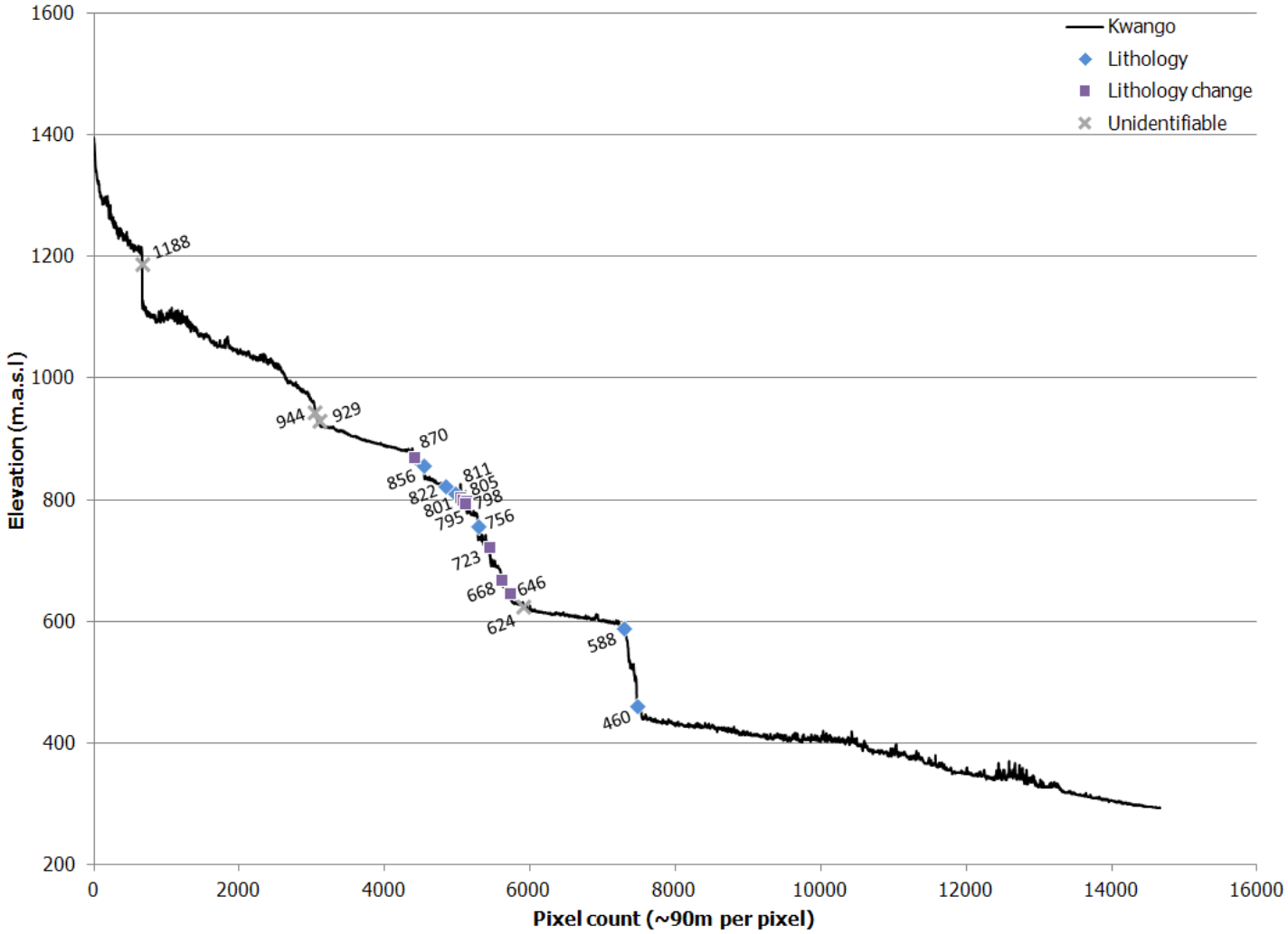

Figure 7.11: The longitudinal profile of the **Kwango** River. The river experiences a 1103 m drop in its elevation over its ~1500 km course. The location, elevation and most probable cause of knickpoints are shown. Of the Kwango's **18** knickpoints, lithology appears to be the main controlling factor, accounting for 14 knickpoints (see **Table 7.7**). Three of the four knickpoints whose cause could not be readily identified occur in the Kwango's headwater region.

Lufira River: Of the 11 knickpoints of the Lufira, eight are associated with lithologic controls (see **Table 7.8)**. These knickpoints are clustered in the two regions of greatest elevation change, and these regions being separated by knickpoint free reaches of very low gradient (see **Figure 7.12**).

Table 7.8: The likely causes of the 11 knickpoints found on along the Lufira River. Two knickpoints identified on the Lufira River are large dams. Of the remaining nine knickpoints, eight were associated with lithology.

Knickpoint category	Primary likely cause of knickpoint : Lufira						
	Fault	Likely fault	Lithology	Lithology change	Unidentifiable	Large dam	Total
-5	-	-	1	1	1	1	**4**
5	-	-	-	1	-	-	**1**
10	-	-	1	-	-	-	**1**
15	-	-	1	-	-	-	**1**
20	-	-	1	-	-	-	**1**
45	-	-	1	-	-	-	**1**
50	-	-	-	1	-	-	**1**
90	-	-	-	-	-	1	**1**
Totals	**-**	**-**	**5**	**3**	**1**	**2**	**11**

Lufupa River: All of the Lufupa's 21 knickpoints appear to be controlled by lithological influences (see **Table 7.9**).The knickpoints occur as three clusters, an upper and lower group that occur on the convex zones of the longitudinal profile and a group occurring between the two on a low gradient portion of the rivers profile, as seen in **Figure 7.13**.

Table 7.9: The likely cause of the knickpoints of the Lufupa River. All of the Lufupa's 21 knickpoints are associated with lithological causes.

Knickpoint category	Primary likely cause of knickpoint : Lufupa						
	Fault	Likely fault	Lithology	Lithology change	Unidentifiable	Large dam	Total
-5	-	-	3	-	-	-	**3**
-1	-	-	2	1	-	-	**3**
0	-	-	5	1	-	-	**6**
5	-	-	1	-	-	-	**1**
10	-	-	-	1	-	-	**1**
15	-	-	2	-	-	-	**2**
25	-	-	3	-	-	-	**3**
30	-	-	1	-	-	-	**1**
40	-	-	1	-	-	-	**1**
Totals	**-**	**-**	**18**	**3**	**-**	**-**	**21**

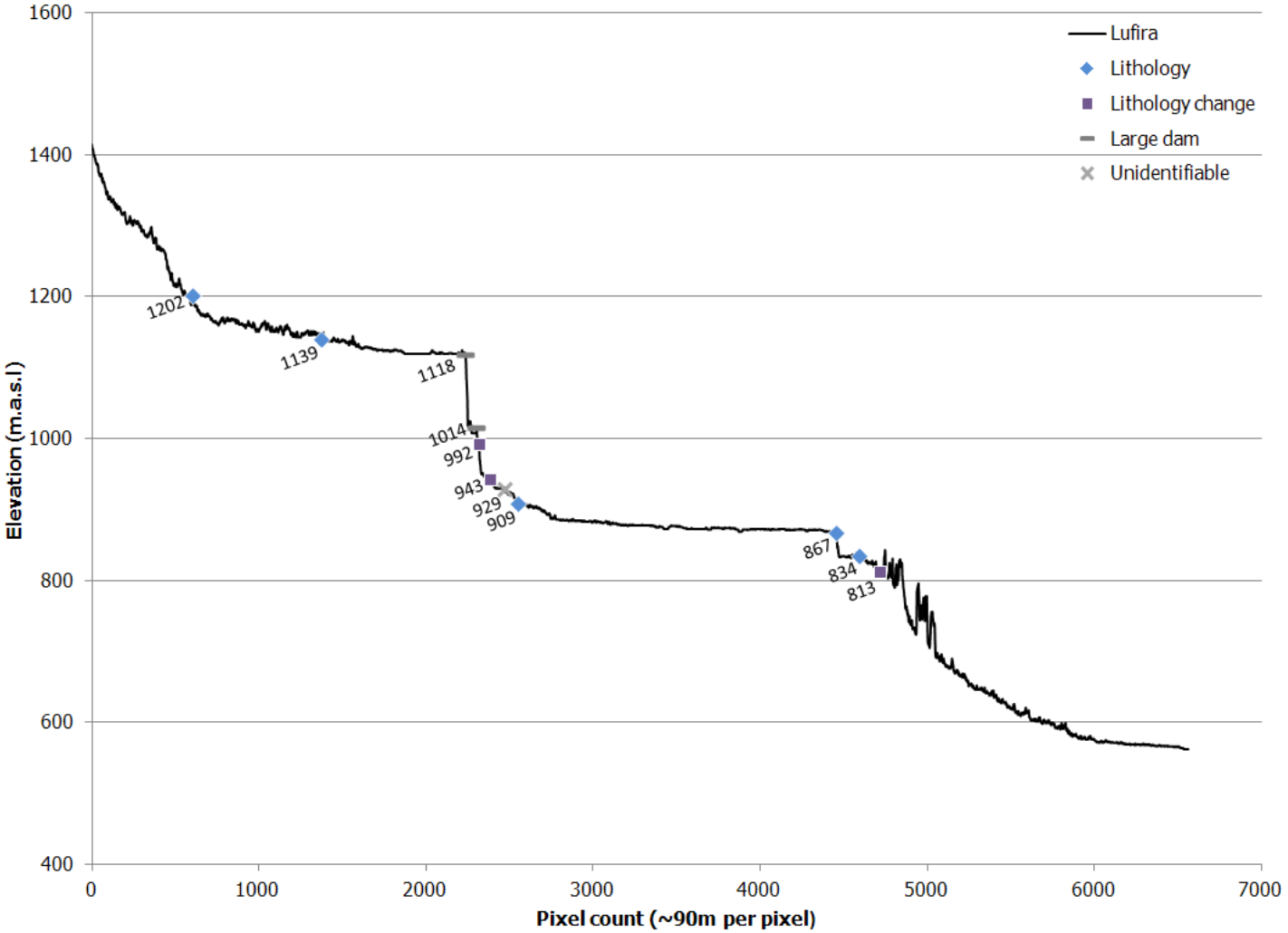

Figure 7.12: The ~ 680 km longitudinal profile of the **Lufira** River experiences an 853 m drop in its elevation. The location, elevation and most probable causes the Lufira's knickpoints are indicated. Of the rivers 11 knickpoints, 8 appear to be related to lithological controls (see **Table 7.8**). Two of the knickpoints are large dams in the upper reaches of the river.

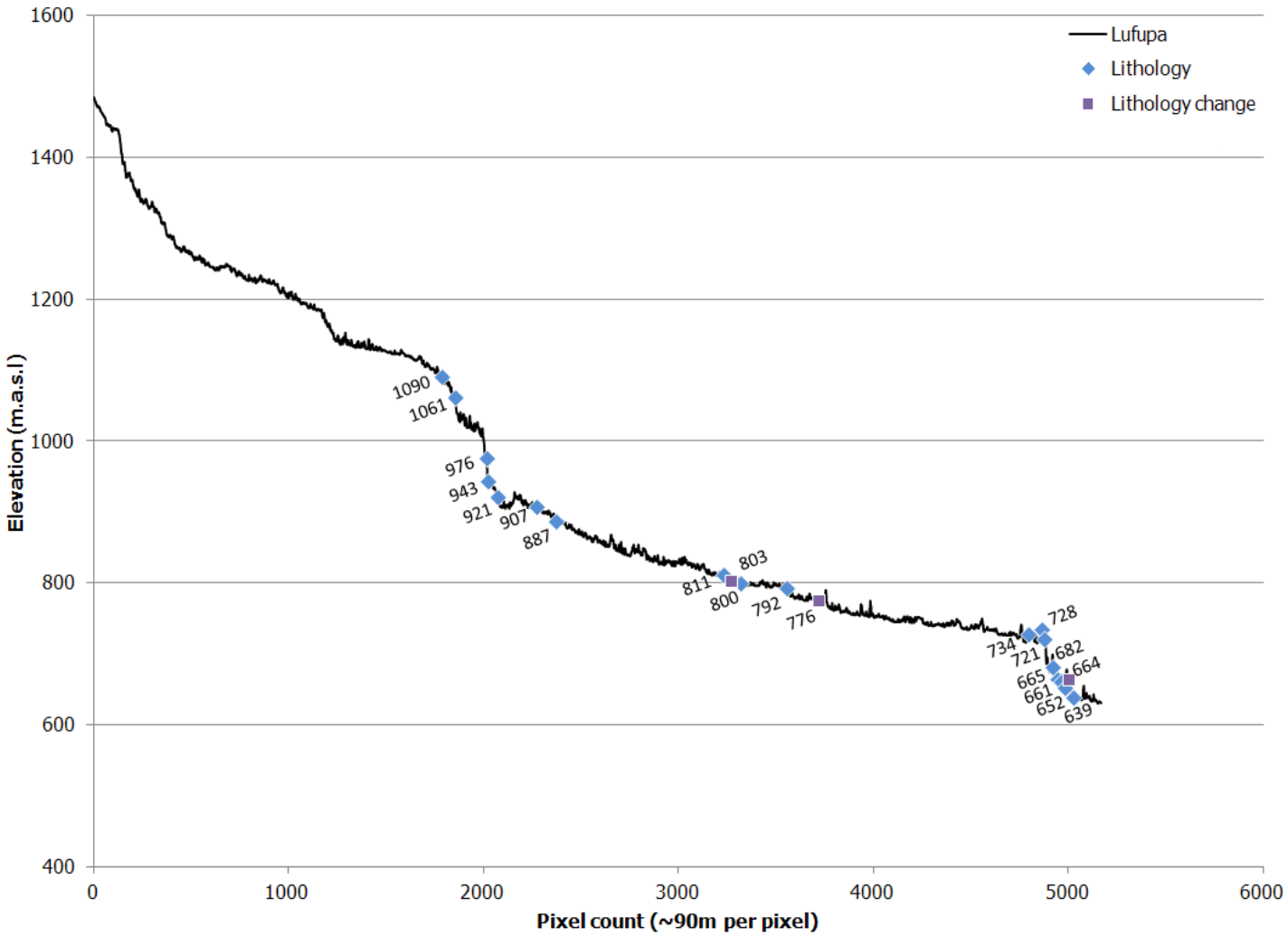

Figure 7.13: The longitudinal profile of the **Lufupa** River. Over its ~ 530 km course it drops a total of 854 m. All of the Lufupa's **21** knickpoints are associated with lithological controls (see **Table 7.9**). The location and elevation of each knickpoint is shown. The knickpoints correspond to the two regions of convexity on the profile, with a cluster of knickpoints occurring approximately half way between the two regions of convexity.

Lukuga River: Of the eight knickpoints of the Lukuga, six are most likely caused by lithologic controls, with five of these knickpoints occurring along the concave region of the profile (see **Table 7.10** and **Figure 7.14**). The last knickpoint is located at 612 m.a.s.l. and no knickpoints occurring below this elevation along the portion of river channel upstream of the Lukuga's confluence with the Congo River.

Table 7.10: The probable causes of the eight knickpoints of the Lukuga River. Six of the knickpoints are associated with lithological controls.

Knickpoint category	Primary likely cause of knickpoint : Lukuga						
	Fault	**Likely fault**	**Lithology**	**Lithology change**	**Unidentifiable**	**Large dam**	**Total**
0	-	1	-	-	-	-	**1**
5	-	-	-	1	1	-	**2**
10	-	-	1	-	-	-	**1**
15	-	-	2	2	-	-	**4**
Totals	**-**	**1**	**3**	**3**	**1**	**-**	**8**

Lulua River: Of the 30 knickpoints of the Lulua, 29 can be explained by lithologic controls, with a single knickpoint occurring on a fault in the lower reaches of the river (see **Table 7.11** and **Figure 7.15**). A single knickpoint occurs on a fault (elevation 752 m.a.s.l.) at the start of river's last zone of rapid elevation change. Most of the river's knickpoints are clustered in this zone, with 16 of the knickpoints occurring downstream of the fault related knickpoint.

Table 7.11: The likely causes of the 30 knickpoints of the Lulua River. Lithologic controls dominate the occurrence of the river's knickpoints, with 29 knickpoints ranging from less than 5 m to 40 m in height.

Knickpoint category	Primary likely cause of knickpoint : Lulua						
	Fault	**Likely fault**	**Lithology**	**Lithology change**	**Unidentifiable**	**Large dam**	**Total**
-5	1	-	7	1	-	-	**9**
-1	-	-	3	-	-	-	**3**
5	-	-	3	-	-	-	**3**
10	-	-	6	-	-	-	**6**
15	-	-	1	-	-	-	**1**
20	-	-	5	-	-	-	**5**
30	-	-	2	-	-	-	**2**
40	-	-	1	-	-	-	**1**
Totals	**1**	**-**	**28**	**1**	**-**	**-**	**30**

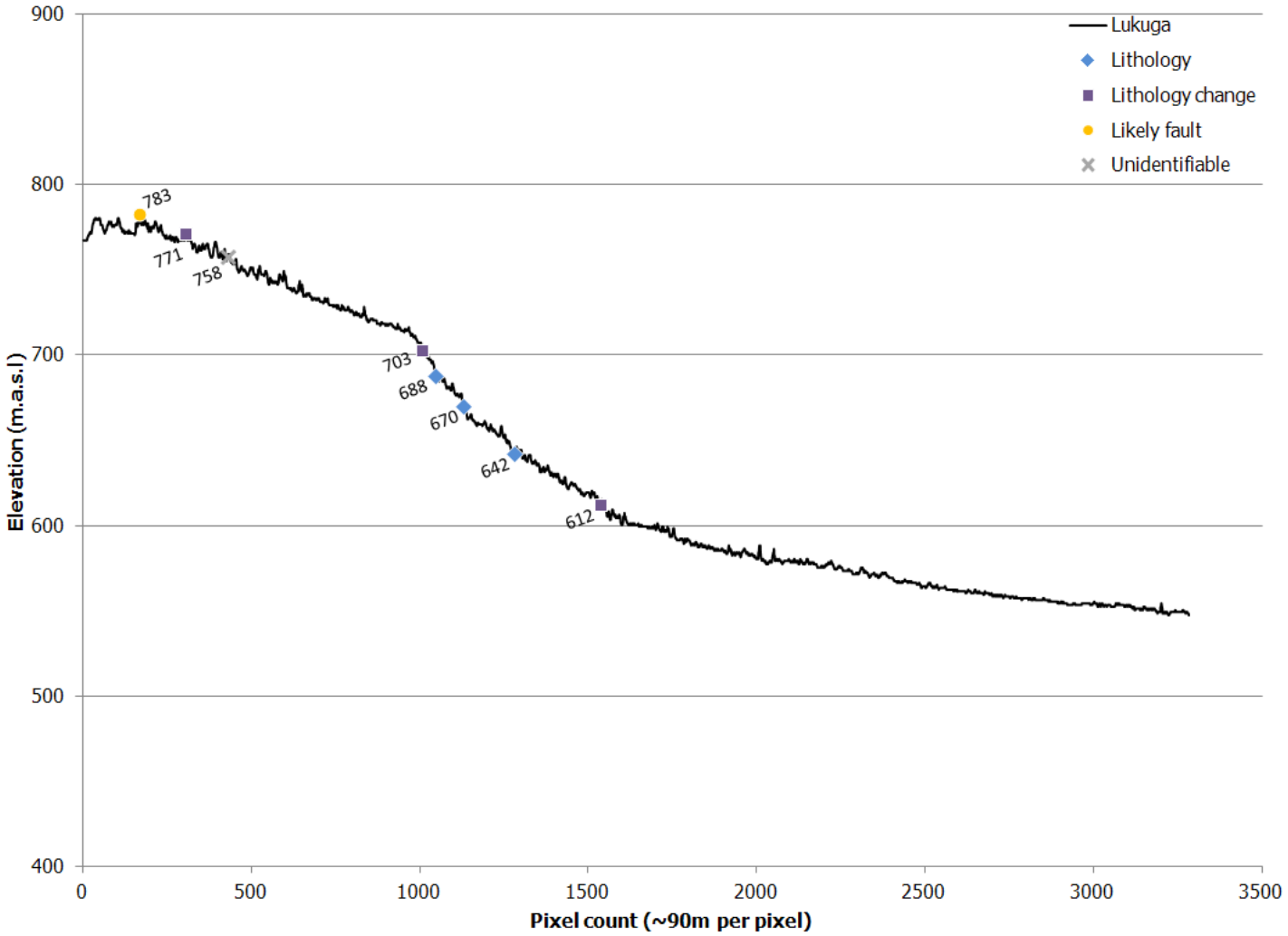

Figure 7.14: The ~340 km long profile of the **Lukuga** River. Over the rivers total elevation drop of 220 m, there is **eight** knickpoints. Six of these knickpoints are associated with lithologic controls with one knickpoint near the beginning of the Lukuga being associated with faulting (see **Table 7.10**). The location and elevation of the knickpoints are shown.

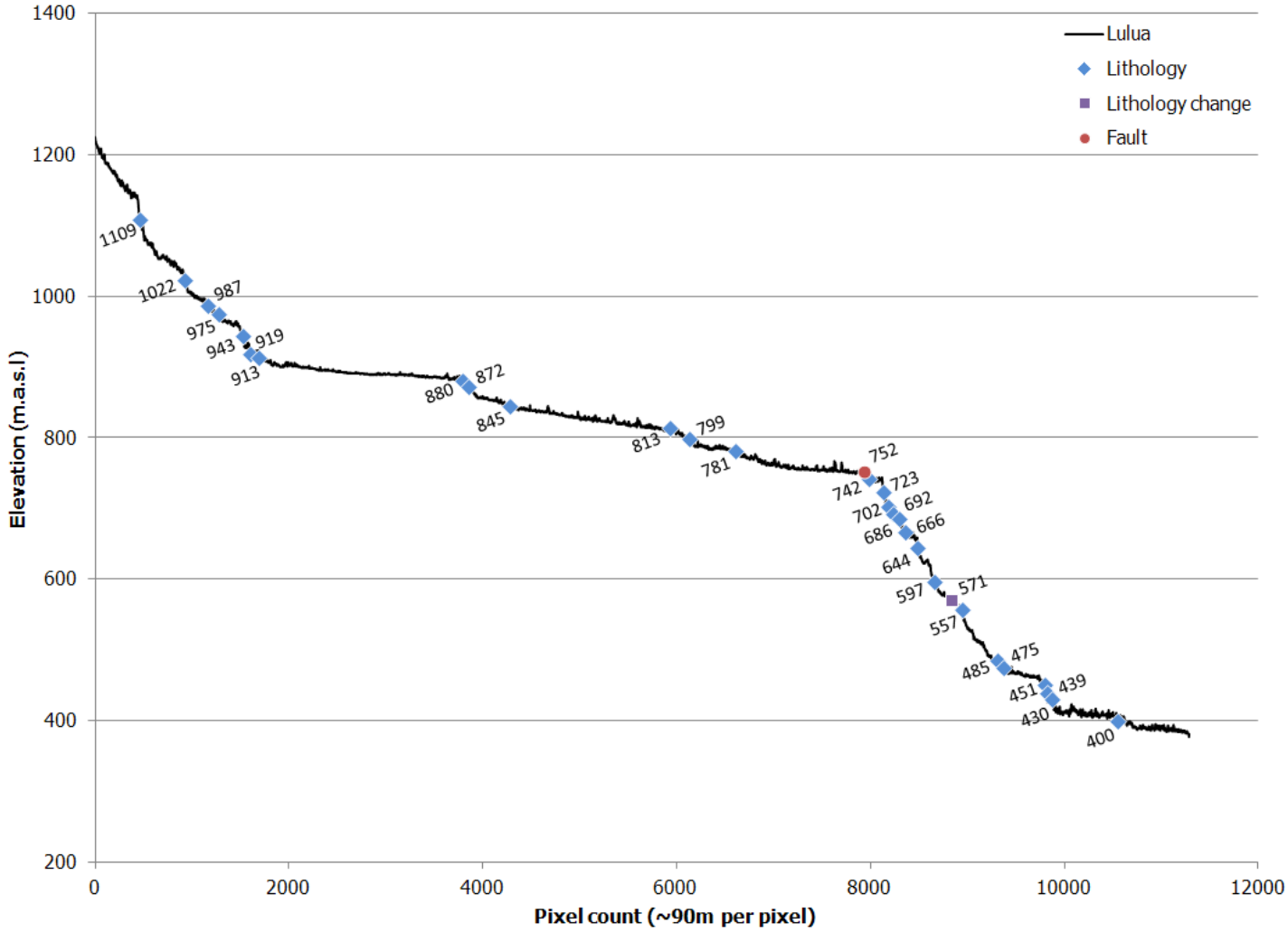

Figure 7.15: The longitudinal profile of the **Lulua** River. The river experiences an 844 m drop in elevation over its ~1100 km course. Of the river's **30** knickpoints, 29 are associated with lithological controls (see **Table 7.11**). The knickpoints occur in spatial clusters, with 7 occurring in close proximity in the river's upper regions and a cluster of 17 in its lower reaches. The location and elevation of the knickpoints is shown.

Wamba River: Of the Wamba River's 21 knickpoints, 15 could not be readily assigned a likely cause (see **Table 7.12**). Ten of these unidentifiable knickpoints occur below 600 m.a.s.l., while the other five occur along river's upper reaches (see **Figure 7.16**). The six knickpoints to which a likely cause could be associated all corresponded to lithologic controls. Three of the lithologically controlled knickpoints occur along the rivers convex upper region.

Table 7.12: The likely causes of the 21 knickpoints of the Wamba River. Most of the knickpoints (15) could not be assigned a likely case.

Knickpoint category	Primary likely cause of knickpoint : Wamba						
	Fault	**Likely fault**	**Lithology**	**Lithology change**	**Unidentifiable**	**Large dam**	**Total**
-5	-	-	1	-	3	-	**4**
-1	-	-	1	-	5	-	**6**
5	-	-	-	-	2	-	**2**
10	-	-	-	1	2	-	**3**
15	-	-	-	1	-	-	**1**
20	-	-	1	-	1	-	**2**
25	-	-	-	-	1	-	**1**
50	-	-	-	1	1	-	**2**
Totals	**-**	**-**	**3**	**3**	**15**	**-**	**21**

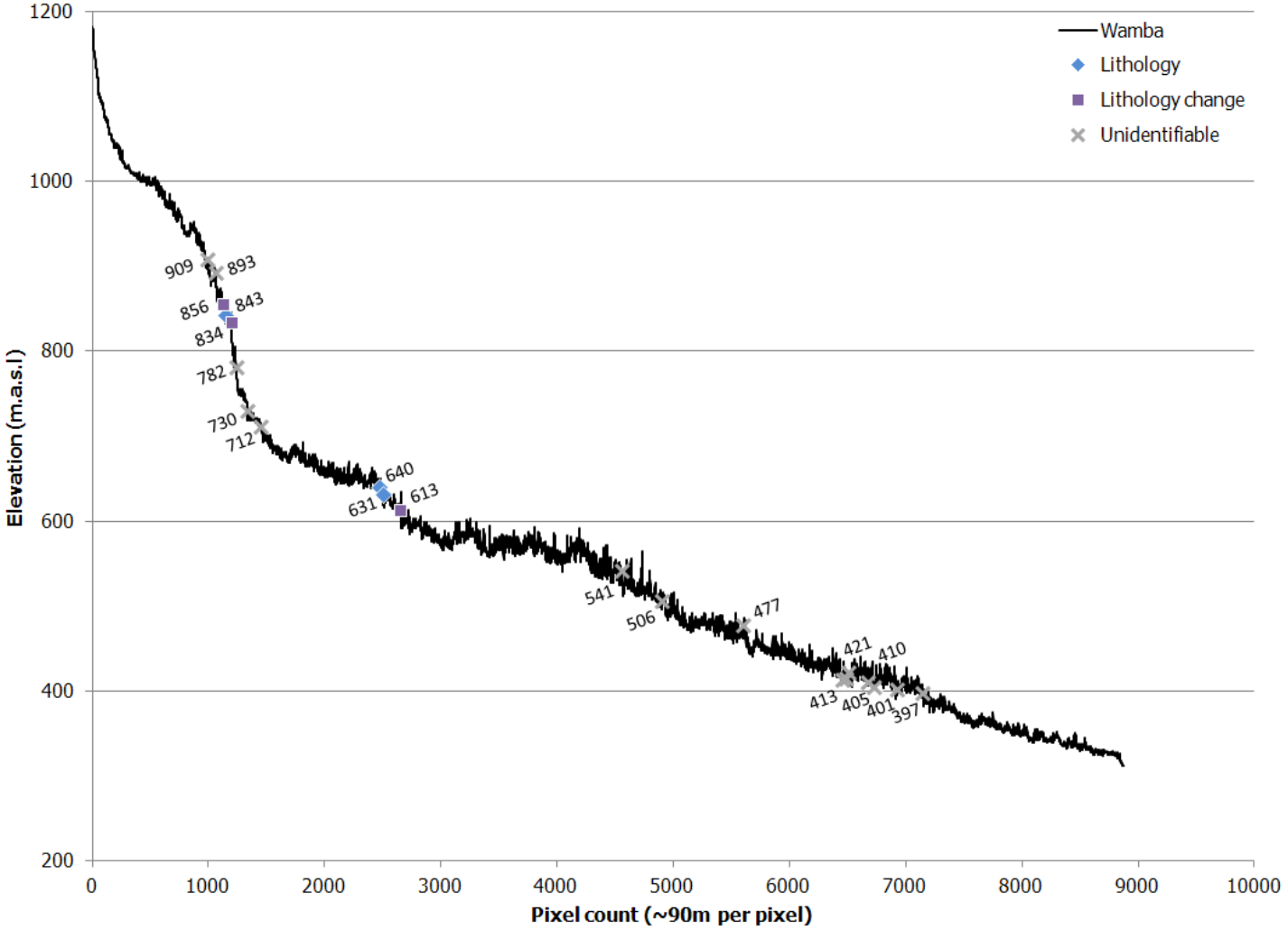

Figure 7.16: The ~920 km longitudinal profile of the **Wamba** River demonstrates an 871 m drop in its elevation over its course. Of the river's **21** knickpoints, 15 could not be readily assigned a likely cause (see **Table 7.12**). Most of these unidentified knickpoints occur below 600 m.a.s.l., in the river's lower course.

The longitudinal profiles and probable causes of the knickpoints in the KB

Of the 121 knickpoints that were identified in the KB, possible causes could be associated with 95 of them (79 %, **Table 7.13**). Knickpoints attributed to lithological controls (both lithologic boundaries or on resistant lithologies) accounted for 74 % of the knickpoints and exhibited a diverse range of knickpoint categories (see **Table 7.13**). By comparison, 12 % of the knickpoints either occurred on known faults or in close proximity to known faults and/or inferred faults (see **Table 7.13**). Over a fifth (21 %) of the knickpoints could not be assigned a cause, with almost all of these knickpoints being found along the Cubango, Luena and Upper Zambezi Rivers. A large proportion of their channels of all three rivers have incised into the Kalahari Group deposits and these unidentifiable knickpoints, 10 of which are smaller than 5 m, may be a result of localised outcrops of resistant layers, such as calcretes and silcretes facies in the Kalahari sediments.

Table 7.13: The most likely causes of knickpoint occurrence in the Kalahari Basin. Lithology appears to be the cause for the majority of the knickpoints identified in the Kalahari Basin.

Knickpoint category	Primary likely cause of knickpoint						
	Fault	Likely fault	Lithology	Lithology change	Unidentifiable	Large dam	Total
-5	3	5	13	12	10	-	**43**
-1	-	-	2	6	3	-	**11**
0	-	-	4	1	1	-	**6**
5	1	-	7	5	4	-	**17**
10	1	-	2	4	4	-	**11**
15	-	-	-	1	2	1	**4**
20	1	-	7	3	1	-	**12**
30	-	-	1	1	-	-	**2**
35	1	-	1	1	-	-	**3**
40	1	-	1	2	-	1	**5**
50	-	-	1	1	-	-	**2**
60	1	-	1	1	-	-	**3**
70	-	1	-	-	1	-	**2**
Totals	**9**	**6**	**40**	**38**	**26**	**2**	**121**

Cubango River: Of the Cubango's 55 knickpoints, 35 are associated with lithologic controls, with nine being related to faulting (see **Table 7.14**). Almost all of the knickpoints (50 of 55) occur in the upper reaches of the river, with only five of the knickpoints occurring in the lower reaches of the river (see **Figure 7.17**). The knickpoints of the upper river region occur as two clusters. The first cluster comprises a headwater concave region of 11 knickpoints, six of which are controlled by lithology and one occurring on a fault. The second, downstream cluster consists of 39 knickpoints, of which 25 knickpoints are related to lithologic controls and nine are related to faulting.

Table 7.14: The likely causes of knickpoint of the Cubango River. Of the rivers 55 knickpoints, 35 are associated with lithologic influences, 6 occur on faults and 11 could not have causes assigned to them.

Knickpoint category	Primary likely cause of knickpoint : Cubango						Total
	Fault	Likely fault	Lithology	Lithology change	Unidentifiable	Large dam	
-5	2	3	2	8	4	-	**19**
-1	-	-	2	4	3	-	**9**
0	-	-	3	1	-	-	**4**
5	1	-	-	2	1	-	**4**
10	1	-	-	2	1	-	**4**
15	-	-	-	1	1	-	**2**
20	1	-	3	3	1	-	**8**
30	-	-	1	1	-	-	**2**
35	-	-	-	1	-	-	**1**
40	1	-	1	-	-	-	**2**
Totals	**6**	**3**	**12**	**23**	**11**	**-**	**55**

Cuchi River: There are 14 knickpoints along the Cuchi River, 11 of which are lithologically controlled (see **Table 7.15**). Apart from two knickpoints related to a change in lithology in the middle of two low gradient reaches, the knickpoints of the Cuchi occur at major changes in the elevation of the longitudinal profile (see **Figure 7.18**). Four knickpoints occur just upstream of the Cuchi junction with the Cubango River, one of which occurs on a fault.

Table 7.15: The probable causes of the 14 knickpoints of the Cuchi River. Almost all of the Cuchi Rivers are related to lithologic controls, with three knickpoints occurring on faults.

Knickpoint category	Primary likely cause of knickpoint : Cuchi						Total
	Fault	Likely fault	Lithology	Lithology change	Unidentifiable	Large dam	
-5	1	-	1	2	-	-	**4**
-1	-	-	-	2	-	-	**2**
5	-	-	-	1	-	-	**1**
20	-	-	2	-	-	-	**2**
35	1	-	-	-	-	-	**1**
40	-	-	-	1	-	-	**1**
50	-	-	-	1	-	-	**1**
60	1	-	-	1	-	-	**2**
Totals	**3**	**-**	**3**	**8**	**-**	**-**	**14**

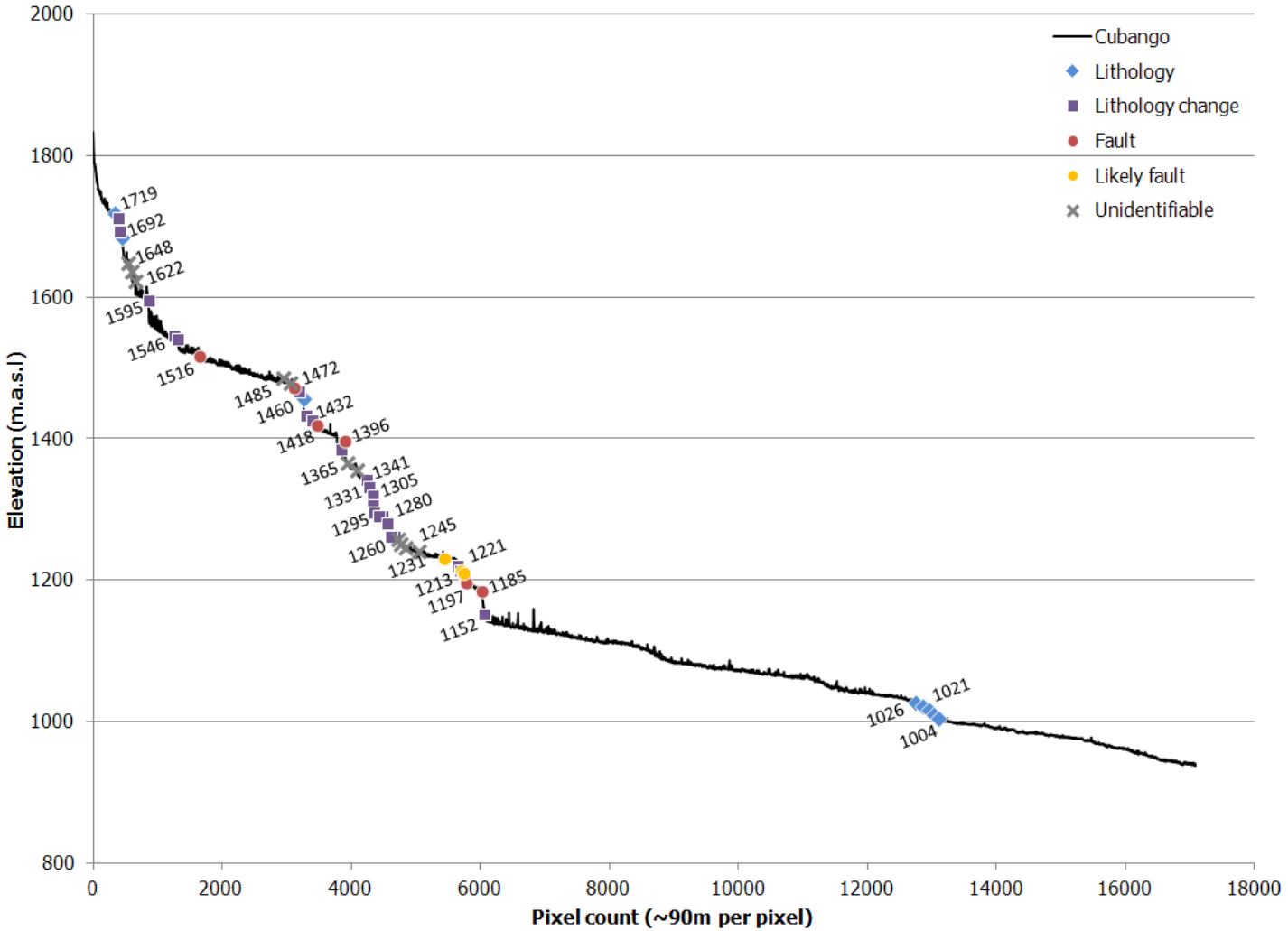

Figure 7.17: The longitudinal Cubango **River** is ~ 1700 km and experiences an 897 m drop in its elevation. Of the rivers **55** knickpoints 35 of them can be associated with lithologic controls (see **Table 7.14**). Nine of the knickpoints occur on known faults. The location and most probable cause of the knickpoints are shown.

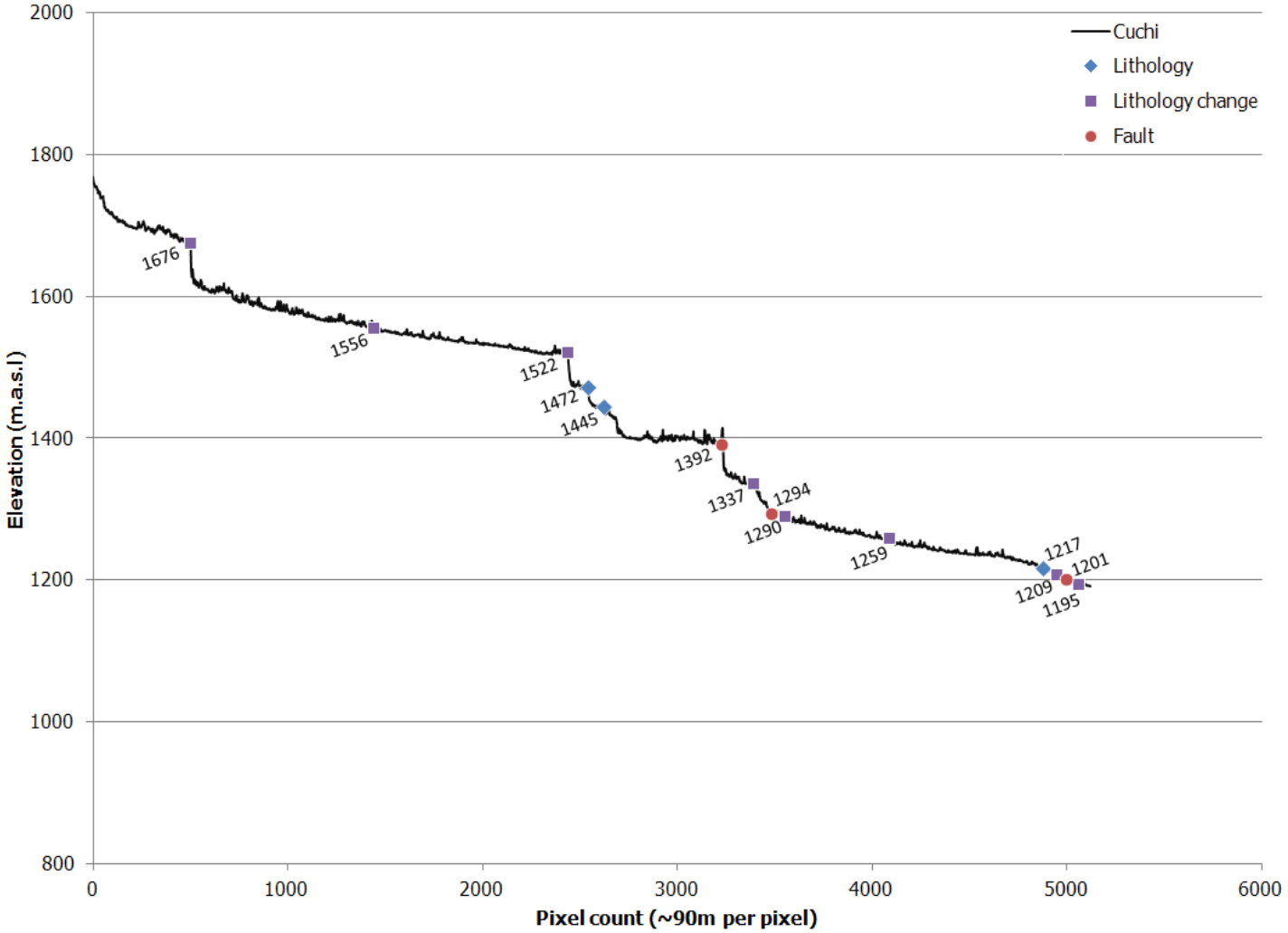

Figure 7.18: The longitudinal profile of the **Cuchi River** is ~520 km and sees a 566 m decrease in its elevation. The river has **14** knickpoints of which 11 are associated with lithological controls (see **Table 7.15**). The location, elevation and most probable cause of knickpoints is shown.

Kabompo River: The Kabompo has three knickpoints that are probably caused by the lithologic controls, with one being probably due to a fault (see **Table 7.16**). Two of these knickpoints (one lithology and one fault) occur in the steep gradient zone of the headwater region and two knickpoints in the lower gradient middle reaches of the river (see **Figure 7.19**).

Table 7.16: All four of the Kabompo River's knickpoints are probably caused by lithologic controls.

Knickpoint category	Primary likely cause of knickpoint : Kabompo						Total
	Fault	Likely fault	Lithology	Lithology change	Unidentifiable	Large dam	
-5	-	-	1	-	-	-	**1**
0	-	-	1	-	-	-	**1**
20	-	-	1	-	-	-	**1**
70	-	1	-	-	-	-	**1**
Totals	**-**	**1**	**3**	**-**	**-**	**-**	**4**

Kafue River: The Kafue has 14 knickpoints of which 11 are likely a result of the rocks over which the river flows (see **Table 7.17**). Large dams account for two of the 14 knickpoints and the cause of the last knickpoint along the river could not be readily identified (see **Figure 7.20**). Despite the change in gradient in the upper Kafue, no knickpoints (as defined in this study) were identified in this upper region, with the knickpoints only occurring from the middle regions onward (see **Figure 7.20**).

Table 7.17: The probable causes of the knickpoints of the Kafue River. Of the river's 14 knickpoints, 11 are possibly due to lithologic controls while two knickpoints are in fact large dams.

Knickpoint category	Primary likely cause of knickpoint : Kafue						Total
	Fault	Likely fault	Lithology	Lithology change	Unidentifiable	Large dam	
-5	-	-	1	1	-	-	**2**
5	-	-	3	1	-	-	**4**
10	-	-	1	1	-	-	**2**
15	-	-		-	-	1	**1**
20	-	-	1	-	-	-	**1**
35	-	-	1	-	-	-	**1**
40	-	-		-	-	1	**1**
60	-	-	1	-	-	-	**1**
70	-	-		-	1	-	**1**
Totals	**-**	**-**	**8**	**3**	**1**	**2**	**14**

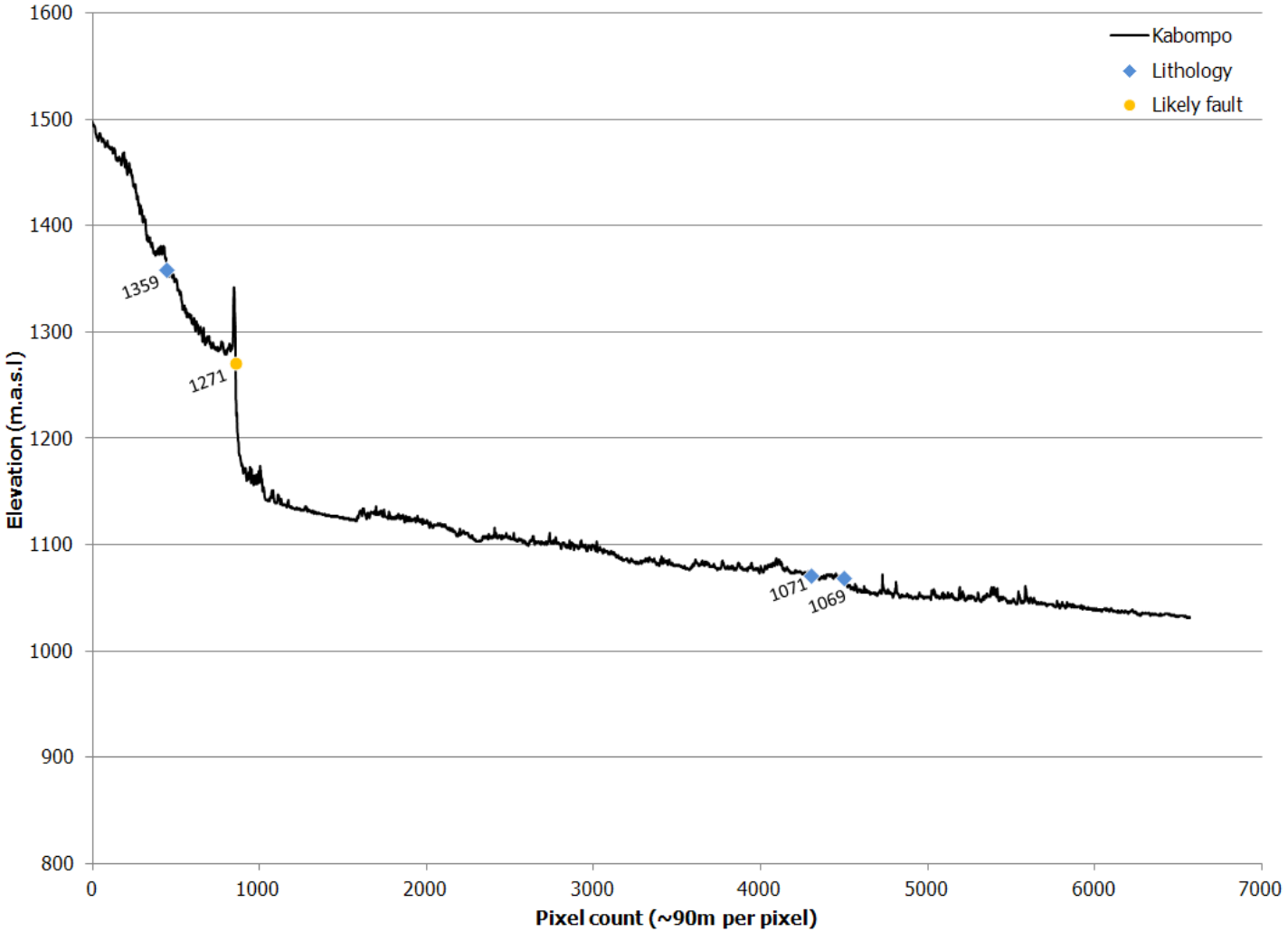

Figure 7.19: The longitudinal profile of the **Kabompo River** drops 464 m over its ~ 650 km length. The Kabompo has four knickpoints, all of which are likely controlled by lithologic controls (see **Table 7.16)**. The location, elevation and most probable cause of knickpoints is indicated. Two of the knickpoints occur in the headwater regions and downstream a further two knickpoints occur in the middle reaches.

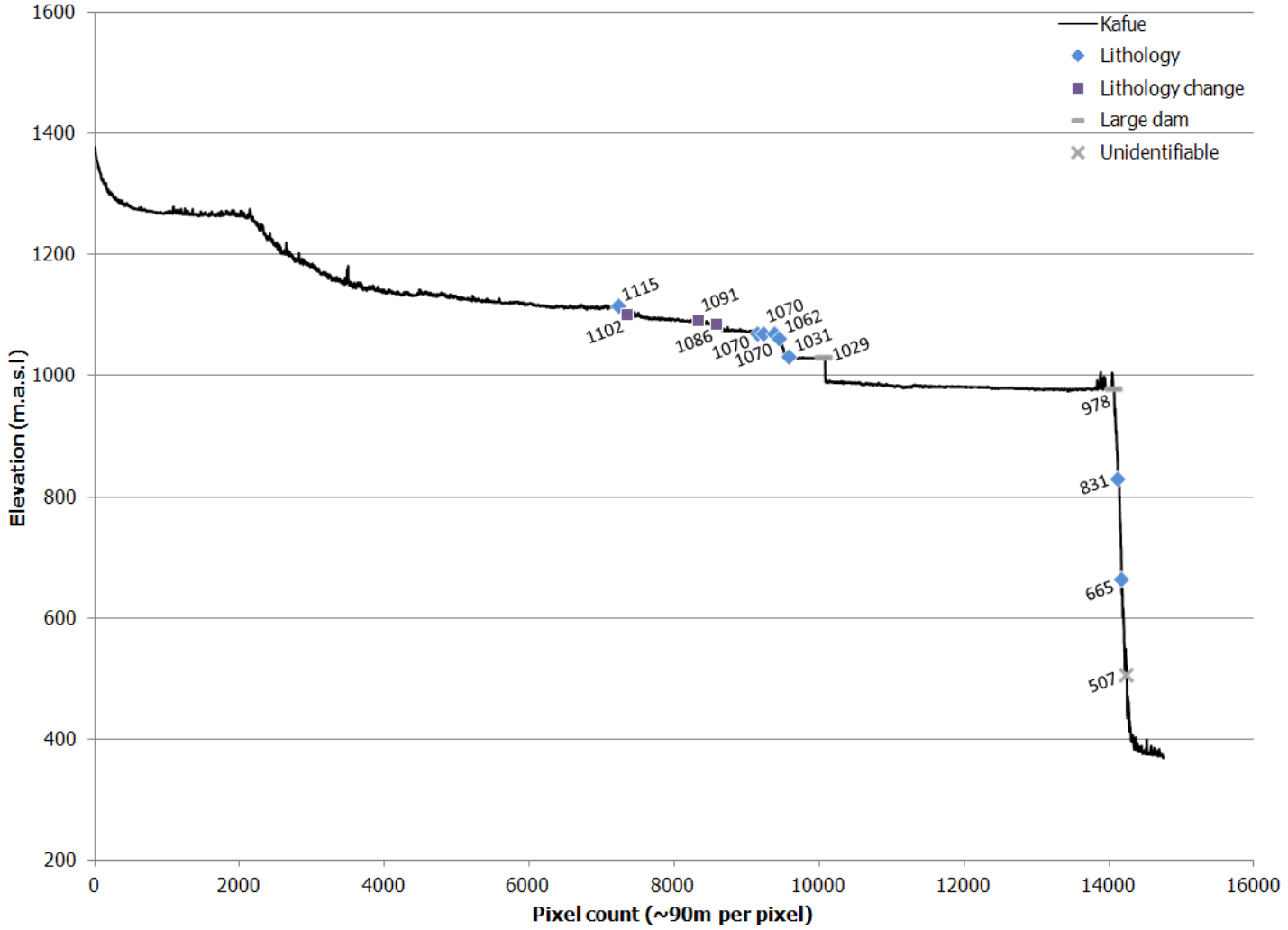

Figure 7.20: Over the **Kafue River's** ~ 1500 km course, the longitudinal profile sees an elevation decrease of 1006 m. The Kafue has **14** knickpoints, 11 of which are probably due to lithologic causes (see **Table 7.17**). The location, elevation and most probable cause of knickpoints are indicated. All of knickpoints occur below elevations of 1120 m.a.s.l. from the middle region of the Kafue River.

Luena River: overall, the Luena is characterised by a low gradient with a total of 10 knickpoints. A possible cause could only be assigned to two of these knickpoints (see **Table 7.18**), located at the start and end of the concave upper regions of the longitudinal profile. They coincide with changes in lithology (see **Figure 7.21**). Seven of the knickpoints whose cause could not be assigned occur within this concave region between these two lithologically controlled knickpoints, with a single knickpoints located immediately upstream of the Luena's junction with the Upper Zambezi River.

Table 7.18: The likely causes of the 10 knickpoints along the Luena River. Of the 10 knickpoints only the cause of two could identified.

Knickpoint category	Primary likely cause of knickpoint : Luena						Total
	Fault	Likely fault	Lithology	Lithology change	Unidentifiable	Large dam	
-5	-	-	-	-	2	-	**2**
0	-	-	-	-	1	-	**1**
5	-	-	-	-	1	-	**1**
10	-	-	-	1	3	-	**4**
15	-	-	-	-	1	-	**1**
40	-	-	-	1	-	-	**1**
Totals	**-**	**-**	**-**	**2**	**8**	**-**	**10**

Upper Zambezi River: The Upper Zambezi River has 24 knickpoints, of which 16 are attributed to due to lithologic influences (see **Table 7.19**). No cause could be readily assigned to 6 of the 24 knickpoints, of which 4 occur in the lower reaches of the river (see **Figure 7.22**). The Upper Zambezi knickpoints occur in four clusters, with three of these groups in close proximity along the lower reaches of the river's course, immediately west of the Machili Flats.

Table 7.19: The probable cause of the knickpoints along the Upper Zambezi. The probable cause of most knickpoints is lithologic

Knickpoint category	Primary likely cause of knickpoint : Upper Zambezi						Total
	Fault	Likely fault	Lithology	Lithology change	Unidentifiable	Large dam	
-5	-	2	8	1	4	-	**15**
5	-	-	4	1	2	-	**7**
10	-	-	1	-	-	-	**1**
50	-	-	1	-	-	-	**1**
Totals	**-**	**2**	**14**	**2**	**6**	**-**	**24**

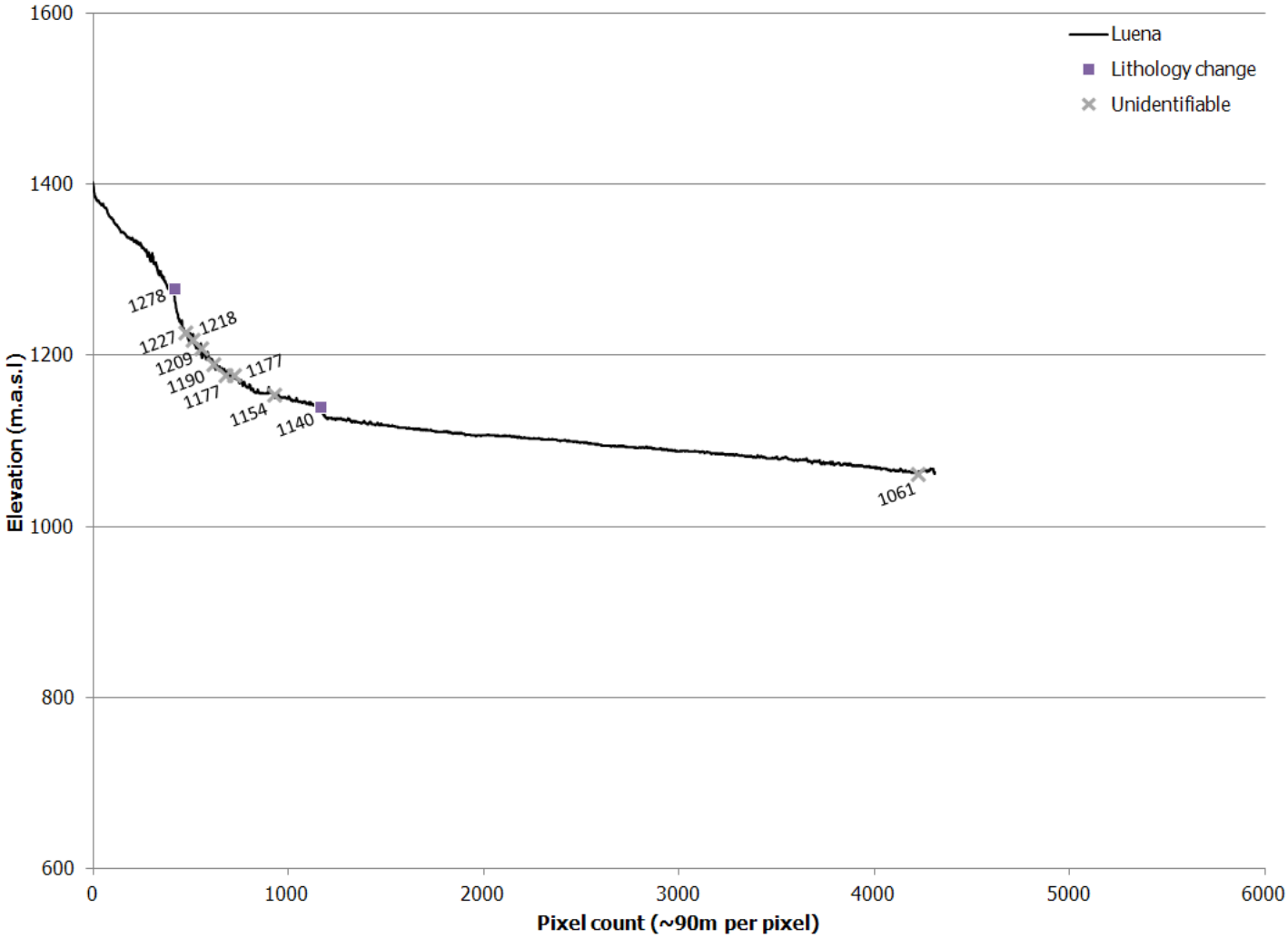

Figure 7.21: The **Luena River**'s longitudinal profile shows a 340 m decrease in elevation over its 430 km course. Of the river's **10** knickpoints only 2 could be assigned a possible cause (see **Table 7.18**). The location and elevation of the knickpoints are shown.

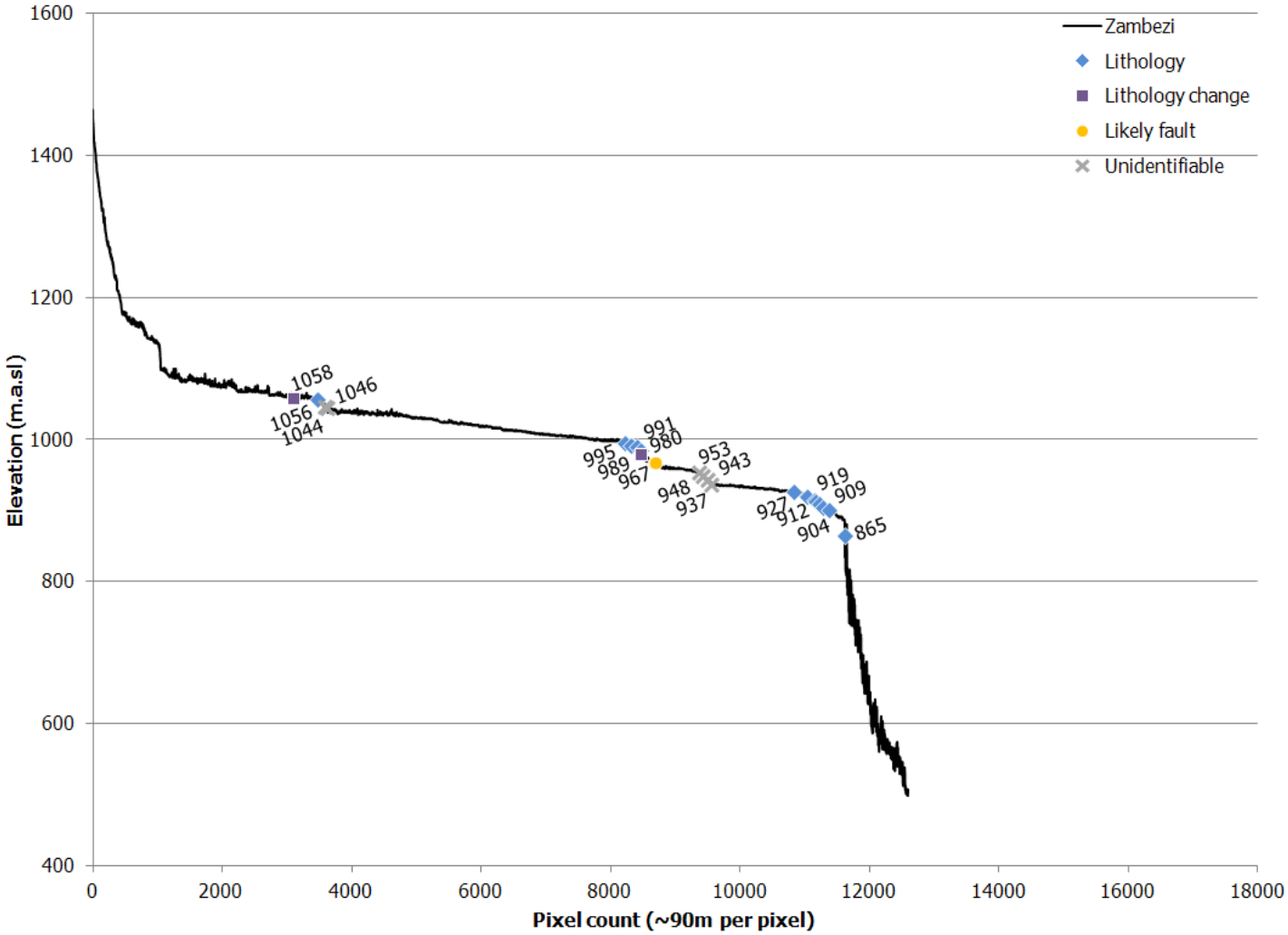

Figure 7.22: The **Upper Zambezi River's** longitudinal profile shows a 959 m decrease in elevation. The ~ 1500 km river has **24** knickpoints of which 16 are controlled by lithology (see **Table 7.19**). The location, elevation and most likely cause of knickpoints is indicated.

7.4 Phylogeographic evidence for landscape changes in south–central Africa

As many of the phylogeographic studies reported events that occurred across watersheds or in broad general areas, no differentiation in terms of presentation was made based on the Congo and Kalahari Basins. **Table 7.20** provides the timings and details of geomorphic events that affected south-central Africa since the Neogene. What is evident from the phylogeographic data is that there have been drainage re-arrangements both within the Congo and Kalahari basins and across drainage divides.

It appears that drainage re–arrangements have occurred around the peripheries of the CB throughout the Neogene (see **Table 7.20**). The eastern margin of the CB has seen disruption of drainage connections to East Africa river systems. Together, the estimated divergence age and genetic affiliations of several fish species, from haplochromine cichlids in the north to eels, tigerfish and mole-rats in the south, indicate a progressive north to south trend of drainage disruption. This disruption began in the late Miocene, if not earlier. The earliest impacts are represented by divergence between species flocks represented today in Lake Victoria and CB haplochromine cichlids. Rifting reached the Tanganyika–Rukwa–Malawi rift triple junction in the late Pliocene (around 3 Ma), as indicated by the congruence in estimates of divergence events that isolated lineages of mastacemalid eels, tigerfishes and mole–rats (Brown et al., 2010; Faulkes et al., 2010; Goodier et al., 2011; Schwarzer et al., 2012). This trend and timing of north to south rift activity broadly corresponds to the geologic evidence that extension of the Western Branch of the EARS occurred during the Neogene (Chorowicz, 2005; Roller et al., 2010; Delvaux, et al., 2012). It is likely that this rift activity caused the re–direction of the early Pliocene Lufubu toward Lake Tanganyika away from the CRS drainages of the Kalungwishi, Bangweulu and Mweru systems (Cotterill and de Wit, 2011). Three fish lineages (mastacemalid eels, southern mouthbrooders and tigerfishes) provide a time estimate range of ca. 3 to 1.5 Ma for this drainage re–arrangement, while the 95 % error of all these estimates collectively constrains the landscape changes within the late Neogene (Koblmüller et al., 2008; Brown et al., 2010; Goodier et al., 2011). The southern, eastern and central margin of the CB (or the KB equivalent) that forms the Congo–Zambezi Watershed saw some substantial changes in river connections during the Pliocene. For example, a substantial portion of the headwaters of the early Neogene Kafue River was captured ca. 3 – 1.8 Myr (based on four fish lineages) by the CRS to create the present day Chambeshi–Luapula–Luvua (including Lakes Mweru and Bangweulu) system of the CB and the Kafue River of the KB (Koblmüller et al., 2008; Day et al., 2009; Brown et al., 2010; Goodier et al., 2011; Cotterill and de Wit, 2011). By ca. 1.5 Ma these rivers were large enough to form a barrier to baboon dispersal between savannah woodlands isolated by

the large rivers (Sithaldeen et al., 2009; Zinner et al., 2009; Keller et al., 2010; Cotterill and de Wit, 2011). The relatively large size of these rivers is also attested by the divergence of *Hydrocynus* Bangweulu population from *H. vittatus* (both tigerfish species) in the Kafue system around 1.4 Ma (Goodier et al., 2011), because these fish are restricted to deep, open water their populations cannot inhabit shallow headwaters. Contemporaneous with these events is the likelihood of several headwater drainage reversals (capture events) that reshaped headwater tributaries across the CKW. These captures are revealed by fishes that currently occur in the Kasai and Lufira Rivers relative to populations who are at present confined in the Zambezi River and its tributaries. The collective phylogeographic evidence is inferred by the locations of hybridisation events between these cichlid fishes and all of the hybridisation occurred during the late Neogene (Schwarzer et al., 2012). Earlier geomorphic studies (e.g. Dixey, 1943; King, 1951; Wellington, 1955) had proposed a multiplicity of drainage reversals across the region; these theories are now supported by the phylogeographic evidence. At a similar time to the Lufira–Zambezi re-arrangements, hybridisation of haplochromine cichlid across the Cuanza–Kwango watershed occurred, suggesting a river capture event in between the Lucalla (part of the coastal Cuanza drainage) and Kwango river systems (Schwarzer et al., 2012).

As detailed in **Table 7.20**, the Pleistocene saw the establishment of the modern day drainage pattern of the *cuvette centrale,* including the arc of the Congo River. The age of this establishment can be estimated by invoking the MCRA of three species complexes of primates. Molecular clocks constrain divergences of their extant representatives at 1.5 – 2.5 Myr (these dates are collated from Hart et al., 2012; Prüfer et al., 2012; Scally et al., 2012). This same time period also saw the severance of hydrological connections between the Bangweulu system and Lake Tanganyika drainage systems (Cotterill and de Wit, 2011; Goodier et al., 2011). In the CB there was partial drainage capture of the basins north–western margin tributaries by headward erosion of the Ogoué River, a coastal river in Gabon, during the late Pleistocene (0.8 Ma) as evidenced by the MCRA age estimate of divergence between the southern and northern mandrills (*Mandrillus sphinx*) (Telfer et al., 2003).

In the KB the late Pleistocene saw the impoundment of the Upper Zambezi by the Bulozi graben (found approximately 300 km upstream of Victoria Fall and the start of the Middle Zambezi) with subsequent restoration of the connection between the Upper and Middle Zambezi Rivers (Cotterill, 2006; Moore et al., 2012). The radiation and dispersal of three fish lineages (*Pseudocrenilabrus*, *Serranochromine* and *Hydrocynus*) date onset of this damming event to be ca. 0.4 Ma (Joyce et al., 2005; Katongo et al., 2007; Koblmüller et al., 2008). The congruence of the divergence ages of

approximately 0.3 Ma for four mammal species lineages, hartebeest (*Alcelaphus spp*); eland (*Taurotragus spp*), giraffes (*Giraffa spp*) and sable antelopes (*Hippotragus spp*) (Flagstad et al., 2001; Pitra et al., 2006; Brown et al., 2007; Lorenzen et al., 2010), can be explained by an independent estimate of 0.3 Ma (Cotterill, 2006; Moore et al., 2012) as to when sustained (perennial) river flow resumed in the Upper Zambezi river; thereafter the Upper Zambezi was permanently linked with the Middle Zambezi River. Thus, the joining of these two rivers formed a barrier to dispersal of many species of terrestrial mammals, but it is argued that the ancestors of these lineages were able to disperse across the Upper Zambezi valley earlier in the middle Pleistocene during the existence of paleo-Lake Bulozi. This large lake was maintained by the impounded Upper Zambezi, such that substantially river flow downstream allowed dispersals of the mammal faunas between central and southern Africa (Moore et al., 2012).

Drainage changes of the western CKW were also occurring during the Pleistocene with the dispersal and speciation of Serranchromine cichlids across the Cunene–Cubango watershed. This capture of part of the Cubango drainage by the coastal Cunene system, the Colui River in particular, led to the dispersal of cichlids into the Cunene system around 0.4 Ma (Koblmüller et al., 2008). The genetic evidence from *Hydrocynus vittatus* indicates dispersal of tigerfish into the Kasai River from the Upper Zambezi system, suggesting a 0.31 Ma age estimation of the capture of the now west to east flowing Kasai River by the southerly flowing Kasai River (Goodier, et al., 2011). Owing to the spatial distribution of these species and the proximity of many of them to one another, it is possible to group disparate species together (see **Appendix 7**, **Section 7.4**, **Table A7.4**) The congruence of species data, so long as a sufficient number and diversity are utilised, may provide unique insights into the landscapes development over Neogene timescales.

Table 7.20: Geomorphic developments of the Congo and Kalahari Basins during the Neogene and Quaternary. The timing of events is based on ages reported by phylogeographic studies. Sources for phylogeographic evidence are indicated by superscript with corresponding references given below the table. Abbreviations in the table are as follows: CRS–Congo River System, CB–Congo Basin; KB–Kalahari Basin; CKW–Congo–Kalahari Watershed

	Estimated time (Ma)	Phylogeographic evidence and age range	Geomorphic interpretation
NEOGENE	early to middle Miocene	**1a)** "*Haplochromis*" species "Yaekama" is distributed in the north-eastern CRS near Kisangani, but groups with Lake Victoria superflocks [21] **1b)** Lake Kivu provides a sistergroup for the modern haplochromines found in Lake Victoria [21]	**1)** Diversion of north-eastern Congo drainage of the Aruwimi River headwaters towards the Nile river system. Probably a result of Miocene rift activity of the Albert Rift in the north of Western Branch (e.g. Roller et al., 2010)
		2a) Close phylogenetic relationship of "*Haplochromis*" species haplotypes of the Fwa-Inkisi-Kwilu Rivers [21] **2b)** Fwa River "*Haplochromis*" closely related to those found in the mid-Kasai and mid-Kwango Rivers and Fwa haplochromides show close genetic affinity to haplochromides from the lower Congo River [21]	**2)** Major drainage re-organisations of the southern CRS including: i) the severing of connections between the Fwa, Inkisi and Kiwul Rivers; presently these rivers are adjacent to one another; ii) disruption of the Sankuru-Lukemie system, with the Sankuru River now flowing into the Kasai system
	ca. 4	**3)** High level of cichlid flock diversification (*Steatocranus* : 0.94 - 4.48 Ma and *Nanochromis* : 1.6 - 2.67 Ma) in the lower Congo River. These cichlids are endemic to rapids [19]	**3)** Establishment of continuous water flow of the CRS to the Atlantic Ocean via the lower Congo River
	late Neogene	**4)** Hybridisation of taxa of northern and southern *Oreochromis torrenticolo* and *Serranochromis* species "red scales" that presently occur either side of the Congo-Cuanza and Congo-Zambezi divides [21]	**4)** Partial drainage re-arrangement of headwaters of the Lucalla River (lower Cuanza system - a coastal drainage) and minor Kwango River tributaries; partial capture minor Zambezi or Kafue tributaries by the the Lufira River headwaters (CB)
	3.9 - 3.3	**5)** *Mastocembalus frenatus* (LT) diverges from M. shiranus (LM) (2.9 - 5.6 Ma) [12] Fukomys cladogenesis (3.2 - 3.8 Ma) [13] Mastocembalus sp nov 3 (Ok) vs M. stappersi (Luongo-Kalungwishi-Lufubu) (2.7 - 3.9 Ma) [12]	**5 - 7)** Enhanced rifting of the Tanganyika-Rukwa-Malawi Rift resulted in widespread drainage disruption. The phylogenetic age estimates broadly correlate with evidence derived from geologic and geomorphic studies (e.g. Chorowicz, 2002; Roller et al., 2010; Delvaux et al., 2012)
	3.1	**6)** Phylogenetic divergence dating of *Hydrocynus tanzania* and *H. vittatus* (1.9 - 6.9 Ma) [2]	
	3.0	**7)** *Mastocembalus* cf *frenatus* vs *M.* cf *frenatus* (2.5 - 3.5 Ma) [7]	

Table 7.20: *continued from above*

	Estimated time (Ma)	Phylogeographic evidence	Geomorphic interpretation
QUATERNARY	2.2 2.1	**1a)** *S. nigromaculata* vs *S. nigro-maculata* (1.4 - 3.4 Ma) [9] **1b)** Serranochromine cladogenesis (1.5 - 2.6 Ma) [7]	**1)** Disruption of drainage connection between the eastern and central rivers of the KB and subsequent isolation of drainages
	2.0	**2)** Founding of *Hydrocynus* "Clade B" and "Clade C" diverges from "Clade D" and *H. vittatus* (0.8 - 3.0 Ma) [16]	**2)** Separation of the drainage connection of Bangweulu and Lufubu from the Upper Congo drainage to the west
	2.0	**3a)** Age of MRCA (2.5 - 1.5 Ma) of chimpanzees on the north Congo River bank and bonobos on the south Congo River bank [18] **3b)** Divergence date of 1.75 Ma between western and eastern lowland gorillas of the CB [20]	**3)** Emplacement of the modern day crescent shape of the Congo River in the region of the Equator
	1.8	**4a)** *Pseudocranilabrus* "lufubu" speciation (1.4 - 2.3 Ma) [7] **4b)** *S. nigromaculata*2 diverges from *S. nigromaculata*3 (1.0 - 2.7 Ma) [9]	**4)** Disruption and isolation of the drainage connection between the Lufubu and Bangweulu river systems
	1.7	**5)** Divergence age of 1.7 Ma (3.2 - 0.8 Ma for TSPY marker) or 2.8 Ma (4.3 - 0.6 Ma for Xq13.3 homolog) for *Cercopithecus lomamiensis* and *C. hamlyni*. These two monkey species are separated by the Congo and Lomami Rivers [17]	**5)** Major south flowing tributaries in the *cuvette centrale* are established and have flowed continuously since the Pleistocene
	1.5	**6a)** Divergence date between *Hydrocynus* clades of Lake Tanganyika and Bangweulu drainage systems [16] **6b)** The Lukuga River appears to be a biogeographic barrier between two chimpanzee populations [8] **6c)** *Hydrocynus* "Clade B" diverges from "Clade C" (0.6 - 2.5 Ma) [16] **6d)** Baboons, *Papio kindae* vs P. cf. cyanocephalus / *P. griseipes* Clade (1.03 - 1.98 Ma) [10; 11; 14]	**6)** Phases of drainage capture and network re-arrangement across the CKW. The Lukuga R. achieves a sufficient size and consistency of flow to prevent chimpanzee movement. Isolation of baboons indicate the emplacement of relatively large in eastern CKW.
	1.4	**7)** *Hydrocynus* "Bangweulu Clade D" diverges from *H. vittatus* (PK) (0.6 - 2.5 Ma) [16]	**7)** Connect of the Kafue and Bangweulu river system by a river sufficiently large to prevent baboon movement and to allow tigerish dispersal
	0.89	**8)** Radiation of *Synodontis* catfishes (0.42 - 1.4 Ma) [9]	**8)** Establishment of (partial?) connections between the Cubango and Zambezi drainage systems
	0.8	**9)** Age of MCRA of southern and northern mandrills [2]	**9)** Establishment of the modern day Ogoue River (coastal river in Gabon) with associated capture north-western tributaries of the CRS
	0.4	**11a)** *Serranochromine* Zambezian radiation [7] **11b)** *Pseudocranilabrus* dispersal [3; 6; 7] **11c)** *Serranochromine* dispersal and speciation (0.2 - 0.6 Ma) [7]	**11)** Onset of impoundment of Upper Zambezi in the Bulozi Graben, allowing for fish radiation and dispersal.Isolation
	0.3	**12)** *Hydrocynus vittatus* dispersal into Congo and Middle Zambezi and undergo cladogenesis [16]	**12)** A single capture event of a Zambezi tributary by the Kasai River and subsequent isolation
	middle Pleistocene (ca. 0.3 Ma)	**13a)** Hartebeests *Alcelaphus* (0.188 - 0.24 Ma) [1] **13b)** Eland *Taurotragus* Southern vs Eastern clades (0.074 - 0.374 Ma) [15] **13c)** Giraffes, *Giraffa camelopardalis giraffe* (S) vs *tippelkirschii* (E) (0.17 - 0.37 Ma) [5] **13d)** *Hippotragus niger* vs *H. kirkii* (0.261 - 0.3 Ma) [4]	**13)** Resumption of sustained flow of the Upper Zambezi into the Middle Zambezi, thus forming a barrier to dispersal

1 – Flagstad et al. (2001); 2 – Telfer et al. (2003); 3 – Joyce et al. (2005); 4 – Pitra et al. (2006); 5 – Brown et al. (2007); 6 – Katongo et al. (2007); 7 – Koblmüller et al. (2008); 8 – UNEP-WCMC and IUCN (2008); 9 – Day et al. (2009); 10 – Sithaldeen et al. (2009); 11 – Zinner et al. (2009); 12 – Brown et al. (2010); 13 – Faulkes et al. (2010); 14 – Keller et al. (2010); 15 – Lorenzen et al. (2010); 16 – Goodier et al. (2011); 17 –Hart et al. (2012); 18 - Prüfer et al. (2012); 19 – Schwarzer et al. (2011); Scally et al. (2012); 21 - Schwarzer et al. (2012)

7.5 The occurrence of knickpoints in south–central Africa

7.5.1 The controls of knickpoints

The results from the amalgamation of geomorphic and geologic data for the 380 knickpoints classified in this study strongly suggest that lithology plays a dominant role (**Table 7.21** and **Figure 7.23**). The apparent lithologic control of knickpoints in south–central Africa has significant consequence for the development of the region's fluvial systems, especially the shape of the rivers' longitudinal profiles, as exemplified in **Figures 7.4** and **7.5**. This is especially true of knickpoints occurring on the Precambrian granitic and gneissic basement (see **Figure 7.6**), as resistant lithologies can effectively limit the denudation of the landscape (e.g. Gilbert, 1877; King, 1951; Hack, 1975; Tooth et al., 2004; Loget and van den Driessche, 2009; Decker et al., 2013). Thus these knickpoints may become effectively fixed to their spatial location as river incision into the basement rocks, preventing lateral migration in the river's course. Rock control also limits vertical incision of the longitudinal profile relative to other regions of less resistant rock. These bedrock knickpoints may therefore dampen changes to baselevel, so they increase the time it takes for the knickpoint to migrate upstream (Loget and van den Driessche, 2009). It could be expected that these knickpoints on Precambrian rocks may become zones where successive baselevel changes merge. This hypothesis can be invoked to explain some of the large knickpoints found on the Precambrian rocks, for example, on the Kwango River (see **Figures 7.5** and **7.11**, **Table 7.7** and **Table A7.2** in Appendix **7**).

The association of knickpoints with lithology in south–central Africa has already been observed by Wellington (1949) for the Upper Zambezi, who noted that where the river was superimposed on resistant rocks, it formed rapids and gorges. The impact of lithologic controls on the development of Zambezi River can be seen by the knickpoint occurring on resistant lithology that is found at the terminus of the alluvial Barotse floodplain (Wellington, 1949). The Barotse floodplain has been recently identified as a large, graben containing late Cenozoic sedimentary infill, representing a large paleo–lake, Lake Bulozi (Cotterill, 2006; Moore et al., 2012). Downstream of the Barotse plain, at distances of approximately 100, 230 and 255 km, knickpoints occur on resistant Batoka basalts, upstream of where the Zambezi flows over the Victoria Falls into the Batoka Gorge (Wellington, 1949). Furthermore, Wellington (1949) also observed that the knickpoint that marks the start of the Okavango Delta system occurs on Proterozoic quartzite. In the CB Linol (2012) confirmed that the last two knickpoints of the Kwango River (see **Figures 7.5** and **7.11**) occur on the Precambrian granitic and gneissic basement, and both the observed Lumangwe and Kaweluma Falls (**Figures 6.9**

and **6.10**) of the Kalungwishi River occur on Proterozoic quartzites. These observations serve as confirmation of the role of lithologic controls of knickpoints of south–central Africa suggested in the discussion above.

Table 7.21: A summary of primary knickpoint causes for the rivers investigated in this thesis. There is strong association of knickpoints with lithologic controls.

	Primary likely cause of knickpoint						
Feature	**Fault**	**Likely fault**	**Lithology**	**Lithology change**	**Unidentifiable**	**Large dam**	**Total**
Chambeshi-Luapula-Luvua	1	3	17	4	5	-	**30**
Congo	7	12	15	17	11	2	**64**
Kalungwishi	-	3	4	1	1	-	**9**
Kasai	1	3	35	8	-	-	**47**
Kwango	-	-	6	8	4	-	**18**
Lufira	-	-	5	3	1	2	**11**
Lufupa	-	-	18	3	-	-	**21**
Lukuga	-	1	3	3	1	-	**8**
Lulua	1	-	28	1	-	-	**30**
Wamba	-	-	3	3	15	-	**21**
Cubango	6	3	12	23	11	-	**55**
Cuchi	3	-	3	8	-	-	**14**
Kabompo	-	1	3	-	-	-	**4**
Kafue	-	-	8	3	1	2	**14**
Luena	-	-	-	2	8	-	**10**
U. Zambezi	-	2	14	2	6	-	**24**
Congo Basin	10	22	134	51	38	4	**259**
Kalahari Basin	9	6	40	38	26	2	**121**
Totals	**19**	**28**	**174**	**89**	**64**	**6**	**380**

Faulting accounts for 47 (12 %) of the studied knickpoints, which is substantially less than those related to lithology (263 or 69 %). Faulting is an important control as evidenced by the large size of several of the faulted knickpoints (see Figure **7.23** and **Table A7.2** in **Appendix 7**). In the CB, nine of the knickpoints 20 m and higher are related to faulting (shown on Table 7.2) and for the KB five knickpoints are 20 m or higher (see **Table 7.13**). These instances of large knickpoints related to faulting suggest that tectonic activity, while playing a lesser role than lithological control in terms of knickpoint numbers, is still a significant controlling factor which as influenced the evolution of south–central Africa's drainage.

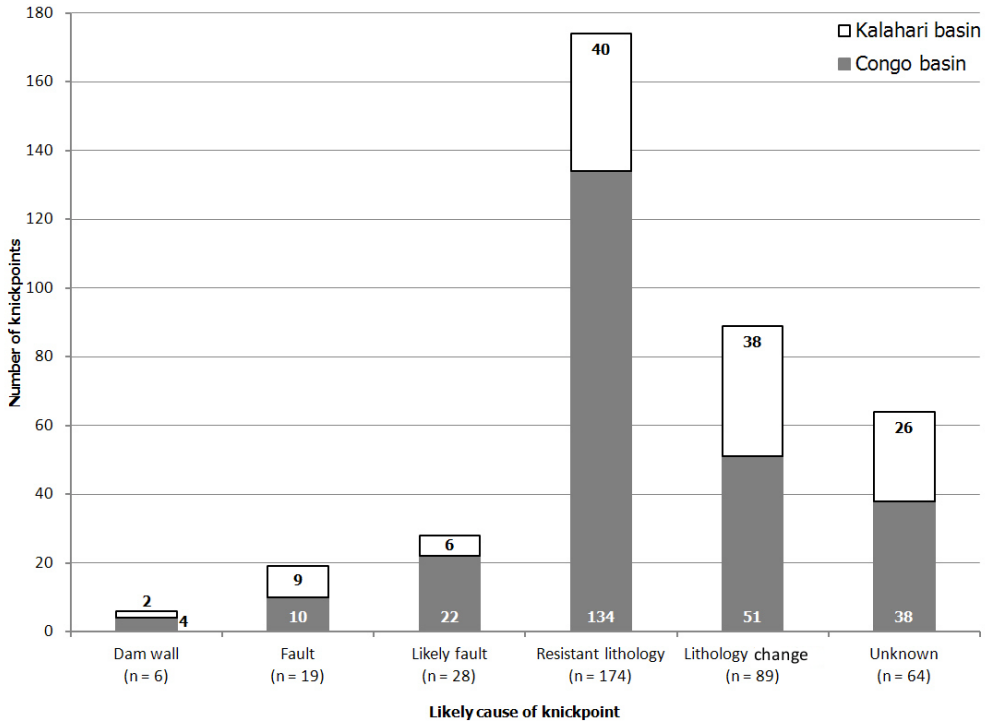

Figure 7.23: The likely causes of knickpoints in the Congo and Kalahari Basins. Lithologic controls (resistant lithologies and changes in lithologies) appear to be the dominant control on knickpoint occurrence.

Of the 380 knickpoints categorised in this study, 64 (17 %) knickpoints could not be readily assigned a cause (see **Figure 7.23**). Of these 64 knickpoints only 10 had heights of 20 m or more with the majority (28) being categorised as -5 (heights less than 5 m), -1 (no discernible height) and 0 (inconclusive). Thus most of the unidentified knickpoints can be considered minor knickpoints. These minor knickpoints may be caused by the initiation of new knickpoints, trunk–tributary relationships or localised faulting. Further investigation into the cause of these knickpoints should focus on the Kwango, Wamba, Cubango, Luena and Upper Zambezi Rivers, which together account for 44 of the 64 unidentified knickpoints. These five rivers all have higher than average incidences of knickpoints whose cause remains unidentified, with the Luena (8 out of 10, or 80 %) and the Wamba (15 out of 21, or 71 %) being the rivers with the highest relative number of unidentifiable knickpoints.

7.5.2 The distribution of knickpoints in south–central Africa

The evidence from this study strongly suggests that the knickpoints of south–central Africa are predominantly controlled by lithology; with faulting playing a lesser but nonetheless important role because some faults appear to have actively created a knickpoints. The association of knickpoints and lithologic controls may be due to fluvial processes resulting in vertical bed erosion and subsequent superimposition on a resistant lithology. The later circumstances result in knickpoint

formation due to vertical erosional differences (e.g. Gilbert, 1877; Horton, 1945; Strahler, 1952; Hack, 1960). The difference in rocks encountered by the rivers in this study may explain the distribution of the knickpoints and difference in the rivers' longitudinal profiles. Collectively these differences can be compared across respective illustrations of the mapped river longitudinal profiles (**Figures 7.7** to **7.22**).

An alternative explanation is that knickpoints are a sole function of changes in the rivers base level brought on by cycles of uplift and subsidence. This explanation suggests that any association of a knickpoint with lithology and/or faulting is co-incidental, and knickpoints occurrence would exhibit a degree of altitudinal correspondence. A comparison of knickpoint occurrence to basin hypsometry should then reveal a pattern of altitudinal association. As shown in **Figure 7.24**, most of the knickpoints occur between the 800 – 1100 m.a.s.l., this altitudinal range corresponds to a change in basin elevation of the CB and KB. For the CB the largest number (37) of its knickpoints occur between 600 – 699 m.a.s.l., with 33, 36, 34 and 30 knickpoints occurring between 400–499, 700–799, 800–899 and 900–999 m.a.s.l. All of these elevation intervals have comparable number of knickpoints. In summary, there does not appear to be a definitive correlation of knickpoint number to the basin elevation. It is notable that the large number of knickpoints (53) occur between 400–599 m.a.s.l., which is the CB's dominant elevation. Nevertheless, if baselevel constituted the sole control of knickpoints position, then most of the knickpoints would occur in the higher, steeper elevations. The small, second peak of the CB's hypsometry is interesting and can most plausibly be attributed to topographic control by Western Branch of the EARS, which has increased the basin's eastern elevation. While the CB's knickpoint distribution is skewed toward the CB's higher elevation, this pattern is not shared with the KB. In contrast to the CB, the KB knickpoints of are skewed to the basin's lower elevations, with 42 of the basin's 121 knickpoints occurring below 1099 m.a.s.l. (see **Figure 7.24**). The highest number of the KB's knickpoints (29) matches the peak elevation distribution but the distribution of knickpoints does not exhibit a clear trend with the rest of the basin's hypsometry. In both basins, this lack of any definitive association between knickpoints elevation and basin hypsometry strongly suggests that knickpoint formation is not solely a function of uplift or subsidence.

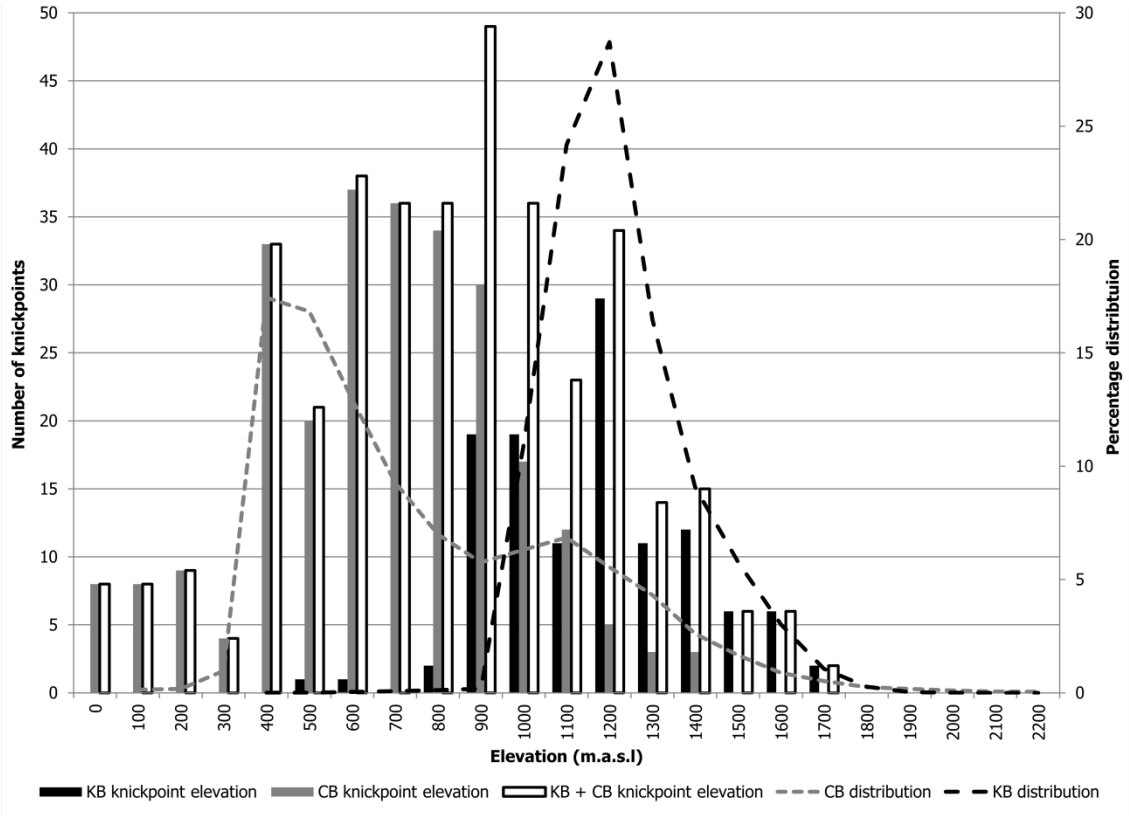

Figure 7.24: The number of knickpoints as a function of the distribution of basin drainage elevation (hypsometry). The highest number of knickpoints appears to fall within a zone 800 – 1100 m.a.s.l, which corresponds to a change in basin elevation distributions, with the Congo Basin having a decreasing distribution at this range while the Kalahari Basin has an increasing distribution. The number of Kalahari knickpoints are indicated by the black bars, the grey bars indicate the number of Congo knickpoints and the white bars indicates the total number of knickpoints for that given elevation interval. The basins' hypsometry is indicated by the grey (Congo) and black (Kalahari) dashed lines.

7.5.3 Controls of knickpoint occurrence in south–central Africa

The association of knickpoints with faults and lithologic controls suggests that in south–central Africa these factors are the dominant controls of the development of the rivers' longitudinal profiles. However, the fact that 17 % of the studied knickpoints could not be readily assigned a cause suggests that other factors may be important controls of knickpoint occurrence. As knickpoints may be related to changes in baselevel, this may be the explanation for these knickpoints. While baselevel changes do not appear to be a dominant influence, they may play a role the occurrence of the knickpoints not explained by faults or lithologies.

The location of knickpoints is probably due to the interplay of several influences interacting in both enhancing and subduing the expression of the knickpoint in terms of its height. Sinha and Parker

(1996) noted that the major changes imposed on a river system may not necessarily result in significant changes in the river's longitudinal profile, as these changes may replace one driving mechanism for another. This study, as discussed in this chapter, has attempted to assign a possible dominant cause to the knickpoint but the interaction between a variety of possible causes needs to be further investigated and this would require more accurate and spatially correct information. Therefore the causes suggested in this study should be considered as a first approximation, using currently available public information. The attribution of knickpoint causes are likely to undergo substantiate revision and refinement in the future.

While lithology and faults are important controls of knickpoint occurrence and distribution in south–central Africa, these two factors do not account for all the knickpoints nor do they provide an explanation of the ultimate drivers of landscape evolution in the region. Significant change has occurred in the fluvial systems of the KB and CB since the Neogene but these changes have not been uniform or constant (see **Section 7.4**). The multiplicity of factors affecting the knickpoint occurrence highlights the need for the further investigation of possible mechanisms responsible for landscape evolution along the CKW. These regional controls on fluvial evolution are investigated and discussed in **Chapter 8**.

The main findings of this thesis can be summarised in the points below:

- The noticeable spatially clustering of knickpoints within a river suggested a non–fluvial control on most of the identified knickpoints.
- Knickpoint location is dominantly controlled by the underlying geology over which the river flows.
- Although faulting influences fewer knickpoints than lithological controls, yet due to higher proportion of knickpoints greater than 20 m faulting plays an important role in river development.
- There have been substantial changes in river networks, particularly in the eastern Congo and Kalahari Basins, as well as along part of their shared watershed since the Neogene.
- The occurrence and extent of many drainage disruptions along the eastern margin of the CB and KB are highly suggestive that rift related of tectonic activity of the EARS, is a regional driver of landscape change.

CHAPTER 8: GEOMORPHIC EVOLUTION OF THE CONGO-KALAHARI WATERSHED

8.1 Introduction

The characterisation of longitudinal river profiles on a continental scale (**Chapter 6**) is strengthened by the addition of meso–scale data (**Chapter 7**); together they provide invaluable insights into the formation and development of the knickpoints and, by extension, the drainage evolution of the Congo and Kalahari Basins. It has been shown that the SRTMv3 data and observations have a high degree of fidelity, as field and digitising observations match closely (**Chapters 5** and **6**). Therefore, inferences based on SRTMv3 and Landsat data can be considered robust. The combination of direct observations of this study with auxiliary maps and literature identified several factors that have influenced the geomorphic evolution of the region. The apparent dominant factors are the underlying geology and tectonics (**Chapter 7**, **Section 7.3.1.3**). While this does not directly inform our understanding of the genesis of these landforms, it sheds light on the ongoing development of the landscape, and specifically the origin and evolution of the CKW. In order to better understand the origin and development of the CKW and its rivers, the geomorphic and biogeographic evidence must be interpreted in relation to the wider context of the African continent. This aim of this chapter is to synthesise the key findings of this study (as discussed in **Chapters 5, 6** and **7**); this chapter proposes a conceptual framework of the evolution of mega-geomorphology of south-central Africa.

8.2 Factors influencing knickpoint locations and river evolution

Of the 374 total knickpoints identified in this study (six knickpoints caused by dams were excluded), lithology appears to be the dominant control accounting for 186 Congo knickpoints and 78 Kalahari knickpoints (see **Table 8.1** and **Chapter 7**, **Figures 7.7** to **7.22**). Meanwhile, faulting accounts for 32 of the Congo knickpoints and 15 of the Kalahari knickpoints.

Of the 374 characterised knickpoints, 37 of the Congo's knickpoints and 26 of Kalahari knickpoints could not be assigned a control (**Table 8.1**). The formation and of these knickpoints may be related to fluvial processes, unmapped localised geological outcrops, and/or faults or wider regional controls such as tectonics, basin subsidence or uplift (see **Chapter 7**, **Section 7.5**).

Table 8.1: Summary of causes knickpoints of Congo and Kalahari basins. Knickpoints caused by dams (four for the Congo and two for the Kalahari Basins) have not been included. See **Section 6.2.4.1** and **Table 6.1** for explanation of the knickpoint categories.

Knickpoint category	Congo (n = 255)			Kalahari (n=119)			
	Tectonics	Lithology	Unidentifiable	Tectonics	Lithology	Unidentifiable	Total
-5	4	38	9	8	25	10	**94**
-1	1	9	5	-	8	3	**26**
0	3	6	-	-	5	1	**15**
5	7	36	7	1	12	4	**67**
10	7	30	5	1	6	4	**53**
15	1	17	3	-	1	2	**24**
20	2	20	5	1	10	1	**39**
25	1	5	1	-	-	-	**7**
30	2	10	-	-	2	-	**14**
35	-	-	-	1	2	-	**3**
40	-	4	-	1	3	-	**8**
45	-	2	-	-	-	-	**2**
50	1	6	1	-	2	-	**10**
60	-	-	-	1	2	-	**3**
70	-	-	-	1	-	1	**2**
75	-	1	-	-	-	-	**1**
80	2	2	-	-	-	-	**4**
90	1	-	1	-	-	-	**2**
Totals	**32**	**186**	**37**	**15**	**78**	**26**	**374**

Of the 374 studied knickpoints, 172 were classed as category 10 or higher (total height equal to or greater than 10 m), with the tallest Congo and Kalahari knickpoints being 90 and 70 m, respectively (**Table 8.1**). Nearly half of all the knickpoints attributed to tectonics (49 %) and lithology (47 %) are category 10 or higher (see **Chapter 7** for details). This indicates that both lithology and tectonics qualify as important controls over the formation of large knickpoints (see **Figure 8.1**). Their relatively high incidence indicates the primary control of knickpoints in the region but interactions between these two controls is a possibility, especially in the east of the study area, and where knickpoints have developed on orogenic belts. Of the knickpoints whose cause was not identified, 62 % are category 5 or lower. Owing to their heights, they are probably related to localised causes, such as fluvial processes (i.e. channel bed incision or knickpoint migration) or local rock outcrops.

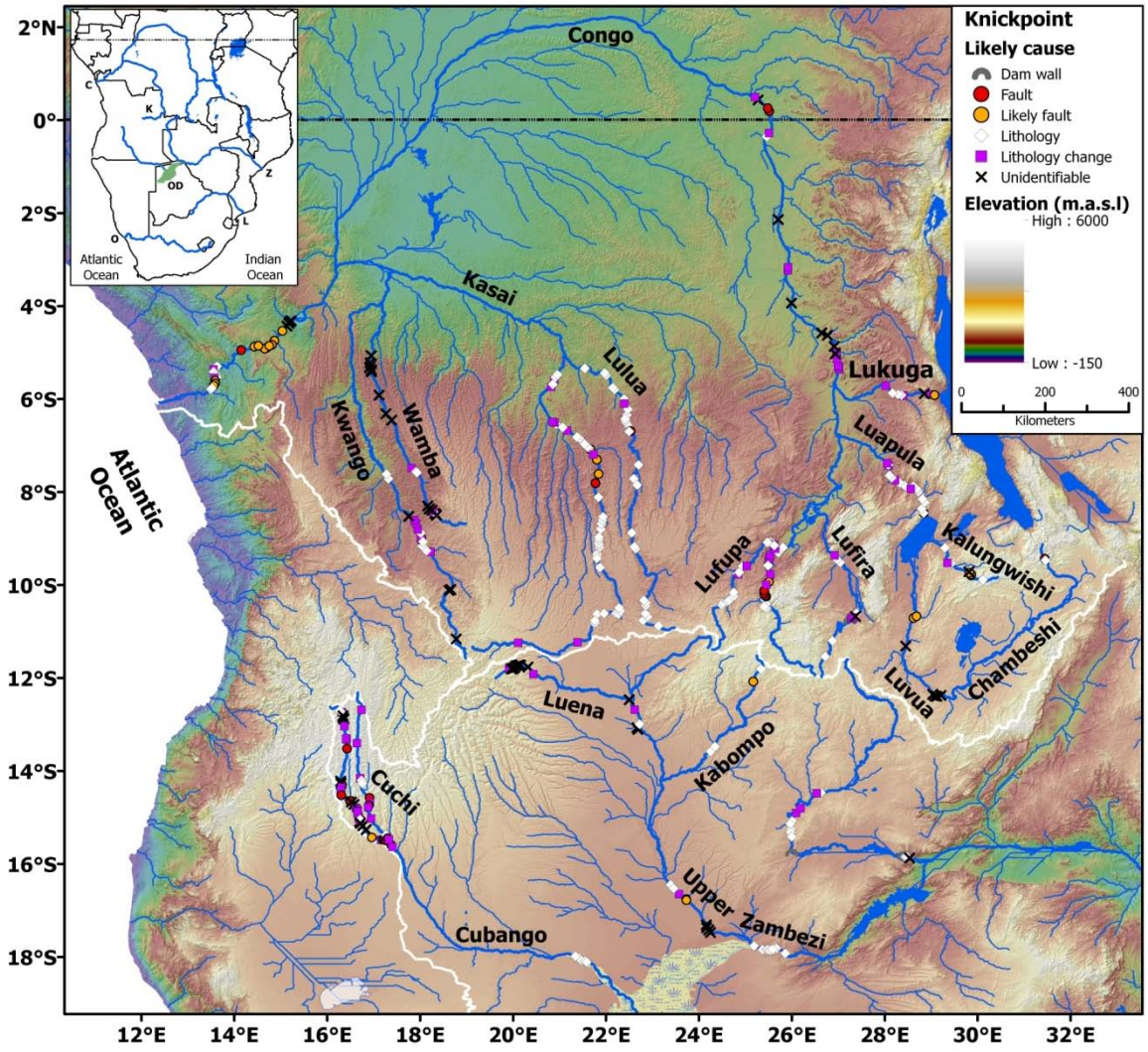

Figure 8.1: The 380 identified knickpoints of south-central Africa and their likely cause. Studied rivers are shown in heavy blue lines, thin blue lines indicated generated river networks and the white line indicates Congo–Kalahari Watershed and the coastal drainage watershed. Inset shows the major rivers and waterbodies in central and southern Africa. Elevation data source is the SRTMv3 DSM. See back sleeve for an A3 print out.

The 374 knickpoints do not show a regular distribution pattern across the basins and along the rivers, and do not exhibit a strong relationship to river length or basin hypsometry (**Figure 8.1**, **Chapter 6, Figure 6.12** and **Chapter 7, Figure 7.24**). Whilst there is a strong link between knickpoint location with lithology and tectonics (as shown by the knickpoint characterisation, see **Chapters 6** and **7**), this association does not fully explain knickpoint occurrence in terms of their distribution. Thus, the determinants of location of these knickpoints need to be investigated in terms of the continental controls on lithology and tectonics.

8.2.1 The role of the Kalahari sedimentary cover in controlling knickpoint formation

The distribution of knickpoints may be better understood by investigating the areas where knickpoints mainly do not occur. Looking at the surface geology, knickpoint formation is limited in areas covered by Kalahari Sands in southern Africa (**Figure 8.2**). Although knickpoints do form in areas of Kalahari Sands and other unconsolidated sediments, there is a relationship between knickpoint occurrence and the depths of these unconsolidated sediments (**Figure 8.2**). Overall, most of the identified knickpoints do not occur on sediments of thicknesses in excess of 30 m, with the majority of the knickpoints either occurring in zones of no Kalahari cover, or limited cover (0 – 30 m isopachs) (**Figure 8.2**). For central Africa, this broad relationship is stronger for the knickpoints occurring along the studied Congo rivers compared to the studied KB knickpoints. Interestingly, this relationship of knickpoint occurrence and the depth of unconsolidated sedimentary cover does not hold true for the extreme west of the CKW. Here the Kwango, Kasai and Kabompo Rivers all have knickpoints in their headwater regions, which flow over sediments ranging in depth from 90 – 210 m (**Figure 8.2**). The cause of the majority of these knickpoints could not be identified (**Figure 8.1**) but may be related to calcrete layers found with the Kalahari sediments (Haddon, 2000; Ringrose et al., 2000) or may be due to the transition in slope changes (topographic control) where these rivers flow off the Angolan Highlands. A similar situation of knickpoints occurring over thick sediments is found along lower reaches of the Upper Zambezi River (**Figure 8.2**). The cause of these anomalous knickpoints should be investigated further, in a future study, because they may provide insights into the geomorphic evolution of these rivers.

The main identified negative relationship of knickpoint occurrence to unconsolidated sedimentary cover suggests that these sediments may inhibit knickpoint formation. In relation to observed knickpoint controls, sedimentary cover in excess of 30 m effectively masks possible underlying geologic controls in the study area. As this cover is deeper and more extensive in southern Africa, it restricts the possible zones where knickpoints may form. This hypothesis explains the observed clustering of the KB knickpoints in areas of shallower sedimentary cover (**Figure 8.2**). The knickpoints of the KB are mainly restricted to the upper reaches of the Cubango and Cuchi Rivers that flow over the Basement rocks of the Angolan Highlands, accounting for 64 of the 119 Kalahari knickpoints (**Figure 8.2, Table 6.8** and **Chapter 7, Figures 7.18 and 7.17**. Additionally none of the 14 knickpoints of the Kafue River occur on Kalahari Sands, meaning that 78 (66 %) of the Kalahari knickpoints occur outside of the range of the main body of the Kalahari sand cover. Of the 41 knickpoints that occur within the main range only 25 are found on Kalahari Sands, the rest being found in zones stripped of the Kalahari sediment cover. While the extent of the Kalahari Sand cover is smaller for the CB than

the KB, a similar situation exists in terms of knickpoint occurrence, with only 10 being found within the sedimentary cover.

Therefore, to summarise, unconsolidated sedimentary cover of the Kalahari Group generally inhibits the formation of knickpoints. The knickpoints that have formed in this area are most appropriately explained by a complimentary cause, such as tectonic events of sufficient magnitude to overcome the dampening effect of the Kalahari sedimentary cover. The inhibition of knickpoints by deep sediments may also explain the lack of knickpoints occurring in the *cuvette centrale*. Thus, in regions of thick sedimentary cover, any changes to the fluvial regime may be accommodated through horizontal changes in the river course, or the effects of these changes may have migrated rapidly upstream, until they encounter pre-existing knickpoints or zones resistant to vertical erosion (e.g. Schumm et al., 2002; Loget and van den Driessche, 2009).

While the unconsolidated sedimentary cover may limit knickpoint development by inhibiting their formation and/or longevity (the unconsolidated allows for the rapid upstream migration of knickpoints or their erosion), some knickpoints do occur within this cover. **Figure 8.2** shows a noticeable trend of knickpoints clustering in a general north–east to south–west direction in the southern CB and eastern KB. This broad trend holds true for areas of Kalahari cover and also zones where the Kalahari is absent, thereby suggesting a second control on knickpoint occurrence that is not solely related to the depth of Kalahari cover or the underlying lithology, as this is heterogeneous across this regional scale. Thus it is probable that these knickpoints, occurring along north–east to south–west axis of orientation across the rivers, are related to tectonic activity linked to the EARS, which shows a similar structural trend. Thus in south–central Africa, it is probable that regional faulting controls some of the knickpoints, despite the absence of faults indicated in the geological maps used.

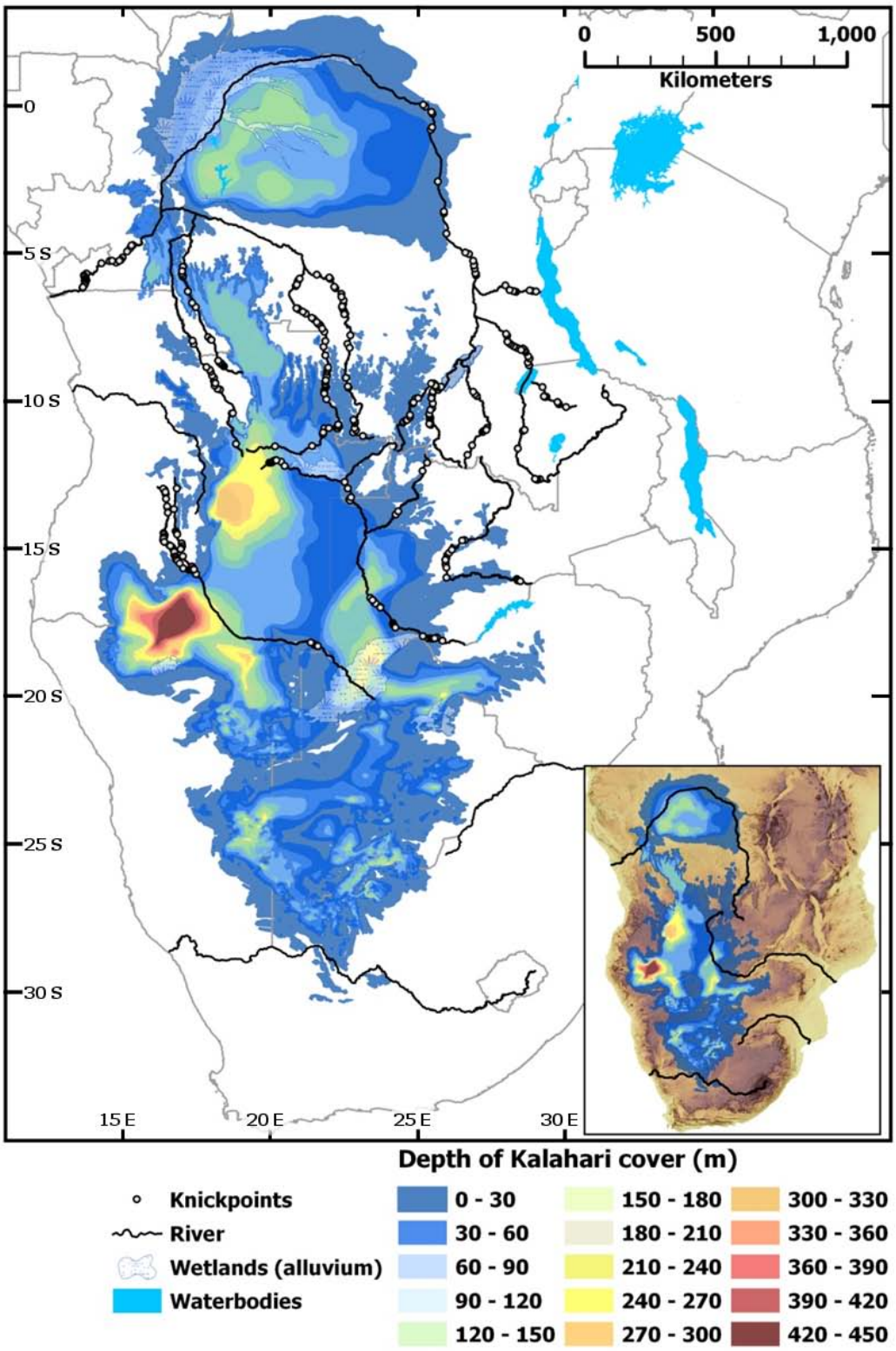

Figure 8.2: Cenozoic sedimentary cover over south and central Africa. The isopachs of the Kalahari sedimentary cover from southern Africa (Angola, Zambia, Namibia, Botswana and South Africa). Sediment isopachs are after Haddon (1999). The depth of the sedimentary cover of central Africa (DRC, CAR and Republic of Congo) from Linol (2013) correlates to the Kalahari cover of southern Africa. White dots indicate knickpoint locations. Inset shows major rivers (Orange, Limpopo, Zambezi and Congo Rivers) in thick black lines, depth of sedimentary cover and topography. Source of elevation data for inset is SRTM 250 m.

8.2.2 The role of tectonics on knickpoint occurrence

This study has demonstrated that faulting is an important cause of knickpoints in south-central Africa (see **Table 8.1** and **Figure 8.1**, and **Chapter 7**). While only accounting for 47 (12 %) of the 374 knickpoints identified, 23 (47 %) of these knickpoints were category 10 or higher, including seven that are 40 m or larger. Thus faulting plays a significant role in knickpoint formation, with the large size of fault related knickpoints suggesting regional faulting rather than localised faulting. As the EARS has been shown to have dramatic and far ranging effects on the landsurface of central and southern Africa, it is plausible that several of these knickpoints may indicate tectonic activity associated with rifting (see **Figure 8.3**). For example, the EARS has been related to the formation of Lake Victoria via regional tilting and faulting of the East African Plateau (Goudie, 2005; Chorowicz, 2005).

The compiled map shown in **Figure 8.3** illustrates the potential seismic hazards across Africa, providing a reliable indicator of this regional activity associated with late Cenozoic tectonism along the EARS. Zones of seismic events extend beyond known surface expressions of the EARS and represent the south–western extension of an incipient rift (Reeves, 1972; Gumbricht et al., 2001; Haddon and McCarthy 2005). Importantly the eastern CKW is situated between two limbs of seismic activity (**Figure 8.3**). Furthermore, several of the knickpoints whose cause was not identified appear within these zones of the seismic activity, so the occurrence of these knickpoints may be related to tectonic activity that has yet to be mapped regionally. This relationship is especially true for the Congo River knickpoints occurring between the junction of the Lukuga River and Kisangani (see **Chapter 6**, **Figure 6.1**). Therefore tectonic activity related to the westward development of the EARS may be responsible for of several knickpoints of the eastern Congo basin whose causes are not readily identifiable (see **Figures 8.1**, **8.2** and **8.3**).

Tectonics may have significant impacts on alluvial river channels (Schumm, 1977), and since much of the KB occurs on Kalahari Sands, these alluvial rivers may exhibit the effects of neotectonics. Schumm et al. (2002) suggest that rivers are sensitive even to slow, aseismic tectonic activity, although it would be expected that the depth of the Kalahari Sands may dampen this activity, the frequency and magnitude of tectonics may play a factor in the degree of the river's response. Thus, neotectonics could be the cause of fault related knickpoints of significant heights (**Table 8.1**) formed over the Kalahari Sands and in the eastern CB. The orientation of the Lufupa–Zambezi headwaters, the Kabompo–Lufira headwaters and the Chambeshi–upper Kafue Rivers as well as the south–west trending limbs of the EARS, are parallel (see **Figure 8.3**). All of these fluvial features have a similar

south–west trend as the incipient Mweru rift. Therefore, in the eastern CKW, regional tectonics (and geodynamics) play a significant role in the evolution of the river systems.

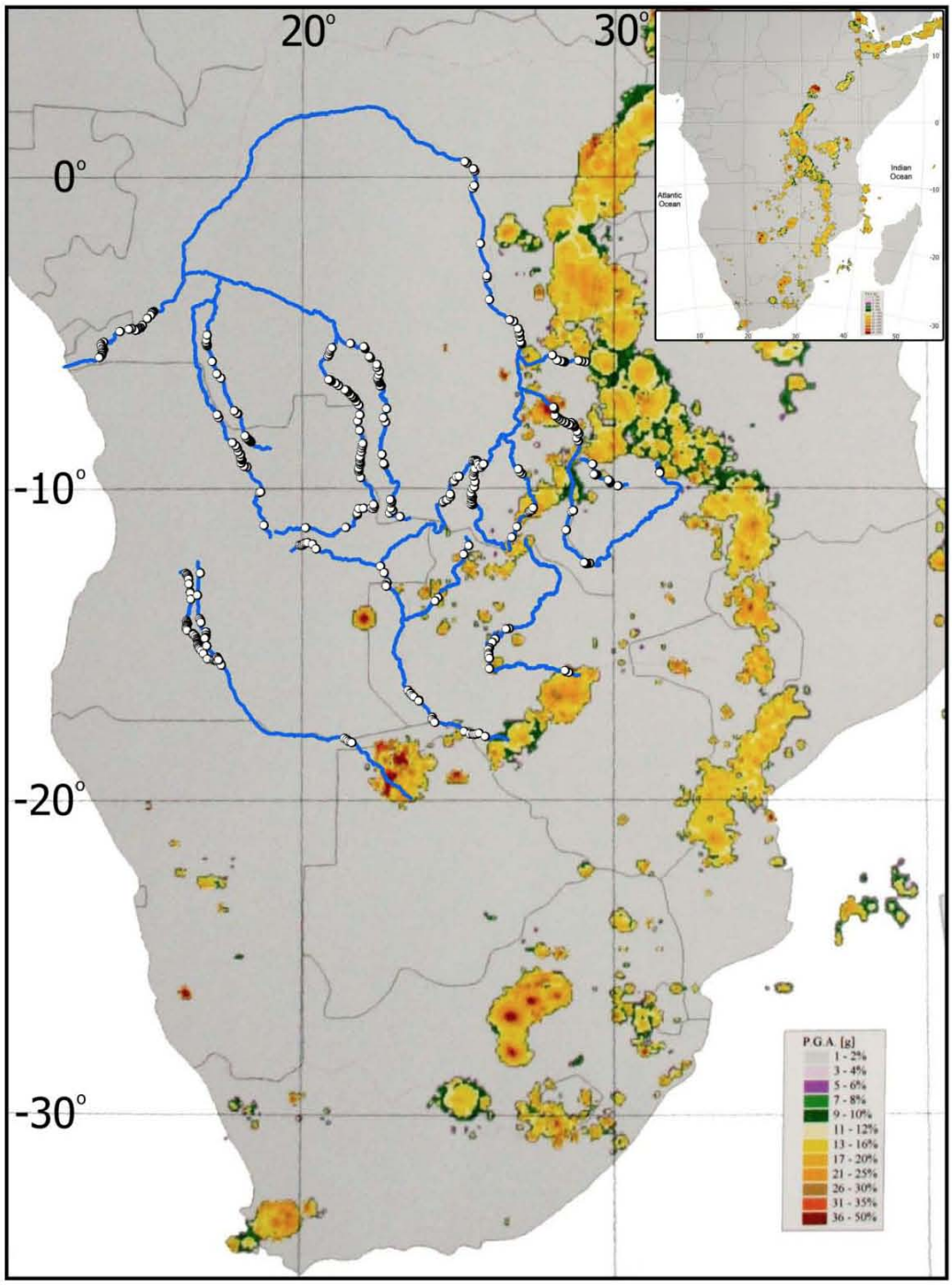

Figure 8.3: Potential seismic hazard map of Africa. It can be seen that seismic hazards follow the East African Rift System (EARS). Note the high probability of seismic hazards around the Okavango Delta region and also in the Kariba valley. This line suggests an incipient western arm of the Western Branch of the EARS. Just north of this line there is an additional line of seismic hazards running through the Upemba swamps and Bulozi wetland Seismic hazards are from Kotze et al. (1999).

8.2.3 Implications for long term river evolution

This study has demonstrated that the combination of lithology and tectonics plays a significant role in the distribution of knickpoints in south-central Africa. This role has implications for the evolution of the studied rivers. Lithology and tectonics affect the morphology of these rivers in different ways, as highlighted by the asymmetric distribution of knickpoints.

In the river longitudinal profiles, knickpoint occurrence was primarily determined by the incidence of resistant rocks or boundaries of rock change (see **Chapter 7**, **Section 7.3.1.3**), which indicates the importance of lithology for river evolution. Resistant lithologies have been shown to limit landscape denudation in southern Africa (see Decker et al., 2013, Table 1 and references therein) and it is reasonable to expect this to hold true in the CB, given the basin's geologic similarities to southern Africa. Vertical incision across these resistant rock outcrops is inhibited, with the horizontal channel migration confined by the bounding lithology. The river is thus effectively pinned (confined) to its current position both vertically and horizontally (Tooth et al., 2002; Schumm, 2005). This confinement limits the river's ability to accommodate changes in its fluvial regime in these zones, forcing changes in channel location and longitudinal profile. For example, the south-to-north flowing segments of the Lulua and upper Kasai both show convex profiles in zones of knickpoint clustering, yet the profiles of both exhibit low, near flat gradients in sections lacking knickpoints (**Chapter 7**, **Figures 7.10** and **7.15**).

The inhibition of knickpoint formation in regions of deep (greater than 30 m) Kalahari Sand cover suggests that these sediments serve as a buffer, limiting the role of lithological and tectonic controls. Where rivers flow over these unconsolidated sediments they are unlikely to form significant valleys and so would not be confined (not pinned into a location), allowing them to accommodate baselevel changes through horizontal adjustments (Montgomery and Buffington, 1997; Tooth et al., 2002). Alternatively, the lack of geological controls on these sections of alluvial channels may result in rapid vertical incision (Schumm, 1977). Thus, changes in fluvial regimes may move rapidly through the rivers sections flowing over the Kalahari Sands, whereas those zones pinned into resistant lithology may only accommodate river changes through vertical incision. This explanation accounts for low gradient stretches and lack of knickpoints of the longitudinal profiles of the Kalahari rivers mapped in this study; several knickpoints only occur in zones where the river has eroded through the sedimentary cover and encountered bedrock (see **Figures 8.1** and **8.2**). Tooth et al. (2002) noted a similar situation for the Klip River of South Africa, which flows over dolerites and sandstones. Where

the Klip River encounters the dolerite outcrops, its valley width narrows and knickpoints occur; in contrast, the river's channel is characterized by a wide river valley, meandering channel and floodplains where the Klip flows across weakly cemented sandstones. Thus, phases of base level change would move rapidly up the river profiles until they encounter, and possibly magnify pre-existing knickpoints or encounter resistant lithologies, thereby forming new knickpoints. Alternatively, these areas of Kalahari Sands, instead of responding to tectonics through longitudinal changes, accommodate to tectonics through horizontal adjustments, including changes in channel pattern, channel depth and width, lateral shifts of the channel, changes in valley width or the formation of lakes (Schumm et al., 2002). However, as alluvial rivers adjust to changes in water and sediment availability in a similar manner, the above geomorphic characteristics of these rivers cannot be invoked as definitive indicators of tectonics without additional evidence (Schumm et al., 2002). The deep Kalahari Sands appear to limit lithologic and tectonic controls, with the degree of negation probably related to river size and depth, pre-existing topography, depth of alluvium over which it flows and tectonic magnitude as well of fluvial processes. An example of this interaction would be the redistribution of unconsolidated sediments through degradation and aggradation along the river longitudinal profile (Schumm et al., 2002). It follows that these Kalahari rivers can be expected to evolve along two contrasting trajectories subject to differences in sediment supply at the local and meso–scale. The evolution of an individual river will reflect the interplay between tectonic control and sediment supply, where fluvial action will redistribute sediments from sources of deeper supply to modify (either increase or decrease) sediment depth under the channel. Thus, a river draining the Kalahari Formation will be expected to exhibit a decrease in sensitivity as its sediment depth increases, and vice versa.

Therefore, where rivers flow over Kalahari Sands any changes must overcome these buffer thresholds, either through the speed of change or its magnitude. Thus the rivers of south-central Africa, especially those flowing over large portions of the unconsolidated Kalahari cover (as shown in **Figure 8.2**) lack evidence of change in baselevel or flow regime (i.e. vertical erosion has been limited), whereas rivers with smaller portions or no Kalahari cover show evidence of these signals. It follows that a comparison of the longitudinal profiles of the rivers could allow a relative magnitude of base level change to be established, if it is assumed that the only variable affecting a river's response to change in draining the KB is the sedimentary cover, and that this variable affects each river equally. While these assumptions do not hold true in practice, some broad comparisons may still be useful in order to refine an explanatory model of river evolution.

Tectonics may influence the landscape from local through regional scales, and in south–central Africa the EARS is the dominating influence (Dixey, 1945; Lavier et al., 2001; Haddon and McCarthy, 2005; Burke and Gunnell, 2008; Delvaux et al., 2012). The combination of multiple phases of tectonic activity related to the reactivation of the EARS and the tectonic quiescence of the cratonic areas has influenced the regional topography (de Wit, 2007). The formation of large knickpoints related to faulting illustrates the important role that tectonics plays in influencing the drainage of south-central Africa, particularly the eastern CB. A possible mechanism is the formation of step faults, which result from the release of lithospheric stress accumulated between faulted blocks. Step faults may form over large areas to radically impact longitudinal profiles and/or lead to river re-arrangement (i.e. Schumm, 1977; Kirby and Whipple, 2012).

The influence of both lithologies and tectonics is exemplified by the lower Cubango River. The part of the course flowing across thick Kalahari sediments has a shallow valley channel, low gradient and no knickpoints. However, where the river changes direction from west-east to northwest-southeast, knickpoints related to lithology and the fault controlled Okavango Delta begin. These lithologically–controlled knickpoints upstream of the Okavango Delta may be responsible for the Cubango's maintaining its easterly flow upstream of its fault-controlled south-easterly delta. These patterns of river control testify to how lateral and vertical river morphology of the Okavango Delta, at the end of the Cubango River, is controlled by neotectonics (Reeves, 1972; McCarthy et al., 1992).

8.3 A conceptual model of the evolution of the Congo-Kalahari Watershed

The development of the longitudinal profiles of rivers has implications for the placement and shape of their watershed. Through time, changes in longitudinal profile will migrate upstream to change the headwater regions of the river's catchment. Therefore, it has been argued repeatedly that the watershed can be seen as a summation of all of the geomorphic development of the landscape (Horton, 1945; King, 1951; Penck, 1953; Howard, 1967; Schumm, 1977). This justifies the investigation of the CKW, the evolution of which is able to be informed by the data compiled in this study.

The lithological and tectonic controls of the present day rivers of south-central Africa provide valuable insights into their development, yet these controls do not explain the origin of the CKW. It can be hypothesised that the precursor landforms of the CKW probably had their origins on the land surfaces and associated slopes that were created during Gondwana's formation. These inherited

surfaces have undergone changes from a sequence of controls. Prospective events include impacts on regional landscape from the break-up of Gondwana, inheritance and persistence of landforms that have formed on the cratons, and the reactivation of structural fabrics, leading today to the younger landforms representing the impacts of the EARS. These two suites of regional controls may be linked to larger geodynamic processes, with the long term stability of the African continent and absence of orogenic subduction zones providing a possible explanation of Africa's mega-geomorphology. In order to better understand the evolution of the CKW, it is helpful to develop a reference model. This section proposes three conceptual models of watershed development. It also outlines possible reasons for deviations from the respective sequence of events in landscape evolution suggested by these respective models. A focus on these deviations (anomalies) in turn identifies regions of the CKW that differ from the model. The valuable insights these anomalies provide can then be exploited to explore factors controlling landscape evolution in south-central Africa, which will be discussed in **section 8.4**.

8.3.1. Conceptual model of watershed development

8.3.1.1 Conceptual model

The multiple spatial and temporal scales of the CKW make the elucidation of its origin a challenging task as similar processes can lead to divergent landforms or dissimilar processes can result in convergent landforms. The CKW may be better understood through the use of a model, deviations from which provide insights into the origin of the divide. This proposed model builds on the ideas and concepts discussed in **Chapter 2**.

Figure 8.4 shows the idealised situation for river evolution through time (e.g. Davis, 1899; Schumm, 1977; Montgomery and Buffington, 1997). According to this model, the lower reaches of a river, owing to their smaller slope, experience a dominance of lateral erosion over vertical erosion, resulting in valley widening and channel flattening (see **Figure 8.4b, $T_1 - T_4$**). This causes a net lowering of the surrounding topography, with plain formation (peneplanation) occurring (see **Figure 8.4a, $T_0 - T_4$**). However, in the upper reaches, vertical erosion dominates, resulting in the eroding backward of the headwater region in a semi-parallel topology, and the river incises into the surrounding topography without substantially lowering it (Gilbert, 1877; King, 1951). Thus, under ideal conditions (such as homogenous substrate and uniform starting slopes), lateral denudation of the surrounding landsurface is focussed in the lower river sections, with the upper reaches

undergoing dominantly vertical incision. The middle river reaches serve as a boundary or transition zone, where at some threshold, the dominance of landscape denudation gives way to vertical incision as one moves upstream. Thus, the middle river experiences a mixture of both vertical and lateral erosion.

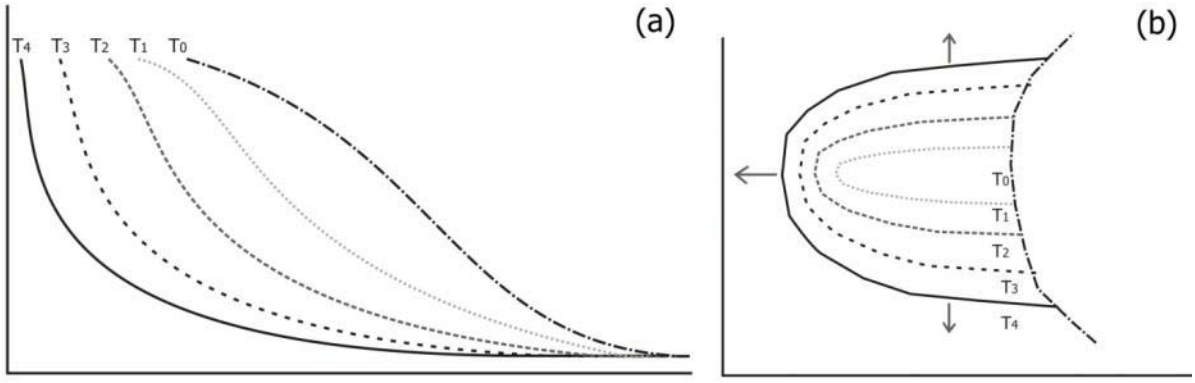

Figure 8.4: The idealised evolution of a river longitudinal profile (a) and a plan view of its associated valley (b). T_0 is the initial slope before channel initiation has occurred. T_1 to T_4 represent the idealised change in river profile through time in (a) and the change in river valley shape (b). Arrows indicate direction of denudation. As the river erodes backward into the slope (a), its lower reaches begin to widen, with its lowest reaches occupying the widest valley section (b). This is due to vertical erosion (river incision) being dominate in the headwater regions, resulting in steep slopes (e.g. T_4 is (a)), whereas the lower regions are dominated by lateral erosion, which lead to valley widening (e.g. T_4 in (b). See Chapter 2, Sections 2.2.1 and 2.3 for treatment of landscape and river longitudinal profile development.

The idealised landscape would therefore develop through vertical incision in the headwater regions, followed by denudation (and valley widening) in lower reaches of the river (see **Figures 8.5 1** and **8.6a**). Owing to basin scaling laws (Horton, 1945; Strahler, 1952), the upper and upper–middle reaches of the river transfer a lower volume of water compared to the lower-middle and lower reaches. In other words, compared to the river mouth, the river headwaters have a lower volume of water, albeit at higher energy levels, acting upon the landsurface. Thus, in terms of water availability, the upper regions of a river may be considered as dry in relation to its wet lower reaches (**Figure 8.5 1a**). The headwater and upper-middle reaches could therefore be thought of as conforming to King–Penck's model, which is based on scarp retreat (backwearing) suggested by observations obtained in arid climates (King, 1951; Penck, 1953), whereas the lower-middle and lower reaches conforms to Davis' model (Davis, 1899) of landscape lowering (downwearing), based on observations made in humid environments. Water availability may be viewed as the determining influence of both these models, producing an idealised river long profile.

Under idealised conditions, backwearing dominates in the upper reaches and downwearing dominates the lower reaches (see **Figures 8.4** and **8.5 1**). Over time the initial slope (T1) becomes graded (T3) and the river profile attains a concave shape. The concave curve between the vertical upper reaches and the horizontal lower reaches marks the transition zone, being a mixture of back- and downwearing, with more backwearing occurring in its upstream zones and downwearing in its downstream areas. For the transition zone, the rate of backwearing is less than in the upper reaches but greater than in the lower river reaches and the rate of downwearing is greater than in the upper reaches but lower than in the lower river (**Figure 8.5 1**). This produces a river in equilibrium, where the rate of backwearing relative to downwearing becomes constant (Hack, 1960; 1975). Valley width is narrow near headwaters with a steady increase in width moving downstream (see **Figure 8.5 1b**, **inset** and **Figure 8.8a**). Under these conditions, the watershed between two rivers would form a well defined apex (see **Figure 8.5b ii** to **iii**). This headwater drainage of a well defined watershed has a definitive directionality; for example, if it falls at (**ii** or **iii**), it will flow effectively to (**i** or **iv**). Therefore, owing to the gradients of the headwaters, drainage of precipitation from the watershed is efficient and wetland formation unlikely.

If the spatial distribution of available water were to change within the profile, the development of the long profile could be expected to change (e.g. Leopold et al., 1964; Schumm, 1977). For example, an increase in water volume may result in the development of flatter longitudinal profile due to increased downwearing (see **Figures 8.5 2** and **8.6 b**). Owing to the increased water supply, the middle and lower reaches are dominated by downwearing, while the upper region becomes a zone of transition with a mix of back- and downwearing, occurring at similar rates. This downwearing of the middle and lower regions results in lower river gradients that then allow for increased lateral erosion and landscape denudation. Additionally, the combination of increased water availability and low gradients (increased residence time of the water) may promote deeper weathering, increasing the rate of topographic downwearing. The result is a low gradient profile and plantation of the surrounding landscape. Thus the long profile would have a lower gradient than the idealised profile, with a wide, shallow catchment throughout creating a broad watershed area between rivers (see **Figure 8.5 2b**, **inset** and **Figure 8.6b**). This watershed may be long-lived owing to the relatively slow rate of backwearing occurring in the transition zone, and the low gradient of the watershed results in inefficient drainage (channel formation is inhibited) allowing for the formation of wetlands in the headwater regions (**Figure 8.5 b ii** to **iii**).

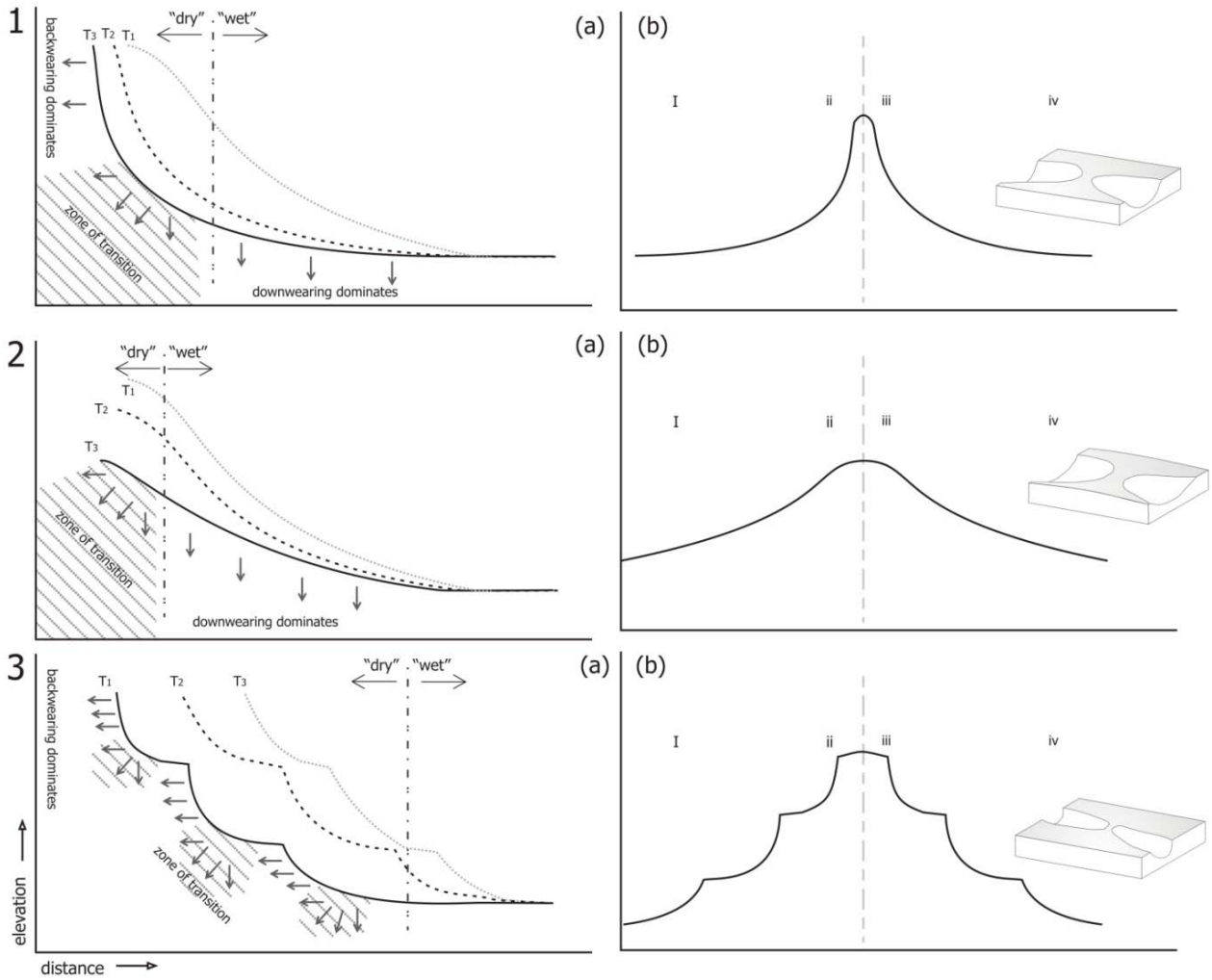

Figure 8.5: **(1)** Three proposed models for the development of the longitudinal profile of the rivers and its associated watershed. (**1a**) The development of a concave river profile ($T_1 – T_3$) and its watershed (**1b**). (**1a**) backwearing dominates in the upper profile where water availability is low ("dry"), resulting in headwater extension of the valley and the formation of a defined watershed. The higher water volume ("wet") of the lower reaches results in downwearing and valley widening (inset). The transition zone is a graded region experiencing both back- and downwearing, producing a concave of near equal rates of back- and downwearing rates. The rate back- and downwearing within the transition zone is lower than backwearing and downwearing of the upper and lower river reaches. (**1b**) The efficiently drained watershed between two long profiles and the resulting valley formation (inset). **(2)** (**2a**) The development of a flat river profile ($T_1 – T_3$) and its watershed (**2b**). An increase in water availability (wet condition) results in the dominance of downwearing over more of the profile (**2b**). The transition zone now occupies the upper regions resulting valley widening occurring concurrently with headwater extension. This creates a broad, flat watershed (**2b**) connected to the river by a gentle slope, resulting in inefficient drainage of the watershed region promoting wetland formations. The inset block diagram highlights the broad nature of this watershed that is associated with flat rivers. (**3a**) The development of a stepped river profile through time, $T_1 – T_3$. **(3)** (**3b**) The resulting watershed of two stepped rivers, (**3a**) backwearing is dominant under dry condition, resulting in scarp retreat. Steps in the profile are created from rock failures owing to channel steepness. These resulting steps experience a mix of vertical and lateral erosion (zone of transition) leading to several concave profiles within the overall long profile. Owing to the combination of back- and downwearing these steps may be enhanced (T_1 vs T_2) before they are completely eroded (T_2 vs T_3). The resulting watershed is flat and narrow near the headwaters (**3b**).

A decrease in water availability may result in a stepped river profile, owing to the dominance in the backwearing and transition zones (see **Figure 8.5 3** and **Figure 8.6 c**). Under dry conditions, backwearing initially dominates (King, 1951), resulting in a large scarp (see **Figure 8.5 3 T_1**). As the slope gradient increases, it eventually exceeds the rock threshold and slope failure occurs, creating steps in the profile (see **Figure 8.5 3 T_2**). The reduced gradients of these steps causes a change in more local erosion controls so that these regions experience a mix of vertical and lateral erosion (zone of transition) between the steep river slopes (see **Figure 8.5 3 T_3**). This creates several concave sub–regions within the overall profile. As the rate of backwearing is greater in the upper regions than the denudation of the transition zone, the tendency is for any steps to be enhanced (see **Figure 8.5 3 T_1** compared to **T_2**) before they are eroded (see **Figure 8.5 3 T_2** compared to **T_3**). This results in the formation of a valley narrower than the idealised valley, separated by a narrow, flat watershed (see **Figure 8.5 3 b**, **inset**). As water availability is limited, wetlands are unlikely to form along the narrow watershed.

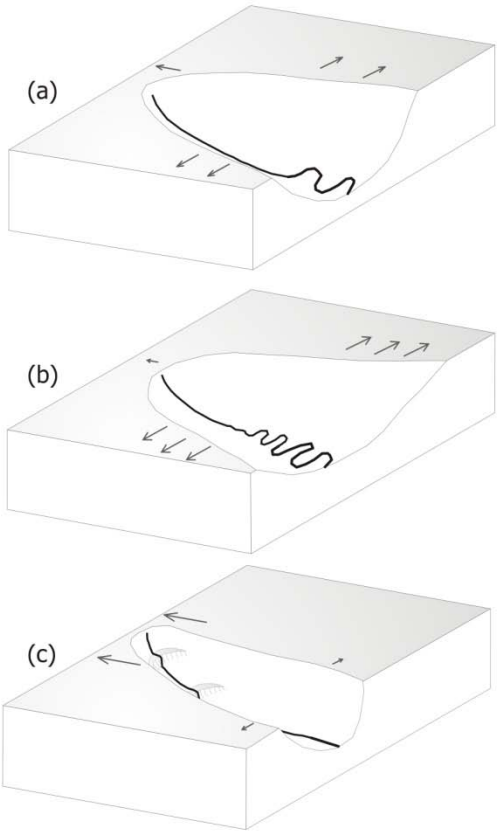

Figure 8.6: A comparison of river valley associated with the three models. (a) An idealised river model; here the rate of headward extension is slower that the rate of valley widening, resulting in a normal, concave valley. (b) The wet river model; here, the rate of valley widening is vastly greater than the rate of headward extension, resulting in a broad but shallow valley. (c) The dry river model; here headward extension is vastly greater than valley widening, resulting in a narrow, deep valley. Steps are introduced by rock strength; where the slope is too great, the rock face breaks away forming steps. Direction and size of arrow indicates the dominant direction of erosion.

8.3.1.2 Confounding factors

The above models apply to the development of rivers under ideal conditions, where the only variable is the amount of water transported through the river system. However, water availability is not the only variable affecting the rivers of the Congo and Kalahari Basins (i.e. Gilbert, 1877; Gilbert, 1914; Zernitz, 1931; Howard, 1967). The characterisation of knickpoints reveals that both (1) lithology and (2) tectonics are important factors controlling landscape evolution (see **Chapter 7**). Other factors include (3) climate, (4) drainage capture, and (5) epeirogeny and geodynamics (see **Chapter 3**).

(1) The underlying lithology influences the degree of back– and downwearing, which then changes what would be the uniform progression of the longitudinal profile (Gilbert, 1877). For example, a concave longitudinal profile may occur under wet conditions as downwearing is retarded in the middle section by the underlying lithology. Under dry conditions, a concave profile may result if lithology is uniformly weak, or if the lithology of the upper and middle reaches is weaker than lithologies incised by the lower river. A low gradient longitudinal profile would occur if the lower lithologies are vastly stronger than those of the upper and middle reaches. Under ideal conditions, if the underlying lithologies consist of alternating strong and weak lithologies, a stepped long profile would develop. Alternating lithologies would result in a stepped profile under wet conditions, because backwearing would be favoured over downwearing in sections of the river.

(2) Tectonic activity may either flatten or steepen the river long profile, depending on whether the activity is producing uplift or subsidence and on the location of the activity (Anderson and Burbank, 2001; Schumm et al., 2002). If subsidence occurs in the upper river reaches or uplift of the lower reaches, the river longitudinal profile would experience an overall decrease in river gradient. Similarly, river gradient would increase, if the upper reaches were uplifted or the lower reaches subsided. If long wavelength horst and graben structures occur, the river profile may become stepped. Also, over time a series of stepped faults may accentuate the concave river scenario by downward displacement of the lower river sections. Impacts of tectonic events along the profile may shift the zone of transition. In all these situations, the magnitudes and frequencies of the tectonics involved are important.

(3) The main effect of changes in climate would be to shift the zones (dry, transition zone and wet) along the river profile (Hack, 1975). If climate changes are sufficiently large and prolonged, it may

have a long lasting effect on the topography; however, if changes are minor, or of a brief duration, there may be no noticeable affects over longer time spans. In summary, climate change will most probably serve to enhance or diminish changes in the longitudinal profile of rivers.

(4) Drainage captures may result in substantial changes in the longitudinal profile of the river (Schumm, 1977). These captures may be related to two types of river rearrangement associated with, firstly, exo-network interference (competition across two or more drainage areas) or, secondly, endo-network interference (competition within a single drainage area). Both types affect the longitudinal profile, through either increasing or decreasing water availability, by introducing new types of lithology to the river profile that may restrain / enhance erosion and by adding to or removing from the longitudinal profile.

(5) Epeirogeny and geodynamics may dramatically alter the characteristics of entire drainage basins (Anderson and Burbank, 2001). Continental uplift may shift the regions of back- and downwearing and the transition regions through river rejuvenation. The effects of epeirogenic uplift and subsidence may be similar to effects experienced by individual rivers impacted by local tectonic changes. There may be a substantial time lag between the uplift or subsidence of an entire drainage basin before its effects become evident in the river's longitudinal profile. This lag effect would occur as the entire basin has been uplifted or subsided and so the basin's rivers would all be equally affected, apart from the basin's drainage outlet, where the change in base level will have more immediate geomorphological impacts. Substantial time may be required for this base level change to migrate throughout the drainage network. Thus, evidence for geomorphic impacts of a large scale (regional) uplift event may not be recognisable throughout the longitudinal profile of a drainage basin.

These confounding factors serve as controls on the spatial distribution of backwearing, downwearing and the location of the transition zone between these two suites of earth surface processes. These factors may enhance backwearing under one set of conditions but diminish it under a different set of conditions, with the expansion or contraction of the transition zone being dependent on the conditions. It is therefore possible to view these controls in terms of where and how they influence the development of the river longitudinal profiles, and by extension the river valleys. Knickpoint characteristics serve as key nodes in determining the influences of these controls.

8.4 The evolution of the Congo-Kalahari Watershed

As the CKW does not follow a continental mountain belt, its evolution cannot be explained solely by topographic controls. By using the combination of knickpoint characteristics, river longitudinal profiles, the above conceptual model and published biogeographic evidence, it is possible to propose a novel model for the development of the CKW. The origin of the CKW is probably a combination of various factors acting at different spatial and temporal scales. This allows for the CKW to be described as a palimpsest (sensu Brunsden, 1996), because its landforms have persisted despite repeated impacts of uplift, deposition and erosion. Different, complementary controls have acted at different points along the continental drainage divide, with these controls occurring at variable rates (impacts, magnitudes and frequencies).

8.4.1 The genesis of the Congo-Kalahari Watershed

Prior to the breakup of Gondwana, it is probable that several continental-scale drainage networks existed across the continent (Cahen, 1954; Deffontaines and Chorowicz, 1991; Burke and Gunnell, 2008). These drainages were the precursors of the drainages that developed during and after the break-up of Gondwana. For south-central Africa, the start of the Atlantic rifting during the Early Cretaceous initiated the development of the west-flowing coastal drainages and what may be termed the proto-Congo-Kalahari watershed (de Wit, et al.,2000; Haddon and McCarthy, 2005; Anka et al., 2010). This proto-watershed was most likely the divide between rivers flowing north toward low Africa and southward across the high African plateau. The position of this proto-watershed probably corresponded to the topographic apex (ridgeline) running west to east that then separated high from low Africa. Based on the distribution of the Karoo aged basins of south–central Africa (see Catuneanu et al., 2005 Figure 1), this proto-watershed is likely to have been U-shaped with a southerly curve and to have been situated around 8˚ S (in terms of the present day latitude).

A possible scenario is that the entire proto-watershed migrated southward subsequent to the break-up of Western Gondwana, experiencing a general flattening of its relief, and that it had reached what is approximately its present location by the late Paleogene. This watershed then attained its modern form during the Neogene. However, many aspects of the development since the north-south divide from the Late Cretaceous to the late Paleogene are unknown. Yet, the inheritance of the forms and preceding landscapes may have exerted significant (but currently inexplicable) controls on the present day CKW. Adding to the limited evidence for the late Cretaceous and early

Cenozoic, the results of this study provide insights into the Neogene evolution of the CKW, and these insights inform and provide the focus for the following section.

8.4.2 The development of the Congo-Kalahari Watershed

The modern CKW has formed through the interplay of a combination of factors acting throughout the Neogene. The interplay of these factors and the spatial extent of the CKW make it difficult to discern details of its evolutionary history. Nevertheless, dividing the CKW into three zones, as proposed in this study, makes it possible to present a sketch of the sequence of events that formed the CKW (see **Figure 8.7**).

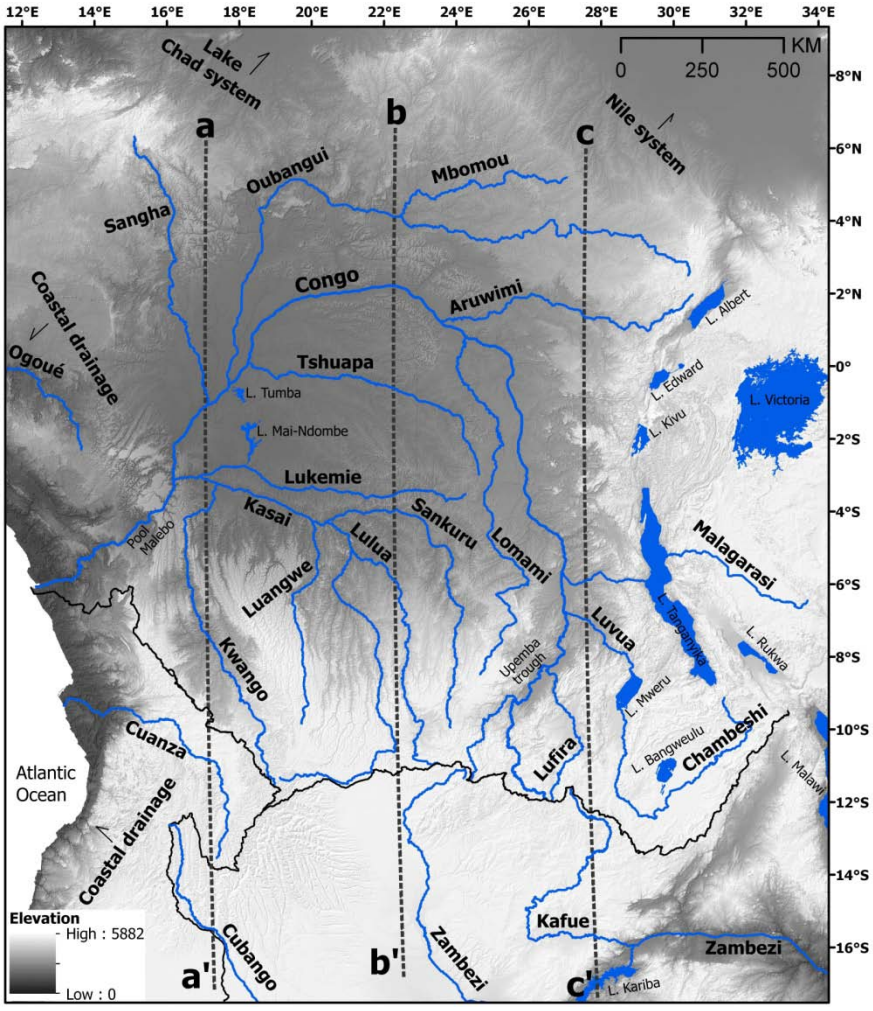

Figure 8.7: An overview of the Congo-Kalahari Watershed (CKW). It is possible to divide the CKW into three zones, western, central and eastern, based on its geomorphic attributes. The western zone corresponds to the drainage between the Kwango-Cuanza-Okavango systems; the eastern zone is associated with the Chambeshi-Luvua-Luapula and Kafue drainage systems. The central zone is the intervening zone between the western and eastern zones.

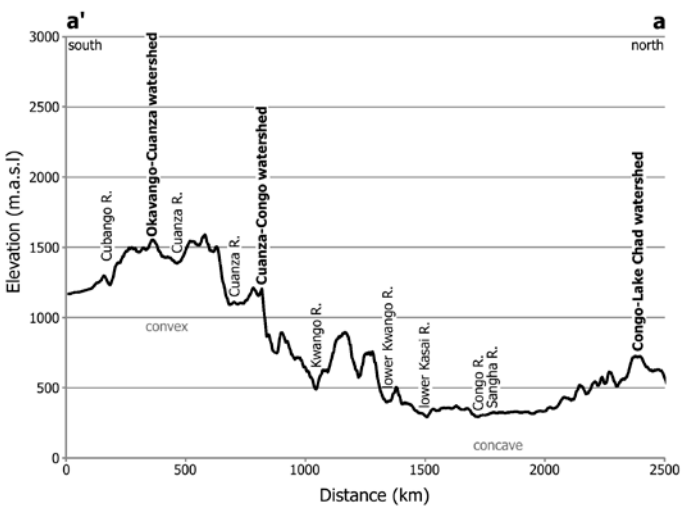

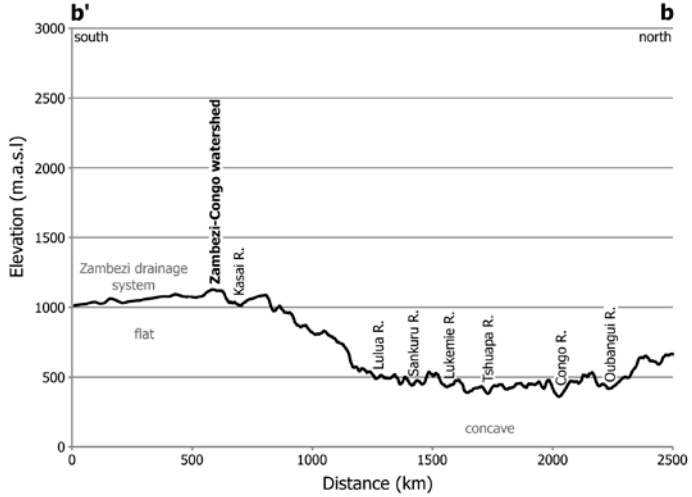

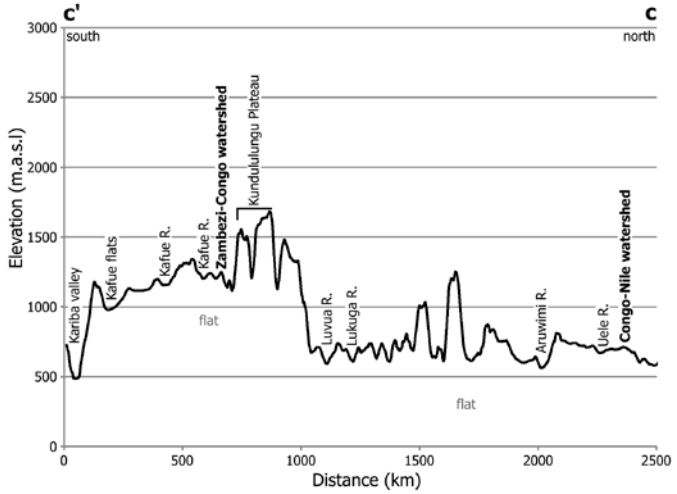

Figure 8.8: (a) The western-most cross section from a (north) to a' (south) with the location of major rivers and major watersheds (Okavango–Cuanza, Cuanza–Congo and Congo-Lake Chad) marked in bold. The overall Angolan highlands are convex while the north, incorporating the Kwango River, is concave. (b) The central cross-section depicts the gentle slopes of the CB in the north, with a gradual transition towards a convex slope below the CKW in the south. (c) In the east there is a high, flat landscape at ca. 1000 m.a.s.l. in the south and a low, flat landscape of ca. 500 m.a.s.l. in the north. The high, flat landscape is punctuated by the topographic spike of the Kundulungu Plateau. The northern, low, flat landscape has several elevation spikes, representing the Western Branch in the form of the eastern highlands of the Congo Basin. The Kundulungu Plateau lies north of the CKW, being of a greater elevation than the watershed itself. This represents a major deviation from the overall cross–section. The transition from the Kalahari to Congo system does not exhibit the general convex nature that is seen in the profiles to the west, with rivers in the region incised to similar elevations.

Figure 8.8 shows three cross–sections, western, central and eastern. The western cross–section illustrates the convex topography of the Angolan highlands region to the south, with the concave profile to the north, which also includes the lower Kwango River (see **Figure 8.8a**). The central north–south cross–section depicts the gentle slopes of the CB to the north, and the gradual transition towards a convex profile below the Zambezi–Congo watershed in the south (see **Figure 8.8b**). The east is characterised by high, flat landscapes at ca. 1000 m.a.s.l. in the south, and a low, flat landscape at ca. 500 m. The high, flat landscape is punctuated by the topographic spike of the Kundulungu Plateau in Katanga, southern DRC (see **Figure 8.8c**). The northern, low, flat landscape has several elevation spikes, representing relief that can be attributed to the Western Branch of the EARS, pertinently the eastern highlands (Mitumba Mountains) of the Congo Basin. It is almost certain that the convex regions of the profiles are undergoing erosion, and are sources of sediment (e.g. the Angolan highlands in the west and the transition zone in the centre), while the concave regions are depositional zones and sediment sinks. In contrast, the flat regions suggest an equilibrium of river degradation and aggradation, with these zones being areas of sediment transport. These equilibrium regions are found in the east and central regions (see **Figures 8.8b** and **c**) and may indicate either low rates of erosion (the central Kalahari rivers) or uplift and/or subsidence that matches fluvial activity (the eastern basins near the EARS). The three differences across the watershed indicate that the CKW is composed of three geomorphic regions.

8.4.2.1 The Congo-Kalahari Watershed

The western zone of the CKW comprises a triple divide; it separates the coastal drainage of the Cuanza system from the continental Congo (mainly the Kwango River) and several Kalahari rivers? (see **Figure 8.7**). The majority of the rivers occur on the Angolan Highlands, which consist dominantly of Precambrian Basement rock. The incised Kwango valley lies to the north of the divide, with the Cuanza valley in the west, and the highlands of the Okavango system in the south, while areas of subdued slope occur to the east. Despite the high volumes of rainfall in the Angolan Highlands, the upper regions of the Kwango, Cuchi and Cubango are convex and the majority of their knickpoints have lithological controls (see **Figure 8.1** and **Chapters 6 and 7**). Thus, while it is possible that the high water volumes may have led to the formation of low gradient and long profiles (see **Figure 8.5a**), the lithology has limited the amount of downwearing across the region, although there is a definitive watershed apex between the drainages (see **Figure 8.5b**). This is in contrast to the low gradient longitudinal profiles of the middle and lower reaches of the Cubango and Cuchi Rivers, both of which, for the most part, flow over Kalahari Sands. A similar reduction in longitudinal slope is seen in the Kwango River, where it flows over the unconsolidated sediments of the central Congo basin.

Therefore, as the entire western CKW has been established on Precambrian rocks, the underlying lithology is the dominant control on its evolution, especially as there is a limited number of knickpoints associated with faulting and river profiles are convex. Thus the western CKW may be currently the most stable part of the divide; here, changes are most likely to be caused by a high incidence of protracted river capture events.

The eastern zone of the divide shows the largest degree of change of its drainage network (see **Figures 8.8c** and **8.9**). This eastern zone consists of numerous uplifted plateaus (such as Kundelungu, Bia, Kibara), subsided basins (i.e. Bangweulu, Mweru and Upemba Swamps) and numerous faults in the area attributable to the south–west extension of the Western Branch of the EARS (De Dapper, 1988). Here, the eastern CKW has been highly modified through a combination of uplift, subsidence, river capture and rejuvenation related to these recent impacts of the EARS. For example, on the Congo side of the drainage divide, the Chambeshi-Luapula-Luvua River system forms a spiral, with five changes in direction and four zones of near horizontal long profiles and only the Luvua shows lithological controls (see **Figure 8.1** and **Chapter 7**). Not only is there a change in river direction at the Chambeshi-Luapula junction but also the knickpoints corresponding to the zones of channel direction change cannot be explained by lithology. Furthermore, the system is associated with the shallow lakes of Bangweulu and Mweru, which have formed in wide, shallow depressions. Lying on top of many of these plateaus are unconsolidated sand deposits of the Neogene Ochreous Sands that were deposited before the plateaus were uplifted (De Dapper, 1988). The region has experienced at least two (probably three) tectonic phases, with the first period occurring during the late Miocene (De Dapper, 1988; Decrée et al., 2010). Decrée et al. (2010) determined a late Miocene (ca. 10 Ma) and Pliocene (5.3–2.6 Ma) age of two uplifts, while acknowledging the possibility of multiple uplifts during the Pliocene.

The stepped nature of the Chambeshi–Luapula–Luvua River longitudinal profile, sudden changes in direction, and the fact that it flows through uplifted Basement rocks suggest a regional tectonic control on the eastern CKW. Given the directionality and proximity of the eastern CKW to the EARS, the eastern CKW in its present form is likely to be a function of the ongoing development of the EARS and should be considered to be of a similar, Neogene age to the Western Branch of the EARS.

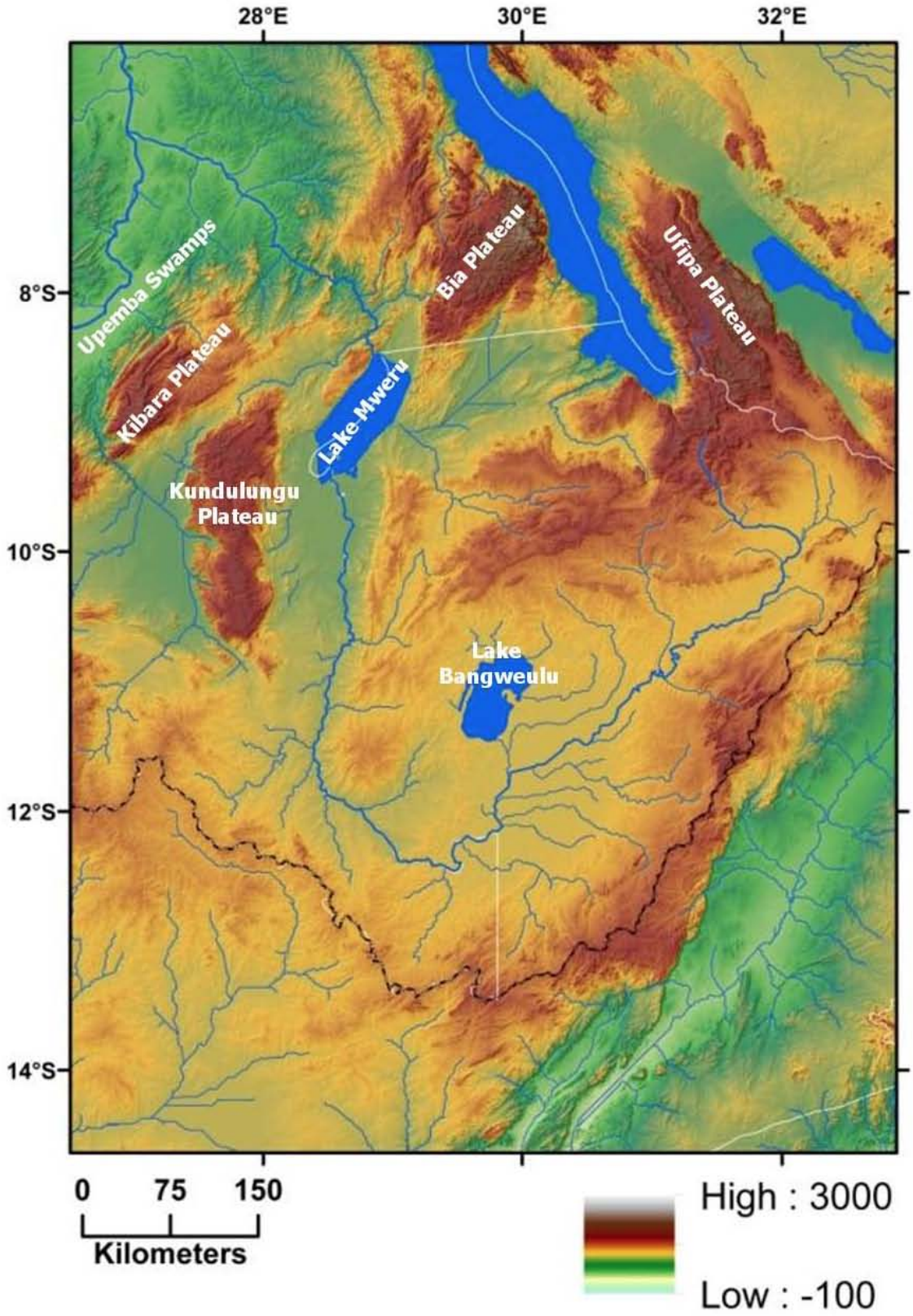

Figure 8.9: The eastern zones of the Congo–Kalahari Watershed (dashed line) are the most topographically rough portion of the CKW. The sharp scarps of plateaus and outlines of Mweru and Bangweulu suggest a recent period of uplift and subsidence.

Finally, the central CKW, which is near linear, comprises of the upper Kasai, upper Lulua, upper Kabompo and parts of the upper Zambezi which flow parallel to one another (see **Figure 8.1**). The presence of low gradients, a limited number of knickpoints (mostly lithologically controlled), broad interfluves and numerous wetlands and floodplains suggest that downwearing is the dominant process here. The dominance of downwearing may be indicative of long term stability of the central CKW, which has led to the development of flat longitudinal profiles (see **Figure 8.6**). Nevertheless, there is evidence of fish fauna exchanges across the headwater of the Zambezi and Congo River system headwaters (Bell–Cross 1965; Skelton 1996), which suggests that drainage captures have occurred in the late Cenozoic, as first proposed by Veatch (1935). Both Veatch (1935) and King (1951) proposed tilting to be the cause for these headwater captures, although the geomorphic evidence suggests that these changes were dominantly localised. The estimated timing of dispersal of Zambezi tigerfish from the Upper Zambezi into the CB at ca. 100 Ka invokes a drainage capture event of a Zambezi headwater by the Kasai (Goodier et al., 2011).

Owing to the apparent fluvial (and by extension geomorphic) stability of the western and central CKW, it is unlikely that any recent major tectonic activity has occurred along this part of the watershed. This suggests that this landscape is a persistent surface on which the modern western and central CKW has formed. In contrast, the eastern CKW shows strong evidence for recent geodynamic activity with major fluvial consequences. These indications allow for the following to be proposed for the development of south-central Africa:

(1) The majority of river courses flow across unconsolidated sands, which appears to allow for geologically rapid adjustment, i.e. lack of knickpoints in Congo Basin and scarcity of the knickpoint for much of KB. Here, climatic and vegetative interactions may form the controls of channel migration and development. Vertical and horizontal channel changes in river channel and location dominate.

(2) However, certain zones of the river act as pegs, these being knickpoints occurring on the eroded surfaces of the cratons. Here, rivers have incised into the Basement rock, thereby pinning the river courses (at least horizontally) into these clusters as shown by the knickpoints. The adjustments to change are dominantly vertical, horizontal changes being limited as channels are locked into bedrock. Therefore rivers have tended to accommodate changes at these points, where they have incised into the Basement rock (in contrast to other areas, for example, the Kalahari Group

sediments). Thus these points may act as zones of convergence whereby successive influences / changes progress along the river rapidly until they converge at these knickpoints / nodes. This may lead to knickpoint enhancement (increasing its height, for example, where several phases of downstream incision converge on a single knickpoint), thereby crossing a threshold that allows for further incision of the Basement rock. In conclusion, the cumulative outcome of these interactive effects will be to magnify the accumulation of impacts of earth surface processes. Alternatively, there may be a decrease in knickpoint height, for example, several successive phases of downstream deposition, with the associated decrease in stream gradient, can be expected to lead to a decrease in erosive stream power; in consequence, knickpoint incision ceases, while channel level increases. The ultimate outcome is that the profile is smoothed out.

(3) While (1) and (2) above, represent a steady state with progressive changes and probably accommodate the majority of the river courses in south-central Africa, a third possibility exists: this would be where geologically rapid events occur, as seen in the eastern CKW. Here, geodynamic activity has overcome lithological controls such that, firstly, the unconsolidated material has been stripped off due to increased erosion associated with ongoing uplift and, secondly, lithological controls have been over-printed through tectonic uplift and subsidence (horst and graben formation), as seen in eastern Katanga (especially the Kundelungu area) and less obviously (as judged by subdued surface expression) in the Okavango Delta.

8.4.2.2 The timing of the development of the CKW

It is possible to assign ages to some of the developments of the CKW that have been outlined above. This is achievable using biogeographic, geologic and geomorphic evidence (see **Chapters 6** and **7**). Due to the south-west extension of the Western Branch, the EARS has had a substantial influence on the drainage of south-central Africa. This is particularly evident in the eastern zones of the Congo and Kalahari Basins and, therefore, it is informative to focus on the timing of the eastern CKW. Not only does the EARS affect existing topography, it is a topographic feature in its own right, because it has created high relief topography, resulting in the formation of numerous, short rivers with steep gradients.

This influence of the EARS should not be seen as affecting a narrow, concentrated strip of the landsurface but rather a 500 km wide, rectangular area oriented to the south-west. The edges of the region are visible in terms of tectonic activity in the form of two near-parallel zones of seismic

hazard that are roughly perpendicular to the main EARS (see **Figure 8.3**) and in the combination of uplifted plateaus and subsided shallow basins (see **Figures 8.9, 8.10** and **8.11**). The extent and nature of disruption and its consequences for drainage are better understood with the use of biogeographic and geomorphic evidence (**Figure 8.9**)

The rate of topographic disruption linked to geodynamic activity associated with the incipient south–west rifting of the Western Branch is geologically rapid, with impacts across the continental land surface having been expressed over a distance of approximately 2000 km within just 8 Myr (see **Figure 8.10**). The biogeographic evidence of this topographic disruption (see **Chapter 7, Section 7.4**) can be clustered into 9 different nodes in a general north-east to south-west direction.

This change in topography and its magnitude can be seen in **Figure 8.11**. There a progressive increase in topographic smoothness moving away from the Western Branch (see **Figure 8.10** and **Figure 8.11 1 – 10**). The topography within and bounding the EARS is rough, consisting of a series of uplifted plateaus, shallow, subsided basins and deep valleys resulting in an elevation range of 1000 – 1200 m (see **Figure 8.10** and **Figure 8.11 1 – 5**). As described above, this combination of uplift and subsidence is tracked by the Chambeshi-Luvua-Luapula River, resulting in its clockwise spiral and abrupt changes in direction (see **Figure 8.9** and **Chapter 7**, **Section 7.3.1.3**, **Figure 7.7**). After 1000 km, the topographic effects of the EARS progressively lessen, with a 400 m elevation change across the profiles (see **Figure 8.10** and **Figure 8.11 6 – 10**). The extent of the topographic disruption in the landscape after 1000 km is generally for the more southerly part of the profiles and there is a substantial reduction in elevation change (see, for example, **Figure 8.11 6** compared to **Figure 8.11 10**). Therefore the geodynamic affects on topography show a long wavelength control in terms of magnitude of disruption and spatial distribution.

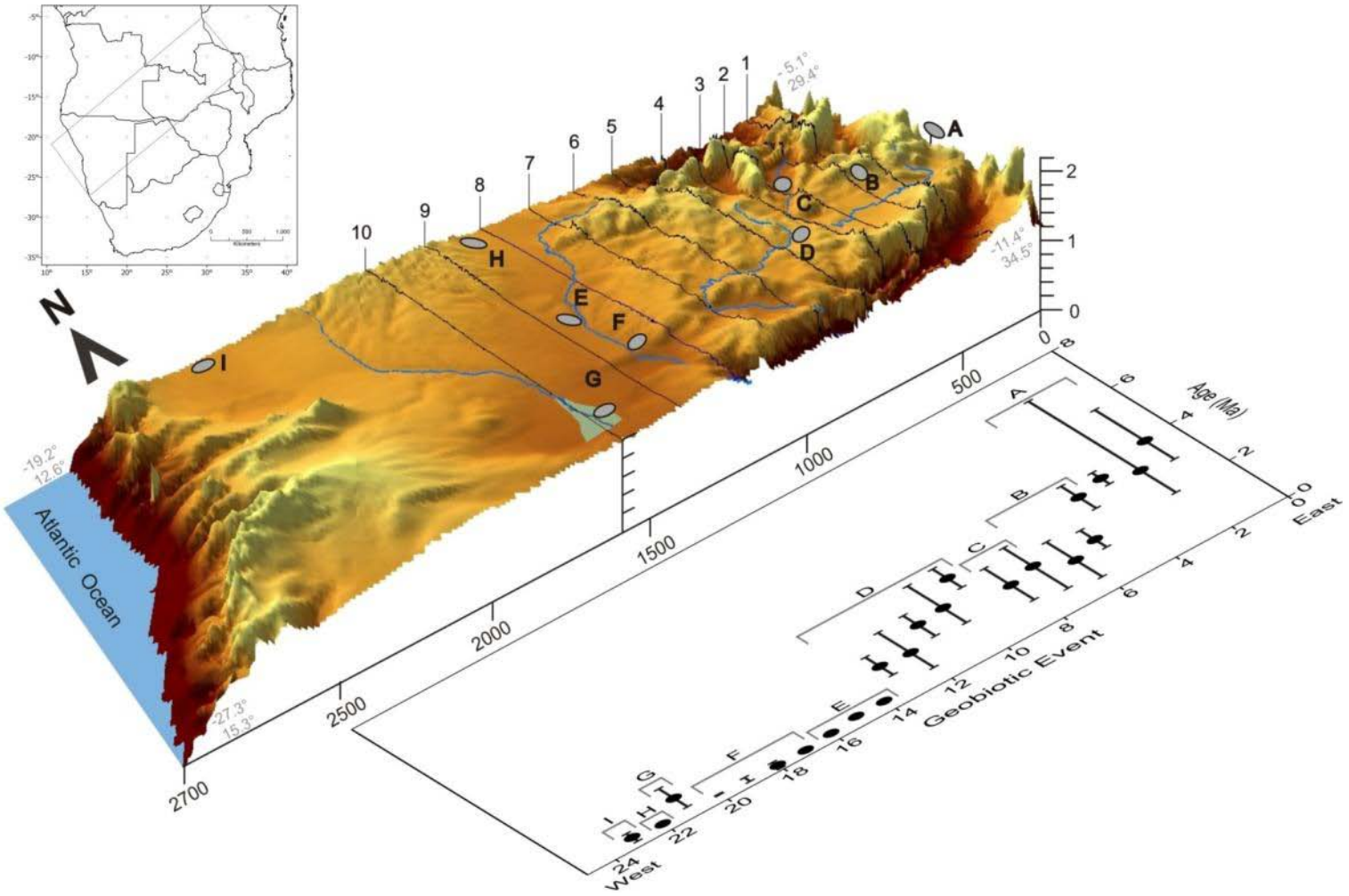

Figure 8.10: Topography and biogeographic events. Inset shows the overview extent of the 3D topographic profile (grey rectangle). Grey ovals represent the combined location of biogeographic events, the various ages of these geobiotic complexes are shown in the table. Species phylogenetic histories suggest a NE to SW trending distribution. This topographic disruption as shown in **Figures 8.9** and **8.11** is due to geodynamic activity associated with the extension of the incipient Western Branch of the EARS. See Chapter 7, Table 7.20 for phylogeographic details and references and Table A7.4 for geobiotic groups.

By looking at the underlying geology of south-central Africa, it is possible to explain the control acting upon the incipient rifting of the Western Branch (see **Figure 8.12**). The development of the incipient rift appears to be tracking the Neoproterozoic Juvenile fabrics, which trend from the north-east to the south-west of the African Plate (see **Figure 8.12**). Much of the rough topography of the eastern CKW, in particular the uplifted plateaus, are spatially linked to the location of suture zones inherited from the assembly of Gondwana, and tectonic episodes related to Gondwana's break–up. Interestingly, the shallow Bangweulu basin (see **Figure 8.9**) corresponds to the Mesoproterozoic shield and the Luvua River course follows the margin between the Neoproterozoic belt and the Mesoproterozoic shield (see **Figure 8.12**). This Neoproterozoic mobile belt has a width of 500 km in the eastern CKW, this 500 km width approximates the distance between the two lines of seismic hazard in shown in **Figure 8.3**. West of the Kafue River, the mobile belt narrows to a small southerly strip, which may explain the change in zones of topographic disruption across its exposed surface (compare **Figure 8.8b** with **Figure 8.8c**, and **Figure 8.11 6** with **Figure 8.11 10**).

The underlying geology with its inherited fabrics is the ultimate control of the development of the eastern CKW, as it determines the zones of influence of geodynamic activity. As the effects of this geodynamic activity are older in the north-east than the south-west (see **Figure 8.10**), the present day eastern CKW is the youngest part of the entire divide. Based on current rate of change and the fact that the topographic disruption of the incipient rifting is migrating south-westward (along pre-existing structural fabrics), the Okavango Delta region will probably undergo substantial topographic change in the future, coming to resemble parts of the eastern CKW, although on a narrower scale, namely, over 7–10 Myr (see **Figure 8.10**). Thus rifting has had a widespread influence on the Neogene evolution of the south-central Africa, especially on those areas closely associated with the EARS.

A point of interest is that the present day rifting of the African continent is occurring in a broadly north to south orientation, which is opposite of its most recent analogue, the South Atlantic Rift. While the South Atlantic rift extended south to north, following the anisotropy of the basement, the majority of the continental border faults (at least in Brazil) are north-east to south-west orientated (De Matos, 1999). Furthermore, the dominant north-east to south-west trending of the Cariri Rift Valleys of Brazil also show overprinting of east-west and north-west to south-east fault sets (De Matos, 1999).

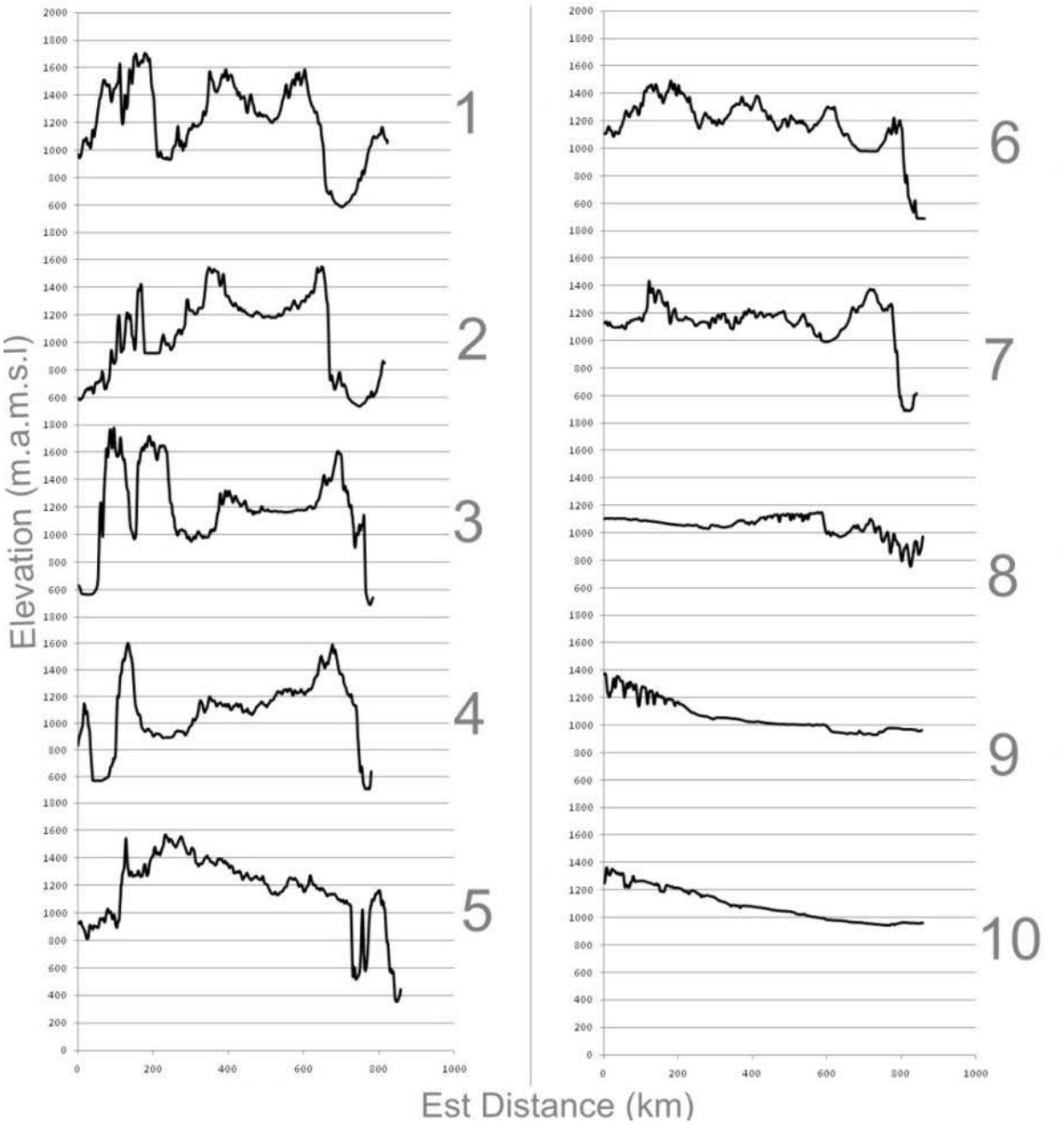

Figure 8.11: Cross sections of lines labelled 1 – 10 in **Figure 8.10**, lines running north-to south with 1 in the east and 10 in the west. As one moves from the east to west there is a smoothing of the landsurface. The central depression in 1 – 4 represents the Lake Bangweulu depression (situated on a small cratonic block). This represents a graben of an incipient western extension of the EARS (see **Figure 8.3** and **Figure 8.10).** The southern valley from 1 – 4 is the Luangwa rift valley. Section 5 shows a reversal of general slope towards the south. The southern drop in elevation in sections 5 – 7 is the Kariba valley. The dip in 7-10 represents the extension of the EARS (**Figure 8.3**), represented by the Kafue flats (7), Sesheke Plain (on the Zambezi River (8), Chobe floodplain (9, bounded by the Linyanti faults), Okavango Delta (10). The collective depression of 8, 9 and 10 is also known as the Mababe Depression. The Angolan highlands are to the north of 9 and 10.

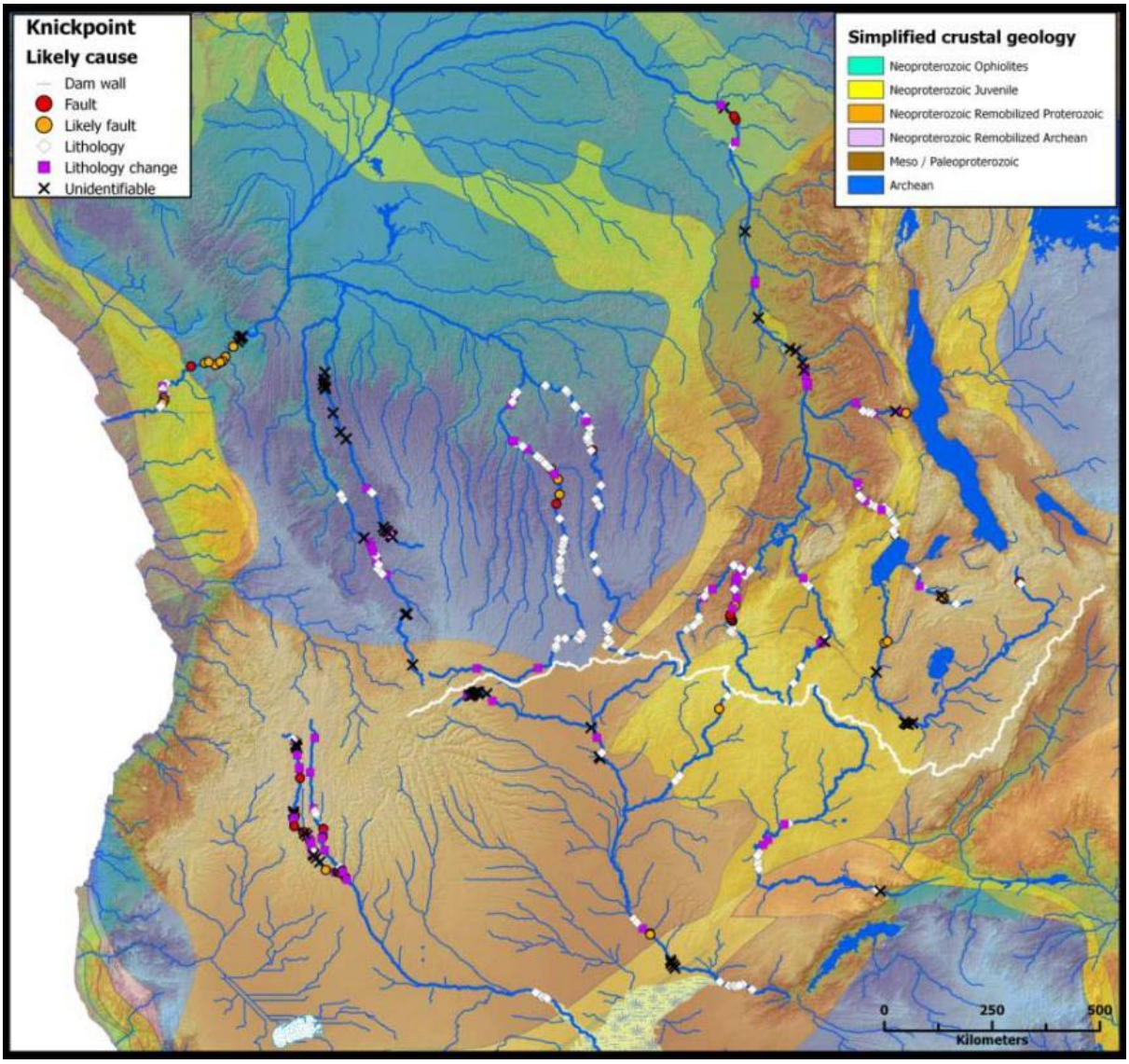

Figure 8.12: The crustal geology of south-central Africa. The western extension of the EARS follows the fabric of the Neoproterozoic juvenile (yellow) belt whereas the Mesoproterozoic shields (brown) and Archean cratons (blue) are tectonically quiescent. Note the clustering of resistant lithology knickpoints on the Archean craton in the Congo Basin, and on the Neoproterozoic Shields. Crustal geology after de Wit, et al. (2008)

8.5 The mega-geomorphology of south-central Africa: inherited, persistent or a new landscape?

The past and ongoing creation of elevated, rough topography associated with the EARS that has led to major drainage changes as discussed above, highlights the complex nature of the mega-geomorphology of south-central Africa. Of particular concern to the CKW is the possibility of the formation of a mosaic of inherited, persistent and new landscapes. Past attempts at elucidating the geomorphic history of Africa invoked various peneplains (or erosion surfaces) (King, 1967; Partridge and Maud, 1987), with the supposed existence of an African Surface being common to them. Yet it may be more beneficial to view the African Surface as a reference plain, with the likelihood that the African Surface did not exist as a true, single surface created by the concurrent activities of processes across a large area of the African continent during a single episode. Rather it should be viewed as the outcome of numerous processes resulting in a convergence of landforms (geomorphic equifinality), which has occurred since the break-up of Gondwana, although some areas might not have been substantially modified since (see, for example, Twidale, 2003), resulting in a variety of surfaces that are loosely connected in terms of their age of initiation. Thus the usefulness of the African Surface is as an idealised point of reference from which deviations in age and process can be quantified.

The evidence to support this suggestion that the African Surface should be regarded as a reference datum lies in the observation that most knickpoints in this study appear to be structurally (lithology and tectonics) controlled and the shared similarities in elevation and knickpoint heights are attributable to lithology and tectonics. Nevertheless, the absolute age of the development of these individual knickpoints has yet to be determined. Quantifying the ages of formation of these knickpoints will indicate the ages of the surrounding regional erosion surfaces and identify scale–dependent differences in ages of these surfaces. This important finding of knickpoint evolution across the CKW agrees with recent studies in southern Africa have shown that lithology controls topography (Decker et al., 2013; Scharf et al., 2013).

The western and central section of the CKW may be explained in terms of fluvial action and landscape inheritance, which is not the case for the eastern section of the divide. The eastern CKW, as evidenced by the Chambeshi-Luvua-Luapula river system (see **Figure 8.9**), indicates several phases of disruption that are not shown by the rest of the divide. This disruption of established, pre-existing drainage by the EARS indicates, along with the biogeography evidence (see **Figure 8.10** and **Chapter 7**), is substantially younger than the drainage systems it is disrupting. The major changes wrought by

the parallel seismic hazard arms (see **Figure 8.3**) suggest that rift associated geodynamic activity dominates the process of drainage rearrangement across the eastern Divide. This re-configuration of the pre-existing Congo and Zambezi drainages is still ongoing as evidenced by the continued adherence (persistence) of parts of these rivers to their previous configuration, for example, the south-westerly flow direction of the Chambeshi and the middle Kafue, the south-easterly flow direction of the Kafue headwaters and the north-westerly flow direction of the upper Congo River headwaters. Thus the EARS is in the process of overprinting drainage configurations that were established prior to the initiation of rift related tectonic activity in south-central Africa. Therefore the drainage, and the landsurface on which it formed, of both the Congo and Kalahari Basins predate the current drainage of the eastern CKW and incipient rifting of the Western Branch. This overprinting of the watershed between high and low Africa strongly suggests that the origin and causation of southern high Africa is vastly different to the origin and causation of eastern high Africa. Therefore, Africa may be considered to comprise three different long wavelength geomorphic zones, represented along the CKW by the low CB, the high KB and the high eastern CKW.

8.5.1 A trimodal Africa?

Africa has been considered to be bimodal (in geomorphic terms), consisting of a high, southern and eastern Africa and a low, central and western Africa. However, as is seen along the CKW, the rift related topography of high eastern Africa is distinct from the homogenous relief of high southern Africa and they have distinct geomorphologies. Therefore, Africa's high relief can be instructively classified into mega–geomorphic regions on the criteria of their distinct topographies. Thus, the surface of the African plate may be described as tri-modal rather than bimodal.

This configuration is especially evident when one examines the topographic roughness (e.g. Iwahashi and Pike, 2007), see **Chapter 3**, of Africa's two high regions. Southern Africa is topographically smooth, especially across central southern Africa, whereas, apart from the East African craton (Lake Victoria region), eastern Africa is topographically rough (see **Figure 8.13**). Not only has the EARS shaped the high topography of east Africa, its impacts have impinged upon the topography of low Africa (CB) and southern high Africa (KB). This affect on the CB can be seen in the numerous steep, westward-flowing rivers. For example, the Lukuga River has an extremely convex slope over its first two thirds, where it drains the flank of the Western Branch; yet its lower third section, flowing within the central CB, is flat. This topographic overprinting of eastern CKW (which includes pre-existing drainages of the Congo and Kalahari Basins) by the EARS has resulted in the eastern CKW

sharing characteristics of both young, active landforms (non-lithological controlled knickpoints, large elbows of capture, sharply defined horst-graben structures) and old, stable landforms (graded river sections with low gradient and no knickpoints, broad plains and wide valleys) (see **Figures 8.9, 8.10** and **8.13**).

Thus, it follows that the origin of the western and central CKW, with its established drainage along the watershed, probably substantially predates the initiation of the activity of the EARS. Therefore, eastern high Africa should be thought of as having a different cause and evolutionary trajectory from that of southern Africa, even though both exhibit a high elevation. The high elevation of southern and eastern Africa can be viewed as convergent outcomes of landscape evolution.

Figure 8.13: Africa's current trimodal topography. The solid, white line delineates the current extent of Old high Africa and the dashed white line shows the probable past margin of old high Africa. The black solid line indicates areas of Old low Africa, with the dashed black line indicating the likely past margin. The solid grey line indicates the extent of Young high Africa with its probable southern extent indicated by the dotted grey line. Young high Africa is a topographically rough high region and as such differs from Old high Africa as this is a topographically smooth, high plateau. The young high is younger than the old low and old high Africa as it can be seen to be imprinting on both these features, as indicated by the dotted line and overlaps. Young high Africa is a north-east trending feature that predominately exploits Gondwana fabrics and has developed with the progression of the EARS; it should be considered a separate feature of the craton and shield dominated features of central and southern Africa.

8.6 Summary

The different developmental histories of the CB and KB have led to Africa being considered bimodal. However, results presented here for the eastern portion of the drainage divide between the Congo and Kalahari Basins suggest an alternative classification (see **Figure 8.12**). This alternative perspective on the geomorphological evolution of Africa is obtained when a temporal component is added to the orthodox physical, elevation based bimodal division. Its addition reveals that a pre-existing watershed between the CB and KB has experienced rapid and ongoing disruption, as evidenced by the Chambeshi–Luapula–Luvua. Here, the drainages of the Congo and Kalahari (in the form of the Zambezi component) have been disrupted by the ongoing extension of the Western Branch of the EARS. As pre-existing drainages have been disrupted, this suggests that the Western Branch is younger than the Congo and Kalahari Basins. In turn, this means that the unaffected central and western CKW is older, having seen less dramatic changes relative to the now heavily modified, and thus reshaped, eastern portions.

The geomorphic evolution of Africa is better understood and contextualised if Africa is reclassified as trimodal. That is as a high, old southern portion (from ~10˚ S to ~35˚ S) with a low, old northern portion (from ~10˚ S to ~35˚ N), both of which have been and are being disrupted by the high, young dominantly north–east to south–west trending EARS (see **Figures 8.9, 8.10** and **8.11**). Therefore, any geomorphic features occurring within the high, new zone would be young; its landforms have undergone substantial rejuvenation or modification or have been newly created, because these landscapes have been, and still are, dominantly controlled by tectonics (geodynamics). In contrast, the landscapes of southern and northern Africa are most likely older, and have been shaped by varying degrees of inheritance and persistence. Furthermore, landscapes that are located within the future sphere of extension of the EARS (i.e. southern Angola, northern Namibia and northern and central Botswana) may experience increasing tectonic influences that will control their future evolution. This tectonic control will be most acutely felt along the mobile zones and shield margins with the cratonic regions remaining comparably stable. Thus, further mixing of landscape controls will occur.

CHAPTER 9: SUMMARY OF FINDINGS AND CONCLUSIONS

9.1 Introduction

This thesis has focused on the geomorphology of 18 selected rivers which share the Congo–Kalahari Watershed and the results presented here provide a better understanding the geomorphic controls, processes and evolution of this sub–continental drainage divide. Use was made of GISs in combination with remotely sensed imagery, the properties of which were reviewed in **Chapter 4**. The validation of the SRTM digital surface model used in this study, as described in **Chapter 5**, provides confidence in the accuracy and precision of the digitisation and mapping of the selected rivers and their longitudinal profiles.

The manual digitisation and characterisation of the river longitudinal profiles in **Chapter 6** allowed for the identification and classification of 380 knickpoints. This in turn resulted in a spatially accurate, searchable geodatabase that can inform future analysis of these rivers. The characterised knickpoints provide insights into the development of the individual rivers and allow for a degree of comparison between rivers. However, the knickpoint characterisation did not allow the Congo Basin to be compared to the Kalahari Basin, nor did it reveal a mechanistic explanation for the evolution of the CKW, as it did not address the formation of the knickpoints themselves. Therefore, the knickpoint geodatabase was combined with additional data from the literature and from published maps to provide insights into factors controlling the development of the CB and KB, as well as time constraints for Neogene events and this integrated data was discussed in **Chapter 7**. The outcomes of **Chapter 6** and **7** were synthesised and contextualised in terms of south–central Africa's geologic and geomorphic history in **Chapter 8** and here an important outcome is the discovery that the continental topography of Africa can be seen as comprised of trimodal relief; this appreciation significantly improves our understanding of the geomorphic development of the Congo and Kalahari Basins.

The key findings of this thesis are summarised in point form below, with reference to the questions outlined in **Chapter 1**, **Section 1.3**. They are followed by several recommendations for future research and concluding remarks.

9.2 The knickpoints of the Congo and Kalahari rivers

9.2.1 What are the spatial distributions and characteristics of the knickpoints of the studied rivers?

- Although time consuming, the manually digitisation of knickpoint identification and characterisation yields results that are currently better contextualised and spatially more accurate than a standard, automated approach.
- The knickpoints in south–central Africa show a degree of spatial structuring within the individual rivers but knickpoint number is not causally related to river length.
- The distribution of knickpoints within and across the Congo and Kalahari Basin do not display a strong, definitive pattern.
- There is a large range in variation of knickpoint density, geomorphic characteristics and heights across south–central Africa, as would be expected for such a vast study area.

9.2.2 Are these knickpoints controlled by structure (lithology and tectonics) or autogenic processes?

- The noticeable spatial clustering of knickpoints within a river suggests non–fluvial controls on the origin and persistence of most of the identified knickpoints.
- Knickpoint location is dominantly controlled by the underlying geology over which the river flows.
- Faulting influences fewer knickpoints than lithological controls, yet of the faulted knickpoints a higher proportion of the knickpoints relative to the lithologically controlled knickpoints have heights greater than 20 m. Therefore, faulting plays an important role in river development.
- However, a cause could not be readily assigned to 63 of the 380 identified knickpoints and their formation could be due to autogenic fluvial processes.
- The spatial distribution of knickpoints across south–central Africa does not exhibit a discernible relationship with landscape elevation, as would be expected if baselevel changes caused by uplift and subsidence were the sole controls of knickpoint formation.
- The river networks of the CB and KB have undergone substantial changes through the Neogene, which provides an explanation for some of the identified knickpoints. However, these changes have not been uniform in terms of spatial extent, magnitude, or frequency. This spatial heterogeneity points to the importance of a regional control in the formation of knickpoints, and by extension the CKW, in south–central Africa.

9.3 The Neogene evolution of the Congo–Kalahari Watershed

9.3.1 How do pre-existing structures influence landscape and river evolution along the CKW?

- The geomorphology of rivers drainage in the Archean cratonic regions of south–central Africa reflects strong controls by the underlying lithology, and those knickpoints shaped by faulting are mainly confined to cratonic margins and orogenic belts.
- The rivers and knickpoints of eastern Congo and Kalahari Basins appear to be significantly influenced by geodynamic activity related to the formation of the EARS, which itself exploits pre–existing structural fabrics that developed during formation of Gondwana.

9.3.2 Is the evolution of the CKW related to the development of Africa's continental geomorphology?

- The origin of the CKW is attributed to the formation of an ancestral watershed that existed between high southern Africa and low central Africa during Gondwana.
- After Gondwana break–up, the western zone of the CKW was modified through the capture of interior river drainage by the coastal Cunene river system.
- In the late Cenozoic the eastern CKW was heavily modified by a south–west trending incipient rift that forms part of the Western Branch.

9.4 Conceptual model of the Neogene evolution of the CKW and its associated landforms

The findings summarised above allow for the development of a conceptual model of the CKW's Neogene evolution, which was an important goal of this study.

The CKW comprises three components, the western, central and eastern zones, each of which are undergoing different rates of modification and thereby reflect distinct evolutionary signals. The central zone is the oldest, having undergone limited modification since the Late Jurassic. The western zone, having become established on the Precambrian basement, has undergone substantial modification during the Cenozoic. The eastern CKW has been modified to such a degree during the Neogene that it would be best considered a new landscape (relative to the central and western zones). Thus, apart from minor modifications, much of the western and central CKW has been stable, in terms of location and overarching morphology, throughout the Neogene. The eastern CKW has undergone significant changes due to horst and graben formation associated with rifting and dramatic changes in drainage, and so should be considered a Neogene landscape.

9.5 Recommendations for future work

While this study has been able to identify and compile a general sequence of events and time constraints on certain events in the geomorphic evolution of the CKW, many details of the area's geomorphic history remain unclear. This study identifies the dominant controls responsible for forming the majority of the rivers' knickpoints, and it provides an example of lithological control by the plotting of the longitudinal profiles of the Kwango and Kasai River. Our understanding the evolution of south–central Africa's landscape may be enhanced by future studies addressing the following issues:

(1) What are the rates of knickpoint migration and river incision in south–central Africa?

This question may be addressed through the use of cosmogenic dating of the exposure age of a sequence of rock outcrops from the knickpoint in a downstream direction. Alternatively the calculation catchment-average denudation rates, by measuring ^{10}Be and ^{26}Al abundances in quartz from stream sediments of suitable rivers, may provide erosion history. Both of these approaches would significantly add to our understanding of the CB and KB river systems by quantifying rates that are currently unknown. The geological geodatabase created for this study provides an invaluable foundation for such future investigation, especially by identifying suitable sample sites.

(2) How do the rivers of the Congo and Kalahari Basin compare to one another, in terms of morphology?

As this study has shown, the rivers of south–central Africa display major differences in their longitudinal profiles. However, a quantified measure of these differences, through the use of morphometric parameters such as slope steepness, the measure of river convexity and concavity, would provide a better understanding of each river's development. This longitudinal information, combined with river valley attributes, such as valley steepness and calculation of width–to–area indices, will allow for the construction of computational models of river evolution in the Congo and Kalahari Basins. This will in turn aid the quantification of the effects of tectonics on these river systems, which will improve our understanding of the development of the CKW.

(3) At what time and in which direction have river re-arrangements occurred?

During this study, the use of phylogeographic data obtained from focal studies of living organisms provided significant insights into the evolution of the CKW and its associated landscapes. Future studies increasing the number of species used and decreasing the spatial distances of species sampled will be likely to provide further valuable insights into the re-arrangements within and across the Congo and Kalahari Basin.

9.6 Concluding remarks

The Congo-Kalahari Watershed is a unique landscape feature, of subcontinental scale, which does not appear to have an analogue elsewhere on the planet. Its current morphology is juxtaposed closely with another uniquely African feature, namely, the East African Rift System. The interplay between these two geological phenomena poses challenges to attempts to elucidate their geomorphologic history, especially the eastern Divide of the CKW. This complex task needs to incorporate as much evidence as possible. The understanding of the structures inherited from the formation, existence and break–up of Gondwana in combination with future research into ongoing geodynamic processes that exploit these inherited, pre–existing fabrics will prove invaluable to our understanding of the unique controls that influence Africa's geomorphology. Already some of these geodynamic controls are recognisable in the creation of new landforms (horst and graben) and the changing mosaic of persistent landforms (pre–existing topographies) and inherited landforms (incongruent river sections). We can expect these patterns to exhibit in both subtle and dramatic phenomena, and this is where cosmogenic and phylogeographic evidence can play a role, as they allow for the dating of landforms (and formative events) and can potentially reconstruct changes at both large and small scales. The cause and evolution of Africa's trimodality is unique and its origins challenge not only today's but also future researchers. The study of rivers will continue to produce new data and insights into Africa's geomorphic development.

REFERENCES

Alexander, D. E. (2008). A brief survey of GIS in mass-movement studies, with reflections on theory and methods. *Geomorphology*, **94**(3–4), pp 261-267.

Anka, Z., Séranne, M. and di Primio, R. (2010). Evidence of a large upper-Cretaceous depocentere across the Continent-Ocean boundary of the Congo-Angola basin. Implications for paleao-drainage and potential ultra-deep source rocks. *Marine and Petroleum Geology*, **27**, pp 601 – 611.

Anka, Z. and Séranne, M. (2004). Reconnaissance study of the ancient Zaire (Congo) deep-sea fan ZaiAngo Project. *Marine Geology*, **209**, pp 223 – 244.

ASTER Global DEM Validation (2009). [online]. Available at: http://gdem.ersdac.jspacesystems.or.jp/>. [Accessed August 2011].

Avise, J. C. (2000). *Phylogeography: the history and formation of species*. Harvard University Press. pp. 447.

Babonneau, N., Savoye, B. and Klein, B. (2002). Morphology and architecture of the present canyon and channel system of the Zaire deep-sea fan. *Marine and Petroleum Geology*, **19**, pp 445 – 467.

Bauer, F.U., Glasmacher, U.A., Ring, U., Schumann, A. and Nagudi, B. (2010). Thermal and exhumation history of the central Rwenzori Mountains, Western Rift of the East African Rift System, Uganda. *International Journal of Earth Science*, **99**, pp 1575 – 1597.

Beckinsale, R.P. and Chorley, R.J. (1991). *The History of Landforms Vol.3: Historical and Regional Geomorphology 1890–1950*, pp 496. London.

Bell-Cross, G. (1965). Movement of fish across the Congo-Zambezi watershed in the Mwinilunga District of Northern Rhodesia. In *Proceedings of the Central African Scientific and Medical Congress*, Lusaka, Northern Rhodesia, pp 415 – 424.

Beyer, H. L. (2010). *Hawth's analysis tools for ArcGIS*. 2004. Freeware from http://wwwspatialecologycom/htools.

Bishop, P. (1980). Popper's principle of falsifiability and the irrefutability of the Davisian cycle. *Professional Geographer,* **32**(3), pp 310 – 315.

Bishop, P. (2007). Long – term landscape evolution: linking tectonics and surface processes. *Earth Surface Processes and Landforms* **32**(3), pp 329 – 365.

Bisnath, S. and Collins, P. (2012). Recent developments in precise point positioning. *Geomatica*, **66**(2), pp 103 – 111.

Blumberg, D.G. (2006). Analysis of large aeolian (wind-blown) bedfors using the Shuttle Radar Topography Mission (SRTM) digital elevation data. *Remote Sensing of the Environment*, **100**, pp 179 – 189.

Bridge, J.S. (2003) *Rivers and Floodplains: Forms, Processes, and Sedimentary Record*. Blackwell Publishing, Cornwall. pp 504.

Brierley, G., Fryirs, K. and Jain, V. (2006). Landscape connectivity: the geographic basis of geomorphic applications. Area, **38**(2), pp 165 – 174.

Brown, D.M., Brenneman, R.A, Koepfli, K., Pollinger, J.P., Milá, B., Georgiadis, N.J., Louis, E.E., Grether,G.F., Jacobs, D.K. and Wayne, R.K. (2007). Extensive population genetic structure in the giraffe. *BMC biology* **5**(1).

Brown, K.J., Rüber, L., Bills, R. and Day, J.J. (2010). Mastacembelid eels support Lake Tanganyika as an evolutionary hotspot of diversification. *BMC evolutionary biology* **10** (1).

Brundsen, D (1990). Tablets of Stone: toward the ten Commandments of Geomorphology. *Zeitschrift für Geomorphologie N.F.*, *Supplementband* **79**, pp 1 – 37.

Brunsden, D. (1996). Geomorphological events and landform change. *Zeitschrift für Geomorphologie N.F.*, **40** pp 273 – 288.

Brundsen, D. (2001). A critical assessment of the sensitivity concept in geomorphology. *Catena*, **42**(2 –4), pp 99 – 123.

Brunsden, D. and Thornes, J. B. (1979). Landscape sensitivity and change. *Transactions of the Institute of British Geographers*, pp 463 – 484.

Bubenzer O. and Bolten, A. (2008). The use of new elevation data (SRTM/ASTER) for the detection and morphometric quantification of Pleistocene megadunes (draa) in the eastern Sahara and the southern Namib. *Geomorphology*, **102**, pp 221 – 231.

Buiter, S.J.H., Steinberger, B., Medvedev, S. and Tetreault, J.L. (2012). Could the mantle have caused subsidence of the Congo Basin? *Tectonophysics*, **514 – 517**, p 62-80.

Burbank, D. W. and Anderson, R. S. (2001). *Tectonic Geomorphology*. Blackwell Science: Oxford. pp 274.

Burke, K. and Gunnell, Y. (2008). The African erosion surface: a continental-scale synethesi of geomorphology, tectonics and environmental change over the past 180 million years. *Geological Society of America Memoir*, **201**, pp 66.

Burke, K.,MacGregor, D.and Cameron, N. (2003) Africa's petroleum systems: four tectonic Aces in the past 600 million years. In: Arthur, T., MacGregor, D. and Cameron, N. (eds). *Petroleum Geology of Africa: New Themes and Developing Technologies*. Geological Society of London Special Publication, **207**, pp 21 – 60.

Cahen, L. (1954). *Géologie du Congo Belge*. H. Vaillant Carmanne, Liège, pp 490.

Cahen, L. and Lepersonne, J. (1952). Équivalence entre le système du Kalahari du Congo belge et les Kalahari beds d'Afrique austral. *Mémoires de la Société Belge Géologique, Paleontologique, et Hydrologique, Tervuren (Belgique)*, Série in-8, Sciences Géologiques, **4**, 63 p.

Castleden, N., Hu, G.R., Abbey, D.A., Wihing, D., Øvstedl, O., Earls, C.J. and Featherstone, W.E. (2004). First results from Virtual Reference Station (VRS) and Precise Point Positioning (PPP) GPS research at Western Australian Centre for Geodesy. *Journal of Global Positioning Systems*, **3**(1-2), pp 79 – 84.

Catuneanu, O., Wopfner, H., Eriksson, P.G., Cairncross, B., Rubidge, B.S., Smith, R.M.H. and Hancox, P.J. (2005). The Karoo basins of south-central Africa. *Journal of African Earth Sciences*, **43**(1-3), p 211 – 253.

Chandler, G. and Merry, C. (2010). The South African Geoid 2010: SAGEOID10. *PositionIT*, **June**, pp 29 – 33.

Chorley, R. J., Schumm, S. A. and David E. S. (1984). *Geomorphology.* Methuen, New York, p 498.

Chorowicz, J. (2005). The East African Rift System. *Journal of African Earth Sciences*, **43**, pp 379 – 410.

Church, M. (2010). The trajectory of geomorphology. *Progress in Physical Geography*, **34**(3) pp 265-286

Cocks, L. R. M. and Torsvik, T. H. (2011). The Palaeozoic geography of Laurentia and western Laurussia: a stable craton with mobile margins. *Earth-Science Reviews*, **106**(1), pp 1 – 51.

Consortium for Spatial Information (CGIAR-CSI). (19 August 2008). SRTM 90m Digital Elevation Data. [online]. Available at: http://srtm.csi.cgiar.org. [Last accesses April 2014]

Consortium for Spatial Information (CGIAR-CSI). (n.d). SRTM Data Processing Methodology http://srtm.csi.cgiar.org/SRTMdataProcessingMethodology.asp. [Accessed date June 2010]

Colin, J.P. (1994). Mesozoic-Cenozoic lacustrine sediments in the Zaïre Interior Basin. In: Gierlowski-Kordesch, E. and Kelts, K. (eds.). *Global Geological Record of Lake Basins*. Cambridge University Press, **4**, pp 31 – 36.

Cotterill, F.P.D. (2006). The evolutionary history and taxonomy of the *Kobus leche* species complex of south–central Africa in the context of palaeo–drainage dynamics. Unpublished PhD thesis, University of Stellenbosch, South Africa. pp 425.

Cotterill, F.P.D. and de Wit, M.J. (2011). Geoecodynamics and the Kalahari epeirogeny: linking its genomic record, tree of life and palimpsest into a unified narrative of landscape evolution. *South African Journal of Geology*, **114**, pp 489 – 514.

Cullum, C., Brierley, G.J., and Thoms, M., (2008). Chapter 4: The Spatial Organization of River Systems. Pp 43- 64. In: Brierley, G.J. and Fryirs, K.A. (eds). *River Futures: An Integrative Scientific Approach to River Repair*. Society For Ecological restoration International. Washington DC, Island Press, pp 304.

Daly, M.C., Lawrence, S.R., Diemu-Tshiband, K. and Matouana, B. (1992). Tectonic evolution of the Cuvette Centrale, Zaire. *Journal of the Geological Society, London*, **149**, pp 539 – 546.

Davis, W.M. (1899). The Geographical Cycle. *Geographical Journal*, **14**(5), pp 481 – 504.

Day, J.J., Bills, R. And Friel, J.P. (2009). Lacustrine radiations in African Synodontis catfish. *Journal of evolutionary biology* **22**(4), pp 805 – 817.

De Carvalho, H. (1981). Geologia de Angola. 4 folhas, escala 1: 1 000 000. Laboratório Nacional de investigação Cientifica Tropical, *Junta de Investigaçãoes Cientifica do Ultramar*.

De Dapper, M. (1988). Geomorphology of the sand-covered plateaux in southern Shaba, Zaire. In: Dardis, G.F. and Moon, B.P. (eds). *Geomorphological Studies in Southern Africa*. Balkema, Rotterdam. pp 115 – 135.

De Matos, R. M. D. (1999). History of the northeast Brazilian rift system: kinematic implications for the break-up between Brazil and West Africa. *Geological Society, London, Special Publications*, **153**(1), pp 55 – 73.

De Wit, M.J. (2007). The Kalahari Eperiogeny and climate change: differentiating cause and effect from core to space. South Africa Journal of Geology, **110**, pp 367 – 392.

De Wit, M. C. J., Marshall, T. R. and Partridge, T. C. (2000). Fluvial deposits and drainage evolution. *Oxford Monographs on Geology and Geophysics*, **40**, pp 55 – 72.

De Wit, M.J., Stankiewicz, J. and Reeves C. (2008). Restoring Pan-African-Brasiliano connections: more Gondwana control, less Trans-Atlantic corruption. In Pankhurst, R.J., Trouw, R.A.J., Brotp Neves, B.B. and de Wit, M.J. (eds) West Gondwana:Pre-Cenozoic Correlations Across the South Atlantic Region. Geological Society, London, Special Publications, **294**, pp 399 – 412.

Decrée, S., Deloule, É., Ruffet, G., Dewaele, S., Mees, F., Marignac, C., Yans, J. and De Putter, T. (2010). Geodynamic and climate controls in the formation of Mio–Pliocene world-class oxidized cobalt and manganese ores in the Katanga province, DR Congo. *Mineralium Deposita*, **45**(7), pp 621 – 629.

Decker, J.E., Niedermann, S. and de Wit, M.J. (2013). Climatically influenced denudation rates of the southern African plateau: Clues to solving a geomorphic paradox. *Geomorphology*, **190**, pp 48 – 60.

Deffontaines, D. and Chorowicz, J. (1991). Principles of drainage basin analysis from multisource data: Application to the structural analysis of the Zaire Basin. *Tectonophysics*, **194**, pp 237 – 263.

DeSalle, R., and Rosenfeld, J. (2013). *Phylogenomics: A Primer*. Garland Science: New York, pp. 338.

Delpomdor, F., Kant, F. and Préat, R. (2014). Neoproterozic uppermost Haut-Shiloango Subgroup (West Congo Supergroup, Democratic Republic of Congo): Misinterpreted stromatolies and implications for sea-level fluctuations before the onset of the Marinoan glaciation. *Journal of African Earth Sciences*, **90**, pp 49 – 63.

Delvaux, D. and Barth A. (2010). African stress pattern from formal inversion of focal mechanism data. *Tectonophysics*, **48**, pp 105 – 128.

Delvaux, D., Kervyn, F., Macheyeki, A.S. and Temu, E.B. (2012). Geodynamic significance of the TRM segment in East African Rift (W-Tanzania): Active tectonics and paleostress in the Ufipa plateau and Rukwa basin. *Journal of Structural Geology*, **37**, pp 161 – 180.

Desthieux F. (1995). Carte Géologique de la République du Congo au 1:1.000.000. *Geological Survey of South Africa*.

Dixey, F. (1938). Some observations on the physiographical development of central and southern Africa. *Transactions of the Geological Society of South Africa*, **41**, pp 113 – 170.

Dixey, F. (1943). The Morphology of the Congo-Zambesi Watershed. *South African Geographical Journal*, **25**(1), pp 20 – 41.

Dixey, F. (1944). African landscape. *Geographical Review*, pp 457 – 465.

Dixey, F. (1945). Miocene sediments in South Turkana. *Journal of the East Africa Natural History Society*, ***18***, pp 13 – 14.

Dixey, F. (1955). Erosion surfaces in Africa; some considerations of age and origin. *Transactions Geological Society South Africa*, ***58***(LVIII), pp 265 – 280.

Dollar, E. S. J. (2000). Progress reports, Fluvial geomorphology. *Progress in Physical Geography*, **24**(3), pp 385 – 407.

Dollar, E. S. (2002). Fluvial geomorphology. *Progress in physical geography*, **26**(1), pp 123 – 143.

Doucouré, C.M. and de Wit, M.J. (2003). Old inherited origin for the present near–bimodal topography of Africa. *Journal of African Earth Sciences*, **36**, pp 371 – 388.

Doyle, M. W. and Bernhardt, E. S. (2010). What is a stream? *Environmental Science and Technology*, **45**(2), pp 354 – 359.

Du Toit, A.L. (1933). Crustal movement as a factor in the geographical evolution of South Africa. *The South African Geographical Journal*, **16**, pp 4 – 20.

Du Toit, A. L., 1937. *Our wandering continents: An Hypothesis of Continental Drifting*.
Edinburgh: Oliver and Boyd, pp 366.

Du Toit, A.L. (1954). *The Geology of South Africa*. Third edition. Oliver and Boyd, Edinburgh. pp 611.

Dupré, B., Gaillardet, J., Rousseau, D. and Allègre, C. J. (1996). Major and trace elements of river-borne material: the Congo Basin. *Geochimica et Cosmochimica Acta*, **60**(8), pp 1301 – 1321.

Ebner, R. and Featherstone, W.E. (2008). How well can online GPS PPP post-processing services be used to establish geodetic survey control networks? *Journal of Applied Geodesy*, **2**, pp 149 – 157.

EGM96 Online Geoid Calculator. (n.d.) [online]. Available at: <http://earth-info.nga.mil/GandG/wgs84/gravitymod/egm96/intpt.html>. [Last accessed 9 July 2013]

Erlanger, E. D., Granger, D. E., and Gibbon, R. J. (2012). Rock uplift rates in South Africa from isochron burial dating of fluvial and marine terraces. *Geology*, **40**(11), pp 1019 – 1022.

Faulkes, C. G., Mgode, G. F., Le Comber, S. C., and Bennett, N. C. (2010). Cladogenesis and endemism in Tanzanian mole-rats, genus Fukomys:(Rodentia Bathyergidae): a role for tectonics? *Biological Journal of the Linnean Society*, **100**(2), pp 337 – 352.

Featherstone, W.E. (2001). Absolute and relative testing of gravimetric geoid models using Global Positioning System and orthometric height data. *Computers and Geosciences*, **27**, pp 807 – 814.

Flagstad, Ø., Syversten, P. O., Stenseth, N. C., and Jakobsen, K. S. (2001). Environmental change and rates of evolution: the phylogeographic pattern within the hartebeest complex as related to climatic variation. *Proceedings of the Royal Society of London. Series B: Biological Sciences*, **268**(1468), pp 667 – 677.

Flowers, R. M., and Schoene, B. (2010). (U-Th)/He thermochronometry constraints on unroofing of the eastern Kaapvaal craton and significance for uplift of the southern African Plateau. *Geology*, **38**(9), pp 827 – 830.

Fouche, J., Bate, K. J., and Van der Merwe, R. (1992). Plate tectonic setting of the Mesozoic Basins, southern offshore, South Africa: A review. *Inversion Tectonics of the Cape Fold Belt, Karoo and Cretaceous Basins of Southern Africa*, pp 27 – 32.

Fuller, A.O. (1999). Alex Logan du Toit. *Journal of African Earth Sciences* **28**(1), pp 3–9.

Gaillardet, J., Dupré, B. and Allèrge, C.J. (1995). A global geochemical mass budget applied to the Congo Basin rivers: Erosion rates and continental crust composition. *Geochemica et Cosmochimica Acta*, **59**(17), pp 3469 – 3485.

Gamache, M. (2004). *Free and Low Cost Datasets for International Mountain Cartography*, Alpine Mapping Guild. Available at: <http://www.terrainmap.com/downloads/Gamache_final_wed.pdf> [Accessed 3 July 2013].

Gardner, R. and Scoging, H. M. (1983). *Mega-geomorphology*. Oxford University Press: USA.

Gesch, D.B. Verding, K.L. and Greenlee, S.K. (1999). New land surface digital elevation model covers the Earth. *Eos Transactions American Geophysical Union*, **80**, pp 69 – 70.

Giresse, P. (2005). Mesozoic-Cenozoic history of the Congo Basin. *Journal of African Earth Sciences*, 43, p 301 – 315.

Gilbert, G.K. (1877). Report on the Geology of the Henry Mountains. Geographical and Geological Survey of the Rocky Mountain Region, Department of the Interior (Washington D.C.), pp 160.

Gilbert, G.K. (1914). *The transportation of debris by running water.* Volume 86, US Government Printing Office. pp 263.

Global Land Cover Facility Earth Science Data Interface. (n.d.). University of Maryland. [online]. Available at: http://glcfapp.glcf.umd.edu:8080/esdi/index.jsp. [Accessed May 2008 - March 2009]

Global Land Cover Facility Landsat Technical Guide (2004). University of Maryland. [online]. Available at: http://glcf.umicas.umd.edu/data/guide/technical/techguide_landsat.pdf. [Accessed 15 April 2008].

Goodier, S.A.M., F.P.D. Cotterill, C. O'Ryan, P. H. Skelton, M. J. de Wit. (2011). Cryptic diversity of African tigerfish (Genus *Hydrocynus*) reveals palaeogeographic signatures of linked Neogene geotectonic events. PLoSONE **6**(12): e28775. doi:10.1371/journal.pone.0028775

Gorokhovich, Y. and Voustianiouk, A. (2006). Accuracy assessment of the processed SRTM-based elevation data by CGIAR using filed data from USA and Thailand and its relations to the terrain characteristics. *Remote Sensing of Environment*, **104**, pp 409 – 415.

Goudie, A.S. (2005). The drainage of Africa since the Cretaceous. *Geomorphology*, **67**, pp 437 – 456.

Gubanov, A. P. and Mooney, W. D. (2009). New global geological maps of crustal basement age. *AGU Fall Meeting Abstracts*, **1**, p 1583.

Gumbricht, T., McCarthy, T. S. and Merry, C. L. (2001). The topography of the Okavango Delta, Botswana, and its tectonic and sedimentological implications. *South African Journal of Geology*, **104**(3), pp 243 – 264.

Gupta, A. (2007). Introduction. In: Gupta, A. (ed). *Large Rivers: Geomorphology and Management*. New York: John Wiley and Sons, Ltd. pp 1 – 4.

Guth, P. (2009) Geomorphometry in MICRODEM, pp 351 – 366. In: Hengl, T. and Reuter H.I. (eds). *Developments in Soil Science Volume 33 – Geomorphometry: Concepts, Software, Applications*. Elesevier, Amsterdam. pp 765.

Hack, J.T. (1960). Interpretation of erosional topography in humid temperate regions. *American Journal of Science*, **258-A**, pp 80-97.

Hack, J.T. (1975). Dynamic equilibrium and landscape evolution. In: Melhorn, W.N. and Flemal, R.C. (eds), 1980. *Theories of Landform Development: A proceedings volume of the Sixth Annual Geomorphology Symposia Series held at Binghamton, New York*. September 26-27, 1975. Allen and Unwin (Boston), p 306.

Haddon, I. (1999). *Isopach map of the Kalahari Group, at a scale of 1: 2.500.000*. Pretoria, South Africa: Council for Geoscience.

Haddon, I.G. (2000). Kalahari Group Sediments pp 173 -181. In: Partridge, T.C. and Maud, R.R (eds). *The Cenozoic of Southern Africa - Oxford Monographs on Geology and Geophysics* No. 40. Oxford University Press: New York. pp 406.

Haddon, I.G. and McCarthy, T.S. (2005). The Mesozoic-Cenozoic interior sag basins of Central Africa: The Late-Cretaceous - Cenozoic Kalahari and Okavango basins. *Journal of African Earth Sciences*, 43 pp 316 – 333.

Hancock, G.R., Martinez, C., Evans, K.G. and Moliere, D.R. (2006). A comparison of SRTM and high-resolution digital elevation models and their use in catchment geomorphology and hydrology: Australian examples. *Earth Surface Processes and Landforms*, **31**, pp 1394 – 1412.

Harcourt, A.H. and Wood, M.A. (2012). Rivers as Barriers to Primate Distributions in Africa. *International Journal of Primatology*, **33**, pp 168 – 183

Hart, J.A., Detwiler, K.M., Gilbert, C.C., Burrell, A.S., Fuller, J.L., Emetshu, M., Hart, T.B., Vosper, A., Sargis, E.J. and Tosi, A.J. (2012). Lesula: A New Species of *Cercopithecus* Monkey Endemic to the Democratic Republic of Congo and Implications for Conservation of Congo's Central Basin. *PloS ONE* 7 (9): e44271

Hayakawa, Y.S., Oguchi, T. and Lin, Z. (2008). Comparison of new and existing global digital elevation modesl: ASTER G-DEM and SRTM-3. *Geophysical Research Letters*, **35**, L17404, pp 5.

Hearn, P., Hare, T., Schruben, P., Sherrill, D., Lamar,C. and Tsushima, P. (2001). *Global GIS, 1:5 000 000*. United States Geological Survey, USA.

Hebeler F. and Purves R.S. (2009). The influence of elevation uncertainty on derivation of topographic indices. *Geomorphology*, **111**, pp 4 – 16.

Hengl, T. and Evans, I.S. (2009). Mathematical and digital models of the land surface. In: Hengl, T. and Reuter H.I. (eds): *Developments in Soil Science Volume 33 – Geomorphometry: Concepts, Software, Applications*. Elesevier, Amsterdam. pp 31 – 63.

Héroux, P. and Kouba, J. (1995). *GPS Precise Positioning with a Difference*. Paper presented at Geomatics '95, Ottawa, Ontario, Canada, June 13-15.

Héroux, P., Kouba, P., Collins, P. and Lahaye, F. (2001). GPS Carrier-Phase Point Positioning with Precise Orbit Products. *Proceedings of the KIS*, Banff Alberta, Canada June 5-8, pp 518 – 528.

Hoffman, P.F., 1999. The break-up of Rodinia, birth of Gondwana, true polar wander and the snowball Earth. *Journal of African Earth Sciences,* **28**(1), pp 17 – 33.

Holbrook, J. and Schumm, S.A. (1999). Geomorphic and sedimentary response of rivers to tectonic deformation: A brief review and critique of a tool for recognizing subtle epeirogenic deformation in modern and ancient settings. *Tectonophysics*, **305**, pp 287 – 306.

Holmes, A. (1965). *Principles of Physical Geology*. Revised Edition. Thomas Nelson: London, pp 1288.

Horton, R.E. (1945). Erosional development of streams and their drainage basins. *Bulletin of the Geological Society of America*, **56**(1), pp 275 – 370.

Howard, A.D. (1967). Drainage analysis in geological interpretation: A summary. *AAPG Bull*etin, **51**, pp 2246 – 2259.

Huang, S., Crabtree, R.L., Swanson, A.K., Halligan, K.Q. and Harmsen, J.A. (2010). Error analysis and correction for extracting the forest height from airborne C-band interferometric SAR and national elevation datasets. *International Journal of Remote Sensing*, **31**(9), pp 2493 – 2512.

Huang, S., Hager, S.A., Halligan, K.Q., Fairweather, I.S., Swanson, A.K. and Crabtree, R.L. (2009). A comparison of individual tree and forest plot height derived from LiDAR and InSAR. *Photogrammetric Engineering and Remote Sensing*, **75,** pp 159 – 167.

Huggett, R. J. (2007). Fundamentals of geomorphology. Routledge.

Iwahashi, J. and Pike, R.J. (2007). Automated classifications of topography from DEMs by an unsupervised nested-means algorithm and a three-part geometric signature. *Geomorphology*, **86**, pp 409 – 440.

Jarvis, A., Reuter, H.I., Nelson, A. and Guevara, E., (2006), Hole-filled seamless SRTM data Version 3, available from the CGIAR-CSI 90 m Database. [online] Available at: <http://srtm.csi.cgiar.org>. [Last accessed April 2006].

Jarvis, A., Reuter, H.I., Nelson, A. and Guevara, E., (2008), Hole-filled SRTM for the globe Version 4, available from the CGIAR-CSI SRTM 90m Database. [online] Available at: <http://srtm.csi.cgiar.org>. [Last accessed January 2012].

Jarvis, A., Reuter, H.I., Nelson, A., Guevara, E., (2011), Hole-filled SRTM for the globe Version 4, available from the CGIAR-CSI SRTM 250m Database. [online] Available at: <http://srtm.csi.cgiar.org>. [Last accessed January 2012].

Jarvis, A., Rubiano, J., Nelson, A., Farrow, A. and Mulligan, M. (2004). *Practical use of SRTM data in the tropics: Comparisons with digital elevation models generated from cartographic data*. Working Document no 198. Cali, Centro Internacional de Agricultura Tropical (CIAT): 32.

Jensen, J.R. (2007). *Remote Sensing of the Environment: An Earth Resource Perspective*, 2nd ed. Upper Saddle River, Pearson Prentice Hall, pp 592.

Jones, C.R. (1980). The Geology of the Kalahari. *Botswana Notes and Records*, **12**, pp 1-14.

Joyce, D.A., Lunt, D.H., Bills, R., Turner, G.F., Katongo, C., Duftner, N., Sturmbauer, C. and Seehausen, O. (2005). An extant cichlid fish radiation emerged in an extinct Pleistocene lake. *Nature*, **435,** pp 90–95.

Kadima, E., Delvaux, D., Sebagenzi, S.N., Tack, L. and Kabeya, S.M. (2011a). Structure and geological history of the Congo Basin: an integrated interpretation of gravity, magnetic and reflection seismic data. *Basin Research*, **23**(5), pp 499 – 527.

Kadima, E., Ntabwoba, S.S.M. and Lucazeau, F. (2011b). A Proterozoic-rift origin for the structure and the evolution of the cratonic Congo basin. *Earth and Planetary Science Letters*, **304**(1-2), pp 240 - 250.

Karner, G. D., and Driscoll, N. W. (1999). Tectonic and stratigraphic development of the West African and eastern Brazilian Margins: insights from quantitative basin modelling. *Geological Society, London, Special Publications*, **153**(1), pp 11 – 40.

Katongo, C., Koblmüller, S., Duftner, N., Mumba, L. and Sturmbauer, C. (2007). Evolutionary history and biogeographic affinities of the serranochromine cichlids in Zambian rivers. *Molecular phylogenetics and evolution*, **45**(1), pp 326 – 338.

Keller, M. M., Moore, D. and Sacks, W. J. (2010). Development of a Data Assimilation System to Study Ecosystem Exchange of Carbon at the National Scale Using Data from the National Ecological Observatory Network. *AGU Fall Meeting Abstracts,* **1**, 0344.

Kenny, F., Matthews, B. and Todd, K. (2008). Routing overland flow through sinks and flats in interpolated raster terrain surfaces. *Computer and Geosciences* **34** pp. 1417 – 1430.

Key, R.M., Pitfield, P.E.J., Thomas, R.J., Goodenough, K.M., De Waele, B., Schofield, D.I., Bauer, W., Horstwood, M. S. A., Styles, M. T., Conrad, J., Encarnacion, J., Lidke, D. J., O'Connor, E. A., Potter, C., Smith, R. A., Walsh, G. J., Ralison, A. V., Randriamananjara, T., Rafahatelo, J. M. and Rabarimanana, M. (2011). Polyphase Neoproterozoic orogensis within the East Africa – Antartica orogeneic Belt in central and northern Madagascar. *Geological Society, London, Special Publications*, **357**(1), pp 49 – 68.

Key, R.M. and Ayres, N. (2000). The 1998 edition of the National Geological Map of Botswana. *Journal of African Earth Sciences*, **30**(3), pp 427-451.

King, L.C. (1951) *South African Scenery: A textbook of geomorphology*. Second edition – revised. Oliver and Boyd LTD: Great Britain. Edinburgh. pp 379.

King, L.C. (1953). Canons of landscape evolution. *Geological Society of America Bulletin*, **64**, pp 721-751.

King, L.C. (1955). Pediplanation and isostasy: an example from South Africa. *Quarterly Journal of the Geographical Society*, **111**, pp 353-359.

King, L.C. (1962). *The Morphology of the Earth: A study and synthesis of world scenery*. Oliver and Boyd LTD: Great Britain. pp 699.

King, L.C. (1967). *Morphology of the Earth (2nd edition)*. Oliver and Boyd:Edinburgh, p 726.

Kirby, E. and Whipple, K. X. (2012). Expression of active tectonics in erosional landscapes. *Journal of Structural Geology*, **44**, pp 54 – 75.

Knighton, D. (1998). *Fluvial forms and processes: a new perspective* (2nd edition). Hodder Headline:Arnold.

Kobrick, M. (2006). On the toes of giants — how SRTM was born, *Photogrammetric Engineering and Remote Sensing*, **72**(3), pp 206 – 210.

Koblmüller, S., Schliewen, U. K., Duftner, N., Sefc, K. M., Katongo, C. and Sturmbauer, C. (2008). Age and spread of the haplochromine cichlid fishes in Africa. *Molecular Phylogenetics and Evolution*, **49**(1), pp 153-169.

Kotze, M., Cole, P. and Robline, D.L. (1999). Sub–Saharan African seismic hazard 1071–1996. 1 : 12 000 000, Council for Geosciences, South Africa.

Kouba, J. and Héroux, P. (2001). Precise Point Positioning using IGS orbit and clock products. *GPS Solutions,* **5**(2), pp 12 – 28.

Lancaster, M. (2000). Eolian deposits. In: Partridge, T.C. and Maud, R.M. (eds). *Cenozoic of Southern Africa*, Oxford Monographs on Geology and Geophysics, Vol 40. Oxford University Press: New York. pp 73 – 87.

Laraque, A., Mahé, G., Orange, D. and Marieu, B. (2001). Spatiotemporal variations in hydrological regimes within Central Africa during the XXth century. *Journal of Hydrology*, **245**, pp 104 – 117

Lavier, L.L., Steckler, M.S. and Briguad, F. (2001). Climate and tectonic control on the Cenozoic evolution of the West African margin. *Marine Geology,* **178**, pp 63 – 80.

Lemoine, F.G., Kenyon, S.C., Factor, J.K., Trimmer, R.G., Pavlis, N.K., Chinn, D.S., Cox, C.M., Klosko, S.M., Luthcke, S.B., Torrence, M.H., Wang, Y.M., Williamson, R.G., Pavlis, E.C., Rapp, R.H. and Olsen, T.R. (1998): The development of the joint NASA GSFC and the National Imagery and Mapping Agency (NIMA) geopotential model EGM96. *NASA Technical Paper NASA/TP-1998-206861*, Goddard Space Flight Center, Greenbelt, USA, pp 575.

Leopold, L. B., and Bull, W. B. (1979). Base level, aggradation, and grade. *Proceedings of the American Philosophical Society*, pp 168 – 202.

Leopold, L. B., and Langbein, W. B. (1962). *The concept of entropy in landscape evolution*. Washington, DC: US Government Printing Office.

Leopold, L.B., Wolman, M.G. and Miller, J.P. (1964). *Fluvial process in geomorphology*. San Francisco, W.H. Freeman, pp 552

Lepersonne, J. (1945). La Stratigraphie du Systeme du Kalahari et du Systeme du Karoo au Congo occidental. *Bulletin du Service Geologique du Congo belge et Ruanda-Urundi*, **1**, pp 27 – 50.

Lepersonne, J. (1951). Les subdivisions du système du Karoo au Kwango (Congo belge).*Annales de la Société Géologique de Belgique*, LXXIV, pp 123 – 138.

Lepersonne, J. (1974a). *Carte géologique du Zaïre au 1: 2.000.000*. Kinshasa, République duZaïre: Direction de la Géologie/Musée Royal de l'Afrique centrale, Tervuren (Belgique).

Lepersonne, J. (1974b). *Notice explicative de la carte géologique du Zaïre au 1: 2.000.000*. Kinshasa, République du Zaïre: Direction de la Géologie/Musée Royal de l'Afrique centrale, Tervuren (Belgique).

Leturmy, P., Lucazeau, F. and Brigaud, F. (2003). Dynamic interactions between the gulf of Guinea passive margin and the Congo River drainage basin: 1. Morphology and mass balance. *Journal of Geophysical Research*, **108**(B8), pp 1-13.

Li, X. and Götze, H. (2001). Ellipsoid, geoid, gravity, geodesy and geophysics. *Geophysics* **66**(6), pp 1660 – 1668.

Lillesand, T.M., Kiefer, R.W. and Chipman, J.W. (2004). *Remote Sensing and Image Interpretation.* 5th Edition. John Wiley and Sons, United States of America, pp 763.

Linol B. (2012). Sedimentology and sequence stratigraphy of the Congo and Kalahari Basins of south-central Africa and their evolution during the formation and break-up of west Gondwana. Unpublished PhD thesis, Nelson Mandela Metropolitan University, South Africa, pp 394.

Loget, N., and Van Den Driessche, J. (2009). Wave train model for knickpoint migration. *Geomorphology*, **106**(3), pp 376 – 382.

Lorenzen, E.D., Masembe, C., Arctander, P. and Siegismund, H.R. (2010). A long–standing Pleistocene refugium in southern Africa and a moscai of refugia in East Africa: insights from mtDNA and the common eland antelope. *Journal of Biogeography* **37**, pp 571 – 581.

Lucazeau, F., Brigaud, F., and Bouroullec, J. L. (2003). High-resolution heat flow density in the lower Congo basin. *Geochemistry, Geophysics, Geosystems*, **5**(3).

Ludwig, R. and Schneider, P. (2006). Validation of digital elevation models from SRTM X-SAR for applications in hydrologic modelling. *ISPRS Journal of Photogrammetry and Remote Sensing,* **60**, pp 339 – 358.

Maufe, H. B. (1935). Some Factors in the Geographical Evolution of Sothern Rhodesia and Neighbouring Countries. *South African Geographical Journal*, **18**(1), pp 3-21.

Mavonga, T. And Durrheim, R.J. (2009). Probabilistic seismic hazard assessment for the Deomocratic Republic of Congo and surrounding areas. *South African Journal of Geology*, **112**, pp 329 – 342.

McCarthy, T.S., Ellery, W.N. and Stanistreet, I.G. (1992). Avulsion mechanisms on the okvango fan, Botswana: control of a river system by vegetation. *Sedimentology* **39**, pp 779 – 795.

McFarlane, M.J. and Eckardt, F.D. (2007). Palaeodune morphology associated with the Gumare fault of the Okavango graben in the Botswana/Namibia borderland: a new model of tectonic influence. *South African Journal of Geology*, **110**, pp 535 – 542.

Meade, R.H., (1996) Chapter 3: River-sediment Inputs to Major Deltas. pp 63 -85 In: Milliman, J.D. and Haq, B.U., (eds). *Sea-level Rise and Coastal Subsidence: Causes, Consequences and Strategies.*, Kluwer, Dordrecht. pp 384.

Merry, C.L. (2007). *Africa*. [online]. Available at: <http://www.iges.polimi.it/Geoid/Africa/africa_pub_g.html>. [Last accessed 31 December 2013].

Miliaresis, G. and Delikaraoglou, D. (2009). Effects of percent tree canopy density and DEM misregistration on SRTM/NED vegetation height estimates. *Remote Sensing*, **1**(2), pp 36 – 49.

Miller, R.McG. (1980). *Geological map of Nambia*. 4 sheets, scale 1: 1 000 000. Reprint 1990. Geological Survey of Namibia, Namibia.

Moore, A.E., Cotterill, F.P.D., Main, M.P.L. and Williams, H.B. (2007). The Zambezi River. In: Gupta, A. (ed). *Large Rivers: Geomorphology and Management*. John Wiley and Sons: New York, Ltd. pp 311 – 332.

Moore, J. M., Polteau, S., Armstrong, R. A., Corfu, F., and Tsikos, H. (2012). The age and correlation of the Postmasburg Group, southern Africa: Constraints from detrital zircon grains. *Journal of African Earth Sciences*, **64**, pp 9 – 19.

Moore, A. and Blenkinsop, T. (2006). Scarp retreat versus pinned drainage divide in the formation of the Drakensberg escarpment, southern Africa. *South African Journal of Geology*, **109**, pp 599 – 610.

Moore, A.,and Blenkinsop, T. (2002). The role of mantle plumes in the development of continental-scale drainage patterns: the southern African example revisited. *South African Journal of Geology*, **105**(4), pp 353 – 360.

Moore, A. E. and Larkin, P. A. (2001). Drainage evolution in south-central Africa since the breakup of Gondwana. *South African Journal of Geology*, **104**(1).

Montgomery, D. R. and Buffington, J. M. (1997). Channel-reach morphology in mountain drainage basins. *Geological Society of America Bulletin*, **109**(5), pp 596 – 611.

National Geospatial-Intelligence Agency. (2013). [online]. Available at: <http://earth-info.nga.mil/GandG/wgs84/gravitymod/egm96/intpt.html>. [Last accessed March 2010].

Natural Resources Canada. (2010). [online]. Available at: http://www.webapp.geod.nrcan.gc.ca/geod/tools-outils/ppp.php>. [Last accessed February 2010].

Natural Resources Canada. (2012). [online]. Available at: http://www.webapp.geod.nrcan.gc.ca/geod/tools-outils/index.php#ppp>. [Last accessed January 2012].

Natural Resources Canada. (2013) [online]. Available at: http://www.webapp.geod.nrcan.gc.ca/geod/tools-outils/index.php#reference_frame>. [Last accessed June 2013].

Nelson, A., Reuter, H.I. and Gessler, P. (2009). DEM production methods and sources. pp 65–85. In *Developments in Soil Science Volume 33 – Geomorphometry: Concepts, Software, Applications* (Hengl, T. And Reuter H.I. eds). Elesevier, Amsterdam, pp 765.

Nibbelink, K. and Budihardjo, S. (2002). Paleo-Congo River Fan in Northern Gabon, *AAPG Annual Meeting*, March, Houston, USA.

Nikora, V. I. (1991). Fractal structures of river plan forms. *Water resources research*, **27**(6), pp 1327 – 1333.

Nugent, C. (1990). The Zambezi River: tectonism, climate change and drainage evolution. *Palaeogeography, Palaeoclimatology, Palaeoecology*, **78**, pp 55 – 69.

Nyblade, A.A. and Robinson, S.W. (1994). The African superswell. *Geophysical Research Letters*, **42**, pp 765 – 768.

O'Brien, E. M. and Peters, C. R. (1999). Landforms, climate, ecogeographic mosaics, and the potential for hominid diversity in Pliocene Africa. *African Biogeography, Climate Change, and Human Evolution*, pp 115 – 137.

Olson, D. M., Dinerstein, E., Wikramanayake, E. D., Burgess, N. D., Powell, G. V., Underwood, E. C., D'amico, J. A., Itoua, I., Strand, H. E., Morrison, J. C., Loucks, C. J., Allnutt, T. F., Ricketts, T. H., Kura, Y., Lamoreux, J. F., Wettengel, W. W., Hedao, P. and Kassem, K. R. (2001). Terrestrial Ecoregions of the World: A New Map of Life on Earth A new global map of terrestrial ecoregions provides an innovative tool for conserving biodiversity. *BioScience*, **51**(11), pp 933 – 938.

Partridge, T.C. (1998). Of diamonds, dinosaurs and diastrophism: 150 million years of landscape evolution in southern Africa. *South African Journal of Geology*, **101**(3), pp 167 – 184.

Partridge, T.C., Dollar, E.S.J., Moolman, J. and Dollar, L.H. (2010). The geomorphoic provinces of South Africa, Lesotho and Swaziland: A physiographic subdivision for earth and environmental scientists. *Transactions of the Royal Society of South Africa*, **65**(1), pp 1-47.

Partridge, T.C. and Maud, R.R. (1987). Geomorphic evolution of southern Africa since the Mesozoic. South African Journal of Geology, **90**, pp 179 – 208.

Partridge, T.C. and Maud, R.R. (2000). Macro-scale geomorphic evolution of southern Africa. In: Partridge, T.C. and Maud, R.R. (eds.). *The Cenozoic of Southern Africa*. Oxford University Press, pp 3 – 18.

Pasyanos, M. E., and Nyblade, A. A. (2007). A top to bottom lithospheric study of Africa and Arabia. *Tectonophysics*, **444**(1), pp 27 – 44.

Penck, W. (1953). *Morphological analysis of landforms: A contribution to physical geology*. Translated by Czech, H. and Boswell, K.C. MacMillan (London), pp 429.

Piégay, H. and Schumm, S. A. (2003) System Approaches in Fluvial Geomorphology. In: Kondolf G. M. and Piégay, H. (eds). *Tools in Fluvial Geomorphology*. John Wiley and Sons, Ltd: Chichester, UK. pp 105 – 134.

Pike, R.J., Evans, I.S. and Hengl, T. (2009). Geomorphomerty: A brief guide pp 3–30. In: Hengl, T. and Reuter H.I. (eds). *Developments in Soil Science Volume 33 – Geomorphometry: Concepts, Software, Applications*. Elsevier: Amsterdam. pp 765.

Pitra, C., VazPinto, P., O'Keeffe, B. W., Willows-Munro, S., van Vuuren, B. J. and Robinson, T. J. (2006). DNA-led rediscovery of the giant sable antelope in Angola. *European Journal of Wildlife Research*, **52**(3), pp 145 – 152.

Potter, P. E. (1978). Petrology and chemistry of modern big river sands. *The Journal of Geology*, pp 423 – 449.

Potter, P. E. and Hamblin, W. K. (2006). *Big rivers worldwide* (Vol. 48). Dept. of Geology, Brigham Young University.

Prüfer, K., Munch, K., Hellmann, I., Akagi, K., Miller, J.R., Walenz, B., Koren, S., Sutton, G., Kodira, C., Winer, R., Knight, J.R., Mullikin, J.C., Meader, S.J., Ponting, C.P., Lunter, G., Higashino, S., Hobolth, A., Dutheil, J., Karakoç, E., Alkan, C., Sajjadian, S., Catacchio, C.R., Ventura, M., Marques-Bonet, T., Eichler, E.E., André, C., Atencia, R., Mugisha, L., Junhold, J., Patterson, N., Siebauer, M., Good, J.M., Fischer, A., Ptak, S.E., Lachmann, M., Symer, D.E., Mailund, T., Schierup, M.H., Andrés, A.M., Kelso, J. and Pääbo, S. (2012). The bonobo genome compared with the chimpanzee and human genomes. *Nature*, **486**, pp 527 – 531 (doi: 10.1038/nature11128)

Reeves, C. (1972). Rifting in the Kalahari? *Nature*, **237**(5350), pp.95-96.

Reeves, C.V. (1999). Aeromagnetic and gravity features of Gondwana and their relation to continental break-up: more pieces, less puzzle. *Journal of African Earth Sciences*, **28**, pp.263 – 277.

Reeves, C.V., de Wit, M.J. and Sahu, B.K. (2004). Tight reassembly of Gondwana exposes Phanerozoic shers in Africa as global tectonic players. *Gondwana Research* **7**(1), pp 7 – 19.

Remondo, J. and Oguchi T. (2009). GIS and SDA applications in Geomorphology. *Geomorphology*, **111**, pp 1 – 3.

Reuter, H.I., Nelson, A. and Jarvis, A. (2007). An evaluation of void filling interpolation methods for SRTM data. *International Journal of Geographic Information Science,* **21**(9), pp 983 – 1008.

Ring, U. (2008). Extreme uplift of the Rwenzori Mountains in the East African Rift, Uganda: Structural framework and possible role of glaciations. *Tectonics* **27**(4).

Ringrose, S., Kampunzu, A.B., Vink, B.W., Matheson, W. And Downey, W.S. (2000). Origin and palaeo-environments of calcareous sediments in the Moshaweng dry valley, southeast Botswana. *Earth Surface Processes and Landforms* **27**, pp 591 – 611.

Robert, M. (1946). *Le Congo Physique* (3é edition). Presse Universitaires de France, Liége. p 499.

Roberts, T.R. (1975). Geographical distribution of African freshwater fishes. *Zoological Jounral of the Linnean Society* **57**(4), pp 249 – 319.

Roberts, E.M., Stevens, N.J., O'Connor, P.M., Dirks, P.H.G.M., Gottfried, M.D., Clydge, W.C., Armstrong, R.A., Kemp, A.I.S. and Hemming, S. (2012). Initiation of the western branch of teh Eater African Rift coeval with the eastern branch. *Nature Geoscience* **5**(4), pp 289 – 294.

Rodrígues-Iturbe, I. And Rinaldo, A. (1997). *Fractal River Basins: Chance and Self-Organisation.* Cambridge University Press, United States of America, pp 547.

Rodríguez, E., Morris, C.S. and Belz, J.E. (2006). A global assessment of the SRTM performance. *Photogrammetric Engineering and Remote Sensing,* **72**(3), pp 249 – 260.

Roller, S., Hornung, J., Hinderer, M. and Ssemmanda, I. (2010). Middle Miocene to Pleistocene sedimentary record of rift evolution in southern Albert Rift (Uganda). *International Journal of Earth Science*, **99**, pp 1643 – 1661 (doi:10.1007/s00531-010-0560-z).

Rossetti, D.F. and Valeriano, M.M. (2007). Evolution of the lowest Amazon basin modelled from the intergration of geological and SRTM topographic data. *Catena*, **70**, pp 253 – 265.

Runge, J. (2007). The Congo River, Central Africa. In: *Large Rivers: Geomorphology and Management*. Gupta A. (ed). New York: John Wiley and Sons, Ltd. pp 293 – 309.

Sachse, D., Billault, I., Bowen, G. J., Chikaraishi, Y., Dawson, T. E., Feakins, S. J., Freeman, K. H., Magill, C. R., McInerney, F. A., van der Meer, M. T. J., Polissar, P., Robins, R. J., Sachs, J. P., Schmidt, H., Sessions, A. L., White, J. W. C., West, J. B. and Kahmen, A. (2012). Molecular paleohydrology: Interpreting the hydrogen-isotopic composition of lipid biomarkers from photosynthesizing organisms. *Annual Review of Earth and Planetary Sciences*, **40**, pp 221 – 249.

Scally, A., Dutheil, J.Y., Hillier, L.W., Jordan, G.E., Goodhead, I.,Herrero, J.,Hobolth, A., Lappalainen, T., Mailund, T., Marques-Bonet, T., McCarthy, S., Montgomery, S.H., Schwalie, P.C., Tang, Y.A., Ward, M.C., Xue, Y., Yngvadottir, B., Alkan, C., Andersen, L.N., Ayub, O., Ball, E.V., Beal, K., Bradley, B.J., Chen, Y., Clee, C.M., Fitzgerald, S., Graves, T.A., Gu, Y., Heath, P., Heger, A., Karakoç, E., Kolb-Kokocinski, A., Laird, G.K., Lunter, G., Meader, S., Mort, M., Mullikin, J.C., Munch, K., O'Connor, T.D., Phillips, A.D., Prado-Martinez, J., Rogers, A.S., Sajjadian, S., Schmidt, D., Shaw, K., Simpson, J.T., Stenson, P.D., Turner, D.J., Vigilant, L., Vilella, A.J., Whitener, W., Zhu, B., Cooper, D.N., de Jong, P., Dermitzakis, E.T., Eichler, E.E., Flicek, P., Goldman, N., Mundy, N.I., Ning, Z., Odom, D.T., Ponting, C.P., Quail, M.A., Ryder, O.A., Searle, S.M., Warren, W.C., Wilson, R.K.,

Schierup, M.H., Rogers, J., Tyler-Smith, C. and Durbin,R., (2012). Insights into hominid evolution from the gorilla genome sequence. *Nature*, **483**, pp 169 – 175.

Scharf, T.E., Codilean, A.T., de Wit, M.J., Jansen, J.D. and Kubik, P.W. (2013). Strong rocks sustain ancient postorogenic topography in southern Africa. *Geology* **41**(3), pp 331 – 334.

Schumm, S. A. (1977). *The fluvial system*. Wiley, New York pp 338.

Schumm, S.A. (1991). *To Interpret the Earth: Ten Ways to be Wrong*. Cambridge University Press: Cambridge, pp 133.

Schumm, S. A. and Lichty, R. W. (1965). Time, space, and causality in geomorphology. *American Journal of Science*, **263**(2), pp 110 – 119.

Schumm, S. A., Dumont, J. F. and Holbrook, J. M. (2002). *Active tectonics and alluvial rivers*. Cambridge University Press.

Schumm, S.A. (2005). *River variability and complexity.* Cambridge University Press.

Schwarzer J., Misof, B., Ifuta, S.N. and Schliewen, U.K. (2011). Time and origin of cichlid colonization of the lower Congo rapids. *PLoSONE,* **6,** e22380.

Schwarzer. J., Swartz, E.R., Vreven, E., Snoeks, J., Cotterill, F.P.D., Misof, B. and Schliewen, U.K. (2012). Repeated trans-watershed hybridization among haplochromine cichlids (Cichlidae) triggered by Neogene landscape evolution. *Proceedings of the Royal Society of London Series B*. Published online, pp 1 – 11. (doi:10.1098/rspb.2012.1667).

Seranne, M., Bruguier, O. and Moussavou, M. (2008). U-Pb single zircon grain dating of Present fluvial and Cenozoic aeolian sediments from Gabon: consequences on sediment provenance, reworking, and erosion processes on equatorial West African margin. *Bulletin de la Société géologique de France*, **179**(1), pp 29 – 40.

Sinha, S. K. and Parker, G. (1996). Causes of concavity in longitudinal profiles of rivers. *Water Resources Research*, **32**(5), pp 1417 – 1428.

Sithaldeen, R., Bishop, J. M. and Ackermann, R. R. (2009). Mitochondrial DNA analysis reveals Plio-Pleistocene diversification within the chacma baboon. *Molecular phylogenetics and evolution*, **53**(3), pp 1042 – 1048.

Skelton, P. H. (1996). A historical review of the taxonomy and biogeography of freshwater fishes in South Africa—the past 50 years. *Transactions of the Royal Society of South Africa*, **51**(1), pp 91 – 114.

Strahler, A. N. (1952). Hypsometric (area-altitude) analysis of erosional topography. *Geological Society of America Bulletin*, **63**(11), pp 1117 – 1142.

Stankiewicz, J. and de Wit, M.J. (2006). A proposed drainage evolution model for Central Africa - Did the Congo flow east? *Journal of African Earth Sciences*, **44**(1), pp 75 – 84.

Stanley, J.R., Flowers, R.M. and Bell, D.R. (2013). Kimberlite (U-Th)/He dating links surface erosion with lithospheric heating, thinning, and metasomatism in southern African Plateau. *Geology* **41**(12), pp 1243 – 1246.

Steel, E. A. (1917). Zambezi-Congo Watershed. *Geographical Journal*, pp 180 – 193.

Summerfield, M.A. (1991). Global geomorphology: an introduction to the study of landforms. Longman (New York), pp 537.

Summerfield, M.A. (2005). A tale of two scales, or the two Geomorphologies. *Transactions of the Institute of British Geographers*, **30**, pp 402 – 415.

Sun, G., Ranson, K.J., Kharuk, V.I. and Kovacs, K. (2003). Validation of surface heights from shuttle radar topography mission using shuttle laser altimeter. *Remote Sensing of Environment,* **88,** pp 401 – 411.

Tack, L., Fernandez-Alonso, M., Trefois, P. and Lavreau, J. (2003) New data raise new question on the regional geology of the Katanga province as figured on the 1974 geological map (112 000 000) of the Democratic Republic of Congo (DRC) in Proterozoic Sediment-hosed Base Metal Deposits of Western Gondwana. 3rd IGCP–450 Conference and Guide Book of the Field Workshop, Lumbumbahsi, Congo.

Tandon, S. K. and Sinha, R. (2007). Geology of large river systems. In: *Large rivers: geomorphology and management.* Gupta, A. (ed), pp 7 – 28.

Tarboton, D.G., Bras, R.L. and Rodrígues-Iturbe, I. (1988). The fractal nature of river networks. *Water Resources Research,* **24**(8), pp 1317 – 1322.

Telfer, P. T., Souquiere, S., Clifford, S. L., Abernethy, K. A., Bruford, M. W., Disotell, D. R., Sterner, K. N., Roques, P., Marx, P. A. and Wickings, E. J. (2003). Molecular evidence for deep phylogenetic divergence in Mandrillus sphinx. *Molecular Ecology*, **12**, pp 2019 – 2024.

Thieme, J.G. and Johnson R.L. (1975). *Geological map of the Republic of Zambia*. 4 sheets, scale 1 : 1 000 000. Geological Survey Department, Zambia

Tinker, J., de Wit, M. and Brown, R. (2008). Linking source and sink: Evaluating the balance between onshore erosion and offshore sediment accumulation since Gondwana break-up, South Africa. *Tectonophysics*, **455**(1-4), pp 94 – 103.

Tooth, S. and McCarthy, T. S. (2007). Wetlands in drylands: geomorphological and sedimentological characteristics, with emphasis on examples from southern Africa. *Progress in Physical Geography*, **31**(1), pp 3 – 41.

Tooth, S., McCarthy, T.S., Brandt, D., Hancox, P.J. and Morris, R. (2002). Geological controls on the formation of alluvial meanders and floodplain wetlands: the example of the Klip River, eastern Free State, South Africa. *Earth Surface Processes and Landforms*, **27**, pp 797 – 815.

Tooth, S., Brandt, D., Hancox, P.J. and McCarthy, T.S. (2004). Geological controls on alluvial river behaviour: a comparative study of three rivers on the South African Highveld. *Journal of African Earth Sciences*, **38**, pp 79 – 97.

Torsvik, T.H. and Cocks, L.R.M. (2009) The Lower Palaeozoic palaeogeographical evolution of the northeastern and eastern peri-Gondwanan margin from Turkey to New Zealand In: Bassett, M.G. (ed.) 2009. *Early Palaeozoic Peri-Gondwana Terranes: New Insights from Tectonics and Biogeography*. Geological Society, London, Special Publication, **325**, pp 3 – 21.

Tucker, J.C., Grant, D.M. and Dykstra, J.D. (2004). NASA's Global Orthorectified Landsat Data Set. *Photogrammetric Engineering and Remote Sensing,* **70**(3), pp 313 – 322.

Turcotte, D.L. (1992). *Fractal and chaos in geology and geophysics*. Cambridge University Press, Great Britain. pp 221.

Twidale, C. R. (2003). "Canons" revisited and reviewed: Lester King's views of landscape evolution considered 50 years later. *Geological Society of America Bulletin*, **115**(10), pp 1155 – 1172.

Tyson, P.D. and Partridge, T.C., 2000. Evolution of Cenozoic Climates. In: Partridge, T.C. and Maud, R.R. (eds.), *The Cenozoic of Southern Africa*. Oxford University Press, pp 371 – 387.

Uenzelmann-Neben, G. (1998). Neogene sedimentation history of the Congo Fan. *Marine and Petroleum Geology*, **15**(7), pp 635 – 650.

UNEP-WCMC and IUCN (International Union for Conservation of Nature) (2008a). Gorilla gorilla. In: IUCN 2013. *IUCN Red List of Threatened Species*. Version 2013.2. [online]. Available at: <http://maps.iucnredlist.org/map.html?id=9404> [Last accessed 7 January 2013]

US Geological Survey (n.d.). [online] Available at: < http://edc.usgs.gov/products/elevation/srtmdted.html>. [Accessed 2009]

van Hinsbergen, D. J., Lippert, P. C., Dupont-Nivet, G., McQuarrie, N., Doubrovine, P. V., Spakman, W. and Torsvik, T. H. (2012). Greater India Basin hypothesis and a two-stage Cenozoic collision between India and Asia. *Proceedings of the National Academy of Sciences*, **109**(20), pp 7659 – 7664.

Veatch, A.C. (1935). Evolution of the Congo Basin. *Memoir Geological Society of America*, **3**, pp 183.

Walker, J.D. and Geissman, J.W., compilers (2009). *Geologic Time Scale*. Geological Society of America. (doi: 10.1130/2009.CTS004R2C).

Wellington, J. H. (1949). A new development scheme for the Okovango Delta, Northern Kalahari. *Geographical Journal*, pp 62 – 69.

Wellington, J.H. (1955). *Southern Africa – a Geographic Study*. Volume 1, Physical Geography. Cambridge University Press, Cambridge, pp 528.

White, R. G. (1983). Foraging patterns and their multiplier effects on productivity of northern ungulates. *Oikos*, pp 377 – 384.

Wichura, H., Bousquet, R., Oberhänsli, R., Strecker, M. R. and Trauth, M. H. (2011). The Mid-Miocene East African Plateau: A pre-rift topographic model inferred from the emplacement of the phonolitic Yatta lava flow, Kenya. *Geological Society, London, Special Publications*, **357**(1), pp 285 – 300.

Zernitz, E.R. (1932). Drainage patterns and their significance. *Journal of Geology,* **40**(6), pp 498 – 521.

Zinner, D., Groeneveld, L. F., Keller, C. and Roos, C. (2009). Mitochondrial phylogeography of baboons (*Papio* spp.) – indication for introgressive hybridization? *BMC Evolutionary Biology*, **9**, pp 83.

APPENDIX 5: PRECISE GPS SURVEY

5.1 Geoid

In order to convert GPS-determined heights to orthometric elevations (that is elevations above mean sea level) a geoid model is required (Li and Götze, 2001; Chandler and Merry, 2010). This is due to the large variation of geodial height relative to ellipsoid surface. This is the surface that is used for elevation by GPS constellations, which for this study was WGS84. The mathematical ellipsoidal surface is a smooth, even surface that measures the distance from the Earth's centre (Featherstone, 2001; Li and Götze, 2001). As this mathematical surface cannot account for variations of the Earth's surface, its height may be above or below the true topographical surface. Therefore in order to achieve true (orthometric) elevations from GPS heights, the deviation of the ellipsoid from the Earth's surface must be accounted for, which requires the use of a geoidal model (Li and Götze, 2001; Chandler and Merry, 2010). The geoidal model may be considered the equipotential surface of the Earth's gravity field that most closely corresponds to the mean sea level of a free-flowing, open ocean (mean sea level) (Featherstone, 2001). The difference in geodial and ellipsoidal heights varies spatially and may be in excess of 100 m. It exists due to the Earth's uneven gravitation field as shown in **Figure A5.1** (Li and Götze, 2001; Chandler and Merry, 2010) This geoid surface may be above or below the ellipsoid surface. (See Lemoine *et al.* (1998) for details regarding the creation of the EGM96 geoidal model.)

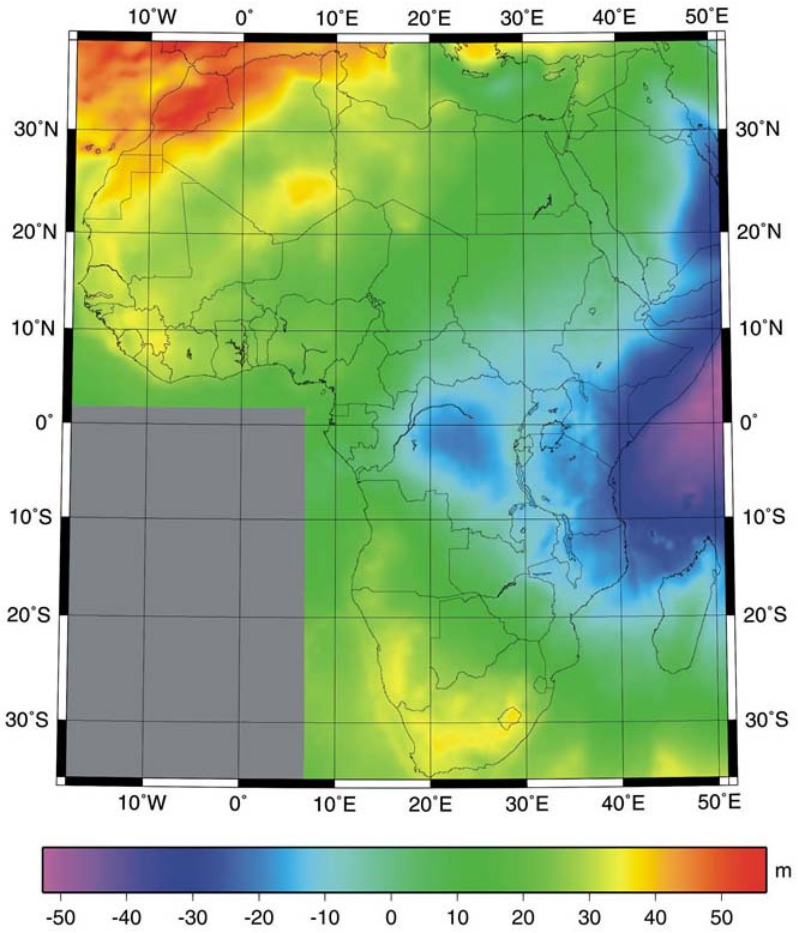

Figure A5.1: The African geoid (Merry, 2007). The geoid shows a -50 to +50 m deviation from the WGS84 ellipsoid. This range of geoidal heights must be accounted for when converting GPS derived heights to accurate elevations above mean sea level (Li and Götze, 2001; Featherstone, 2001; Chandler and Merry, 2010. Of interest are the negative deviations of up to *c.* -30 m for the central Congo basin and northern Zambia.

5.2 Precision GPS survey

Table A5.1 below shows the results of post-processing correction of the 39 GPS surveyed positions. The processed elevations of the GPS positions (**GS20 (Ellipsoid)(m)**) and the calculated error for each point is shown (**GS20 Error (m)**). The average GS20 error is 0.406 m, with a range of 0.252 to 0.627 m. The GPS elevations are given as ellipsoidal elevations, therefore geoid correction for the positions have been included (**EGM96 Height**) to allow for the calculation of the orthometric elevation (**Orthometric (m)**). The corresponding SRTMv3 elevation (uncorrected) is given (**SRTMv3 (m)**). A comparison of the SRTMv3 elevations to the orthometric elevations (**Difference (SRTMv3 – Orth)** indicates an average error of positive 5m. That is, the SRTM elevations are, on average, 5m higher than the true, orthometric elevation in southern Africa. The range is -1 to +34m.

Table A5.1: The results of the GPS surveys (n = 39).The resulting orthometric elevations are shown and compared to the corresponding SRTMv3 elevations. The difference between SRTMv3 and orthometric is positive 5 m. See **Chapter 5** for further details.

Latitude	Longitude	Name of Point	GS20 (Ellipsoid) (m)	GS20 Error (m)	EGM96 Height (m)	Orthometric (m)	SRTMv3 (m)	Difference (SRTMv3 - Orth)
-8.477121	30.44967	Ndola Bay	753.993	0.279	-14.64	768.633	778	9
-8.662692	30.6554	Lufubu	760.877	0.279	-14.63	775.507	782	6
-9.524446	29.3515	**Kabawene Falls ***	1086.011	0.371	-12.20	1098.211	1119	21
-9.539162	29.38572	**Below Lumangwe Falls ***	1106.549	0.297	-11.93	1118.479	1152	34
-9.542712	29.38759	Lumangwe Falls	1146.986	0.283	-11.93	1158.916	1165	6
-9.798755	28.74045	Chipipa	916.613	0.306	-8.84	925.453	926	1
-9.813422	28.76684	Orphange	968.279	0.411	-8.87	977.149	978	1
-10.57092	28.67479	**Mambilima Falls ***	936.789	0.373	-7.76	944.549	955	10
-10.92385	31.07421	Chambeshi River (by old bridge)	1175.39	0.326	-11.12	1186.51	1189	2
-11.34464	29.56265	Samfya Bay Lodge 1	1155.546	0.342	-9.17	1164.716	1166	1
-11.34555	29.56236	Samfya Bay Lodge 2	1155.869	0.378	-9.17	1165.039	1168	3
-11.7186	29.66902	Twingi Wetland	1155.278	0.310	-8.81	1164.088	1168	4
-11.71755	29.6695	Twingi Landing	1159.053	0.305	-8.81	1167.863	1167	-1
-12.50181	30.13068	Luwombwa	1168.222	0.452	-7.37	1175.592	1179	3
-12.53799	30.36637	**Malembo River (near Kasanka GP) ***	1185.717	0.393	-7.96	1193.677	1208	14
-12.55428	30.37639	**Kasanka GP Edu Centre ***	1193.769	0.263	-7.96	1201.729	1213	11
-12.57391	30.23454	**Pontoon Camp ***	1172.35	0.252	-7.45	1179.8	1188	8
-13.72202	29.15666	Forrest Inn	1229.909	0.358	-4.91	1234.819	1240	5
-15.83632	28.23766	Kafue R Queen	978.788	0.321	1.04	977.748	981	3
-16.64223	27.02985	Ian's	1208.582	0.349	6.15	1202.432	1203	1
-16.64735	27.00445	Emma's	1225.045	0.472	6.22	1218.825	1221	2
-19.72741	26.06854	946TP	950.4	0.319	10.40	940	944	4
-19.91659	26.14536	943TP	948.7	0.535	10.8	937.9	940	2

Latitude	Longitude	Name of Point	GS20 (Ellipsoid) (m)	GS20 Error (m)	EGM96 Height	Orthometric (m)	SRTM3 (m)	Difference (SRTM3 - Ortho)
-20.28762	26.3004	Nata	924.205	0.459	11.93	912.275	913	1
-20.30708	24.79511	919TP	930.9	0.427	13.4	917.5	919	2
-20.43565	25.25265	Ice 20	924.3	0.388	13.5	910.8	917	6
-20.46256	25.18766	Ice 36	921.7	0.525	13.7	908	912	4
-20.47575	25.98042	905TP	915.4	0.627	12.8	902.6	907	4
-20.4874	25.26587	Ice 22	920.3	0.410	13.6	906.7	911	4
-20.65005	25.11882	Ice 19	916.5	0.439	14.1	902.5	904	2
-20.75517	25.70443	Ice X1	916.4	0.505	13.7	902.6	905	2
-20.91684	26.25917	Ice (1)	912.9	0.525	14	898.9	903	4
-21.01795	24.26318	Ice 42	968.6	0.536	15.8	952.8	954	1
-21.01795	24.26318	954TP	968.6	0.536	15.8	952.8	954	1
-21.16056	25.96321	**980TP ***	987.7	0.466	14.3	975.4	982	7
-21.22099	24.99371	910TP	924.7	0.470	14.9	909.7	914	4
-21.44428	24.72664	Ice 26	970.9	0.467	15.7	955.2	960	5
			Average error	0.406		**Average difference**		**5**

***** indicate those points in areas of high topographic relief (i.e. near large waterfalls such as Kabawene and Mambilima Falls) or riparian forest (i.e. Malembo River and Kasanka GP Edu) or dense, sustained woodland (i.e. Pontoon Camp and 980TP).

Table A5.2: Comparison of orthometric elevations, predicted orthometric and SRTMv3 elevations; and comparison of the squares of the difference of predicted orthometric and orthometric, and SRTMv3 and orthometric. All readings (n = 39) were used as they were indicative of on the ground conditions of the study region. Note the SRTMv3 elevation data is to rounded to the nearest metre. P_Orth = predicted orthometric; Orth = orthometric.

Orth (m)	P_Orth (m)	SRTMv3 (m)	Difference (P_Orth – Orth)	Difference (SRTMv3 – Orth)	Difference from mean (P_Orth)	Difference from mean (SRTMv3)	square of difference (P_Orth – Orth)	square of difference (SRTMv3 – Orth)
768.633	775.0	778	6.4	9.4	-6.4	-4.1	40.9	16.5
775.507	779.0	782	3.5	6.5	-3.5	-1.2	12.1	1.4
1098.211	1112.8	1119	14.5	20.8	-14.5	-15.5	211.5	239.7
1118.479	1145.4	1152	27.0	33.5	-27.0	-28.2	726.8	796.0
1158.916	1158.3	1165	-0.6	6.1	0.6	-0.8	0.4	0.6
925.453	921.6	926	-3.8	0.5	3.9	4.7	14.8	22.7
977.149	973.1	978	-4.0	0.9	4.0	4.5	16.3	19.9
944.549	950.3	955	5.8	10.5	-5.8	-5.1	33.4	26.5
1186.51	1182.1	1189	-4.4	2.5	4.4	2.8	19.6	7.9
1164.716	1159.3	1166	-5.4	1.3	5.4	4.0	29.3	16.2
1165.039	1161.3	1168	-3.8	3.0	3.8	2.3	14.1	5.5
1164.088	1161.3	1168	-2.8	3.9	2.8	1.4	7.9	1.9
1167.863	1160.3	1167	-7.6	-0.9	7.6	6.2	57.3	38.1
1175.592	1172.2	1179	-3.4	3.4	3.4	1.9	11.6	3.6
1193.677	1200.9	1208	7.2	14.3	-7.2	-9.0	52.2	81.3
1201.729	1205.9	1213	4.1	11.3	-4.1	-6.0	17.0	35.6
1179.8	1181.1	1188	1.3	8.2	-1.3	-2.9	1.7	8.4
1234.819	1232.6	1240	-2.2	5.2	2.2	0.1	5.0	0.0
977.748	976.1	981	-1.7	3.3	1.7	2.0	2.8	4.2
1202.432	1195.9	1203	-6.5	0.6	6.5	4.8	42.0	22.5
1218.825	1213.8	1221	-5.0	2.2	5.1	3.132	25.5	9.8
940	939.4	944	-0.6	4.0	0.6	1.307	0.3	1.7

Orth (m)	P_Orth (m)	SRTMv3 (m)	Difference (P_Orth – Orth)	Difference (SRTMv3 – Orth)	Difference from mean (P_Orth)	Difference from mean (SRTMv3)	square of difference (P_Orth – Orth)	square of difference (SRTMv3 – Orth)
937.9	935.5	940	-2.4	2.1	2.4	3.207	5.9	10.3
905.4	905.8	910	0.4	4.6	-0.4	0.707	0.1	0.5
916.2	914.7	919	-1.5	2.8	1.5	2.507	2.3	6.3
912.275	908.7	913	-3.5	0.7	3.6	4.582	12.5	21.0
917.5	914.7	919	-2.8	1.5	2.9	3.807	8.0	14.5
910.8	912.7	917	1.9	6.2	-1.9	-0.893	3.6	0.8
908	907.7	912	-0.3	4.0	0.3	1.307	0.1	1.7
902.6	902.8	907	0.2	4.4	-0.2	0.907	0.0	0.8
906.7	906.8	911	0.1	4.3	-0.047	1.007	0.0	1.0
902.5	899.8	904	-2.7	1.5	2.685	3.807	7.2	14.5
902.6	900.8	905	-1.8	2.4	1.795	2.907	3.2	8.5
898.9	898.8	903	-0.1	4.1	0.076	1.207	0.0	1.5
952.8	949.3	954	-3.5	1.2	3.465	4.107	12.0	16.9
952.8	949.3	954	-3.5	1.2	3.465	4.107	12.0	16.9
975.8	977.1	982	1.7	6.6	-1.666	-1.293	2.8	1.7
909.7	909.7	914	0.0	4.3	-0.019	1.007	0.0	1.0
955.2	955.3	960	0.1	4.8	-0.077	0.507	0.0	0.3

Average difference (mean)	0.0	5.3

Variance	**36.2**	**37.9**
1σ Standard deviation (m)	**6.0**	**6.2**
2σ Standard deviation (m)	**12.0**[a]	**12.3**[b]

[a] 12 m accuracy at the 95 % confidence limit [b] 12 m accuracy at the 95% confidence limit

APPENDIX 6

6.1 River courses and longitudinal profile creation

6.1.1 Manual digitisation of river courses and longitudinal profiles

- In order to geographically link the three viewer : *View > Link/Unlink Viewers > Geographical*.
- The Spatial Profile tool created an associated table, accessible by: *Spatial Profile > View > Tabular Data*. This table contained information regarding the Map X (longitude) Map Y (latitude) File X (pixel row) File Y (pixel column) Distance (straight line distance) Surface Distance (the actual on the ground distance) and Layer 1 (DSM elevations).
- Adding the tabular XY into ArcGIS : *Tools > add XY data >* and the Geographic Co-ordinate System (GCS) WGS 1984 was selected as the Coordinate system. The created an events layers that was then exported as a shapefile : *Right click on events layer > Export Data*. This assigned each row entry a FID (unique feature identifier) allowing it to be queried.
- Converting a point shapefile to a polyline shapefile : *HawthsTools > Animal movements > Convert locations to paths (points to line)*. The "Create a single output path (one line)" option was chosen.
- To project the river polyline shapefile: *ArcToolbox > Data Management Tools > Projections and Transformations > Feature > Project > UTM* was chosen for the "Output Coordinate System". The UTM zone chosen depended upon the location of the river being projected).
- Length determination of the projected river polyline: *HawthsTools > Table Tools > Add LENGTH field to table*. The "Convert length units (multiply by this constant)" was checked and 0.001 selected so that the lengths were given in kilometres.
- To merge : *ArcToolbox > Data Management Tools > General > Merge*
- To add the names of the river : *Editor > Start Editing >* open attribute table and double click on cell to be edited.

6.1.2 Generation of rivers networks and long profile

6.1.2.1 Generated river networks

Derived stream networks are based on configuration of the landscape, representing the pattern of flow accumulation and potential location of river networks. The tools used to generate the required output files can be found in : ArcToolbox > Spatial Analyst Tools > Hydrology (see **Table A6.1**).

To resample the SRTMv3 3 arc-second DSM to 30 arc-seconds the SRTMv3 data was exported with a different cell size : in the Layer Display window > *Right Click > Data > Export Data > Change cell size from 0.000833 to 0.00833*.

Table A6.1: List of the ArcGIS tools, there outputs and required intputs. Table modified from ArcGIS Online help.

Tool	**Output**	**Required input**
Basin	Creates a raster delineating all drainage basins.	Flow direction raster.
Fill	Fills sinks in a surface raster to remove small imperfections in the data.	Surface raster.
Flow Accumulation	Creates a raster of accumulated flow to each cell.	Flow direction raster.
Flow Direction	Direction from each cell to its steepest downslope neighbour.	Surface raster.
Flow Length	Calculates the distance, or weighted distance, along flow path.	Flow direction raster.
Sink	Creates a raster identifying all sinks or areas of internal drainage.	Flow direction raster.
Snap Pour Points	Snaps pour points to the cell of highest flow accumulation within a specified distance.	Accumulation raster and raster pour point data.
Stream Link	Assigns unique values to sections of a raster linear network.	Stream raster and flow direction.
Stream Order	Assigns a numeric order to segments of a raster representing branches of a linear network.	Stream raster and flow direction raster.
Stream to Feature	Converts a raster representing a linear network to features representing the linear network.	Stream raster and flow direction raster.
Watershed	Determines the contributing area above a set of cells in a raster.	Flow direction raster, raster pour point.

No z option was used for the Fill tool.

- To convert the stream raster networks to shapefiles: *Conversion Tool > Raster to Polyline > Background value left as 'Zero' and Minmum dangle length left as' 0' with Simplify polylines unchecked.*

6.1.2.2 Generated river long profiles

Issues regarding river long profile generation

Raster output issues

After extraction, the elevation values were visually using the attribute table of the output rasters. This involved the comparison the elevation of pixels in the individual raster attribute tables. It was expected that using the stream network shapefiles to extract the DSM elevations, the correct sequence of the elevations in relation to the river would have been maintained. However, the elevation in the raster attribute values were stored in a descending order without regard to sequential ordering of the elevations in along the river. The elevation data was put into a spreadsheet and plotted, which showed some anomalous spikes and troughs in the resulting river profile, further highlighting the incorrect sequencing of the elevation values.

In an attempt to overcome the raster ordering issue, the stream polyline shapefile was converted to points using Hawth's Tools (Beyer, 2004) (**Appendix: River long profiles**).

- To convert raster data to point data using Hawths Tools : *Conversion Tool > Raster to Point > Field > Value*

This conversion of the polyline to points was expected to produce separate points with a unique, sequentially correct value. Potting the river long profiles indicated that the elevation order was still out-of-sequence. An attempt to fix the segment order using Arc/INFO 's Build/Clean routines but these did not work.

After creating a new polyline shapefile by tracing the generate river courses (using the Trace Tool). The identifying field, RivID, was added and then manually filled in using the Editor tool. The steps below were followed in order to extract the elevation data in the correct sequential order.

- To convert polylines into point data using Haths Tools: *Hawths Tools > Animal Movements > Convert Path to Points (lines to points)* > the RivID was chosen as the unique field > Interval between points was set too 900 (as this would created a point every 900 m or roughly 30 arc seconds). Thus a single point corresponded to a single pixel
- To spatially join the two point shapefiles: *Right click on the shapefile > Joins and Relates > Join > Join data from another layer based on spatial location* > chose the relevant layer > check "Each point will be given all the attributes…"

6.2. **Comparison of generated and manually digitised longitudinal profiles**

The following figures are the graphical comparisons of rivers, as determined from three techniques (Chapter 6). For a detailed treatment of each river see Chapter 6, section 6.3.2.

6.2.1 Profiles of the Congo Basin

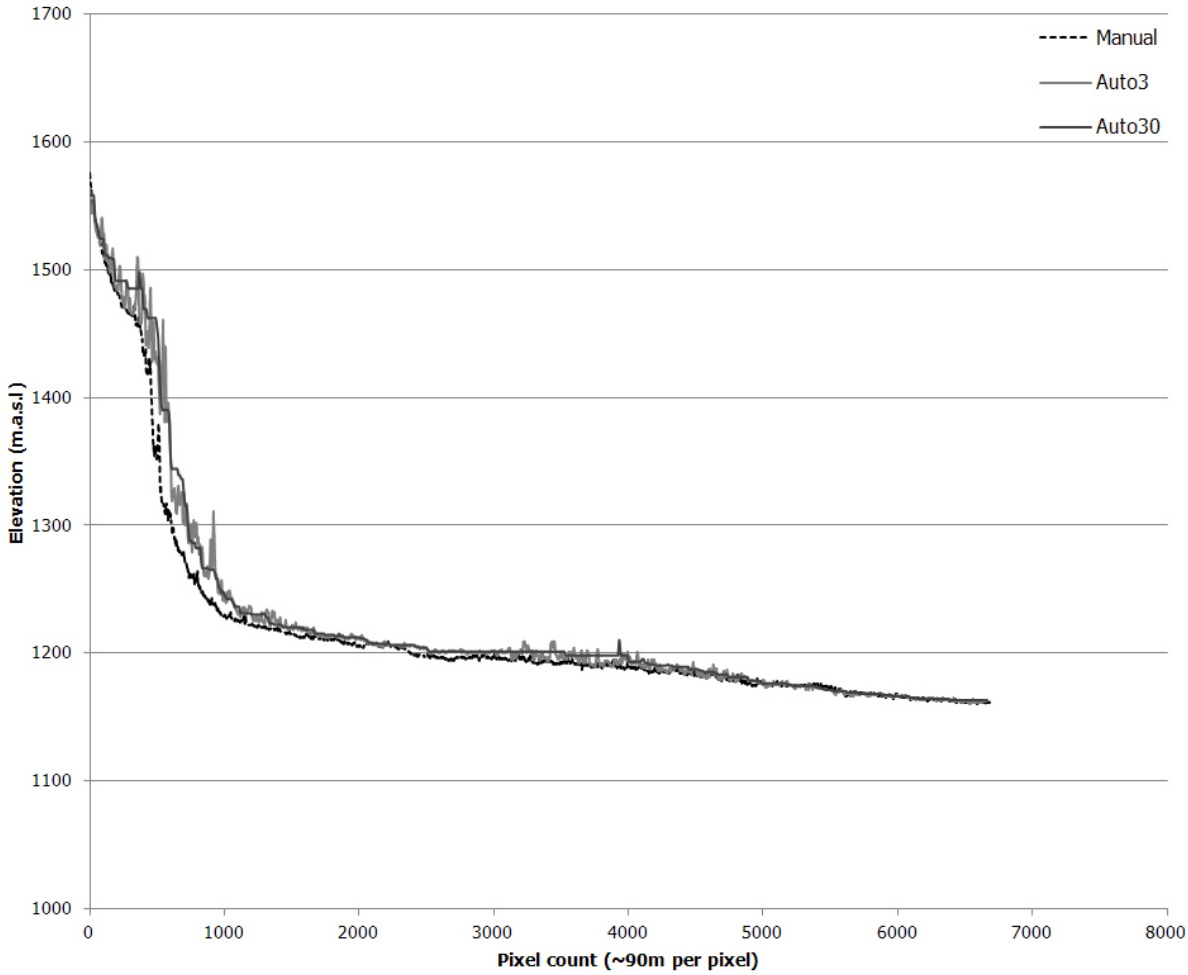

Figure A6.1: Comparison between the manually digitised and automatically generated river profiles of the **Chambeshi river**. Note the overall similarities in shape of the three profiles, with the

automated profiles being offset in term of higher elevation in the upper and middle reaches. Vertical exaggeration : x 1029

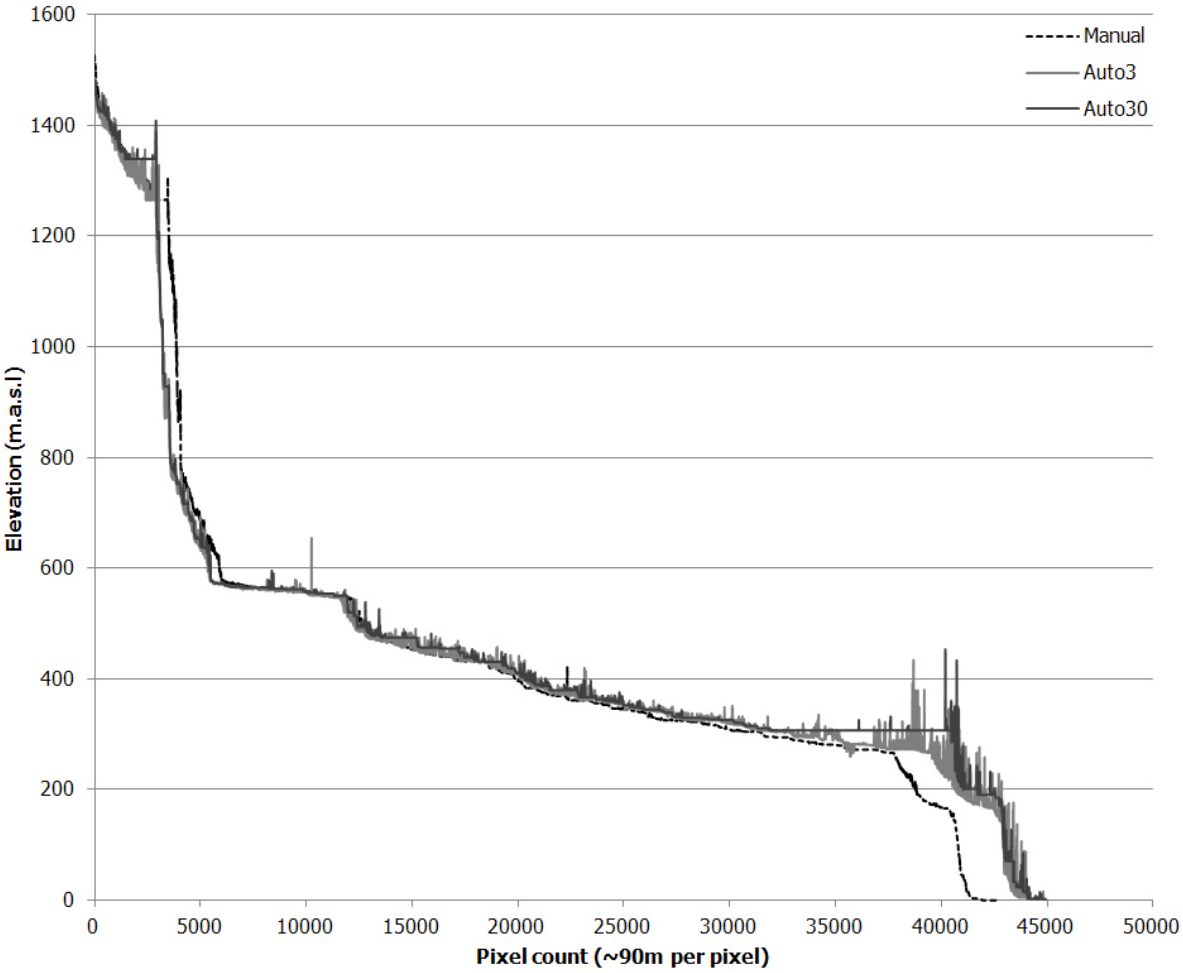

Figure A6.2: The manually digitised and automatically generated river profiles of the **Congo river**. Note the overall similarities in shape of the three profiles, with the automated profiles being offset in term of higher elevation in the middle and lower reaches. Vertical exaggeration : x2813

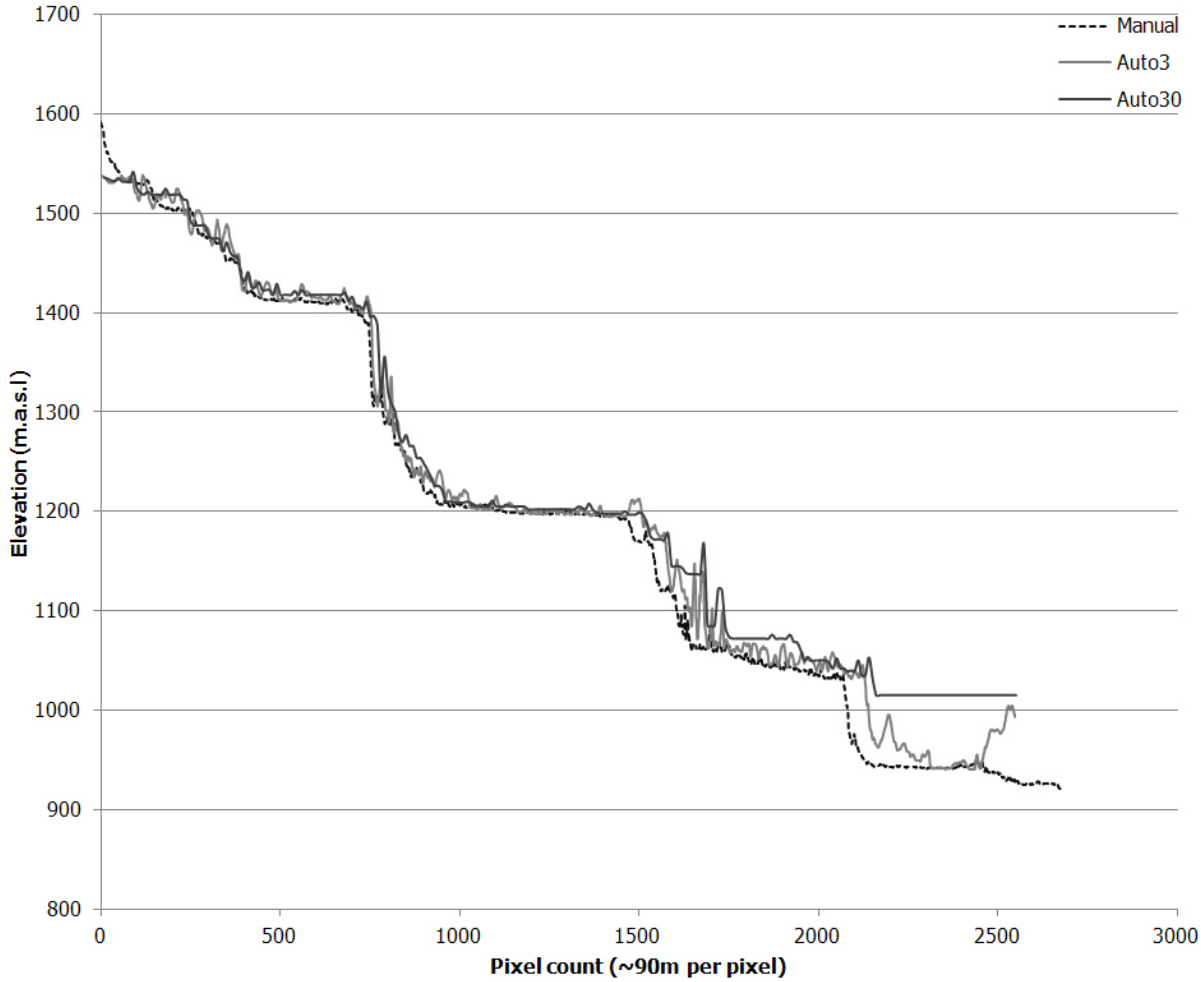

Figure 6.3: Comparison between the manually digitised and automatically generated river profiles of the **Kalungwishi river**. The three profiles have good fit in term of shape for the upper and middle reaches, yet the shape of the lower reaches is dissimilar. The last section of Auto30 has is highly elevated compared to Manual, while the Auto3 is very noisy in the lower section. Vertical exaggeration : x300

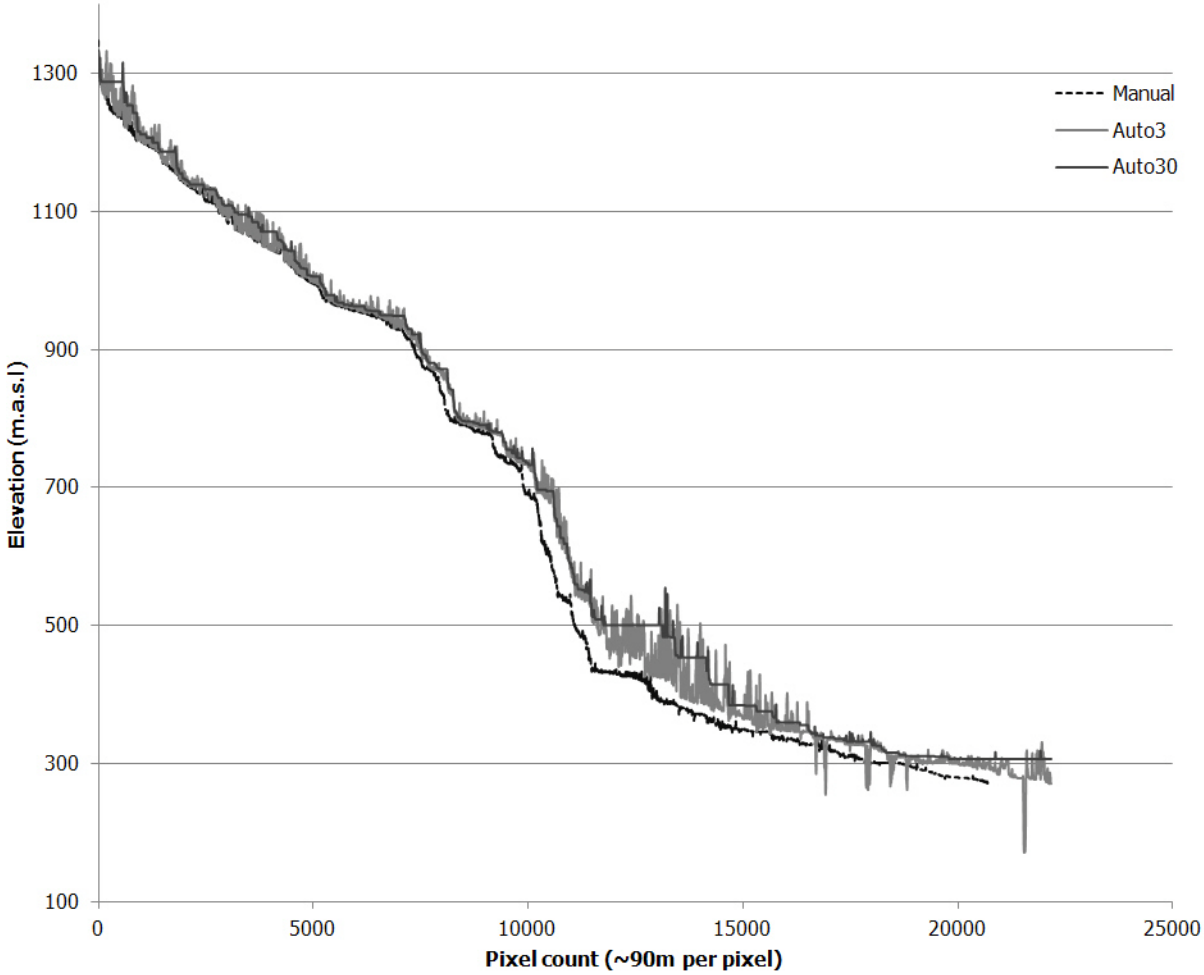

Figure A6.4: Comparison between the manually digitised and automatically generated river profiles of the **Kasai river**. For the upper and middle reaches the three profiles have good fit in term of shape, yet the shape begin to diverge in the lower, especially for Auto3. Auto3 is extremely noisy, with large 'holes' in the foot of the profile. Vertical exaggeration : x1875

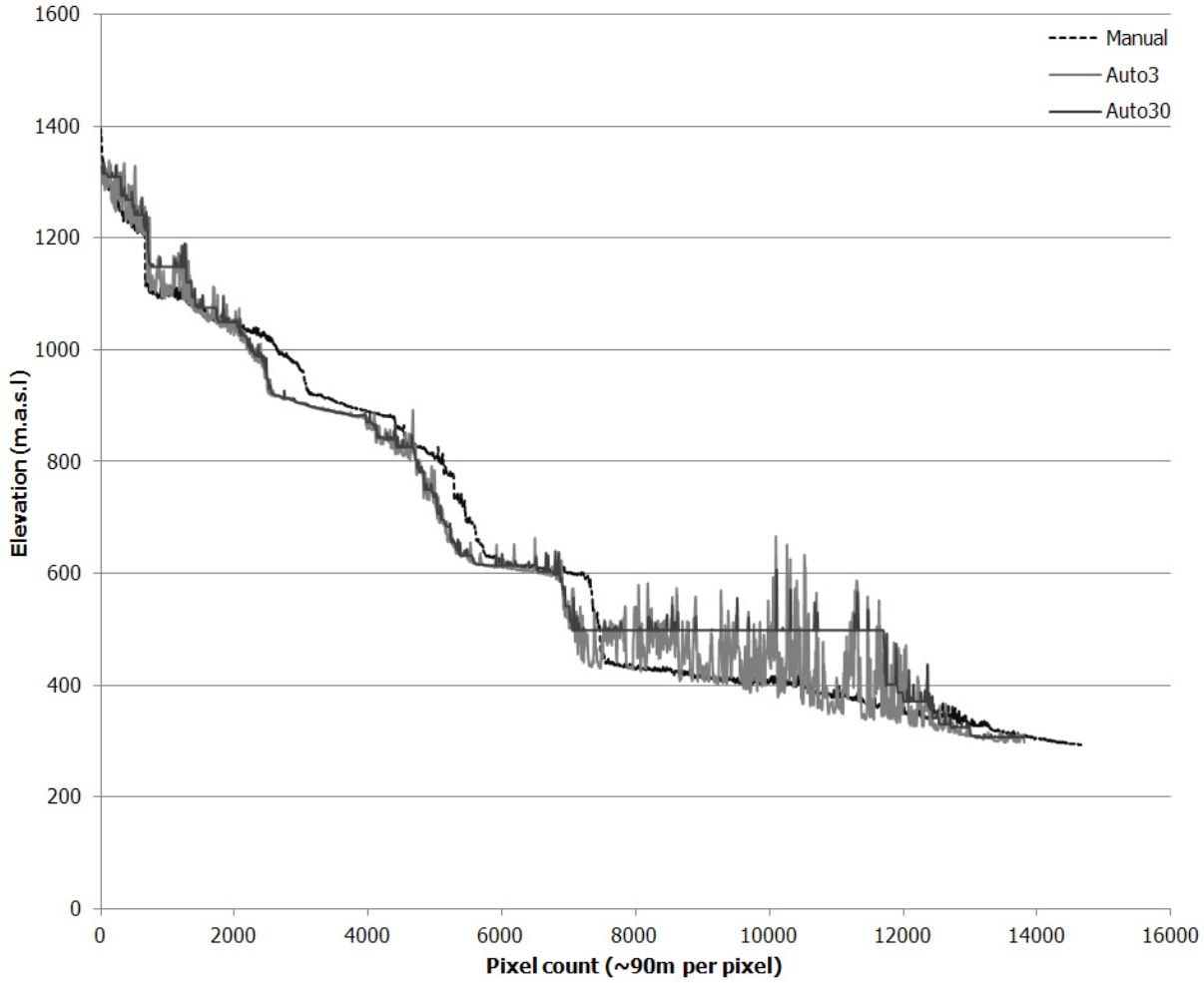

Figure A6.5: Comparison between the manually digitised and automatically generated river profiles of the **Kwango river**. While some sections of the three profiles are comparable, there are large deviations in terms of shape between the three. This is especially true of the lower-middle and lower reaches. Auto3 is extremely noisy, with the lower reaches having variation too large to be useful. Vertical exaggeration : x900

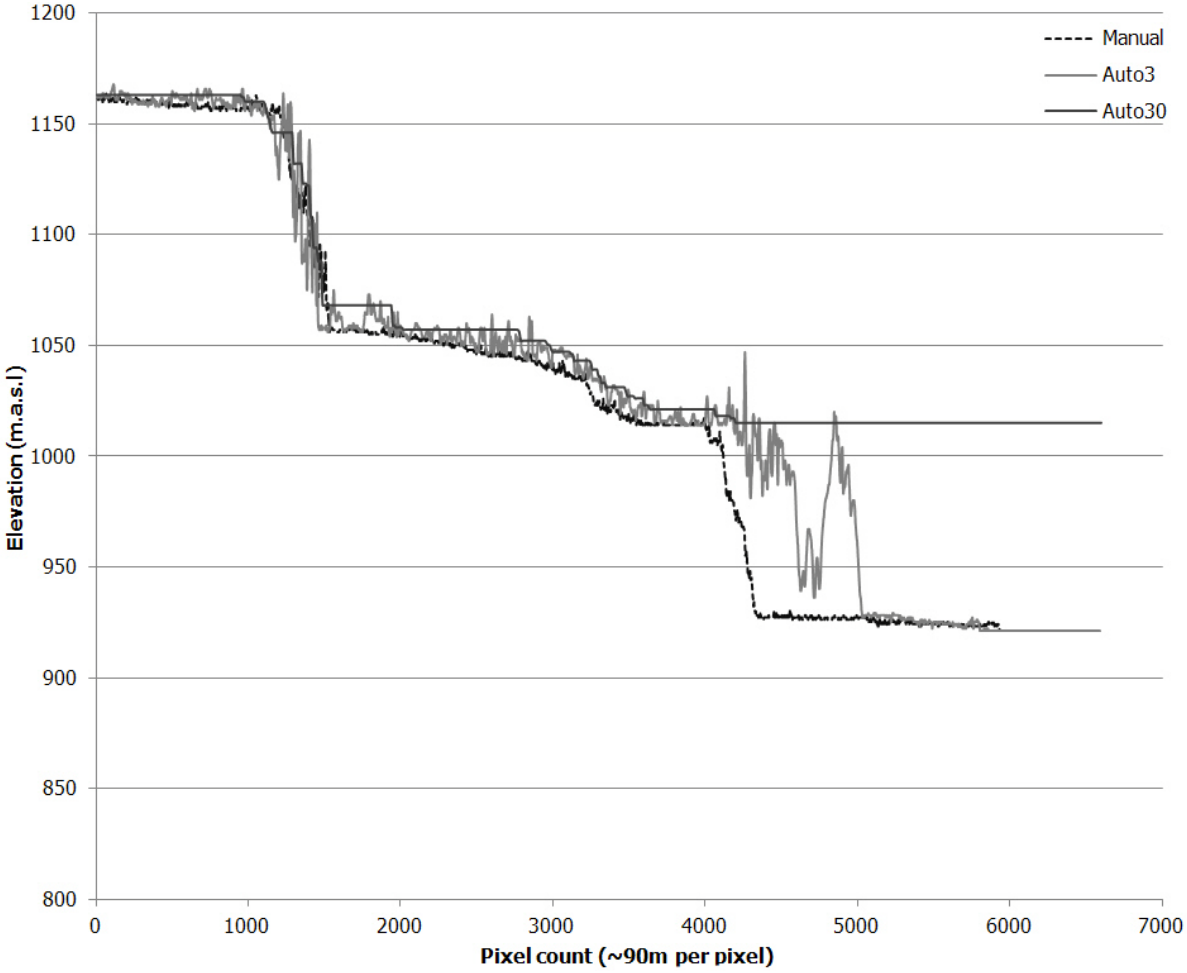

Figure A6.6: Comparison between the manually digitised and automatically generated river profiles of the **Luapula river**. Both Auto3 and Auto30 show large deviation in terms of shape from the manually derived profile. Auto3 is very noisy, with erratic variations in elevation while Auto30 has a distinct stepped form with its lower reach 96 m higher than Manual. Vertical exaggeration : x1575

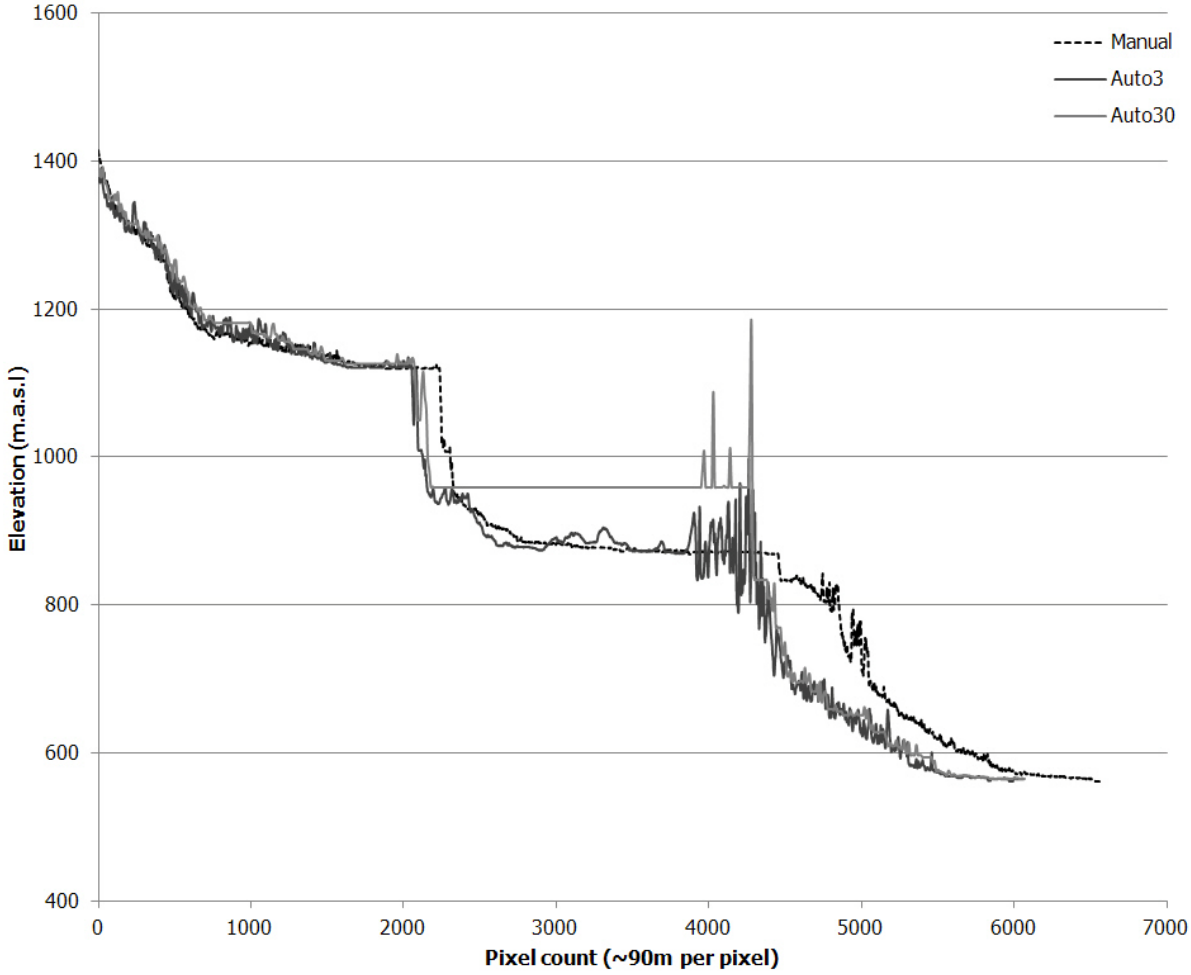

Figure A6.7: Comparison between the manually digitised and automatically generated river profiles of the **Lufira river**. There is close agreement in terms of shape and elevation values between the three profiles for the upper reaches. For the middle and lower reaches both Auto3 and Auto30 are very noisy with large spikes in elevation. Additionally Auto3 and Auto30 underestimate the length of the Lufira and show an offset in terms of the large drops in elevation of the profile compared to Manual. Vertical exaggeration : x525

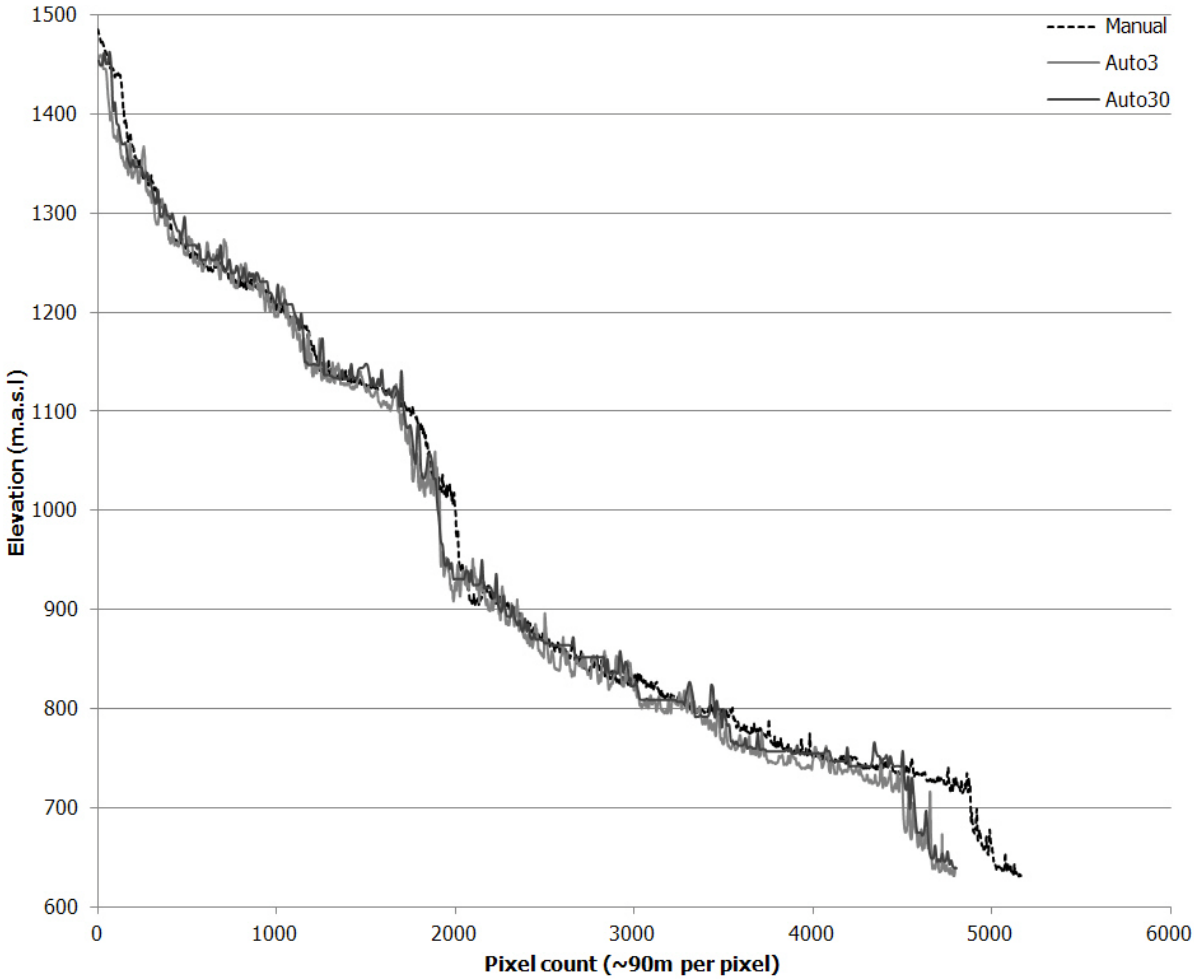

Figure A6.8: Comparison between the manually digitised and automatically generated river profiles of the **Lufupa river**. Overall there is close agreement between the three profiles in terms of shape and elevation values. For the middle and lower reaches both Auto3 and Auto30 underreport the elevation and length of the river compared to Manual. Vertical exaggeration : x600

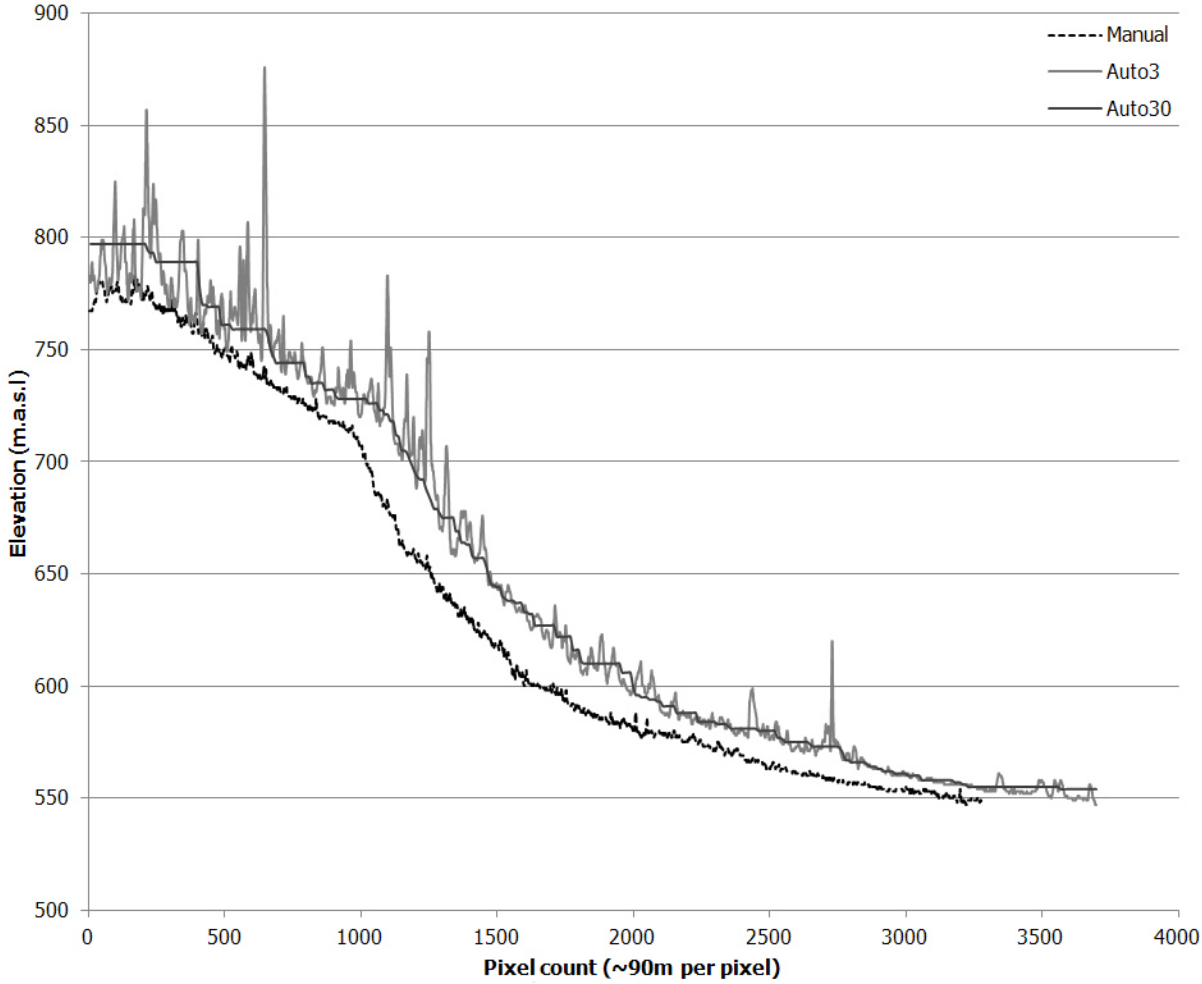

Figure A6.9: Comparison between the manually digitised and automatically generated river profiles of the **Lukuga river**. There is close agreement between the Auto30 and Manual in terms of shape but Auto30 shows a consistent offset in terms of elevation. Auto3 is very noisy, with large spikes in elevation, only matching the shape of Auto30 in the lower reaches. Both Auto3 and Auto30 are longer than the manually extracted river profile. Vertical exaggeration : x900

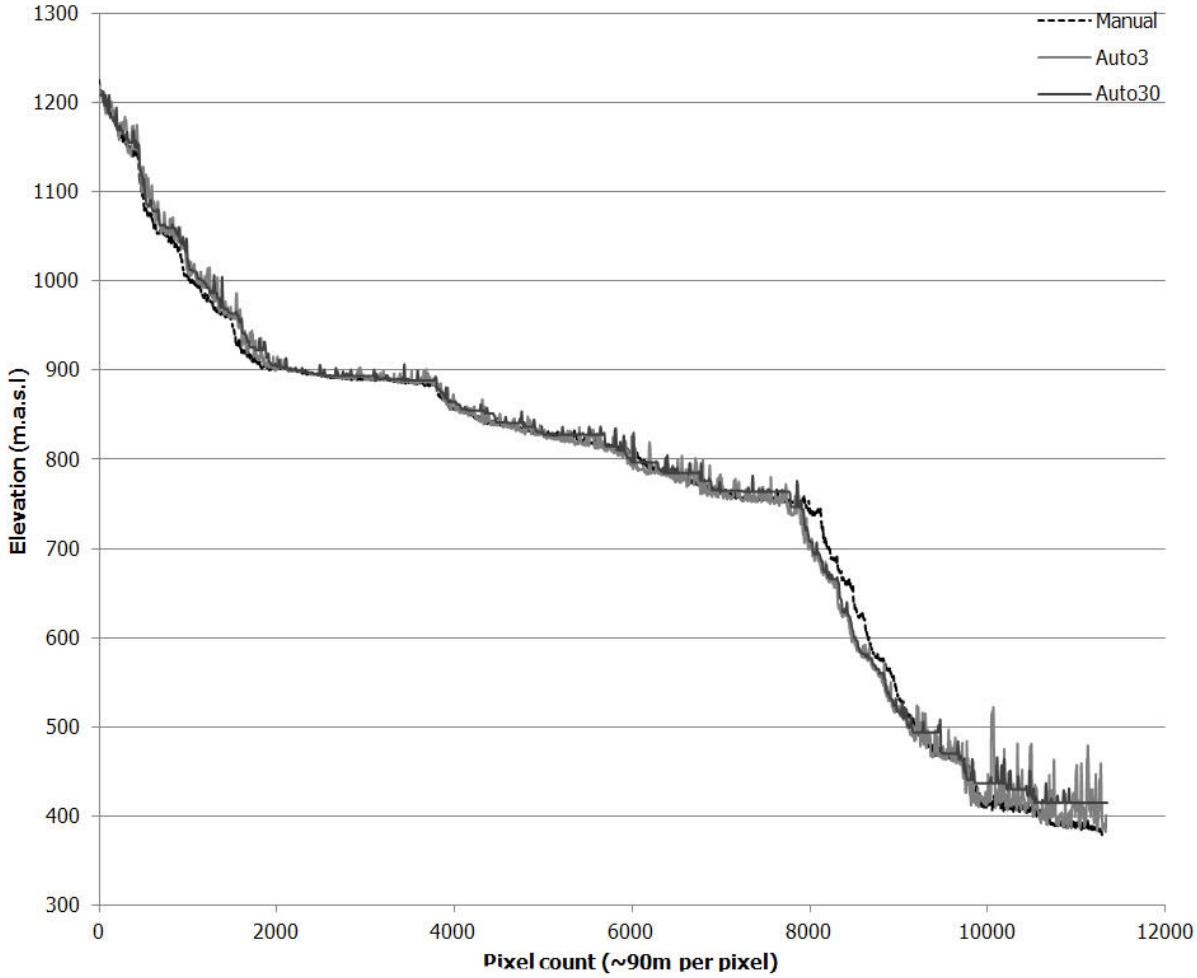

Figure A6.10: Comparison between the manually digitised and automatically generated river profiles of the **Lulua river**. In terms of shape all three profiles match closely, with only the extreme lower section of Auto2 and Auto30 differing substantially from Manual. A similar situation applies for comparisons of elevation, wit the greatest differences being seen in the lower section of the profiles. Vertical exaggeration : x1080

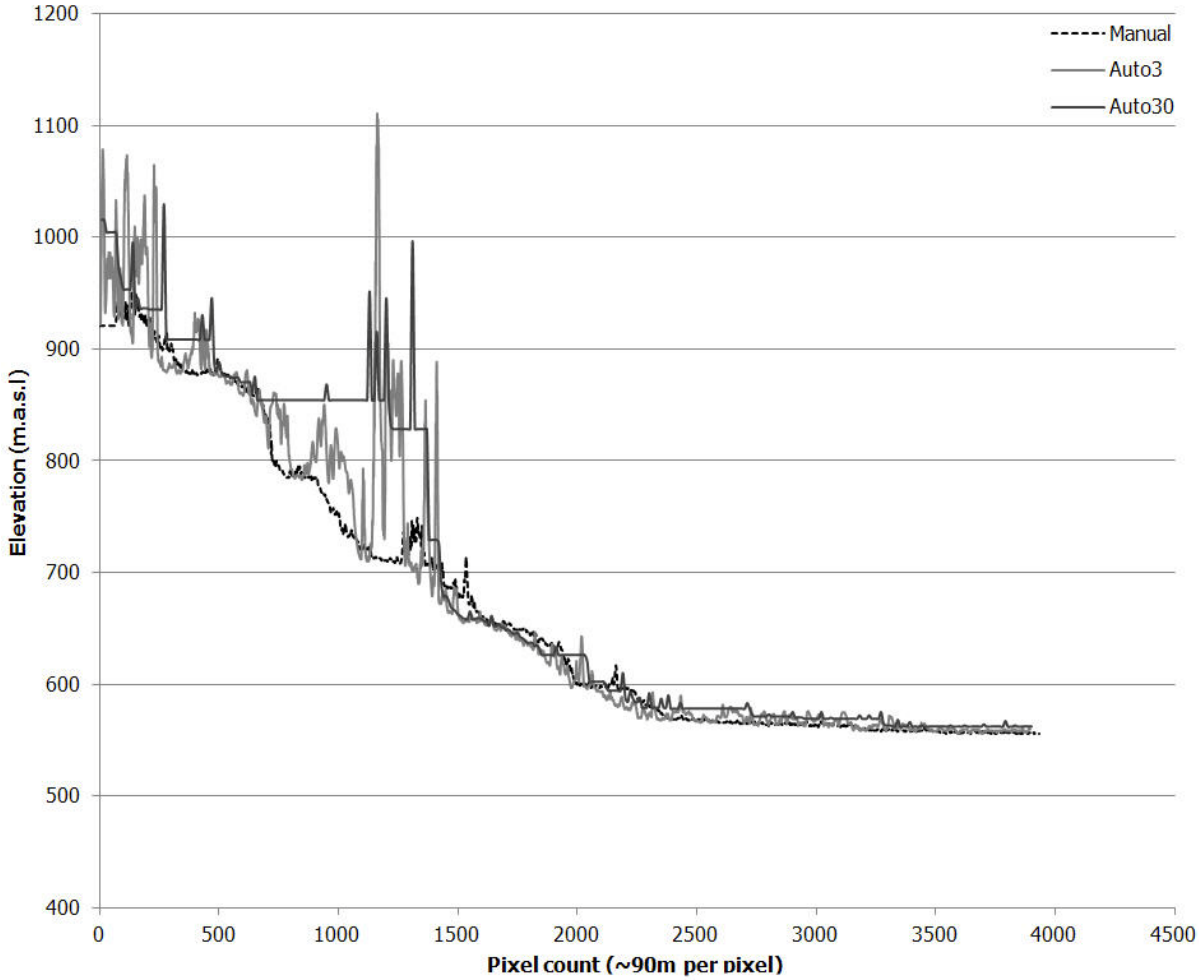

Figure A6.11: Comparison between the manually digitised and automatically generated river profiles of the **Luvua river**. There is a significant mismatch with regards to the elevations and shape of the three profiles in the upper and middle reaches. Both Auto3 and Aitho30 show large spikes in elevations for the upper and middle reaches. The profiles become more similar in the lower sections. Vertical exaggeration : x506

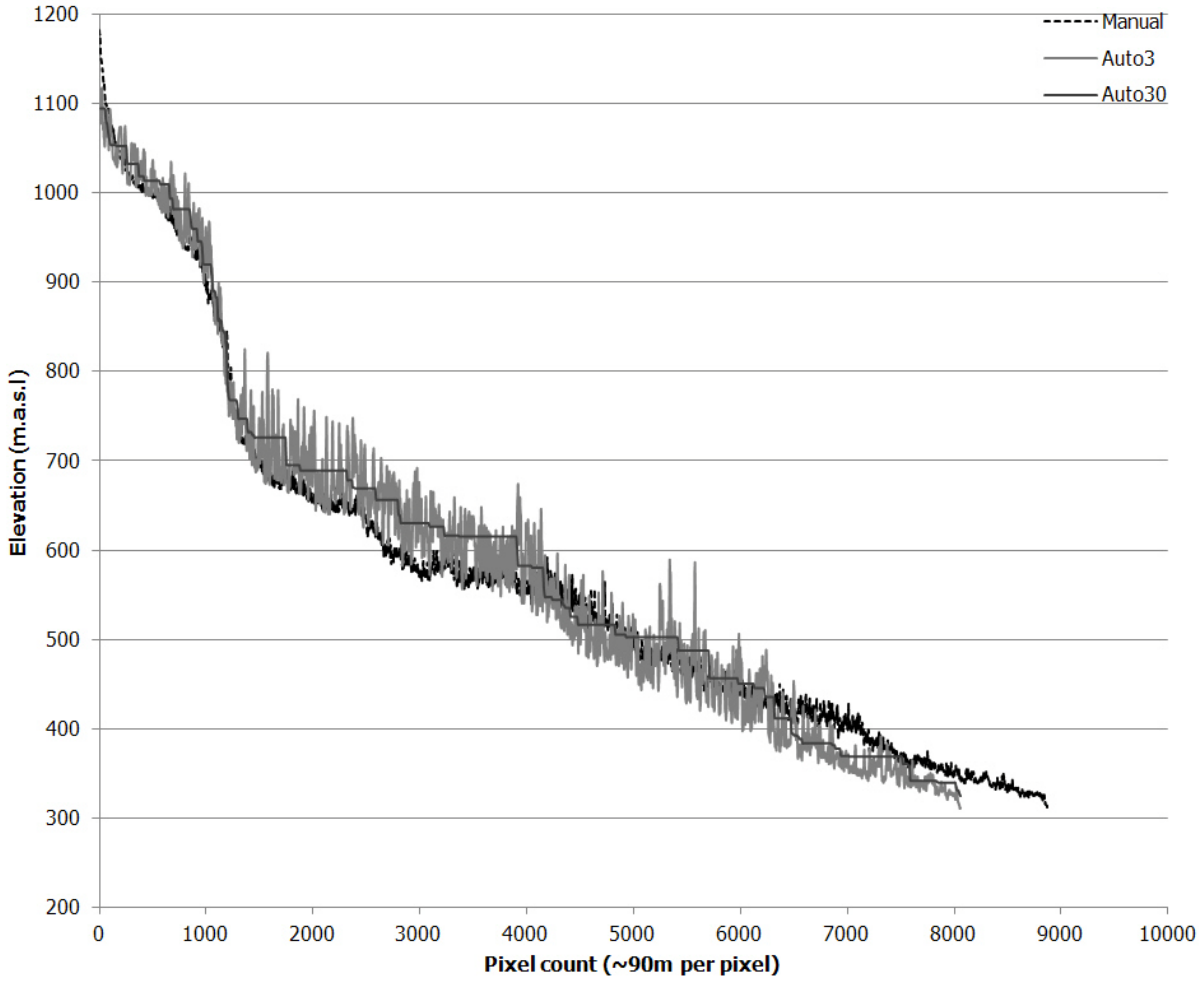

Figure A6.12: Comparison between the manually digitised and automatically generated river profiles of the **Wamba river**. The manually extracted profile is itself noisy yet Auto3 is substantially noisy, to the point of no clear profile being discernable. Auto30 has a markedly stepped nature, with elevations above Manual in the upper and middle reaches and elevations below Manual in the lower reaches. Both automatically generated rivers are shorter than the manually extracted river. Vertical exaggeration : x900

6.2.2 Kalahari basin

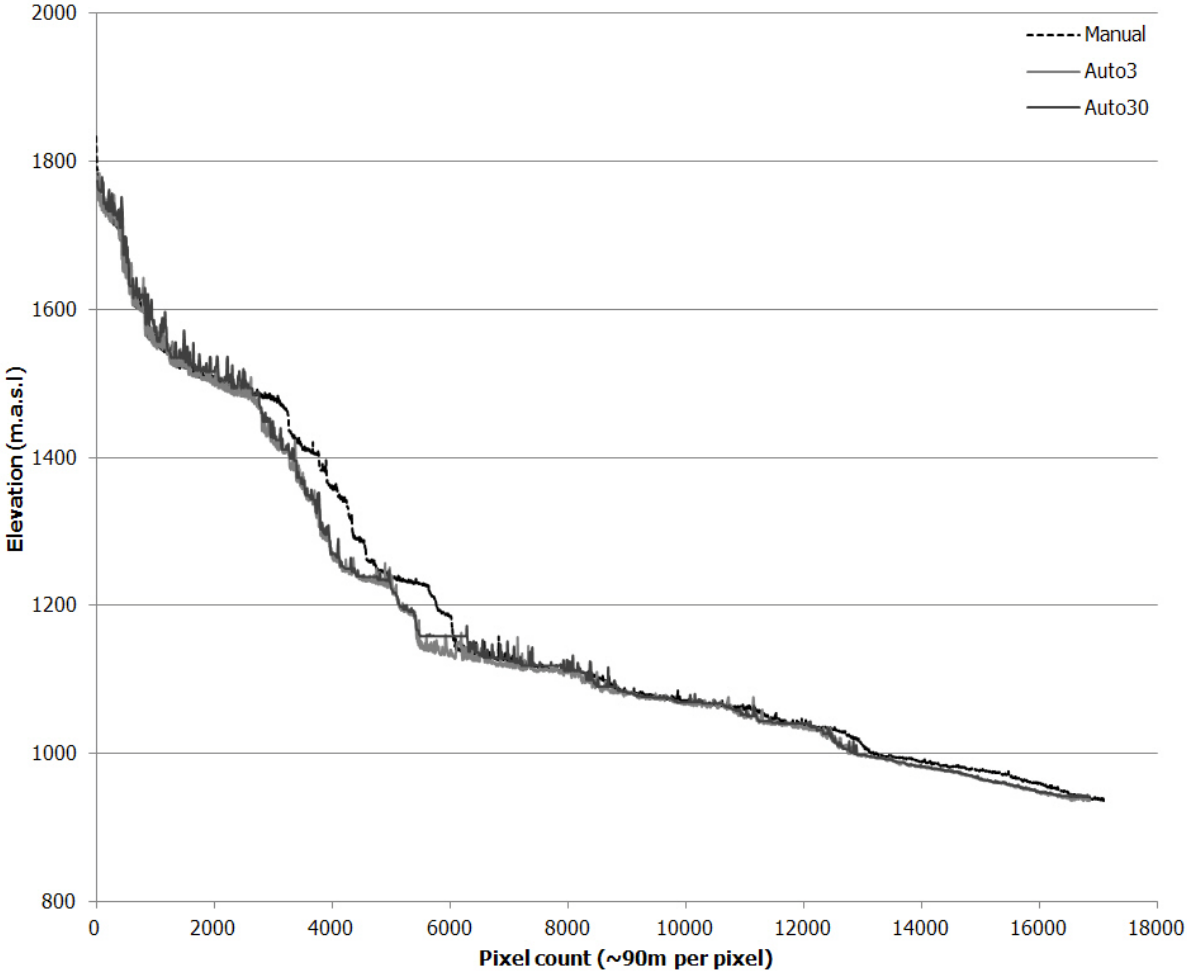

Figure A6.13: Comparison between the manually digitised and automatically generated river profiles of the **Cubango river**. Note the general similarities in shape of the three profiles, although there is a major discrepancy in the middle reaches with the automated profiles being offset in term of lower elevations. Vertical exaggeration : x1350

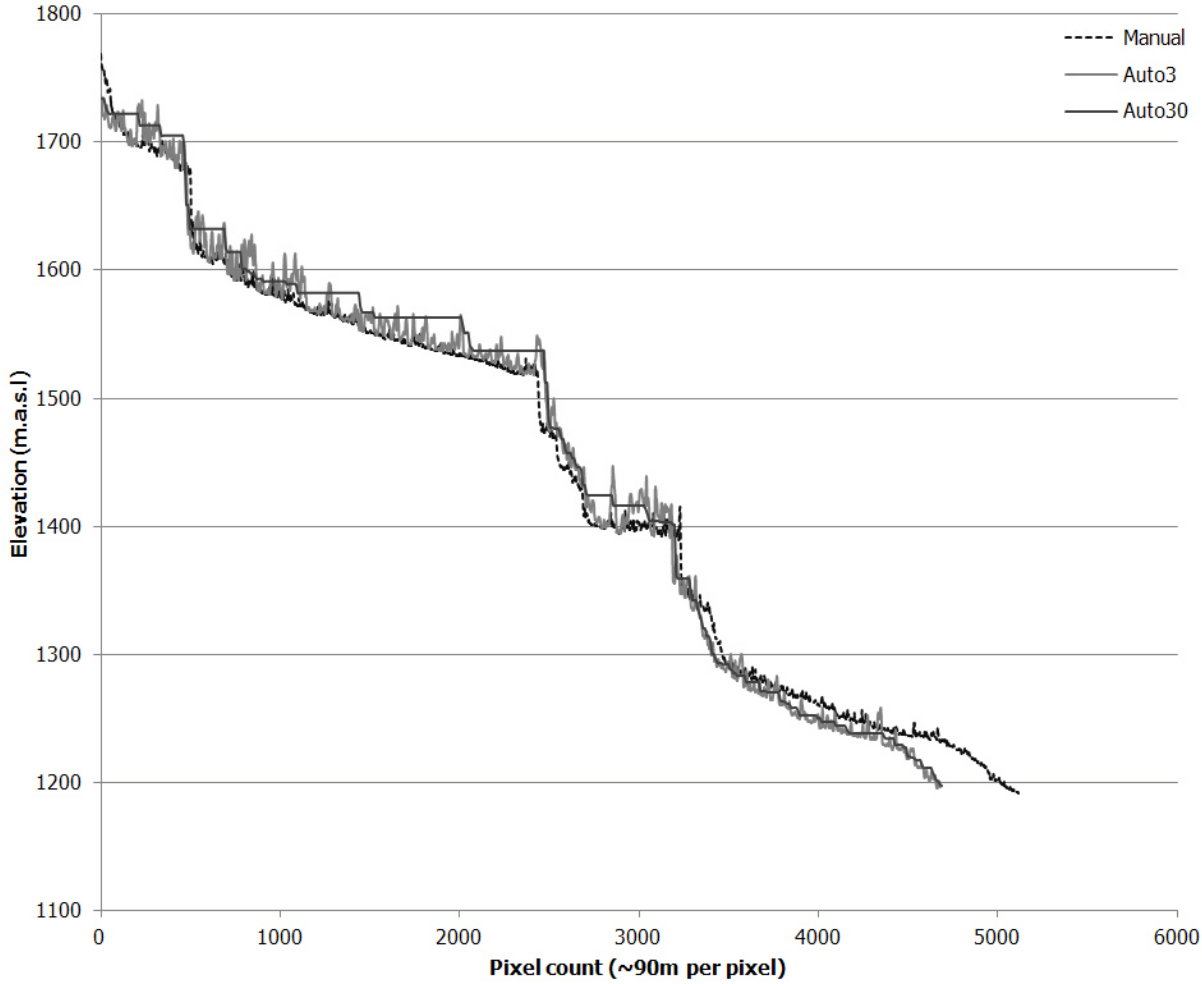

Figure A6.14: Comparison between the manually digitised and automatically generated river profiles of the **Cuchi river**. Note the stepped nature of Auto30 compared to Auto3 and Manual. While profiles broadly match, the automatic profiles are noticeably shorter and noisier. Vertical exaggeration : x771

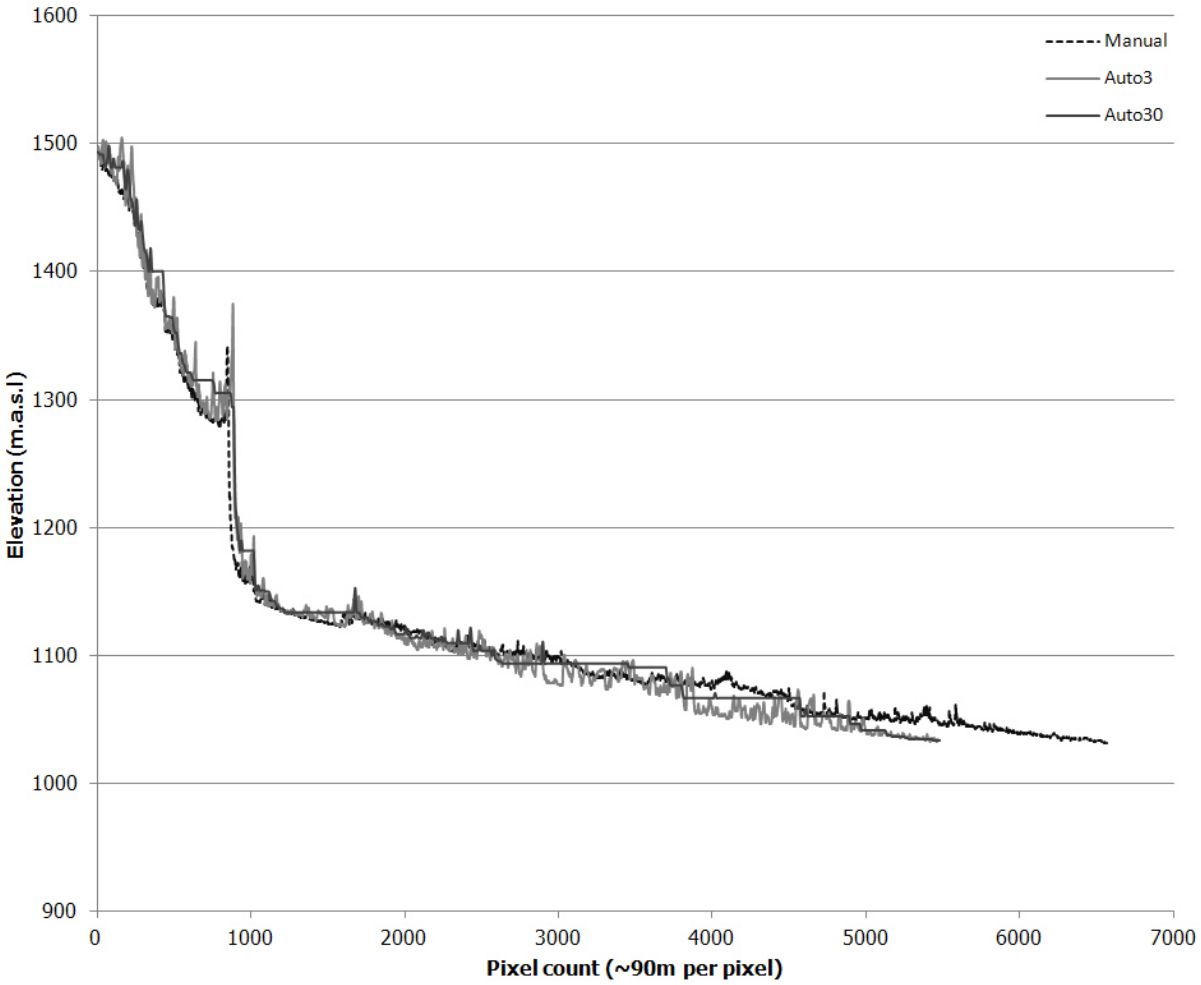

Figure A615: Comparison between the manually digitised and automatically generated river profiles of the **Kabompo river**. Note the distinct stepped nature of Auto30 compared to Auto3 and Manual. The profile match reasonably well for the upper and upper-middle reaches, thereafter the automatic profiles are noticeably shorter, noisier and at lower elevation than the manual river. Vertical exaggeration : x900

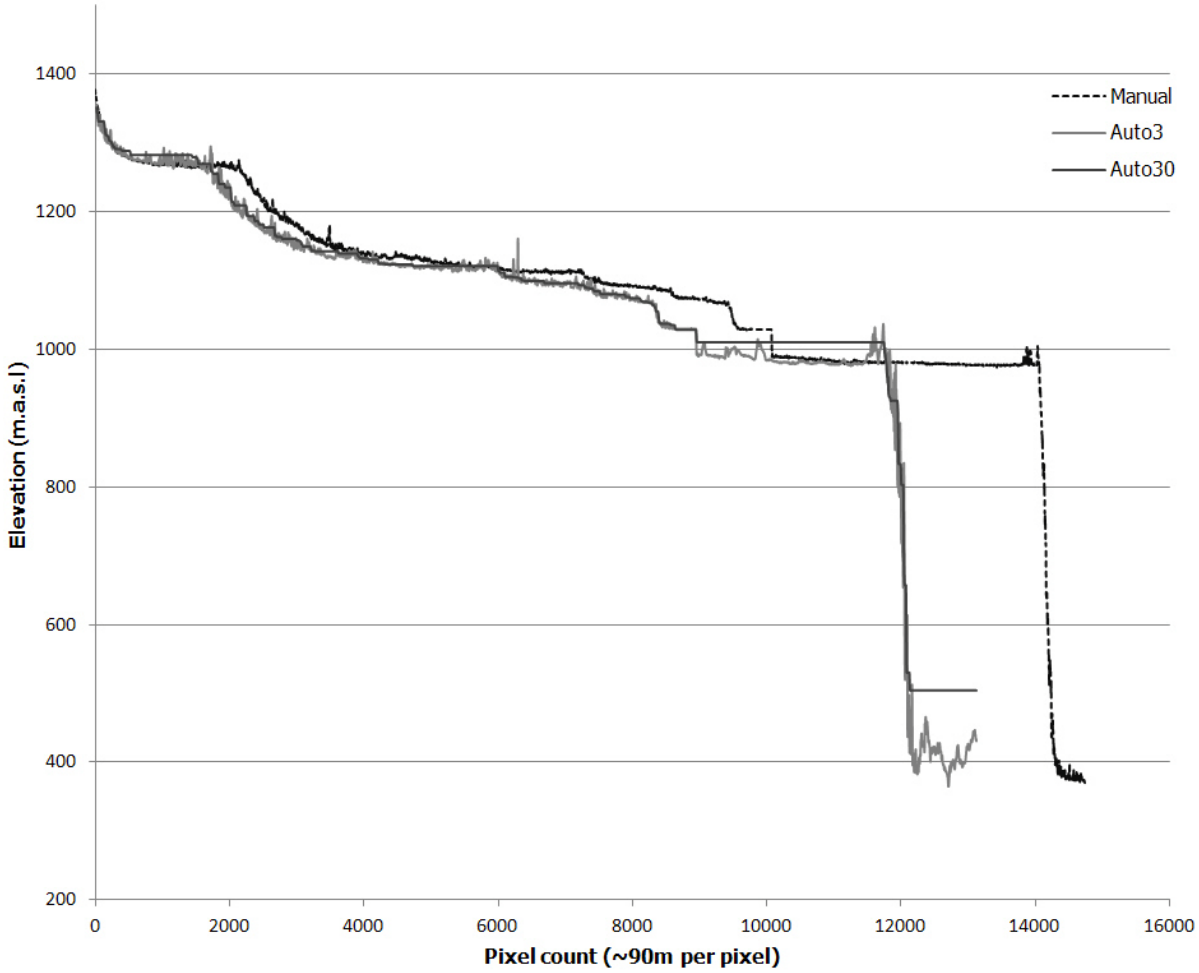

Figure A6.16: Comparison between the manually digitised and automatically generated river profiles of the **Kafue river**. While all three profiles have similar shapes, due to the shorter lengths of the generated profiles there is a large offset in the lower reaches. This gives the generated river a more compressed form relative to the Manual. Auto3 is the nosiest profile of the three. Vertical exaggeration : x1200

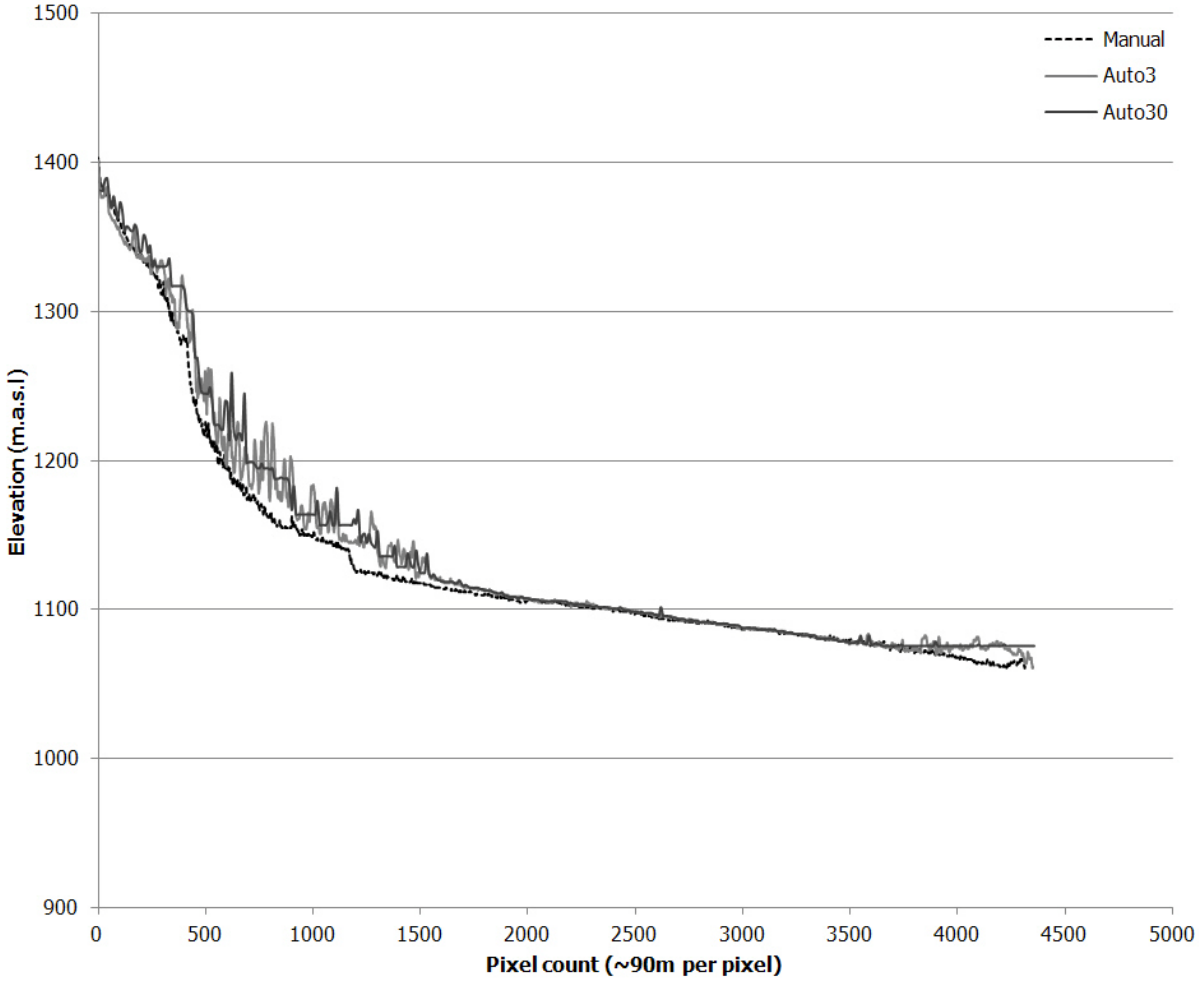

Figure A6.17: Comparison between the manually digitised and automatically generated river profiles of the **Luena river**. Both Auto3 and Auto30 appear very noisy with large spikes in elevation. There is some agreement of profiles for the lower section of the river, with most of the difference in shapes between the profiles occurring in the upper reaches. Vertical exaggeration : x750

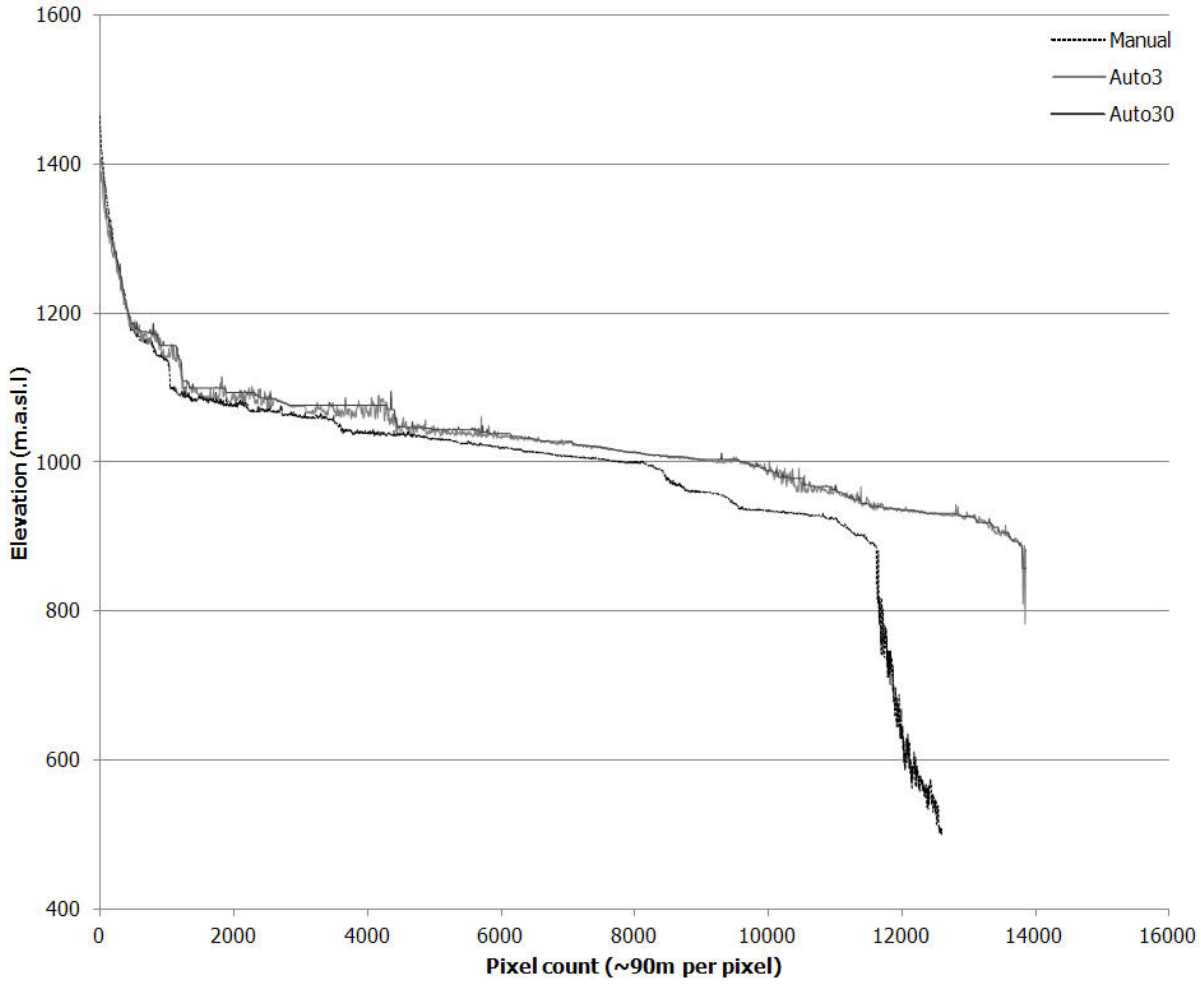

Figure A6.18: Comparison between the manually digitised and automatically generated river profiles of the **Upper Zambezi river**. While the shape of the three profiles (excluding the extreme lower reach) is comparable, Auto3 and Auto30 show a sustained offset with regards to elevation. There is a mismatch with regards to the elevations and shape of the three profiles in the upper and middle reaches. Both Auto3 and Aitho30 show large spikes in elevations for the upper and middle reaches. The profiles become more similar in the lower sections. Vertical exaggeration : x1200

6.3 Database of knickpoints

The table below (Table A6.2) shows all the knickpoints identified in the study. Recorded attributes include location, knickpoint height, elevation of knickpoint occurrence and a brief geomorphic description.

Table A6.2 : The qualitative directory of the 380 characterised knickpoints. Knickpoints are primarily listed by alphabetical order of the river names and there after their elevation. Co-ordinates are given in decimal degrees. The majority of the entries have a corresponding image reference. Unfortunately a small percentage of the image references were not capture adequately. Class guides : Knick = knickpoint, m. = minor knickpoint. See **Chapter 6** for description on how knickpoint heights were determined and what the categories mean.

N$^{o.}$	Name	Class	Height (m)	Elevation (m.a.s.l)	Longitude	Latitude	Description
1	Chambeshi	knick	15	1429	31.4577	-9.4683	>15 m drop; high topographic region
2	Chambeshi	knick	10	1422	31.4475	-9.4389	>10 m drop; angular channel: high topographic region
3	Chambeshi	knick	50	1397	31.4622	-9.4753	>50 m drop; high topographic region
4	Congo	1 st dam wall	15	1287	25.4620	-10.4994	Dam wall; primary dam wall of Lac Nzoli; dam 46km long; wall likely to have replaced or flooded natural knickpoints at the beginning of gorge; white-water
5	Congo	knick	80	1231	25.4394	-10.4950	>80 m drop; angular channel; angular islands; bare rock or soil on channel margins, islands & linear ridges; linear drainage; white-water
6	Congo	knick	30	1147	25.4447	-10.4036	>30 m drop; angular isle. fan; white-water; several knickpoints close together; channel flow parallel to linear ridge; bare rock or soil on channel margin & linear ridges
7	Congo	m. knick	-5	1143	25.4080	-10.4664	Minor; angular island fan; channel change direction downstream of knick: white-water; bare rock or soil on islands, channel margin & linear ridges; linear drainage; incised channel flow across ridge orientation
8	Congo	2nd dam wall	25	1090	25.4269	-10.3243	Dam wall; secondary dam wall of Lac Nzoli; in gorge downstream of main dam; wall likely to have replaced or flooded natural knickpoints in the gorge; white-water; linear ridges orientated NNE SSW
9	Congo	knick	30	1019	25.4491	-10.2539	>30 m drop; 2 knickpoints; knick at end of high gradient straight channel; channel change direction at knick; white-water; bare rock/soil on linear ridges & channel margin; channel cut across lineaments
10	Congo	knick	50	999	25.4358	-10.2326	>50 m drop; series of continuous knickpoints; channel cut through 3 linear ridges perpendicularly; channel change direction at knick; bare rock or soil on channel margin
11	Congo	knick	0	890	25.4072	-10.1851	Height undetermined; knick; white-water; angular channel; bare rock or soil on channel margin; river step in two places & knickpoints at each change in direction; gorge noise hide height of knick
12	Congo	knick	90	862	25.4101	-10.1254	>80 m drop; 2 falls close together; one 30m drop the other 60m drop; white-water; bare rock/soil on channel margin; deeply incised in linear ridge; last knick before river flows into smoother basin

13	Congo	m. knick	-5	758	25.4485	-9.9873	Minor; white-water; angular island on channel margin; channel steps at just upstream & just downstream of knick; bare rock or soil visible on channel margin
14	Congo	knick	10	748	25.5080	-9.9343	10 m drop; white-water; angular island on channel margin; channel step at knickpoint; channel narrow & become angular at knickpoint; downstream of knick there is a floodplain
15	Congo	knick	15	718	25.5361	-9.7682	15 m drop; several falls close together; white-water; angular channel; bare rock or soil on channel margin; angular channel
16	Congo	m. knick	-5	695	25.4885	-9.5831	Minor; angular island fan; angular channels; knick occur where channel has cut into linear ridge; bare rock or soil on channel margin; channel follow lineaments for most part but knickpoints occur when cut across them
17	Congo	knick	15	679	25.5196	-9.4058	>15 m drop; angular islands; bare rock or soil on channel margins & angular islands; channel widens where it changes direction; channel skirts linear ridge than cuts through it; lineaments
18	Congo	knick	20	675	25.5028	-9.4698	20 m drop; near continuous series of minor knickpoints; white-water; angular islands; bare rock or soil on channel margin; channel steps twice; lineaments visible
19	Congo	knick	5	653	25.5374	-9.3544	>5 m drop; white-water; angular island & channel; channel runs parallel to linear ridge before crossing it; bare rock/soil on margins & surrounds; channel steps in S; change of direction downstream of knick
20	Congo	m. knick likely	-1	639	25.6438	-9.2202	Minor likely; channel diverted by linear ridge; angular channel; angular islands downstream of the ridge; rapids likely; bare rock or soil on channel margin & islands; possibly white-water; channel change direction downstream of ridge
21	Congo	knick	5	625	25.7141	-9.3062	5 m drop; start of a set 1a; 45m total drop; change of direction; white-water; angular island fan; channel flow parallel to large linear ridge after knick; knick where channel crosses linear ridge; bare rock/soil on channel margins & islands
22	Congo	knick	10	605	25.7803	-9.2350	>10 m drop; middle of set of knickpoints 1a; angular island; narrow angular channel; white-water; several falls close; channel parallel to linear ridge; linear drainage 90 to channel; bare rock/soil on channel margin; possibility of paleo-channels flow
23	Congo	knick	30	591	25.8097	-9.1965	>10 m drop; end of set of knickpoints 1a total drop 45m; angular narrow channel; white-water; channel parallel to linear ridge; linear drainage 90 to channel; bare rock/soil on channel margin; end in Upemba wetland; change direction near swamps; lineament parallel
24	Congo	knick	5	541	27.0144	-5.3600	5 m drop; start of series of knickpoints 2a total drop of 25m; white-water; angular island fan; angular channel; bare rock or soil visible on channel margins & islands; channel change direction downstream of knick; river stops flowing due N & start return
25	Congo	knick	10	530	27.0184	-5.3099	10 m drop; middle of series of knickpoints 2a total drop of 25m; white-water;

							angular island fan; angular channel; bare rock or soil visible on channel margins & islands; channel change direction downstream of knick; lineaments; linear drainage; river steps
26	Congo	knick	10	530	26.9934	-5.2916	10 m drop; end of series of knickpoints 2a total drop of 25 m; white-water in linear formation in sections; angular island fan; angular channel; bare rock/soil on margins & islands; lineaments; linear drainage; channel narrows & begins to curve after knick
27	Congo	m. knick	-5	511	26.9716	-5.1266	Minor; angular island; white-water; channel step at knick; angular channel; bare rock or soil dominate surrounds; linear drainage perpendicular to channel; lineaments
28	Congo	m. knick	-5	504	26.9383	-5.0244	Minor; angular island; white-water; channel step at knick; angular channel; bare rock or soil dominate surrounds; linear drainage perpendicular to channel; lineaments
29	Congo	knick	15	500	26.9610	-4.9793	15 m drop; white-water; continuous series of knickpoints; angular channel; bare rock or soil on channel margin; channel step at knick to flow NW from NNW; white-water in linear formations in some sections running with the stream & as a continuation of lineaments
30	Congo	m. knick	-5	490	26.9142	-4.8647	Minor; white-water; channel step at knick; angular channel; bare rock or soil dominate surrounds; linear drainage perpendicular to channel; lineaments; channel is narrow before knick & very wide after knick
31	Congo	knick	10	478	26.7701	-4.6253	10 m drop; single fall; channel steps at knick; channel constricted at knick; white-water; bare rock or soil on channel margin; angular channel; lineaments
32	Congo	m. knick	-5	474	26.6477	-4.5760	Minor; white-water in a linear formation; angular islands fan; linear drainage; bare rock or soil on channel margins & surrounds; channel run roughly parallel to southern linear ridges
33	Congo	m. knick	-5	468	25.9943	-3.9316	Minor; white-water; angular island on channel margin & in channel; channel constricted at knick almost pinched shut; channel cut through ridge at knick; angular channel; sedimentary islands downstream of knick
34	Congo	m. knick	-5	454	25.9132	-3.2327	Minor; white-water; rapids; angular channel; channel narrows at knick; channel steps downstream of knick; knick occur where channel crosses a linear ridge; angular islands
35	Congo	m. knick	-5	452	25.9182	-3.1650	Minor; white-water; rapids; angular channel; channel narrows at knick; channel steps at knick; angular island; large islands downstream of knick are sedimentary based on shape & do not occur directly upstream of knick
36	Congo	knick	5	440	25.7106	-2.1362	>5 m drop; white-water in a linear formation; islands downstream of knick; channel changes direction downstream of knick
37	Congo	knick	5	414	25.4596	-0.3563	5 m drop; white-water in linear formation; 3km long stretch; angular islands; channel step; knick occur where channel cuts through a broad ridge; bare rock/soil on islands & margins; channel narrow at knick start broadening at main section of

							knick
38	Congo	m. knick	-5	413	25.5087	-0.2781	Minor; white-water; angular channels; angular island fan; bare rock or soil on channel margin; channel narrows at knick; knick occur as channel exits broad ridge
39	Congo	knick	10	404	25.5188	0.1874	>10 m drop; continuous series of minor knickpoints 5km long stretch; angular islands at channel margin; channel constricts at knick; in channel sedimentary islands stop at knick; channel begin to change direction at knick
40	Congo	knick	5	398	25.4851	0.2546	5 m drop; below 10m knick; series of continuous rapids; white-water; channel narrows at knick; angular island on channel margin
41	Congo	knick	5	389	25.2734	0.4386	>5 m drop; over a 4km long stretch; channel change direction after knick; large island below knick; small section of white-water; small section of angular islands on channel margin
42	Congo	m. knick	-5	386	25.2066	0.4931	Minor; at Kisangani; white-water in irregular line; angular island; channel change direction downstream of knick; channel constricts at knick
43	Congo	knick	5	255	15.2272	-4.3172	>5 m drop; white-water; angular island; angular channels; bare rock or soil on channel margins & surrounds; channel changes direction at knick; first knick downstream of Malebo pool
44	Congo	knick	10	254	15.1760	-4.3687	>10 m drop; start of a continuous series of rapids 3a; white-water; angular channel; bare rock or soil on channel margin; channel change direction at knick; dendritic drainage; channel flows across linear ridge
45	Congo	m. knick	-5	253	15.1852	-4.3399	Minor; angular islands; angular channel; change in channel direction downstream of knick; bare rock or soil on islands & channel margin; diamond pattern of channels on SRTM
46	Congo	knick	10	239	15.1359	-4.4310	>10 m drop; end of a continuous series of rapids 3b; white-water; angular channel; bare rock or soil on channel margin; channel change direction at knick; dendritic drainage; channel flows across linear ridge
47	Congo	m. knick	-5	231	15.0385	-4.5379	Minor; angular island; white-water; channel step at knick; angular channel; bare rock or soil on channel margin; mainly linear drainage perpendicular to channel with some dendritic drainage; incised channel
48	Congo	knick	5	220	14.8694	-4.7504	>5 m drop; angular island; bare rock or soil on channel margin; white-water; angular channel; channel constricted at knick; incised channel with tributaries having visible knickpoints before they flow into trunk
49	Congo	knick	10	210	14.8140	-4.8360	10m drop; white-water; linear islands; channel step at knick; channel constricted at knick but widen after knick; linear drainage; incised channel; bare rock or soil on channel margins & hilltops
50	Congo	m. knick	-5	206	14.7585	-4.8584	Minor; white-water in near linear formation; angular channel; bare rock or soil on channel margins & dominates surrounds; channel narrows at knick & widens after

							knick; incised channel; trellis drainage
51	Congo	knick	5	203	14.7057	-4.8997	>5 m drop; channel narrows at knick; faint white-water; bare rock or soil on channel margin; channel changes direction downstream of knick; incised channel
52	Congo	knick	5	196	14.6570	-4.9193	>5 m drop; channel step at knick; channel angular; channel constricted at knick; bare rock or soil visible on channel margin & hilltops; incised channel; short linear tributaries
53	Congo	m. knick	-5	189	14.5222	-4.8590	Minor; white-water in near linear formation; angular channel; bare rock or soil on channel margins & dominates surrounds; channel narrows at knick & widens after knick; knick occur as channel flow through a mountainous region
54	Congo	knick	5	187	14.4375	-4.8776	>5 m drop; continuous sets of knickpoints for 4km; mainly short linear drainage; incised channel; bare rock or soil on channel margins & hilltops; white-water in a liner formation at start
55	Congo	m. knick likely	-1	175	14.1517	-4.9516	Minor likely; channel flows across a mini escarpment; rapids likely; channel changes direction just upstream of knick
56	Congo	knick	5	157	13.6287	-5.2977	>5 m drop; white-water in semi linear formation; 90 degree bend just upstream of knick; channel flows parallel to linear ridges upstream of knick cutting across them at knick; angular channel; constricted channel at knick; angular island; bare rock
57	Congo	knick	5	155	13.5493	-5.3606	>5 m drop; single continuous fall; channel angular; channel changes direction at knick; channel cut through large ridge at knick; linear landscape structures; bare rock or soil on channel margins & islands; angular islands
58	Congo	knick	5	143	13.5577	-5.4143	5 m drop; start of a continuous series of knickpoints 4a; angular channel; bare rock or soil on channel margins & islands; angular island; channel flow parallel with linear ridges; channel begin to branch out on the southern edge; white-water
59	Congo	knick	20	120	13.6104	-5.4770	20 m drop; middle of a continuous series of knick 4b; angular channel with northern margin parallel to linear ridge; bare rock/ soil on margins & islands; angular islands; channel broadens to south; white-water; linear island formations; possible pal
60	Congo	knick	40	81	13.6345	-5.5317	40 m drop; end of a continuous series of knickpoints 4c; total drop of 65m + over 1km; angular channel; bare rock or soil on channel margins & islands; angular island; channel change direction cutting across a broad ridge; lots of white-water; linear form
61	Congo	knick	40	81	13.6154	-5.5312	40 m drop total; start of continuous series of knickpoints over 5km; 5a; white-water; angular channel; channel steps; direction change after knick; linking with other knickpoints make a Z shape; channel crosses broad ridge; linear ridges; bare rock/soil on channel
62	Congo	knick	40	47	13.5695	-5.5460	40 m drop in total; end of continuous series of knickpoints over 5km; 5b; white-water; angular channel; channel steps; direction change after knick; knickpoints

							make Z shape when linked with others not of this series; linear ridges; bare rock or soil on channel
63	Congo	knick	5	45	13.5899	-5.6087	5 m drop; angular channel; small angular islands; channel changes direction upstream of knick; incised channel; linear drainage due to linear landscape features; bare rock or soil on channel margins & ridge tops; white-water
64	Congo	knick	10	39	13.5888	-5.6651	10 m drop; angular channel; small angular islands; channel changes direction downstream of knick; incised channel; linear drainage due to linear landscape features perpendicular to channel ; bare rock or soil on channel margins & ridge tops; white-water
65	Congo	knick	15	30	13.5588	-5.7134	>15 m drop; three falls close together; white-water in linear formation across entire channel width; channel angular; channel flows across large ridges; highly incised channel; angular islands; bare rock or soil on channel margins & ridges
66	Congo	m. knick	-5	16	13.5161	-5.7697	Minor; white-water; channel narrows at knick; channel steps at knick; angular islands; angular channel; channel cuts through a high ridge
67	Congo	knick	5	15	13.4964	-5.7928	5 m drop; white-water; channel narrows at knick; channel changes direction at knick; angular islands; angular channel; last knick of the Congo
68	Cubango	knick likely	-1	1719	16.2660	-12.7029	Knick likely; as meander before & after but here channel straighten angular; bare rock; SRTM drops rapidly
69	Cubango	knick	0	1712	16.3001	-12.7387	Height undetermined; Knick; structural control; change direction; angular channel rapids begin
70	Cubango	m. knick	-5	1692	16.3165	-12.7430	Minor as cascades; white-water visible; angular channel
71	Cubango	knick	40	1684	16.3220	-12.7631	40 m drop; bare rock; angular channel likely geol control; change in direction indicates river capture
72	Cubango	knick likely	-1	1648	16.3397	-12.8114	Knick likely rapids & noise & bare rock white-water angular channel
73	Cubango	knick	15	1637	16.3415	-12.8511	>15 m drop; with meander below
74	Cubango	knick	20	1622	16.3612	-12.8846	>20 m drop; channel narrow & angular; above & below meanders; likely geol controls or blocks
75	Cubango	knick	35	1595	16.3668	-13.0385	35 m drop; white-water with angular channel with straight sections
76	Cubango	knick likely	-1	1546	16.4052	-13.2977	Knick likely or rapids ; as channel angular; bare rock & no meanders; hidden by terrain spike
77	Cubango	knick	10	1541	16.4113	-13.3266	>10 m drop; terrain spike before; bare rock & linear channel
78	Cubango	knick	10	1516	16.4303	-13.5257	10 m drop; channel meander after; knick in line with ridge
79	Cubango	knick likely	-1	1485	16.2889	-14.2168	Knick likely; as angular island with two channels; bare rock & light-water line

80	Cubango	knick likely	-1	1479	16.2965	-14.2692	Knick likely; minor drop & water lighter blue & on straight channel usually equals rapids
81	Cubango	knick	5	1472	16.3203	-14.2973	5 m drop; angular island fan; bare rock
82	Cubango	m. knick	-5	1466	16.3025	-14.3508	Minor; rapids upstream; angular island fan; bare rock
83	Cubango	knick	0	1460	16.2874	-14.3746	Height undetermined; knick ; drop unsure; 3 angular island fan & bare rock & hidden on SRTM by ridges
84	Cubango	knick	30	1456	16.2865	-14.3862	30 m drop; change in flow direction after; gorge with rapids bare rock downstream
85	Cubango	m. knick	-5	1432	16.2853	-14.4146	Knick minor; likely large rapids; white-water; bare rock & perpendicular tributaries
86	Cubango	knick likely	-1	1427	16.2715	-14.4613	Knick likely; rapids; 2 minor knickpoints downstream seen; similar marked channel, narrow white-water
87	Cubango	knick	5	1425	16.2846	-14.4729	>5 m drop; angular island fan; bare rock; change direction
88	Cubango	m. knick	-5	1418	16.3079	-14.5265	Minor; likely rapids; angular island fan & white-water
89	Cubango	knick	20	1396	16.5005	-14.6501	>20 m drop; two cascades; angular island; straight channel through ridge giving terrain spike
90	Cubango	knick	30	1385	16.4831	-14.6336	30 m drop; multi cascades & some rapids directly upstream; lots open soil or rock
91	Cubango	m. knick	-5	1365	16.5206	-14.6666	Minor; likely rapids; has angular island
92	Cubango	knick	10	1355	16.5765	-14.7180	10 m drop; angular island fan
93	Cubango	knick	5	1341	16.6120	-14.7860	>5 m drop; angular island fan; tributaries on east trellis
94	Cubango	knick	10	1331	16.6342	-14.8104	10 m drop; river distributary to 2 with angular island but continuous drop; steep rapids
95	Cubango	knick	20	1320	16.6505	-14.8538	20 m drop; cut through ridge; gorge effects spike & channel change
96	Cubango	m. knick	-5	1305	16.6522	-14.8611	Minor; angular island fan
97	Cubango	m. knick	-5	1295	16.6549	-14.8773	Minor; angular island fan
98	Cubango	knick likely	-1	1291	16.6600	-14.9517	Knick likely; due white-water & narrow channel & tree
99	Cubango	knick likely	-1	1290	16.6591	-14.9303	Knick likely; minor with narrow channel white-water & riparian vegetation
100	Cubango	knick	0	1286	16.6526	-14.9793	Height undetermined; Knick; angular island fan; massive geology; not resolved on SRTM
101	Cubango	knick	20	1280	16.6705	-14.9940	>20 m drop; combination of falls & rapids in angular island fan
102	Cubango	knick likely	-1	1262	16.7113	-15.0750	Knick likely; likely rapids; white-water & tree with angular island upstream
103	Cubango	m. knick	-5	1261	16.6898	-15.0340	Minor; likely rapids in low flow; likely two sets; visible on Landsat; part 1 start

104	Cubango	m. knick	-5	1260	16.7038	-15.0497	Minor; likely rapids in low flow; likely two sets; visible on Landsat; part 2 end
105	Cubango	knick	5	1258	16.6964	-15.0954	>5 m drop; two such drops; white-water; angular island fan; firefront upstream
106	Cubango	m. knick	-5	1251	16.7136	-15.1246	Minor; rapids less 5m ;white-water & channel narrow
107	Cubango	m. knick	-5	1245	16.7639	-15.1787	Minor; rapids; angular island
108	Cubango	m. knick	-5	1241	16.8376	-15.2636	Minor; rapids; angular island in channel; no noticeable drop in SRTM
109	Cubango	m. knick	-5	1231	16.9638	-15.4376	Minor; large angular island with white-water; narrow channel; geol ctrl
110	Cubango	m. knick	-5	1221	17.1565	-15.4804	Minor; likely rapids due to angular island series; narrowing channel; part 1a
111	Cubango	m. knick	-5	1214	17.1917	-15.4857	Minor; likely rapids due angular island series; narrowing channel; part 2a
112	Cubango	m. knick	-5	1213	17.2085	-15.4798	Minor; likely rapids due angular fan series; just before major knick; part 1b
113	Cubango	m. knick	-5	1210	17.2366	-15.4829	Minor; likely rapids due angular fan series; just before major knick; part 2b
114	Cubango	knick	15	1206	17.2455	-15.4897	>15 m drop; single fall; angular rock outcrops within channel
115	Cubango	m. knick	-5	1197	17.2688	-15.5005	Minor 3m drop; angular island; rapids up & downstream on same stretch
116	Cubango	knick	40	1185	17.3761	-15.5939	40 m drop; part 1; angular island fan begin; gorge downstream; landforms look warped
117	Cubango	knick	20	1152	17.4019	-15.6343	>20 m drop; part 2; deformed landscape & spikes caused by flowing through ridge
118	Cubango	m. knick	-5	1026	21.3410	-17.9854	Minor; rapids with angular island fan
119	Cubango	knick	20	1021	21.4227	-18.0243	Knick; three part 1a; 20m total drop; start; protracted knick as Cub turns into Okavango; many distributaries
120	Cubango	knick	20	1016	21.4740	-18.0757	Knick; three part 1b; 20m total drop; middle ; angular island fan
121	Cubango	knick	20	1009	21.5467	-18.0909	Knick; three part 1c; 20m total drop; toe; downstream channel becomes wide & shallow
122	Cubango	knick	0	1004	21.5835	-18.1142	Height undetermined; knick; shelf like maybe weir ; eastern direction; last before floodplain
123	Cuchi	knick	50	1676	16.7339	-12.6858	>50 m drop; single fall with short gorge before & after
124	Cuchi	m. knick likely	-1	1556	16.6350	-13.4010	Minor likely; unresolved height due to noise on SRTM; angular channel & floodplain meanders; rapids likely & mini gorge effects
125	Cuchi	knick	40	1522	16.7048	-14.1543	>40 m drop; looks like 3 drops with rapids between; meander above below; straight tributaries from E
126	Cuchi	knick	20	1472	16.7350	-14.2064	20 m drop; angular island at begin; narrow rapids fill gorge downstream white-water
127	Cuchi	knick	20	1445	16.7545	-14.2675	>20 m drop; convex series of drops & rapids; white-water & angular channel
128	Cuchi	knick	35	1392	16.9150	-14.5821	>35 m drop; 90 degree turn; straight channel; one major & minor knick close
129	Cuchi	knick	60	1337	16.9181	-14.6789	knick series; total drop 60m; start ; rumpled ridge outcrops & angular island fans;

							riparian vegetation
130	Cuchi	knick	60	1294	16.9009	-14.7453	knick series; total drop 60m; end ; rumpled ridge outcrops & angular island fans; riparian vegetation
131	Cuchi	m. knick likely	-1	1290	16.8784	-14.7795	Minor likely rapids or small knick; not seen on SRTM & two angular island fans with angular channel
132	Cuchi	m. knick	-5	1259	16.9414	-15.0213	Minor; angular isle narrow channel & heavy rip vegetation
133	Cuchi	m. knick	-5	1217	17.2635	-15.3781	Minor ; a shelf projection in stream; angular island fan
134	Cuchi	knick	5	1209	17.2879	-15.4189	>5 m drop; angular island fan
135	Cuchi	m. knick	-5	1201	17.3055	-15.4525	Minor ; 1 of 2 ; angular fan on land; knick lost in noise on SRTM
136	Cuchi	m. knick	-5	1195	17.3228	-15.4732	Minor ; 2 of 2 ; angular fan on land; knick lost in noise on SRTM
137	Kabompo	knick	20	1359	25.3374	-11.8097	>20 m drop; linear drainage; tributaries 90 to channel; bare rock/soil on channel margin
138	Kabompo	knick	70	1271	25.1748	-12.0820	70 m drop; picked out in mountain & gorge; bare rock/soil on channel margin & surrounds; angular channel; white-water; drop from highlands to lowlands across catchment
139	Kabompo	m. knick	-5	1071	24.3475	-13.4755	Minor; angular island fan; near confluence with tributaries trunk connecting at knick: linear drainage; channel step at knick
140	Kabompo	knick	0	1069	24.2540	-13.5840	Height undetermined; knick; hidden due to radar shadow in gorge; Landsat visible as knick; angular island on channel margin; channel step at knick; white-water; bare rock/soil on channel margin; change direction downstream
141	Kafue	knick	10	1115	26.6278	-14.4657	>10 m drop; angular island fan; angular channel
142	Kafue	knick	5	1102	26.5350	-14.4797	>5 m drop; angular island fan; bare soil or rock
143	Kafue	m. knick	-5	1091	26.1882	-14.8012	Minor; rapids; angular island fan; channel flatten out suddenly then form fan
144	Kafue	knick	10	1086	26.0895	-14.9060	10 m drop; large angular island fan; channel widen upstream of knick & narrower downstream; perpendicular tributaries downstream of knick
145	Kafue	knick	5	1070	26.0026	-15.0787	>5 m drop; channel widen to form large angular island fan; trellis tributaries
146	Kafue	knick	5	1070	25.9796	-15.2544	5 m drop to start; begin massive angular island fan; angular channel
147	Kafue	m. knick	-5	1070	25.9660	-15.1372	Minor; rapids; 3m drop; island form as channel split into two & then form a angular island fan
148	Kafue	knick	35	1062	25.9716	-15.3176	>35 m drop; middle of large angular fan; high density distributaries forming angular island fan covering large area; bare rock or soil
149	Kafue	knick	5	1031	25.9963	-15.4160	5m drop; toe of 35m drop; thin linear island in channel
150	Kafue	1st dam wall	40	1029	26.0017	-15.7567	Dam wall; primary dam wall of 40m drop

151	Kafue	2nd dam wall	15	978	28.4188	-15.8053	Dam wall; secondary dam wall of 15m drop with natural knickpoints below it
152	Kafue	knick	20	831	28.4448	-15.8479	>20 m drop; natural knick after dam wall; angular channel
153	Kafue	knick	60	665	28.4803	-15.8475	>60 m drop; angular gorge; white-water; many smaller knickpoints close together
154	Kafue	knick	70	507	28.5355	-15.8722	>70 m drop; angular gorge; white-water; many smaller knickpoints close together; form part of same gorge as the 60m drop connected by lesser knickpoints
155	Kalungwishi	knick	30	1440	30.1146	-9.8927	>30 m drop; near source
156	Kalungwishi	knick	80	1361	29.8626	-9.7967	>80 m drop; single fall as river enters main valley; linear landforms ENE WSW; bare rock visible
157	Kalungwishi	knick	25	1317	29.8687	-9.7790	>25 m drop; in gorge after low gradient section after bigger fall; linear landforms ENE WSW
158	Kalungwishi	knick	20	1263	29.8269	-9.7456	>20 m drop; angular channel; series of rapids & cascades; downstream of gorge valley; linear landforms ENE WSW
159	Kalungwishi	knick	10	1239	29.8142	-9.7140	>10 m drop; white-water; angular channel; series of rapids & cascades
160	Kalungwishi	knick	20	1187	29.4323	-9.5384	>20 m drop; single drop with angular islands above & below
161	Kalungwishi	knick	50	1164	29.3875	-9.5423	>50 m drop; single fall with mini angular island fan above & below; angular channel; beginning of a gorge
162	Kalungwishi	knick	40	1119	29.3515	-9.5248	>40 m drop; radar effects; angular island fan; angular channel; enter gorge as river flow to escarpment
163	Kalungwishi	knick	80	1006	29.3004	-9.2038	>80 m drop; like 3 sets in a gorge; gorge orientated NE SW
164	Kasai	knick	10	1177	20.1073	-11.2422	10 m drop; angular channel; narrow channel
165	Kasai	knick	5	1075	21.3870	-11.2312	5 m drop; narrow channel; knick on part where channel flow around a ridge
166	Kasai	knick	10	1046	21.7529	-10.8246	>10 m drop; angular channel; channel change direction after knick from NE to N
167	Kasai	m. knick	-5	1032	21.7625	-10.7651	Minor; angular island; white-water; narrow channel
168	Kasai	knick	10	1028	21.7688	-10.8071	10 m drop; rapids downstream drop another 5m; angular island fan; angular channel; incised channel
169	Kasai	knick	5	1018	21.8088	-10.6243	>5 m drop; channel change direction; surrounding channels also change direction in line with this point
170	Kasai	m. knick	-5	1008	21.9577	-10.6105	Minor; angular channel; white-water
171	Kasai	knick	15	993	22.2157	-10.6073	>15 m drop; angular island; bare soil or rock
172	Kasai	knick	10	987	22.2711	-10.6246	10 m drop; change in channel direction; angular channel at knick section
173	Kasai	knick	5	976	22.3088	-10.5543	5 m drop; channel become straighter at knick; channel pool at knick & is narrow after knick

174	Kasai	knick	5	973	22.2841	-10.4947	> 5 m drop; river change direction
175	Kasai	knick	5	939	21.8720	-9.6260	>5 m drop; angular channel with perfectly straight section; zig-zag effect
176	Kasai	m. knick	-5	931	21.8038	-9.4296	Minor; bare rock & white-water; angular channel
177	Kasai	knick	5	930	21.8093	-9.3723	> 5m drop; angular block island in channel
178	Kasai	knick	5	923	21.8078	-9.3317	>5 m drop; angular block island in channel
179	Kasai	knick	10	912	21.8568	-9.2116	>10 m drop; angular island fan; white-water
180	Kasai	knick	5	905	21.8596	-9.1929	5 m drop; single fall
181	Kasai	knick	10	899	21.8500	-9.1455	10 m drop; single fall; angular island fan after knick; channel almost backflow after knick
182	Kasai	knick	5	888	21.8399	-9.1062	>5 m drop; angular island in channel; angular channel
183	Kasai	knick	5	884	21.8465	-9.0246	>5 m drop; angular island fan; bare rock or soil; trellis tributaries
184	Kasai	m. knick	-5	875	21.8495	-8.9721	Minor; angular island fan; white-water; bare rock or soil
185	Kasai	knick	5	867	21.8873	-8.8016	>5 m drop; angular island fan; concave drop; angular channel
186	Kasai	knick	20	842	21.9026	-8.6825	20 m drop; two stages of 10m drops; angular island fan; white-water
187	Kasai	knick	20	829	21.9250	-8.6073	20 m plus drop; angular island fan; trellis tributaries: angular channel
188	Kasai	knick	5	803	21.9374	-8.5351	5 m drop; angular island fan; large island; trellis tributaries
189	Kasai	m. knick likely	-1	786	21.8381	-8.1157	Minor likely; angular island fan; bare rock
190	Kasai	knick	30	774	21.7775	-7.8129	30m drop; large angular island fan; many distributaries; angular channel sections
191	Kasai	knick	5	745	21.8437	-7.6165	>5 m drop; angular island fan; tow tributaries join at knick site
192	Kasai	knick	20	727	21.8072	-7.3072	>20 m drop; large angular island fan; angular channel; distributaries; horizontal channel flow at one stage; bare rock or soil
193	Kasai	m. knick	-5	697	21.7264	-7.1962	Minor; angular island fan; angular channel; white-water; channel narrows only to widen again
194	Kasai	knick	10	682	21.6677	-7.0852	Knick 10m plus drop; several angular island fans; downstream tributary join after its own knick
195	Kasai	knick	10	655	21.6281	-7.0493	> 10 m drop; several close cascades; channel change direction; bare rock or soil; large gorge valley
196	Kasai	knick	20	632	21.5956	-7.0303	>20 m drop; channel zig-zag at knick; one continuous fall
197	Kasai	m. knick	-5	612	21.5415	-6.9731	Minor; angular island fan; white-water; bare rock or soil; channel narrows then widens again
198	Kasai	knick	5	596	21.4618	-6.8871	5m drop; white-water; angular islands; angular channel

199	Kasai	knick	25	571	21.4219	-6.8440	>25 m plus drop; large angular island fan; sinuous channel through fan possibly old angular fan
200	Kasai	knick	5	548	21.3737	-6.8194	5 m drop; single drop; angular channel
201	Kasai	knick	15	522	21.1629	-6.6755	15 m drop; channel narrows & widens; angular island fan; white-water
202	Kasai	m. knick	-5	491	21.0689	-6.6111	Minor; white-water; large angular island fans
203	Kasai	knick	10	478	20.9317	-6.5412	Knick 10m plus drop; single fall; channel constricted at knick but is wide upstream & downstream of the knickpoint
204	Kasai	knick	10	466	20.8932	-6.5058	>10 m drop; chute drop in that channel wider upstream & downstream but narrows greatly to form knick
205	Kasai	knick	15	452	20.8486	-6.4966	>15 m drop; two knickpoints close together of similar size; channel constricts at each knickpoint only to widen substantially
206	Kasai	m. knick	-5	434	20.853	-5.6862	Minor; white-water; block island; channel narrows
207	Kasai	m. knick	-5	426	20.8217	-5.7387	Minor; white-water; block island; channel narrows
208	Kasai	knick	5	416	20.8847	-5.5961	5 m drop; angular island; angular channel
209	Kasai	knick	15	400	20.9100	-5.5327	15 m drop; channel change direction; single fall
210	Kasai	knick	10	400	20.9541	-5.4787	10 m drop; angular island fan; several falls close together
211	Kwango	knick	90	1188	18.7748	-11.1594	>90 m drop; continuous series of knickpoints close together; near vertical; drop down the escarpment of the African high to the start of the Congo basin; bare rock
212	Kwango	knick	20	944	18.6216	-10.1157	20 m drop; part 1; total drop 40m plus; series of drops; bare rock or soil; connected to downstream knick via rapids; the dropping down to the true Congo basin
213	Kwango	knick	20	929	18.6603	-10.0976	20 m drop; part 2; total drop 40m plus; series of drops; bare rock or soil; connected to downstream knick via rapids; the dropping down to the true Congo basin
214	Kwango	knick	20	870	18.2228	-9.2874	>20 m drop; white-water; angular channel; series of cascades close together; channel change direction; angular island fans
215	Kwango	knick	20	856	18.1360	-9.2665	>20 m drop; white-water; angular channel; series of falls very close together; knick where straight channel curves around ridge
216	Kwango	knick	5	822	18.0374	-9.1605	5 m drop; white-water; large angular island in channel
217	Kwango	m. knick	-5	811	18.0601	-9.0719	Minor; white-water; region of settlement maybe weir; straight channel
218	Kwango	knick	5	805	18.0398	-9.0381	>5 m drop; channel change direction; angular channel; bare rock or soil
219	Kwango	knick	5	801	18.0312	-9.0159	5 m drop; channel constricted; bare rock or soil
220	Kwango	knick	15	798	18.0158	-8.9806	15 m plus drop; single fall; angular channel; white-water; narrow channel; bare rock or soil
221	Kwango	knick	5	795	18.0163	-8.9982	5 m drop; channel flow around ridge white-water; bare rock or soil

222	Kwango	knick	45	756	18.0107	-8.8856	45 m drop; single fall; angular island downstream of knick; channel zig zag; linear island in channel; bare rock
223	Kwango	knick	30	723	17.9466	-8.8060	>30 m drop; linear island in channel; white-water: channel change direction in zig-zag manner
224	Kwango	knick	25	668	17.9090	-8.6778	>25 m drop; white-water; angular channel; bare rock or soil; linear island channel
225	Kwango	knick	10	646	17.8697	-8.6035	10m drop; white-water; bare rock or soil; linear islands in the channel
226	Kwango	knick	5	624	17.7560	-8.5199	5m drop; angular islands; widening & narrowing of channel; change in channel direction
227	Kwango	knick	75	588	17.3179	-7.7162	>75 m drop; multiple cascades close together; angular channel; angular island fans; white-water; bare rock or soil
228	Kwango	knick	50	460	17.2723	-7.6153	>50 m drop; two knickpoints close together; one 15m the other 35m; white-water; bare rock
229	Luapula	knick	15	1138	29.2118	-12.3738	>15 m drop; in two sections; white-water; angular island fan; angular channel
230	Luapula	knick	20	1114	29.1214	-12.3940	20 m drop; knick positioned at 90 degree bend in channel; trellis tributaries; bare rock or soil
231	Luapula	knick	15	1087	29.0800	-12.3866	>15 m drop; multiple falls close together; white-water; angular channel: channel zig-zag
232	Luapula	knick	15	1067	29.0354	-12.3524	15 m drop; knick at escarpment; angular channel; white-water; single fall; narrow gorge with radar effects on SRTM;
233	Luapula	knick	20	1033	28.4532	-11.3129	> 20 m plus drop; single fall; angular island; mini islands on the channel edges; bare rock or soil
234	Luapula	knick	10	1011	28.6254	-10.7156	>10 m drop; angular island fan; bare rock or soil; knick positioned at 90 degree bend in channel; upstream of knick river very low gradient
235	Luapula	knick	80	997	28.6890	-10.6785	>80 m drop; several large drops close together; large angular island fan in the beginning with smaller ones following; likely indications of structural controls
236	Luena	knick	40	1278	19.9139	-11.8028	>40 m drop; the beginning of a section of white-water; total drop 85m; series of knickpoints close together; bare rock or soil at channel margins; angular channel
237	Luena	knick	15	1227	19.9637	-11.8024	15 m drop; section 2 of white-water; bare rock or soil; angular channel; series of falls
238	Luena	knick	10	1218	19.9955	-11.7987	10 m drop; section 3 of white-water; perpendicular incised tributaries; angular channel; series of drops
239	Luena	knick	10	1209	20.0313	-11.7785	10 m drop; section 4 of white-water; perpendicular incised tributaries; angular channel; series of drops; river begin to change direction
240	Luena	knick	10	1190	20.0662	-11.7382	10 m drop; section 5; last section; angular channel: many pools: white-water continue with change of river direction
241	Luena	m. knick	-5	1177	20.1198	-11.7230	Minor; white-water; angular channel; narrow channel; incised channel

242	Luena	m. knick	-5	1177	20.1570	-11.7205	Minor; white-water; angular channel; narrow channel; incised channel; trellis drainage
243	Luena	knick	5	1154	20.3225	-11.7627	5 m drop; single drop by an angular island; narrow channel; incised channel; river flow into gorge then knickpoint then floodplain
244	Luena	knick	10	1140	20.4365	-11.9154	>10 m drop; incised channel; angular channel with knick on channel 90 degree bend; white-water; bare rock or soil; floodplain after knick
245	Luena	knick	0	1061	22.5012	-12.4688	Height undetermined; knick single drop; gorge effects hide knick height; last knick before flow into the Zambezi with the difference in height 5m between knick & Zambezi thalweg
246	Lufira	m. knick	-5	1202	26.7190	-11.5376	Minor; angular channel; knick at 90 degree turn in channel; first major confluence; bare rock or soil visible
247	Lufira	knick	10	1139	26.8771	-11.2001	>10 m drop; single fall; channel straight & narrow then knickpoint; bare rock or soil on channel margin
248	Lufira	1st dam wall	90	1118	27.2443	-10.7524	Dam wall; primary wall for Lac de le Lufira; wall horizontal although surrounding linear structures are orientated NW SE; likely flooded natural knickpoint or replaced it
249	Lufira	2nd dam wall	50	1014	27.2687	-10.7221	Dam wall; secondary wall for Lac de le Lufira; wall parallel with the linear structures; likely resulted in back flooding of natural knickpoints & replaced a natural knick as there is are knickpoints downstream
250	Lufira	knick	50	992	27.2809	-10.7184	>50 m drop; two falls close together; fall after secondary dam wall for Lac de le Lufira; gradient nearly 0 after dam wall upstream of falls; river flow through linear ridges; angular channel
251	Lufira	m. knick	-5	943	27.3182	-10.6943	Minor; angular channel stepping to the east; landforms are linear; bare rock or soil visible in lines
252	Lufira	m. knick	-5	929	27.3721	-10.6750	Knick minor; 4 knickpoints dropping 10m; white-water; angular island; channel flowing out of a floodplain
253	Lufira	knick	15	909	27.3984	-10.6072	Knick 15m + drop; series of cascading falls; angular islands; angular channel
254	Lufira	knick	45	867	27.04037	-9.5169	Knick 45m + drop; single fall; exiting Kundelungu swamp as Kiubo falls; angular island; channel narrows; channel look underfit in valley downstream of knick; river exit square toe of swamp into a floodplain gorge
255	Lufira	knick	20	834	26.9752	-9.4538	20 m drop; single fall; channel underfit in valley; old river terraces visible; bare rock or soil visible
256	Lufira	knick	5	813	26.9208	-9.3638	5 m drop; angular island; white-water; in gorge; angular channel that has curved zig-zag morphology
257	Lufupa	knick	15	1090	24.4966	-10.4297	>15 m drop; start of a set of 4; series of falls close together; convex profile; overall series start where river changes direction & this is the position of this knick; bare

							rock or soil
258	Lufupa	knick	25	1061	24.5217	-10.3922	>25 m drop; single fall; set 1 of 4; channel change direction again; bare rock or soil
259	Lufupa	knick	25	976	24.6076	-10.3459	>5 m drop; single drop; set 2 of 4; angular channel; channel flow through lineaments & folds; white-water
260	Lufupa	knick	25	943	24.6156	-10.3524	>25 m drop; single drop; set 3 of 4; angular channel; channel flow through lineaments & folds; white-water; knick at 90 degree bend of channel; downstream of knick channel flow parallel to lineaments
261	Lufupa	knick	30	921	24.6510	-10.3314	30 m drop; several falls close together; set 4 of 4; convex profile; angular channel; channel flow through lineaments & folds; lost of white-water; bare rock or soil; channel now in angular valley orientated NNE SSW with linear features
262	Lufupa	m. knick	-5	907	24.7500	-10.2404	Minor; series of white-water rapids; steep channel gradient; trellis drainage
263	Lufupa	m. knick	-5	887	24.7481	-10.1633	Minor; angular island; white-water; narrowing of channel; bare rock or soil; angular channel
264	Lufupa	m. knick	-5	811	24.8214	-9.7544	Minor; river change direction; as flow into a linear valley; white-water; angular channel; drop in SRTM
265	Lufupa	m. knick likely	-1	803	24.8461	-9.7679	Minor knick likely; river change direction; as flow into a linear valley; tear shaped island; angular channel
266	Lufupa	m. knick likely	-1	800	24.8671	-9.7330	Minor knick likely; angular island; white-water; angular channel; likely rapids
267	Lufupa	knick	15	792	24.9365	-9.6039	>15 m drop; angular island on channel margins; single fall; angular channel; knick occur as channel flow into a depression in line with southern linear valley
268	Lufupa	knick	10	776	25.0278	-9.5904	>10 m drop; 2 falls close together; angular island; angular channel
269	Lufupa	knick	0	734	25.5185	-9.0862	Height unknown as occur on a terrain spike; knickpoint, bare rock or soil visible on channel margins; angular channel; white-water; narrow channel flow through lineaments; just upstream of a 40m fall
270	Lufupa	knick likely	-1	728	25.4734	-9.0849	Knick likely; angular island; white-water; bare rock or soil; knickpoints downstream
271	Lufupa	knick	40	721	25.5306	-9.0819	>40m drop; single fall; channel narrow as cut through ridge; white-water
272	Lufupa	knick	0	682	25.5674	-9.0848	height unknown as occur on terrain spike ; knick; angular island; height difference upstream & downstream is between 5 to 10m; channel cut through lineament; bare rock or soil on channel margin & in parallel lines; begin of change in flow direction of river
273	Lufupa	knick	0	665	25.5839	-9.0985	Height unknown as occur on terrain spike; knick; single fall; white-water; height difference upstream & downstream is between 5 to 10m; channel cut through lineaments; bare rock or soil on channel margin & in parallel lines

274	Lufupa	knick	0	664	25.6150	-9.1312	Height unknown as occur on terrain spike; height difference upstream & downstream is between 5 to 15m; channel cut through ridge in a curve; white-water; bare rock or soil on channel margin & in parallel lines
275	Lufupa	knick	0	661	25.5984	-9.1049	Height unknown due to terrain spike; difference between the upstream and downstream is 5m; white-water; angular channel; bare rock or soil on margin; flow through lineament
276	Lufupa	knick	0	652	25.6058	-9.1218	Height unknown due to terrain spike; difference between the upstream and downstream is 10m; white-water; angular channel; bare rock or soil on margin; flow through lineament
277	Lufupa	knick	5	639	25.6211	-9.1514	5m drop; angular island fan; multiple distributaries; bare rock or soil; channel angular
278	Lukuga	m. knick	0	783	29.0745	-5.9214	Minor likely; height unknown due to gorge & ridge noise; difference in height upstream & downstream of knickpoint is 5m; white-water; bare rock or soil; high topographic area
279	Lukuga	knick	5	771	28.9590	-5.9014	5m drop; angular island; channel width alternates; angular islands on channel margin; angular channel
280	Lukuga	knick	5	758	28.8543	-5.8830	5m drop; angular island; white-water; bare rock or soil; linear drainage; angular channel
281	Lukuga	knick	15	703	28.3947	-5.9238	>15m drop; white-water; high density distributaries become a single channel abruptly at a linear impoundment; angular islands; bare rock/soil; white-water; channel narrows downstream; convex profile
282	Lukuga	knick	15	688	28.3582	-5.9168	>15m drop; white-water; angular islands; angular channel; narrow channel widens downstream of knick; bare rock or soil; continuous set of knicks
283	Lukuga	knick	15	670	28.2891	-5.9036	>15m drop; angular island fans; several drops close together; white-water; linear landscape structures; incised channel; trellis drainage; bare rock/soil; angular stepping channel; narrows at knick
284	Lukuga	knick	10	642	28.1698	-5.8733	>10m drop; angular island fans; angular channel; channel zig zags; white-water; linear drainage perpendicular to channel; bare rock or soil
285	Lukuga	knick	15	612	28.0192	-5.7124	>15 m drop; angular island fans; several drops close together; downstream of 90 degree bend in channel; flow into a linear valley; trellis drainage; bare rock or soil
286	Lulua	knick	10	1109	23.1339	-10.8790	>10 m drop; angular channel; bare rock or soil on channel margin; single fall; channel abruptly step north in direction at knickpoint only to flow in line with upstream section downstream of knickpoint
287	Lulua	knick	40	1022	22.7981	-10.7603	> 40 m plus drop; series of continuous falls; diagonal profile; channel change direction in this section twice; possible past river capture; bare rock or soil; angular channel

288	Lulua	knick	5	987	22.8990	-10.6828	>5m drop; angular island; bare rock or soil on channel margin; white-water; angular channel; change in flow direction at knickpoint; incised channel
289	Lulua	knick	10	975	22.8475	-10.6162	10m drop; angular island; white-water; angular channel; flow direction change at knick; bare rock or soil at channel margin
290	Lulua	knick	30	943	22.8576	-10.4424	>30 m drop; a continuous series of knicks; angular channel; angular islands; bare rock or soil; channel has rounded zig zag morphology
291	Lulua	knick	10	919	22.8610	-10.3813	10 m drop; a short series of continuous knicks; angular channel with knick occurring on the straight section; bare rock or soil visible
292	Lulua	m. knick	-5	913	22.8158	-10.3344	Minor; angular channel; white-water; bare rock or soil on channel margin; linear drainage on the west side more dendritic on the east side
293	Lulua	knick	20	880	22.6361	-9.2274	> 20 m drop; start of 2 knick set; set 1 of 2; total drop of 50m plus; 3 knicks close together; bare rock or soil, on channel margin; angular island at each knick; white-water; angular channel; channel step at each knickpoint
294	Lulua	knick	30	872	22.6117	-9.1812	>30m drop; 2 set of 2; total drop 50m plus; continuous series of 5 knicks; angular channel; angular islands; bare rock or soil on channel margin; channel alternates between wide & narrow sections; white-water
295	Lulua	m. knick	-5	845	22.5554	-8.8807	Minor; 2 minor knicks close together; white-water; angular islands; bare rock or soil on channel margin; linear drainage
296	Lulua	m. knick likely	-1	813	22.6718	-7.8501	Minor likely; rapids likely; large angular islands in channel; angular channel; bare rock or soil on channel margin
297	Lulua	m. knick	-5	799	22.5962	-7.7168	Minor; rapids likely; large angular islands in channel; angular channel; white-water; steep river gradient; bare rock or soil on channel margin
298	Lulua	m. knick likely	-1	781	22.6997	-7.4199	Minor likely; rapids likely; large angular islands in channel; angular channel; bare rock or soil on channel margin
299	Lulua	m. knick	-5	752	22.5330	-6.6945	Minor; angular island fan; white-water; change in river flow direction at knickpoint; bare rock or soil
300	Lulua	m. knick	-5	742	22.4960	-6.6981	Minor; angular island fan; white-water; change in river flow direction at knickpoint; bare rock or soil
301	Lulua	knick	20	723	22.4761	-6.5882	20 m drop; 3 falls close together an seen as one; large angular island in channel; white-water; angular channel; bare rock or soil on channel margin; knickpoint at change of direction; 90 degree bend
302	Lulua	knick	5	702	22.4597	-6.5489	5 m drop; angular island fans; angular distributaries; white-water; single fall; bare rock or soil on in channel islands; bare rock or soil
303	Lulua	knick	10	692	22.4366	-6.5207	>10 m drop; angular island fan; white-water; single fall; angular channel; bare rock or soil on channel margin at knickpoint;bare rock or soil; knickpoint where channel step up

304	Lulua	knick	15	686	22.4180	-6.4725	>15 m drop; 2 drops close together; white-water; 2 angular island fans one upstream with rapids & the other at the knickpoint; angular channel; 90 degree turn in flow direction at knickpoint; bare rock or soil at channel margin
305	Lulua	m. knick	-5	666	22.4140	-6.4274	Minor; angular island fan; white-water; angular channel with round zig zag form; bare rock or soil
306	Lulua	knick	20	644	22.4494	-6.3440	>20 m drop; single fall; angular island fan; angular channel; bare rock or soil at channel margin
307	Lulua	knick	20	597	22.4693	-6.2214	>20 m drop; in middle of large distributary fan with high gradient; only section with white-water; angular channels; bare rock
308	Lulua	m. knick	-5	571	22.3924	-6.0970	Minor; large angular island fan; white-water; bare rock or soil; steep profile gradient
309	Lulua	knick	5	557	22.3914	-6.0048	5 m drop; single fall; angular island; angular channel; bare rock or soil
310	Lulua	m. knick	-5	485	22.1834	-5.8009	Minor; single drop; white-water; angular island fan; linear drainage; bare rock or soil
311	Lulua	m. knick	-5	475	22.1474	-5.7589	Minor; white-water; angular island fan; bare rock or soil on channel margin; angular channel; river alternate between wide & narrow channel
312	Lulua	knick	10	451	22.0074	-5.4922	10 m drop; angular channel; angular island fan; bare rock or soil on channel margin; white-water
313	Lulua	knick	20	439	21.9897	-5.4784	>20 m plus drop; 2 drops close together with a total drop of 20m; white-water; linear landscape feature; zig zag morphology; angular island fans; bare rock or soil
314	Lulua	knick	10	430	21.9709	-5.4405	>10 m drop; single drop; angular island on channel margin; angular island fan; white-water; bare rock or soil; trellis drainage
315	Lulua	m. knick likely	-1	400	21.5446	-5.3406	Minor; angular island in channel; apparent white-water; bare rock or soil on channel margin
316	Luvua	knick	0	930	28.8459	-8.4577	Undetermined elevation; white-water; height unresolved due to noise from gorge & effects of flattening of Lk Mweru; bare rock/soil; terraces; underfit channel; knickpoint +10m lower than closest spike
317	Luvua	knick	10	928	28.8380	-8.4531	10m drop; white-water; channel has smoothed zig zag morphology; several knicks close together; bare rock or soil; terraces visible next to channel; channel incised
318	Luvua	knick	5	885	28.7986	-8.3624	>5 m drop; knick might be +10m gorge effects make resolving this difficult; white-water in linear formation; 2 knicks close together; bare rock/soil; cliffs next to channel; channel incised; angular island
319	Luvua	knick	15	873	28.8615	-8.2265	>15 m drop; several knicks close together giving a total drop of >15 m; large angular island fan; bare rock or soil; white-water; angular channels
320	Luvua	knick	50	852	28.8125	-8.1523	>50 m drop; 3 continuous falls; angular channels; angular island fans; bare rock/soil on channel margin & islands; river steps north; linear drainage & landscape features; channel narrows at knick

321	Luvua	knick	10	785	28.7216	-8.0014	>1 0m drop; begin of rapids with total drop of 20 m; angular island fan; angular channel; white-water; channel widens at knick; linear drainage; channel crosses several lineaments; channel has steep gradient after knick
322	Luvua	knick	5	755	28.6947	-7.9568	>5 m drop; end of rapids with total drop of 20 m in rapids; rapids end in knick; angular channel; white-water; angular island fan; channel change direction at knick to flow around a ridge
323	Luvua	knick	20	732	28.6818	-7.9274	>20 m drop; white-water; angular island fan; angular distributaries; bare rock or soil on islands and channel margin; channel cut across lineaments; linear drainage
324	Luvua	knick	20	719	28.6185	-7.8805	>20 m drop; white-water; large angular island fan; angular distributaries; bare rock/soil on islands & channel margin; linear drainage; series of smaller knicks with a larger 5m drop at the end going through a lineament
325	Luvua	m. knick	-5	711	28.5591	-7.9324	Minor; white-water as river flows into gorge; 90 degree bend into gorge; bare rock or soil visible on channel margin; angular channel; angular island in channel & on channel margin
326	Luvua	knick	20	703	28.4426	-7.8733	20 m drop; 2 knicks; white-water; angular island; deeply incised channel; linear drainage; tableland topography; terraces near channel
327	Luvua	knick	20	701	28.4166	-7.8553	>20 m drop; actually 2 knicks of 10m + each; white-water; angular channel; angular island fans; channel changes direction at knick points in a rounded zig zag morphology; linear drainage; table land topography;
328	Luvua	m. knick	-5	665	28.3198	-7.8039	Minor; white-water; angular island fan; angular channel; 2 sets of minor knicks close together; bare rock or soil; linear drainage
329	Luvua	m. knick	-5	654	28.2219	-7.7505	Minor; angular island fan; angular distributaries; bare rock or soil on islands; 2 sets of knicks close together; white-water; knick occur with lineament visible on either bank; linear drainage
330	Luvua	m. knick	-5	638	28.1530	-7.6921	Minor; likely rapids; angular channel; angular island fan; white-water; floodplain terrace; linear drainage perpendicular to channel; bare rock or soil on channel margin & islands
331	Luvua	m. knick	-5	619	28.1007	-7.6422	Minor; angular island fan; white-water; bare rock or soil on islands & channel margins; linear drainage; terrace
332	Luvua	knick	20	618	28.1023	-7.6403	20 m drop; continuous drops; white-water; knick where river stop flowing NW to flow SW in very narrow channel to flow W to then abruptly flow N with a 90 degree bend; angular island fan; linear drainage; angular channel
333	Luvua	knick	30	589	28.0870	-7.4374	>30 m drop; continuous set of rapids & falls dropping a total of 30m +; angular channels; angular island fan; white-water; bare rock or soil; 5m drops at start & end of angular fan
334	Luvua	knick	10	584	28.0773	-7.4198	10 m drop; white-water; start of angular island fan of 30m drop; single fall; angular

							island; channel change direction downstream of knick; bare rock or soil; linear drainage
335	Luvua	knick	5	578	28.0504	-7.3814	5 m drop; end of angular fan dropping 30m; white-water; angular island; downstream river gradient near horizontal; angular islands; linear drainage
336	Wamba	knick	10	909	18.3509	-8.4951	10 m drop; very incised channel; angular channel; channel change direction at knick; terrain is flat hills with deep ravines; main drainage linear interfluves drainage dendritic
337	Wamba	knick	25	893	18.3172	-8.4606	25 m drop; angular zig zaggin channel; deeply incised; white-water; river change direction at knickpoint; flat hill deep ravine topography
338	Wamba	knick	15	856	18.2906	-8.4357	15 m drop; sinuous angular channel; deeply incised channel; river change direction at knicpoint;bare rock or soil at channel margin; white-water
339	Wamba	knick	20	843	18.2856	-8.4276	20 m drop; sinuous angular channel; deeply incised channel; river change direction at knicpoint;bare rock or soil at channel margin
340	Wamba	knick	50	834	18.2630	-8.4052	>50 m drop; white-water; angular channel with knick in straight section; river change direction just downstream of knick; bare rock or soil visible
341	Wamba	knick	50	782	18.2534	-8.3883	>50 m drop; white-water; angular channel; river change direction just downstream of knick; bare rock or soil; linear drainage in parts
342	Wamba	knick	20	730	18.1973	-8.3640	20m drop; deeply incised channel; linear drainage & some dendritic drainage; bare rock/soil on the surrounding highlands; direction change just downstream of knick
343	Wamba	m. knick	-5	712	18.1630	-8.2978	Minor; single drop; white-water; bare rock or soil on surrounding highlands; linear drainage perpendicular to channel; channel change direction downstream
344	Wamba	m. knick likely	-1	640	17.9293	-7.5833	Minor likely; deeply incised channel; white-water just downstream of confluence; bare rock or soil on channel margin
345	Wamba	m. knick	-5	631	17.9071	-7.5702	Minor; white-water; deeply incised channel; angular island; bare rock/soil on channel margin; angular channel; channel constricted at knick; downstream direction change
346	Wamba	knick	10	613	17.8144	-7.4907	10m drop; angular channel; white-water; bare rock/soil on channel margin; river steps at knick in a S manner; topography is flat hills with deeply incised & forested gorges
347	Wamba	knick	10	541	17.3860	-6.4526	10m drop; white-water; plunge pool visible; channel narrow just upstream of plunge pool than downstream or upstream; bare rock or soil visible in pool
348	Wamba	m. knick likely	-1	506	17.2651	-6.3135	Minor likely; plunge pool; drop in SRTM but very noisy; angular channel; channel narrow as enter angular section
349	Wamba	knick	5	477	17.1152	-5.9181	>5 m drop; channel narrows than widens into plunge pool; white-water; river change direction just upstream of knick; knick may be greater than 10m but SRTM noisy
350	Wamba	m. knick	-1	421	16.9532	-5.3723	Minor likely; angular island on channel margin; drop in SRTM but noisy; river change

		likely					direction just downstream of knick; bare rock or soil visible on islands
351	Wamba	m. knick	-5	414	16.9488	-5.3849	Minor; angular island; white-water; drop in SRTM but noisy; river change direction just downstream of knick; channel cut through a ridge
352	Wamba	m. knick	-5	413	16.9503	-5.4116	Minor; angular island; white-water; drop in SRTM but noisy; river change direction just upstream of knick
353	Wamba	m. knick likely	-1	410	16.9118	-5.3205	Minor likely; angular island on channel margin; drop in SRTM but noisy; deeply incised meanders; river cuts through 4 ridges in this section; outer bank incision visible
354	Wamba	m. knick likely	-1	405	16.9240	-5.3017	Minor likely; drop in SRTM but noisy; deeply incised meanders; river cuts through lineament in this section; outer bank incision visible; channel narrows & widens alternately
355	Wamba	m. knick likely	-1	401	16.9211	-5.2212	Minor likely; 20m drop in SRTM but noisy; deeply incised meanders; river cuts through lineament; angular island; outer bank incision; channel narrows & widens alternately
356	Wamba	knick	5	397	16.9477	-5.0683	>5 m drop; river steps abruptly at knick; knick may be greater than 10m but SRTM noisy; river flows through ridge
357	Zambezi	m. knick	-5	1058	22.6167	-12.6833	Minor; white-water; river step at knick; linear drainage; bare rock or soil on channel margin
358	Zambezi	m. knick	-5	1056	22.7196	-12.9929	Minor; white-water in a linear formation; angular island; linear drainage; bare rock or soil on channel margin; knickpoint where river flows near a flat topped hill
359	Zambezi	knick	5	1046	22.6681	-13.0717	Knick 5m drop; white-water; continuous series of rapids; bare rock or soil on channel margin; knick occur where river flows semi parallel to a flat topped ridge
360	Zambezi	knick	5	1044	22.6894	-13.1050	>5 m drop; white-water; single drop; bare rock or soil on channel margin; river enter a floodplain after knick where channel meanders
361	Zambezi	m. knick	-5	995	23.3889	-16.4505	Minor; rapids; white-water; angular island on channel margin
362	Zambezi	knick	5	992	23.4822	-16.5570	5 m drop; white-water; continuous series of rapids; several small angular islands with larger island that may be sedimentary or geological
363	Zambezi	m. knick	-5	991	23.4565	-16.5322	Minor; rapids; white-water; angular island on channel margin; channel change direction just upstream of knick
364	Zambezi	knick	5	989	23.5266	-16.6086	5m drop; lots white-water; angular islands; bare rock or soil on islands & on channel margin; channel in process of stepping; white-water in linear arrangement
365	Zambezi	knick	10	984	23.5681	-16.6467	> 10 m drop; white-water in linear formation; bare rock visible in channel; channel abruptly step south; channel changes from a very broad width to a very narrow channel at knickpoint
366	Zambezi	knick	5	980	23.5700	-16.6505	>5 m drop; white-water; near continuous series of rapids; angular island; bare rock or soil on channel margin; angular narrow channel with broad zig zag morphology

367	Zambezi	m. knick	-5	967	23.7306	-16.7634	Minor; white-water; angular islands; bare rock or soil islands; angular channels; river step at knickpoint
368	Zambezi	m. knick	-5	967	23.7349	-16.7835	Minor; white-water; angular islands; bare rock or soil islands; angular channels; river step at knickpoint
369	Zambezi	m. knick	-5	953	24.1586	-17.3093	Minor; angular islands; angular channels; white-water in linear formation; river steps at knick; bare rock or soil on surrounds & islands
370	Zambezi	m. knick	-5	948	24.1674	-17.3716	Minor; angular islands on channel margins; larger islands in channel more rounded; angular channels; white-water; river steps just downstream of knick; bare rock or soil on islands
371	Zambezi	m. knick	-5	943	24.2144	-17.4196	Minor; angular islands; bare rock or soil islands; angular channels; river step just downstream of knick
372	Zambezi	m. knick	-5	937	24.2498	-17.4740	Minor; angular islands; angular channels; white-water in linear formation; river steps at knick; bare rock or soil on islands
373	Zambezi	m. knick	-5	927	25.1871	-17.7652	Minor; angular islands; angular channels; white-water; river changes direction downstream of knick; bare rock or soil on islands; channel cuts through a lineament at knick
374	Zambezi	knick	5	919	25.3726	-17.8444	5 m drop; angular island fan; white-water; bare rock/soil on islands & surrounds; river steps at knick; angular channels
375	Zambezi	m. knick	-5	914	25.4604	-17.8445	Minor; angular island; angular channel; channel contricted as change direction with 90 degree bend; incised floodplain; bare rock or soil on channel margins & islands
376	Zambezi	m. knick	-5	912	25.4862	-17.8501	Minor; angular islands; angular channels; white-water in a linear formation; river changes direction just downstream of knick; bare rock or soil on islands
377	Zambezi	m. knick	-5	909	25.5352	-17.8511	Minor; angular islands; angular channels; white-water; bare rock or soil on islands & channel margins
378	Zambezi	m. knick	-5	904	25.5914	-17.8382	Minor; angular islands; angular channels; white-water; bare rock or soil on islands & channel margins; channel narrows at knickpoint
379	Zambezi	knick	5	901	25.6657	-17.8152	5m drop; angular island fan; white-water; bare rock or soil on islands & surrounds; knick occurs where river steps; angular channels; linear drainage perpendicular to channel; channel narrows at knick
380	Zambezi	knick	50	865	25.8594	-17.9255	>50 m drop; Victoria falls; white-water; single drop; white-water in a linear formation; angular islands; angular channel; channel zig zag heavily below falls in a deeply incised gorge; SRTM very noisy after the Victoria falls due to gorge effects

Table A6.3: The ranking of rivers based on the number of knickpoints, comparing all knickpoints categories identified to just those assigned a height (categories **-5**, **5**, **10** etc). Kalahari basin rivers shown in bold

River name	Basin	Knickpoint count(Total)	Knickpoint count (excl. categories **-1** & **0)**	Rank change (total vs excl. categories **-1** & **0**)
Congo	Congo	64	61	1 / 1
Cubango	**Kalahari**	**55**	**41**	**2 / 3**
Kasai	Congo	47	46	3 / 2
Lulua	Congo	30	27	4 / 4
Upper Zambezi	**Kalahari**	**24**	**24**	**5 / 5**
Wamba	Congo	21	15	6 / 8
Lufupa	Congo	21	12	7 / 10
Luvua	Congo	20	19	8 / 6
Kwango	Congo	18	18	9 / 7
Kafue	**Kalahari**	**14**	**14**	**10 / 9**
Cuchi	**Kalahari**	**14**	**12**	**11 / 11**
Lufira	Congo	11	11	12 / 12
Luena	**Kalahari**	**10**	**9**	**13 / 13**
Kalungwishi	Congo	9	9	14 / 14
Lukuga	Congo	8	7	15 / 15
Luapula	Congo	7	7	16 / 16
Kabompo	**Kalahari**	**4**	**3**	**17 / 17**
Chambeshi	Congo	3	3	18 / 18

APPENDIX 7: GEOSPATIAL DATASETS

7.1 Detailed geology geodatabase

Due to the large size of this database, **Table A7.1** has been stored on attached the CD-R

7.2 Simplified geology database

Table A7.2: The simplified lithostratigraphy and rock type of the 380 knickpoints identified in this study. River names, and knickpoint categories and elevations are given as well as coordinates. See Chapter 6 for details on this data. Simplfied lithostratigraphy and rock types have been assigned to each knickpoint using mainly scanned and georectified maps. Abbreviations for maps used are: A– Angola; DRC– Democratic Republic of Congo, N– Namibia; RC– Republic of Congo; Z– Zambia; D– digital

N°.	River name	Knickpoint category	Elevation (m.a.s.l.)	Longitude	Latitude	Simple lithostratigraphy	Rocky type	Map
1	Chambeshi	10	1422	31.4475	-9.4389	Precambrian	volcanic-sedimentary	Z (D)
2	Chambeshi	15	1429	31.4577	-9.4683	Precambrian	volcanic-sedimentary	Z (D)
3	Chambeshi	50	1397	31.4622	-9.4753	Precambrian	volcanic-sedimentary	Z (D)
4	Congo	15	1287	25.4620	-10.4994	Precambrian	volcanic-sedimentary	DRC
5	Congo	25	1090	25.4269	-10.3243	Precambrian	volcanic-sedimentary	DRC
6	Congo	80	1231	25.4393	-10.4950	Precambrian	volcanic-sedimentary	DRC
7	Congo	30	1147	25.4447	-10.4036	Precambrian	volcanic-sedimentary	DRC
8	Congo	30	1019	25.4491	-10.2539	Precambrian	volcanic-sedimentary	DRC
9	Congo	50	999	25.4358	-10.2326	Intrusion	igneous & metamorphic	DRC
10	Congo	0	890	25.4072	-10.1851	Precambrian	volcanic-sedimentary	DRC
11	Congo	90	862	25.4101	-10.1253	Precambrian	volcanic-sedimentary	DRC
12	Congo	10	748	25.5080	-9.9343	Precambrian	volcanic-sedimentary	DRC
13	Congo	15	718	25.5361	-9.7682	Karoo	sandstone & glacial dwyka	DRC
14	Congo	20	675	25.5028	-9.4697	Precambrian	volcanic-sedimentary	DRC
15	Congo	15	679	25.5196	-9.4058	Precambrian	volcanic-sedimentary	DRC
16	Congo	5	653	25.5374	-9.3544	Karoo	sandstone & glacial dwyka	DRC
17	Congo	5	625	25.7141	-9.3062	Intrusion	igneous & metamorphic	DRC
18	Congo	10	605	25.7803	-9.2349	Intrusion	igneous & metamorphic	DRC
19	Congo	30	591	25.8097	-9.1965	Intrusion	igneous & metamorphic	DRC
20	Congo	5	541	27.0144	-5.3600	Karoo	sandstone & glacial dwyka	DRC
21	Congo	10	530	27.0184	-5.3099	Precambrian	granitic / gneissic	DRC
22	Congo	10	530	26.9934	-5.2916	Precambrian	granitic / gneissic	DRC
23	Congo	15	500	26.9610	-4.9793	Karoo	sandstone & glacial dwyka	DRC
24	Congo	10	478	26.7702	-4.6253	Karoo	sandstone & glacial dwyka	DRC

25	Congo	5	440	25.7106	-2.1362	Karoo	sandstone & glacial dwyka	DRC
26	Congo	5	414	25.4596	-0.3563	Intrusion	igneous & metamorphic	DRC
27	Congo	10	404	25.5188	0.1874	Precambrian	volcanic-sedimentary	DRC
28	Congo	5	398	25.4851	0.2546	Precambrian	volcanic-sedimentary	DRC
29	Congo	5	389	25.2734	0.4386	Karoo	sandstone & glacial dwyka	DRC
30	Congo	5	255	15.2272	-4.3172	Karoo	sandstone & glacial dwyka	RC
31	Congo	10	254	15.1760	-4.3687	Karoo	sandstone & glacial dwyka	RC
32	Congo	10	239	15.1359	-4.4310	Kalahari	sand & silcrete	RC
33	Congo	5	220	14.8694	-4.7504	Karoo	sandstone & glacial dwyka	RC
34	Congo	10	210	14.8140	-4.8360	Karoo	sandstone & glacial dwyka	RC
35	Congo	5	203	14.7059	-4.8997	Karoo	sandstone & glacial dwyka	RC
36	Congo	5	196	14.6570	-4.9193	Karoo	sandstone & glacial dwyka	RC
37	Congo	5	187	14.4371	-4.8776	Precambrian	Sedimentary	RC
38	Congo	5	157	13.6287	-5.2977	Precambrian	Sedimentary	DRC
39	Congo	5	155	13.5493	-5.3606	Intrusion	igneous & metamorphic	DRC
40	Congo	5	143	13.5577	-5.4143	Intrusion	igneous & metamorphic	DRC
41	Congo	20	120	13.6104	-5.4770	Intrusion	igneous & metamorphic	DRC
42	Congo	40	81	13.6345	-5.5317	Intrusion	igneous & metamorphic	DRC
43	Congo	40	81	13.6154	-5.5312	Precambrian	volcanic-sedimentary	DRC
44	Congo	40	47	13.5695	-5.5460	Precambrian	volcanic-sedimentary	DRC
45	Congo	5	45	13.5899	-5.6087	Precambrian	volcanic-sedimentary	DRC
46	Congo	10	39	13.5888	-5.6651	Precambrian	volcanic-sedimentary	DRC
47	Congo	15	30	13.5588	-5.7134	Precambrian	volcanic-sedimentary	DRC
48	Congo	5	15	13.4964	-5.7928	Precambrian	volcanic-sedimentary	DRC
49	Congo	-5	1143	25.4080	-10.4664	Precambrian	Sedimentary	DRC
50	Congo	-5	758	25.4485	-9.9873	Karoo	sandstone & glacial dwyka	DRC
51	Congo	-5	695	25.4885	-9.5831	Karoo	sandstone & glacial dwyka	DRC
52	Congo	-5	511	26.9716	-5.1266	Precambrian	volcanic-sedimentary	DRC
53	Congo	-5	504	26.9383	-5.0244	Karoo	sandstone & glacial dwyka	DRC
54	Congo	-5	490	26.9142	-4.8647	Karoo	sandstone & glacial dwyka	DRC
55	Congo	-5	474	26.6477	-4.5760	Karoo	sandstone & glacial dwyka	DRC
56	Congo	-5	468	25.9943	-3.9316	Karoo	sandstone & glacial dwyka	DRC
57	Congo	-5	454	25.9132	-3.2327	Precambrian	Sedimentary	DRC
58	Congo	-5	452	25.9181	-3.1650	Precambrian	Sedimentary	DRC
59	Congo	-5	413	25.5086	-0.2781	Intrusion	igneous & metamorphic	DRC
60	Congo	-5	386	25.2066	0.4931	Precambrian	Sedimentary	DRC

61	Congo	-5	253	15.1852	-4.3399	Karoo	sandstone & glacial dwyka	RC
62	Congo	-5	231	15.0385	-4.5379	Karoo	sandstone & glacial dwyka	RC
63	Congo	-5	206	14.7585	-4.8584	Karoo	sandstone & glacial dwyka	RC
64	Congo	-5	189	14.5222	-4.8590	Precambrian	Sedimentary	RC
65	Congo	-5	16	13.5161	-5.7697	Precambrian	volcanic-sedimentary	DRC
66	Congo	-1	639	25.6438	-9.2202	Precambrian	volcanic-sedimentary	DRC
67	Congo	-1	175	14.1517	-4.9516	Precambrian	Sedimentary	DRC
68	Cubango	-5	1692	16.3165	-12.7429	Precambrian	granitic / gneissic	A
69	Cubango	0	1712	16.3001	-12.7383	Precambrian	granitic / gneissic	A
70	Cubango	40	1684	16.3220	-12.7631	Precambrian	granitic / gneissic	A
71	Cubango	15	1637	16.3415	-12.8511	Recent alluvium	Recent alluvium	A
72	Cubango	20	1622	16.3612	-12.8846	Recent alluvium	Recent alluvium	A
73	Cubango	35	1595	16.3668	-13.0385	Precambrian	granitic / gneissic	A
74	Cubango	10	1541	16.4113	-13.3265	Precambrian	granitic / gneissic	A
75	Cubango	10	1516	16.4303	-13.5257	Precambrian	granitic / gneissic	A
76	Cubango	5	1472	16.3203	-14.2973	Recent alluvium	Recent alluvium	A
77	Cubango	0	1460	16.2874	-14.3745	Precambrian	granitic / gneissic	A
78	Cubango	30	1456	16.2865	-14.3862	Precambrian	granitic / gneissic	A
79	Cubango	5	1425	16.2846	-14.4728	Precambrian	granitic / gneissic	A
80	Cubango	30	1385	16.4831	-14.6336	Precambrian	volcanic-sedimentary	A
81	Cubango	20	1396	16.5005	-14.6501	Recent alluvium	Recent alluvium	A
82	Cubango	10	1355	16.5765	-14.7180	Recent alluvium	Recent alluvium	A
83	Cubango	5	1341	16.6110	-14.7860	Precambrian	volcanic-sedimentary	A
84	Cubango	10	1331	16.6342	-14.8104	Precambrian	volcanic-sedimentary	A
85	Cubango	20	1320	16.6505	-14.8538	Precambrian	volcanic-sedimentary	A
86	Cubango	0	1286	16.6526	-14.9793	Precambrian	granitic / gneissic	A
87	Cubango	20	1280	16.6705	-14.9940	Precambrian	granitic / gneissic	A
88	Cubango	5	1258	16.6964	-15.0954	Recent alluvium	Recent alluvium	A
89	Cubango	15	1206	17.2455	-15.4897	Precambrian	granitic / gneissic	A
90	Cubango	40	1185	17.3761	-15.5939	Precambrian	volcanic-sedimentary	A
91	Cubango	20	1152	17.4019	-15.6343	Precambrian	granitic / gneissic	A
92	Cubango	20	1021	21.4227	-18.0243	Precambrian	sedimentary	N
93	Cubango	20	1016	21.4740	-18.0757	Precambrian	sedimentary	N
94	Cubango	20	1009	21.5466	-18.0909	Precambrian	sedimentary	N
95	Cubango	0	1004	21.5835	-18.1142	Precambrian	sedimentary	N
96	Cubango	-1	1719	16.2660	-12.7029	Precambrian	granitic / gneissic	A

97	Cubango	-1	1648	16.3397	-12.8114	Recent alluvium	Recent alluvium	A
98	Cubango	-1	1546	16.4052	-13.2979	Precambrian	granitic / gneissic	A
99	Cubango	-1	1485	16.2889	-14.2168	Recent alluvium	Recent alluvium	A
100	Cubango	-1	1479	16.2965	-14.2692	Recent alluvium	Recent alluvium	A
101	Cubango	-1	1427	16.2714	-14.4612	Precambrian	volcanic-sedimentary	A
102	Cubango	-1	1290	16.6591	-14.9303	Precambrian	granitic / gneissic	A
103	Cubango	-1	1291	16.6600	-14.9517	Precambrian	granitic / gneissic	A
104	Cubango	-1	1262	16.7113	-15.0750	Precambrian	granitic / gneissic	A
105	Cubango	-5	1466	16.3025	-14.3508	Precambrian	granitic / gneissic	A
106	Cubango	-5	1432	16.2853	-14.4145	Precambrian	granitic / gneissic	A
107	Cubango	-5	1418	16.3079	-14.5265	Precambrian	granitic / gneissic	A
108	Cubango	-5	1365	16.5206	-14.6666	Recent alluvium	Recent alluvium	A
109	Cubango	-5	1305	16.6522	-14.8611	Precambrian	granitic / gneissic	A
110	Cubango	-5	1295	16.6549	-14.8773	Precambrian	granitic / gneissic	A
111	Cubango	-5	1261	16.6898	-15.0340	Precambrian	granitic / gneissic	A
112	Cubango	-5	1260	16.7038	-15.0497	Precambrian	granitic / gneissic	A
113	Cubango	-5	1251	16.7136	-15.1246	Recent alluvium	Recent alluvium	A
114	Cubango	-5	1245	16.7639	-15.1787	Recent alluvium	Recent alluvium	A
115	Cubango	-5	1241	16.8376	-15.2636	Recent alluvium	Recent alluvium	A
116	Cubango	-5	1231	16.9638	-15.4376	Recent alluvium	Recent alluvium	A
117	Cubango	-5	1221	17.1565	-15.4803	Precambrian	granitic / gneissic	A
118	Cubango	-5	1214	17.1917	-15.4857	Precambrian	granitic / gneissic	A
119	Cubango	-5	1213	17.2085	-15.4798	Recent alluvium	Recent alluvium	A
120	Cubango	-5	1210	17.2366	-15.4829	Recent alluvium	Recent alluvium	A
121	Cubango	-5	1197	17.2687	-15.5005	Precambrian	volcanic-sedimentary	A
122	Cubango	-5	1026	21.3410	-17.9854	Precambrian	sedimentary	N
123	Cuchi	50	1676	16.7339	-12.6858	Precambrian	granitic / gneissic	A
124	Cuchi	40	1522	16.7048	-14.1543	Precambrian	granitic / gneissic	A
125	Cuchi	20	1472	16.7350	-14.2064	Precambrian	granitic / gneissic	A
126	Cuchi	20	1445	16.7545	-14.2675	Precambrian	granitic / gneissic	A
127	Cuchi	35	1392	16.9150	-14.5821	Precambrian	granitic / gneissic	A
128	Cuchi	60	1337	16.9181	-14.6789	Precambrian	granitic / gneissic	A
129	Cuchi	60	1294	16.9009	-14.7453	Precambrian	granitic / gneissic	A
130	Cuchi	5	1209	17.2879	-15.4189	Precambrian	volcanic-sedimentary	A
131	Cuchi	-5	1259	16.9414	-15.0213	Precambrian	granitic / gneissic	A
132	Cuchi	-5	1217	17.2635	-15.3780	Precambrian	volcanic-sedimentary	A

133	Cuchi	-5	1201	17.3055	-15.4525	Recent alluvium	Recent alluvium	A
134	Cuchi	-5	1195	17.3228	-15.4732	Precambrian	granitic / gneissic	A
135	Cuchi	-1	1556	16.6350	-13.4010	Precambrian	granitic / gneissic	A
136	Cuchi	-1	1290	16.8784	-14.7795	Precambrian	granitic / gneissic	A
137	Kabompo	20	1359	25.3374	-11.8097	Precambrian	granitic / gneissic	Z (D)
138	Kabompo	70	1271	25.1748	-12.0820	Precambrian	Sedimentary	Z (D)
139	Kabompo	0	1069	24.2540	-13.5840	Precambrian	Sedimentary	Z (D)
140	Kabompo	-5	1071	24.3474	-13.4755	Precambrian	Sedimentary	Z (D)
141	Kafue	10	1115	26.6278	-14.4657	Precambrian	Sedimentary	Z (D)
142	Kafue	5	1102	26.5350	-14.4797	Precambrian	Sedimentary	Z (D)
143	Kafue	10	1086	26.0895	-14.9060	Precambrian	Sedimentary	Z (D)
144	Kafue	5	1070	26.0026	-15.0787	Intrusion	(igneous & metamorphic)	Z (D)
145	Kafue	5	1070	25.9796	-15.2544	Intrusion	(igneous & metamorphic)	Z (D)
146	Kafue	35	1062	25.9716	-15.3176	Intrusion	(igneous & metamorphic)	Z (D)
147	Kafue	5	1031	25.9963	-15.4160	Intrusion	(igneous & metamorphic)	Z (D)
148	Kafue	40	1029	26.0016	-15.7567	Precambrian	Sedimentary	Z (D)
149	Kafuel	15	978	28.4188	-15.8053	Precambrian	granitic / gneissic	Z (D)
150	Kafue	20	831	28.4448	-15.8479	Precambrian	granitic / gneissic	Z (D)
151	Kafue	60	665	28.4803	-15.8475	Precambrian	granitic / gneissic	Z (D)
152	Kafue	70	507	28.5355	-15.8722	Precambrian	Sedimentary	Z (D)
153	Kafue	-5	1091	26.1881	-14.8012	Intrusion	(igneous & metamorphic)	Z (D)
154	Kafue	-5	1070	25.9659	-15.1372	Intrusion	(igneous & metamorphic)	Z (D)
155	Kalungwishi	30	1440	30.1146	-9.8927	Precambrian	volcanic-sedimentary	Z (D)
156	Kalungwishi	80	1361	29.8626	-9.7967	Precambrian	volcanic-sedimentary	Z (D)
157	Kalungwishi	25	1317	29.8686	-9.7790	Precambrian	volcanic-sedimentary	Z (D)
158	Kalungwishi	20	1263	29.8269	-9.7456	Precambrian	volcanic-sedimentary	Z (D)
159	Kalungwishi	10	1239	29.8142	-9.7140	Precambrian	volcanic-sedimentary	Z (D)
160	Kalungwishi	20	1187	29.4323	-9.5384	Precambrian	volcanic-sedimentary	Z (D)
161	Kalungwishi	50	1164	29.3875	-9.5423	Precambrian	volcanic-sedimentary	Z (D)
162	Kalungwishi	40	1119	29.3515	-9.5248	Precambrian	volcanic-sedimentary	Z (D)
163	Kalungwishi	80	1006	29.3004	-9.2038	Precambrian	Sedimentary	Z (D)
164	Kasai	10	1177	20.1073	-11.2422	Intrusion	igneous & metamorphic	A
165	Kasai	5	1075	21.3870	-11.2312	Kalahari	sand & silcrete	A
166	Kasai	10	1046	21.7529	-10.8246	Precambrian	granitic / gneissic	A
167	Kasai	10	1028	21.7688	-10.8071	Precambrian	granitic / gneissic	A
168	Kasai	5	1018	21.8088	-10.6243	Precambrian	granitic / gneissic	A

169	Kasai	15	993	22.2157	-10.6073	Precambrian	granitic / gneissic	A
170	Kasai	10	987	22.2711	-10.6246	Precambrian	granitic / gneissic	A
171	Kasai	5	976	22.3088	-10.5543	Precambrian	granitic / gneissic	A
172	Kasai	5	973	22.2841	-10.4947	Precambrian	granitic / gneissic	A
173	Kasai	5	939	21.8720	-9.6260	Precambrian	volcanic-sedimentary	A
174	Kasai	5	930	21.8093	-9.3723	Precambrian	granitic / gneissic	A
175	Kasai	5	923	21.8078	-9.3317	Precambrian	granitic / gneissic	A
176	Kasai	10	912	21.8568	-9.2116	Precambrian	granitic / gneissic	A
177	Kasai	5	905	21.8596	-9.1929	Precambrian	granitic / gneissic	A
178	Kasai	10	899	21.8500	-9.1455	Precambrian	granitic / gneissic	A
179	Kasai	5	888	21.8399	-9.1062	Precambrian	granitic / gneissic	A
180	Kasai	5	884	21.8465	-9.0246	Precambrian	granitic / gneissic	A
181	Kasai	5	867	21.8872	-8.8016	Precambrian	granitic / gneissic	A
182	Kasai	20	842	21.9026	-8.6825	Precambrian	granitic / gneissic	A
183	Kasai	20	829	21.9250	-8.6073	Precambrian	granitic / gneissic	A
184	Kasai	5	803	21.9373	-8.5351	Precambrian	granitic / gneissic	A
185	Kasai	30	774	21.7775	-7.8129	Precambrian	granitic / gneissic	A
186	Kasai	5	745	21.8437	-7.6165	Precambrian	granitic / gneissic	A
187	Kasai	20	727	21.8072	-7.3072	Precambrian	granitic / gneissic	A
188	Kasai	10	682	21.6677	-7.0852	Precambrian	granitic / gneissic	DRC
189	Kasai	10	655	21.6281	-7.0493	Precambrian	granitic / gneissic	DRC
190	Kasai	20	632	21.5956	-7.0303	Precambrian	granitic / gneissic	DRC
191	Kasai	5	596	21.4618	-6.8871	Precambrian	granitic / gneissic	DRC
192	Kasai	25	571	21.4219	-6.8440	Precambrian	granitic / gneissic	DRC
193	Kasai	5	548	21.3737	-6.8194	Precambrian	granitic / gneissic	DRC
194	Kasai	15	522	21.1629	-6.6755	Precambrian	granitic / gneissic	DRC
195	Kasai	10	478	20.9317	-6.5412	Precambrian	granitic / gneissic	DRC
196	Kasai	10	466	20.8932	-6.5058	Precambrian	granitic / gneissic	DRC
197	Kasai	15	452	20.8486	-6.4966	Precambrian	granitic / gneissic	DRC
198	Kasai	5	416	20.8847	-5.5961	Precambrian	granitic / gneissic	DRC
199	Kasai	15	400	20.9100	-5.5327	Precambrian	granitic / gneissic	DRC
200	Kasai	10	400	20.9541	-5.4787	Precambrian	granitic / gneissic	DRC
201	Kasai	-5	1032	21.7625	-10.7651	Precambrian	granitic / gneissic	A
202	Kasai	-5	1008	21.9577	-10.6109	Precambrian	granitic / gneissic	A
203	Kasai	-5	931	21.8037	-9.4296	Precambrian	granitic / gneissic	A
204	Kasai	-5	875	21.8495	-8.9721	Precambrian	granitic / gneissic	A

205	Kasai	-5	697	21.7264	-7.1962	Precambrian	granitic / gneissic	DRC
206	Kasai	-5	612	21.5415	-6.9731	Precambrian	granitic / gneissic	DRC
207	Kasai	-5	491	21.0689	-6.6111	Precambrian	granitic / gneissic	DRC
208	Kasai	-5	426	20.8217	-5.7387	Precambrian	granitic / gneissic	DRC
209	Kasai	-5	434	20.8533	-5.6862	Precambrian	granitic / gneissic	DRC
210	Kasai	-1	786	21.8381	-8.1157	Precambrian	granitic / gneissic	A
211	Kwango	90	1188	18.7748	-11.1594	Kalahari	sand & silcrete	A
212	Kwango	20	944	18.6216	-10.1157	Karoo	sandstone & glacial dwyka	A
213	Kwango	20	929	18.6603	-10.0976	Karoo	sandstone & glacial dwyka	A
214	Kwango	20	870	18.2228	-9.2874	Precambrian	granitic / gneissic	A
215	Kwango	20	856	18.1360	-9.2665	Precambrian	volcanic-sedimentary	A
216	Kwango	5	822	18.0374	-9.1605	Precambrian	volcanic-sedimentary	A
217	Kwango	5	805	18.0398	-9.0381	Precambrian	granitic / gneissic	A
218	Kwango	5	801	18.0312	-9.0159	Precambrian	granitic / gneissic	A
219	Kwango	5	795	18.0163	-8.9982	Precambrian	granitic / gneissic	A
220	Kwango	15	798	18.0158	-8.9806	Precambrian	granitic / gneissic	A
221	Kwango	45	756	18.0107	-8.8856	Precambrian	volcanic-sedimentary	A
222	Kwango	30	723	17.9466	-8.8060	Precambrian	volcanic-sedimentary	A
223	Kwango	25	668	17.9090	-8.6778	Precambrian	volcanic-sedimentary	A
224	Kwango	10	646	17.8697	-8.6035	Precambrian	volcanic-sedimentary	A
225	Kwango	5	624	17.7560	-8.5199	Karoo	sandstone & glacial dwyka	A
226	Kwango	75	588	17.3179	-7.7162	Precambrian	granitic / gneissic	A
227	Kwango	50	460	17.2723	-7.6152	Precambrian	granitic / gneissic	A
228	Kwango	-5	811	18.0601	-9.0719	Precambrian	volcanic-sedimentary	A
229	Luapula	15	1138	29.2117	-12.3738	Precambrian	Sedimentary	DRC
230	Luapula	20	1114	29.1214	-12.3940	Precambrian	Sedimentary	DRC
231	Luapula	15	1087	29.0800	-12.3866	Precambrian	Sedimentary	DRC
232	Luapula	15	1067	29.0354	-12.3524	Precambrian	Sedimentary	DRC
233	Luapula	20	1033	28.4532	-11.3129	Precambrian	Sedimentary	DRC
234	Luapula	10	1011	28.6254	-10.7156	Intrusion	igneous & metamorphic	DRC
235	Luapula	80	997	28.6890	-10.6785	Intrusion	igneous & metamorphic	DRC
236	Luena	40	1278	19.9139	-11.8028	Kalahari	sand & silcrete	A
237	Luena	15	1227	19.9637	-11.8024	Kalahari	sand & silcrete	A
238	Luena	10	1218	19.9955	-11.7984	Kalahari	sand & silcrete	A
239	Luena	10	1209	20.0313	-11.7785	Kalahari	sand & silcrete	A
240	Luena	10	1190	20.0662	-11.7382	Kalahari	sand & silcrete	A

241	Luena	5	1154	20.3225	-11.7623	Kalahari	sand & silcrete	A
242	Luena	10	1140	20.4365	-11.9154	Intrusion	igneous & metamorphic	A
243	Luena	0	1061	22.5012	-12.4688	Recent alluvium	Recent alluvium	A
244	Luena	-5	1177	20.1198	-11.7230	Kalahari	sand & silcrete	A
245	Luena	-5	1177	20.1570	-11.7205	Kalahari	sand & silcrete	A
246	Lufira	90	1118	27.2443	-10.7524	Precambrian	Sedimentary	DRC
247	Lufira	50	1014	27.2687	-10.7221	Precambrian	Sedimentary	DRC
248	Lufira	10	1139	26.8771	-11.2000	Precambrian	Sedimentary	DRC
249	Lufira	50	992	27.2809	-10.7184	Precambrian	Sedimentary	DRC
250	Lufira	15	909	27.3984	-10.6072	Precambrian	Sedimentary	DRC
251	Lufira	45	867	27.0404	-9.5169	Precambrian	Sedimentary	DRC
252	Lufira	20	834	26.9752	-9.4538	Precambrian	Sedimentary	DRC
253	Lufira	5	813	26.9208	-9.3638	Precambrian	Sedimentary	DRC
254	Lufira	-5	1202	26.7189	-11.5376	Precambrian	Sedimentary	DRC
255	Lufira	-5	943	27.3182	-10.6943	Precambrian	Sedimentary	DRC
256	Lufira	-5	929	27.3720	-10.6750	Precambrian	Sedimentary	DRC
257	Lufupa	15	1090	24.4966	-10.4297	Precambrian	granitic / gneissic	DRC
258	Lufupa	25	1061	24.5217	-10.3922	Precambrian	granitic / gneissic	DRC
259	Lufupa	25	976	24.6076	-10.3459	Precambrian	volcanic-sedimentary	DRC
260	Lufupa	25	943	24.6156	-10.3524	Precambrian	volcanic-sedimentary	DRC
261	Lufupa	30	921	24.6510	-10.3314	Precambrian	volcanic-sedimentary	DRC
262	Lufupa	15	792	24.9365	-9.6039	Precambrian	volcanic-sedimentary	DRC
263	Lufupa	10	776	25.0278	-9.5904	Precambrian	volcanic-sedimentary	DRC
264	Lufupa	0	734	25.5185	-9.0862	Precambrian	volcanic-sedimentary	DRC
265	Lufupa	40	721	25.5306	-9.0819	Precambrian	volcanic-sedimentary	DRC
266	Lufupa	0	682	25.5673	-9.0848	Precambrian	volcanic-sedimentary	DRC
267	Lufupa	0	665	25.5839	-9.0985	Precambrian	volcanic-sedimentary	DRC
268	Lufupa	0	661	25.5984	-9.1049	Precambrian	volcanic-sedimentary	DRC
269	Lufupa	0	652	25.6058	-9.1217	Precambrian	volcanic-sedimentary	DRC
270	Lufupa	0	664	25.6150	-9.1312	Precambrian	volcanic-sedimentary	DRC
271	Lufupa	5	639	25.6211	-9.1514	Precambrian	volcanic-sedimentary	DRC
272	Lufupa	-1	728	25.4734	-9.0848	Precambrian	volcanic-sedimentary	DRC
273	Lufupa	-5	907	24.7500	-10.2404	Precambrian	volcanic-sedimentary	DRC
274	Lufupa	-5	887	24.7481	-10.1633	Precambrian	volcanic-sedimentary	DRC
275	Lufupa	-5	811	24.8214	-9.7544	Precambrian	volcanic-sedimentary	DRC
276	Lufupa	-1	803	24.8461	-9.7679	Precambrian	volcanic-sedimentary	DRC

277	Lufupa	-1	800	24.8671	-9.7330	Precambrian	volcanic-sedimentary	DRC
278	Lukuga	5	771	28.9590	-5.9014	Precambrian	granitic / gneissic	DRC
279	Lukuga	5	758	28.8543	-5.8829	Karoo	sandstone & glacial dwyka	DRC
280	Lukuga	15	703	28.3947	-5.9238	Intrusion	igneous & metamorphic	DRC
281	Lukuga	15	688	28.3582	-5.9168	Intrusion	igneous & metamorphic	DRC
282	Lukuga	15	670	28.2891	-5.9035	Intrusion	igneous & metamorphic	DRC
283	Lukuga	10	642	28.1698	-5.8733	Intrusion	igneous & metamorphic	DRC
284	Lukuga	15	612	28.0192	-5.7124	Intrusion	igneous & metamorphic	DRC
285	Lukuga	0	783	29.0745	-5.9214	Karoo	sandstone & glacial dwyka	DRC
286	Lulua	10	1109	23.1338	-10.8790	Precambrian	granitic / gneissic	DRC
287	Lulua	40	1022	22.7981	-10.7603	Precambrian	granitic / gneissic	DRC
288	Lulua	5	987	22.8990	-10.6828	Precambrian	granitic / gneissic	DRC
289	Lulua	10	975	22.8475	-10.6162	Precambrian	granitic / gneissic	DRC
290	Lulua	30	943	22.8575	-10.4424	Precambrian	granitic / gneissic	DRC
291	Lulua	10	919	22.8610	-10.3813	Precambrian	granitic / gneissic	DRC
292	Lulua	20	880	22.6361	-9.2274	Precambrian	granitic / gneissic	DRC
293	Lulua	30	872	22.6117	-9.1812	Precambrian	granitic / gneissic	DRC
294	Lulua	20	723	22.4761	-6.5882	Precambrian	granitic / gneissic	DRC
295	Lulua	5	702	22.4597	-6.5489	Precambrian	granitic / gneissic	DRC
296	Lulua	10	692	22.4366	-6.5207	Precambrian	granitic / gneissic	DRC
297	Lulua	15	686	22.4180	-6.4725	Precambrian	granitic / gneissic	DRC
298	Lulua	20	644	22.4494	-6.3440	Precambrian	granitic / gneissic	DRC
299	Lulua	20	597	22.4693	-6.2214	Precambrian	granitic / gneissic	DRC
300	Lulua	5	557	22.3914	-6.0048	Precambrian	granitic / gneissic	DRC
301	Lulua	10	451	22.0074	-5.4922	Precambrian	granitic / gneissic	DRC
302	Lulua	20	439	21.9897	-5.4784	Precambrian	granitic / gneissic	DRC
303	Lulua	10	430	21.9709	-5.4405	Precambrian	granitic / gneissic	DRC
304	Lulua	-5	913	22.8158	-10.3344	Precambrian	granitic / gneissic	DRC
305	Lulua	-5	845	22.5553	-8.8807	Precambrian	granitic / gneissic	DRC
306	Lulua	-5	799	22.5962	-7.7168	Intrusion	igneous & metamorphic	DRC
307	Lulua	-5	752	22.5330	-6.6945	Precambrian	granitic / gneissic	DRC
308	Lulua	-5	742	22.4960	-6.6981	Precambrian	granitic / gneissic	DRC
309	Lulua	-5	666	22.4140	-6.4274	Precambrian	granitic / gneissic	DRC
310	Lulua	-5	571	22.3924	-6.0970	Precambrian	granitic / gneissic	DRC
311	Lulua	-5	485	22.1834	-5.8009	Precambrian	granitic / gneissic	DRC
312	Lulua	-5	475	22.1474	-5.7589	Precambrian	granitic / gneissic	DRC

313	Lulua	-1	813	22.6718	-7.8501	Intrusion	igneous & metamorphic	DRC
314	Lulua	-1	781	22.6997	-7.4199	Intrusion	igneous & metamorphic	DRC
315	Lulua	-1	400	21.5446	-5.3406	Precambrian	granitic / gneissic	DRC
316	Luvua	0	930	28.8459	-8.4577	Precambrian	Sedimentary	DRC
317	Luvua	10	928	28.8380	-8.4531	Precambrian	Sedimentary	DRC
318	Luvua	5	885	28.7986	-8.3624	Precambrian	Sedimentary	DRC
319	Luvua	15	873	28.8615	-8.2265	Precambrian	Sedimentary	DRC
320	Luvua	50	852	28.8125	-8.1523	Precambrian	Sedimentary	DRC
321	Luvua	10	785	28.7216	-8.0014	Precambrian	volcanic-sedimentary	DRC
322	Luvua	5	755	28.6947	-7.9568	Precambrian	volcanic-sedimentary	DRC
323	Luvua	20	732	28.6818	-7.9274	Precambrian	volcanic-sedimentary	DRC
324	Luvua	20	719	28.6185	-7.8805	Precambrian	volcanic-sedimentary	DRC
325	Luvua	20	703	28.4426	-7.8733	Precambrian	Sedimentary	DRC
326	Luvua	20	701	28.4166	-7.8553	Precambrian	Sedimentary	DRC
327	Luvua	20	618	28.1023	-7.6403	Intrusion	igneous & metamorphic	DRC
328	Luvua	30	589	28.0870	-7.4374	Precambrian	volcanic-sedimentary	DRC
329	Luvua	10	584	28.0773	-7.4198	Precambrian	volcanic-sedimentary	DRC
330	Luvua	5	578	28.0504	-7.3814	Intrusion	igneous & metamorphic	DRC
331	Luvua	-5	711	28.5592	-7.9323	Precambrian	volcanic-sedimentary	DRC
332	Luvua	-5	665	28.3198	-7.8039	Precambrian	volcanic-sedimentary	DRC
333	Luvua	-5	654	28.2219	-7.7505	Intrusion	igneous & metamorphic	DRC
334	Luvua	-5	638	28.1530	-7.6921	Intrusion	igneous & metamorphic	DRC
335	Luvua	-5	619	28.1007	-7.6422	Intrusion	igneous & metamorphic	DRC
336	Wamba	10	909	18.3509	-8.4951	Karoo	sandstone & glacial dwyka	A
337	Wamba	25	893	18.3171	-8.4606	Karoo	sandstone & glacial dwyka	A
338	Wamba	15	856	18.2906	-8.4357	Precambrian	granitic / gneissic	A
339	Wamba	20	843	18.2856	-8.4276	Precambrian	granitic / gneissic	A
340	Wamba	50	834	18.2630	-8.4052	Precambrian	granitic / gneissic	A
341	Wamba	50	782	18.2534	-8.3883	Karoo	sandstone & glacial dwyka	A
342	Wamba	20	730	18.1973	-8.3640	Karoo	sandstone & glacial dwyka	A
343	Wamba	10	613	17.8144	-7.4907	Precambrian	granitic / gneissic	DRC
344	Wamba	10	541	17.3860	-6.4526	Karoo	sandstone & glacial dwyka	DRC
345	Wamba	5	477	17.1152	-5.9181	Karoo	sandstone & glacial dwyka	DRC
346	Wamba	5	397	16.9477	-5.0683	Karoo	sandstone & glacial dwyka	DRC
347	Wamba	-5	712	18.1630	-8.2978	Karoo	sandstone & glacial dwyka	A
348	Wamba	-5	631	17.9071	-7.5702	Precambrian	granitic / gneissic	DRC

349	Wamba	-5	413	16.9503	-5.4116	Karoo	sandstone & glacial dwyka	DRC
350	Wamba	-5	414	16.9488	-5.3849	Karoo	sandstone & glacial dwyka	DRC
351	Wamba	-1	640	17.9293	-7.5833	Precambrian	granitic / gneissic	DRC
352	Wamba	-1	506	17.2651	-6.3135	Karoo	sandstone & glacial dwyka	DRC
353	Wamba	-1	421	16.9532	-5.3723	Karoo	sandstone & glacial dwyka	DRC
354	Wamba	-1	410	16.9118	-5.3205	Karoo	sandstone & glacial dwyka	DRC
355	Wamba	-1	405	16.9240	-5.3017	Karoo	sandstone & glacial dwyka	DRC
356	Wamba	-1	401	16.9211	-5.2213	Karoo	sandstone & glacial dwyka	DRC
357	Zambezi	5	1046	22.6681	-13.0717	Kalahari	sand & silcrete	Z (D)
358	Zambezi	5	1044	22.6894	-13.1050	Kalahari	sand & silcrete	Z (D)
359	Zambezi	5	992	23.4822	-16.5570	Recent alluvium	Recent alluvium	Z (D)
360	Zambezi	5	989	23.5265	-16.6086	Recent alluvium	Recent alluvium	Z (D)
361	Zambezi	10	984	23.5681	-16.6467	Recent alluvium	Recent alluvium	Z (D)
362	Zambezi	5	980	23.5699	-16.6505	Recent alluvium	Recent alluvium	Z (D)
363	Zambezi	5	919	25.3726	-17.8444	Intrusion	igneous & metamorphic	Z (D)
364	Zambezi	5	901	25.6657	-17.8152	Intrusion	igneous & metamorphic	Z (D)
365	Zambezi	50	865	25.8594	-17.9255	Intrusion	igneous & metamorphic	Z (D)
366	Zambezi	-5	1058	22.6167	-12.6833	Kalahari	sand & silcrete	A
367	Zambezi	-5	1056	22.7196	-12.9929	Precambrian	granitic / gneissic	A
368	Zambezi	-5	995	23.3889	-16.4505	Recent alluvium	Recent alluvium	Z (D)
369	Zambezi	-5	991	23.4565	-16.5322	Recent alluvium	Recent alluvium	Z (D)
370	Zambezi	-5	967	23.7306	-16.7634	Kalahari	sand & silcrete	Z (D)
371	Zambezi	-5	967	23.7349	-16.7835	Kalahari	sand & silcrete	Z (D)
372	Zambezi	-5	953	24.1586	-17.3093	Kalahari	sand & silcrete	Z (D)
373	Zambezi	-5	948	24.1674	-17.3716	Kalahari	sand & silcrete	Z (D)
374	Zambezi	-5	943	24.2144	-17.4196	Kalahari	sand & silcrete	Z (D)
375	Zambezi	-5	937	24.2498	-17.4740	Kalahari	sand & silcrete	Z (D)
376	Zambezi	-5	927	25.1871	-17.7652	Recent alluvium	Recent alluvium	Z (D)
377	Zambezi	-5	914	25.4604	-17.8445	Intrusion	igneous & metamorphic	Z (D)
378	Zambezi	-5	912	25.4862	-17.8501	Intrusion	igneous & metamorphic	Z (D)
379	Zambezi	-5	909	25.5352	-17.8511	Intrusion	igneous & metamorphic	Z (D)
380	Zambezi	-5	904	25.5914	-17.8382	Intrusion	igneous & metamorphic	Z (D)

Section 7.3

Table A7.3: The causes and confidence scores of the identified knickpoints of south–central Africa. The assigned causes should be considered as a first order classification and may undergo substantial revision as better geological mapping is done in the region. A confidence score of 1 = highly confident; 3 – moderately confident and; 5 – limited confidence. Abbreviations for maps used are: A– Angola; DRC– Democratic Republic of Congo, N– Namibia; RC– Republic of Congo; Z– Zambia; D– digital

N$^{o.}$	River	Category	Elevation (m.a.s.l)	Longitude	Latitude	Most likely cause	Confidence score	Map
1	Chambeshi	10	1422	31.4475	-9.4389	Fault	1	Z (D)
2	Chambeshi	15	1429	31.4577	-9.4683	Lithology	1	Z (D)
3	Chambeshi	50	1397	31.4622	-9.4753	Lithology	1	Z (D)
4	Congo	15	1287	25.4620	-10.4994	Lithology	3	DRC
5	Congo	25	1090	25.4269	-10.3243	Lithology	1	DRC
6	Congo	80	1231	25.4393	-10.4950	Lithology	1	DRC
7	Congo	30	1147	25.4447	-10.4036	Lithology	1	DRC
8	Congo	30	1019	25.4491	-10.2539	Fault	1	DRC
9	Congo	50	999	25.4358	-10.2326	Fault	3	DRC
10	Congo	0	890	25.4072	-10.1851	Fault	3	DRC
11	Congo	90	862	25.4101	-10.1253	Fault	3	DRC
12	Congo	10	748	25.5080	-9.9343	fault	5	DRC
13	Congo	15	718	25.5361	-9.7682	Lithology change	5	DRC
14	Congo	20	675	25.5028	-9.4697	Lithology change	1	DRC
15	Congo	15	679	25.5196	-9.4058	Lithology change	1	DRC
16	Congo	5	653	25.5374	-9.3544	Lithology change	3	DRC
17	Congo	5	625	25.7141	-9.3062	Lithology	1	DRC
18	Congo	10	605	25.7803	-9.2349	Lithology	1	DRC
19	Congo	30	591	25.8097	-9.1965	Lithology	1	DRC
20	Congo	5	541	27.0144	-5.3600	Lithology change	1	DRC
21	Congo	10	530	27.0184	-5.3099	Lithology change	3	DRC
22	Congo	10	530	26.9934	-5.2916	Lithology change	3	DRC
23	Congo	15	500	26.9610	-4.9793	Lithology change	1	DRC
24	Congo	10	478	26.7702	-4.6253	other	5	DRC
25	Congo	5	440	25.7106	-2.1362	other	5	DRC

26	Congo	5	414	25.4596	-0.3563	Lithology	1	DRC
27	Congo	10	404	25.5188	0.1874	Fault		DRC
28	Congo	5	398	25.4851	0.2546	Fault	3	DRC
29	Congo	5	389	25.2734	0.4386	other	5	DRC
30	Congo	5	255	15.2272	-4.3172	other	5	RC
31	Congo	10	254	15.1760	-4.3687	other	5	RC
32	Congo	10	239	15.1359	-4.4310	other	5	RC
33	Congo	5	220	14.8694	-4.7504	fault	5	RC
34	Congo	10	210	14.8140	-4.8360	fault	3	RC
35	Congo	5	203	14.7059	-4.8997	fault	3	RC
36	Congo	5	196	14.6570	-4.9193	fault	3	RC
37	Congo	5	187	14.4371	-4.8776	fault	5	RC
38	Congo	5	157	13.6287	-5.2977	Lithology	3	DRC
39	Congo	5	155	13.5493	-5.3606	Lithology change	5	DRC
40	Congo	5	143	13.5577	-5.4143	Lithology	1	DRC
41	Congo	20	120	13.6104	-5.4770	Lithology	1	DRC
42	Congo	40	81	13.6345	-5.5317	Lithology	5	DRC
43	Congo	40	81	13.6154	-5.5312	Lithology	3	DRC
44	Congo	40	47	13.5695	-5.5460	Lithology change	3	DRC
45	Congo	5	45	13.5899	-5.6087	fault	1	DRC
46	Congo	10	39	13.5888	-5.6651	fault	1	DRC
47	Congo	15	30	13.5588	-5.7134	fault	1	DRC
48	Congo	5	15	13.4964	-5.7928	Lithology	1	DRC
49	Congo	-5	1143	25.4080	-10.4664	Lithology	1	DRC
50	Congo	-5	758	25.4485	-9.9873	Lithology change	5	DRC
51	Congo	-5	695	25.4885	-9.5831	Lithology	1	DRC
52	Congo	-5	511	26.9716	-5.1266	Lithology change	3	DRC
53	Congo	-5	504	26.9383	-5.0244	other	5	DRC
54	Congo	-5	490	26.9142	-4.8647	other	5	DRC
55	Congo	-5	474	26.6477	-4.5760	other	5	DRC
56	Congo	-5	468	25.9943	-3.9316	other	5	DRC
57	Congo	-5	454	25.9132	-3.2327	Lithology change	3	DRC
58	Congo	-5	452	25.9181	-3.1650	Lithology change	3	DRC
59	Congo	-5	413	25.5086	-0.2781	Lithology change	3	DRC
60	Congo	-5	386	25.2066	0.4931	Lithology change	3	DRC
61	Congo	-5	253	15.1852	-4.3399	other	5	RC

62	Congo	-5	231	15.0385	-4.5379	fault	3	RC
63	Congo	-5	206	14.7585	-4.8584	fault	3	RC
64	Congo	-5	189	14.5222	-4.8590	fault	1	RC
65	Congo	-5	16	13.5161	-5.7697	Lithology	1	DRC
66	Congo	-1	639	25.6438	-9.2202	Lithology change	1	DRC
67	Congo	-1	175	14.1517	-4.9516	Fault	3	DRC
68	Cubango	-5	1692	16.3165	-12.7429	Lithology change	3	A
69	Cubango	0	1712	16.3001	-12.7383	Lithology change	3	A
70	Cubango	40	1684	16.3220	-12.7631	Lithology	1	A
71	Cubango	15	1637	16.3415	-12.8511	other	5	A
72	Cubango	20	1622	16.3612	-12.8846	other	5	A
73	Cubango	35	1595	16.3668	-13.0385	Lithology change	1	A
74	Cubango	10	1541	16.4113	-13.3265	Lithology change	1	A
75	Cubango	10	1516	16.4303	-13.5257	Fault	3	A
76	Cubango	5	1472	16.3203	-14.2973	Fault	1	A
77	Cubango	0	1460	16.2874	-14.3745	Lithology	1	A
78	Cubango	30	1456	16.2865	-14.3862	Lithology	1	A
79	Cubango	5	1425	16.2846	-14.4728	Lithology change	1	A
80	Cubango	30	1385	16.4831	-14.6336	Lithology change	1	A
81	Cubango	20	1396	16.5005	-14.6501	Fault	3	A
82	Cubango	10	1355	16.5765	-14.7180	other	5	A
83	Cubango	5	1341	16.6110	-14.7860	Lithology change	1	A
84	Cubango	10	1331	16.6342	-14.8104	Lithology change	1	A
85	Cubango	20	1320	16.6505	-14.8538	Lithology change	1	A
86	Cubango	0	1286	16.6526	-14.9793	Lithology	1	A
87	Cubango	20	1280	16.6705	-14.9940	Lithology change	1	A
88	Cubango	5	1258	16.6964	-15.0954	other	5	A
89	Cubango	15	1206	17.2455	-15.4897	Lithology change	3	A
90	Cubango	40	1185	17.3761	-15.5939	Fault	1	A
91	Cubango	20	1152	17.4019	-15.6343	Lithology change	1	A
92	Cubango	20	1021	21.4227	-18.0243	Lithology	3	N
93	Cubango	20	1016	21.4740	-18.0757	Lithology	3	N
94	Cubango	20	1009	21.5466	-18.0909	Lithology	3	N
95	Cubango	0	1004	21.5835	-18.1142	Lithology	3	N
96	Cubango	-1	1719	16.2660	-12.7029	Lithology	3	A
97	Cubango	-1	1648	16.3397	-12.8114	other	5	A

98	Cubango	-1	1546	16.4052	-13.2979	Lithology change	1	A
99	Cubango	-1	1485	16.2889	-14.2168	other	5	A
100	Cubango	-1	1479	16.2965	-14.2692	other	5	A
101	Cubango	-1	1427	16.2714	-14.4612	Lithology	1	A
102	Cubango	-1	1290	16.6591	-14.9303	Lithology change	1	A
103	Cubango	-1	1291	16.6600	-14.9517	Lithology change	3	A
104	Cubango	-1	1262	16.7113	-15.0750	Lithology change	3	A
105	Cubango	-5	1466	16.3025	-14.3508	Lithology change	3	A
106	Cubango	-5	1432	16.2853	-14.4145	Lithology change	3	A
107	Cubango	-5	1418	16.3079	-14.5265	Fault	3	A
108	Cubango	-5	1365	16.5206	-14.6666	other	5	A
109	Cubango	-5	1305	16.6522	-14.8611	Lithology change	1	A
110	Cubango	-5	1295	16.6549	-14.8773	Lithology change	1	A
111	Cubango	-5	1261	16.6898	-15.0340	Lithology change	1	A
112	Cubango	-5	1260	16.7038	-15.0497	Lithology	1	A
113	Cubango	-5	1251	16.7136	-15.1246	other	5	A
114	Cubango	-5	1245	16.7639	-15.1787	other	5	A
115	Cubango	-5	1241	16.8376	-15.2636	other	5	A
116	Cubango	-5	1231	16.9638	-15.4376	fault	5	A
117	Cubango	-5	1221	17.1565	-15.4803	Lithology change	3	A
118	Cubango	-5	1214	17.1917	-15.4857	Lithology change	3	A
119	Cubango	-5	1213	17.2085	-15.4798	fault	3	A
120	Cubango	-5	1210	17.2366	-15.4829	fault	3	A
121	Cubango	-5	1197	17.2687	-15.5005	Fault	3	A
122	Cubango	-5	1026	21.3410	-17.9854	Lithology	1	N
123	Cuchi	50	1676	16.7339	-12.6858	Lithology change	1	A
124	Cuchi	40	1522	16.7048	-14.1543	Lithology change	3	A
125	Cuchi	20	1472	16.7350	-14.2064	Lithology	3	A
126	Cuchi	20	1445	16.7545	-14.2675	Lithology	3	A
127	Cuchi	35	1392	16.9150	-14.5821	Fault	1	A
128	Cuchi	60	1337	16.9181	-14.6789	Lithology change	1	A
129	Cuchi	60	1294	16.9009	-14.7453	Fault	1	A
130	Cuchi	5	1209	17.2879	-15.4189	Lithology change	3	A
131	Cuchi	-5	1259	16.9414	-15.0213	Lithology change	1	A
132	Cuchi	-5	1217	17.2635	-15.3780	Lithology	3	A
133	Cuchi	-5	1201	17.3055	-15.4525	Fault	1	A

134	Cuchi	-5	1195	17.3228	-15.4732	Lithology change	3	A
135	Cuchi	-1	1556	16.6350	-13.4010	Lithology change	3	A
136	Cuchi	-1	1290	16.8784	-14.7795	Lithology change	3	A
137	Kabompo	20	1359	25.3374	-11.8097	Lithology	1	Z (D)
138	Kabompo	70	1271	25.1748	-12.0820	fault	1	Z (D)
139	Kabompo	0	1069	24.2540	-13.5840	Lithology	5	Z (D)
140	Kabompo	-5	1071	24.3474	-13.4755	Lithology	3	Z (D)
141	Kafue	10	1115	26.6278	-14.4657	Lithology	3	Z (D)
142	Kafue	5	1102	26.5350	-14.4797	Lithology change	3	Z (D)
143	Kafue	10	1086	26.0895	-14.9060	Lithology change	3	Z (D)
144	Kafue	5	1070	26.0026	-15.0787	Lithology	1	Z (D)
145	Kafue	5	1070	25.9796	-15.2544	Lithology	1	Z (D)
146	Kafue	35	1062	25.9716	-15.3176	Lithology	1	Z (D)
147	Kafue	5	1031	25.9963	-15.4160	Lithology	1	Z (D)
148	Kafue	40	1029	26.0016	-15.7567	Dam wall	1	Z (D)
149	Kafue	15	978	28.4188	-15.8053	Dam wall	1	Z (D)
150	Kafue	20	831	28.4448	-15.8479	Lithology	1	Z (D)
151	Kafue	60	665	28.4803	-15.8475	Lithology	1	Z (D)
152	Kafue	70	507	28.5355	-15.8722	UNKOWN	5	Z (D)
153	Kafue	-5	1091	26.1881	-14.8012	Lithology change	3	Z (D)
154	Kafue	-5	1070	25.9659	-15.1372	Lithology	1	Z (D)
155	Kalungwishi	30	1440	30.1146	-9.8927	Lithology	3	Z (D)
156	Kalungwishi	80	1361	29.8626	-9.7967	fault	3	Z (D)
157	Kalungwishi	25	1317	29.8686	-9.7790	fault	3	Z (D)
158	Kalungwishi	20	1263	29.8269	-9.7456	fault	3	Z (D)
159	Kalungwishi	10	1239	29.8142	-9.7140	other	1	Z (D)
160	Kalungwishi	20	1187	29.4323	-9.5384	Lithology	1	Z (D)
161	Kalungwishi	50	1164	29.3875	-9.5423	Lithology	1	Z (D)
162	Kalungwishi	40	1119	29.3515	-9.5248	Lithology change	1	Z (D)
163	Kalungwishi	80	1006	29.3004	-9.2038	Lithology	1	Z (D)
164	Kasai	10	1177	20.1073	-11.2422	Lithology change	3	A
165	Kasai	5	1075	21.3870	-11.2312	Lithology change	3	A
166	Kasai	10	1046	21.7529	-10.8246	Lithology	1	A
167	Kasai	10	1028	21.7688	-10.8071	Lithology	1	A
168	Kasai	5	1018	21.8088	-10.6243	Lithology	1	A
169	Kasai	15	993	22.2157	-10.6073	Lithology	1	A

170	Kasai	10	987	22.2711	-10.6246	Lithology	1	A
171	Kasai	5	976	22.3088	-10.5543	Lithology	1	A
172	Kasai	5	973	22.2841	-10.4947	Lithology	11	A
173	Kasai	5	939	21.8720	-9.6260	Lithology	1	A
174	Kasai	5	930	21.8093	-9.3723	Lithology	1	A
175	Kasai	5	923	21.8078	-9.3317	Lithology	1	A
176	Kasai	10	912	21.8568	-9.2116	Lithology	1	A
177	Kasai	5	905	21.8596	-9.1929	Lithology	1	A
178	Kasai	10	899	21.8500	-9.1455	Lithology	1	A
179	Kasai	5	888	21.8399	-9.1062	Lithology	1	A
180	Kasai	5	884	21.8465	-9.0246	Lithology	1	A
181	Kasai	5	867	21.8872	-8.8016	Lithology	1	A
182	Kasai	20	842	21.9026	-8.6825	Lithology	1	A
183	Kasai	20	829	21.9250	-8.6073	Lithology	1	A
184	Kasai	5	803	21.9373	-8.5351	Lithology	1	A
185	Kasai	30	774	21.7775	-7.8129	Fault	3	A
186	Kasai	5	745	21.8437	-7.6165	fault	5	A
187	Kasai	20	727	21.8072	-7.3072	fault	3	A
188	Kasai	10	682	21.6677	-7.0852	fault	3	DRC
189	Kasai	10	655	21.6281	-7.0493	Lithology	1	DRC
190	Kasai	20	632	21.5956	-7.0303	Lithology	1	DRC
191	Kasai	5	596	21.4618	-6.8871	Lithology	1	DRC
192	Kasai	25	571	21.4219	-6.8440	Lithology	1	DRC
193	Kasai	5	548	21.3737	-6.8194	Lithology	1	DRC
194	Kasai	15	522	21.1629	-6.6755	Lithology change	1	DRC
195	Kasai	10	478	20.9317	-6.5412	Lithology	1	DRC
196	Kasai	10	466	20.8932	-6.5058	Lithology change	3	DRC
197	Kasai	15	452	20.8486	-6.4966	Lithology change	3	DRC
198	Kasai	5	416	20.8847	-5.5961	Lithology change	3	DRC
199	Kasai	15	400	20.9100	-5.5327	Lithology	1	DRC
200	Kasai	10	400	20.9541	-5.4787	Lithology	1	DRC
201	Kasai	-5	1032	21.7625	-10.7651	Lithology	1	A
202	Kasai	-5	1008	21.9577	-10.6109	Lithology	1	A
203	Kasai	-5	931	21.8037	-9.4296	Lithology	1	A
204	Kasai	-5	875	21.8495	-8.9721	Lithology	1	A
205	Kasai	-5	697	21.7264	-7.1962	Lithology change	1	DRC

206	Kasai	-5	612	21.5415	-6.9731	Lithology	1	DRC
207	Kasai	-5	491	21.0689	-6.6111	Lithology	1	DRC
208	Kasai	-5	426	20.8217	-5.7387	Lithology change	3	DRC
209	Kasai	-5	434	20.8533	-5.6862	Lithology		DRC
210	Kasai	-1	786	21.8381	-8.1157	Lithology	1	A
211	Kwango	90	1188	18.7748	-11.1594	other	5	A
212	Kwango	20	944	18.6216	-10.1157	other	5	A
213	Kwango	20	929	18.6603	-10.0976	other	5	A
214	Kwango	20	870	18.2228	-9.2874	Lithology change	1	A
215	Kwango	20	856	18.1360	-9.2665	Lithology	1	A
216	Kwango	5	822	18.0374	-9.1605	Lithology	1	A
217	Kwango	5	805	18.0398	-9.0381	Lithology change	1	A
218	Kwango	5	801	18.0312	-9.0159	Lithology change	1	A
219	Kwango	5	795	18.0163	-8.9982	Lithology change	1	A
220	Kwango	15	798	18.0158	-8.9806	Lithology change	1	A
221	Kwango	45	756	18.0107	-8.8856	Lithology	1	A
222	Kwango	30	723	17.9466	-8.8060	Lithology change	1	A
223	Kwango	25	668	17.9090	-8.6778	Lithology change	1	A
224	Kwango	10	646	17.8697	-8.6035	Lithology change	3	A
225	Kwango	5	624	17.7560	-8.5199	other	5	A
226	Kwango	75	588	17.3179	-7.7162	Lithology	3	A
227	Kwango	50	460	17.2723	-7.6152	Lithology	1	A
228	Kwango	-5	811	18.0601	-9.0719	Lithology	1	A
229	Luapula	15	1138	29.2117	-12.3738	other	5	DRC
230	Luapula	20	1114	29.1214	-12.3940	other	5	DRC
231	Luapula	15	1087	29.0800	-12.3866	other	5	DRC
232	Luapula	15	1067	29.0354	-12.3524	other	5	DRC
233	Luapula	20	1033	28.4532	-11.3129	other	5	DRC
234	Luapula	10	1011	28.6254	-10.7156	fault	5	DRC
235	Luapula	80	997	28.6890	-10.6785	fault	3	DRC
236	Luena	40	1278	19.9139	-11.8028	Lithology change	5	A
237	Luena	15	1227	19.9637	-11.8024	other	5	A
238	Luena	10	1218	19.9955	-11.7984	other	5	A
239	Luena	10	1209	20.0313	-11.7785	other	5	A
240	Luena	10	1190	20.0662	-11.7382	other	5	A
241	Luena	5	1154	20.3225	-11.7623	other	5	A

242	Luena	10	1140	20.4365	-11.9154	Lithology change	3	A
243	Luena	0	1061	22.5012	-12.4688	other	5	A
244	Luena	-5	1177	20.1198	-11.7230	other	5	A
245	Luena	-5	1177	20.1570	-11.7205	other	5	A
246	Lufira	90	1118	27.2443	-10.7524	Dam wall	1	DRC
247	Lufira	50	1014	27.2687	-10.7221	Dam wall	1	DRC
248	Lufira	10	1139	26.8771	-11.2000	Lithology	1	DRC
249	Lufira	50	992	27.2809	-10.7184	Lithology change	1	DRC
250	Lufira	15	909	27.3984	-10.6072	Lithology	1	DRC
251	Lufira	45	867	27.0404	-9.5169	Lithology	3	DRC
252	Lufira	20	834	26.9752	-9.4538	Lithology	1	DRC
253	Lufira	5	813	26.9208	-9.3638	Lithology change	1	DRC
254	Lufira	-5	1202	26.7189	-11.5376	Lithology	1	DRC
255	Lufira	-5	943	27.3182	-10.6943	Lithology change	3	DRC
256	Lufira	-5	929	27.3720	-10.6750	other	3	DRC
257	Lufupa	15	1090	24.4966	-10.4297	Lithology	1	DRC
258	Lufupa	25	1061	24.5217	-10.3922	Lithology	1	DRC
259	Lufupa	25	976	24.6076	-10.3459	Lithology	1	DRC
260	Lufupa	25	943	24.6156	-10.3524	Lithology	1	DRC
261	Lufupa	30	921	24.6510	-10.3314	Lithology	1	DRC
262	Lufupa	15	792	24.9365	-9.6039	Lithology	1	DRC
263	Lufupa	10	776	25.0278	-9.5904	Lithology change	1	DRC
264	Lufupa	0	734	25.5185	-9.0862	Lithology	1	DRC
265	Lufupa	40	721	25.5306	-9.0819	Lithology	1	DRC
266	Lufupa	0	682	25.5673	-9.0848	Lithology	1	DRC
267	Lufupa	0	665	25.5839	-9.0985	Lithology	1	DRC
268	Lufupa	0	661	25.5984	-9.1049	Lithology	1	DRC
269	Lufupa	0	652	25.6058	-9.1217	Lithology	1	DRC
270	Lufupa	0	664	25.6150	-9.1312	Lithology change	1	DRC
271	Lufupa	5	639	25.6211	-9.1514	Lithology	1	DRC
272	Lufupa	-1	728	25.4734	-9.0848	Lithology	1	DRC
273	Lufupa	-5	907	24.7500	-10.2404	Lithology	1	DRC
274	Lufupa	-5	887	24.7481	-10.1633	Lithology	1	DRC
275	Lufupa	-5	811	24.8214	-9.7544	Lithology	1	DRC
276	Lufupa	-1	803	24.8461	-9.7679	Lithology change	1	DRC
277	Lufupa	-1	800	24.8671	-9.7330	Lithology	1	DRC

278	Lukuga	5	771	28.9590	-5.9014	Lithology change	1	DRC
279	Lukuga	5	758	28.8543	-5.8829	other	1	DRC
280	Lukuga	15	703	28.3947	-5.9238	Lithology change	1	DRC
281	Lukuga	15	688	28.3582	-5.9168	Lithology	1	DRC
282	Lukuga	15	670	28.2891	-5.9035	Lithology	1	DRC
283	Lukuga	10	642	28.1698	-5.8733	Lithology	1	DRC
284	Lukuga	15	612	28.0192	-5.7124	Lithology change	3	DRC
285	Lukuga	0	783	29.0745	-5.9214	fault	3	DRC
286	Lulua	10	1109	23.1338	-10.8790	Lithology	1	DRC
287	Lulua	40	1022	22.7981	-10.7603	Lithology	1	DRC
288	Lulua	5	987	22.8990	-10.6828	Lithology	1	DRC
289	Lulua	10	975	22.8475	-10.6162	Lithology	1	DRC
290	Lulua	30	943	22.8575	-10.4424	Lithology	1	DRC
291	Lulua	10	919	22.8610	-10.3813	Lithology	1	DRC
292	Lulua	20	880	22.6361	-9.2274	Lithology	1	DRC
293	Lulua	30	872	22.6117	-9.1812	Lithology	1	DRC
294	Lulua	20	723	22.4761	-6.5882	Lithology	1	DRC
295	Lulua	5	702	22.4597	-6.5489	Lithology	1	DRC
296	Lulua	10	692	22.4366	-6.5207	Lithology	1	DRC
297	Lulua	15	686	22.4180	-6.4725	Lithology	1	DRC
298	Lulua	20	644	22.4494	-6.3440	Lithology	1	DRC
299	Lulua	20	597	22.4693	-6.2214	Lithology	1	DRC
300	Lulua	5	557	22.3914	-6.0048	Lithology	1	DRC
301	Lulua	10	451	22.0074	-5.4922	Lithology	1	DRC
302	Lulua	20	439	21.9897	-5.4784	Lithology	1	DRC
303	Lulua	10	430	21.9709	-5.4405	Lithology	1	DRC
304	Lulua	-5	913	22.8158	-10.3344	Lithology	1	DRC
305	Lulua	-5	845	22.5553	-8.8807	Lithology	1	DRC
306	Lulua	-5	799	22.5962	-7.7168	Lithology	1	DRC
307	Lulua	-5	752	22.5330	-6.6945	Fault	1	DRC
308	Lulua	-5	742	22.4960	-6.6981	Lithology	3	DRC
309	Lulua	-5	666	22.4140	-6.4274	Lithology	1	DRC
310	Lulua	-5	571	22.3924	-6.0970	Lithology change	3	DRC
311	Lulua	-5	485	22.1834	-5.8009	Lithology	1	DRC
312	Lulua	-5	475	22.1474	-5.7589	Lithology	1	DRC
313	Lulua	-1	813	22.6718	-7.8501	Lithology	1	DRC

314	Lulua	-1	781	22.6997	-7.4199	Lithology	1	DRC
315	Lulua	-1	400	21.5446	-5.3406	Lithology	1	DRC
316	Luvua	0	930	28.8459	-8.4577	fault	3	DRC
317	Luvua	10	928	28.8380	-8.4531	Lithology	1	DRC
318	Luvua	5	885	28.7986	-8.3624	Lithology	1	DRC
319	Luvua	15	873	28.8615	-8.2265	Lithology	1	DRC
320	Luvua	50	852	28.8125	-8.1523	Lithology	1	DRC
321	Luvua	10	785	28.7216	-8.0014	Lithology	1	DRC
322	Luvua	5	755	28.6947	-7.9568	Lithology	1	DRC
323	Luvua	20	732	28.6818	-7.9274	Lithology	1	DRC
324	Luvua	20	719	28.6185	-7.8805	Lithology	1	DRC
325	Luvua	20	703	28.4426	-7.8733	Lithology	3	DRC
326	Luvua	20	701	28.4166	-7.8553	Lithology	3	DRC
327	Luvua	20	618	28.1023	-7.6403	Lithology	1	DRC
328	Luvua	30	589	28.0870	-7.4374	Lithology change	3	DRC
329	Luvua	10	584	28.0773	-7.4198	Lithology	1	DRC
330	Luvua	5	578	28.0504	-7.3814	Lithology change	3	DRC
331	Luvua	-5	711	28.5592	-7.9323	Lithology change	3	DRC
332	Luvua	-5	665	28.3198	-7.8039	Lithology	1	DRC
333	Luvua	-5	654	28.2219	-7.7505	Lithology change	3	DRC
334	Luvua	-5	638	28.1530	-7.6921	Lithology	1	DRC
335	Luvua	-5	619	28.1007	-7.6422	Lithology	1	DRC
336	Wamba	10	909	18.3509	-8.4951	other	5	A
337	Wamba	25	893	18.3171	-8.4606	other	5	A
338	Wamba	15	856	18.2906	-8.4357	Lithology change	3	A
339	Wamba	20	843	18.2856	-8.4276	Lithology	3	A
340	Wamba	50	834	18.2630	-8.4052	Lithology change	1	A
341	Wamba	50	782	18.2534	-8.3883	other	5	A
342	Wamba	20	730	18.1973	-8.3640	other	5	A
343	Wamba	10	613	17.8144	-7.4907	Lithology change	3	DRC
344	Wamba	10	541	17.3860	-6.4526	other	5	DRC
345	Wamba	5	477	17.1152	-5.9181	other	5	DRC
346	Wamba	5	397	16.9477	-5.0683	other	5	DRC
347	Wamba	-5	712	18.1630	-8.2978	other	5	A
348	Wamba	-5	631	17.9071	-7.5702	Lithology	1	DRC
349	Wamba	-5	413	16.9503	-5.4116	other	5	DRC

350	Wamba	-5	414	16.9488	-5.3849	other	5	DRC
351	Wamba	-1	640	17.9293	-7.5833	Lithology	1	DRC
352	Wamba	-1	506	17.2651	-6.3135	other	5	DRC
353	Wamba	-1	421	16.9532	-5.3723	other	5	DRC
354	Wamba	-1	410	16.9118	-5.3205	other	5	DRC
355	Wamba	-1	405	16.9240	-5.3017	other	5	DRC
356	Wamba	-1	401	16.9211	-5.2213	other	5	DRC
357	Zambezi	5	1046	22.6681	-13.0717	other	5	Z (D)
358	Zambezi	5	1044	22.6894	-13.1050	other	5	Z (D)
359	Zambezi	5	992	23.4822	-16.5570	Lithology	1	Z (D)
360	Zambezi	5	989	23.5265	-16.6086	Lithology	1	Z (D)
361	Zambezi	10	984	23.5681	-16.6467	Lithology	1	Z (D)
362	Zambezi	5	980	23.5699	-16.6505	Lithology change	3	Z (D)
363	Zambezi	5	919	25.3726	-17.8444	Lithology	1	Z (D)
364	Zambezi	5	901	25.6657	-17.8152	Lithology	1	Z (D)
365	Zambezi	50	865	25.8594	-17.9255	Lithology	1	Z (D)
366	Zambezi	-5	1058	22.6167	-12.6833	Lithology change	3	A
367	Zambezi	-5	1056	22.7196	-12.9929	Lithology	1	A
368	Zambezi	-5	995	23.3889	-16.4505	Lithology	3	Z (D)
369	Zambezi	-5	991	23.4565	-16.5322	Lithology	3	Z (D)
370	Zambezi	-5	967	23.7306	-16.7634	fault	3	Z (D)
371	Zambezi	-5	967	23.7349	-16.7835	fault	3	Z (D)
372	Zambezi	-5	953	24.1586	-17.3093	other	5	Z (D)
373	Zambezi	-5	948	24.1674	-17.3716	other	5	Z (D)
374	Zambezi	-5	943	24.2144	-17.4196	other	5	Z (D)
375	Zambezi	-5	937	24.2498	-17.4740	other	5	Z (D)
376	Zambezi	-5	927	25.1871	-17.7652	Lithology	1	Z (D)
377	Zambezi	-5	914	25.4604	-17.8445	Lithology	1	Z (D)
378	Zambezi	-5	912	25.4862	-17.8501	Lithology	1	Z (D)
379	Zambezi	-5	909	25.5352	-17.8511	Lithology	1	Z (D)
380	Zambezi	-5	904	25.5914	-17.8382	Lithology	1	Z (D)

Section 7.4 Geobiotic groupings

Table 7.4: Selected groupings of species lineages forming coherent spatial ranges. See Chapter 7 for full details. Refer to **Table 7.20** for references to species divergence dates. Spatial groupings of divergence dates were used in **Figure 8.10** to date landscape events.

Geographic centre	Geobiotic complex	Groupings	Phylogeographic event	Divergence data (Ma)	Lower 95 % (Ma)	Upper 95 % (Ma)
TRM Triple Junction	A	A 1	*Mastocembalus frenatus* diverges from M. *shiranus*	**3.9**	**2.9**	**5.9**
TRM Triple Junction		A 2	*H. tanzaniae* diverges from *H. vittatus* complex	3.1	**1.9**	**6.9**
TRM Triple Junction		A 3	*Fukomys* cladogenesis	**3.5**	**3.2**	**3.8**
Kalungwishi - Lufubu Watershed	B	B 1	*Mastocembalus* sp nov 3 vs *M. stappersi*	**3.3**	**2.7**	**3.9**
Kalungwishi - Lufubu Watershed		B 2	*Pseudocranilabrus* "lufubu" speciation	**1.8**	**1.4**	**2.3**
Kalungwishi - Lufubu Watershed		B 3	*Hydrocynus* "Clade B" diverges from "Clade C"	**1.5**	**0.6**	**2.5**
Mweru-Bangweulu	C	C 1	Founding of *Hydrocynus* "Clade B" and "Clade C" diverges from "Clade D" and *H. vittatus*	**2**	**0.8**	**3**
Mweru-Bangweulu		C 2	*S. nigromaculata2*) diverges from *S. nigromaculata*3	**1.8**	**1**	**2.7**
Bangweulu – Upper Zambezi	D	D 1	*Mastocembalus* cf *frenatus* vs *M.* cf *frenatus*	**3**	**2.5**	**3.5**
Bangweulu - Upper Zambezi		D 2	*S. nigromaculata* vs *S. nigromaculata*1	**2.2**	**1.5**	**2.6**
Bangweulu - Upper Zambezi		D 3	Serranochromine cladogenesis	**2.1**	**1.5**	**2.6**
Bangweulu - Upper Zambezi		D 4	*Hydrocynus* "Bangweulu Clade D" diverges from *H. vittatus*	**1.4**	**0.6**	**2.5**
Bangweulu - Upper Zambezi		D 5	Baboons, *Papio kindae* vs *P.* cf. *cyanocephalus* / *P. griseipes* Clade	**1.49**	**1.03**	**1.98**
Bulozi Plain	E	E 1	Serranochromine Zambezian radiation	**0.4**		
Bulozi Plain		E 2	*Pseudocranilabrus* dispersal	**0.4**		
Bulozi Plain		E 3	*Hydrocynus vittatus* cladogenesis	**0.3**		

Table 7.4: *continued from previous page*

Geographic centre	Geobiotic complex	Groupings	Phylogeographic event	Divergence data (Ma)	Lower 95 % (Ma)	Upper 95 % (Ma)
Machili Flats	F	F 1	Hartebeests *Alcelaphus*	**0.212**	**0.188**	**0.24**
Machili Flats		F 2	Eland *Taurotragus Southern vs Eastern clades*	**0.209**	**0.074**	**0.374**
Machili Flats		F 3	Giraffes, Giraffa camelopardalis giraffe (S) vs tippelkirschii		**0.374**	**0.17**
Machili Flats		F 4	*Hippotragus niger* vs *H. kirkii*		**0.261**	**0.3**
Okavango Graben	G	G 1	Radiation of *Synodontis* catfishes	**0.89**	**0.42**	**1.4**
Kasai – Upper Zambezi	H	H 1	*Hydrocynus vittatus* dispersal into Congo and Mzambezi	**0.31**		
Cunene - Cubango	I	I 1	Serranochromine (Kunene Flock) dispersal and speciation	**0.4**	**0.2**	**0.6**

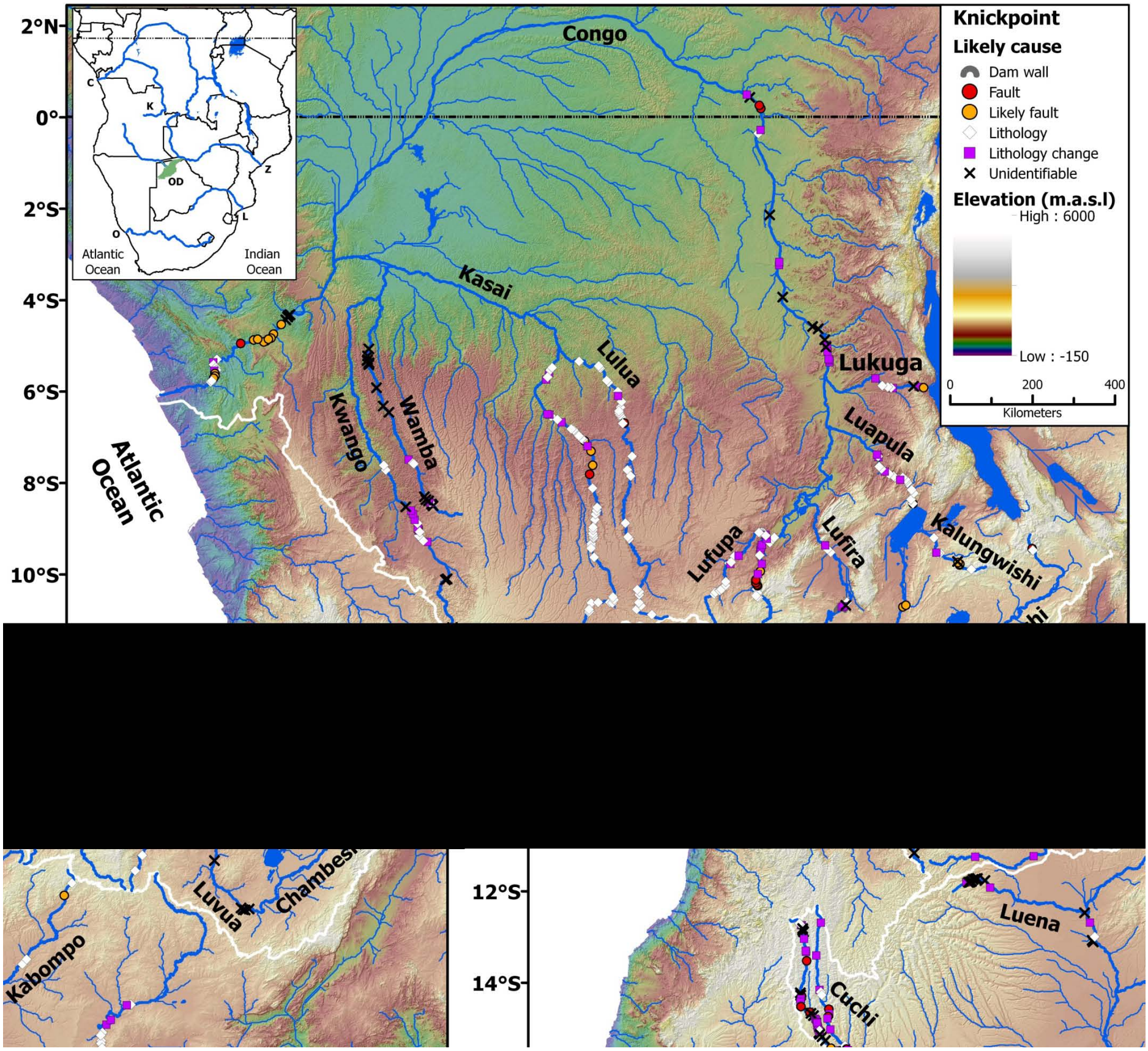

Figure 8.1: The 380 identified knickpoints of south-central Africa and their likely cause. Studied rivers are shown in heavy blue lines, thin blue lines indicated generated river networks and the white line indicates Congo–Kalahari Watershed and the coastal drainage watershed. Inset shows the major rivers and waterbodies in central and southern Africa. Elevation data source is the SRTMv3 DSM. Details regarding this data are discussed in **Chapter 8**, **Section 8.2**.